ANALYSIS AND IMPLICATIONS OF LARGE MARTIAN AND TERRESTRIAL LANDSLIDES

Thesis by

Philip John Shaller

In Partial Fulfillment of the Requirements

for the Degree of

Doctor of Philosophy

California Institute of Technology

Pasadena, California

1991

(Submitted April 8, 1991)

Acknowledgments

To acknowledge the assistance of everyone who has played a positive part in a 5+ year process is by no means a trivial task. I first must acknowledge the efforts of my wife, Ann Smith Shaller, who, at various times throughout this endeavor, has acted as my field assistant, typist, editor, advisor, antelope collision avoidance system and much more, especially my friend. She has been at my side continuously for the last four years, figuratively and literally, and this thesis belongs as much to her as to me.

I also acknowledge the support, encouragement, and sometimes prodding, of my primary thesis advisor, Bruce Murray, who has had the vision to guide us through the long-runout landslide minefield as capably as anyone could possibly have done. Without his unflagging enthusiasm and input into this project, we would never have gotten this far. I believe that we have both come a long way in the course of this thesis work.

My geology thesis advisor, Arden Albee, has played an equally important role in this project, especially as the quality control regulator of all parts of this thesis research. His efforts have kept this thesis on the most solid geological foundation possible. I am indebted to his input for making this thesis a worthy scientific document and for the insight he has given me on the nature of good science and on the making of a good scientist.

There are a number of other individuals without whose help, wisdom and friendship I don't believe I ever would have made it through Caltech. Michele Vogt has played an important role in my life throughout these years. I owe her deep gratitude for getting me on track in my early years at Caltech, for her assistance in the field and in our efforts at image processing, and especially for her everpresent enthusiasm, friendship and willingness to help out in matters both personal and professional. I also wish to thank many of those with whom I started Caltech: Joel Blum, Sally McGill, Diane Knott, Mike Wolf, Yigal Erel, Jackie Dixon and Charlie Rubin. They all deserve special credit, for each made important contributions in getting me through at one time or another in my stay at Caltech.

I also wish to add my thanks to a number of professors at Caltech who have given me critical advise, support and guidance. Bob Sharp, Ron Scott and Kerry Sieh all deserve thanks for buoying my spirit and enthusiasm for this subject.

Finally, I wish to thank the support of my parents and the rest of my family, who have supported me down all the roads I have chosen to follow. Their encouragement and example have provided me the enthusiasm and drive to succeed and the willpower to never give up on anything.

I dedicate this work to all of those who have played an influential role in my life, especially those no longer here to witness this achievement.

Abstract

I address two long-standing scientific problems in this thesis: the mechanism(s) of long-runout in large landslides; and the activity of water on the surface of Mars late in its history. Long-runout landslides form significant geologic risks. My research has aimed at understanding the factors that control the initiation and runout of large landslides wherever they occur. A second objective of this research has been to use martian landslides to gauge the activity of liquid water on Mars' surface over the past quarter of its history. To achieve these objectives, I made field observations of six moist and dry landslides in the western United States, I studied all the high-resolution Viking Orbiter images for large landslides on Mars and I collated all the available literature data on large landslides, to develop the clearest view possible of the nature of the large landslide process. I then used this information to evaluate all the previously published models of long runout, and to develop my own theory when I found that none of the existing theories provided an adequate explanation of the observations.

I conclude that large landslides primarily slide and spread into place over fluidized natural basal lubricants. This concept follows upon the air-layer lubrication theory of Shreve, but does not call upon a gas lubricant, a possibility ruled out by the presence of Blackhawk-like long-runout landslides on Mars. Rather, the lubricants appear to be fine-grained materials from the substrate or from the landslide debris itself that deform plastically at the high shear stresses and strain rates present beneath large rapid landslides. Large dry landslides grade into moist debris flows as water becomes incorporated into their fine-grained component. Moist and dry landslides differ markedly in sedimentology and morphology, but not in a variety of quantitative relations. Seven landslide events on Mars appear to have involved water during runout, based on comparisons with water-bearing landslides of similar morphology and volume on Earth. These deposits occur primarily in Valles Marineris and indicate that liquid water has been sporadically available on Mars at various times over the last ~1 billion years of its history.

Table of Contents

List of Figures

List of Tables

Chapter I. Introduction

Two subjects are investigated in this thesis. The mechanism(s) of "long-runout" landslides forms the first and paramount problem. The role of water on the martian surface as reflected in the behavior of large (>10^6 m^3) and giant (>10^9 m^3) landslides comprises the second problem addressed in this thesis.

A. Background and Motivation

The static and dynamic coefficients of friction of dry geologic materials usually lie near 0.6 (tan 31°), so that mass movements whose travel is governed by dry frictional interactions with the substrate should normally exhibit center of gravity lines (connecting final and initial centers of gravity of the slidemass) with slopes of about 31°. The term "long-runout landslides" refers to rapid landslides in which the center of gravity of the slidemass travels through an angle of less than 31° from the beginning to the cessation of movement. Long runout is actually characteristic of large landslides; most landslides containing more than 10^6 m^3 of debris exhibit center of gravity line slopes of less than 31°. In addition, the center of gravity lines of large landslides generally decrease in inclination with increasing volume; larger landslides travel farther for a given fall height than smaller slides. The volume threshold for long runout varies for different starting materials. Landslides that begin movement in a loosely aggregated condition may experience long runout at volumes as low as 10^4 m^3. Long-runout landslide deposits occur on Earth's continents, in terrestrial lakes and oceans, on Mars and perhaps on the Moon.

Because of their great destructive potential, long-runout landslides have received much attention in the geologic literature ever since Heim (1882) described the characteristics of the 1881 Elm, Switzerland, landslide, a catastrophic event that killed 116 persons. Much of the interest in these landslides has centered on the mechanics of their high-velocity transport. This interest has led to the publication of nearly twenty separate theories on the mechanism of long runout in large landslides. These efforts have followed two principal approaches: some workers have viewed all large landslides as behaving according to a single, unique process, while others have viewed the process on a case-by-case basis. Workers who have espoused a general mechanism have proposed bulk fluidization models, basal lubrication models

and a distributed mass loss theory to explain the long runout phenomenon. The individual-case models, in turn, have proposed either basal lubrication or earthquake fluidization to explain the long runout of individual landslides or small groups of slides. In the body of the thesis, I have collated both new and previously published data to evaluate each of these theories, and I have determined that none of the proposed general theories can adequately explain all the important characteristics of these landslides. Specifically, I have ruled out one of the theories currently considered a prime candidate for explaining the phenomenon: air-layer lubrication (Shreve, 1968a). Furthermore, I show that the concept of acoustic fluidization as currently developed (Melosh, 1979; 1983; 1986; 1987) appears inadequate to explain long-runout landslides generally. I have therefore developed my own concepts for explaining long runout as a group phenomenon. My concept, which is explained in Chapter VI of this thesis, explains long runout as resulting from two processes: distributed deposition of the brecciated landslide debris; and non-turbulent spreading of landslide debris over naturally-occurring basal lubricants. The latter half of Chapter VI lists specific field, laboratory and computer studies that should be conducted to test my hypothesis.

Liquid water seems to have been sporadically available at the surface of Mars through much of its geologic history. Most of the evidence for surficial water comes from erosive features interpreted to have been cut by flowing water early in Mars' history. Three types of channels occur on Mars: 1) runoff channels, limited to the ancient cratered terrain and probably formed as a result of groundwater sapping; 2) outflow channels, distributed around the planet, and apparently formed by catastrophic floods from the rapid extrusion of underground water onto the surface from pressurized aquifers; and 3) fretted channels, which seem to represent runoff channels subsequently modified by mass wasting processes (Carr, 1981). Carr (1981) suggests that the runoff channels probably formed at the same time as the ancient cratered terrain, roughly 3.4 to 4.0 billion years ago. In contrast, the outflow channels formed over an extended period of time, mostly early in Mars' history, but with late events perhaps occurring as recently as 0.5 billion years ago (Baker, 1982). At high latitudes (>30°) on Mars, numerous features, such as polygonal ground, fretted terrain, patterns of impact ejecta, debris flows, terrain softening and arrays of parallel ridges suggest the presence of near-surface ground ice (Carr, 1986). However, theoretical studies and a lack

of these ice-related features in the cratered uplands at low latitudes suggest that the upper 1 km of the uplands at low latitudes is ice poor (Carr, 1986).

A number of features in Valles Marineris also appear related to ground ice or liquid water. The walls of Valles Marineris are marked by three basic morphologies: spur-and-gulley topography, tributary canyons and giant slump scars (Blasius, et al., 1977). The slump scars generally cut through and thus postdate the other two types of canyon-wall textures. Along with the slump scars, Sharp (1973) interpreted the spur-and-gulley morphology as resulting primarily from mass movement processes, while he viewed the tributary canyons as probably resulting from sapping processes, caused either by seepage of liquid water or sublimation of ground ice at the heads of the tributary canyons. Subsequent to the erosion of the canyon wall rock into the spur-and-gulley and tributary canyon morphologies, but prior to emplacement of the giant slumps, layered terrain filled Valles Marineris in places and then became partially eroded. The origin of the chasma layered terrains has been attributed to lacustrine deposition (McCauley, 1978), perhaps in ice-covered lakes (Nedell, et al., 1987), though other processes, such as aeolian and volcanic activity cannot conclusively be ruled out (Nedell, et al., 1987). Fluvial erosion, perhaps during catastrophic emptying of the hypothetical lakes, has been proposed to explain the majority of their subsequent erosion (McCauley, 1978). The large landslides in Valles Marineris, the most recent form of mass movement in the equatorial chasmas, were deposited within the last ~1 billion years (Lucchitta, 1987a). They have been variously argued to have been water-saturated (Lucchitta, 1987a) and totally dry (McEwen, 1989) at deposition.

Giant ($> 10^9$ m^3) long-runout landslides were first recognized on Mars by Lucchitta (1978a; 1979). Their giant volumes were initially thought anomalous in the solar system, but recent findings of giant landslides from Hawaiian Ridge volcanoes (Lipman, et al., 1988; Moore, et al., 1989) have shown that landslides with giant volumes can occur in other environments having large-scale relief (Shaller, et al., 1989). Although Lucchitta (1978a) initially compared the giant landslides on Mars with dry long-runout slides on Earth, she subsequently interpreted the morphologies of many of the martian landslides to represent mudflow deposits, emplaced in a water-saturated condition. Because the martian landslides formed in roughly the last ~1 billion years of Mars' geologic history, a proven water-saturated origin for the

landslides would suggest that water was available in Valles Marineris much more recently than the ~3 billion year old age of the chasma layered terrains, with serious implications for the internal geological evolution of Mars (Lucchitta, 1987a). McEwen (1989) countered the proposal that large martian landslides were water saturated at emplacement. He used a variety of quantitative measures of landslide properties to show that long-runout landslides on Mars have more in common with large dry terrestrial slides than with moist or water-saturated terrestrial mass movements. These quantitative measures included: velocity data from overtopped obstacle heights; estimated plastic yield strength data from deposit thickness and depositional slope measurements; and log(volume) vs. fall height to runout length (H/L) measurements. I have evaluated the arguments of both Lucchitta and McEwen in this thesis, using data from my field study of the Carlson landslide, together with morphological and quantitative data from other large terrestrial landslides described in the literature. My research has discovered, in *contradiction to the conclusions* of McEwen (1989), that common quantitative measures of landslide properties fail to distinguish dry from moist or water-saturated landslides. Furthermore, based on morphology, five martian landslide events specifically appear to have involved water in Valles Marineris, and two others on Olympus Mons. These observations imply that liquid water was involved in martian crustal processes as late as a few tens or hundreds of millions of years ago.

B. Method

I began my work on this thesis by collating all possible sources of information on terrestrial, martian and lunar long-runout landslides and placing this information into a database with approximately twenty fields, containing data on landslide locations, dimensions and morphologies (Chapter II). Using this database as a basis for observation, I then undertook a systematic search of all the high-resolution (<100 m/picture element) Viking Orbiter images of Mars in search of landslide deposits. The two Viking Orbiters took a total of about 50,000 images of the martian surface (Blasius, et al., 1980); probably 1/4 to 1/5 of these were of the necessary high resolution and quality to observe landslides in the ~10^9 m^3 volume range, while giant landslides could be observed on lower-resolution images. In this survey I located about 100 previously unrecognized landslides on Mars, most having volumes between

0.25 and 2 x 10^9 m^3, roughly the volume range of larger terrestrial subaerial landslides (Appendix A). Using the combined dataset of literature data and new martian landslide images, I then developed my own classification scheme for large landslides based solely on morphology (Chapter II). This scheme is a departure from other landslide classifications, which have previously been based upon landslide composition (soil vs. bedrock), water content, and emplacement speed, all unknown factors for the martian landslides.

By applying the morphological classification scheme to each landslide in the database, I recognized for the first time that landslides on Earth and Mars exhibit a common range of morphologies and volumes, with the exception that Mars contains none of the planar landslides common in folded sedimentary mountain belts on Earth. Three groups of landslides with common morphologies and comparable volumes on Earth and Mars were then singled out for concentrated study: large lobate landslides, "Blackhawk-like" landslides, and giant slumps.

Large lobate landslides had previously been noted on Earth (Shelton, 1966: Bock, 1977), but no previous field work had focused on the lobate terrestrial landslides most analogous in morphology to those on Mars. This led me to conduct field studies on a large lobate landslide in east-central Idaho, informally termed the Carlson landslide (Appendix B). Study of the Carlson landslide, which began motion as a dry rock avalanche and concluded as a large moist debris flow, indicated to me that large moist and dry landslides exhibit no characteristic differences in quantitative properties such as log(volume) vs. H/L trends or plastic yield strength estimates, but that they do differ significantly in morphology and sedimentology. These results rule out the proposition by McEwen (1989) that his quantitative measures of landslide properties support a dry origin for all Valles Marineris landslides; such quantitative measures fail to distinguish moist from dry landslides on Earth, and so could hardly be expected to separate them on Mars. The morphological results, in turn, showed me that the lobate martian landslides most likely traveled in a moist state during runout, not dry as concluded by McEwen (1989), nor water-saturated as suggested by Lucchitta (1987a).

The gradational dry-to-moist behavior of the Carlson landslide, combined with its quantitative similarities to dry long-runout landslides, furthermore indicated to me that the mechanism of long runout in dry and moist landslides must be quite similar. However, comparison of the sedimentology of the

Carlson landslide (Appendix B) with data I collected from a field survey of the Martinez Mountain rock avalanche of southern California (Chapter III: Figure 23) showed the two deposits to exhibit considerable textural differences. These seemingly contradictory findings led me back to the literature and to other field sites in an effort to fully document the variety of sedimentary data available on the interior and basal geologic relations of large landslides (Chapter III). The additional field sites I visited include the Blackhawk landslide of southern California, a pair of megabreccia deposits in the Avawatz Mountains of southern California, and the El Capitan landslide of east-central Arizona. The data I collected from these sources were crucial to my subsequent detailed analysis of proposed long-runout mechanisms in large landslides.

The observation of large landslides on Mars with morphologies remarkably similar to the Blackhawk dry rock avalanche of southern California led to another revolution in my thinking on the long runout process. I ultimately located thirteen "Blackhawk-like" landslides on Earth and Mars that exhibited similar morphological development (Chapter IV), probably reflecting similar origins as coherent rockfalls onto unconfined depositional surfaces. I discovered that the only characteristic difference between the martian and terrestrial landslides is that the martian landslides ended movement with approximately 2-3 times the thickness of their terrestrial counterparts. Because I found that similar thickness relations exist between terrestrial and martian lobate landslides, this finding strongly suggested to me that the transport of the landslides on both planets required the development of threshold basal shear stresses, values dictated in part by the thickness of a landslide and the gravitational acceleration of its environment.

The presence of fresh-appearing Blackhawk-like landslides on Mars also allowed me to evaluate the air-layer lubrication model of Shreve (1959; 1968a), which was originally developed to explain the long runout and morphological development of the Blackhawk landslide of southern California (Shreve, 1959). I submit that this provides an important and valid test of the theory because of the high acceptance the air-layer lubrication theory has achieved among geologists and because of the close morphological and volumetric similarities of the martian examples to their terrestrial counterparts. Shreve (1966; 1968a) later extended the theory to several other large long-runout landslides, notably the Sherman, Frank, Elm and Saidmarreh deposits. Shreve (1968a) summarized the air-layer lubrication theory as follows:

> According to this idea a landslide of the Blackhawk type starts as a huge rockfall which acquires such high speed in its descent that at a projecting shelf of rock or sudden steepening of slope it leaves the ground, overriding and trapping a cushion of compressed air upon which it traverses the gentler slopes below with little friction, much as the slipper in a thrust bearing slides on a cushion of oil with no metal-to-metal contact. The distance and direction travelled after launching depends upon the initial velocity, the gradient and smoothness of the land surface, and the amount, redistribution and leakage of the trapped air.

The air-layer lubrication theory describes the geological relations of the Blackhawk landslide quite well (Shreve, 1959; 1968a), but is much less satisfactory in its explanation of relations observed in other terrestrial long-runout landslides, such as Saidmarreh (Watson and Wright, 1969), Sherman (Shreve, 1966; McSaveney, 1978) and Frank (Cruden and Hungr, 1986). In addition, I show in Chapter IV and Appendix D that the air-layer lubrication theory also fails materially to explain the occurrence and unique characteristics of landslides with Blackhawk-like morphologies that I have discovered on Mars. The calculations made in Appendix D force me to conclude that air-layer lubrication cannot explain the runout of martian Blackhawk-like landslides because of the tremendous volumes of atmosphere the landslides would have had to capture during runout to provide an effective gas cushion. These results lead me to conclude that the mechanism of air-layer lubrication, though possible on Earth, probably is not the cause of the runout and morphological development of terrestrial long-runout landslides.

Giant slumps form a third class of landslides which I discovered to exhibit similar volumes and morphologic development on Earth and Mars. On Mars, the giant slumps are confined almost entirely to the walls of Valles Marineris, while on Earth bedrock slumps form almost entirely on large subaerial and subaqueous volcanic piles. The debris aprons emanating from large terrestrial slumps exhibit a variety of morphologies. Of these, I found three distinct debris apron morphologies that always appear to signal a role for water in emplacement of the landslide debris. A distal gradation from landslide debris to mud- or debris flows implies the presence of water-saturated matrix material; a large-scale lobate-terraced morphology appears related to emplacement within an aqueous medium; and a morphology in which large blocks of landslide debris lie outside the distal margin of a landslide deposit reflects either the presence of water-saturated matrix

material and/or water-saturated substrate sediments (Chapter IV). I also found these morphologies on some landslides in Valles Marineris: (1) an interconnected group of three fresh-appearing landslides at the north end of Ophir Chasma with debris that transitions gradationally into probable mudflow or debris flow deposits; (2) a landslide in Ganges Chasma that disaggregated into a mass of blocks along its distal margin upon entering a shallow basin; and (3) a large landslide in Tithonium Chasma that displays a lobate-terraced morphology that closely mimics similar textures imaged by GLORIA side-scan sonar (Lipman, et al., 1988) on the surface of a large landslide several thousand meters below sea level in the Hawaiian Trough (Chapter IV). The morphological development of these unique martian landslides leads me to conclude that liquid water was involved in their runout. In each case the water probably originated in chasma wall rock, and either was mixed with the landslide debris from the outset of motion, or, for the Ganges and Tithonium slides, fed large temporary ice-covered lakes into which the landslide debris traveled during runout. Together with evidence from the lobate landslides described previously, these observations lead me to suggest that liquid water has been available at high pore pressures behind wall rock in Valles Marineris at very infrequent intervals over the past ~1 billion years, perhaps in response to long-term volcanic or tectonic processes. Over this time interval, at least five landslide events in Valles Marineris appear to have involved liquid water.

The systemized data on long-runout landslide morphologies (Chapter II), their sedimentologies, eyewitness accounts and quantitative relations (Chapter III), together with the comparative planetology data (Chapter IV) and the observations on the gradational nature of dry, moist and water-saturated landslides (Chapter IV; Appendix B), have allowed me to fully evaluate the various mechanisms previously proposed to explain the long runout phenomenon in large landslides (Chapter V). These models have followed two principal approaches: some workers have viewed all large landslides as behaving according to a single, unique process, while others have viewed the process on a case-by-case basis. Workers who have espoused a general mechanism have proposed bulk fluidization models (Heim, 1932; Kent, 1966; Hsü, 1975; Davies, 1982; Melosh, 1979; 1983 1986; 1987; Krumdieck, 1984; Trunk, et al., 1986; Campbell, 1989; McEwen, 1989; Potapov and Ivanov, 1991), basal lubrication models (Shreve, 1968a; Erismann, 1979) and a distributed mass loss

theory (Van Gassen and Cruden, 1989) to explain the long runout phenomenon. The individual-case models, in turn, have proposed either basal lubrication (Watson and Wright, 1969; Habib, 1975; Goguel, 1978; Johnson, 1978; McSaveney, 1978) or earthquake fluidization (Solonenko, 1972; Hazlett, et al., in press) to explain the long runout of individual landslides or small groups of slides. As published, however, none of the proposed general theories can adequately explain all the important characteristics of these landslides. The bulk fluidization models, for example, all fail because they cannot explain the preservation of stratigraphy in dry long-runout landslides. While some (Davies, 1982; Melosh, 1979; 1983; 1986; 1987) state that fluidization may occur only along the bases of large landslides, such mechanical basal fluidization models remain experimentally unproven and are thus ad hoc. The proposed general basal lubrication models also fail because of a lack of a universal lubricant for long-runout landslides. As written (Van Gassen and Cruden, 1989), a proposed general model of long runout caused by distributed deposition fails as well because it wrongly predicts that landslide travel distances should vary with deposit profile shape, with tapered landslides predicted to travel the greatest distance for a given volume and fall height.

The acoustic fluidization concept of Melosh (1979; 1983; 1986; 1987) is currently among the most popular theories for explaining long runout in large landslides (c.f. Curry and Melhorn, 1990; Hazlett, et al., in press). The concept postulates a method of granular flow for long-runout landslides which requires much less energy than other proposed mechanisms of mechanical fluidization (Melosh, 1983). The concept is outlined in Melosh (1986) as follows:

> The fluid-like flow of large rock debris masses, even *in vacuo*, may be explained by the presence of strong acoustic waves or 'noise' within the slide mass. Acoustic waves, generated by the shear flow, diffuse through the strongly-scattering rock debris. Because rocks in the slide remain largely in contact during flow, these waves may transmit large pressure fluctuations elastically without simultaneously transporting large amounts of energy. The pressure fluctuations allow the dry rock debris to yield under a differential stress much smaller than the average overburden. The overburden is briefly relieved by any unusually large pressure fluctuation and a local slippage may take place in the debris mass...

Melosh (1987) goes on to state that:

> It appears that large, high-frequency pressure fluctuations due to irregularities in the flow of the debris may locally relieve overburden pressures in the rock mass and allow rapid pseudoviscous flow of even dry rock debris. If the avalanche volume is large enough, the rate of production of this vibrational (acoustic) energy exceeds its loss rate, and sustained motion is possible...

Melosh (1987) also states that acoustic fluidization can explain several of the general geological observations of long-runout landslides:

> ...The high power law rheology of acoustically fluidized debris accounts for the frequent observation that large rock avalanches slide, preserving gross stratigraphic relations [preserved stratigraphy] in the debris mass. It accounts naturally for the scale-dependence of large avalanches, since acoustic energy is lost too easily from small volumes of debris due to their large surface-to-volume ratio...
>
> ...[The] basal zone is very active, in contrast to the overlying debris mass...Small amounts of the underlying ground surface may be incorporated here and mixed with the laterally transported rock debris...

Unlike the air-layer lubrication model of Shreve (1959; 1968a), however, the acoustic fluidization concept does not make any other specific morphological or textural predictions on the nature of long-runout landslide deposits. It does not take into account effects of landslide debris properties, substrate properties, confinement or initiation style. Unlike Shreve's theory, therefore, acoustic fluidization remains conceptual, and is not yet sufficiently well constrained to allow field testing of the concept on long-runout landslide deposits. In addition, some doubt (Melosh, personal communication, 1990) remains as to whether the process can actually generate basally-concentrated flow as predicted in Melosh (1987). As currently documented, therefore, acoustic fluidization does not provide a testable explanation for long runout in large landslides.

Because of the failure of all the previously proposed general theories of long runout to explain the full range of geologic field relations of large landslides, I have developed my own concepts for explaining long runout as a general phenomenon. My concept, which is explained in Chapter VI of this thesis, explains long runout as resulting from the operation of two processes: distributed deposition of the brecciated landslide debris, which, in larger landslides, grades into non-turbulent spreading of landslide debris over naturally-occurring basal lubricants. The distributed deposition concept is an

outgrowth of the low-velocity mass loss model of Van Gassen and Cruden (1989). Their model states that the long runout of large landslides occurs as an outgrowth of gradual deposition of landslide debris caused by momentum transfer between individual particles making up the landslides, with particles at the rear coming to rest first. Distributed deposition explains a few critical observations of long-runout landslides not explained by basal lubrication, but the basal lubrication portion of the concept forms an equally important part of the theory and accounts for many of the geological details of these deposits. My basal lubrication concept is an outgrowth of the air-layer lubrication theory of Shreve (1968a) and of several other basal lubrication theories promoted to explain long runout on an individual-case basis (Watson and Wright, 1969; Johnson, 1978; McSaveney, 1978; Evans, personal communication, 1990). The basal lubrication concept I develop in Chapter VI extends these earlier models by suggesting that long-runout landslides can be lubricated by a variety of natural substances that yield and flow under the high shear stresses and strain rates encountered beneath large, rapidly moving landslides. Where a substrate consists of weak materials, such as soil, snow or mud, this material yields and forms the lubricant, whereas comminuted debris from the landslides themselves may form the basal lubricant where landslides travel over bedrock substrates.

The research I have conducted for this thesis should open new doors on our perceptions of long-runout landslides on Earth and Mars. The distributed deposition and basal lubrication concepts I present in Chapter VI explain many of the previously disparate observations concerning long-runout landslides and provides a reasonable conceptual framework for predicting the behavior of future events. The distributed deposition and basal lubrication concepts should prove testable in centrifuge simulations of large landslides, as well as in future field and computer-modeling studies. Laboratory investigations of the rheological properties of natural materials under the pressure, shear rate and shear stress conditions existing beneath large landslides await the development of devices capable of experimentally reproducing these conditions.

Chapter II. Database of Giant Landslides

A. A Comprehensive Database of Large Landslides

The "Database of Giant Landslides" (Appendix A) incorporates information on large (>10^6 m^3) lunar, martian and terrestrial landslides. Each landslide record in the database consists of a number of field entries. The field entries include condensed data on a landslide's name and rank, dimensions, velocity, estimated friction coefficient, morphological classification, location, degree of confinement, age, composition, moisture content, substrate properties and literature references. In addition, a "Notes" section is provided for supplementary information, such as eyewitness accounts and depositional characteristics. Information for the landslide records in Appendix A is extracted from the literature, except for data on the Carlson landslide and on a number of martian landslide deposits studied for the thesis.

The database records in Appendix A provide the most complete compilation of data yet available on the subject of large landslides. This database is unique as compared with other collections of data on large landslides, as it is the first database to combine information on large landslides from all the solar system environments known to contain them: the surface of Mars, including highland locations, Valles Marineris and volcanoes; the lunar surface; and terrestrial subaerial and subaqueous occurrences, including Tertiary megabreccias and large volcanic landslides. Previous significant compilations of landslide data have concentrated principally on subgroups of large landslides, such as Alpine landslides (Heim, 1932; Eisbacher and Clague, 1984), Canadian landslides (Eisbacher, 1979), giant (>10^9 m^3) subaqueous landslides (Lipman, et al., 1988; Moore, et al., 1989), lunar landslides (Howard 1973 a; b), martian Valles Marineris landslides (Lucchitta, 1979; 1987a; McEwen, 1989), megabreccias (Yarnold and Lombard, 1989), terrestrial non-volcanic subaerial landslides (Scheller, 1971; Scheidegger, 1973; Hsü, 1975) or volcanic landslides (Ui, 1983; Siebert, 1984), though several of these studies incorporated terrestrial non-volcanic subaerial landslides as a basis for comparison (Howard, 1973a; b; Lucchitta, 1978a; Eisbacher, 1979; Ui, 1983; Siebert, 1984; McEwen, 1989). Appendix A incorporates data from all of these sources, and, in contrast to most previous studies, Appendix A incorporates information on nearly all aspects of large landslide phenomena, not just dimensional figures. This database builds on the Alpine landslide database of Heim (1932) and upon

the terrestrial and martian landslide database of Lucchitta (1978a). In addition, it incorporates new data on martian and terrestrial landslides published since 1978.

This comprehensive overview of large landslides is warranted by the fact that the large landslide "facies" has previously been very poorly constrained. This has led to a proliferation of mechanical models which attempt to explain the long runout (long runout is defined as occurring when the ratio of fall height, H, to runout length, L of a landslide has a value of less than 0.6) of large landslides but fail to consider other critical dimensional or depositional characteristic(s) of large landslide deposits. The systematics of the data in Appendix A (Chapters III and IV) allow a comprehensive review of previously proposed mechanical models (Chapter V), and demonstrate the need for a new model that considers all the observations (Chapter VI). In addition, this compilation of data provides the groundwork for future studies of large landslides, including field studies, kinematic investigations in the laboratory using geotechnical centrifuges, and field instrumentation of the actual emplacement of large landslides.

B. Database Fields

The following chapter defines the fields occurring in each record and describes their method of collection. Where appropriate, the common methods for estimating values such as the velocity and average friction coefficient are evaluated and compared with values obtained from other methods.

1. *Rank*

The rank field of the database (Appendix A, Field 1) provides information on the planetary locations of landslides and for each planet gives a numerical ranking of landslides based on their relative volume. The database contains three basic locations: "E" stands for Earth ("u" indicating a terrestrial subaqueous landslide), "L" indicates a lunar landslide and "M" stands for martian landslides. For each of the three basic locations, every landslide having a volume estimate also has a numerical rank based on its relative volume, beginning at 1 for the largest landslides. Thus, the ranks E(u)1, L1 and M1 designate the largest landslides on Earth, the Moon and Mars, respectively. Landslides having no volume estimate or which lack critical

straight length or fall height values are given only a basic location symbol and are arranged according to name after the ranked landslides.

2. *Name*

Giant terrestrial landslides are named after nearby towns or villages (often ones buried by landslide debris), local district names, adjacent geographic features or mines carved into them (Appendix A, Field 2). Respective examples include: the Usoy landslide, U.S.S.R., named after a village buried by the slide; the South Kona landslide, named after the adjacent district on the island of Hawaii; the Martinez Mountain landslide, CA, named after the geographic feature; and the Silver Reef landslide, CA, named after the Silver Reef gold mine. Where multiple landslide events have recurred in the same area, individual deposits are often referred to by a name and number, as, for example, the Chaos Jumbles I, II and III deposits (Eppler, et al., 1987).

Lunar landslides are named either for the crater they occur in or near (i.e., Tsiolkovsky), or, in the case of the Apollo 17 landslide, by the name of a nearby manned landing site (Howard, 1973a; b). The process of naming a landslide on the Moon after a nearby geographic feature is aided by the large number of formally named features on the Moon.

In contrast with lunar and terrestrial landslides, the lack of sufficient formal place names on Mars has prevented the naming of most martian landslides. Thus, the format Mars (number) is used in place of a formal name when referring to martian landslides. The Mars 1 to Mars 31 and Mars 33 deposits all retain the numbers given them in Lucchitta (1979). Mars 32 in this reference was misidentified and is not a landslide deposit (Lucchitta, personal communication, 1988). The few officially named martian landslides occur on 1:500,000-series photomosaic maps of Valles Marineris. These names are included parenthetically next to their numerical designation in Appendix A. The deposits have local names followed by the descriptor "labes," Latin for "a falling in or sinking in of the earth." Named martian landslides include: Ophir Labes, Coprates Labes (U. S. Geological Survey, 1984a), Melas Labes (U. S. Geological Survey, 1984b), Candor Labes (U. S. Geological Survey, 1986a) and Ius Labes (U. S. Geological Survey, 1986b).

3. *Dimensions*

The landslide database includes seven dimensional fields for the quantitative description and comparison of giant landslide deposits: volume, area, average and maximum thickness, maximum elevation drop, and straight and curved length. Other useful measurements have been made on giant landslide deposits, but the seven listed fields comprise the most readily determined properties, available for most landslide deposits from the literature or from topographic maps or images of the deposits.

Volume, measured in km^3, is the primary dimensional property in the database because of its importance to the mobility (H/L) and morphology of large landslides (Appendix A, Field 3). Several methods exist to estimate the volume of a giant landslide. The method used depends greatly upon the date and location of the landslide.

The most simple and exact volume estimates are made for historical landslides occurring in locations having preexisting topographic map coverage. Comparison of the original data with the post-landslide topography in such locations allows for highly exact determinations of both the in situ volume of the slidemass prior to failure as well as that of the resultant comminuted rubble deposit. Data collected for the 17 August 1959 Madison, Montana landslide provides an excellent example of the use of this method. The landslide involved $21 \times 10^6 m^3$ of in situ rock, which expanded upon collapse to form a rubble accumulation of $28 \times 10^6 m^3$, a volume expansion of approximately 30% (Hadley, 1960). The 18 May 1980 Mt. St. Helens landslide is the only other historic landslide to have sufficiently detailed topographic data from before and after emplacement to obtain the volume dilation. Voight, et al. (1983) estimated the final deposit volume at 2.8 km^3, and the missing volcanic cone volume at 2.3 km^3, indicating that a bulking of 20% accompanied emplacement. A 30% bulking factor probably represents the volume expansion for a change from in situ rock to landslide breccia; the smaller value observed for the Mt. St. Helens landslide probably reflects the fact that large slump blocks at the head of the deposit failed to disaggregate at collapse, so that the proximal portions of the slide maintained a relatively constant volume at emplacement. Unfortunately, these two landslides are the only deposits for which sufficiently detailed topographic data exist to

determine such accurate volumetric data. Much more commonly, post-event topographic maps provide the only means to estimate landslide volumes.

The accuracy of a volume estimate produced from a post-event topographic map depends on the youth and geometry of a landslide. For example, the volume of the prehistoric Carlson landslide (Appendix B) was determined from an isopach map of the deposit constructed from the present and estimated pre-landslide topography of the depositional surface developed from the geometries of neighboring drainage basins. This volume estimate was then cross-checked with a geometric reconstruction of the missing mass in the landslide's headscarp region. Allowance for moderate gullying of the old surface of the slidemass made the volume estimates consistent at 100×10^6 m^3. Many difficulties arise in attempting to estimate the volume of a landslide strictly on the basis of missing headscarp volume, primarily because extrapolation from post-landslide topography cannot account for the many original irregularities of the former surface. For example, Heim (1932) experienced considerable difficulty estimating the volume of the prehistoric Kandertal landslide:

> The volume of the zone of depletion of the landslide cannot be determined with any certainty. It is impossible to know if the lower edge of the slab of rock that slipped was situated at 2100 m, or if it reached to the Dolderhorn cabin at 1920 m before failure, or if it even reached to Biberg at 1550 m. It is also impossible to know if the sequence of sliding layers reached a width of 700 m or 1000 m in its strike direction. Even the estimate of the thickness of the fallen deposits varies between 150 and 300 m. Using the minimum values, I arrive at a break-out volume of approximately 200,000,000 m^3. But it could be as much as three times this much, and TURNAU has calculated 900 millions!

Clearly, many difficulties may complicate landslide volume estimation, particularly if the landslide is partially buried or eroded. In this case, no means exists to cross-check volumes estimated from missing headscarp mass with that estimated from the zone of deposition.

Two other methods of landslide volume estimation exist for landslides having little or no topographic coverage, as, for example, for many landslides on Mars and on the terrestrial ocean floor. The first method is useful for estimating the volume of smaller, uniform thickness landslides. The largest landslide deposits generally vary greatly in thickness, ruling out the use of this method, which simply involves obtaining the product of landslide area

and marginal thickness (McEwen, 1989). For remotely sensed images of landslides with known sun zenith and azimuth angles, the marginal thickness may be determined by the careful use of shadow length measurements.

The second method is appropriate for 100 km^3 and larger landslides covered only by wide-contour topographic maps. Such topographic data details the steep headscarp regions, but provides little information about the thin, extensive landslide deposits themselves. It is also useful when landslide deposits are difficult to discern from visible or imaging sonar data, either because of low resolution or because landslide lobes with different sources overlap. Equation 1 gives an estimate of the volume of large landslides from the missing volume of well-defined landslide slump scars (McEwen, 1989):

$$V = ZA + 0.5WZ^2(\tan[90 - \beta_1] - [90 - \beta_2]) \quad (1)$$

Here, Z gives the elevation difference in km between the plateau surface and the canyon floor (measured in a nearby region not covered by landslide debris), A the estimated plateau surface area in km^2 removed by the landslide, W the width of the scarp embayment in km, β_1 the estimated pre-landslide slope angle and β_2 the post-landslide slope angle in degrees. A is estimated by assuming that a straight line across the scarp indentation into the plateau surface marks the pre-landslide plateau edge, and β_1 is measured from the slopes of canyon walls adjacent to a landslide scarp (Figure 1). Though rather approximate, this method allows for order-of-magnitude estimates of landslide volumes for deposits covered only by wide-contour topographic maps. Examples include a 200 m contour interval map covering landslides in part of Valles Marineris (U. S. Geological Survey, 1980) and a 200 fathom (366 m) base map showing mass wasting features off the Hawaiian Islands (Moore, et al., 1989).

Compared with volume, the other landslide dimensions recorded in the database typically require much less effort to extract from the topographic and imaging data. **Area**, measured in km^2, refers to the horizontally projected area of a landslide deposit only and does not include exposed in situ rock in the headscarp scar (Appendix A, Field 4). Landslide area measurement is straightforward for all deposits on topographic maps. For many martian landslides, controlled photomosaic maps exist which also allow for rapid area determinations. These maps consist of mosaics of digitally processed Viking

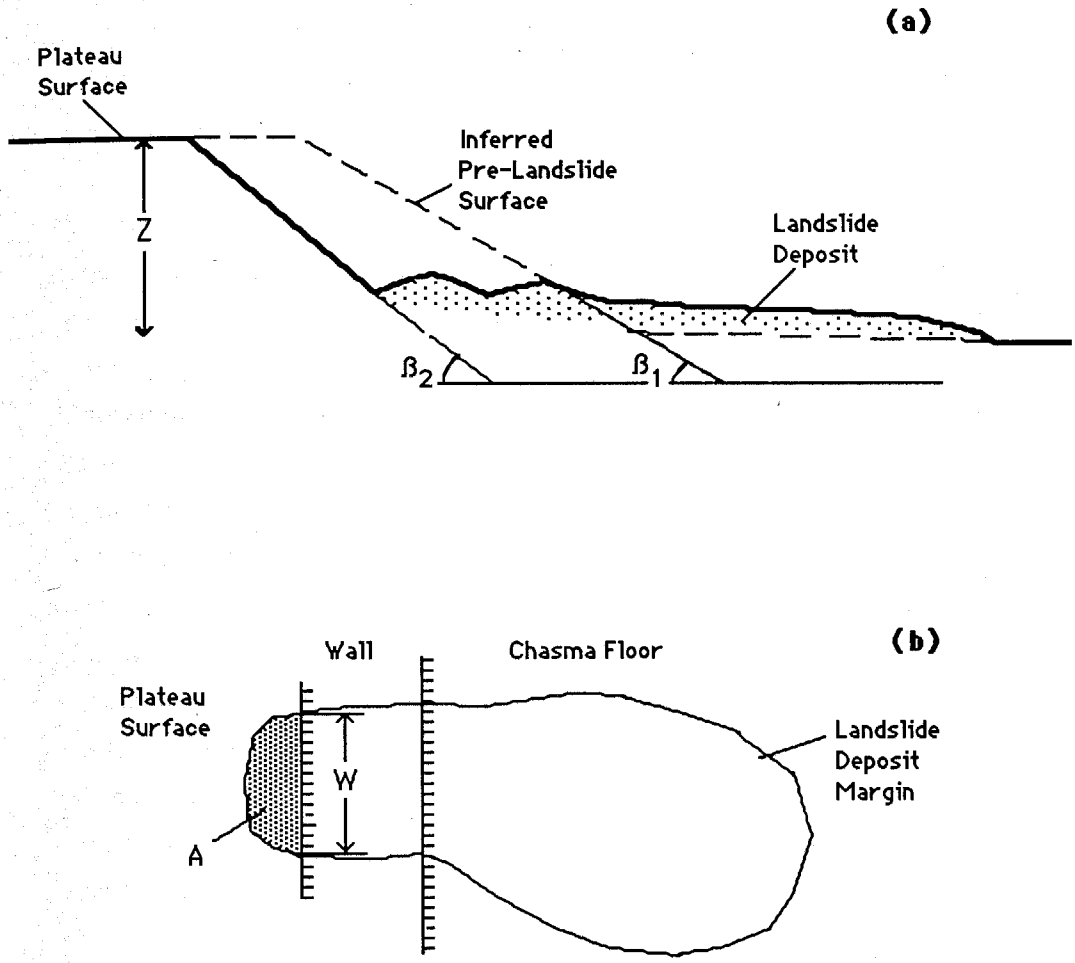

Figure 1. Sketch of volume estimate for large landslides by way of missing headscarp volume calculation (Equation 1). **a**: Cross-section; **b**: Plan view (modified from McEwen, 1989).

Orbiter images that have an average sun angle of 20° from the horizontal, and which are set to the same scale using global control points (U. S. Geological Survey, 1979). Somewhat greater difficulty surrounds area measurements for small martian landslides that do not show up well on photomosaics or topographic maps. These landslides require study from Viking Orbiter frames, which often exhibit variable, difficult to determine scales. In most cases, however, larger features in a frame can be matched with topography on a controlled photomosaic map, allowing a scale to be determined for the image.

Two measures of landslide thickness, given in meters, are included in each database record; the **average** and the **maximum thickness** (Appendix A, Fields 5a, b). The database program calculates the average thickness by dividing a landslide's volume by its area. For the few cases in which landslide volume is estimated from the product of the area and the marginal thickness, the average thickness reports only the thickness along the deposit margin. The maximum thickness typically originates as a by-product of the volume estimation. It is determined from field measurements, from topographic data or from shadow measurements.

The **maximum elevation drop**, measured in meters, reports the total vertical distance between the uppermost point of the headscarp and the lowermost point along the toe of the deposit (Appendix A, Field 6). Together with volume, fall height has a strong influence on the length of runout of a landslide. The maximum elevation drop may be readily obtained from landslides with topographic coverage, while shadow length measurements can be used to obtain relative height data for martian landslides lacking topographic coverage. Obtaining a more valuable figure, the center of gravity drop of a landslide mass, faces the difficulty or impossibility of determining the centers of gravity of the zone of depletion and of deposition, especially for partially eroded landslides (Heim, 1932).

The **straight** and **curved lengths** of large landslide deposits, measured in meters, record the distances traveled by landslide debris from the uppermost point of the headscarp to the lowermost point along the toe of the deposit (Appendix A, Fields 8a, b). The straight length gives the straight-line horizontal distance between these points, while the curved length estimates the actual distance travelled by a landslide between these two points by following bends in the travel path. The straight and curved lengths will coincide for straight, unconfined landslides, but will contrast markedly for

confined landslides constrained to follow a sinuous path by deposition in narrow canyons and channels. The curved length actually travelled by a landslide can generally be estimated from the margins and surficial textures of the deposit (Figure 2). Estimations of the straight and curved length of a landslide follow the same criteria as landslide area determinations.

4. *Velocity*

Large landslides typically move at high speeds at emplacement. Except for some instrumented observations of large landslides triggered by the Soviets, however (Figure 35), neither eyewitness nor geological evidence yield entirely reliable quantitative estimates of landslide velocities. The velocity estimates made from these sources typically provide only the average speed of a landslide or its velocity over a short distance of its length, with little known of its overall movement history. Except where noted, the velocity values reported in the database (Appendix A, Field 7) are derived from the height of obstacles climbed and/or overtopped by landslides, because this is the easiest and most common method used for estimating landslide speeds. Other velocity estimation techniques for large landslides include eyewitness accounts, superelevation of channeled debris, spattering of individual boulders and use of the average estimated friction coefficient (Appendix C).

The most common velocity estimation method makes use of obstacles climbed and/or overtopped by landslide debris, and therefore only gives an estimate for one short segment of a landslide. It assumes conservation of energy for the packet of material that climbed the obstacle, with the energy required to overcome gravity originating in the kinetic energy of the landslide (Shreve, 1966). For an obstacle climbed but not overtopped by landslide debris, Equation 2a provides a velocity estimate:

$$\text{kinetic energy} = \text{potential energy}$$

$$(1/2)mv^2 = mgh$$

$$v^2 = 2gh$$

$$v = \sqrt{2gh} \qquad (2a)$$

For obstacles completely overtopped by debris, the equation becomes an inequality:

Figure 2. Sketch map of the strongly channelled 1749 Diablerets landslide, Switzerland, highlighting the contrast between the 4.9 km straight length (sl) and the 6.2 km curved length (cl). Also marked are the uppermost point of the headscarp (H) and the most distal point along the toe (T) of the landslide. Diagram modified from Heim (1932).

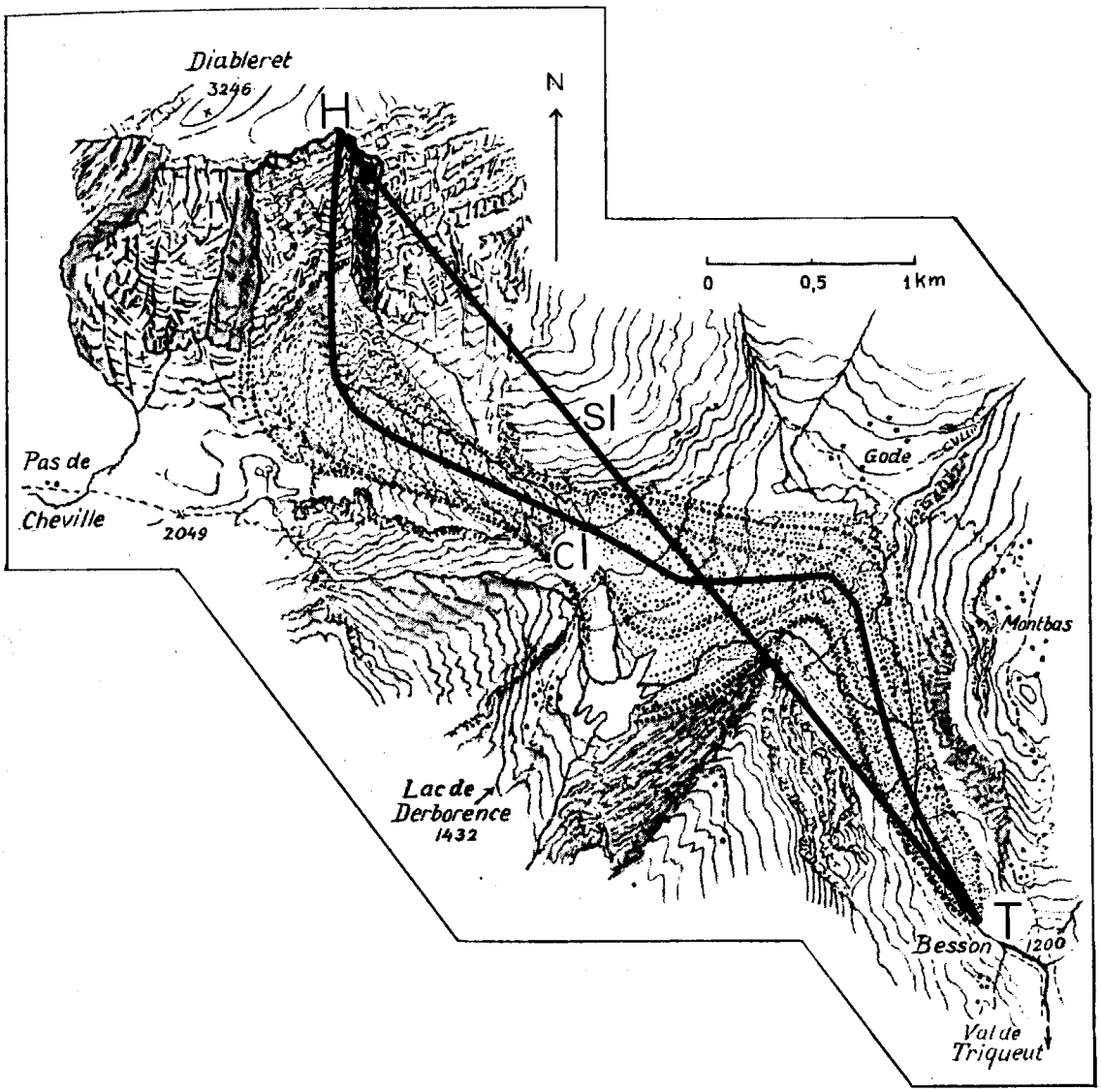
Diableret
3246
H
N
0
0,5
1 km
SI
CI
Pas de
Cheville
2049
Gode
Montbas
Lac de
Derborence
1432
T
1200
Besson
Val de
Triqueut

$$v > \sqrt{2gh} \qquad (2b)$$

For both Equations 2a and 2b, v gives the velocity estimate in m/s, g the gravitational acceleration in m/s^2 and h the height of the obstacle in m.

To the extent that such a unit volume of debris moves independently of the body of the landslide, Equation 2a yields a minimum velocity estimate (Shreve, 1966). This is because the equation fails to account for the restraining frictional force of debris over its bed that would have to be overcome in addition to the force of gravity. Conversely, large landslides clearly move cohesively, in some respects like a viscous fluid (Heim, 1932), so that portions of them might be pushed up and over obstacles by the momentum of trailing debris having an unknown, lower velocity than that estimated by Equations 2a and 2b (Figure 3). Because the effects of friction and of pushing from behind operate in different directions, the velocity estimates from Equations 2a and 2b should be considered rough until further data are obtained from centrifuge or model studies to determine the relative magnitudes of these competing influences.

5. *Estimated Friction*

Numerous analyses of the kinematics of giant landslides point to unusually low apparent coefficients of friction as a common characteristic of these deposits. The actual average friction coefficient experienced by a landslide, ignoring possible effects of pore pressure, is given by the tangent of the slope connecting the pre- and post-event centers of gravity of a slidemass (Cruden, 1980). Unfortunately, unless detailed topographic maps exist for an area from before and after a large landslide, determination of the pre- and post landslide centers of gravity may be difficult or impossible to obtain (Heim, 1932). To get around this problem, Heim (1932) suggested the use of the **fahrböschung** (Appendix A, Field 9), the tangent of the slope connecting the crown of the headscarp with the toe of the landslide, in lieu of the center of gravity gradient, because in his experience the fahrböschung was easy to obtain and the slopes of the two gradients often coincided.

Unfortunately, the data in Table 1 fail to support Heim's contention that the fahrböschung and the center of gravity lines commonly coincide, as the few known true friction coefficients average 22% greater than the corresponding fahrböschung estimates. The fahrböschung and the center of gravity

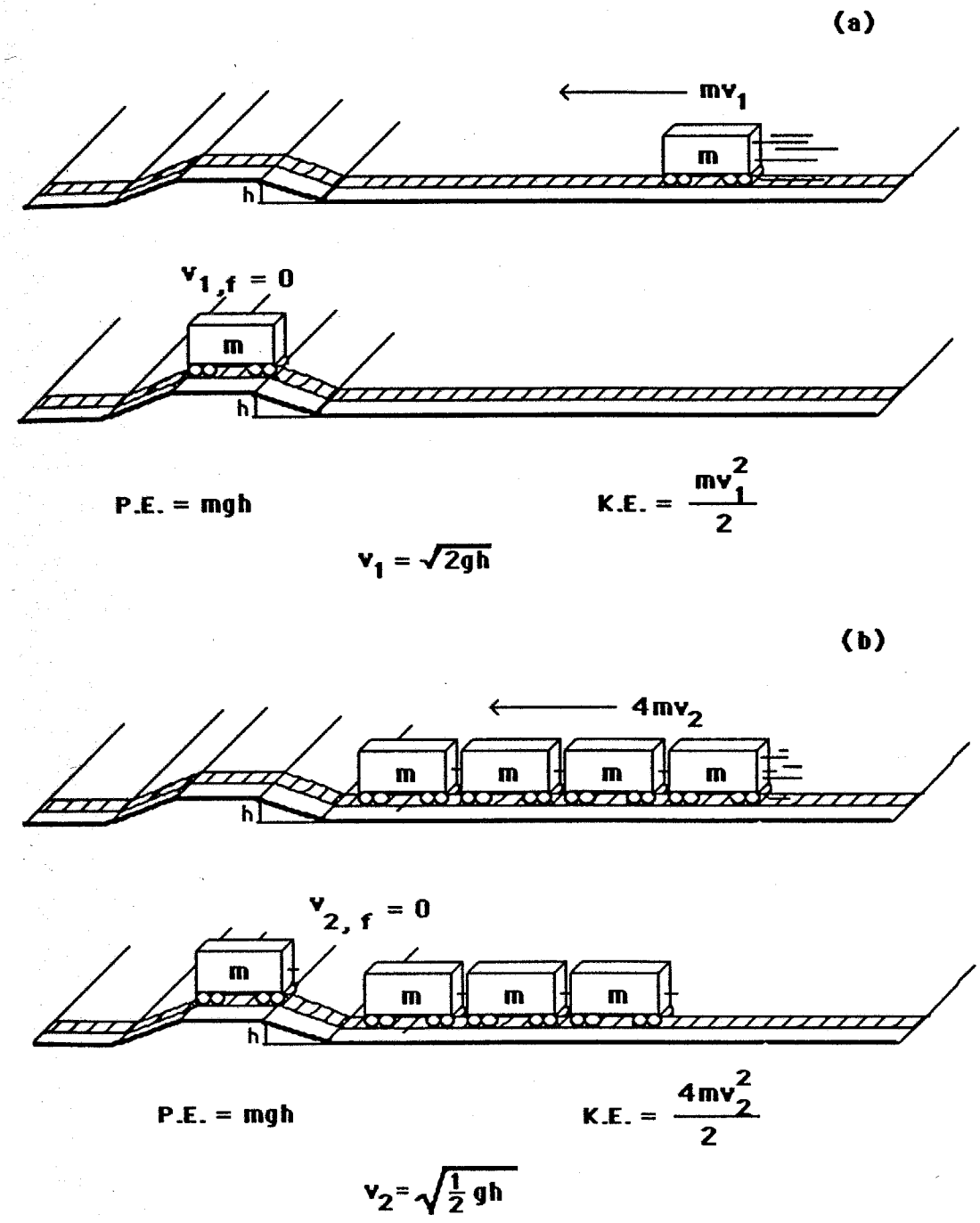

Figure 3. This diagram illustrates different ways to interpret the velocity of a landslide from overtopped obstacles. Part **(a)** shows the typically assumed case, in which a packet of landslide debris, here modelled by a frictionless railroad car, climbs a hill using its own kinetic energy, yielding velocity v_1. Part **(b)** illustrates an equally plausible case, in which the debris packet is in part pushed up hill by trailing debris. In this case, the landslide moves at a rate v_2, $1/\sqrt{n}$ times the velocity in **(a)**, where n is the number of linked packets reaching the obstacle.

Table 1. Comparison of Fahrböschung and Actual Friction for Several Giant Landslides

Name	Fahr-böschung	Actual Friction	References
Elm	0.29	0.42	Hsü, 1978
Hope	0.40	0.44	Mathews and McTaggart, 1969; Cruden, 1980
Mt. Granier	0.17	0.23	Cruden and Antoine, 1984
Rubble Creek	0.15	0.18	Moore and Mathews, 1978
Sherman	0.22	0.19	McSaveney, 1978
Usoy	0.24	0.33	Preobrajensky, 1920

gradient will, in fact, coincide only for those landslides whose center of gravity lies rather close to the toe. The discrepancy between the two values is especially severe for distally-tapering landslides, as in this case the line joining the crown of the landslide to its toe will nearly always slope less steeply than the line joining the centers of gravity of a slide mass before and after sliding (Figure 4). Nevertheless, the fahrböschung remains a convenient approximation of the true friction for comparing the behavior of large landslides because it collectively underestimates landslide friction coefficients. However, the use of these values in landslide mechanical modeling studies requires great caution.

6. *Morphological Classification*

The Type field of the database gives a shorthand notation for the morphological characteristics of landslide deposits (Appendix A, Field 10). The notation is based on a morphological classification developed for this thesis as a strictly descriptive method for describing large landslide deposits, without typical references to the rapidity of movement or the type of material involved (Sharpe, 1938; Varnes, 1958). This scheme allows for ready comparison and contrast of giant landslide characteristics, and for outlining the various components of the mechanical behavior of individual landslides. It contains codes for the form of the headscarp, for the relationship between the headscarp and the breccia debris apron, and for textures and structures found on the debris apron (Table 2). The Type field uses one of three different nomenclature forms depending on whether the landslide has an absent, attached or detached debris apron. Figure 5 illustrates the method for classifying the three basic forms.

A landslide may begin its movement in a variety of ways. The form of the **headscarp** commonly reveals the mode of initiation. The three primary modes of headscarp failure, rotational slumps, translational slides and rockfalls, are coded and defined below:

I. A ***rotational slump*** refers to a shearing and rotary movement of a mass of rock of any size, moving as a unit or as several subsidiary units (multiple slump), usually with backward rotation along a curved concave-upward slip surface, around a more or less horizontal axis parallel to the cliff or slope from which it descends, often resulting in a reversed slope facing uphill;

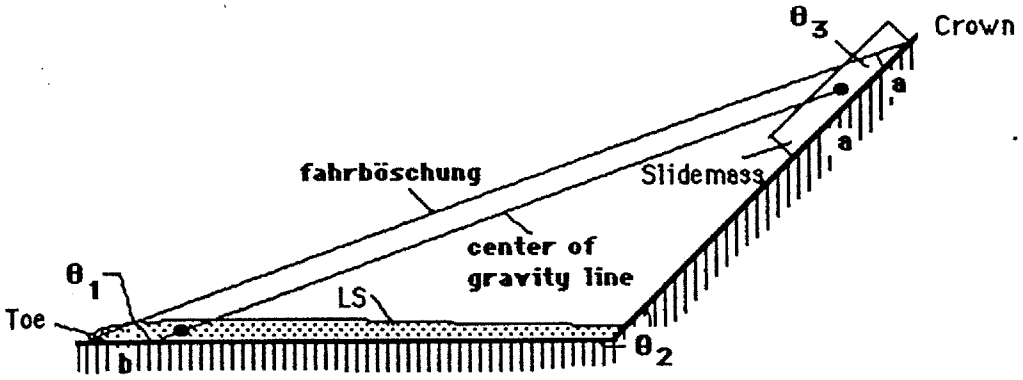

a = the half length of a symmetrical slab slidemass
b = the distance from the landslide center of gravity to the toe of the deposit

Figure 4a. This simplified diagram of a slidemass and resultant landslide illustrates that for the fahrböschung and center of gravity gradient to coincide, the final center of gravity of the mass must lie near the toe of the deposit. Making the simplifying assumption that the initial and final centers of gravity lie near the slide plane, the two gradients will coincide when:

$$a = \frac{b \sin \theta_1}{\sin (\theta_2 - \theta_1)}$$

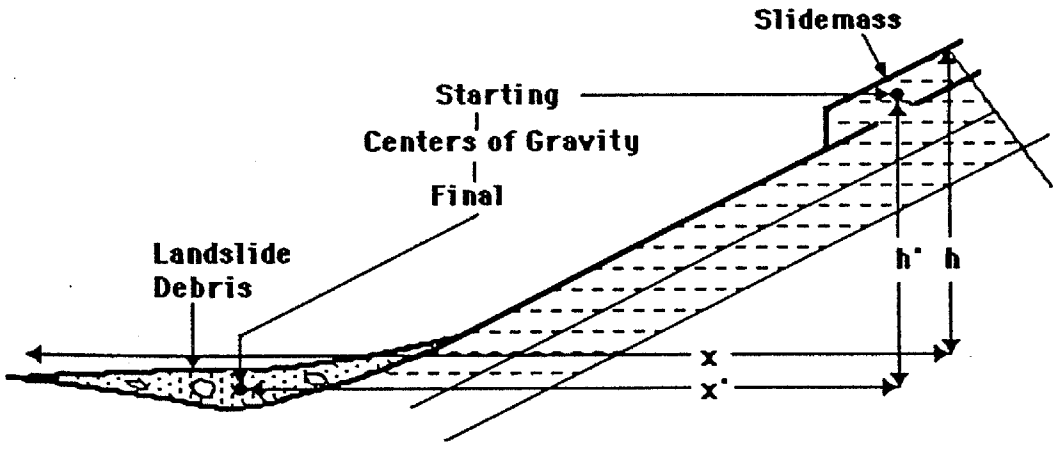

Figure 4b. Sketch of idealized landslide geometry illustrating that the center of gravity gradient, h'/x' will typically exceed the fahrböschung, h/x, because of thinning and spreading of the slidemass away from the scarp (modified from Cruden, 1980).

Basic Form:

Headscarp. Headscarp/Debris Apron Relationship. Surficial Texture(s)

Examples:

1. Simple slump, no debris apron:

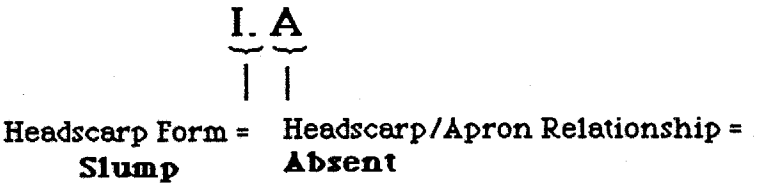

2. Slump-type headscarp with attached debris apron and longitudinally-ribbed and smooth debris apron:

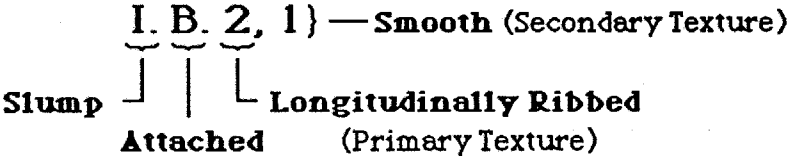

3. Fall-type headscarp with a detached debris apron, lobate plan form, planar major relief and longitudinally-ribbed debris apron:

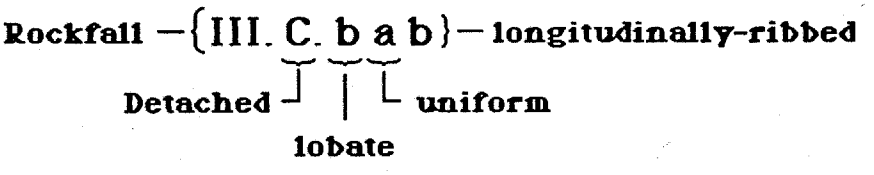

Figure 5. Illustration of morphological classification scheme.

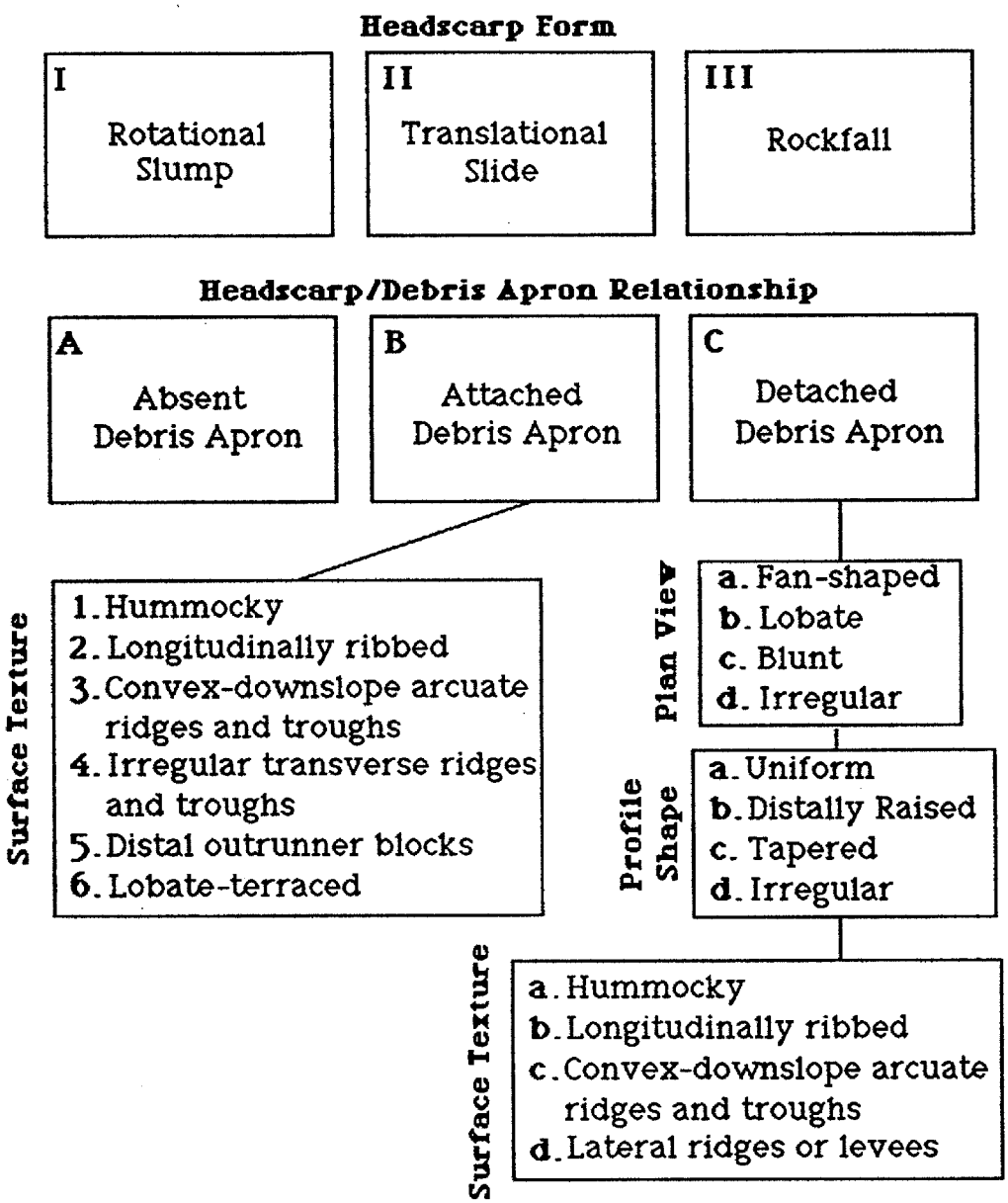

Table 2. Morphological classification table for large landslides. Landslides are classified using one headscarp form and one headscarp/debris apron relationship. For attached debris apron landslides, one or more of six possible surficial textures are applied, and for detached debris apron landslides, one plan form, one profile shape and one or more surficial textures are used to give a full classification. Figure 5 gives a more complete explanation with examples.

II. A ***translational slide*** is defined as the downslope displacement of a rock mass of any size on a surface that is roughly parallel to the general ground surface, most often along a pre-existing plane of weakness, such as bedding, foliation, joints or faults; and

III. A ***rockfall*** indicates the relatively free falling or precipitous movement of a detached segment of bedrock (usually massive, homogeneous or jointed) of any size from a cliff or other steep slope not guided by a unique plane of failure.

The **headscarp/debris apron relationship** provides the second morphological characteristic for use in the classification of giant landslides. Three possible relationships, absent, attached and detached, exist between the headscarp and the debris apron:

A. The term ***absent*** refers to rotational or translational landslides which remained cohesive during movement, failing to form a debris apron; simple slump blocks or block glides;

B. An ***attached*** relationship refers to circumstances in which proximal material has strictly rotated or translated into place and remains cohesive, but grades distally into a disaggregated rock debris apron; and

C. A ***detached*** relationship, in which the entire deposit consists of a brecciated rock debris apron without any material that simply rotated or slid into place.

In addition to the two framework characteristics defined in I-III and A-C above, landslide deposits exhibit a myriad of **debris apron morphologies**. Larger landslides typically have attached debris aprons and exhibit extremely complex morphologies, while smaller landslides more often have detached debris aprons and display variations on a few simple morphologies. These characteristics require a separate handling of textures associated with attached and detached debris apron landslides.

Attached debris apron landslides exhibit six basic textures. Many attached debris apron landslides display only one of these textures, but some of the largest landslides display combinations of these patterns:

1. A ***hummocky*** texture, which refers to landslides without any consistently oriented surficial relief at the best available scale of resolution;

2. ***Longitudinally ribbed*** texture, describing landslides displaying movement-parallel ridges and troughs;

3. ***Convex-downslope transverse arcuate ridges and troughs*** texture;

4. ***Irregular transverse ridges and troughs*** texture, which consists of relatively evenly spaced craggy ridges aligned perpendicular to the landslide movement direction;

5. ***Distal outrunner blocks*** texture, which describes large isolated blocks situated outside the apparent distal margin of a large landslide but which appear from their distribution to have originated from the landslide; and

6. ***Lobate-terraced*** texture, a step-like morphology in which individual risers are rounded in profile and in plan view.

Detached debris apron landslides also exhibit a variety of morphologies, but with far fewer observed variations than the attached debris apron landslides. This allows for a more detailed morphological description of each deposit, using data on the plan form, profile shape and surficial texture. Detached debris aprons exhibit four gradational ***plan forms***, defined as follows:

a. *Fan-shaped*, displaying proximally to distally diverging linear lateral margins and a digitate distal margin;

b. *Lobate*, having linear to smoothly curving lateral margins and a smoothly curved distal margin;

c. *Blunt*, which exhibits parallel lateral margins and a smoothly curved distal margin; and

d. *Irregular* in plan form, having no well defined shape.

In addition, four primary ***profile shapes*** exist for detached debris apron landslides:

a. *Uniform*, which refers to debris aprons of relatively uniform thickness;

b. *Distally raised*, where the thickest portion of the debris apron lies near the distal margin of the deposit;

c. *Tapered*, displaying a proximally to distally thinning debris apron; and

d. *Irregular* changes in thickness.

The third set of characteristics, the ***surficial textures***, complete the morphological description of giant landslides. Four basic surficial textures exist for detached debris apron slides, and as with attached debris apron landslides, they can occur together in any combination:

a. *Hummocky* texture, consisting of irregularly distributed mounds and depressions;

b. *Longitudinally ribbed* texture, describing landslides having movement-parallel ridges and troughs;

c. *Convex-downslope transverse arcuate ridges and troughs* texture; and

d. *Prominent lateral levees or ridges* texture.

Figures 6a-6k give prints and drawings of giant landslides illustrating the many morphological categories of landslides discussed above and outlined in Table 2.

7. *Location*

Four database fields describe the location of landslide deposits: the basic environment, the geographic place name, the latitude and the longitude. The planetary location of a giant landslide deposit is contained in the Rank field (Section II. A. 1; Appendix A, Field 1). Field 11 of Appendix A gives the **geographic location** or place name of landslide deposits. For terrestrial landslides, the database gives the country in which the deposit lies, preceded for large countries by the specific state, province, republic or territory name. For large subaqueous landslides, the geographic location field reports the closest named undersea geographic feature to the landslide, including island

Figure 6a. Type I.A landslide deposit. The Mars 31 deposit is a simple slump block in eastern Tithonium Chasma, Mars (4°56'S, 79°14'W). Viking Orbiter frame 065A24. In this image and in all other Viking Orbiter images reproduced in this work, the direction of solar lighting is represented by the arrow pointing away from the circled dot (representing the sun). An observer on the ground looking in the same direction as the arrow is pointing would have his back to the sun. The sun zenith angle, the angle between the vertical and the sun as viewed from the ground, measures 27.18° in this image.

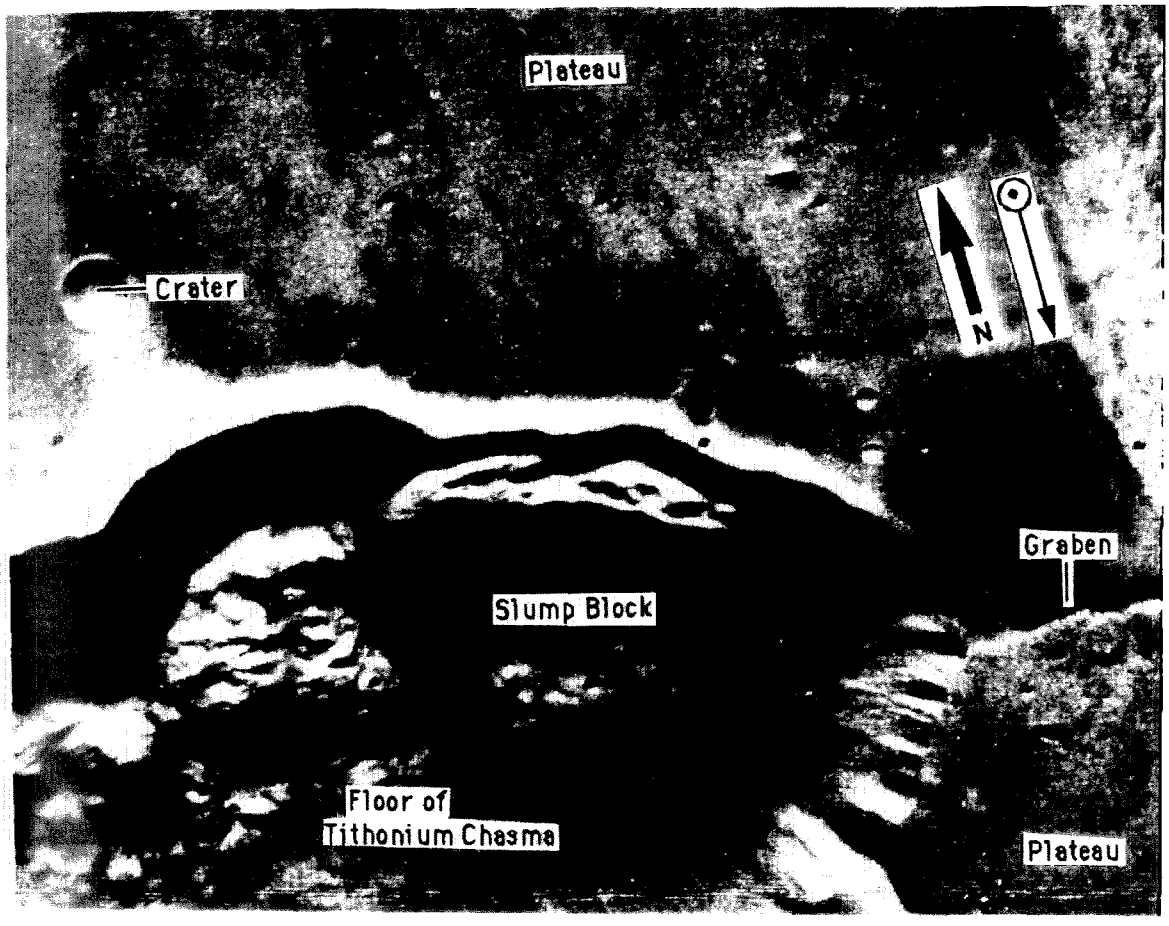
Plateau
Crater
N
Graben
Slump Block
Floor of
Tithonium Chasma
Plateau
0
km
30

Figure 6b. Type I.B.1,5 landslide. Geologic map of the Alika slide complex, SW flank of Hawaii Island, shows two giant landslides with slump-type headscarps and attached debris aprons dominated by hummocky and isolated glide-block textures (Lipman, et al., 1988).

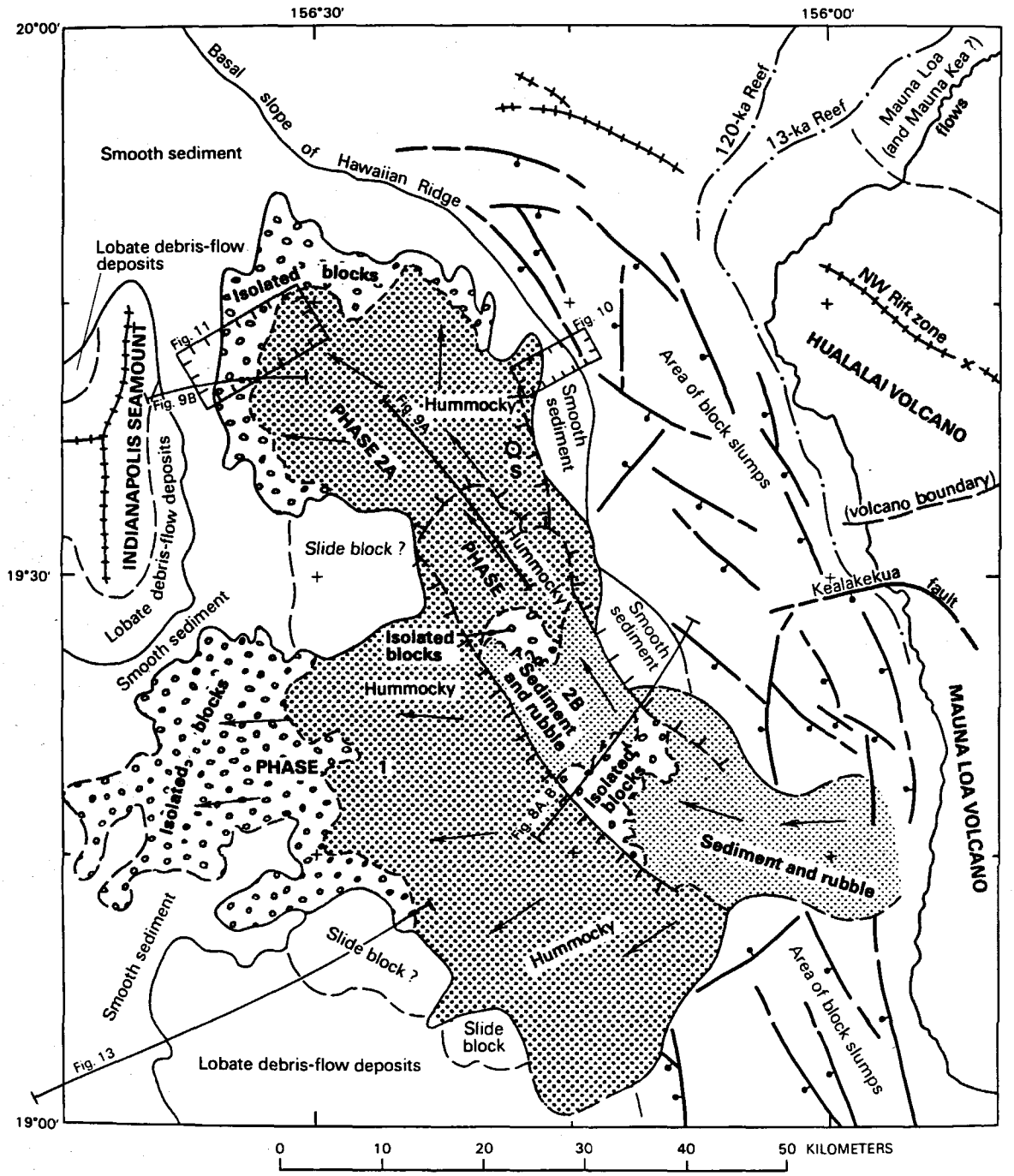
156°30'
156°00'
20°00'
19°30'
19°00'
Basal slope of Hawaiian Ridge
Smooth sediment
120-ka Reef
13-ka Reef
Mauna Loa (and Mauna Kea ?) flows
Lobate debris-flow deposits
Isolated blocks
Fig. 11
Fig. 10
NW Rift zone
HUALALAI VOLCANO
INDIANAPOLIS SEAMOUNT
Fig. 9B
Fig. 9A
PHASE 2A
Hummocky
Smooth sediment
Area of block slumps
(volcano boundary)
Slide block ?
Kealakekua fault
Lobate debris-flow deposits
Smooth sediment
Isolated blocks
Hummocky
PHASE 2B
Sediment and rubble
MAUNA LOA VOLCANO
Isolated blocks
PHASE 1
Fig. 8A
Sediment and rubble
Smooth sediment
Slide block ?
Hummocky
Area of block slumps
Fig. 13
Slide block
Lobate debris-flow deposits
0 10 20 30 40 50 KILOMETERS

Figure 6c. Type I.B.1,6 landslide. The Mars 24 deposit, a slump-block landslide with an attached debris apron and a hummocky, lobate-terraced surficial texture. The landslide is situated in western Tithonium Chasma, Mars (4°10'S, 87°34'W). Viking Orbiter frame 063A67. Solar zenith angle 28.61°.

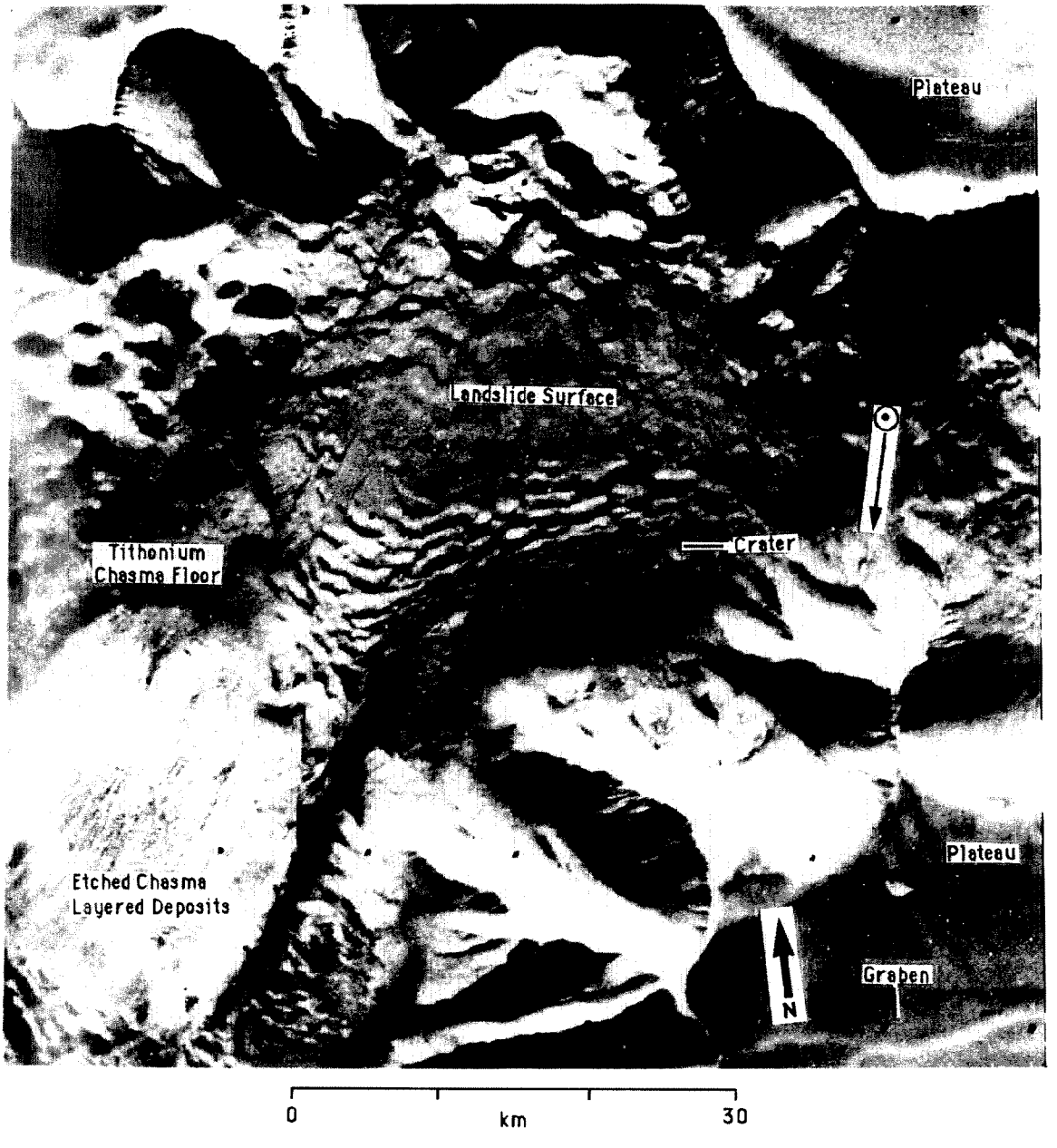
Plateau
Landslide Surface
Crater
Tithonium
Chasma Floor
Etched Chasma
Layered Deposits
Plateau
Graben
N
0
km
30

Figure 6d. Type I.B.2 landslide. The Mars 1 deposit (overlying Mars 2 and Mars 3 landslides), a slump-block landslide with an attached debris apron and a longitudinally ribbed debris apron texture. These three landslides are situated in Ganges Chasma, Mars (8°45'S, 44°38'W). Viking Orbiter images 014A29-32. Solar zenith angle ranges between 63.48° and 65.29° for the four images.


Plateau
Crater
Mars 2
Mars 1
N
Plateau
Mars 3
Chasma Wall
Floor of Gangis Chasma
0
50
km

Figure 6e. Type I.B.4,3 landslide. The Mars 18 deposit is a multiple-slump landslide with an attached debris apron dominated by irregular transverse ridges and troughs and secondarily by convex-downslope arcuate ridges and troughs. This landslide lies in western Ius Chasma, Mars (6°48'S, 85°12'W). Viking Orbiter images 064A19 and 065A10. Solar zenith angles measure 29.68° and 30.62° for the two images, respectively.

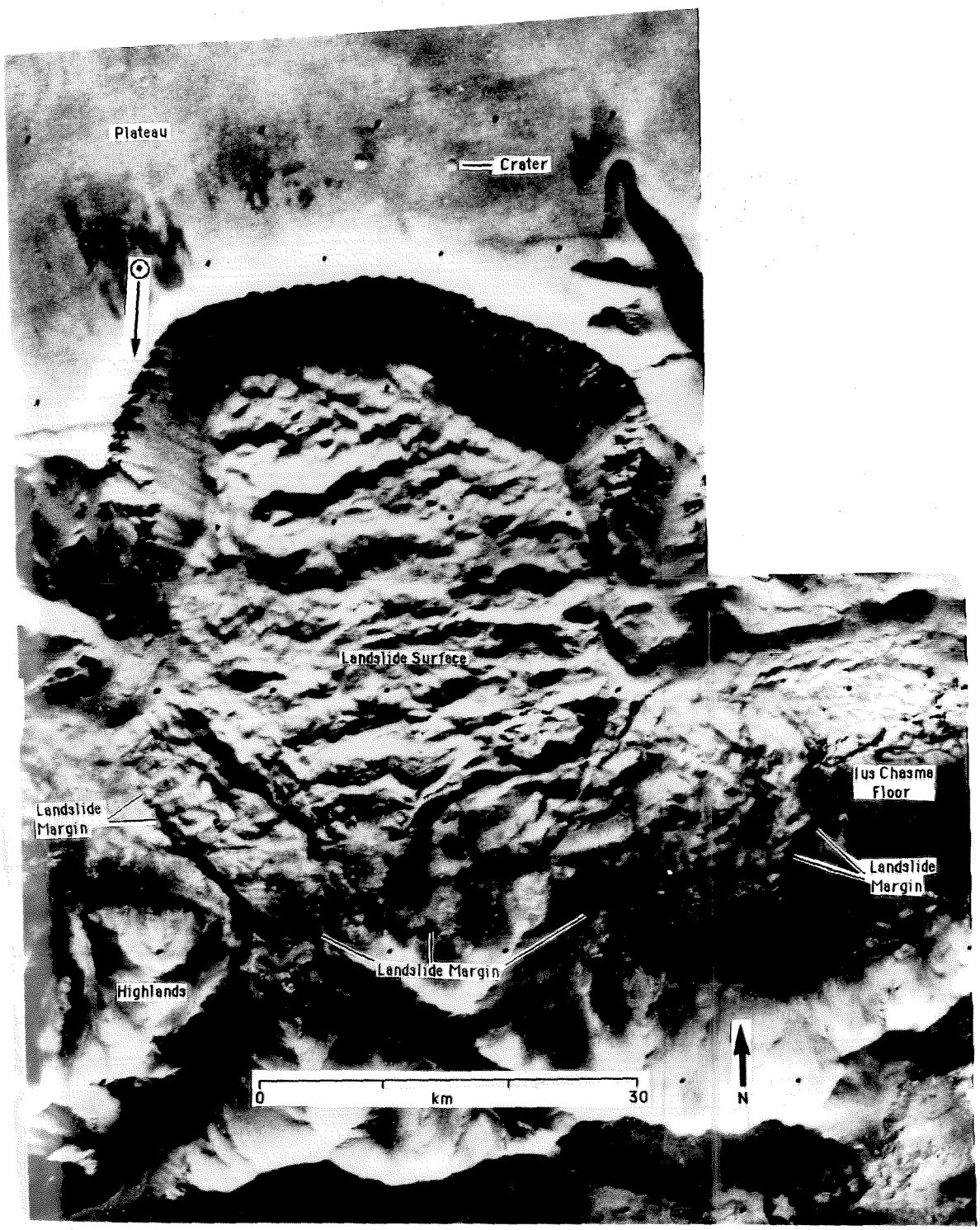
Plateau
Crater
Landslide Surface
Ius Chasma Floor
Landslide Margin
Landslide Margin
Landslide Margin
Highlands
0
km
30
N

Figure 6f. Type II.C.dda landslide. The Saidmarreh, Iran landslide has a translational headscarp and a detached debris apron that is irregular in plan form and in profile and displays a hummocky surface texture. Arrows show direction of movement of landslide. The original microtopography of the slide is partially preserved as a series of faint troughs trending parallel to the direction of sliding (pattern A). Elsewhere the slide surface is overprinted by a series of small northwest-southeast oriented ridges and troughs (pattern B) as well as large grabens (pattern C) having the same orientation. The development and collapse of solution cavities in the limestone landslide appears responsible for the formation of pattern B and C features. Geomorphic map of the landslide modified from Watson and Wright (1969).

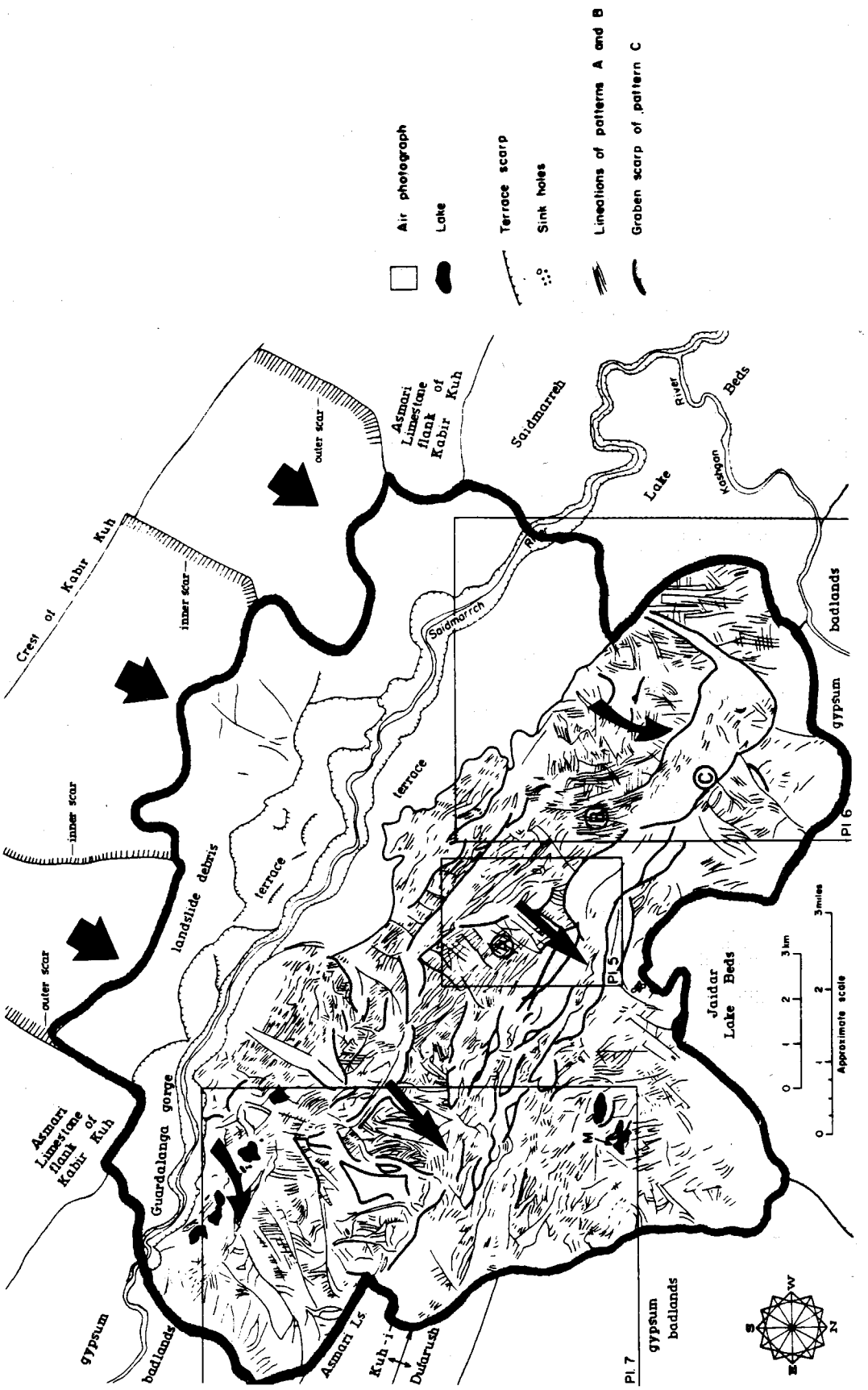
Air photograph
Lake
Terrace scarp
Sink holes
Lineations of patterns A and B
Graben scarp of pattern C
Crest of Kabir Kuh
outer scar
inner scar
inner scar
outer scar
Asmari Limestone flank of Kabir Kuh
Saidmarreh
River
Lake
Kashgan
Beds
Saidmarreh
landslide debris
terrace
terrace
gypsum badlands
Pl. 6
Guardalanga gorge
Asmari Limestone flank of Kabir Kuh
Jaidar Lake Beds
Pl. 5
Approximate scale
0 1 2 3 km
0 1 2 3 miles
gypsum badlands
Asmari Ls
Kuh-i-Dufarush
Pl. 7
gypsum badlands
N
NW
W
SW
S

Figure 6g. Type III.C.aab landslide. The Sherman, Alaska landslide had a rockfall-type headscarp and a detached debris apron that was fan-shaped in plan view, had uniform thickness in profile and exhibited a longitudinally-ribbed surface texture. Geomorphic map from McSaveney (1978) was drawn from aerial photographs taken shortly after the landslide. Deposit subsequently was disrupted by activity of underlying Sherman glacier.


SHERMAN GLACIER
1250m SHATTERED PEAK
LEGEND
Rock Avalanches and Rock Falls
Bedrock
Outwash
Avalanche Source and Direction
Transverse Folds
Direction of flow
Longitudinal Grooves
Transverse Fissures
500 0 meters 1000 1500
Contour interval 25meters on glacier, 50meters on valley wall
Datum is mean sea level
500
450
400
350
300
250
200
150
N

Figure 6h. Two type III.C.bab landslides, the Mars 84 and 85 deposits. These landslides both have rockfall-type headscarps and detached debris aprons. Their debris aprons are lobate in plan view, planar in profile and have longitudinally ribbed surface textures. These deposits lie in eastern Candor Chasma, Mars (8°19'S, 66°29'W and 8°17'S, 66°17'W). Viking Orbiter image 910A15. Solar zenith angle 55.92°.

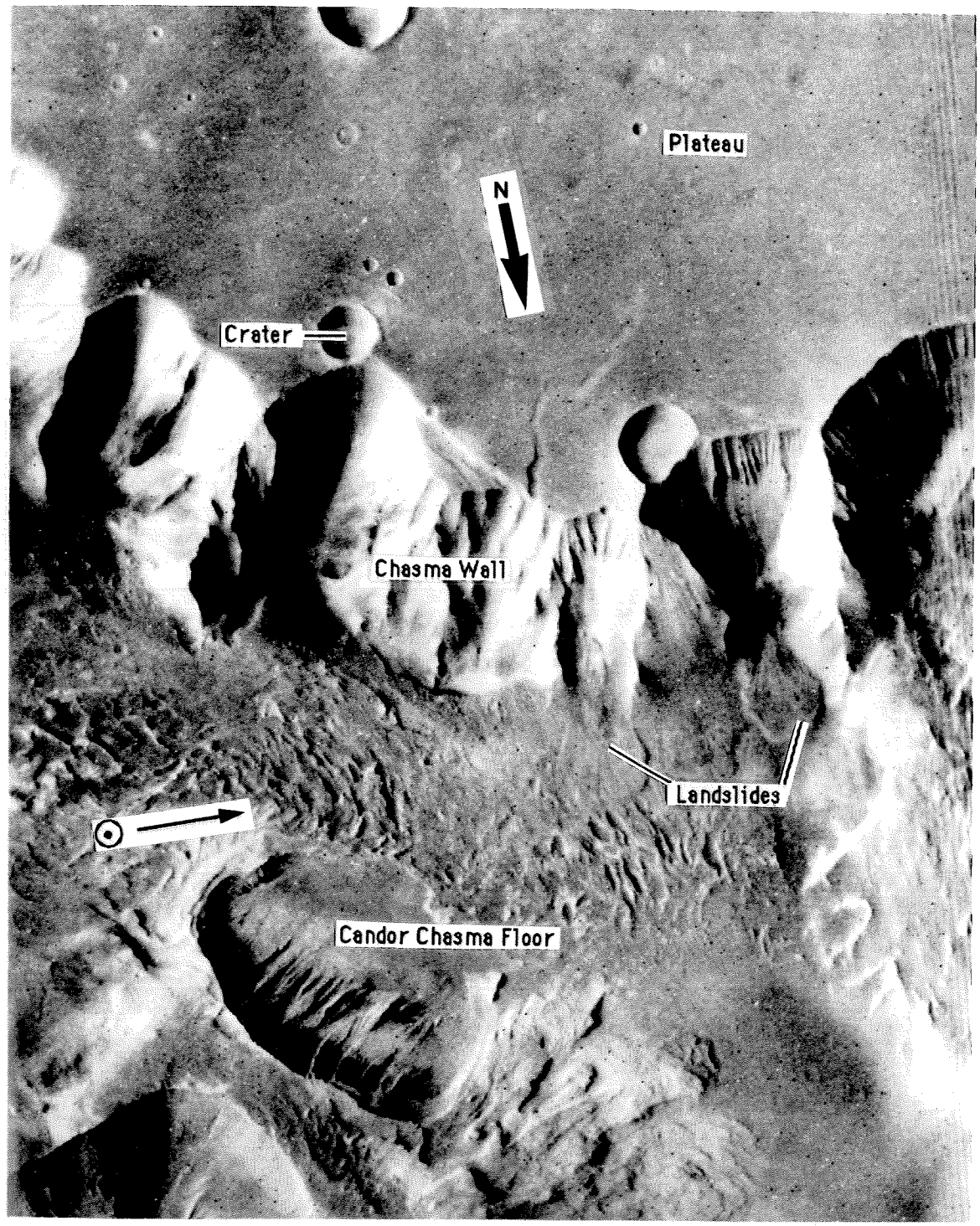
Plateau
N
Crater
Chasma Wall
Landslides
Candor Chasma Floor
0
km
30

Figure 6i. Type III.C.cbd,a landslide, the Mars 141 deposit. This landslide has a rockfall-type headscarp and a detached debris apron that is blunt in plan form, distally raised in profile and exhibits lateral levees and a hummocky surface texture. The landslide is situated in the summit caldera of Olympus Mons volcano, Mars (18°05'N, 133°32'W). Viking Orbiter image 474S22. Solar zenith angle 25.34°.

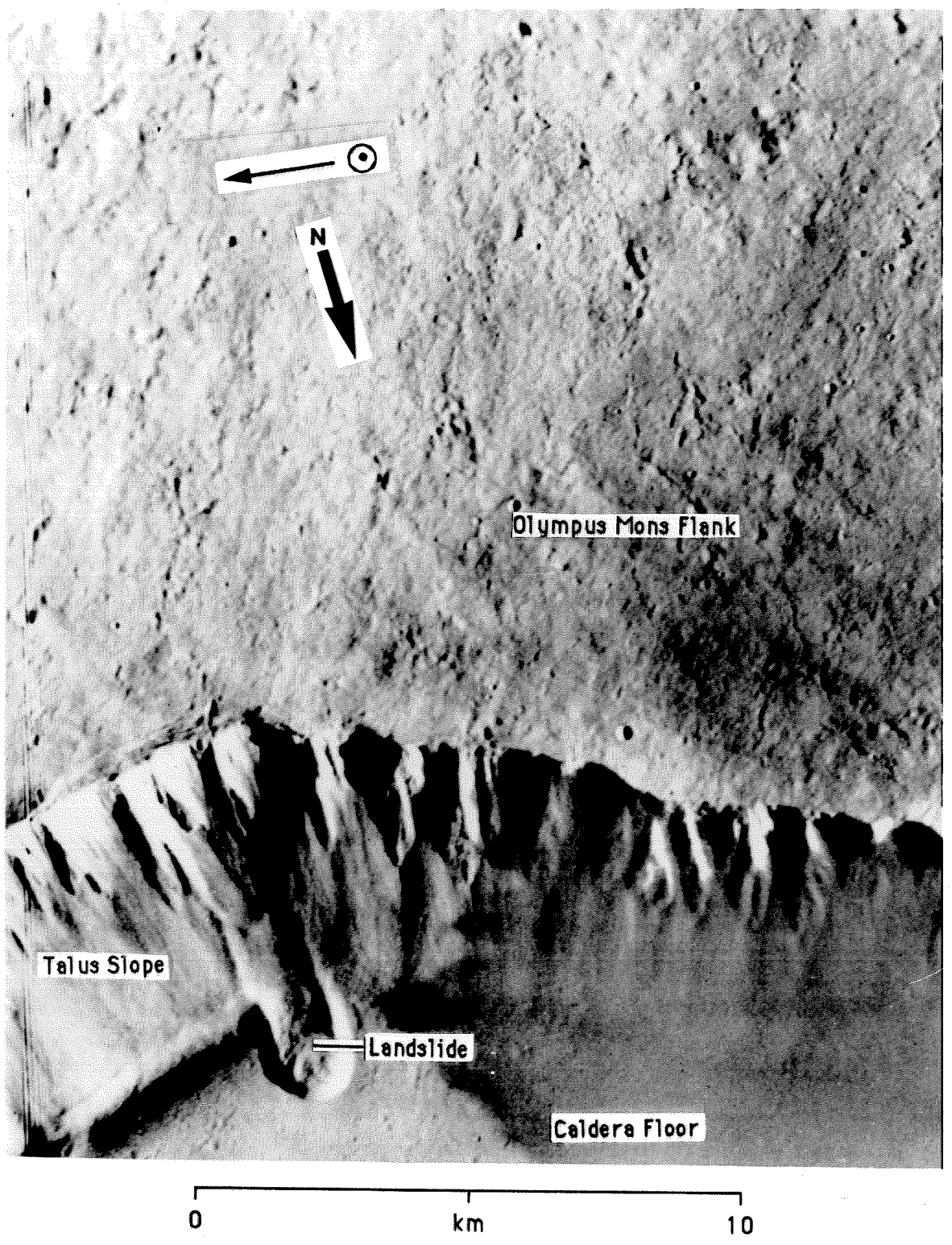
N
Olympus Mons Flank
Talus Slope
Landslide
Caldera Floor
0
km
10

Figure 6j. Type III.C.dcc landslide. The Elm landslide had a rockfall-type headscarp and a detached debris apron that was irregular in plan form, tapered in profile and surfaced with a convex-downslope pattern of ridges and troughs. The landslide was subsequently significantly modified during reclamation by local inhabitants (Heim, 1932).

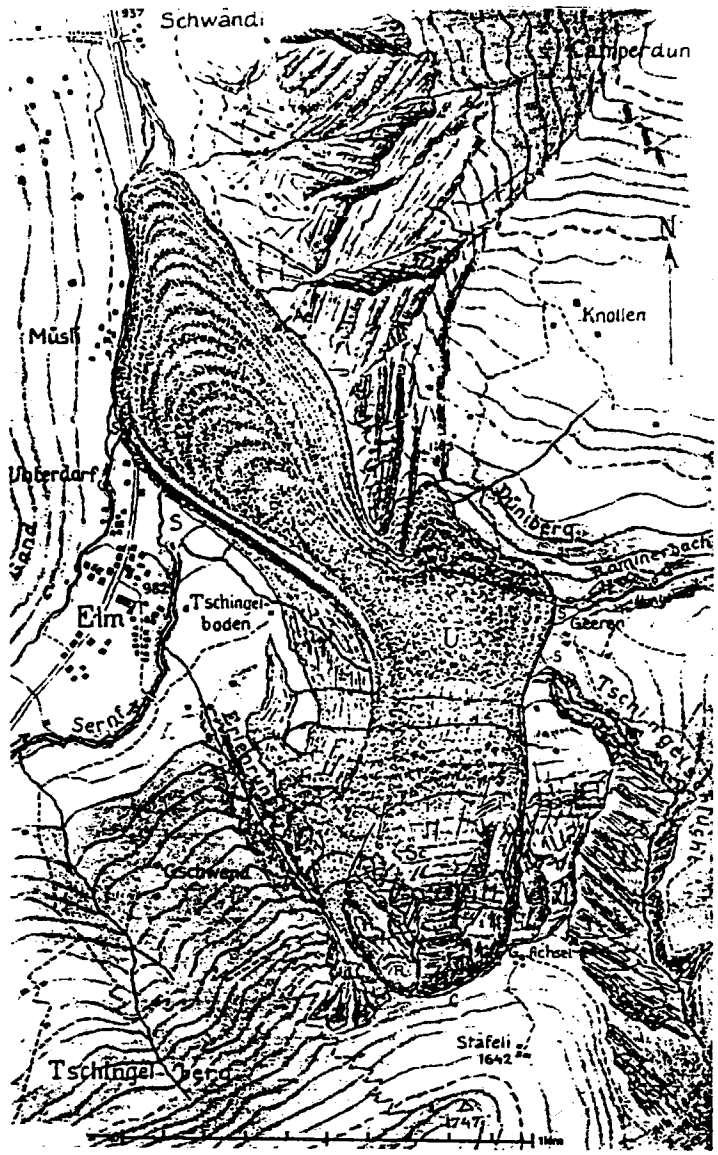

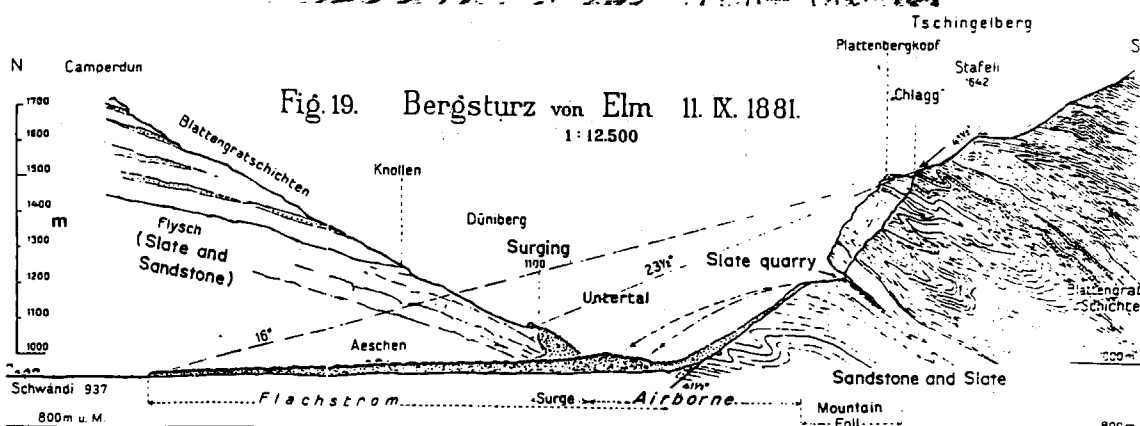

Fig. 19. Bergsturz von Elm 11. IX. 1881.
1 : 12.500

Figure 6k. Type III.C.dda landslide. The Madison, Montana landslide has a rockfall-type headscarp, detached debris apron, irregular plan form and profile shape and a hummocky surface texture. This topographic map of the landslide includes figures that give the thickness of the deposit at various locations, as well as the depth of the present scar beneath the former surface in feet (Hadley, 1978).

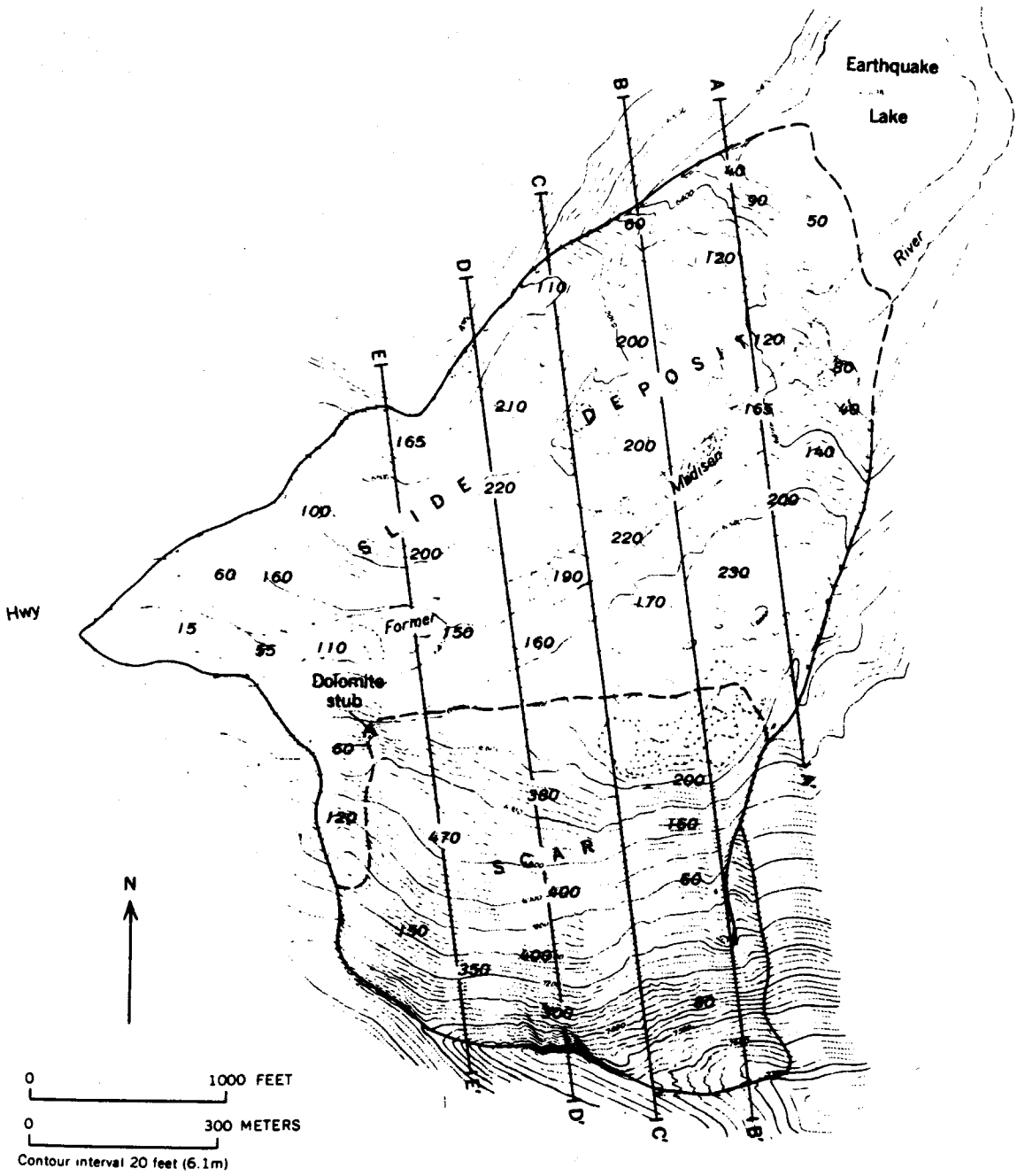
Earthquake
Lake
River
Hwy
Former
Dolomite stub
SLIDE DEPOSIT
SCAR
Madison
A
A'
B
B'
C
C'
D
D'
E
E'
N
0 1000 FEET
0 300 METERS
Contour interval 20 feet (6.1m)

names for landslides shed from the submerged flanks of oceanic islands. The geographic location field for lunar and martian landslides is provided by the most specific place name available. Especially for Mars, these locations vary from highly detailed, for example "Olympus Mons caldera," to extremely general, such as "NE Terra Cimmeria." Scott and Tanaka (1986), Greely and Guest (1987) and Tanaka and Scott (1987) provide martian place names, while Wilhelms (1987) gives lunar geographic data.

The **latitude** and **longitude** fields in the database provide precise locational data for each landslide deposit on Earth, Mars and the Moon (Appendix A, Fields 12a and 12b). For each planet, the latitude and longitude fields give the coordinates of a landslide in *decimal* degrees. A positive sign refers to north latitude or to west longitude, while negative values are assigned to south latitude and east longitude. As on Earth, latitudes on Mars and the Moon measure from 0° to 90° from the equator to the poles. Longitudes on the Moon range from 0° to 180° east and west, with 0° lying at the sub-Earth point. Martian longitudes, in contrast, measure from 0° to 360° west, with the prime meridian marked by a small, dark feature in Terra Meridiani (Mutch, et al., 1976). Examples of landslide coordinates reported normally and as in the database include: the Blackhawk landslide, at 34°25'N, 116°47'W, which is reported in the database as 34.42, 116.78, while the landslide just outside the crater Tsiolkovsky on the lunar farside, at 22°S, 128°E, is reported in the database as -22,-128.

The geographic coordinates of large landslide deposits in Appendix A are drawn mostly from a variety of topographic and geologic maps, from aircraft navigational charts and from photomosaic maps for martian landslides. Viking Orbiter frames provide latitude/longitude data for martian landslides too small for identification from available maps.

8. *Confinement*

Heim (1932) stated that three primary factors influence the distance travelled by a large landslide: the mass of the landslide, its fall height and the regularity of its travel path. Of the three, the regularity of the travel path often plays the critical role in determining the ultimate runout length of a giant landslide. However, even though Heim recognized that "Bends, deflections, divisions, surging [climbing obstacles], especially blockages use

up a lot of energy, decreasing the distance hurled, causing a steeper fall path," he found no brief parameter to describe the travel path regularity.

To more simply describe the regularity of the travel path, Lucchitta (1978a) abbreviated observations of this parameter in a comparative plot of potential energy versus fahrböschung for 38 large landslide deposits. She gave a qualitative estimate of the confinement of 30 of these deposits, which ranged from "unconfined" to "Landslides confined by obstacles or in valleys," to "Highly confined landslides. Confined by opposite valley wall in narrow, steep valley." Unfortunately, this scheme lacks definitions of "obstacles" and "unconfined landslides," making this scheme difficult to apply to other landslides with confidence.

The confinement field in the database (Appendix A, Field 13) uses a series of terms to express the degree of regularity of the travel path of large landslides. Satellite images, aerial photographs, detailed maps and sketches of large landslides provide data for evaluation of the confinement. The systematics of the assignment expand on the method of Lucchitta (1978a), providing more concise definitions for terms she proposed and adding additional terms to her original list. The gradational confinement values used in the database are discussed below, with definitions and terrestrial examples (Appendix A) provided for each term:

Heavy confinement: This term refers to a landslide strongly restrained by falling into a valley and impacting the opposite canyon wall. A heavily confined landslide comes to a rapid halt while still travelling normal to the headscarp and does not spread appreciably up- and down-valley. These landslides have essentially "fallen into a hole," and have transferred their energy to the ground through impact. Examples include: Gohna, India; Usoy, U.S.S.R.; Vaiont, Italy; and Madison, Montana.

Deflected path: This new term refers to a landslide that falls into a valley and deflects off a canyon wall, either as a single stream or as a divided stream that moves up- and down-canyon from the point of impact. The deflection angle of a landslide is provided where known. For example: "deflected-90°" designates a landslide which made a single deflection of 90°; "deflected-45°-50°" indicates a double deflection, the first impact deflecting it 45°, the second 50°; and "deflected-55°, 35°" describes the deflection angles of two lobes of a landslide

moving separately after collision with a valley wall, one moving 35° off the original movement direction, the other 55°. Examples of deflected landslides include: Flims, Switzerland; Gros Ventre, Wyoming; and Mayunmarca, Peru.

Partial Confinement: This term describes landslides that encounter and bodily overrun broad obstacles in their paths without significant deflection, such as hilly terrain or river terraces on the opposite bank of a valley. Examples include the Saidmarreh, Iran and Frank, Alberta landslides.

Unconfined: This term describes the confinement of landslides emplaced on relatively low-relief surfaces such as glaciers and alluvial fans. Examples include: Blackhawk, California, and Avalanchia del Zarzo I, Argentina.

Two additional terms modify these basic descriptors:

Channeled, "CH:" This term indicates a landslide that travelled 10% or more of its movement length in a well-defined channel with transverse movement checked by the canyon walls. Channeling has a profound effect on the morphology of large landslides (Appendix B), but little effect on their mobility (Chapter III). Examples of channeled landslides include: Martinez Mountain, California; Diablerets, Switzerland; and Huascaran, Peru.

Divided, "DI:" This term is used for landslides that separate into two or more large-scale lobes during the deposition of a single pulse of debris. The term does not refer to landslides with small, marginal digitations or to multiple-pulse deposits. Division sometimes occurs as a direct result of an impact with a valley wall, while in other cases it seems to occur spontaneously, usually near the end of movement. Where it is known, the angle between the lobes is also provided in the database. For example, the Bormio, Italy, landslide divided into two lobes upon impact with a canyon wall. One lobe deflected 75° to the left, the other 15° to the right, making an angle of 90° between the lobes (Heim, 1932). This information is provided in the database by the designation DI-90°. Other examples of divided landslides include the Silver Reef, California and El Capitan, Arizona deposits.

These modifiers are added parenthetically at the end of the primary confinement term in Appendix A. For example, the Martinez Mountain

landslide was channelized and deflected at emplacement, so its confinement may be expressed as "Deflected(CH)."

Unfortunately, no quantitative method has been devised to describe the confinement of large landslides. The ratio of the curved length to the straight length provides one quantitative method, but this has value only for deflected and channelized landslides. Many large, highly confined landslides having almost no transverse deflection would group with unconfined landslides on the basis of curved to straight length ratio.

9. *Age*

The age field of the database (Appendix A, Field 14) provides the best available date or age of emplacement of a landslide. For observed historical events, the database provides the day, month and year of the landslide. More commonly, the age must be estimated from available geologic data. For subaerial terrestrial landslides, the age is typically estimated from dateable materials, such as charcoal or fossils, in deposits surrounding the landslides. Playa deposits, which commonly form in closed basins or swales on the surfaces of large landslides, typically provide the best sites for obtaining minimum age estimates. The landslide deposits themselves rarely preserve dateable materials, even though most or all subaerial landslides must incorporate some organic detritus during movement from overrun trees and plants. Either the landslide deposits fail to isolate the detritus from the oxidizing surficial environment or the landslides have such great internal energy that they comminute and disseminate the material into a large volume of material, making detection difficult.

The ages of giant terrestrial suaqueous landslides must also be estimated from the surrounding geology; none have been dated directly (Moore, et al., 1989). One common dating technique involves estimating the accumulated sediment thickness overlying a landslide and dividing this value by the sedimentation rate. Unfortunately, this method yields large error bars in regions of extremely low sedimentation rate, such as the 1 mm/1000 yr mid-ocean accumulation rate applicable to landslides off the Hawaiian Ridge (Lipman, et al., 1988). Another method uses dated near-surface deposits in the headscarps of giant landslides to estimate the emplacement age. Age dates from lava flows, coral reefs and marine terraces partially filling old slide scars provide minimum emplacement ages, while dated deposits cut by the slide scars

provide maximum ages. A third technique allowed for an age estimate of the Alika 2 landslide off the southwestern coast of Hawaii Island. The large size, youth and location of the Alika 2 landslide make it a reasonable source for extensive tsunami deposits found up to 326 m above sea level on nearby Lanai Island, dated at 105,000 B.P. (Moore and Moore, 1984; 1988; Moore, et al., 1989).

Only two lunar landslides have been dated, Tsiolkovsky and the Apollo 17 "light mantle deposit." Crater counts from lunar orbiter photos on the former give it an Imbrian age (Guest, 1971), corresponding to an absolute age in the range of 3.2 to 3.85 by (Tanaka, 1986). In comparison, cosmic ray exposure ages for returned lunar samples stratigraphically bracketing the Apollo 17 landslide yielded a much younger age of about 50 to 100 my for this deposit.

The number and size of superposed impact craters and the textural/ morphologic sharpness observed from Viking Orbiter images provide the principle means to estimate the ages of martian landslides. Most martian landslides have superposed impact craters, mostly with 1/2- to 2-km diameters. However, because of the relatively limited area of individual landslides, not even the largest deposits provide sufficient cratering statistics for dating purposes, though the presence of any superposed craters in itself suggests considerable age (Lucchitta, 1978a). Based on similarities in the overall freshness of Valles Marineris landslides, Lucchitta (1979) assumed that they all belonged to about the same era of martian geologic history. By combining cratering statistics for 0.3- to 3.8-km diameter craters littering 33 larger landslide deposits in Valles Marineris, she obtained a density of 570 ± 130 craters larger than 1 km diameter per 10^6 km^2. This crater number indicates a Middle Amazonian age, corresponding to absolute ages between 250 and 2300 my (Tanaka, 1986), and suggests that the landslides correlate roughly in age with major late eruptive activity on the Tharsis volcanoes and with the formation of some channels (Lucchitta, 1979). Smaller martian landslides in Valles Marineris and elsewhere provide even less surface area for crater count statistics. The ages of these deposits can only be said to post-date the surfaces upon which they are deposited. Many smaller landslides occur in craters in the ancient highlands, but these probably do not date from early in martian history because they do not exhibit the severe mantling and degradation exhibited by the surrounding ancient terrain (Murray, personal communication, 1989).

While these data suggest that, at least for larger landslides in Valles Marineris, landslide activity was concentrated in a late phase of martian geologic history, a considerable range in ages is nevertheless implied by superposition of multiple landslide events and a range of surficial textural appearances, from clear and sharp to rather subdued. For this reason, the age field for martian landslides provides a simple qualitative description of their degree of degradation. The terms "fresh," "moderate" and "degraded" refer to the general appearance of the landslides, but no attempt is made to further divide or quantify these descriptions because of the variable resolution and clarity of the Viking Orbiter images.

10. *Composition*

The Composition field of the database gives the lithologies of terrestrial landslide deposits (Appendix A, Field 15). Where landslides involved multiple lithologies, the database reports all the major components, starting with the dominant rock type.

Lunar landslides occur inside craters, on the outer slopes of crater ejecta rims and on other steep slopes (Guest, 1971; Howard, 1973a; b). The lunar surface consists of brecciated rock of two primary types, "regolith" breccia and bedrock breccia, or "megabreccia." The former measures 5-6 m thick on the maria and thicker on the terra and formed by innumerable small impacts, while the bedrock breccia formed from fewer and larger impacts and extends several kilometers into the surface on the terra (Wilhelms, 1987). The Apollo 17 landslide, for example, took place in regolith breccia (Howard, 1973a), while the Tsiolkovsky landslide occurred in the bedrock breccia forming the raised rim of the 180 km-diameter crater.

The compositions of martian landslides cannot be determined with certainty. Landslides in craters in the terra, like the lunar landslides, likely consist of impact breccia, while those few landslides in volcanic calderas and from volcanic slopes probably consist primarily of basalt breccia. These two occurrences are labeled "breccia?" and "basalt?" in the database. The majority of the landslides, however, fell from "wall rock" of unknown composition in Valles Marineris. The walls of Valles Marineris commonly expose crudely layered deposits near the surface, underlain by many kilometers by massive, lighter-albedo rock. One widely held theory is that the near-surface layers consist of lava flows, while the massive deposits consist of highly brecciated,

much finer-grained materials of the old cratered terrain (Carr, 1981), akin to the lunar megabreccia.

11. *Moisture*

The Moisture field of the database (Appendix A) provides a general estimate of the water content for large martian and terrestrial landslides. Three terms are used in the database to indicate the moisture content: dry, moist and wet. The term "dry" refers to landslides having no perceptible water content. "Moist" refers to landslides that contained water, but not in sufficient quantities that the water drained away after the cessation of motion. "Wet" refers to landslides having a water-saturated matrix. At the cessation of motion, water separates from the matrix of these landslides and travels beyond the margin of the slides as mudflows, debris flows, or perhaps, as turbidity currents. Data for these assignments are obtained from field observations of landslide sedimentologies for terrestrial subaerial deposits, and from remotely-sensed morphological data for terrestrial subaqueous and martian landslide occurrences.

12. *Substrate*

The Substrate field (Appendix A) provides a general term for the nature of the substrate overrun by a landslide during its travel. These terms are largely self-explanatory. They include snow, soil, mud (water-saturated sediment), bedrock and alluvium. The nature of the substrate has a strong influence on the behavior of large landslides during runout.

13. *References*

The References field of the database gives the shorthand form of published data on given landslide deposits. The full references are given in Appendix F.

14. *Notes*

The Notes database field provides important supplementary data for landslide deposits, covering the many different sorts of data not otherwise recorded in the database. For one, this field gives necessary supplementary information on data reported in other database fields. It also includes a variety of data not included in any other database field, including:

1) abbreviated eyewitness accounts of large landslide behavior during movement, such as associated windgusts;

2) details of local conditions that might have helped set up an unstable slope and/or trigger a landslide;

3) the sedimentological characteristics of a deposit;

4) the effects of large landslides, such as the triggering of tsunamis or the numbers of associated deaths; and

5) kinematic or mechanical models of movement.

C. Landslide Database

Table 3 provides a summary of the database records in Appendix A, using a few of the most critical fields discussed above. The database records are arranged principally by volume. For landslides of the same volume or for landslides having no volume estimate, the name forms a second key field for alphabetically sorting the landslide records. Table 3 is meant to serve as a rapid source of basic data on giant landslide deposits and to facilitate direct comparisons between the various landslide deposits.

D. Conclusions-Chapter II

The data contained in Appendix A and summarized in Table 3 provides the groundwork for the remaining chapters of the thesis. Chapter III specifies the systematics of the database information, while Chapter IV describes the comparative planetology of martian, terrestrial and lunar landslides. The data and observations presented in these chapters are then used to evaluate the numerous mechanisms that have been proposed to explain the long runout and other unusual features of large landslides (Chapter V). Finally, the combined results of Chapters III-V provide the foundation upon which a new model of long runout is formulated (Chapter VI).

Table 3: Synopsis of Critical Data for Long-Runout Landslides in the Inner Solar System

Rankt	Name	Volume (cu. km.)	Fall (m)	Length (m)	H/L	References
M 1	Mars 19	17880	7000	119000	0.06	Lucchitta, 1979; 1987a; McEwen, 1989
M 2	Mars 15 (Ius Labes)	5800	7000	117000	0.06	Lucchitta, 1979; 1987a; U.S.G.S., 1986b
M 3	Mars 35	4880	7000	70000	0.10	Lucchitta, 1987a; McEwen, 1989
M 4	Mars 36	4183	8400	82500	0.10	Lucchitta, 1987a; McEwen, 1989
M 5	Mars 18	4047	6800	95000	0.07	Lucchitta, 1979; 1987a; McEwen, 1989
M 6	Mars 33	3267	7200	76000	0.09	McEwen, 1989
M 7	Mars 37	2960	8000	64000	0.13	Lucchitta, 1987a; McEwen, 1989
M 8	Mars 26	2761	6800	63000	0.11	Lucchitta, 1979; McEwen, 1989
E 1	Nuuanu	1600	5267	180000	0.03	Lipman, et. al., 1988; Moore, et al., 1989
M 9	Mars 34	1282	8200	63000	0.13	McEwen, 1989
E 2	Wailau	1100	5572	125000	0.04	Lipman, et. al., 1988; Moore, et al., 1989
M 10	Mars 24	833	5400	56000	0.10	Lucchitta, 1979; McEwen, 1989
M 11	Mars 30	688	3600	45000	0.08	Lucchitta, 1979; 1987a; McEwen, 1989
M 12	Mars 25	668	4400	31000	0.14	Lucchitta, 1979; McEwen, 1989
M 13	Mars 38	655	7600	54000	0.14	McEwen, 1989
E 3	Alika 1	400	5700	92000	0.06	Lipman, et. al., 1988
E 4	Alika 2	200	4800	90000	0.05	Lipman, et. al., 1988
M 14	Mars 1	200	2000	60000	0.03	Lucchitta, 1978a; 1979
M 15	Mars 28	157	2800	33000	0.08	Lucchitta, 1979; McEwen, 1989
E 5	Mt. Shasta	45	3550	49000	0.07	Siebert, 1984; Crandell, 1988
E 6	Ka Lae-E	40	5200	65000	0.08	Lipman, et. al., 1988; Moore, et al., 1989
E 7	Papa'u	39	1350	24400	0.06	Fornari, et. al., 1979
M 16	Mars 65	32	3600	29000	0.12	McEwen, 1989
M 17	Mars 97	29	4000	20000	0.20	Lucchitta, 1987a; McEwen, 1989
E 8	Saidmarreh	20	1200	15000	0.08	Harrison and Falcon, 1938
E 9	Langtang	15	3400	30000	0.11	Heuberger, et. al., 1984
E 10	Meru Volcano	15	3900	50000	0.08	Siebert, 1984
E 11	Socompa Volcano	15	3000	25200	0.12	Francis, et. al., 1985
M 18	Mars 22	14	2000	18000	0.11	McEwen, 1989
E 12	Colima Volcano	12.5	4000	40000	0.10	Siebert, 1984
E 13	Flims	12	2120	16000	0.13	Heim, 1932
M 19	Mars 64	11	1200	8000	0.15	Lucchitta, 1979; McEwen, 1989
E 14	Sur	10.5	1650	80950	0.02	Normark and Gutmacher, 1988
E 15	Yatsugatake-A	9	2400	32000	0.08	Ui, 1983
E 16	Egmont Volcano-A	7.5	2600	31000	0.08	Siebert, 1984
E 17	Pungarehu	7.5	2600	27000	0.10	Ui, et. al., 1986
E 18	Mawenzi Volcano	7.1	4500	60000	0.08	Siebert, 1984
M 20	Mars 66	5.5	6400	21000	0.30	McEwen, 1989
M 21	Mars 67	5.3	6200	20000	0.31	McEwen, 1989

M 22	Mars 68	4.3	6200	19000	0.33	McEwen, 1989
E 19	Akagi Volcano	4	2400	19000	0.13	Siebert, 1984
M 23	Mars 69	3.3	5000	16000	0.31	McEwen, 1989
E 20	Koefels	3	600	5364	0.11	Heuberger, et. al., 1984
E 21	Galunggung Volcano	2.9	1900	25000	0.08	Siebert, 1984
E 22	Mt. St. Helens	2.8	2550	24000	0.11	Voight, et al., 1983; Siebert, 1984
E 24	Engelberg	2.75	1650	7500	0.22	Heim, 1932
E 25	Asama Volcano	2	2250	20000	0.11	Siebert, 1984
E 26	Usoy	2	1650	6800	0.24	Preobrajensky, 1920; Gaziev, 1984
E 27	Tin Mtn.	1.8	620	5900	0.11	Burchfiel, 1966
E 28	Iriga Volcano	1.5	1050	11000	0.10	Siebert, 1984
E 29	Bandai Volcano	1.5	1200	11000	0.11	Schuster and Crandell, 1984; Siebert, 1984
M 24	Mars 109	1.5	1800	15000	0.12	This paper
E 30	Siders	1.5	2450	17500	0.14	Lucchitta, 1978a
E 31	Shiveluch Volcano	1.5	2000	12000	0.17	Siebert, 1984
M 25	Mars 70	1.4	6200	17000	0.36	McEwen, 1989
E 32	Iwaki Volcano	1.3	1500	15000	0.10	Ui, 1983
E 33	Tamins	1.3	1280	13500	0.09	Lucchitta, 1978a
E 34	Egmont Volcano-B	1	2400	21000	0.11	Siebert, 1984
E 35	Camen	1	2700	23000	0.12	Adushkin, personal communication, 1990
E 36	Bezymianny Volcano	1	2200	28000	0.08	Ui, 1983
E 37	Fempass	1	1400	15500	0.09	Lucchitta, 1978a
E 38	Mombacho Volcano	1	1300	12000	0.11	Siebert, 1984
E 39	Mayunmarca	1	1870	8250	0.23	Kojan and Hutchinson, 1978
E 40	Ircht	1	1000	4000	0.25	Adushkin, personal communication, 1990
M 26	Mars 71	0.9	2200	7000	0.31	McEwen, 1989
E 41	Papandajan Volcano	0.9	1150	12000	0.10	Siebert, 1984
E 42	Glarnisch Guppen	0.8	1920	5275	0.36	Heim, 1932
M 27	Mars 133	0.8	1900	10000	0.19	This paper
E 43	Myoko Volcano-A	0.8	2000	19000	0.11	Siebert, 1984
E 44	Glarnisch Gleiter	0.77	2460	8000	0.31	Heim, 1932
E 45	Deyen	0.6	740	6600	0.11	Hsü, 1975
M 28	Mars 101	0.5	1600	6600	0.24	This paper
E 46	Mt. Granier	0.5	1600	7500	0.21	Eisbacher and Clague, 1984
E 47	Soufriere Volcano	0.5	1350	9500	0.14	Siebert, 1984
E 48	Maligne Lake	0.498	920	5470	0.17	Cruden, 1976
E 49	Unzen Volcano	0.48	850	5700	0.15	Siebert, 1984
E 50	Rockslide Pass	0.45	750	5500	0.14	Eisbacher, 1979
E 51	Avalanche Lake	0.4	800	4600	0.17	Eisbacher, 1979
E 52	Khait	0.4	1500	8700	0.17	Seed, 1968; Solonenko, 1972; 1977
E 53	Sawtooth 1	0.37	910	3700	0.25	Mudge, 1965
E 54	Egmont Volcano-C	0.35	2500	27000	0.09	Siebert, 1984
E 55	Blackhawk	0.3	1200	9000	0.13	Shreve, 1968a; Johnson, 1978
M 29	Mars 72	0.3	2200	6000	0.37	McEwen, 1989
E 56	Usu Volcano	0.3	750	6500	0.12	Siebert, 1984

E57	Gohna	0.29	1520	3050	0.50	Holland, 1894
E58	Sawtooth 2	0.275	670	1570	0.43	Mudge, 1965
E59	Yatsugatake-B	0.27	1400	12500	0.11	Siebert, 1984
E60	Komagatake Volcano	0.25	1200	12000	0.10	Siebert, 1984
M30	Mars 108	0.25	900	5700	0.16	This paper
E62	Vaiont	0.25	540	1600	0.34	Mueller, 1964; 1968
E63	Martinez Mtn.	0.24	1555	7900	0.20	Bock, 1977; Baldwin, 1986
E64	Myoko Volcano-B	0.23	1400	8000	0.18	Siebert, 1984
E65	Silver Reef	0.23	900	7000	0.13	Shreve, 1968a
M32	Mars 141	0.2	2500	5500	0.45	This paper
L2	Apollo 17	0.2	1900	9000	0.21	Howard, 1973a;b; Lucchitta, 1977
E66	Rarz	0.2	675	2400	0.28	Gregorian, et al., 1983
M31	Mars 74	0.2	1100	4800	0.23	This paper
E67	Bormio	0.18	1620	5140	0.32	Heim, 1932
M33	Mars 118	0.15	2000	4900	0.41	This paper
E68	Huascaran 1	0.15	4200	20000	0.21	Hsü, 1975; Plafker and Erickson, 1978
E70	Poschiavo	0.15	1500	4350	0.34	Heim, 1932
E70	Parpan	0.15	1560	5800	0.27	Heim, 1932
E71	Kandertal	0.14	2210	11000	0.20	Heim, 1932
E72	Upper Kananaskis	0.13	650	2560	0.25	Locat and Cruden, 1977
E73	Kurohime Volcano	0.12	800	6000	0.13	Siebert, 1984
E74	Obersee	0.12	1840	6350	0.29	Heim, 1932
M34	Mars 73	0.1	4200	7500	0.56	McEwen, 1989
E75	Magian	0.1	708	2340	0.30	Gregorian, et al., 1983
E76	Ainy	0.1	725	2970	0.24	Adushkin, personal communication, 1990
E77	Carlson	0.1	750	4400	0.17	Shaller, in press
E78	Medicine Lake	0.086	320	1220	0.26	Cruden, 1976
E79	Scima di Saoseo	0.08	1450	5500	0.26	Heim, 1932
E80	U.S.S.R. Artificial 1	0.08	750	2200	0.34	Adushkin, personal communication, 1990
E81	Huascaran 3	0.075	4000	18600	0.22	Plafker and Erickson, 1978
E82	Loma Redonda	0.065	700	7000	0.10	Fauque and Strecker, 1988
E83	U-turn	0.065	550	3200	0.17	Eisbacher, 1979
E84	Mageik	0.054	800	6500	0.12	Griggs, 1922
E85	Chaos Jumbles 2	0.05	651	3476	0.19	Eppler, et. al., 1987
E86	Nozzle	0.05	850	5800	0.15	Eisbacher, 1979
E87	Sale Mountain	0.05	300	1350	0.22	Gongxian and Bangdong, 1984
E88	Hope	0.047	1220	3080	0.40	Mathews and McTaggart, 1969
E89	Chaos Jumbles 1	0.044	770	4550	0.17	Eppler, et. al., 1987
E90	El Capitan	0.04	1300	6800	0.19	Krieger, 1977; Yarnold and Lombard, 1989
E91	Stalk Lakes	0.04	700	3000	0.23	Eisbacher, 1971; Mollard, 1977
E92	Mount Kitchener	0.0391	660	3220	0.20	Cruden, 1976
E93	Gros Ventre	0.038	610	3400	0.18	Alden, 1928; Voight, 1983
E94	Avalancha del Zarzo 1	0.037	900	6500	0.14	Fauque and Strecker, 1988
E95	Frank	0.0365	830	3000	0.28	Daly, et al., 1912; Cruden and Hungr, 1986
E96	Goldau	0.035	1100	5175	0.21	Heim, 1932

E97	Triple	0.035	450	2660	0.17	Eisbacher, 1979
E98	Panum	0.033	183	2515	0.07	Sieh and Bursik, 1986
E99	North Arm	0.03	950	4100	0.23	Eisbacher, 1979
E100	Diablerets 2	0.03	1900	5450	0.35	Heim, 1932; Eisbacher and Clague, 1984
E101	Voralpsee	0.03	1050	3900	0.27	Heim, 1932
E102	Sherman	0.03	1100	5000	0.22	Shreve, 1966; McSaveney, 1978
E103	Madison	0.028	425	1550	0.27	Hadley, 1960; 1978
E104	Schwan	0.027	1550	6100	0.25	Post, 1967
E105	Chaos Jumbles 3	0.026	430	2910	0.15	Eppler, et. al., 1987
E106	Fairweather	0.026	3350	10500	0.32	Post, 1967
E107	Cadomin	0.025	400	1000	0.40	Locat and Cruden, 1977
E108	Rubble Creek	0.025	1035	6900	0.15	Moore and Mathews, 1978
E109	Allen 4	0.023	1300	7700	0.17	Post, 1967
E110	Loma de la Aspereza	0.021	800	7000	0.11	Fauque and Strecker, 1988
E111	Stanley	0.021	800	2666	0.30	Adams, 1981
E112	Damocles	0.02	290	2850	0.10	Eisbacher, 1979
E113	Como di Dosde	0.02	1190	2670	0.45	Heim, 1932
E114	Steller	0.02	1200	6700	0.18	Post, 1967
E115	Pasayten	0.02	790	3600	0.22	Waitt, 1979
E116	Biasca	0.015	1900	3333	0.57	Eisbacher and Clague, 1984
E117	Disentis	0.015	740	1950	0.38	Heim, 1932
E118	Huascaran 2	0.013	4200	19000	0.22	Plafker and Erickson, 1978
E119	Angarakan	0.012	500	1700	0.29	Solonenko, et. al., 1984
E120	Antronapiana	0.012	1600	3704	0.43	Eisbacher and Clague, 1984
E121	Jonas Creek South	0.0102	920	2490	0.37	Cruden, 1976
E122	Corbeyrier-Yvorne	0.01	800	3400	0.24	Eisbacher and Clague, 1984
E123	Bualtar 1	0.01	1490	4560	0.33	Hewett, 1988
E124	Elm	0.01	610	2130	0.29	Buss and Heim, 1881; Heim, 1932
E125	Twin Slides 1	0.01	950	4500	0.21	Eisbacher, 1979
E126	Twin Sildes 2	0.01	900	3600	0.25	Eisbacher, 1979
E127	U.S.S.R. Artificial 2	0.008	600	1500	0.40	Adushkin, personal communication, 1990
E128	Bualtar 2	0.007	1430	3550	0.40	Hewett, 1988
E129	North Nahanni	0.007	400	1550	0.26	Evans, et. al., 1987
E130	Chibins 9	0.006	650	3000	0.22	Adushkin, personal communication, 1990
E131	Sioux	0.006	1400	4500	0.31	Post, 1967
E132	Wengen 2	0.0055	590	1400	0.42	Hsü, 1975
E133	Jonas Creek North	0.0054	880	3250	0.27	Cruden, 1976
E134	Avalancha del Zarzo 2	0.005	850	5000	0.17	Fauque and Strecker, 1988
E135	Antelao	0.005	750	2350	0.32	Eisbacher and Clague, 1984
E136	Simplon	0.005	2300	5200	0.44	Eisbacher and Clague, 1984
E137	Ennetbühl	0.005	300	1700	0.18	Heim, 1932
E138	Beaver Flats South	0.00482	300	1220	0.25	Cruden, 1976
E139	Beatty	0.0046	427	1113	0.38	Hector, 1989
E140	Altels	0.0045	1100	3850	0.29	Heim, 1932; Eisbacher and Clague, 1984
E141	Brazeau Lake	0.0045	884	2720	0.33	Cruden, 1982

E142	Beaver Flats North	0.00413	350	1100	0.32	Cruden, 1976
E143	Chibins 17	0.004	500	1600	0.31	Adushkin, personal communication, 1990
E144	Pisque River	0.0036	500	1125	0.44	Plaza-Nieto, et al., 1990
E145	Plurs	0.0035	950	2000	0.48	Heim, 1932; Eisbacher and Clague, 1984
E146	Bualtar 3	0.003	1300	2400	0.54	Hewett, 1988
E147	Clavans	0.003	700	1200	0.58	Eisbacher and Clague, 1984
E148	Chibins 8	0.0026	370	900	0.41	Adushkin, personal communication, 1990
E149	Wengen 1	0.0025	500	1100	0.45	Hsü, 1975
E150	Chibins 6	0.0024	400	1100	0.36	Adushkin, personal communication, 1990
E151	Chibins 1	0.002	400	1100	0.36	Adushkin, personal communication, 1990
E152	U.S.S.R. Artificial 4	0.002	500	800	0.63	Adushkin, personal communication, 1990
E153	Puget Peak	0.0018	1215	2130	0.57	Hoyer, 1971
E154	Chibins 4	0.0015	400	1000	0.40	Adushkin, personal communication, 1990
E155	Kootenay 1	0.0014	300	1600	0.19	Campbell and Shaw, 1978
E156	Chibins 5	0.0013	250	500	0.50	Adushkin, personal communication, 1990
E157	Vesuvius 7	0.0012	410	820	0.50	Hazlett, et al., in press
E158	Chibins 3	0.0011	350	700	0.50	Adushkin, personal communication, 1990
E159	Vesuvius 6	0.0011	360	680	0.53	Hazlett, et al., in press
E160	U.S.S.R. Artificial 3	0.001	750	1400	0.54	Adushkin, personal communication, 1990
E161	Vesuvius 5	0.001	636	1240	0.51	Hazlett, et al., in press
E162	Chibins 14	9E-4	200	400	0.50	Adushkin, personal communication, 1990
E163	Vesuvius 2	9E-4	505	940	0.54	Hazlett, et al., in press
E164	Chibins 10	8E-4	250	450	0.56	Adushkin, personal communication, 1990
E165	Vesuvius 4	7.9E-4	470	960	0.49	Hazlett, et al., in press
E166	Monbiel	7.5E-4	400	1300	0.31	Heim, 1932; Eisbacher and Clague, 1984
E167	Chibins 2	7E-4	250	400	0.63	Adushkin, personal communication, 1990
E168	Val Lagone	6.5E-4	1050	2400	0.44	Hsü, 1975
E169	Zarera	6.5E-4	1200	2700	0.44	Eisbacher and Clague, 1984
E170	Chibins 13	6E-4	300	550	0.55	Adushkin, personal communication, 1990
E171	Vesuvius 3	5.5E-4	285	500	0.57	Hazlett, et al., in press
E172	Altdorf-Spiringen	5E-4	1300	2100	0.62	Eisbacher and Clague, 1984
E173	Airolo	5E-4	820	1290	0.64	Heim, 1932; Eisbacher and Clague, 1984
E174	Schachental	5E-4	1800	3100	0.58	Hsü, 1975
E175	Chibins 7	5E-4	240	500	0.48	Adushkin, personal communication, 1990
E176	Chibins 15	3E-4	170	240	0.71	Adushkin, personal communication, 1990
E177	Summit Lake	2.5E-4	745	5800	0.13	Curry and Melhorn, 1990
E178	Vesuvius 1	1.8E-4	375	640	0.59	Hazlett, et al., in press
E179	Kootenay 2	1.3E-4	213	700	0.30	Campbell and Shaw, 1978
E180	Kootenay 3	1.2E-4	190	530	0.36	Campbell and Shaw, 1978
E181	Kootenay 4	1.1E-4	125	310	0.40	Campbell and Shaw, 1978
E182	U.S.S.R. Artificial 5	1E-4	425	925	0.46	Adushkin, personal communication, 1990

† Landslide location: M = Mars; E = Earth; L = Moon

Chapter III. Systematics of Database Information

A. Importance of Pattern Delineation in the Database

The following chapter describes the systematics of the large landslide observations collected in Appendix A. The landslide observations discussed below are grouped into five primary sections. The first portion considers the systematics of the log(volume) vs. H/L relations of large landslides. This section includes a description of prominent relationships within and between certain subgroups of data on the plots, as well as tests of the effects of initiation style, confinement, deposit morphology, composition and setting on the log(volume) vs. H/L relationship of long-runout landslides. The following four sections concentrate on the four major stages in the history of a large landslide: 1) slope preparation and the initiation of movement; 2) runout; 3) stopping; and 4) post-depositional degradation. These four sections combine data from a variety of sources, including eyewitness accounts of historical landslide emplacement, the depositional characteristics of large landslides and the effects of setting for terrestrial, martian and lunar landslides. These systematics are referenced in later chapters which concern the mechanics of initiation and travel of large landslides on Earth, Mars and the Moon.

The systemization of the data of Appendix A into well-defined patterns provides the primary means currently available to determine the mechanics of long-runout landslides, one of the principle goals of this research. Of principle concern is the commonly observed "long-runout" (landslides with fall height, H/runout length, L ratios below 0.6) phenomenon exhibited by large rock landslides ($>10^6$ m^3), in which a mass of brecciated rock debris can appear to flow or slide as a thin sheet at high speed down a mildly dipping depositional plain. The large diversity of models proposed to explain long runout (Chapter V) is in part a result of the limitations of the datasets used by previous researchers. A unified model to explain the behavior of large landslides must take into account the many new, obscure and disparate facts and observations contained in Appendix A. Modeling from the geologic data is the only means presently available to establish the mechanics of long runout, as this phenomenon has not yet been experimentally reproduced in the laboratory. The means to do so potentially exists in the use of detailed computer simulations or large geotechnical centrifuges. The latter could conceivably mimic the behavior of 10^5-10^6 m^3 landslides (Scott, personal

communication, 1990), the lower size limit of long-runout landslides. While such detailed experiments remain in the planning stage, the systemized data presented below will provide a critical reference for the development of these lines of experimental research.

B. The Log(Volume) vs. H/L Relationship in Large Landslides

1. *Introduction*

One of the most significant characteristics of large long-runout landslides is that their H/L values generally decrease with their volume. Heim (1932) was the first to note this characteristic of large landslides, but it was first quantified by Scheller (1971), who observed a linear relationship in the log(volume) vs. H/L ratios of long-runout landslides. The cause of this semi-log relationship forms one of the primary questions in understanding the nature of long runout in large landslides.

Throughout the following discussion, trends of landslide data plotted on log(volume) vs. H/L diagrams are used to distinguish the behavior of different groups of long-runout landslides. In order to determine the comparative trends of various groupings of the data on these plots and the significance of differences in observed trends, each dataset is plotted with an associated regression line. These regression lines are calculated according to the reduced major axis (RMA) method. Davis (1986) stated that this is one of the appropriate methods to follow when it is not possible "to rationally decide which variable should be X and which should be Y [in a regression analysis]." He further stated that:

> This occurs, for example, in biometry, where it may be useful to know the relationship between two sets of measurements, such as the lengths and widths of shells, but it is not obvious which set of measurements should be expressed as a function of the other...
> An appealing solution would be to fit a line that minimizes the deviations of the observations from the line in both the X and Y directions simultaneously. Such a line would split the difference between the regression lines of X on Y and Y on X. It would conform more closely to the visual impression of the trend in the observations, and it would attribute the scatter of the datapoints to both variables, rather than assigning all the deviations from the fitted line to a single variable.

An estimation of the expected variation in H/L and in log(volume) measurements indicates that both should have about equivalent degrees of

uncertainty, as assumed in the RMA regression method. For example, the uncertainty in H and L for terrestrial landslides having existing topographic map coverage probably ranges around 5%, giving an estimated uncertainty in H/L of about 10%. In comparison, the volume of large landslides probably cannot be measured to better than 30% in most cases (Chapter II). The uncertainty in log(volume) therefore has a minimum of about 5-10%. Thus, the H/L and log(volume) values reported for most large landslides should have approximately equivalent magnitudes, supporting the use of the RMA method for regression analysis.

The RMA procedure minimizes the product of the deviations in both the X and Y directions. This procedure has the effect of minimizing the sum of the triangular areas formed between the observations and the fitted line (Figure 7). The reduced major axis is defined by an ordinary linear equation (Davis, 1986):

$$Y = b_0 + b_1 X \tag{3}$$

in which b_0 gives the Y-intercept and b_1 the so-called RMA slope, defined as the ratio of the standard deviations (*standard deviation* describes the dispersion or spread of data around the mean, and has the same units of measurement as the data), s, of the two variables X and Y:

$$b_1 = s_Y / s_X \tag{4}$$

The intercept of the reduced major axis is given by:

$$b_0 = \overline{Y} - b_1 \overline{X} \tag{5}$$

in which X-bar and Y-bar are the mean values of the X and Y datasets, respectively. Equation 6 gives the standard error of the RMA slope and Equation 7 the standard error of the intercept:

$$se_{b_1} = b_1 \sqrt{\left(\frac{1 - r^2}{n}\right)} \tag{6}$$

Figure 7. Criteria for fitting a reduced major axis (RMA) line. The reduced major axis line is that which minimizes the product of deviations (X - *X*) and (Y - *Y*) from the fitted line, equivalent to minimizing the areas of the triangles (shaded). Modified from Davies (1986).

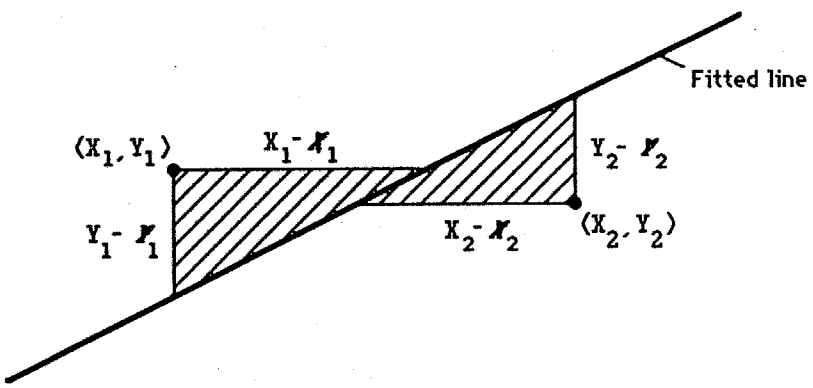
Fitted line
(X_1, Y_1)
$X_1 - \bar{X}_1$
$Y_2 - \bar{Y}_2$
$Y_1 - \bar{Y}_1$
$X_2 - \bar{X}_2$
(X_2, Y_2)

$$se_{b_o} = s_Y \sqrt{\frac{1 - r^2}{n} \left[1 + \frac{\bar{X}^2}{s_X^2} \right]} \qquad (7)$$

in which r^2 is the correlation coefficient and n the number of paired X, Y values in the dataset. The standard error describes the variability that can be expected in the means of samples by repeated random collection from the same sample. The r^2-correlation coefficient is given by Equation 8 (Size, 1987):

$$r^2 = \frac{[\Sigma(X_i - \bar{X})(Y_i - \bar{Y})]^2}{[\Sigma(X_i - \bar{X})^2][\Sigma(Y_i - \bar{Y})^2]} \qquad (8)$$

The value of r^2 varies with the scatter in the plotted dataset. These values vary from 0.000 for a circular distribution of points for which no best-fit line exists, to 1.000 for datapoints that fall precisely along a straight line. To test whether the slopes of two reduced major axis lines, b_1 and b_2, vary significantly from one another, one may make use of the test statistic Z (Davis, 1986):

$$Z = \frac{b_1 - b_2}{\sqrt{se_{b_1}^2 + se_{b_2}^2}} \qquad (9)$$

Z is approximately normally distributed and its significance can be determined from a table of the standardized normal distribution (Davis, 1986; Appendix G). For example, if the slopes of two calculated RMA lines are compared and a Z-value of 0.5 is determined, the associated value of A, 0.1915 (Appendix G), indicates that there is only a 19.15% probability that the slopes of the lines representing the two plotted datasets vary from one another. Conversely, the A-value can be interpreted to mean that there is a 80.85% probability that the slopes of the RMA lines representing the two datasets are actually identical. For each of the RMA best-fit lines plotted in the following diagrams, the equation of the line, the standard error of the slope of the line, se_s, the standard error of the y-intercept, se_i, and the r^2-correlation coefficient are reported. Where necessary, the significance of variations in slope between different best-fit lines are checked using the Z test.

In the following sections, detailed information on long-runout landslides collected in the large landslide database (Appendix A) provides the means for detailed assessment of the factors that influence their log(volume) vs. H/L relations. This analysis begins with a discussion of two sets of prominent log(volume) vs. H/L relationships. The initial discussion reviews previously recognized variations between the log(volume) vs. H/L relations of landslides from four widely differing solar system environments. Next, the subset of terrestrial subaerial landslides is investigated for prominent log(volume) vs. H/L relations. The terrestrial subaerial data also provides the source of data for the following section, in which a variety of factors are tested to determine their influence on the degree of long runout experienced by large landslides. This information should in large part also apply to the less complete datasets of terrestrial subaqueous landslides and martian landslides. The observations discussed below will be referenced in later chapters which discuss proposed mechanical models for understanding long runout in large landslides.

2. *Prominent Relationships*

Scheller (1971), Scheidegger (1973) and Hsü (1975) all noted that terrestrial non-volcanic subaerial landslides exhibit a trend towards decreasing H/L with increasing volume using slightly different datasets. Similar relationships have been noted for large terrestrial volcanic landslides (Ui, 1983) and also for large martian Valles Marineris landslides (McEwen, 1989). Based on data from 17 volcanic and 31 non-volcanic landslides, Ui (1983) stated that terrestrial volcanic deposits exhibit lower H/L values on average than non-volcanic landslides of equivalent volume. Log(volume) vs. H/L data for 134 non-volcanic and 37 volcanic landslides (Appendix A) plotted in Figure 8a, however, indicates that the best-fit trend through the volcanic landslide data actually closely matches that of the non-volcanic deposits. The trends through these two intersecting datasets have equivalent slopes at the 95% confidence interval on a 2-tailed normal distribution. In contrast, the log(volume) vs. H/L trend observed for martian landslides varies markedly from the trends of the terrestrial datasets (Figure 8a), as observed by McEwen (1989). The martian landslides exhibit higher average H/L values for a given landslide volume than their terrestrial counterparts. In addition to these studies, Lipman, et al. (1988) showed that five giant ($>10^9$ m^3) subaqueous landslides (those landslides that were initiated and traveled primarily or entirely under water) in basalt

Figure 8a. This diagram plots the log(volume) versus H/L relations of four groups of long-runout landslides. The diagram plots data for terrestrial subaerial non-volcanic and volcanic landslides, for subaqueous landslides and for martian landslides. Best-fit lines through the data are provided by the reduced major axis method. Also included are the equations of the RMA best-fit lines, the r^2-correlation coefficients of each line and the standard errors of the slopes and intercepts of the lines.

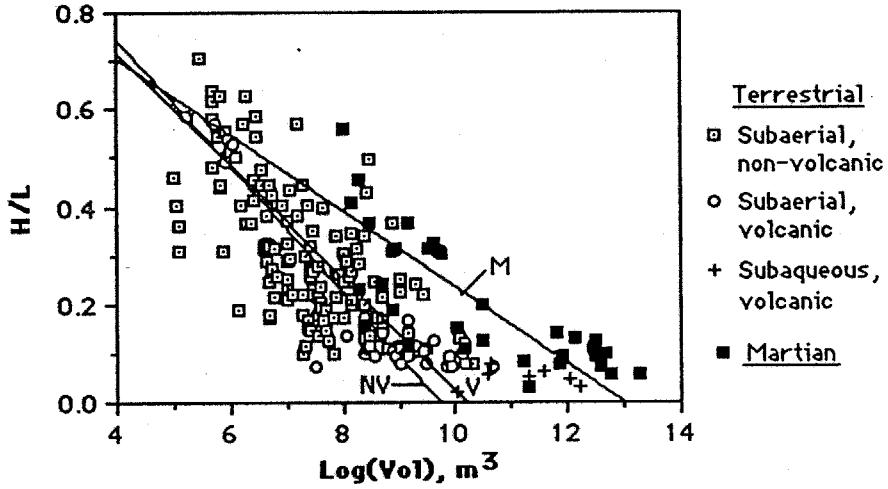

Non-volcanic: H/L = -0.129 Log V + 1.250, R^2 = 0.440, se_s = 0.008, se_i = 0.062

Volcanic: H/L = -0.116 Log V + 1.178, R^2 = 0.831, se_s = 0.008, se_i = 0.068

Martian: H/L = -0.078 Log V + 1.017, R^2 = 0.608, se_s = 0.008, se_i = 0.089

bedrock shed from the Hawaiian Islands roughly followed the extension of the log(volume) vs. H/L trend of the terrestrial subaerial landslides. Because of the small number of datapoints, no regression analysis has been performed on these data. Subaqueous landslides in marine sediments yield entirely dissimilar log(volume) vs. H/L trends, however (Lipman, et al., 1988), and will not be considered further because their movement appears to be a water-dominated process.

The data collated in Appendix A allow for more detailed considerations of trends of terrestrial landslide data on log(volume) vs. H/L plots. Figures 8a and 8b give the log(volume) vs. H/L relations for 134 terrestrial subaerial non-volcanic landslides. The five groups of landslide deposits exhibiting the most prominent relationships are highlighted in Figure 8b, with their RMA best-fit slopes given in Figure 8c. These five sets of data consist of heavily confined landslides, landslides emplaced on snow/ice substrates, those consisting of ice/rock mixtures, a group having Blackhawk-like morphologies and a group consisting of landslides in coal mine tailings. This grouping of the data indicates that a number of factors, including morphology, confinement, substrate properties and landslide composition, have an influence on the log(volume) vs. H/L relations demonstrated by long-runout landslides. These groups of data generate an envelope in log(volume) vs. H/L space that contains all the other unclassified deposits. Blackhawk-like landslides along with the Kootenay mine tip landslides define the low-H/L boundary over a wide range in volumes, while heavily confined landslides make up the high H/L boundary. Large landslides composed of ice/rock mixtures, in turn, demark the low-volume end of the envelope for the great majority of long-runout landslides.

A variety of factors probably play a role in producing the variations between the five prominent groups of data highlighted in Figure 8b. The degree of confinement clearly forms one of the important controls. Heavily confined landslides, which fall into narrow gorges during emplacement, have essentially fallen into a deep hole. Their runout is restricted by their depositional geometry. All the landslides in the Blackhawk-like morphology class, in turn, are unconfined (Appendix A). However, these deposits comprise only a small percentage of the unconfined landslides plotted in Figures 8b and 8c (c.f., Figure 10a), indicating that some other factor in addition to a lack of confinement must operate in these landslides to give them their exceedingly

Figure 8b. This diagram plots the log(volume) versus H/L relations of 134 terrestrial subaerial non-volcanic landslides, and highlights five prominent clusters of datapoints.

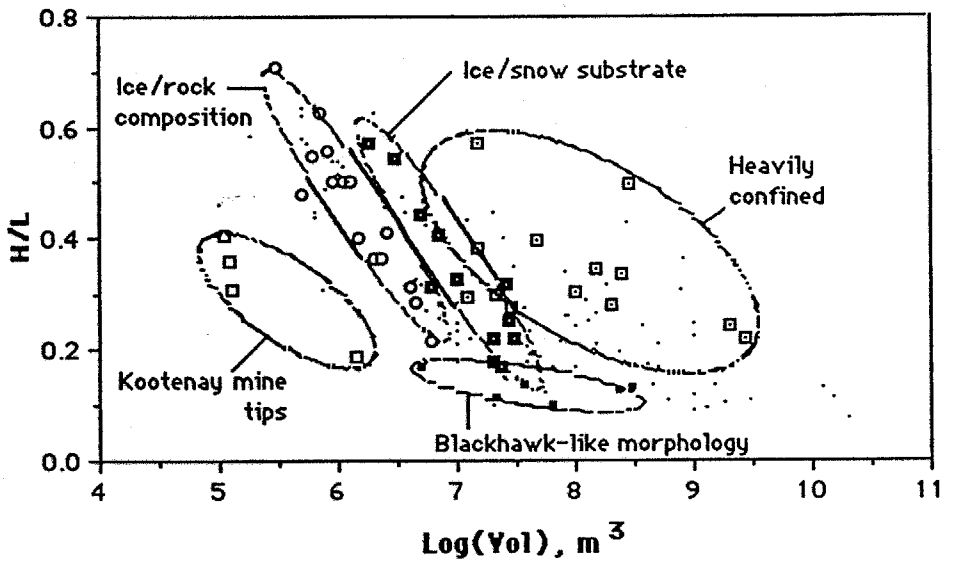

- Heavy Confinement
- Ice/Rock Composition
- Landslides on Ice/Snow-Covered Ground
- Blackhawk-Like Morphology
- Coal Mine Tips
- Unclassified

Figure 8c. This diagram plots the log(volume) versus H/L relations for 134 terrestrial subaerial non-volcanic landslides. Best-fit lines through five prominent clusters of data are provided by the reduced major axis method. Also included are the equations of the RMA best-fit lines, the r^2-correlation coefficients of each line and the standard errors of the slopes and intercepts of the lines.

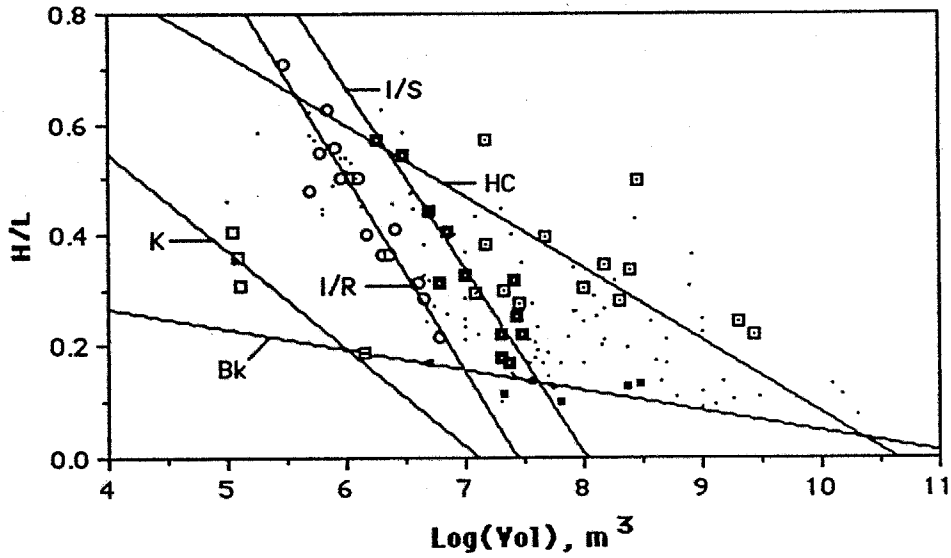

- Heavy: H/L = -0.128 Log V + 1.365, R^2 = 0.164, se_s = 0.032, se_i = 0.261
- Ice/Rock: H/L = -0.349 Log V + 2.594, R^2 = 0.876, se_s = 0.032, se_i = 0.195
- Ice/Snow Subst: H/L = -0.327 Log V + 2.627, R^2 = 0.827, se_s = 0.039, se_i = 0.276
- Blackhawk-Like: H/L = -0.036 Log V + 0.408, R^2 = 0.218, se_s = 0.079, se_i = 0.101
- Coal Mine Tips: H/L = -0.174 Log V + 1.244, R^2 = 0.862, se_s = 0.032, se_i = 0.173

low average H/L values. Composition, comprising elements of both grain size and lithology (of landslide debris as well as of the substrate), forms another probable influence on the observed log(volume) vs. H/L trends. The Kootenay mine dumps, for example, which formed from heaps of loose, fine-grained detritus, consistently exhibited lower H/L values for given volumes of debris than landslides formed from coarsely jointed bedrock, indicating that a decrease in grain size and initial inter-clast cohesion may cause an increase in the runout length of a landslide for a given volume and fall height. In addition, the similarity in the trends of the data on log(volume) vs. H/L plots for ice/rock landslides and those that traveled over icy substrates indicates that the nature of the material along the base of a moving landslide must have a pronounced influence on its runout behavior. These preliminary findings are investigated in more depth below. In the following section, the effects of confinement, lithology, and grain size, as well as a number of other possible relationships, are tested for their influence on the log(volume) vs. H/L trends of long-runout landslides.

3. Tests for Relationships

The preceding discussion considered several prominent groupings of data on log(volume) vs. H/L plots for long-runout landslides on Earth, Mars and the Moon. The following section, in contrast, tests for inconspicuous log(volume) vs. H/L relationships hidden in the data for 134 terrestrial subaerial non-volcanic landslides. The characteristics tested for their possible effects on log(volume) vs. H/L trends include: headscarp form, degree of confinement, morphology, lithology, grain size and travel during seismic activity.

Effects of Initiation Style

This section describes the effects of initiation style on the log(volume) vs. H/L relations of large terrestrial subaerial non-volcanic landslides. These landslides begin only as translational slips and as rockfalls, never as slumps, and all have detached debris aprons. The deposits considered here range in volume from 10^5 m^3, at the lower limit of long-runout behavior, up to the Saidmarreh landslide, at 2×10^{10} m^3. Of the 94 terrestrial subaerial non-volcanic landslides with known headscarp relations, 40 have translational headscarps with detached debris aprons (Type IIC), and 56 have rockfall-type headscarps with detached debris aprons (Type IIIC). The data for these

landslides is tabulated in Tables 4a and 4b, and their log(volume) vs. H/L relations are plotted in Figure 9.

Figure 9 allows comparison of the log(volume) vs. H/L relations for landslides initiated as rockfalls with those initiated as translational-slip landslides. This plot illustrates that the two sets of data display very similar overall trends on the log(volume) vs. H/L plot, but that the translational landslide data exhibits much less scatter than the rockfall data. Specifically, a Z-test value of 1.67 for the intersecting RMA lines indicates that the slopes of the lines are not significantly different at the 95% confidence level. In addition, the much lower r^2-correlation coefficient for the rockfall landslides (0.22) relative to that of the translational landslides (0.66) illustrates that the translational landslides exhibited much more consistent behavior during runout than the rockfall landslides. Perhaps the more highly variable headscarp geometries of the rockfall landslides gave these landslides an initial positive or negative energy bias relative to the translational landslides, which all began movement along uniform planar discontinuities with dip slopes of 20°-35°.

Effects of Confinement

Together with the volume and the fall height, the travel path exerts an extremely strong influence on the distance traveled by a landslide during emplacement (Heim, 1932). The degree of tortuosity of a large landslide's travel path is reflected in its qualitative confinement term in the large landslide database (Appendix A). The database contains four primary confinement terms: unconfined, partially confined, deflected and heavily confined, as well as two modifying terms, channeled and divided (Chapter II). Figures 10a-10c illustrate the influence of confinement on the log(volume) vs. H/L relations of large terrestrial subaerial non-volcanic landslides. The data for the diagrams are displayed in Tables 4a and 4b.

Figure 10a plots data for long-runout landslides according to confinement grade. As observed previously, heavily confined landslides generally exhibit high H/L values, and unconfined landslides exhibit low H/L values over a broad range in volumes. Although each dataset exhibits considerable scatter, leading to the crossing of RMA lines in the middle of the highest concentration of points, the plot nevertheless gives some interesting results. For instance, the slope of the RMA line through the data for deflected

Table 4a. Some Critical Statistics on Translational-Slip (Type IIC) Landslides

Name	Log(Vol) (m^3)	Type	H/L	Confinement
Bualtar 3	6.48	IICbab	0.54	unconfined(DI-110°)
Beaver Flats N.	6.62	IICd-a	0.32	partial
Brazeau Lake	6.65	IICdda	0.33	unconfined
Beaver Flats S.	6.68	IIC-ba	0.25	partial
Ennetbühl	6.70	IIC---	0.18	NA
Antelao	6.70	IICb--	0.32	unconfined
Jonas Creek N.	6.73	IICda-	0.27	partial
North Nahanni	6.85	IICdda	0.26	deflected-90°(CH)
Bualtar 2	6.85	IICbab	0.40	deflected-35°(CH)
Twin Sildes 2	7.00	IICdca	0.25	deflected-50°(CH)
Twin Slides 1	7.00	IICdca	0.21	deflected-45°(CH)
Bualtar 1	7.00	IICdaa	0.33	deflected-35°(CH)
Corbeyrier-Yvorne	7.00	IICdd-	0.24	unconfined(CH)
Jonas Creek S.	7.00	IIC-a-	0.37	unconfined
Pasayten	7.30	IICdda	0.22	deflected-40°(CH)
Damocles	7.30	IICdca	0.10	deflected-30°-30°-20°(CH)
Cadomin	7.40	IIC---	0.40	NA
North Arm	7.48	IICdda	0.23	deflected-35°,125°(CH,DI-190°)
Triple	7.54	IICa-a	0.17	deflected-35°-15°
Goldau	7.54	IICada	0.21	unconfined(CH)
Gros Ventre	7.58	IICdda	0.18	deflected-90°,90°(CH,DI-180°)
Mount Kitchener	7.59	IICdd-	0.20	partial
Stalk Lakes	7.60	IICb-b	0.23	unconfined
El Capitan	7.60	IIC---	0.19	unconfined(DI-20°)
Hope	7.67	IICddc,a	0.40	heavy
Nozzle	7.70	IICaca	0.15	deflected-90°(CH)
U-turn	7.81	IICdda	0.17	deflected-100°(CH)
Medicine Lake	7.93	IICcbd	0.26	unconfined
Obersee	8.08	IIC---	0.29	deflected-98°,74°(CH,DI)
Upper Kananaskis	8.11	IICaa-	0.25	unconfined
Kandertal	8.15	IIC---	0.20	deflected-35°(CH)
Vaiont	8.40	IICdda	0.34	heavy
Avalanche Lake	8.60	IICdda	0.17	deflected-20°,55°(CH,DI-30°)
Rockslide Pass	8.65	IICdca	0.14	deflected-90°-40°(CH)
Maligne Lake	8.70	IICdc-	0.17	partial
Deyen	8.78	II----	0.11	NA
Tin Mtn.	9.26	IICdda	0.11	partial
Engelberg	9.44	IIC---	0.22	heavy
Flims	10.1	IICdca	0.13	deflected-120°,60°(CH,DI-180°)
Saidmarreh	10.3	IICdda	0.08	partial

Table 4b. Some Critical Statistics on Rockfall (Type IIIC) Landslides

Name	Log(Vol) (m^3)	Type	H/L	Confinement
Altdorf-Spiringen	5.70	IIICd--	0.62	deflected-80°(CH)
Airolo	5.70	IIIC---	0.64	unconfined
Zarera	5.81	IIICb-a	0.44	unconfined(CH)
Monbiel	5.88	IIICb--	0.31	unconfined
Puget Peak	6.26	IIICbab	0.57	unconfined(CH)
Clavans	6.48	IIICbaa	0.58	unconfined
Plurs	6.54	IIICdda	0.48	unconfined
Altels	6.65	IIICbab	0.29	unconfined(CH)
Beatty	6.66	IIICc--	0.38	deflected-30°(CH)
Simplon	6.70	IIICaaa	0.44	partial
Aval. del Zarzo 2	6.70	IIICcbd	0.17	unconfined
Sioux	6.78	IIICda-	0.31	deflected-40°(DI-5°)
Elm	7.00	IIICdcc	0.29	deflected-50°(CH)
Antronapiana	7.08	IIICba-	0.43	deflected-80°(CH)
Angarakan	7.08	IIICdda	0.29	heavy
Huascaran 2	7.11	IIIC---	0.22	deflected-50°-70°(CH)
Disentis	7.18	IIICdda	0.38	heavy
Biasca	7.18	IIICdda	0.57	heavy
Steller	7.30	IIICba-	0.18	unconfined(DI-30°)
Corno di Dosde	7.30	IIIC---	0.45	deflected-70°(CH)
Loma de la Aspereza	7.32	IIICcbd	0.11	unconfined
Allen 4	7.36	IIICbab	0.17	unconfined(CH)
Rubble Creek	7.40	IIICbaa	0.15	deflected-20°-50°-60°(CH)
Fairweather	7.41	IIICaab	0.32	deflected-45°-60°-35°(CH)
Chaos Jumbles 3	7.41	IIICbac	0.15	deflected-50°(CH)
Schwan	7.43	IIICba-	0.25	unconfined
Madison	7.45	IIICdda	0.27	heavy
Voralpsee	7.48	IIIC---	0.27	deflected(CH)
Sherman	7.48	IIICaab	0.22	unconfined
Diablerets 2	7.48	IIICdcc	0.35	deflected-65°-50°(CH)
Frank	7.56	IIICaac	0.28	partial
Aval. del Zarzo 1	7.57	IIICbbd	0.14	unconfined
Chaos Jumbles 1	7.64	IIICbac	0.17	deflected-50°(CH)
Chaos Jumbles 2	7.70	IIICbac	0.19	deflected-50°(CH)
Mageik	7.73	IIICbca	0.12	unconfined(CH)
Loma Redonda	7.81	IIICbbd	0.10	unconfined(CH)
Huascaran 3	7.88	IIIC---	0.22	deflected-multiple(CH,DI-35°)
Scima di Saoseo	7.90	IIIC---	0.26	deflected-110°-75°(CH)
Carlson	8.00	IIICbab,d	0.17	unconfined(CH)
Poschiavo	8.18	IIICdda	0.34	heavy
Parpan	8.18	IIICdda	0.27	deflected-90°,90°(CH,DI-180°)
Huascaran 1	8.18	IIIC---	0.21	deflected-multiple(CH)
Bormio	8.26	IIICd--	0.32	deflected-75°,15°(CH,DI-90°)
Silver Reef	8.36	IIICbbd	0.13	unconfined(DI-20°)
Martinez Mtn.	8.38	IIICbdd,b	0.20	deflected-40°(CH)
Sawtooth 2	8.44	IIICdd-	0.43	unconfined
Gohna	8.46	IIICdda	0.50	heavy
Blackhawk	8.48	IIICbbd,a	0.13	unconfined(CH)

Table 4b, con't.

Name	Log(Vol) (m^3)	Type	H/L	Confinement
Sawtooth 1	8.57	IIIC---	0.25	unconfined
Khait	8.60	IIICa-a	0.17	deflected-90°(CH,DI-70°)
Glarnisch Gleiter	8.89	IIIC---	0.31	deflected(CH)
Glarnisch Guppen	8.90	IIIC---	0.36	deflected(CH)
Mayunmarca	9.00	IIICdab,c	0.23	deflected-90°,90°(CH,DI-180°)
Usoy	9.30	IIICdda	0.24	heavy

Figure 9. Comparison of log(volume) vs. H/L relations of terrestrial subaerial landslides having translational and rockfall-type headscarps.

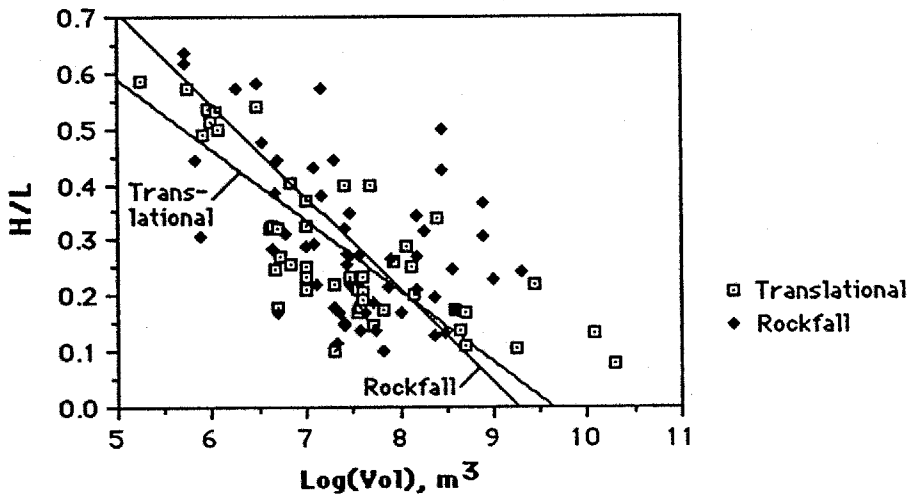

Translational: H/L = -0.126 Log V + 1.218, R^2 = 0.557, se_s = 0.012, se_i = 0.093

Rockfall: H/L = -0.165 Log V + 1.534, R^2 = 0.226, se_s = 0.020, se_i = 0.150

Figure 10a. Diagram illustrating the effects of confinement on the log(volume) vs. H/L relations of terrestrial non-volcanic subaerial landslides.

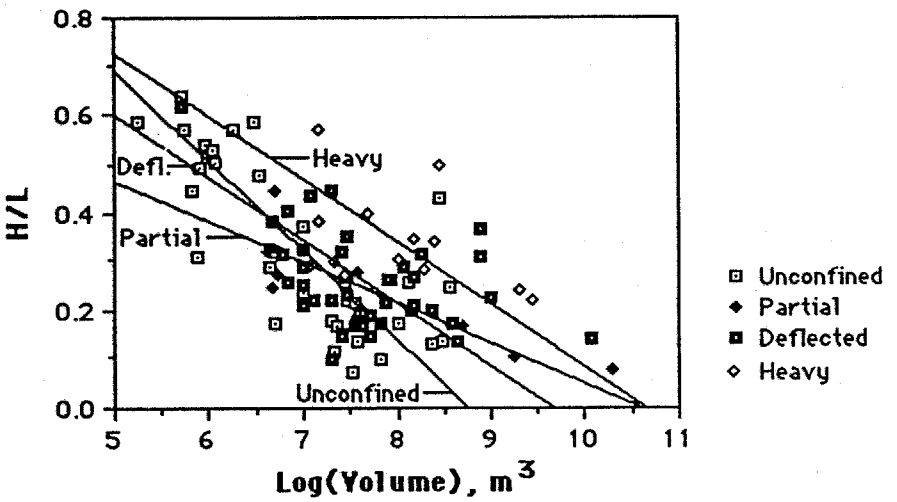

Unconfined: H/L = -0.184 Log V + 1.611, R^2 = 0.581, se_s = 0.020, se_i = 0.140

Partial: H/L = -0.083 Log V + 0.882, R^2 = 0.730, se_s = 0.014, se_i = 0.114

Deflected: H/L = -0.129 Log V + 1.249, R^2 = 0.220, se_s = 0.018, se_i = 0.138

Heavy: H/L = -0.128 Log V + 1.365, R^2 = 0.164, se_s = 0.032, se_i = 0.261

landslides does not differ from that of the heavily confined landslides at the 95% confidence level (Z = 0.03). In addition, the standard errors of the intercepts of the two groups of landslides overlap, indicating that deflected and heavily confined landslides behave in a very similar manner during runout.

Figure 10b investigates the effect of channeling on the log(volume) vs. H/L behavior of large landslides. All of the channeled and unchanneled deposits plotted in the diagram are unconfined, as unconfined landslides form the only confinement grade having significant numbers of both channeled and unchanneled deposits. The channeled unconfined landslides refer to those deposits originating within a drainage basin, which travel directly down a channel and out upon an alluvial surface without significant deflections. RMA regression lines through the data plotted in Figure 10b have slopes that do not vary significantly from one another, as well as standard errors for their intercepts that completely overlap. These observations indicate that channeling has very little influence on the log(volume) vs. H/L relations of large landslides.

In addition to channeling, large unconfined and deflected landslides sometimes also divide into two or more lobes during runout. The division of a large landslide into independently moving lobes occurs under different circumstances for unconfined and deflected landslides. Unconfined landslides often split into two lobes when travelling down an upwardly-convex surface, such as a volcanic cone or an alluvial fan. The landslides usually travel downslope as a coherent mass for most of their length, then split into broad lobes distally which diverge at about 20°. Deflected landslides, in contrast, commonly divide into lobes only upon impact with some obstruction. Beyond the point of impact, the divided lobes of these landslides may travel away from one another at angles in excess of 180°. Figure 10c plots log(volume) vs. H/L data for all terrestrial subaerial non-volcanic divided landslides. Comparison of the RMA best-fit lines through the divided data can be seen to coincide closely with the trend plotted for all terrestrial subaerial non-volcanic landslides. A Z-test value of 0.553 indicates that the slopes of the two lines actually coincide at the 95% confidence level. These observations indicate that the division of a landslide into two or more separately moving lobes during runout does not significantly influence the distance traveled by the toe of the landslide for a given landslide volume and fall height.

Figure 10b. Diagram illustrating the effects of channelized movement on the log(volume) vs. H/L relations of terrestrial non-volcanic subaerial landslides.

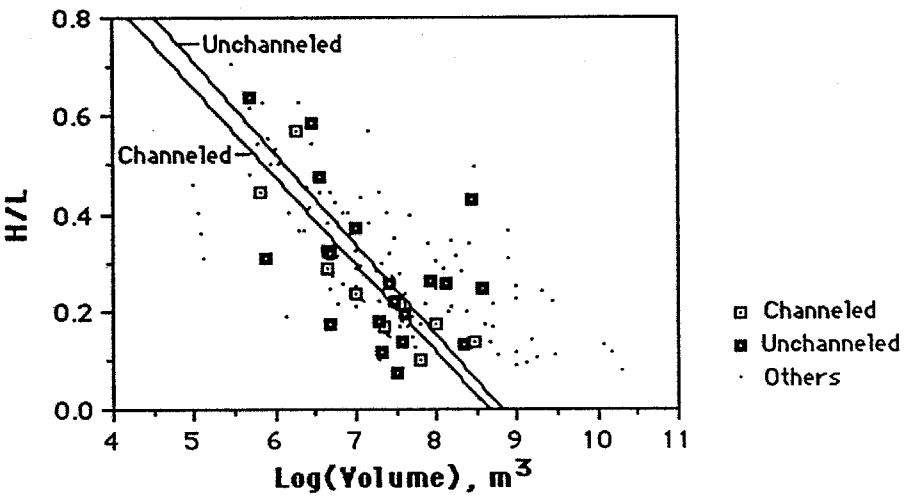

Channeled: H/L = -0.180 Log V + 1.556, R^2 = 0.743, se_s = 0.030, se_i = 0.221

Unchanneled: H/L = -0.188 Log V + 1.650, R^2 = 0.270, se_s = 0.036, se_i = 0.263

Figure 10c. Diagram illustrating the effects of division on the log(volume) vs. H/L relations of terrestrial non-volcanic subaerial landslides.

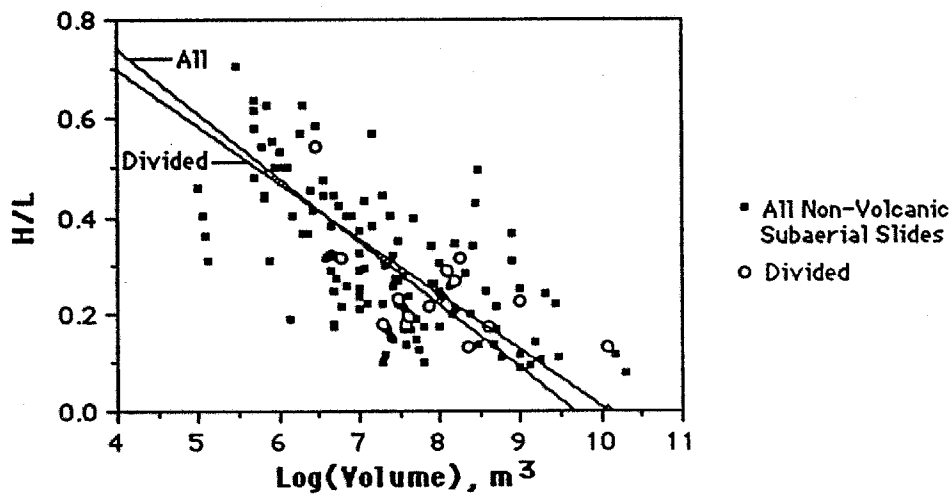

All Non-volcanic: H/L = -0.129 Log V + 1.250 , R^2 = 0.440 , se_s = 0.008 , se_i = 0.062

Divided: H/L = -0.115 Log V + 1.159 , R^2 = 0.366 , se_s = 0.024 , se_i = 0.191

Effects of Debris Apron Morphology

Observations of numerous photographs, images and maps of large martian, terrestrial and lunar landslides has allowed the development of a morphological classification for these deposits (Chapter II: Table 2, Figure 5). One outcome I have realized from this morphological classification is that the geometry of the depositional path followed by a large landslide at emplacement often has a large impact on the final morphology expressed by these deposits. For example, a correlation exists between channeling and lobate plan form, as well as between unconfined, unchanneled movement and a distally-raised profile shape. Because the confinement of the travel path can influence the log(volume) vs. H/L relations of large landslides (Figure 10a), the expectation arises that the morphology, which is at least somewhat controlled by the travel path, may also relate to variations in log(volume) vs. H/L relations. This section therefore considers the possibility of relationships between morphology (plan form, profile shape and surface texture) and log(volume) vs. H/L relations for terrestrial subaerial non-volcanic landslides.

Figure 11a illustrates the relationship between plan form and log(volume) vs. H/L relations for terrestrial subaerial landslides. The diagram includes data on three of the four debris apron plan forms: fan-shaped, lobate, irregular. A fourth plan form, the blunt shape, has too few terrestrial subaerial members to allow for useful comparisons. The log(volume) vs. H/L plot in Figure 11a illustrates that data from landslides having lobate and fan-shaped debris aprons generate similar RMA best-fit lines. A Z-test value of 0.118 indicates that the two slopes coincide at about the 85% level. Both RMA slopes vary markedly from the RMA trend of irregular landslides. For the most part these trends appear to relate to the differing confinement grades represented by the landslides forming each of the three groups of landslides. For example, 22 out of 28 of the lobate landslides are unconfined, while of the ten fan-shaped landslides, four are unconfined, two are partially confined and four are deflected. This mixture of confinement grades provides the fan-shaped and lobate landslides RMA best-fit trends close to the trend for unconfined landslides plotted in Figure 10a. In comparison, most of the landslides with irregular plan form forms were heavily confined or deflected during runout. Irregular landslides therefore appear to have inherited the high average H/L values and large scatter of deflected and heavily confined landslides (Figure 10a).

Figure 11a. Diagram illustrating the effects of plan form on the log(volume) vs. H/L relations of terrestrial non-volcanic subaerial landslides.

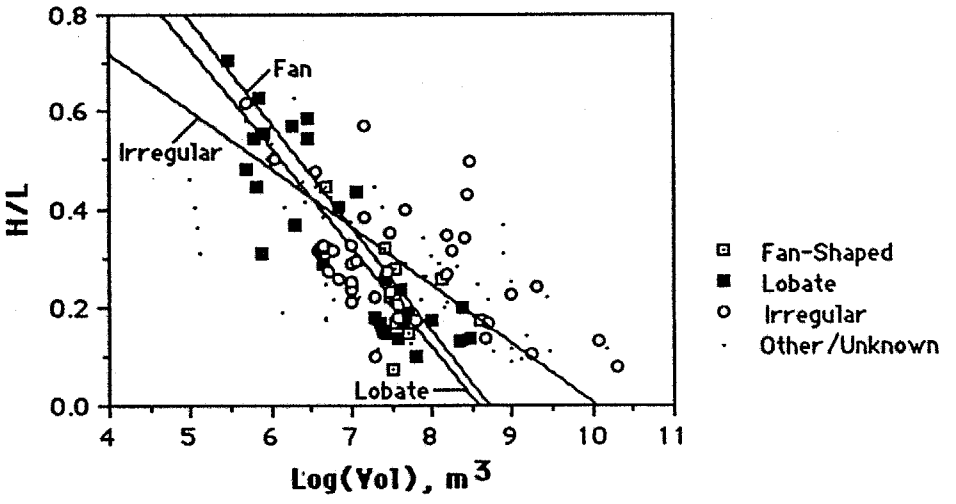

Fan-Shaped: H/L = -0.211 Log V + 1.836 , R^2 = 0.293 , se_s = 0.056 , se_i = 0.427

Lobate: H/L = -0.204 Log V + 1.746 , R^2 = 0.730 , se_s = 0.020 , se_i = 0.138

Irregular: H/L = -0.120 Log V + 1.210 , R^2 = 0.281 , se_s = 0.016 , se_i = 0.125

The relationship of profile shape to the log(volume) vs. H/L relations of terrestrial subaerial non-volcanic landslides is plotted in Figure 11b. The diagram includes data on the four debris apron profile shapes: distally-raised, tapered, uniform and irregular. Of the four profile shapes, uniform landslides, the most common of the four types, exhibit by far the most linear log(volume) vs. H/L relations. The uniform-thickness landslides also display the strongest trend towards decreasing H/L with increasing volume of any of the four groups. The distally-raised landslides mostly consist of unconfined, unchanneled deposits, characterized by the Blackhawk landslide of southern California (Figure 8b; Chapter IV). These deposits have consistently low H/L values and exhibit only a minor trend towards decreasing H/L with increasing volume. Landslides with tapered and irregular profile shapes also fail to show a strong tendency towards decreasing H/L with increasing volume. It is interesting to note that while all but one of the tapered landslides was deflected during emplacement and that the irregular landslides generally consist of deflected and heavily confined landslides, the log(volume) vs. H/L trends of these data do not come close to approximating the trends of deflected and heavily confined landslides shown in Figure 10a. Unlike the plan view shape, therefore, factors other than the degree of confinement must play a critical role in the development of the profile shape of a long-runout landslide.

The third element of morphology is surface texture. Long-runout landslides exhibit four common debris apron surface textures: hummocky, longitudinally ribbed, convex-downslope ridges/troughs and lateral levees. Two of the textures, the convex-downslope ridges/troughs and lateral levees patterns plot with such large degrees of scatter on log(volume) vs. H/L diagrams (r^2-correlation coefficients<0.1), that no sensible trend exists for them. In addition, the hummocky texture forms a catch-all category for landslides having no distinct surface texture. Figure 11c therefore plots the log(volume) vs. H/L trend of long-runout landslides having a longitudinally ribbed surface texture against data from all terrestrial subaerial non-volcanic landslides. A Z-test (Z = 1.52) for the two intersecting trends plotted in the diagram fails to demonstrate a significant difference between the trends. Taken together, these observations appear to indicate surface texture and log(volume) vs. H/L trends of large landslides are not related.

Figure 11b. Diagram illustrating the effects of profile shape on the log(volume) vs. H/L relations of terrestrial non-volcanic subaerial landslides.

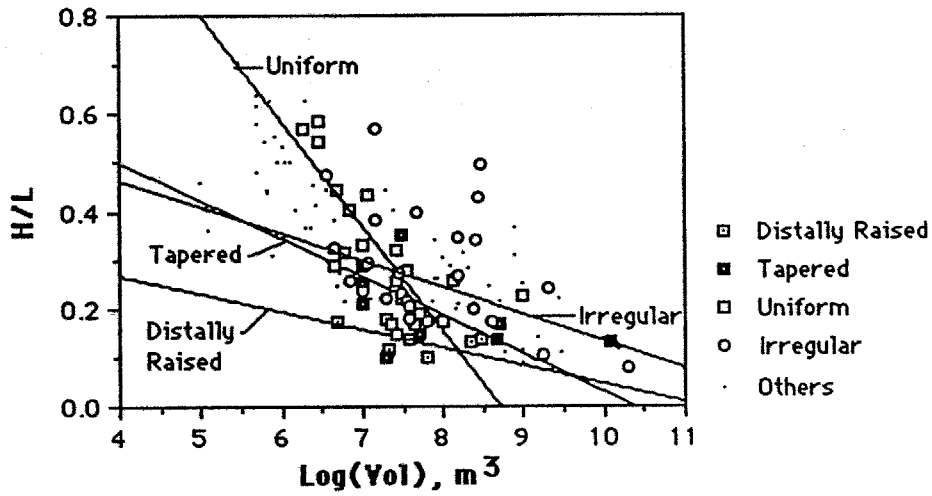

Dist Raised: H/L = -0.036 Log V + 0.408 , R^2 = 0.218 , se_s = 0.079 , se_i = 0.101
Tapered: H/L = -0.078 Log V + 0.813, R^2 = 0.247 , se_s = 0.023 , se_i = 0.178
Uniform: H/L = -0.214 Log V + 1.864 , R^2 = 0.513, se_s = 0.033 , se_i = 0.238
Irregular: H/L = -0.055 Log V + 0.685, R^2 = 0.164, se_s = 0.010 , se_i = 0.076

Figure 11c. Diagram illustrating the effect of longitudinal ribbing on the log(volume) vs. H/L relations of terrestrial non-volcanic subaerial landslides.

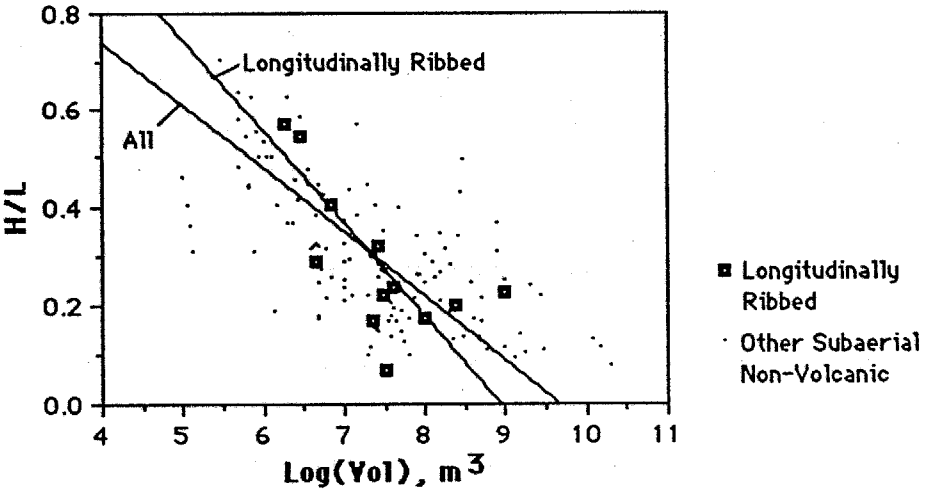

All Non-volcanic: H/L = -0.129 Log V + 1.250, R^2 = 0.440, se_s = 0.008, se_i = 0.062

Ribbed: H/L = -0.191 Log V + 1.700, R^2 = 0.473, se_s = 0.040, se_i = 0.298

Effects of Composition

The following section investigates the effects of composition, including aspects of both lithology and clast size, on the runout behavior of large landslides. Three different plots are used to investigate these effects. The first two diagrams respectively report the influence of lithology and grain size on the log(volume) vs. H/L relations of long-runout landslides. In the third plot, H/L values are plotted directly against the modal (most common) clast size surfacing large landslides, to directly investigate the effect of varying clast size on the effective coefficient of friction experienced by large landslides during runout.

Figure 12a displays the log(volume) vs. H/L relations of terrestrial subaerial non-volcanic landslides with known lithologies. The various lithologies composing these deposits (Appendix A) were divided into four categories related to the primary materials involved in each deposit: carbonate, granitic, metamorphic and sedimentary rock (Table 5). The "carbonate" group includes landslides composed primarily of limestone, dolomite, marl and other undivided carbonate rocks. The "granitic" class incorporates landslides composed of intrusive rocks more acidic than gabbro, such as granodiorite and true granite. A "metamorphic" lithology describes several rock types, broadly incorporating metavolcanic and metasedimentary rocks such as greenstone, slate and quartzite, while the "sedimentary" category encompasses sandstone and siltstone lithologies. The RMA trends of the data plotted in Figure 12a reveal that the best-fit lines through the sedimentary, metamorphic and granitic landslide data do not vary significantly from one another in slope nor in intercept value. These lithologies appear indistinguishable according to their log(volume) vs. H/L relations. The best-fit trend through the carbonate landslides varies markedly from the trends of the other lithologies. The RMA slope through the carbonate landslide data differs at the 95% confidence level with the slope through the metamorphic landslide data, but differs less significantly from the slopes for other lithologies. Much of the difference between the trends of the metamorphic and carbonate landslide datasets probably results from the fact that the average volume of the carbonate landslides is much higher than that of the metamorphic landslides. Thus, the trends through the data must largely reflect the fact that landslides with greater volumes have lower average H/L

Table 5. Terrestrial Landslide Lithologies and Modal Clast Sizes

Name	Log(Vol) (m^3)	H/L	Primary Lithology	Modal Clast Size (cm)
Monbiel	5.88	0.31	carbonate	
Bualtar 3	6.48	0.54	"	200
Beaver Flats N.	6.62	0.32	"	
Brazeau Lake	6.65	0.33	"	
Beaver Flats S.	6.68	0.25	"	
Ennetbühl	6.70	0.18	"	
Antelao	6.70	0.32	"	
North Nahanni	6.85	0.26	"	
Bualtar 2	6.85	0.40	"	200
Twin Sildes 2	7.00	0.25	"	
Twin Slides 1	7.00	0.21	"	
Bualtar 1	7.00	0.33	"	200
Damocles	7.30	0.10	"	
Madison	7.45	0.27	"	150
Voralpsee	7.48	0.27	"	
Diablerets 2	7.48	0.35	"	
North Arm	7.48	0.23	"	
Triple	7.54	0.17	"	
Goldau	7.54	0.21	"	
Frank	7.56	0.28	"	100
Mount Kitchener	7.59	0.20	"	
El Capitan	7.60	0.19	"	
Nozzle	7.70	0.15	"	
U-turn	7.81	0.17	"	
Medicine Lake	7.93	0.26	"	
Obersee	8.08	0.29	"	
Upper Kananaskis	8.11	0.25	"	
Kandertal	8.15	0.20	"	
Parpan	8.18	0.27	"	
Bormio	8.26	0.32	"	
Silver Reef	8.36	0.13	"	2.5
Vaiont	8.40	0.34	"	
Sawtooth 2	8.44	0.43	"	
Gohna	8.46	0.50	"	
Blackhawk	8.48	0.13	"	2.5
Sawtooth 1	8.57	0.25	"	8
Avalanche Lake	8.60	0.17	"	
Rockslide Pass	8.65	0.14	"	
Maligne Lake	8.70	0.17	"	
Glarnisch Gleiter	8.89	0.31	"	
Tin Mtn.	9.26	0.11	"	10
Engelberg	9.44	0.22	"	
Usoy	9.30	0.24	"	
Flims	10.1	0.13	"	
Saidmarreh	10.3	0.08	"	
Plurs	6.54	0.48	granitic	
Aval. del Zarzo 2	6.70	0.17	"	200

Table 5, con't.

Name	Log(Vol) (m^3)	H/L	Primary Lithology	Modal Clast Size (cm)
Angarakan	7.08	0.29	granitic	
Huascaran 2	7.11	0.22	"	
Loma de la Aspereza	7.32	0.11	"	200
Aval. del Zarzo 1	7.57	0.14	"	200
Loma Redonda	7.81	0.10	"	200
Huascaran 3	7.88	0.22	"	
Huascaran 1	8.18	0.21	"	
Martinez Mtn.	8.38	0.20	"	300
Airolo	5.70	0.64	metamorphic	
Zarera	5.81	0.44	"	
Puget Peak	6.26	0.57	"	90
Clavans	6.48	0.58	"	
Simplon	6.70	0.44	"	
Jonas Creek N.	6.73	0.27	"	
Jonas Creek S.	7.00	0.37	"	
Elm	7.00	0.29	"	
Antronapiana	7.08	0.43	"	
Disentis	7.18	0.38	"	
Biasca	7.18	0.57	"	
Madison	7.45	0.27	"	10
Sherman	7.48	0.22	"	30
Hope	7.67	0.40	"	60
Altdorf-Spiringen	5.70	0.62	sedimentary	
Beatty	6.66	0.38	"	
Corbeyrier-Yvorne	7.00	0.24	"	
Pasayten	7.30	0.22	"	
Cadomin	7.40	0.40	"	
Gros Ventre	7.58	0.18	"	
Stalk Lakes	7.60	0.23	"	
Mayunmarca	9.00	0.23	"	

Figure 12a. Illustration of the effects of generalized lithology on the log(volume) vs. H/L trends of terrestrial subaerial non-volcanic landslides.

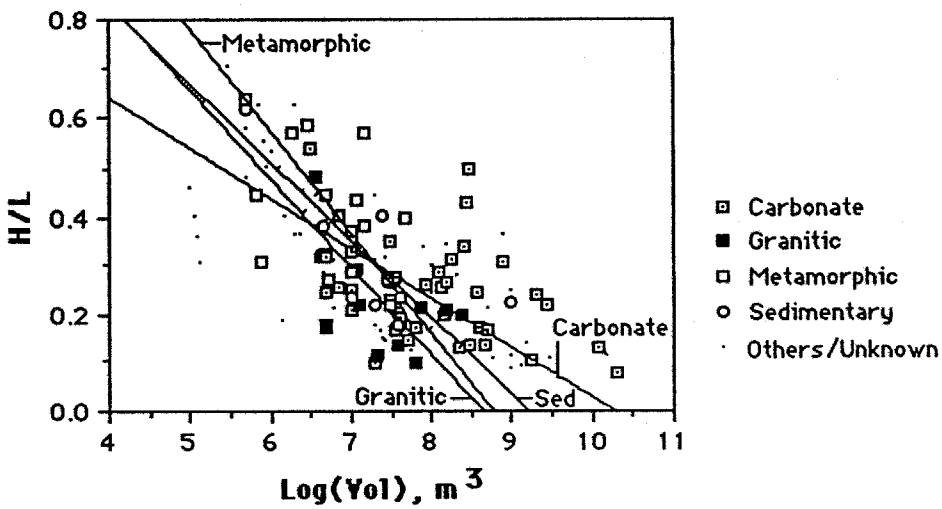

Carbonate: H/L = -0.102 Log V + 1.050 , R^2 = 0.154 , se_s = 0.014, se_i = 0.111
Granitic: H/L = -0.180 Log V + 1.556 , R^2 = 0.240, se_s = 0.050, se_i = 0.371
Metamorphic: H/L = -0.207 Log V + 1.814 , R^2 = 0.215, se_s = 0.047 , se_i = 0.322
Sedimentary: H/L = -0.158 Log V + 1.462 , R^2 = 0.542 , se_s = 0.038 , se_i = 0.278

values than those with smaller volumes. Apparently, carbonate massifs break off in bigger masses on average than those composed of metamorphic rock.

Figure 12b depicts the effect of estimated modal (most common) surficial clast size on the log(volume) vs. H/L relations of terrestrial subaerial landslides. The modal clast sizes reported were in some cases estimated by general field surveillance, but in other cases their sizes were estimated at various points by precise clast counts (Shreve, 1968a; Cruden and Hungr, 1986). Very few large dry landslides have been noted to exhibit large-scale variations in surficial clast size from one area to another, suggesting that the estimates of clast size determined at one or a few locations on a deposit should prove largely representative of the surface of a landslide as a whole (c.f., Shreve, 1968a). As shown later in this chapter, the geologic evidence suggests that the clasts situated on the surface of a large landslide deposit probably traveled on top of the slide surface during runout and did not migrate there as a result of dispersive grain pressure. The size of the clasts surfacing of a large landslide therefore seem to closely represent the state of coherency of the bedrock in the source slope and only minimally reflect the effects of comminution processes acting during runout.

The landslide data in the diagram are separated into three groups: 1) "small," with modal clast size less than ten centimeters; "medium," having modal clast sizes between ten and one hundred centimeters; and "large," with a modal clast size larger than one meter. The best-fit RMA trends through the data in Figure 12b indicate that landslides with medium and large modal clast sizes exhibit rather similar log(volume) vs. H/L behavior, while deposits with small clast sizes exhibit a much lower log(volume) vs. H/L slope over the same range of volume. This pattern relates in part to the fact that the largest landslides with known modal clast sizes have small grain sizes, whereas those surfaced by medium- and large-sized boulders occur with about the same frequency over an overlapping intermediate range of volume. This observation may indicate that larger landslides somehow generate smaller clasts during transport than smaller landslides. More likely this observation is a statistical problem resulting from the small number of available datapoints.

If volume is discounted and modal surficial clast size is plotted directly against H/L, several interesting trends appear between rock type, modal clast size and H/L values (Figure 12c). In the diagram, the terms "metamorphic," "carbonate" and "granitic" refer to the same rock types as in Figure 12a. Each

Figure 12b. Illustration of the effects of variations in modal (most common) surficial clast size on the log(volume) vs. H/L trends of terrestrial subaerial non-volcanic landslides.

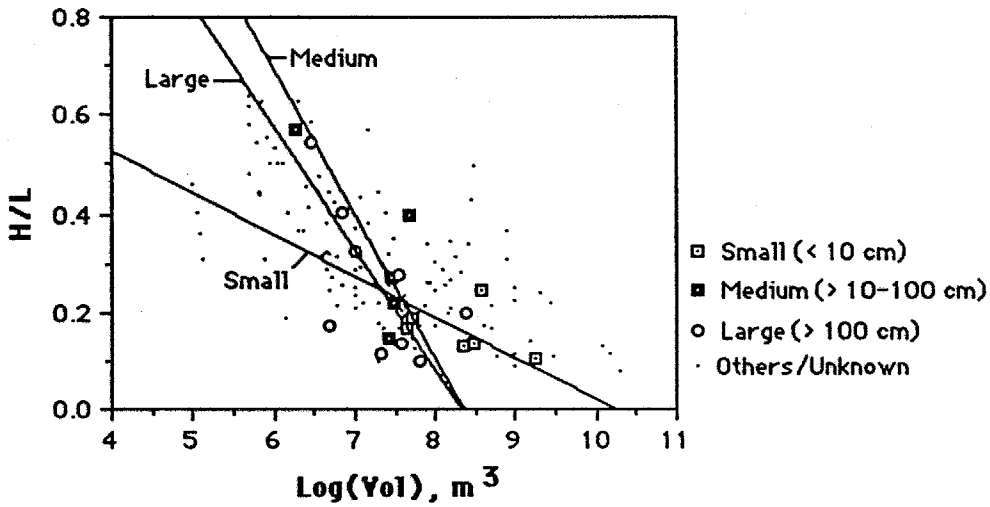

Small: H/L = -0.085 Log V + 0.870, R^2 = 0.149, se_c = 0.032, se_i = 0.267

Medium: H/L = -0.293 Log V + 2.447, R^2 = 0.542, se_s = 0.089, se_i = 0.645

Large: H/L = -0.247 Log V + 2.054, R^2 = 0.383, se_s = 0.065, se_i = 0.474

Figure 12c. Illustration of the effects of modal (most common) surficial clast size and generalized lithology on the H/L values of a number of terrestrial subaerial landslides.

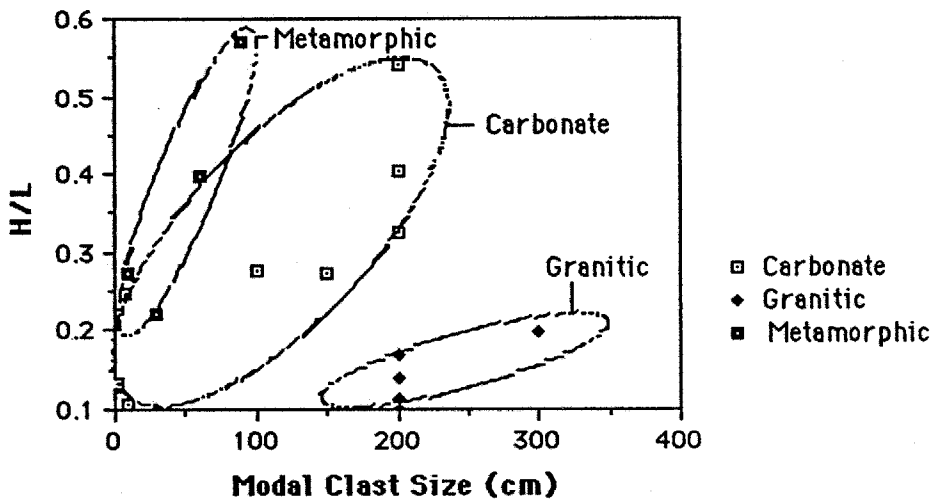

Carbonate: H/L = 0.00154 Log V + 0.122, R^2 = 0.748, se_s = 0.000258, se_i = 0.025

Granitic: H/L = 0.000894 Log V -0.0527, R^2 = 0.554, se_s = 0.000267, se_i = 0.060

Metamorphic: H/L = 0.00443 Log V + 0.155, R^2 = 0.852, se_s = 0.000852, se_i = 0.050

of the lithologies exhibits a trend of decreasing H/L with a decreasing modal (most commonly observed) surficial clast size. A lithology-related variation in landslide H/L trends also exists. For a given modal surface clast size, granitic landslides have the lowest H/L values, followed by carbonate landslides and then by landslides with metamorphic lithologies. The data plotted in Figure 12c come from landslides that traveled over a variety of different substrates, including bedrock, dry alluvium, and moist or wet alluvium.

The trends that appear in Figure 12c indicate that for a given rock type, the most common surficial clast size of a landslide relates strongly to its H/L value: the lower the modal clast size, the lower the H/L value, on average. Assuming that the modal clast size decrease causes the drop in H/L allows one to explain the role of lithology in influencing H/L values. A more easily fragmented rock type would cause the creation of smaller clast sizes in a landslide during runout, therefore diminishing its H/L value for a given slide volume. Thus, the durability of the rock comprising a large landslide might have a significant impact on its H/L. A landslide composed of readily comminuted rock would experience a lower H/L value than one consisting of less easily brecciated material. Unfortunately, it is rather difficult to assess the relative durabilities of the various rock types represented in Figure 12c in the interiors of moving landslides. Clasts may fragment due to crushing in the interior or, on the other hand, due to sudden stress release when an initially deeply buried fragment is quickly unloaded during runout. Factors influencing rock durability include: hardness (resistance to gouging), toughness (resistance to impact), resistance to plucking, tensile strength, compressive strength, shear strength, the number and spacing of discontinuities such as fractures and grain boundaries, and perhaps other factors (Mathewson, 1981; Carmichael, 1982). Interestingly, the modal clast size vs. H/L trends plotted in Figure 12c appear despite the fact that the landslides traveled across different substrate materials at emplacement. This observation is reconsidered in Chapter VI, where a comprehensive concept of landslide long runout is proposed.

Effects of Setting

Landslides occur in a variety of tectonic and climatic settings. Two such settings have been qualitatively connected with highly mobile long-runout landslides. One environmental condition proposed to decrease the H/L values

of large landslides is emplacement during active seismic groundshaking (Solonenko, 1972; McSaveney, 1978). Earthquakes certainly can trigger large landslides, but this theory suggests that seismic energy added to a landslide in its runout phase could significantly lower its fall height to runout length ratio. The other setting thought to have an effect on the H/L of large landslides is emplacement on ice and snow (Post, 1967). The log(volume) vs. H/L relations of these landslides are shown in Figures 8b and 8c.

Figure 13 illustrates the effects of emplacement during seismic shaking on the log(volume) vs. H/L relations of terrestrial subaerial landslides. Table 6 summarizes the data on large landslides known to have traveled during earthquakes or during underground explosions (Appendix A; Solonenko, 1972; Keefer, 1984; Evans, et al., 1987, Adushkin, personal communication, 1990). Landslides U.S.S.R. #1-#5 were all initiated and began their travel during seismic activity caused by the detonation of nuclear(?) explosives about 1 kilometer below the surface (Adushkin, personal communication, 1990). The landslides listed in the table are plotted together in Figure 13 with landslides known *not* to have been traveled in the presence of externally-generated seismic energy. The trends plotted in Figure 13 indicate that emplacement during seismic groundshaking appears to have little effect upon the H/L values of long-runout landslides as compared with those known not to have occurred during seismic events; the slopes of the intersecting trends do not differ with great significance. Seismic energy from earthquakes and underground explosions therefore does not seem to characteristically decrease landslide H/L values as proposed by such workers as Solonenko (1972) and McSaveney (1978) (Chapter V).

4. *Summary*

Large terrestrial subaerial landslides exhibit a distinct trend towards decreasing H/L values with increasing volume. Terrestrial volcanic and non-volcanic landslides exhibit rather similar behavior on log(volume) vs. H/L plots, in contradiction to earlier reports. Martian landslides, however, exhibit log(volume) vs. H/L trends that differ significantly from the terrestrial trends. The martian landslides do not runout as far on average for a given volume and fall height than do the terrestrial subaerial landslides. A plot of terrestrial subaerial non-volcanic landslides on a log(volume) vs. H/L diagram reveals several prominent groups of data that vary markedly in their runout

Table 6. Some Critical Statistics on Landslides Emplaced During Seismic Shaking from Large Earthquakes and Underground Explosions

Name	Volume ($\times 10^6$ m^3)	H/L	Earthquake or Explosion		
			Date	Location	Magnitude
USSR #5	0.1	0.46	?	USSR	NA
Vesuvius 1	0.18	0.59	1944	Italy	NA
Vesuvius 3	0.5	0.57	1944	Italy	NA
Vesuvius 4	0.8	0.49	1944	Italy	NA
Vesuvius 2	0.9	0.54	1944	Italy	NA
USSR #3	1.0	0.54	?	USSR	NA
Vesuvius 5	1.0	0.51	1944	Italy	NA
Vesuvius 6	1.1	0.53	1944	Italy	NA
Vesuvius 7	1.2	0.50	1944	Italy	NA
Puget Peak	1.8	0.57	27 Mar. 1964	Alaska, USA	9.2
USSR #4	2.0	0.63	?	USSR	NA
Beatty	4.5	0.38	18 Apr. 1906	California, USA	7.9
Sioux	6	0.31	27 Mar. 1964	Alaska, USA	9.2
North Nahanni	7	0.26	5 Oct. 1985	N.W.T., Canada	6.6
USSR #2	8	0.40	?	USSR	NA
Steller	20	0.18	27 Mar. 1964	Alaska, USA	9.2
Schwan	27	0.25	27 Mar. 1964	Alaska, USA	9.2
Madison	28	0.27	17 Aug. 1959	Montana, USA	7.1
Sherman	30	0.22	27 Mar. 1964	Alaska, USA	9.2
Huascaran 3	75	0.22	31 May 1970	Peru	7.9
USSR #1	80	0.34	?	USSR	NA
Khait	400	0.17	10 July 1949	Tadzhikistan, USSR	7.6
Usoy	2000	0.24	18 Feb. 1911	Tadzhikistan, USSR	~7

Figure 13. Comparison of the log(volume) vs. H/L trends of terrestrial subaerial landslides known to have travelled during earthquakes with trends for landslides known *not* to have been associated with seismic activity.

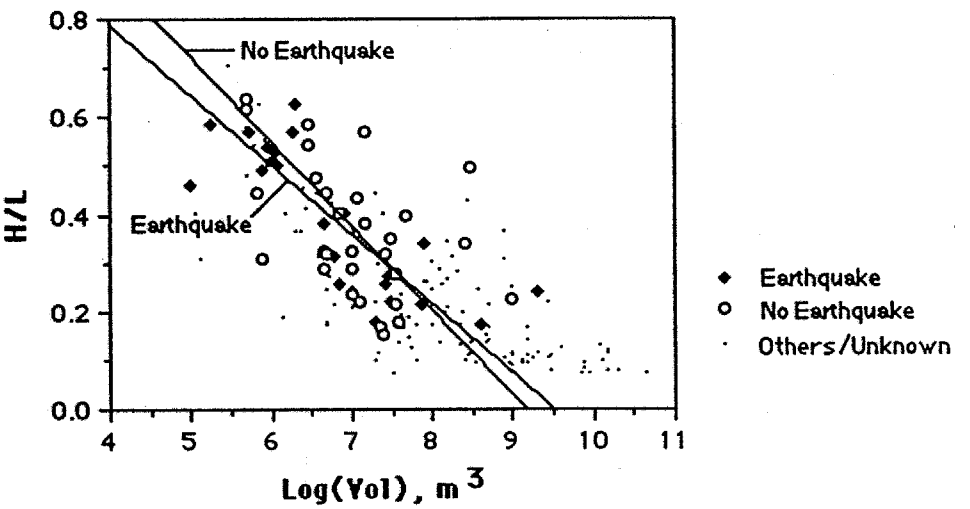

Earthquake: H/L = -0.142 Log V + 1.357 , R^2 = 0.660, se_s = 0.017, se_i = 0.118

No Earthquake: H/L = -0.175 Log V + 1.601 , R^2 = 0.220 , se_s = 0.028 , se_i = 0.200

behavior. Heavily confined landslides consistently have the highest H/L values for a given volume, whereas unconfined "Blackhawk-like" landslides and coal-mine tip landslides consistently exhibit the lowest observed H/L values. Landslides composed of ice/rock mixtures and those that traveled across ice and snow exhibited very similar log(volume) vs. H/L relations. This observation indicates that material located along the contact between a moving landslide and the substrate plays a crucial role in the runout behavior of long-runout landslides.

A number of variable features of long-runout landslides were also studied to determine which other factors might influence the log(volume) vs. H/L trends of large landslides. These factors include: initiation style, degree of confinement, debris apron morphology, composition and depositional environment.

The style of initiation, whether by a translational or rockfall mechanism, has a minor effect on the log(volume) vs. H/L trends of long-runout landslides. Comparison of the two groups of data indicates that, on average, landslides of similar volume exhibit about the same H/L regardless of the headscarp form. Datapoints for rockfall-type landslides, however, exhibit significantly greater scatter on the log(volume) vs. H/L plot than the translational deposits. This observation indicates that initiation by a rockfall mechanism typically may give a landslide an initial positive or negative energy bias relative to a translational mechanism, probably because of the relatively variable headscarp geometries of the rockfall landslides.

The degree of confinement has a more important influence on H/L values than the headscarp form. Observed H/L values generally increase with the degree of confinement for a given landslide volume. Heavily confined and deflected landslides yield essentially the same trends on log(volume) vs. H/L plots. Partially confined landslides exhibit a log(volume) vs. H/L trend in which H/L values do not decrease dramatically with increasing volume. Channeling apparently does not have much effect on H/L values, nor does division, despite the fact that division seemingly should decrease the volume and thus increase H/L values of individual lobes of divided debris streams.

Landslide debris apron morphology, which consists of different combinations of plan forms, profile shapes and surficial textures, generally appears to exhibit little correlation with landslide log(volume) vs. H/L trends. Landslides with irregular plan forms and profile shapes had the greatest

average H/L values for the range of landslide volumes because these deposits included all the heavily confined landslides. Unconfined landslides with a distally raised profile shape all have extremely low H/L values and exhibit little trend towards decreasing H/L with volume, perhaps suggesting a specialized form of long-runout landslide. The composition of long-runout landslides has an important influence on the H/L values achieved by these mass movements, although in some cases log(volume) vs. H/L trends do not give a good demonstration of this fact. While little demonstrable correlation exists between lithology or modal clast size and H/L values when landslide data are plotted on log(volume) vs. H/L diagrams, when modal surface grain size is plotted directly against H/L, two clear trends emerge. First, the H/L values of large landslides decrease with modal surface grain size. Also, for a given modal surface grain size, H/L varies with changes in composition. Both observations, only made possible with the complicating factor of volume removed, suggest that small grain size, in addition to volume, may play an important role in the runout length of large landslides.

The effects of emplacement during seismic groundshaking form the remaining category of investigated influences on the log(volume) vs. H/L relations of long-runout landslides. Landslides known to have traveled during natural and artificially-triggered seismic events exhibited log(volume) vs. H/L relations equivalent to the trend for landslides known to have traveled in the absence of such activity. Apparently, external seismic energy has little influence on the runout distance traveled by a large landslide.

C. Systematics of Landslide Travel and Degradation

1. *Introduction*

This portion of Chapter III presents the systematics of the geological and eyewitness observations of large landslides. Together with the comparative planetology data presented in Chapter IV, these data provide the means for testing the various published theories of landslide runout discussed in Chapter V, and for substantiating the long-runout concept I develop in Chapter VI. The systematized observations made in this section come from a variety of sources: from literature descriptions of terrestrial, lunar and martian landslides, from my studies of martian landslides from Viking Orbiter images

and from field observations I made on large landslide deposits in the western United States in the course of this thesis research.

In this section I have separated the process of rapid large-scale landsliding into four gradational intervals. In chronological order, these four phases include: 1) slope preparation and slide initiation; 2) runout of the landslide as a mobile debris stream; 3) stopping; and 4) post-depositional degradation of the landslide deposit. Division of the large landslide process into these four intervals facilitates discussion of the topic and follows upon the structure of previous landslide research. The first area is mainly concerned with the problem of slope stability; how large masses of rock become unstable and begin to move as a cohesive unit. The second interval considers the special evolution of long-runout landslides as high-velocity debris streams that exhibit low, volume-dependent apparent coefficients of friction. The stopping phase is distinguished from the runout/travel phase because the geological relations preserved on and within large landslides primarily reflect the last few moments of a landslide's evolution. The nature of large landslides while moving, in contrast, has to be surmised from their final condition and from any available eyewitness accounts of their movement. The thorough description of stopping-phase phenomena has particular importance to the evaluation of certain published theories of landslide runout (Chapter V). The post-depositional phase considers those geological processes that act to modify landslides after deposition. Especially important are those processes that strongly modify the initial geometry, morphology or internal structures of large landslides. Each of the four discussed intervals is subdivided into a group of observations important to that phase in the development of large landslides. These observations include such details as the geology of landslide source regions, the sedimentology of landslide deposits, eyewitness accounts and specific effects of the environment of deposition. The information presented below occurs in abbreviated form in Appendix A.

2. *Slope Preparation and Slide Initiation*

Slope preparation forms the first stage in the chronology of a large landslide. Because slope preparation grades into and critically relates to the initiation of movement of a landslide, the two phases are described together here. By comparison, although slide initiation also grades into the runout phase of a large landslide, the mode of initiation generally exerts only minor

control on phenomena occurring in the runout phase. The following examination of slope preparation and slide initiation is divided into three major sections: slidemass characteristics, initiation mechanisms, and eyewitness accounts. Important slidemass characteristics include: the relationship between the volume of a large landslide and its headscarp form, a discussion of the monolithologic nature of most large terrestrial landslides, and a description of the geological structures critical to isolating the large, unstable bedrock masses that ultimately form large landslides. The initiation mechanisms important for large landslides include those factors that increase the shearing stresses on rock masses or those that reduce their shearing resistance to movement. Finally, eyewitness accounts of landslide initiation, which document the gradation from slope preparation to rapid slide movement, complete the discussion of this initial phase.

Slidemass Characteristics

Volume/Headscarp Form Relationship

Landslides on Earth have three common headscarp forms. They may initiate movement as slumps, as translational slides and as rockfalls. All three types occur commonly in small landslide events ($<10^5$-10^6) m^3 in soils and other unconsolidated materials. The large landslides in which long-runout is commonly observed, however, typically originate from well-indurated bedrock outcrops. Slope failures in these materials exhibit different characteristics than those in unconsolidated materials. A primary difference is that slumps are rather rare in bedrock over the volume range from 10^5 to 10^9 m^3, but they become the dominant form of slope failure in giant landslides having volumes in excess of 10^9 m^3. This basic relationship occurs for all large landslides, on Earth, Mars and the Moon. Translational and rockfall-type headscarps characterize landslides over the volume range from 10^5 to 10^9 m^3, while larger landslides, such as those in Valles Marineris and off the Hawaiian Ridge, commonly have slump-type headscarps (Figure 14). Most of the data in Figure 14 originate from terrestrial landslide occurrences. This is significant because the only known large ($>10^6$ m^3) translational landslides occur in terrestrial environments; none have been found on Mars or the Moon. Translational landslides begin their movement along valley-dipping bedding or foliation planes. The absence of large translational landslides on the Moon and Mars relates to the lack of tilted sedimentary or metamorphic

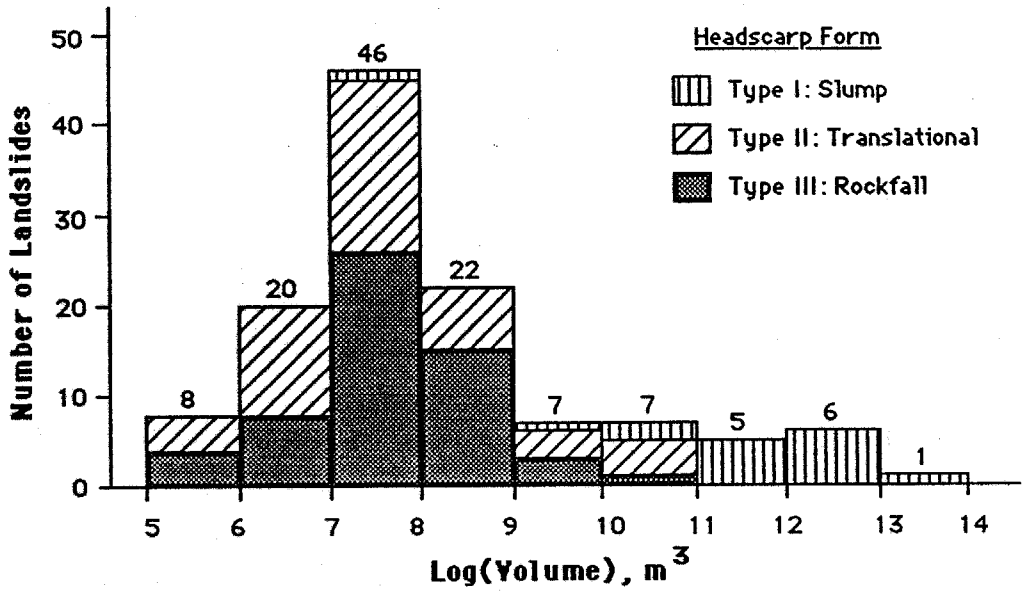

Figure 14. Histogram showing relative numbers of landslides having slump, translational and rockfall-type headscarp forms as a function of volume. The plotted values include data from terrestrial subaerial, terrestrial subaqueous, martian and lunar landslide occurrences.

bedrock outcrops on these planets. In spite of the absence of large translational landslides on Mars and the Moon, a similar trend exists between landslide volume and headscarp form on the two bodies; large landslides over the volume range from 10^5 to 10^9 m^3 have rockfall-type headscarps, while those larger than 10^9 m^3 usually have slump-type headscarps.

The shape of a landslide's failure surface reflects the rock strength and geological relations of the failed slope. Slumps occur where the strength of the solid rock nearly equals the strength along discontinuities in the rock mass. The failure surface of a slump is often uncontrolled, although some rotational slip surfaces may be controlled by the local geology and the mechanical properties of the geologic units. Failure of the slope occurs along a circular or spoon-shaped surface because the maximum shear stress develops along such a surface (Mathewson, 1981). Also, because slumps remove support from the overlying slope, they can promote a retrogressive series of failures of the slope incised by the initial slope failure. Translational and rockfall landslides, in contrast, have an initial solid rock strength that commonly exceeds the shear strength along discontinuities in the rock mass (Mathewson, 1981). Thus, failure takes place along the weaker structural discontinuities in the rock mass; planar discontinuities lead to translational headscarps, whereas rockfalls occur in bedrock having dual or multiple sets of major discontinuities.

The preceding discussion permits an analysis of the observed relationship between landslide volume and headscarp form illustrated in Figure 14. The 10^{10}-10^{11} m^3 upper volume limit for landslides having rockfall- and translational-type headscarps apparently relates to the strength of downhill-oriented discontinuities in a rock mass. The upper volume limit suggests an ultimate strength for the rock discontinuities; rockfalls and translational-slip landslides do not occur in volumes greater than ~10^{10} m^3 because the slopes fail in smaller masses first, precluding the development of such high-volume events.

These observations can be extended to explain why slumps always form the largest solar system landslides, but only rarely occur in the 10^5-10^9 m^3 volume range. Where downhill-oriented structures are lacking in a bedrock outcrop, the erosion of elevated bedrock regions is significantly constrained. Bedrock slope failures can then only occur by way of slumps. These can occur in two ways. Where vigorous erosion or fault-related tectonic uplift of a slope occurs,

slopes can become severely oversteepened (steepened beyond the angle of repose for loose, granular material, >30°). Under these conditions, the driving moment for failure can outweigh the resisting moment, even in homogeneous bedrock (Terzaghi, 1950). Such circumstances appear to have occurred in the single large bedrock slump reported in the 10^5-10^9 m^3 volume range in Figure 14. The 50 x 10^6 m^3 Sale Mountain loess slump (Appendix A) took place where the slope, an exposed normal fault plane, stood at an angle of 60° (Gongxian and Bangdong, 1984). Slumping could occur on this slope because of the vigorous fault-related uplift of the cliff and because of the relatively low shear strength of the loess bedrock, approximately two orders of magnitude less than that of common bedrock, such as limestone (Heard, 1960; Gongxian and Bangdong, 1984).

Few environments exhibit such combinations of vigorous uplift and weak, but homogeneous, bedrock. Most terrestrial and martian bedrock slopes lie at or below the angle of repose for granular material (Lucchitta, 1978a), precluding failure by dramatic oversteepening as indicated for the Sale Mountain landslide. In homogeneous bedrock that has not experienced oversteepening, slump failure of such slopes can only occur in the presence of strong seismic activity (Terzaghi, 1950) or when a potential slip surface intersects a plane of weakness in the slope (Reiche, 1937; Varnes, 1958). Thus, the giant slumps in Valles Marineris and from the Hawaiian Ridge volcanoes must have formed because of one or the other of these factors. The fact that the bedrock slumps from the Hawaiian Islands only occur in huge pieces, however, indicates to me that giant-scale planes of weakness must be responsible for their initiation, not earthquake activity. If earthquake activity was responsible, I believe that a whole family of slumps should affect the islands, not just giant ones. Thus, the Hawaiian slumps apparently only occur when a potential slip surface can intersect a major plane of weakness within an island, causing the slumps to form only at very large scales. Numerous such tectonic-scale discontinuities exist in the Hawaiian shield volcanoes, including major rift zones and the volcanic pile-oceanic sediment boundary at the bases of the volcanoes. This interpretation is supported by observations by Lipman et al. (1988) and Moore et al. (1989), who state that the crowns of many of the giant slumps from the Hawaiian Islands corresponded to major island rift zones. Also, Eissler and Kanamori (1987) and Delaney, et al. (1990) suggest that the initial motion of the large slump which caused the 1975

Kalapana earthquake was centered at a depth of about 9-10 km below sea level, along the volcanic pile-oceanic sediment interface. These observations suggest that the Valles Marineris landslides probably occurred because of the presence of major discontinuities in the walls of Valles Marineris, a possibility further investigated in Chapter IV.

Thus, where valley-dipping bedrock discontinuities exist, mass movements in highland regions will occur by means of rockfalls and translational landslides having volumes up to $\sim 10^{10}$ m^3. Where such discontinuities do not exist, landslides will have a slump form. Most slopes will not fail as slumps because of oversteepening, however, because slopes are usually too shallow and bedrock has too much strength. However, slumps can form if a potential slip surface can intersect a major, tectonic-scale bedrock discontinuity.

Monolithology

A large percentage of long-runout landslides are characterized by a single dominant rock type. This trait characterizes the majority of terrestrial subaerial landslides, excluding most volcanic landslides (Table 7). Volcanic landslides instead commonly incorporate a variety of materials, including shallow intrusive bodies, lava flows, ash, blocks, etc., having a variety of mechanical properties. Only those volcanic landslides originating from individual volcanic domes of comparatively homogeneous composition are considered here. As for extraterrestrial landslides, the one lunar landslide with a known lithology, the Apollo 17 deposit, consists of regolith derived from the surficial materials of an adjacent mountainside. In a sense this landslide is monolithologic, consisting entirely of regolith, but the material itself is quite heterogeneous on a small scale. No lithologic information exists for any martian landslides.

Table 7 lists the terrestrial subaerial landslides known to exhibit a single dominant lithology, and the rock type composing the deposit (Appendix A). Of terrestrial subaerial landslides with known lithologies, the majority (56%) are monolithologic. The preponderance of single-lithology terrestrial subaerial landslides was recognized some time ago by workers in Tertiary sedimentary sequences in the western United States. These deposits were commonly termed "monolithologic breccias" (Sharp, 1976) prior to their widespread recognition as deposits of ancient long-runout landslides.

Table 7. Monolithologic Terrestrial Long-Runout Landslides and Their Rock Types

Name	Lithology	Environment
Adair Park mb*	granite	arid
Altels	ice	glacial
Avalanche Lake	carbonate	glacial
Avalancha del Zarzo 1	granite	arid
Avalancha del Zarzo 2	granite	arid
Avawatz Mtns. mb	metavolcanic rock	arid
Bormio	dolomite	glacial
Brazeau Lake	dolostone	glacial
Carlson	basalt	periglacial
Chaos Jumbles 1	dacite	volcanic
Chaos Jumbles 2	dacite	volcanic
Chaos Jumbles 3	dacite	volcanic
Damocles	carbonate	glacial
Engelberg	limestone	glacial
Flims	limestone	glacial
Frank	limestone	glacial
Glärnisch-Gleiter	limestone	glacial
Kandertal	limestone	glacial
Loma de la Aspereza	granite	arid
Loma Redonda	granite	arid
Martinez Mtn.	granite gneiss	arid
North Arm	carbonate	glacial
Nozzle	carbonate	glacial
Panum	rhyolite	volcanic
Pasayten	arkose	glacial
Rubble Creek	dacite	glacial
Sawtooth 1	limestone	glacial
Sawtooth 2	limestone	glacial
Triple	carbonate	glacial
Twin Slides	carbonate	glacial
U-Turn	carbonate	glacial

* : mb = megabreccia deposit, interbedded in sedimentary strata.

The data presented in Table 7 demonstrate that only a few bedrock lithologies yield large monolithologic landslides. By far the greatest number of monolithologic landslides consist of carbonate rocks, followed by much smaller groups of landslides composed of granite, dacite and other rock types. The predominance of carbonate rocks in monolithologic long-runout landslides has several probable causes. For example, all of these deposits lie in glacially-carved terrain in the Rocky Mountains and the Alps. These landslides are all of late Pleistocene to Holocene age and all date from episodes of glacial retreat, either interstadial or interglacial periods, including the Holocene (Appendix A). One possible cause for this correlation is that carbonate strata might have greater susceptibility to glacial erosion than other rock types, leading to greater unsupported topographic relief following the recession of glaciers, and thus to more large landslides. Another possible cause, mentioned by Cruden (1976), is the ability of cold water to solvate calcium carbonate more efficiently than warm water. The action of cold subsurface waters during glacial regimes on discontinuities in carbonate rock masses might also have helped promote the observed concentration of carbonate landslides in formerly glaciated regions. In addition to these observations it is noteworthy that most large landslides with mixed lithologies also consist in part of carbonate rocks. These deposits occur in both currently arid regions as well as in formerly glaciated locations. That large carbonate landslides are not limited to formerly glaciated regions suggests that carbonate rocks probably contain, on average, more widely spaced major rock discontinuities than other rock types. This property would promote carbonate uplands to erode by way of rare major mass movements more frequently than other rock types. The carbonate bedrock discontinuities in both glacial and arid environments could be exacerbated by special ice age conditions. Several of the glacial-climate factors are mentioned above. In addition, many currently arid environments experienced pluvial conditions during the ice ages, which might have helped promote many of the largest and most familiar late Pleistocene long-runout landslides in carbonate terrains, such as the Blackhawk, Silver Reef (Stout, 1977), and Saidmarreh landslides (Watson and Wright, 1969). Thus, in regions of high topographic relief underlain by great sequences of carbonate rock where the topography is controlled by the erosional properties of the carbonate rock alone, much erosion might be expected to occur by way of large monolithologic carbonate landslides.

The second most common monolithologic landslides have granitic lithologies. Interestingly, all six granitic landslides listed in Table 7 took place in arid environments where rapid granular decomposition of the granites should have dominated their weathering patterns, leading to slow continuous erosion rather than to catastrophic denudation by large landslides. Each of these landslides, however, occurred from rapidly rising faulted mountain fronts (Bock, 1977; Fauque and Strecker, 1988; Yarnold and Lombard, 1989). The steep topography built by the rapid uplift along these faults apparently favored the triggering of large landslides. In these cases monolithology resulted from the fact that the uplifted granitic batholiths that shed the landslides have large areal dimensions. Basically, the tectonic environment set up the conditions for the development of large landslides and the rocks involved just happened to have a single lithology. This leads to the conclusion that many large monolithologic landslides occur because a single rock type outcrops over a large, tectonically active area.

The final common group of monolithologic landslides is those composed of dacite. Three of these occur in the Chaos Crags region of Lassen National Volcanic Park, northern California. Each was shed from a different phase in the growth of the same dacite volcanic dome (Eppler, et al., 1987). The landslides from the dome shared its relatively uniform dacite lithology. The other landslide with a dacite lithology, the Rubble Creek deposit, like many of the carbonate landslides, resulted from glacial activity. Near the end of the Wisconsin glacial advance, a dacite lava flow in British Columbia, Canada, pooled against the side of a valley glacier. When the ice receded, it left behind a wall of dacite standing at an angle near 60°. The rock mass later became sufficiently weathered and jointed to fail in a large landslide (Moore and Mathews, 1977).

The data outlined above, as well as from other landslides listed in Table 7, indicate that large monolithologic landslides form in three principle environments: 1) in regions widely underlain by a single lithology that has undergone severe terrain oversteepening due to glacial erosion; 2) in areas subject to strong tectonic uplift that happen to be widely underlain by a single rock type and 3) where volcanic activity constructs gravitationally unstable jointed rock masses.

Critical Structures

Most of the large landslides described in Appendix A began their movement along major bedrock discontinuities. Some of the giant martian slump-type landslides lack obvious structural controls for their headscarps, but, for the most part, fractures and joints, primary surfaces and faults control the collective detachment of large rock masses at the initiation of movement. In order to be important to the movement of large rock landslides, fractures must be macroscopic and of considerable areal extent (i.e., meters or tens of meters in length). Tensional fractures developing along the crown of a potential headscarp must open centimeters or tens of centimeters before failure becomes imminent (Hadley, 1978; Keefer, personal communication, 1991).

Fractured rock includes rock shattered by impact events, volcanic explosions and shearing in fault zones. Joints in a rock mass refer to those fractures along which no observable relative motion has occurred. Three primary types of joints exist: "shrinkage joints," caused by tensional forces set up in a rock body as a result of cooling (e.g., columnar joints in basalt) or desiccation; "sheet joints," which develop more or less parallel to the ground surface as a result of unloading of a rock mass when the cover is eroded away; and "tectonic joints," which arise as a direct result of folding or thrusting in rocks. Three sets of tectonic joints may be recognized: a strike set, parallel to the fold axes; a dip set, perpendicular to the strike set; and a conjugate set of oblique joints (Whitten and Brooks, 1983). In general, joints intersect primary surfaces, which include such features as bedding planes, cleavage and schistosity. The following section investigates the correlation between large landslides and large-scale geologic structures such as faults, folds and impact craters important to developing the bedrock discontinuities that control the detachment of large landslide masses. On Earth, inclined bedding planes, fold axes, inclined foliation planes and slope-intersecting faults (especially thrust faults with carbonate hanging walls) form the most important large-scale geologic structures, while on Mars, impact craters, graben-bounding faults, wrinkle ridges, dikes(?) and sills(?) form the structures most important to large landslide initiation.

A number of large-scale geological structures appear important to the detachment of large landslide masses on Earth. In order of importance, these structures include: sloping bedding planes, variously oriented faults or fault

zones, sloping foliation planes, and fold axes. Downslope-oriented bedding planes form by far the most common geological structures associated with large terrestrial landslides. The bedding planes include both the normal discontinuities in sedimentary strata as well as the sloping layers of ash and lava composing large stratovolcanoes. In many cases bedding planes form preferred sites of decoupling of a rock mass because of special conditions along the plane, such as elevated pore pressure (see below) or the presence of a thin but areally widespread weak stratum. Examples of weak materials in which bedding plane failures initiated include clay, marl, silt and shale. Water moving downhill through these zones may have additionally reduced the shear strength of these already weak materials.

The surface trace of fault planes in regions of steep topography create the second most common major structure associated with large landslides. Most large landslides associated with faults are initiated on the hanging walls of thrust or reverse-faulted mountain blocks. A particularly unstable situation develops when carbonate rocks form the hanging block of a thrust fault (Figure 15). The resistant overthrust carbonate block can become undermined when weak subjacent cataclastic rocks along the fault plane weather out preferentially. Two such locations are known, at Sawtooth Ridge, Montana (Mudge, 1965) and at Blackhawk Mountain, California (Shreve, 1968a). Both locations have been the sites of repeated large rockfall-type landslides due to this chronically unstable geological situation. An additional factor in both sites is the fact that the plane of the thrust fault rolls over just prior to daylighting. At Sawtooth Ridge, this antiformal shape was probably responsible for opening wide tensional joints along the crest of the carbonate massif, promoting the development of solution cavities and caves in the body of the carbonate rock and perhaps along the thrust plane (Mudge, 1965).

Other unstable geometries result when fault planes intersect slopes at high angles. In several such situations, such as for the North Nahanni landslide (Evans, et al., 1987) and for several of the large Hawaiian Ridge landslides (Moore, et al., 1989), a fault dipping in the same direction but more steeply than the overlying slope formed the upper bound of the headscarps of these slope failures where the faults intersected the ground surface. Material fell away below the trace of the fault on the slope, as no cohesion existed between rocks on opposite sides of the fault trace. The giant Usoy landslide in Tadzhikistan, U.S.S.R., also fell away below the intersection of a steeply dipping

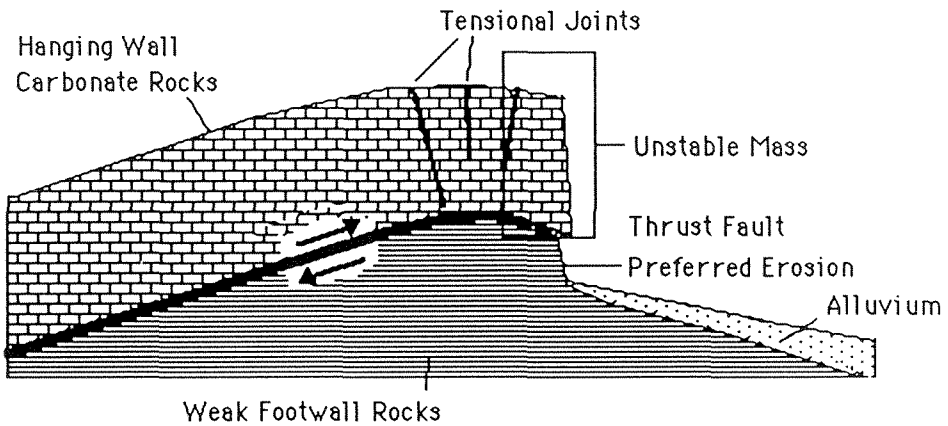

Figure 15. Generalized cross-section of unstable slope development such as occurred at Sawtooth Ridge, Montana and at Blackhawk Mountain, California. Resistant rocks with carbonate lithologies thrust over weaker rocks result in overhang and eventual massive failure of headwall rocks.

fault trace and a canyon wall. The Usoy slide, the largest known terrestrial subaerial rockfall-type landslide and the largest historical landslide on dry land exhibited the additional risk factor of upper-plate thrust-faulted carbonate rocks (Gregorian, et al., 1983; Figure 16). These structures combined to destabilize a huge slope area, which collapsed in a magnitude ~7 earthquake on 18 February 1911 (Solonenko, 1972; Table 6).

Two other structures have been found to promote large landslides on Earth. Downslope-oriented foliation planes controlled the detachment of three large landslides, at Martinez Mountain, California (Bock, 1977), at Pandemonium Creek (Evans, et al., 1989) and at Hope (Mathews and McTaggart, 1969), British Columbia. Like bedding planes, the downhill-oriented structures provided slope-parallel discontinuities and natural detachment surfaces for the landslides. The last important geological structures in the development of large terrestrial landslides are anticlinal and synclinal fold axes. The crowns of the headscarps of both the Frank, Alberta (Cruden and Krahn, 1978) and the Carlson, Idaho (Appendix B) landslides corresponded with anticlinal fold axes, while the lower ends of the headscarps of the Diablerets 1 and 2 landslides coincided with the axis of a large recumbent fold (Heim, 1932). Presumably, tensional joints along the hinges of a fold provide discontinuities along which the adjacent rocks can readily detach. In addition, the presence of such joints would have provided an avenue for meteoric waters to migrate into the subsurface at critical locations, perhaps aiding in the processes leading to these slope failures.

The headscarp locations of large martian landslides are also often correlated with major geologic structures. The association of major geological structures with landslide headscarps, collated in Appendix A, was determined for seventy-seven large martian landslides with detached debris aprons and for fifty-six having attached debris aprons. A high slope forms the primary requirement for the development of large landslides. On Mars, high slopes occur in association with five principal land forms: chasmas, outflow channels, volcanoes, impact craters and erosional remnant mountains and mesas in regions of chaotic terrain.

Of the seventy-seven detached debris apron landslides with observed headscarp relations, fifty (65%) were found to have originated from chasma walls, chasma erosional spurs and erosional remnant mountains and mesas. Twenty-nine of these landslides originated from unremarkable plateau

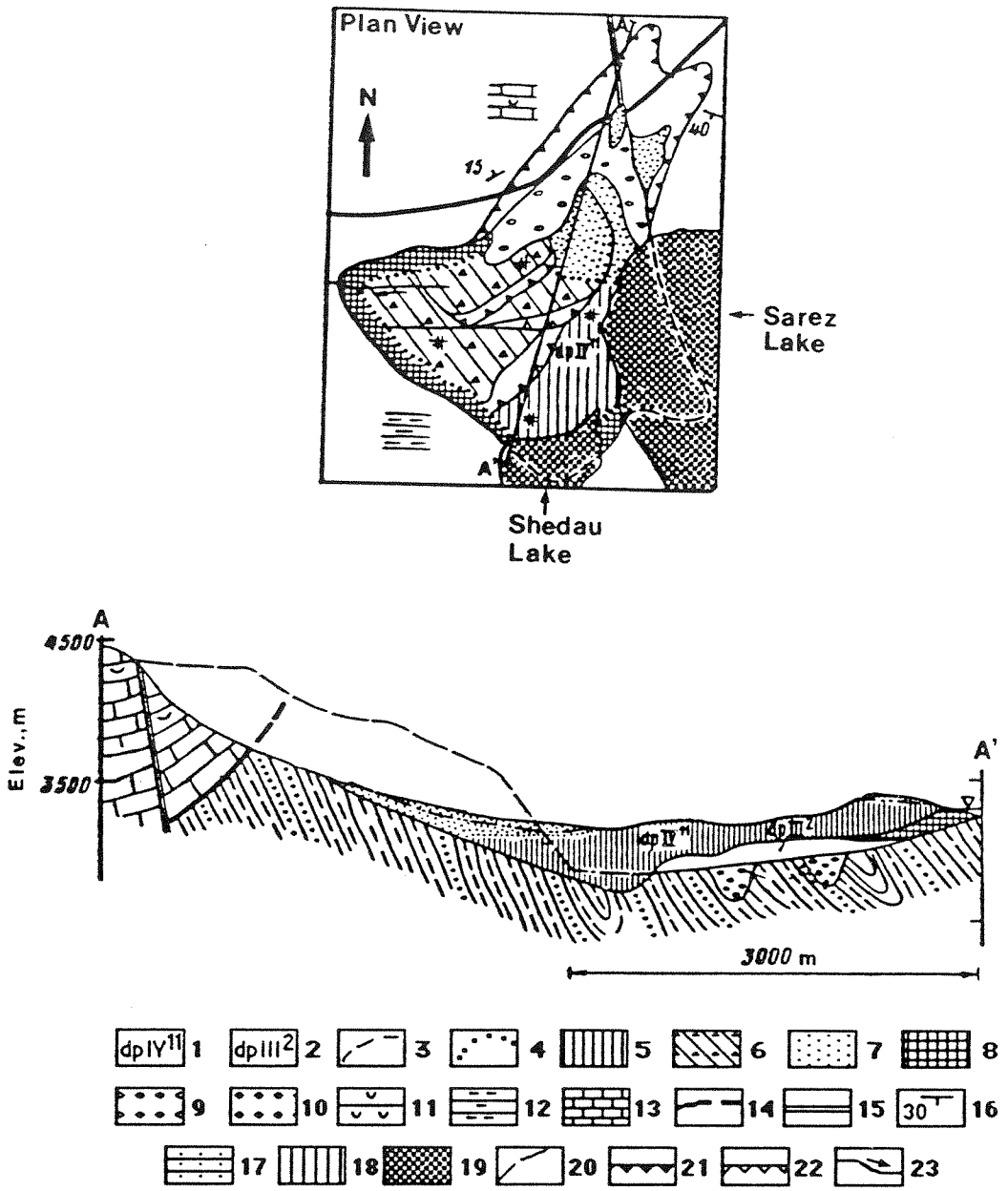

Figure 16. Geologic sketch map and cross section through the Usoy landslide, Tadzhikistan, U.S.S.R., which occurred on 18 Feb. 1911. Definitions: 1) Usoy landslide; 2) a prehistoric, post-Pleistocene landslide; 3) inundated margin of landslide deposit; 4) gradational unit contact; 5) Usoy landslide deposit in cross-section; 6) detrital blocks facies of landslide deposit; 7) tail-end landslide debris facies; 8) leading-edge landslide debris facies; 9) talus; 10) alluvium; 11) gypsum; 12) sileceous shale; 13) limestone; 14) thrust fault, dashed where approximate; 15) Quaternary fault trace; 16) strike and dip of tilted strata; 17) sandstone; 18) contorted Paleozoic bedrock landslide blocks; 19) lake waters; 20) pre-landslide slope profile; 21) primary landslide breakaway scarp; 22) secondary landslide scarps; 23) stream channels. From Grigorian, et al. (1983) and Gaziev (1984).

margins, while the remaining twenty-one deposits had headscarps that occurred at the intersections of plateau margins and major plateau structures.The three primary plateau-edge structures observed to intersect landslide headscarps are (with number of landslides from each intersecting structure in parentheses): impact craters (14; Chapter II: Figure 6h); dark, linear, cross-cutting features resembling intrusive dikes (5; Figure 17a); and graben-bounding faults (2). The remaining twenty-seven detached debris apron landslides fell from volcanic constructs (5; Chapter II: Figure 6i) and from the inner walls of impact craters (22; Chapter IV: Figure 43). The impact craters containing these landslides have varying diameters and morphologies, but most of the slides (73%) occurred within fresh-appearing 50 km- or smaller-diameter craters.

In comparison, of the fifty-six attached debris apron landslides with observed headscarp relations, forty-eight (86%) were found to have originated from chasma walls, chasma erosional spurs and outwash valley walls. Only twenty-two of these slides originated from unremarkable plateau margins, while the remaining twenty-six deposits had headscarps that occurred at the intersection of a plateau margin and one or more major plateau structures. The primary plateau-edge structures observed to intersect landslide headscarps are (with number of landslides from each intersecting structure in parentheses): graben-bounding faults (13; Chapter II: Figure 6e); impact craters (8; Chapter II: Figure 6d); multiple features (4); and a dark, linear, horizontal feature resembling a sill (1). Landslide headscarps that cut multiple plateau-surface structures (Figure 17b) incised two or more of the following structures: wrinkle ridges, impact craters, graben-bounding faults, and a possible sill. The remaining eight attached debris apron landslides fell from the inner walls of impact craters.

The preceding discussion indicates that, while detached and attached debris apron landslides were controlled by many of the same structures, the structures differed in importance for the two types of deposit. Detached debris apron landslides on Mars occurred most frequently in impact craters, while a much smaller proportion of the attached debris apron landslides took place there. Also, for landslides originating at the intersection of plateau margins and plateau-surface structures, the great majority of the detached debris apron slides fell away from impact craters, while attached debris apron landslides occurred primarily at the intersections of plateau margins and

Figure 17a. Illustration of location of landslide headscarps at the intersection of a sill(?) and a chasma wall for four closely-spaced martian landslides. Possible sill is marked by small arrows. Martian landslides labeled with identification numbers (Appendix A); fall directions are marked by large open arrows. Dark patch to west of landslide complex appears to be dark sand dune complex. Viking Orbiter image 014A31. Solar zenith angle 63.99°.

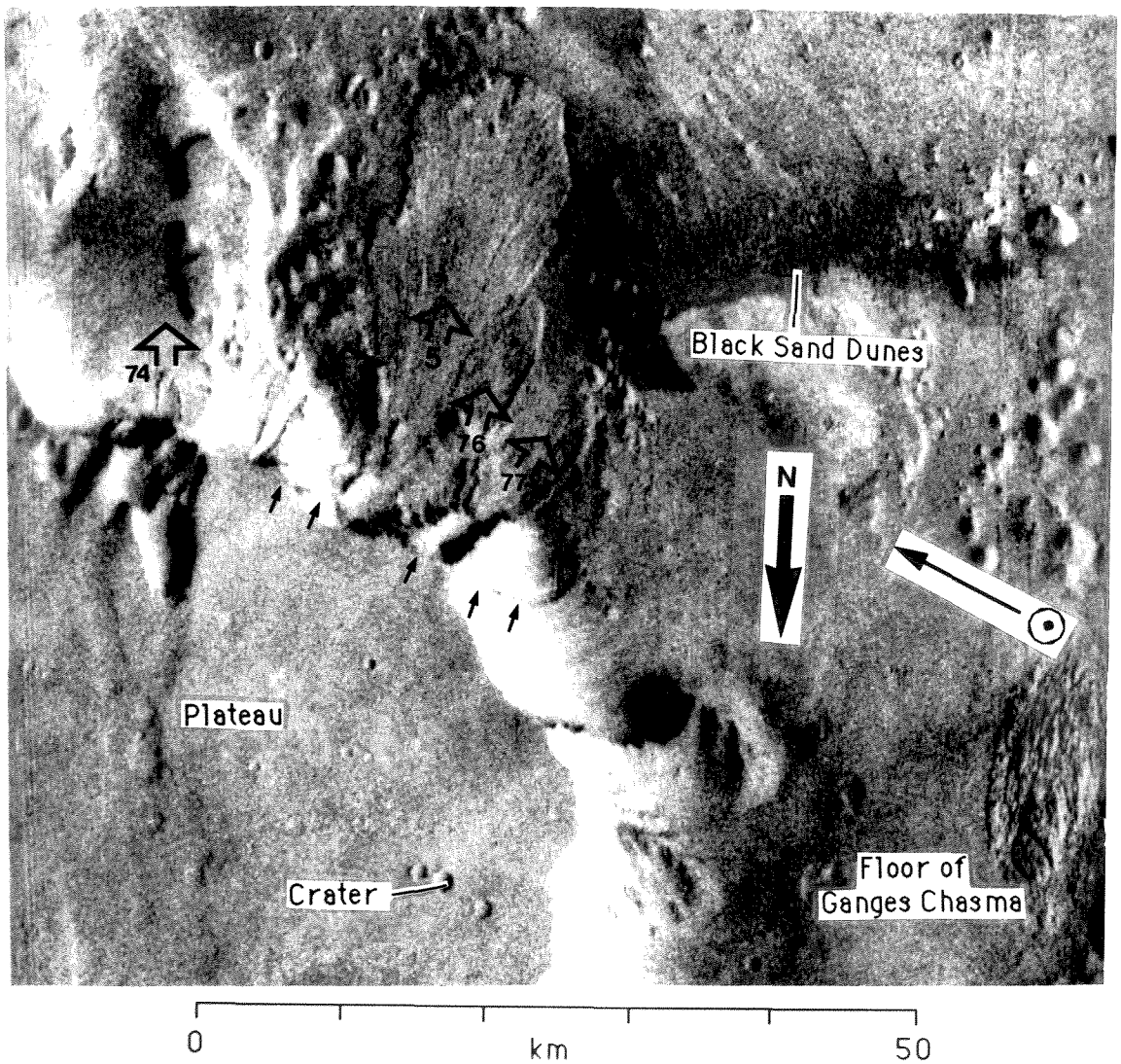
74
5
76
77
Black Sand Dunes
N
Plateau
Crater
Floor of
Ganges Chasma
0
km
50

Figure 17b. Illustration of location of landslide headscarps at the intersection of multiple plateau-surface structures and a chasma wall. Landslides Mars 35 and Mars 37 are associated with multiple structures, while Mars 34 and Mars 36 are associated with only one primary structure. Plateau surface is marked by "P," floor of Ophir Chasma by "C," and landslide debris by "L." Possible sill is marked by "S," grabens by "G," wrinkle ridge by "W." Martian landslides labeled with identification numbers (Appendix A); fall directions are marked by large open arrows. Portion of a controlled photomosaic of part of the Valles Marineris region of Mars, U. S. G. S. Misc. Inv. Map I-1592. The lighting in the center of the image is from near due east, at a solar zenith angle of approximately 55°.


N
P
P
P
G
G
W
S
C
L
L
L
L
C
30 km
20
10
0
10

graben-bounding faults. Many of the differences between the two groups of landslides probably relate to the fact that detached debris apron landslides contain on average much smaller volumes of material than attached debris apron slides. Thus, only those structures with large linear dimensions, such as large impact craters and long, continuous, graben-bounding faults, could normally influence the initiation of attached debris apron landslides. Also, since detached debris apron landslides normally began as rockfalls and the attached debris apron landslides as slumps, the various different types of major structure would tend to favor mass wasting by one or the other of the two types of mechanism. The heavily fractured inner walls of an impact crater, for example, would tend to fail more commonly by a rockfall mechanism than by slumping. Therefore, detached debris apron landslides are the common form of mass wasting of impact craters. Similar arguments could be made for the dominance of one or the other type of landslide from other specific structures. Generally, smaller, detached debris apron landslides are favored by smaller structures where shattering and jointing of bedrock is important, whereas larger, attached debris apron landslides are favored by larger structural discontinuities without accompanying shattered bedrock.

Initiation mechanisms

Most of the processes believed responsible for triggering large landslides are the same as those that operate at more pedestrian scales. Unlike the runout phase, therefore, during which large landslides exhibit much greater mobilities than their smaller counterparts, most of the same initiation mechanics operate for all sizes of landslides, from small road-cut failures to those containing cubic kilometers of rock. Initiation thus forms the only phase in the movement of large landslides in which the operative mechanisms may be extended with some confidence from a knowledge of smaller deposits.

The development of an unstable slope is dominated by different processes in the various environments where large landslides occur. In the terrestrial subaqueous environment large landslides nearly always occur as a result of constructional processes, such as overloading of a slope by lava. In terrestrial continental environments, in comparison, landslides are shed from volcanic constructs or from tectonically uplifted mountain ranges. In non-volcanic environments, the local instability leading to large landslides usually forms in response to erosional oversteepening of slopes. In the absence of significant

erosion by ice or running water, talus deposits created by innumerable small mass movements typically form stable slopes at the angle of repose of the loose material, normally precluding the triggering of large landslides. However, where weak materials exist at the proper orientation in a slope, or if large transitory earth stresses occur, large landslides can form even on gentle slopes. For example, the Goldau and Gros Ventre landslides began movement along weak, silt- and clay-rich strata exhibiting only 20° dip slopes (Heim, 1932; Voight, 1978). Slumps can also form on gentle slopes (Albee, et al., 1981), either when a potential slip surface intersects a low-strength bed (Reiche, 1937; Varnes, 1958) or during an earthquake (Terzaghi, 1950). Interestingly, because of the lack of stable water or ice on the surface of Mars, most of the slopes on the planet indeed lie at or near the angle of repose for granular material. Nevertheless, large slumps have occurred on these slopes, suggesting that zones of weak material may underlie many martian slopes or that marsquakes have struck these slopes. These possibilities are considered in detail in Chapter IV.

The initiation of a landslide is controlled both by materials in the slope, such as the geology, structures and groundwater, and by external processes, like climate, seismic shaking and human activity. A useful approach is to divide these processes into those that increase the shearing stress on a slope and others that decrease the shearing resistance of the materials composing a slope. The processes that act to increase shear stresses in a large rock mass include: 1) the removal of lateral or underlying support; 2) increased loading; 3) seismic activity (Mathewson, 1981); 4) oversteepening due to volcanic activity (Voight, et al., 1983); and 5) dike intrusion (Lipman, et al., 1985). Factors that decrease the shearing resistance of slope materials include: 1) an increase in pore water pressure; 2) rock weathering; 3) the effects of long-term creep; and 4) fracture development (Mathewson, 1981). In most cases, several of these processes act together to destabilize a slope and initiate landslide motion. In the following discussion, descriptions of the listed initiation processes are provided, together with examples of each from the large landslide database (Appendix A).

The removal of lateral or underlying support from a slope serves as one of the primary means of triggering large landslides. Slide initiation could conceivably occur immediately upon the removal of support, but in all known cases the loss of support has led to a period of creep (see below), culminating

in a large slope failure only after a considerable time delay. Several mechanisms are responsible for removing lateral support from broad areas, triggering large landslides. These include: the wasting of valley glaciers after a major glaciation, the rapid draw-down of a neighboring water body, human excavations, previous landslides, stream erosion and long-term differential erosion of slopes underlain by strata with differing weathering properties.

The interglacial or interstadial wasting of glacial ice in valleys deeply eroded during Pleistocene glacial epoches clearly provided a triggering mechanism for many large landslides. These landslides date from periods of major glacial retreat, which removed the buttressing ice masses from the eroded valleys. Numerous examples occur in the Alps, including: Glärnisch-Guppen, Glärnisch-Gleiter, Flims, Engelberg, Kandertal, Parpan (Heim, 1932); in the Rocky Mountains: Pasayten (Waitt, 1979); and in the Himalaya: Koefels (Heuberger, et al., 1984).

A second means of decreasing lateral support is the draw-down of a neighboring water body, such as a reservoir, lake or even an ocean. This process could have many influences on a slope, but primarily it removes a heavy buttress of water from the lower, stabilizing portions of a slope. The Vaiont landslide, for example, resulted from an acceleration of creep motion triggered by the alternate raising and lowering of the water level of an abutting reservoir (Müeller, 1964). Circumstantial evidence also points to the triggering of some giant landslides from oceanic islands by the draw-down of sea level during Pleistocene glaciations. Fairbridge (1950) suggested this mechanism from his studies of a landslide off Goenoeng Api, a volcanic island in the East Indies. The slow rate at which oceanic draw-down occurs at the onset of a major glaciation, however, makes this mechanism somewhat questionable (Moore, personal communication, 1991).

Human activities can also trigger large landslides. The removal of underlying support via mining activities led to accelerated creep and failure of the Elm (Heim, 1932) and also probably the Frank landslides (Daly, et al., 1912).

Large landslides can also occur where previous landslides from the lower regions of a slope have removed subjacent support from a rock mass. This ultimately leads to failure as the upper part of the bedrock mass experiences rock fatigue following collapse of the lower part of the slope. Examples include the Hope landslide, which occurred from an oversteepened slope above

the headscarp of a prehistoric landslide, and the 1970 Huascaran 3 landslide, that fell from an overhanging cliff left by the earlier 1962 Huascaran 2 event (Plafker and Ericksen, 1978).

Another means by which lateral support is removed from a slope resulting in a large slope failure is undercutting of a slope by stream erosion. The toe of the Gros Ventre landslide was, for example, apparently undercut by the Gros Ventre river, which ran along the base of the failed slope (Voight, 1978). A similar situation probably instigated the giant Saidmarreh landslide. In this location, the Saidmarreh River, which flowed down the axis of a synclinal trough, eroded the toe of the adjacent anticlinal carbonate ridge (Harrison and Falcon, 1938). The headscarp region of Carlson landslide, in comparison, was undercut and oversteepened by the headward erosion of a stream channel (Appendix B).

A related process is the oversteepening of slopes by long-term differential erosion of slope-forming strata that experience different responses to weathering processes. In arid climates, for example, carbonate rocks consistently develop great relief because of their resistance to erosion in a dry climate. Many large Tertiary and Quaternary landslides in arid regions have carbonate lithologies for this reason (Jahns and Engel, 1949; Albee, personal communication, 1991). Other cliff-forming rock types in arid climates include gneiss schist and quartzite (Jahns and Engel, 1949; Longwell, 1951; Yarnold and Lombard, 1989).

Increased loading of a slope provides a second principal means for triggering large landslides. Large landslides have occurred from slopes overloaded by several processes, including: 1) volcanic activity; 2) human activity; 3) rainfall; 4) snowfall/glaciation; and 5) prior landslides. Overloading of slopes by way of volcanic activity provides a very effective means of destabilizing large slope regions. For example, the overloading of slopes by fluid basaltic lava flows probably played a major role in the initiation of the numerous giant landslides from the Hawaiian shield volcanoes. This is suggested by the coincidence in time between the landslides and the major shield building periods of their host volcanoes. In these periods, the volcanoes stood 2-4 km above sea level and were extending their shorelines most vigorously (Moore, et al., 1989). The extrusion of blocks and ash from stratovolcanoes forms another example of slope overloading by volcanic activity. The blocks and ash may form loose, stratified accumulations

near source vents that slough off due to oversteepening and eruption-related seismic shaking. Several examples of such landslide deposits have been described from the 1944 eruption of Mt. Vesuvius, Italy (Hazlett, et al., in press). Where erupting lavas are yet more sialic, large landslides may occur from partially or fully cooled volcanic domes. Highly viscous rhyolitic or dacitic lavas often form steep-sided domes which may become gravitationally unstable as they cool and develop a system of joints and fractures. Large landslides may occur from fully cooled domes, such as the Chaos Jumbles 1-3 landslides (Eppler, et al., 1987). Others, such as the Panum block and ash landslide, may fall from hot, recently extruded domes (Sieh and Bursik, 1986).

Human mining activities form a second means by which slopes may become sufficiently overloaded to produce large landslides. In regions of large-scale mining activities, landforms are often altered to an unstable geometry in the process of redistributing mine tailings. The sub-ore quality rock removed from a mine often simply gets bulldozed off the side of a hill. Ultimately this poorly consolidated material may build up into large accumulations, or "tips." If these accumulations become overloaded due to addition of material from above or if they are poorly drained and become weighted with pore waters, they may experience catastrophic failure, leading to long-runout landslides. Figure 18 presents an example of one such mining region on the Kola Peninsula, U.S.S.R., which gave rise to numerous large landslides. The topographic map exhibits fifteen long-runout landslides originating from a plateau leveled off in the course of mining activities. Loose dross was deposited all along the edge of the plateau, which overloaded the slopes and led to the numerous large-scale failures of the plateau margin over time (Adushkin, personal communication, 1990).

Heavy rainfall often triggers small landslides when rain waters infiltrate and overload permeable slopes (Mathewson, 1981). However, this mechanism apparently plays only a minor role in the triggering of large landslides. The only large landslide believed triggered by rainfall was the 1893 Gohna, India landslide, which actually appears to have formed as a series of rockfall-type landslides over a three-day period of heavy rains (Holland, 1894). The role of rainfall in triggering the Gohna landslides is unknown, but it probably acted both to overload the carbonate slope and to increase the pore pressure of water along discontinuities in the rock mass. The relative rarity of large, rainfall-induced landslides probably relates to two important factors. First, because

Figure 18. Topographic map of the Chibins mine, Kola Peninsula, U.S.S.R., showing large landslides shed from the margins of the strip-type mine. Loose debris bulldozed off the edge of the plateau became unstable over time, generating numerous long-runout landslides (Adushkin, personal communication, 1990).

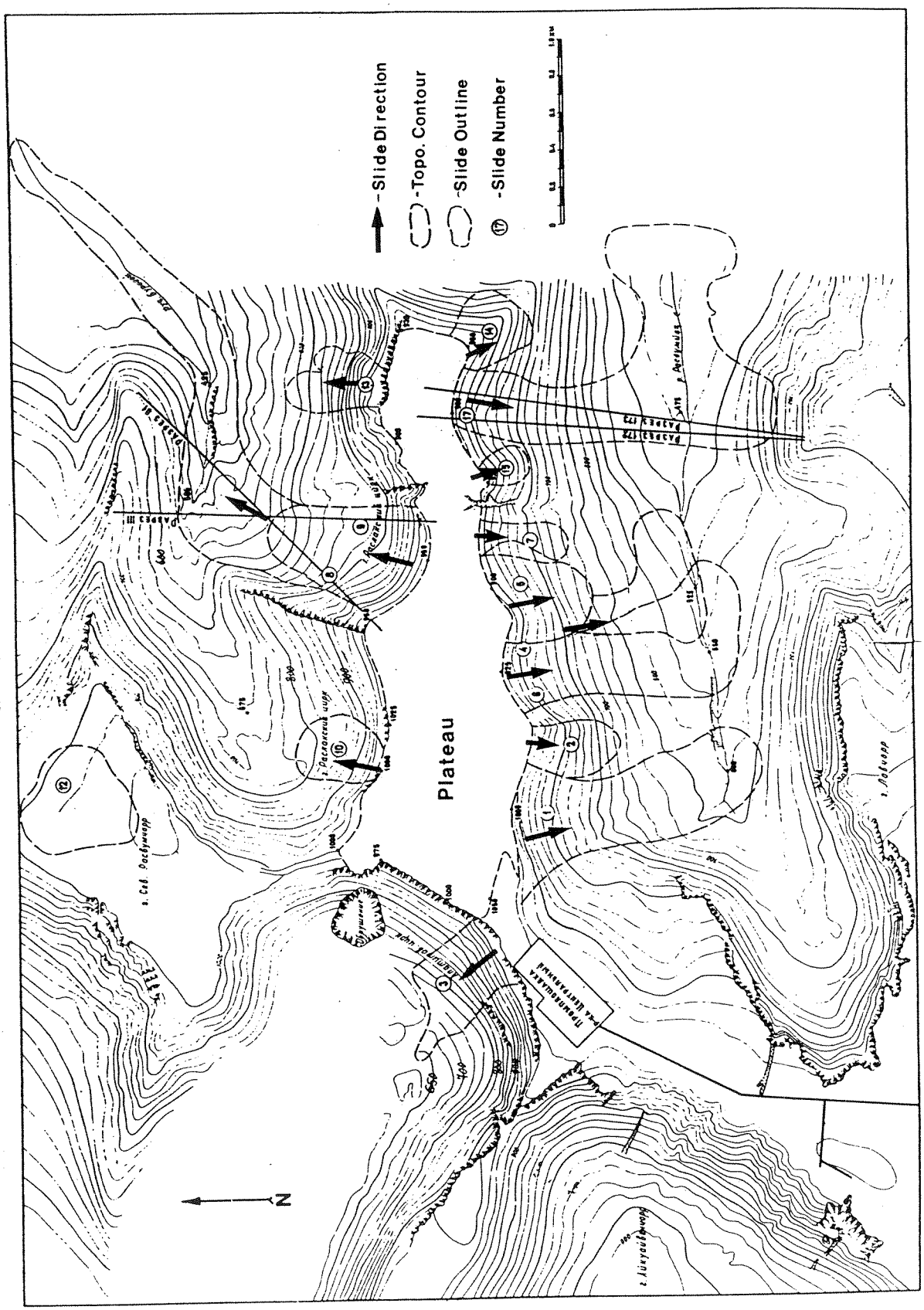
-Slide Direction
-Topo. Contour
-Slide Outline
-Slide Number
Plateau
N

long-runout landslides have slidemasses of large dimensions, only great quantities of added water could supplement the weight sufficiently to trigger failure. This may explain the occurrence of the Gohna landslides. Second, as compared with many types of surficial materials subject to failure in small landslides, the large rock masses probably have less available pore space per unit volume for surface waters to infiltrate.

Multi-year accumulations of snow and ice provide another means by which a slope may become overweighted. With regard to large landslides, multi-year snowpacks and glaciers are a much more effective climate-related means of overloading a slope than rainfall because much more weight is ultimately brought to bear on the underlying slope (see above). Numerous large landslides have occurred from steep rock faces topped by glaciers. In these cases the bedrock usually became oversteepened due to Pleistocene glacial erosion and gave way later after most of the buttressing ice melted away (see above). In the resultant landslides the ice and rock typically mix together to some extent in the final deposit, though the glacial ice rarely appears to have time to melt and modify the movement behavior. Such landslides have occurred historically in many mountainous region on the Earth. Examples include the Diablerets 1 and 2 landslides in the Swiss Alps (Heim, 1932); the Sherman glacier landslide in Alaska (Shreve, 1966; McSaveney, 1978); and the Huascaran 3 landslide in the Peruvian Andes (Plafker and Ericksen, 1978).

The last reported means by which slope overloading triggered a large landslide occurred by means of a two-stage process. In the first stage a rockfall from a high limestone peak fell during an earthquake onto an alluvial terrace halfway down the mountainside. On the following two days, a large rainstorm moved into the area and soaked the landslide-covered terrace. The weight of the landslide debris and the rainwater together overloaded the alluvial terrace, leading to a period of creep (described below) which ended in failure of the alluvial slope. The slope failure generated the Corbeyrier-Yvorne long-runout landslide (Eisbacher and Clague, 1984).

Seismic groundshaking comprises the third slope-external force known to trigger large landslides. Seismic events important for initiating large landslides may originate by way of earthquakes and possibly "marsquakes," human-triggered chemical or nuclear explosions, bolide impacts or by the movement of very large landslides themselves. Such seismic events trigger large landslides in several ways: by rapidly cycling the shear stresses along a

potential failure surface, by reducing cohesion in unconsolidated granular or blocky material, by causing large fluctuations in pore water pressure, or by rupturing cohesive fracture fillings (Mathewson, 1981).

Earthquakes provide an important, though somewhat overrated means for triggering large terrestrial landslides. It is important to note that an earthquake in itself usually only triggers the failure of metastable bedrock slopes, although seismic activity can fluidize poorly consolidated, water-saturated or thrixotropic materials in place to cause major slope failures (Mathewson, 1981). Thus, the distribution of large landslides triggered by an earthquake relates primarily to the distribution of metastable slopes in the affected region, and only secondarily to the magnitude of the earthquake, the distance of a slope from the epicenter of the quake or the orientation of the affected slope relative to the direction of first motion of the earthquake. The distribution of large bedrock landslides triggered in the 1964 Alaska earthquake supports these conclusions. Despite the large magnitude of the event, there was no predominant direction of initial movement of the landslides and no simple function of slide distribution with distance from the epicenter, suggesting that local structures and bedrock weaknesses primarily controlled the landslide distribution, rather than the local strength of the seismic shaking (Post, 1967). Presumably there is a threshold of seismic groundshaking necessary to trigger a metastable slope that relates to the secondary factors, but this value has not been established and must vary from slope to slope depending on local conditions. Table 6 gives a list of the numerous large historical landslides known to have been triggered by earthquakes. Note that all of the bedrock landslides listed in Table 6 occurred during large earthquakes having Richter magnitudes in excess of 6.6.

It is unknown whether marsquakes, either fault- or volcano-related, have been important in triggering large landslides on Mars. The great majority of large landslide deposits on Mars are situated in areas where geological evidence suggests that seismic activity could have once been significant. In particular, the great majority of martian landslides lie in Valles Marineris, a system of chasmas formed by some combination of extensional tectonics and erosion. Faulting seems to have played a key role in the formation of the chasmas, both by providing sites for preferential erosion and by providing much of the vertical relief necessary for erosion to occur. In many locations, faulting and erosion apparently proceeded simultaneously rather than

succeeding each other, because some erosional features which could not have formed until after faulting started are themselves cut by faults (Carr, 1981). Seismic activity along chasma-bounding faults may therefore have played a role in triggering some of the landslides in Valles Marineris. However, while some of the chasmas containing large landslides, such as Coprates, Ius and Tithonium, show distinct linear scarps along their margins suggestive of fault scarps, many others also containing landslides, including Hebes, Ophir, Candor, Melas (Carr, 1981) and Ganges show little evidence of faulting and must have been significantly enlarged by erosion. In addition, many of the large landslides in the scarp-lined chasmas cut through, and apparently post-date, the scarps. Also, few of the landslides in the chasmas can be shown to be overlapped by later products of erosion of the chasma walls. Because many of the Valles Marineris landslides occurred away from apparent fault scarps and because most of them post-date the opening of the chasmas, the majority of landslides in Valles Marineris landslides probably were not triggered by fault-related seismic activity. Elsewhere, a few large landslides occur on and around martian volcanoes. The majority of these are associated with Olympus Mons; two fell from the flank of the landslide onto a neighboring plain and one fell into the summit caldera from the caldera wall (Appendix A). These landslides may have been triggered by eruption-related seismic activity, or, conversely, they may have simply occurred as a result of long-term creep and failure of local, steep constructional slopes on the volcano.

Large landslides may also be triggered by seismic events originating in nuclear or chemical explosions. Both these methods seemingly have been used to trigger large landslides in the Soviet Union. The five landslides listed as "U.S.S.R. Artificial" in Appendix A, for example, were all apparently triggered by underground nuclear explosions centered approximately one kilometer below ground in the vicinity of the landslides (Adushkin, personal communication, 1990). As a component of a more recent project, by which large, heavily confined landslides are to be triggered to create large dams for hydroelectric power generation, another large landslide in the Soviet Union was triggered by the detonation of 1900 tons of chemical explosives in two ~120 meter long galleries situated parallel to the trend of the underlying valley floor (Figure 19; Muratova, personal communication, 1990; Zykov, personal communication, 1990). In this case, and perhaps also for the earlier artificial landslides and maybe some natural ones as well, the movement of the landslide

Figure 19. Cross-section through the artificially-triggered Uchterek landslide, Kirghizia, U.S.S.R. (41°45'N, 73°10'E). The landslide was triggered in 1988 by the detonation of 1900 metric tons of chemical explosives as a test of a project to build hydroelectric dams using artificial landslides. The explosives were detonated in two ~120 m-long slope-parallel galleries (circles), the lower gallery first, followed 4 seconds later by detonation of the upper tunnel. The hatched line shows the original ground surface, the plain solid line the final profile. The heavily confined landslide contained 3 million cubic meters of sandstone breccia (Zykov, personal communication, 1990).

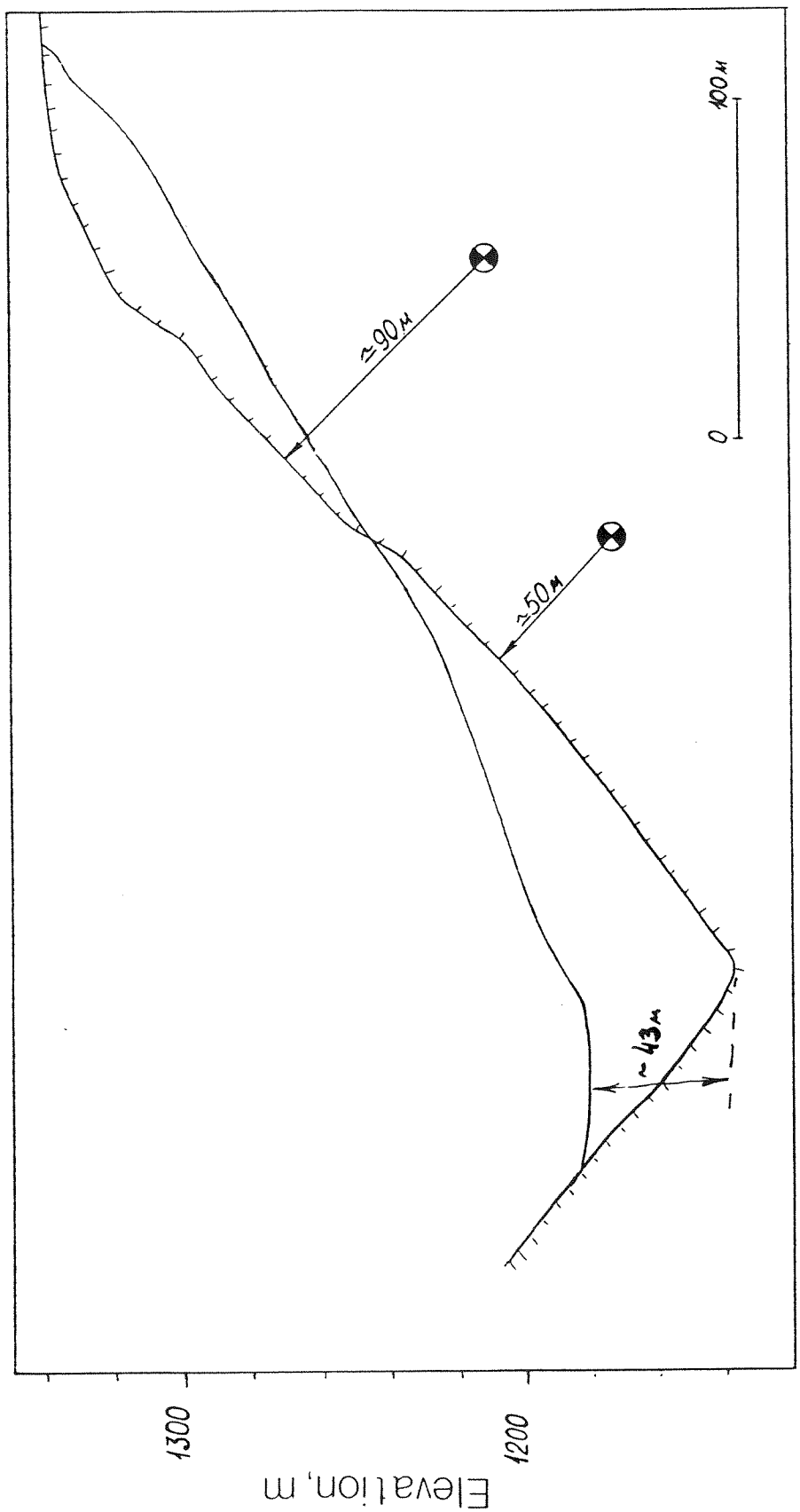
Elevation, m
1300
1200
≃90м
≃50м
~43м
100м
0

was actually induced by the initial slope-normal impulse of the explosion rather than by the vibratory loading effects normally associated with seismic triggering of landslides. It seems possible that some natural landslides were triggered in a like manner because observers noted that the landslides began moving with the arrival of the first motions of earthquakes (see Eyewitness Accounts, below). Naturally-occurring examples include the Huascaran 3 (Plafker and Ericksen, 1978) and Madison (Hadley, 1978) landslides.

Bolide impacts, naturally-occurring explosions, provide yet another source for seismic waves that could trigger large landslides. No known terrestrial landslides could have been triggered by meteorite impacts, as none occurs near known terrestrial impact craters of similar age. However, bolide impacts probably triggered both the lunar landslides listed in Appendix A, as well as many martian landslides. The lunar landslide Tsiolkovsky, for example, formed from a rotational failure of the outer rim of the crater of the same name. Because the age of the landslide corresponds closely with the age of the crater, the landslide may have occurred as a direct result of the cratering event. In fact, Guest (1971) considered the landslide to be a modified ejecta deposit. The other known large lunar landslide, the Apollo 17 deposit, was also apparently triggered by an impact cratering event, when secondaries from Tycho impacted at the top of a ridge and dislodged a layer of regolith from the subjacent slope (Lucchitta, 1977).

Although seismic events associated with bolide impacts doubtless triggered many of the martian landslides listed in Appendix A, none can be proven to have been triggered in this manner. However, while it might be argued that landslide deposits from the walls of Valles Marineris and from the slopes of martian volcanoes might have been triggered by endogenic seismic energy or by other mechanisms, most of the landslides in impact craters on the old cratered terrain occurred in the absence of any other common process of slope destabilization. Note that the impact events that triggered most of these landslides were probably not those that formed the craters, but rather were much later events. This observation is supported by two facts: that the landslides typically exhibit much sharper morphologies than the nearby degraded crater walls and that many of the landslide deposits overlie dark, flat plains on the interiors of the craters that probably represent solidified impact melt or later volcanic infilling. It is more difficult to discern whether the source of the seismic activity was nearby secondary impacts, such as triggered

the Apollo 17 landslide on the Moon, or whether more distant primary events might have been the trigger. To give some idea of the seismic effects associated with impact craters of various sizes, Schultz and Gault (1975) compared the energies released in impacts to the amount released in large terrestrial earthquakes. For lunar craters, they found that a 1-km impact corresponds to a magnitude 5.8 earthquake, and a 35-km diameter cratering event to a magnitude 10 earthquake. Schultz and Gault (1975) also calculated the ground displacements from the latter event for points 140 km from ground zero. By assuming that the seismic surface waves generated by the impact propagated as sawtooth waves, they calculated surface displacements of 2, 0.7 and 7 m for frequencies of 0.2, 0.5 and 0.05 Hz, respectively. Given the great age of deposits in the cratered plains, many such impact events must have been available to trigger the observed landslide deposits.

The last means of triggering large landslides with seismic activity is by the movement of giant landslide masses themselves. This idea originates with the work of Galitzin (1915) for the Usoy landslide, and was later extended by Kanamori and Given (1982), who explained the long-period surface waves associated with the Mt. St. Helens eruption as the "single-force" seismic signature of the giant landslide that initiated the eruption. Later, Eissler and Kanamori (1987), interpreted the seismic energy released in the 1975 (M_S = 7.1) Kalapana, Hawaii, earthquake as similarly being the energy released in large-scale slumping of the south flank of Kilauea volcano. The volume of material involved in the Hawaiian slump amounted to between 300 and 3000 km^3, the same order of magnitude as the giant long-runout Valles Marineris and Hawaiian landslide slumps (Appendix A). However, while the slump which created the 1975 Hawaiian earthquake only traveled on the order of 10 m, the giant slumps that produced long-runout landslides in Valles Marineris and off the Hawaiian Ridge traveled thousands of meters, both vertically and horizontally. Eissler and Kanamori (1987) modeled the first impulses of seismic waves as originating from the decoupling of the slump block from Hawaii Island along a shallowly dipping slide plane near the base of the volcanic pile, at a depth of 9-10 km:

> Sliding motion is triggered by a sudden reduction of friction between the upper block and the slope. The reduction of friction causes the block to be accelerated downdip and reduces the downdip force exerted

> by the block on the slope. This sudden reduction of the downdip force is equivalent to a sudden application of an updip force on the slope. Since the block is decoupled mechanically from the slope, this updip force alone contributes to seismic radiation as a single force...
>
> The peak acceleration for the slide mass inferred from the seismic force is then 0.1 m s^{-2}. This is comparable with the acceleration due to gravity on a gently inclined plane (0.85 m s^{-2} for $\alpha=5°$)...
>
> Although the entire event may have been initiated by a small tectonic earthquake caused by magmatic stresses, gravity must play an important role in driving this sustained slumping process.

After movement began, at least five more subevents were recorded by seismographs in Hilo during the 75-second duration of the earthquake. After fully investigating the seismic signature of the slump and its aftershocks, Eissler and Kanamori (1987) concluded that the partially decoupled slump initially moved on a deep-seated slide plane, but subsequently lost coherency as a unit and experienced internal failure on many planes, producing a complex and sustained seismic event.

These observations lead me to conclude that the giant long-runout Valles Marineris and Hawaiian landslides probably were also associated with strong self-generated seismic activity as the slumps decoupled from the substrate. Because Kanamori and Given (1982) and Eissler and Kanamori (1987) successfully modeled the seismic signatures of the 1980 Mt. St. Helens and 1975 Kalapana landslide-related earthquakes as originating from the temporary decoupling of the landslides from their substrate and their subsequent acceleration under gravity, it appears that the acceleration of gravity should play an important role in the seismic signature of such an event. This observation suggests to me that the martian slumps probably produced events of lower peak magnitude than slumps of similar scale on Earth. However, the large travel distances involved also suggest to me that these landslides probably each produced a series of seismic disturbances that lasted much longer than the 75 seconds of activity triggered by the Kalapana slump/earthquake. One possible implication of this analysis is that such large, long-duration seismic events could trigger the failure of nearby slopes, perhaps explaining why some chasma areas on Mars, such as eastern Ganges

Chasma, exhibit clusters of large landslides of similar freshness, while similar areas elsewhere contain no landslides. The seismic disturbances produced by individual large landslides might trigger others locally, leading to groups of closely-spaced large landslides of similar age.

Two remaining processes, both related to volcanic activity, act to increase the shearing stresses on a slope and induce large landslides. Both processes occur in large active volcanic edifices when magma is pumped into the volcano from depth preceding an eruption. If the slopes of a volcano are initially rather steep, such as in a stratovolcano, the inflation of an edifice due to magmatic injection can oversteepen the slopes of the volcano and induce creep and catastrophic failure of an entire sector of a volcanic cone. The Mt. St. Helens landslide appears to have formed in just this fashion. The landslide followed about two months of intense bulging and strength deterioration associated with magmatic intrusion, seismicity and gravitational creep (Voight, et al., 1983). The giant slope failure that ensued on 18 May 1980 released the overburden pressure on the gas-rich magma in the volcano and produced a tremendous directed blast that modified the slide scar produced by the landslide. Figure 20 gives the profile of the Mt. St. Helens landslide scar as well as those from other large volcanic landslides and from some representative non-volcanic landslides, showing the comparatively great depth of slide scars in stratovolcanoes. This diagram illustrates that landslides from stratovolcanoes commonly leave deep slide scars due to the directed explosions that accompany the landslides (Siebert, 1984).

Another, related, volcanic process that can increase the shear stresses on a slope and induce slope failure is vertical wedge-like dike intrusion headward of the potential slide surface of a giant landslide. Lipman, et al. (1985) and Delaney, et al. (1990) have suggested such a mechanism as one causative factor in the previously discussed 1975 Kalapana, Hawaii slump/earthquake. The headscarp of the slump coincided with the east and southwest rift zones of Hawaii Island. Because the rifts form major structural discontinuities on Hawaii, they provide preferred sites of near-vertical magmatic intrusion from depth (Delaney, et al., 1990). Lipman, et al. (1985) believed that the long-term addition of magma to this site acted to wedge the slump region away from the rest of the island; ultimately, the slump slipped out away from the island as a result of accumulation of stresses from the magmatic wedging. The connection between the movement of the slump and the volcanic plumbing

Figure 20. Comparison of cross-sections of volcanic (left) and non-volcanic (right) terrestrial subaerial landslide scars. All of the volcanic landslides shown were accompanied by slide-related directed blasts. Shaded portion indicates volume removed by slope failure. Vertical scale equals horizontal scale (right column drawn at 2X scale). Diagram from Siebert (1984).

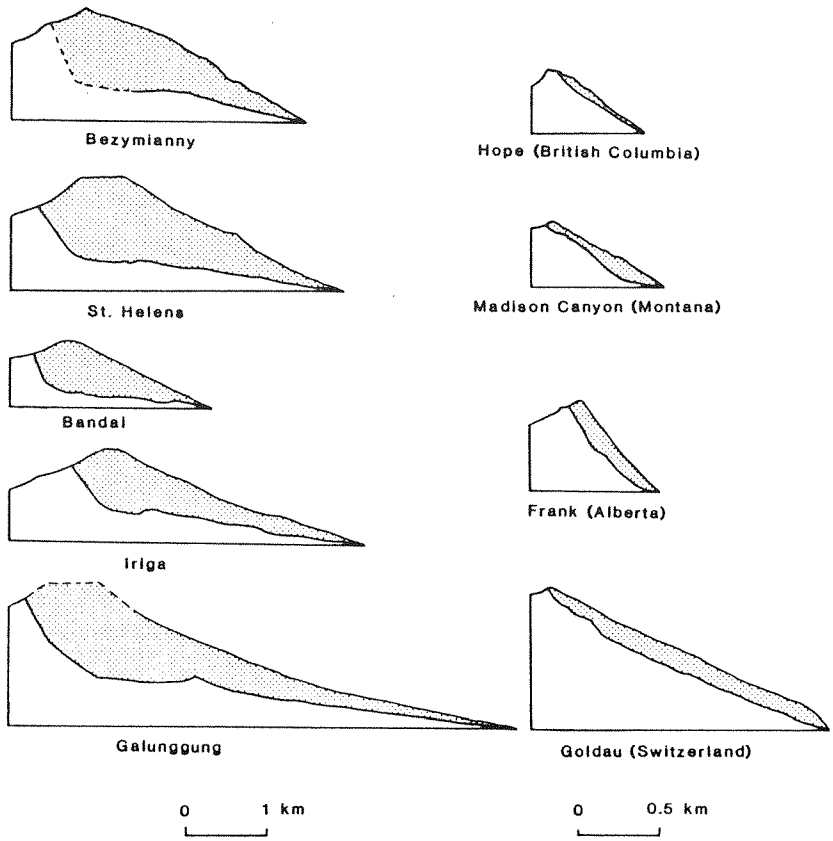
Bezymianny
Hope (British Columbia)
St. Helens
Madison Canyon (Montana)
Bandai
Frank (Alberta)
Iriga
Galunggung
Goldau (Switzerland)
0 1 km
0 0.5 km

system on Hawaii is supported by the observation that a small eruption broke out on the floor of Kilauea caldera half an hour after the earthquake. The eruption continued for 21 hours after the earthquake (Eissler and Kanamori, 1987).

The other group of processes that act to destabilize slopes are those that decrease the shearing resistance of slope materials. These processes include pore water pressure increases, rock weathering, the effects of long-term creep, and fracture development (Mathewson, 1981). As mentioned and illustrated previously, many of these processes can act together and with other factors that increase the shear stresses on slope-forming materials to induce landslides.

An increase in pore water pressure is one of the most common causes of instability in small slope failures, but it appears to be a relatively rare cause of large landslides on Earth. An increase in pore water pressure induces slope failures by reducing the effective normal stress acting across a given potential failure surface. As hypothesized earlier, pore water pressure increases tend to be less important for triggering large landslides than for smaller landslides because large landslides almost always occur in jointed bedrock outcrops with little true porespace. To destabilize a large bedrock slope, water pressure would have to increase throughout a large interconnected system of joints and fractures passing through a rock mass. The only known terrestrial landslides in which pore water pressure increases may have played triggering roles are the Gohna and Vaiont landslides. The former occurred during a three-day deluge of rain, suggesting a possible correlation between the rain water and initiation of the slide (Holland, 1894). The Vaiont landslide, in comparison, was strongly influenced by a man-made reservoir at its toe. Fluctuations in the reservoir level during filling both varied the water pressures in the interior of the rock mass and fluctuated the level of the restraining buttress of water at the toe of the slide. These combined influences apparently caused the slide mass to begin creeping, ultimately leading to catastrophic failure of the slope (Müeller, 1964; 1968).

While pore pressure increases are of minor importance to the triggering of large terrestrial landslides, the situation with respect to martian landslides in Valles Marineris is less clear. As is discussed in detail in Chapter IV, some Valles Marineris landslides have morphologies strongly suggestive of emplacement as moist landslides or debris flows (Lucchitta, 1987a). In some

locations, these unusual landslides fell into structural depressions which might have supported ice-covered lakes (Shaller, et al., 1989), thus providing one possible source of water. Other landslides have geometries that seemingly require that the slide masses themselves contained water at the time of failure, derived from wall rock in Valles Marineris. One possible origin for this water is subsurface ice melted and mobilized by internal heat flow at distances as little as 1-2 km beyond exposed chasma wall rock faces (Lucchitta, 1987a). Such waters might have triggered landslides by increasing pore pressures at depth over wide areas of jointed bedrock in Valles Marineris. The landslides could then have been moistened by these waters in the subsequent slump and runout phases of movement of the landslides.

Long-term weathering of bedrock outcrops, at least under subaerial conditions on Earth, provides another source of slope instability that could lead to large landslides. Weathering can reduce the shear strength of a rock mass by way of both chemical and physical processes. On Earth's surface, chemical weathering can alter silicate rocks to clays, thus reducing the strength of in situ rock. Also, chemical dissolution of bedrock along joints, especially in carbonate outcrops, would decrease the strength of the rock mass along these discontinuities. Physical weathering could also play a role in generating slope failures, such as by decreasing the strength of rock discontinuities via the seasonal freezing and thawing of joint-filling waters. It is much less clear whether environmental conditions on Mars might produce significant weathering of martian rock. In general, the preservation of ancient geological structures on Mars provides a testament that weathering is very inefficient in altering landforms on the planet (Malin, 1977). This is a result of the scarcity of atmospheric water on the planet and of the relative inefficiency of aeolian weathering in the low-density martian atmosphere. However, the presence of wide-spread atmospheric dust and the observation that soil at the Viking landing sites contains superoxidizing compounds (Carr, 1981) suggests that some degree of chemical weathering is or has been active on Mars. Whether it is of significant magnitude to alter the strengths of martian rock outcrops is unknown.

Creeping motion of rock masses apparently plays a very important role in the initiation of large landslides. Except for some landslides triggered by earthquakes, very few large witnessed terrestrial landslides have taken place without some prior evidence of creep of the slope (see below). Creep

represents a steady-state response of a rock mass to gravitational loading. Once creep is initiated, it progressively weakens the rock mass until it experiences sudden failure along a discontinuity or slip plane (Mathewson, 1981). Like metal parts in engineering structures, the load-bearing capabilities of rock depend on the time-duration of loading, as well as on the applied differential stress, the effective confining pressure and the moisture content (Carmichael, 1982). Laboratory investigations of low-porosity crystalline rocks loaded to a constant differential stress near the short-term breaking strength generally show such time-delayed failures. In these rocks, the creep strains are due to extension of preexisting cracks and by the production and growth of new tensile cracks. Once crack density exceeds some critical value, the cracks become close enough to interact on a large scale and they coalesce into a macroscopic fracture on which failure occurs (Carmichael, 1982). Thus, an oversteepened rock mass may ultimately undergo failure over time simply due to "rock fatigue," though other natural or human-related processes acting on a slope often accelerate the process.

Fracture development forms the fourth and final known means by which the shearing resistance of slope materials may be reduced sufficiently to cause failure of a large rock mass. Unfavorable fracture or fault orientation and density can develop in a rock mass responding to unloading or strain relief or as ice wedging or chemical weathering occur. Because the discontinuities in a rock mass control its stability, any activity that increases the structure in a slope will decrease its shearing resistance (Mathewson, 1981). Structures can develop in a rock mass in a variety of ways, and not all structures are equally important in causing the instability of large rock masses. These structures are discussed fully in the "Critical Structures" section, above.

Eyewitness Accounts

As mentioned in the introduction to this section, the processes of slope preparation and slide initiation are gradational in nature. Creep processes, for example, can suddenly accelerate into rapid sliding, or seismic waves can arrive from an earthquake and instantaneously destabilize a metastable slope. However, the actual kinematics of the transition from preparation to initiation are not readily discerned from a study of a landslide deposit or its source area. Eyewitness accounts of the initial phases of large landslides therefore provide critical information to fill the gap on this important phase in the movement

history of a large landslide. One interesting theme of the eyewitness accounts is that few large landslides took place without some advance warning, even though several were triggered by earthquakes. Noises, ground fissuring, small-scale earth movements and other related phenomena preceded most of the observed historical landslides (Table 8).

The Elm and Frank landslides are two of the most well-known and perhaps well-observed long-runout landslides. They also provided what were perhaps the most profound warning signals prior to failure of any of the observed landslides. Both events involved the failure of large rock masses directly overlying active mining operations. Slate mining activities at Elm directly led to the Elm landslide (Heim, 1932), while the coal mines under Turtle Mountain probably contributed to triggering the Frank slide (Voight and Pariseau, 1978). At Elm, an improperly excavated mine undermined a steep mountain face; the excavation measured 180 m in width and extended 65 m into the rock face (Chapter II: Figure 6j). Five years prior to the landslide a large fissure opened a few hundred meters above the mine workings. Prior to the landslide, the slidemass had crept 5 m downward along the fissure ("Chlagg," Chapter II: Figure 6j) and a creek poured into the fissure from above. In the days leading up to the disaster, chunks of mine ceiling began to fall and a crackling and banging could be heard within the mountain. By the morning of the disaster, 11 September 1881, rockfalls occurred at fifteen minute intervals, and later a continuous roaring noise issued from the mountainside. A small rock avalanche then occurred, followed by another seventeen minutes later. Four minutes after the second avalanche, the entire undermined section broke off in a single coherent ($\sim 10 \times 10^6$ m^3) rockfall, which dropped onto the floor of the mine and shattered, forming a highly mobile and destructive long-runout landslide (Heim, 1932). A similar series of events recurred twenty-two years later at Frank, Alberta (Figure 20). There, miners observed slight movements in the seven months preceding the landslide, and ground tremors even drove some of them away. The coal in the mine also began to "mine itself" due to ground squeeze, and hanging wall breaks became more frequent in the days leading up to the landslide (Voight and Pariseau, 1978). No one actually observed the initial movement of the landslide on 29 April 1903, however, because it took place in the early hours of the morning. Unfortunately, both the Elm and the Frank landslides led to considerable loss of life, 115 people at Elm, 66 at Frank, despite the clear signs that the mountainsides were showing

Table 8. Historical Observations of Large Landslide Initiation

Name	Date	Observations	Reference
Mayunmarca, Peru	25 Apr. 1974	pre-slide creep	Kojan and Hutchinson, 1978
Huascaran 3, Peru	31 May 1970	earthquake trigger	Plafker and Ericksen, 1978
Vaiont, Italy	9 Oct. 1963	pre-slide creep	Müeller, 1964
Huascaran 2, Peru	10 Jan. 1962	no precursor effects	Plafker and Ericksen, 1978
Madison, MT	17 Aug. 1959	ground fissuring, earthquake trigger	Hadley, 1978
Khait, U.S.S.R.	10 July 1949	earthquake trigger	Solonenko, 1977
Gros Ventre, WY	23 June 1925	pre-slide noises	Voight, 1978
Frank, Alberta	29 April 1903	pre-slide noises	Voight and Pariseau, 1978
Elm, Switz.	11 Sept. 1881	pre-slide noises	Heim, 1882; 1932
Goldau, Switz.	2 Sept. 1806	pre-slide noises	Heim, 1932
Diablerets 2, Switz.	23 June 1749	pre-slide noises	Heim, 1932
Diablerets 1, Switz.	23 Sept. 1714	pre-slide noises,	Heim, 1932
Plurs, Italy	4 Sept. 1618	pre-slide noises,	Heim, 1932; Eisbacher and Clague, 1984
Corbeyrier-Yvorne, Switz.	4 Mar. 1584	pre-slide noises,	Heim, 1932

imminent signs of giving way. People could not grasp the possible magnitude of the coming events because long-runout landslides were not a recognized threat.

Rather similar warnings had preceded three large, naturally occurring Alpine landslides centuries prior to the events at Elm. At Corbeyrier-Yvorne, in 1584, an earthquake preceded the main landslide by three days. The earthquake shook loose a small carbonate landslide that fell onto an alluvial terrace below. Over the next two days, heavy rains soaked the area, saturating and overloading the rockfall-covered terrace. Three days after the earthquake, the skies cleared and workers returned to the fields, where they observed the opening of mud-emitting fissures on the terrace slopes and experienced constant earth tremors that brought down many additional rockfalls. Ultimately a moistened landslide broke loose from the hillside and swept across tended fields and through the villages of Corbeyrier and Yvorne, killing 330 persons (Heim, 1932; Eisbacher and Clague, 1984). The two Diablerets landslides, in 1714 and again in 1749 were also preceded by ominous signs from the source region. Creaks, pops and other noises originated near the glacier-covered Diablerets ridge prior to failure. The 20 x 10^6 m^3 1714 landslide fell onto a summer cattle pasture, killing 20 herdsmen. People fled the larger, second Diablerets landslide (Chapter II: Figure 2) in time, however, because the symptoms of the 1714 fall were repeated and understood by the local inhabitants (Heim, 1932).

Pre-slide events at Gros Ventre, Goldau and Plurs had a somewhat more insidious nature. In each place, the mountains had given signs of eventual failure for many years, but no one was quite prepared when the landslides eventually fell. At Gros Ventre, a local prospector predicted the landslide five years before the event from his observations of spring-fed waters disappearing into the upper surface of the slidemass (Voight, 1978):

> Yes, I have noticed that and I cannot see where the water can be going to unless it is following the formation between two different stratifications [Figure 21] and coming to the surface at some other water-level point. If not, this mountain side would be a mushy, woozy boil. However it may be, there is a wet line running between these stratas and the time will come when the entire mountain will slip down into the canyon below. For instance, some of these times, these earthquake tremors that are coming so often are going to hit at about the right time when the mountain is wooziest, and down she'll come.

Figure 21. Cross-section of the Gros Ventre landslide, Wyoming. The initial movement of the mass of soil-covered sandstone took place on a moist shale bedding-plane surface (Alden, 1928).

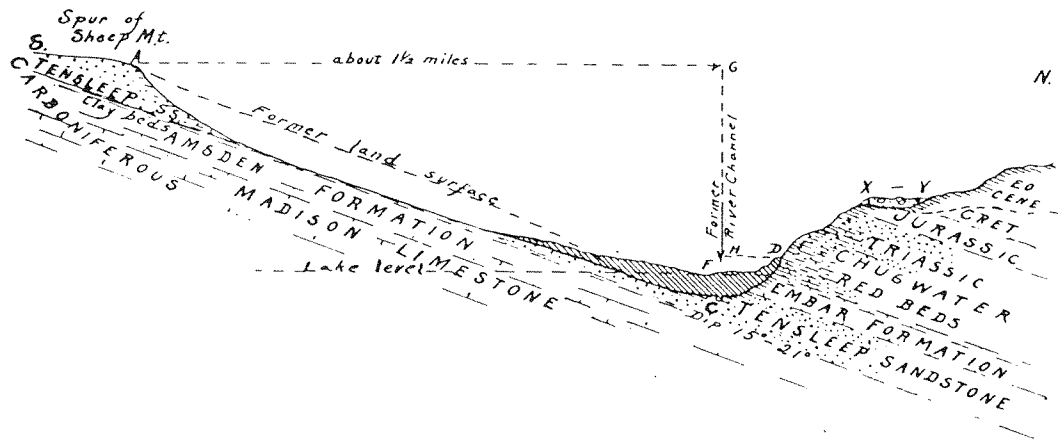
Spur of Sheep Mt.
about 1½ miles
N.
Former land surface
Former River Channel
TENSLEEP SS.
Clay beds
AMSDEN FORMATION
CARBONIFEROUS
MADISON LIMESTONE
Lake level
EOCENE
CRET.
JURASSIC
TRIASSIC
CHUGWATER RED BEDS
EMBAR FORMATION
TENSLEEP SANDSTONE
Dip 15°-21°
A
G
F
X
Y

On the day of the landslide, the symptoms became much more evident. Cracks opened and seepage began along a several hundred meter stretch of the Gros Ventre river at the base of the slidemass. The landslide initiated movement with a low rumble, a dust cloud and failure along the base of the hill along the riverbank (Voight, 1978).

Like the Gros Ventre slide, the Goldau landslide (Figures 20, 22) also gave many premonitions of eventual large-scale failure. For thirty years prior to the landslide, loggers on the mountain had noticed the growth of slowly widening cracks near the slidemass. In the months prior to the landslide, the cracks filled with water, and many roots could be heard snapping as the fissures widened. On the day of the landslide, new cracks opened, including some particularly large transverse fissures, and small rockfalls began and became continuous. Eventually, another transverse fissure opened low on the slope, triggering the large landslide that killed 457 persons despite the lengthy warning time (Heim, 1932).

As at Goldau and Gros Ventre, the hillslope that yielded the Plurs landslide had given years of advance warning. Ten years before the landslide, mining activity and clearing of the uplands initiated creep and the opening of fissures on the slope above the adits. Just prior to the landslide, a ten-day period of heavy rains drenched the area and probably overloaded the slope. On the morning of the landslide, persons tending the fields on the lower slope noticed ground vibrations, snapping and rumbling noises coming from the mountain and the agitated behavior of animals. Later that day one eyewitness observed a huge crack propagate across the slope. Unfortunately he was not believed, and the village of Plurs was wiped out by the landslide later that evening along with 1200 inhabitants (Eisbacher and Clague, 1984).

Two other large landslides, Mayunmarca and Vaiont, were not observed at emplacement but were nonetheless also observed to exhibit significant creep motion prior to the primary slope failure. At Mayunmarca, residents observed the progressive development of scarps, fissures and slumps starting four years prior to the landslide throughout a large portion of the source region (Kojan and Hutchinson, 1978). Similarly, three years of creep motion preceded the Vaiont landslide. Because the hillslope that failed bordered on the Vaiont reservoir, the creep rate was closely monitored and found to increase from millimeters to a few centimeters per day depending upon the elevation and

Figure 22. Cross-section of the Goldau landslide, Switzerland. Movement of the conglomeratic slide block began along a weak, valley-dipping bed of marl (Heim, 1932).

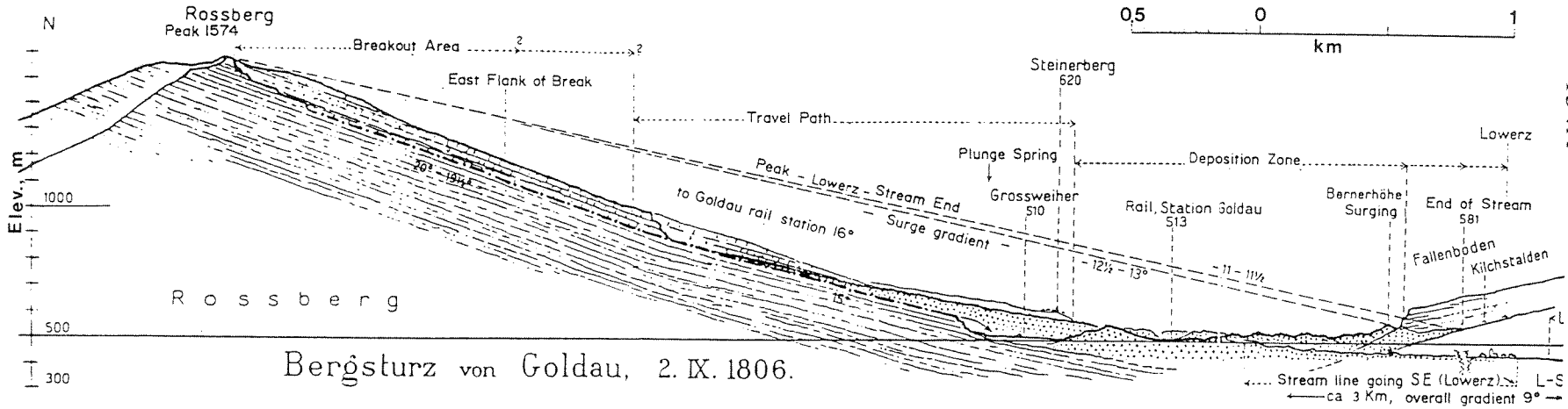

Bergsturz von Goldau, 2. IX. 1806.

rate of change of water level in the reservoir. On the day of the landslide, the creep rate had peaked at 20 cm/day (Müeller, 1964).

Based on data from six of the deposits described above (Table 9), I infer that the duration of pre-slide creep preceding catastrophic landslides relates strongly to the headscarp geometry. Goldau and Gros Ventre, which experienced the longest episodes of pre-slide creep, had the lowest slab thicknesses and smallest gradients, giving them the most stable initial slopes. The Frank and Diablerets 2 rockfall landslides, in comparison, had much greater slab thicknesses, larger slip-surface gradients and smaller slab contact areas and correspondingly low preparation times. The Vaiont and Elm landslides, with intermediate characteristics, experienced a moderate duration of pre-slide creep. The duration of pre-slide creep prior to failure is apparently a function of rock strength, stress per unit area and time, much as the case in metal fatigue (Carmichael, 1982). The detection of acoustical emissions during creep, as observed at several of the landslides described above, is actually an indirect way of monitoring crack growth and development. The rate of emissions correspond to changes in creep rate and style. Laboratory investigations of creep in brittle rocks indicate that creep takes place in two styles, an initial "hardening stage," during which creep rates decrease with time followed by a "stage of accelerating creep," in which creep rates increase continually with time until failure occurs. Microshocks are randomly located throughout the uniformly stressed sections of samples in the hardening stage, but in the accelerating stage they tend to localize on the future surface of failure. Because the observed acoustical emissions prior to rockfalls appear to increase with time until failure, the eyewitness accounts appear to me to document macroscale fracturing along the future failure surfaces of the rock masses during creep acceleration (Carmichael, 1982).

Although large landslides are often thought to be triggered by earthquake shocks, the available eyewitness accounts suggest that earthquake triggering is not an especially common phenomenon. Of the fourteen natural landslides listed in Table 8, only three, the Madison, Huascaran 3 and Khait events, definitely coincided directly with earthquake shocks. The Madison landslide (Figure 20) occurred almost immediately following the first and strongest shock of the M_S = 7.1 Hebgen Lake earthquake. The epicenter of the earthquake was located about 20 km east of the landslide (Hadley, 1978). The Huascaran 3 landslide also began almost as soon as the first tremors arrived

Table 9. In-Situ Characteristics of Large Rockfalls and Translational Landslides

Name	Preparation Time	Approximate Slide Block Dimensions: Thickness (meters)	Approximate Slide Block Dimensions: ContactArea (sq. meters)	Contact Slope (degrees)	References
Goldau	30 yr	70	500,000	20	Heim, 1932
Gros Ventre	5+ yr	70	550,000	20	Voight, 1978
Vaiont	3 yr	125	2,000,000	0 - 40	Müeller, 1964
Elm	3 yr	90	110,000	45	Heim, 1932
Frank	7 mo	100	300,000	35	Cruden and Krahn, 1978
Diablerets	2 days	200	150,000	30 - 65	Heim, 1932

from a M_S = 7.7 subduction zone earthquake originating 130 km west of Nevados Huascaran mountain (Plafker and Ericksen, 1978). A M_S = 7.7 earthquake triggered the Khait landslide as well; ground shaking at the site of the slope failure had a Modified Mercalli Index above 8 (Gubin, 1960).

In each of these three landslides, the slidemasses that collapsed seem to have reached high degrees of instability by the time they were struck by the triggering earthquake activity. The available evidence suggests that these landslides would have eventually taken place even in the absence of seismic shocks. Aerial photographs of the Madison landslide area taken in 1956, for example, show that creeping movements had already begun on at least three breaks, each of 100 m or greater length, parallel to the eastern edge of the slide (Hadley, 1978). Similarly, the massif which collapsed to form the Huascaran 3 landslide in 1970 had been photographed eight years earlier by a glaciological expedition. Their observations showed that the rock exposed in the face after the January 1962 Huascaran 2 landslide was pervasively fractured, with a system of open sheet joints oriented roughly parallel to the face. The collapse of the lower part of the face in 1962 had left a tremendous 1 km-high overhanging cliff, suggesting to expedition members the potential of a future rockfall even larger than the 1962 landslide. The subsequent 1970 rockfall had a volume between three and seven times that of the 1962 landslide (Plafker and Ericksen, 1978). At Khait, paleoseismic evidence gathered after the earthquake and landslide provided evidence that two similar collapses had occurred in the same location previously and that the district center built in the way was condemned to destruction by its placement. In fact, new rock masses are near to collapse for the fourth time, and may be triggered in the next large earthquake to hit the region (Solonenko, 1979). Thus, even though earthquakes may trigger large landslides, much gradual preparation of a slope must occur prior to the shock to prepare it for failure.

The two remaining large observed landslides, the Gohna and Huascaran 2 deposits, apparently gave no observed indications of imminent failure and were not triggered by seismic activity, though the Gohna landslide did occur during a three-day period of heavy rains (Holland, 1894; Plafker and Ericksen, 1978). Both landslides originated in remote locations, however, suggesting the possibility that creep movements, noises, etc., might have preceded the landslides without notice. The Huascaran 2 landslide, though initiated in a remote location, fell into a river valley and moved rapidly down a valley into

the community of Ranrahirca, killing 4000 persons (Plafker and Ericksen, 1978).

Summary

Slope preparation and its gradation to slide initiation forms the first stage in the chronology of a large landslide. This initial stage is controlled both by slidemass characteristics as well as by those external processes that increase the shearing stresses or decrease the shearing resistance of slope materials and trigger landslide motion. Eyewitness accounts of large landslide initiation document the gradation from slope preparation to the initiation of rapid sliding or falling movement of the large slidemasses.

Elevated regions shed large landslides for a variety of reasons. These include potential source rock lithology and structures, as well as the long-term tectonic and climatic environments in which the highlands are located. One characteristic feature of large landslide deposits I have documented is that their volume and their headscarp forms are related properties. Large bedrock landslides with volumes greater than about 10^{10}-10^{11} m^3 usually have slump-type headscarps, while bedrock landslides in the volume range of 10^5-10^9 m^3 typically exhibit rockfall-type, or, on Earth, translational headscarp forms. Giant slumps form in regions of high relief having an absence of basin-dipping structural discontinuities. These generally form when a potential slip surface can intersect a major, tectonic-scale bedrock discontinuity. Apparently this only occurs at large scales, leading to the observed predominance of slumps at volumes greater than ~10^9 m^3. On Earth, another characteristic feature of large landslides is that most consist of a single dominant lithology. Most of the terrestrial monolithologic landslides consist of limestone, and most of these occur in arid climates and in glacially eroded highlands. Elsewhere, monolithologic landslides occur when single rock types outcrop over a large, tectonically active regions. A number of critical source region geologic structures also play a role in the development of large landslides. On Earth, the important structures include sloping bedding planes, faults, foliation and fold axes. The headscarp locations of large martian landslides are also often correlated with major geologic structures. In particular, they concentrate in impact craters and where high chasma slopes intersect plateau-surface structures such as impact craters, graben-bounding faults, wrinkle ridges, and, possibly, dikes and sills.

Thus, elevated regions having certain lithologies, structural relations and tectonic and climatic histories form favorable sites for the development of large landslides. In addition to these source characteristics, a number of processes act on favorable slopes to prepare restricted areas for large-scale failure. These properties include those that increase the shearing stresses on a slope, such as the removal of lateral support, increased loading, transitory earth stresses, volcanic oversteepening, dike intrusion and differential erosion, as well as those that decrease the shearing resistance of slope materials, such as pore water pressure increases, weathering, creep and fracture development.

The actual kinematics of the transition from preparation to initiation caused by the long-term action of these processes cannot readily be discerned from a study of a landslide deposit or its source area. Eyewitness accounts of large landslide initiation thus provide an important source for understanding this critical gradational phase. The common theme of these accounts is that large landslides are often foreseeable because they are usually preceded by noises, ground fissuring, small-scale earth movements and other phenomena related to the accelerating creep of a slidemass prior to catastrophic failure. This is even true of landslides triggered in large earthquakes. In the absence of an earthquake trigger, the duration of creep preceding catastrophic failure may vary from a few days to tens of years, depending on the thickness of the potential slide block and the geometry of the potential detachment surface.

3. *Runout Phase*

The runout phase comprises the second step in the chronology of a large landslide. It is the most important, but also most poorly understood step. The discussion here of the runout phase starts with a highly detailed description of the everpresent, common and rare depositional characteristics associated with this phase in the movement of large landslides. The effects of differing substrate properties on the observed depositional characteristics are also described, together with a facies model of long-runout landslide sedimentology (extended from that of Yarnold and Lombard, 1989) that places many of these observations into their stratigraphic context within the bodies of large landslide debris streams. Description of the runout phase concludes with eyewitness accounts of the long-runout motion of large landslides as ground-

hugging debris streams and the numerous associated phenomena that accompany their movement.

Depositional Characteristics

Eighteen runout-phase depositional characteristics are described below. These features most likely originated during the runout phase, but may have also occurred to some degree in the gradationally following stopping phase. These observations are subdivided into three groups: characteristics common to all large landslides, those features common to many landslide deposits, and other depositional characteristics shared by only two or three large landslide deposits. This section concludes with a facies model of arid climate long-runout sedimentation (Yarnold and Lombard, 1989) and how I infer the model might vary for different climates. The model places the various depositional characteristics described in this section into their context in the body of a large landslide deposit.

Two of the runout-phase depositional characteristics listed in Table 10 are **everpresent** in large landslide deposits: brecciated rock and cohesive movement behavior. Brecciated rock composes the first everpresent characteristic of large landslides. Landslide breccia is commonly angular, randomly oriented, very poorly sorted and sometimes displays voidspace between the fragments. Clast sizes range from coherent blocks tens to hundreds of meters on a side, down to rock flour (Figures 23a-c). Generally, the larger the landslide, the more compact is the packing of rock flour and clasts (Heim, 1932). The debris in a large landslide behaves in a brittle fashion and clasts often exhibit conchoidal fractures and percussion marks (Heim, 1932). Sometimes the rock in a large landslide can be so severely sheared that rock flour produced in the process behaves locally in a rather fluid manner. This is illustrated in Figure 23c, where microscopic grains are seen to float in and be intruded by a fine, mobile groundmass. This fine grain size fraction is apparently rather mobile on a larger scale as well. For example, in the lithologically-banded Bualtar 1-3 landslide deposits, Hewett (1988) found that the fine grain size fraction consists primarily of the same materials as the surrounding coarse fraction, but that in addition the fines contain a significant admixture of "exotic" minerals from other lithologic bands (see below). X-ray diffraction and grain size analyses indicated that powdered talc, calcite and chlorite grains smaller than intermediate sand had diffused to all

Table 10: Runout-Phase Depositional Characteristics of Large Landslides

I. Everpresent:

A) Brecciated rock, very poorly sorted, locally ungraded, ranging in size from huge blocks down to rock flour;

B) Cohesive nature of movement and deposition, exhibiting distinct deposit borders.

II. Common (number and names of deposits with characteristic in parentheses):

A) Terrain mantling in the zone of deposition (**all but heavily confined**);

B) Preserved stratigraphy, either 1) slope-normal bedding (**7**: Bualtar 1-3, Elm, Madison, Silver Reef, Usoy), 2) slope-parallel bedding (**15**: Ales mb, El Capitan, Goldau, Gros Ventre, Hope, Rockslide Pass, Saidmarreh, Sherman, Vesuvius 1-7), or 3) cross-slope bedding (**2**: Parpan, Tin Mtn.) (**24 total**);

C) Reverse grading (**19**: Adair Park mb, Avalancha del Zarzo 1-2, Black Canyon mb, Blackhawk, Bualtar 1-3, Cross Hill mb, El Capitan, Frank, Goldau, Gros Ventre, Loma de la Aspereza, Loma Redonda, Madison, Martinez Mtn., Saidmarreh, Sherman);

D) Incorporated substrate material mixed into debris: 1)Inert (**10**: Adair Park mb, Artillery Mtns. mb, Black Canyon mb, Blackhawk, Buckskin Mtn. mb, Cross Hill mb, El Capitan, Puget Peak, Sherman, Tahoma Peak) and 2) Mobile (**6**: Carlson, Frank, Huascaran 2-3, Mageik, Simplon) (**16 total**);

E) Three-dimensional jigsaw puzzle breccia (**15**: Adair Park mb, Artillery Mtns. mb, Avawatz Mountains mb, Black Canyon mb, Blackhawk, Buckskin Mtn. mb, Carlson, Cross Hill mb, El Capitan, Pungarehu, Sherman, Silver Reef, Split Mtn. mb, Tin Mtn., Vallecito Mtns. mb,);

F) Spattering of rock, dust or ice beyond the margins of the deposit (**11**: Allen 4, Altels, Avalanche Lake, Damocles, Elm, Huascaran 3, Mayunmarca, Nozzle, Puget Peak, Schwan, Triple);

G) Proximal trough, separating main deposit from base of cliff or scar (**11**: Angarakan, Disentis, Elm, Hope, Kandertal, Koefels, Madison, Medicine Lake, Parpan, Poschaivo, Usoy);

H) Dozed marginal ridges (**7**: Avalanche Lake, Blackhawk, Elm, Frank, Plurs, Sherman, Silver Reef);

I) Proximal-Distal size decrease, an average change occurring gradationally (**7**: Bandai Volcano, Carlson, Mt. Shasta, Mt. St. Helens, North Nahanni, Panum, Pungarehu);

J) Oriented clasts (**6**: Carlson, Chaos Jumbles 1-3, Sawtooth 2, Sherman);

Table 10, con't.

K) Block bands, either 1) radial (**4**: Carlson, Elm, Hope, Sherman), or 2) concentric (**1**: Bualtar 2); (**5 total**)

L) Striations (**4**: Adair Park mb., Ales mb, Black Cyn. mb, Martinez Mtn.).

III. Rare (number and names of deposits with characteristic in parentheses):

A) Rock-crested hummocks (**3**: Carlson, Mt. Shasta, Pungarehu);

B) Foliated texture, displaying aligned tabular fragments (**3**: Adair park mb, Blackhawk, Bonelli Peak mb);

C) Clast rounding (**2**: Altels, Pungarehu);

D) Fused rock (**2**: Koefels, Langtang).

Figure 23a. Large boulder on the surface of the Martinez Mountain landslide. Compare with breccia from lower reaches of same landslide in Figure 23b. The boulder has a tough, smooth surface that develops thick coatings of desert varnish. The good condition of the boulder suggests that it was transported the several kilometers from the source region on top of the landslide and thus experienced little abrasion.

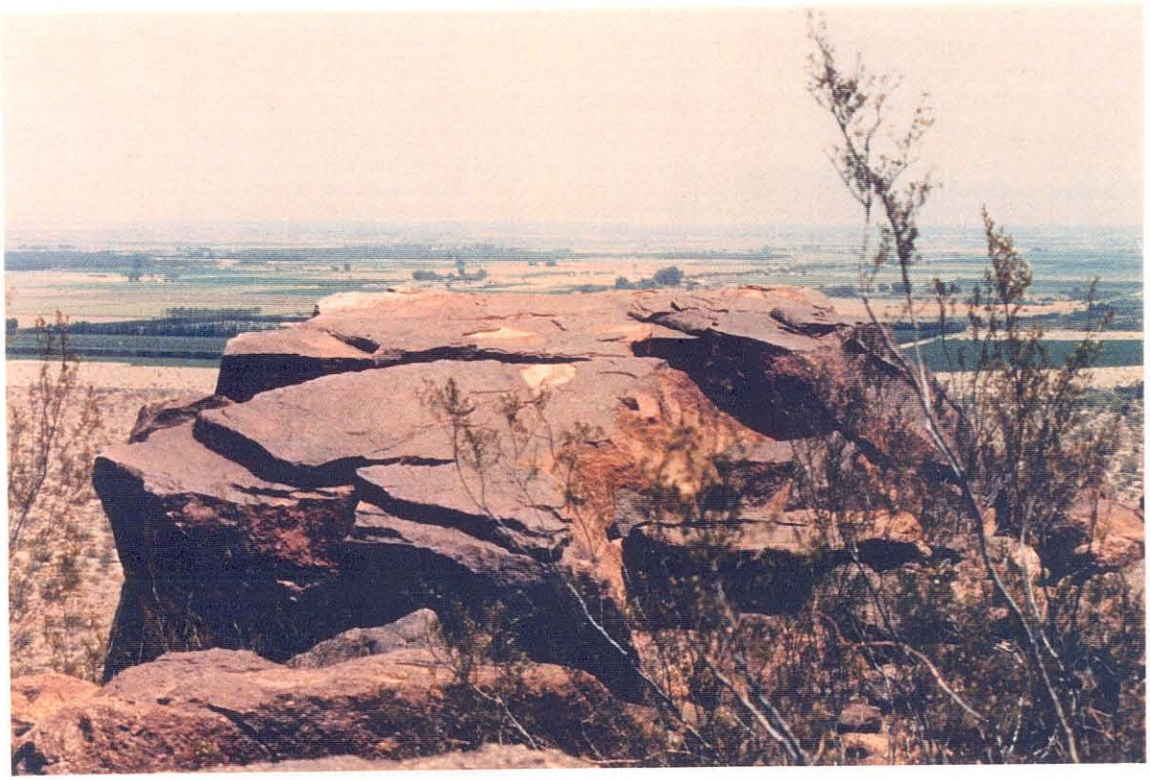

Figure 23b. Granite gneiss landslide breccia in an exposure very close to the boulder in Figure 23a on the Martinez Mountain landslide. Lens cap provides scale. Debris below the surface of the slide exhibits significantly greater abrasion, rounding of edges and smaller grain size than clasts forming the surface of the slide.

Figure 23c. Photograph of thin section of granite gneiss microbreccia sampled from near the base of the Martinez Mountain landslide. The groundmass apparently acted rather fluidly during travel of the landslide with respect to fractured microscopic grains, as indicated by the observation that microscopic grains float in and were intruded by the highly mobile fine-grained component. Width of field of view approximately 8.5 mm.

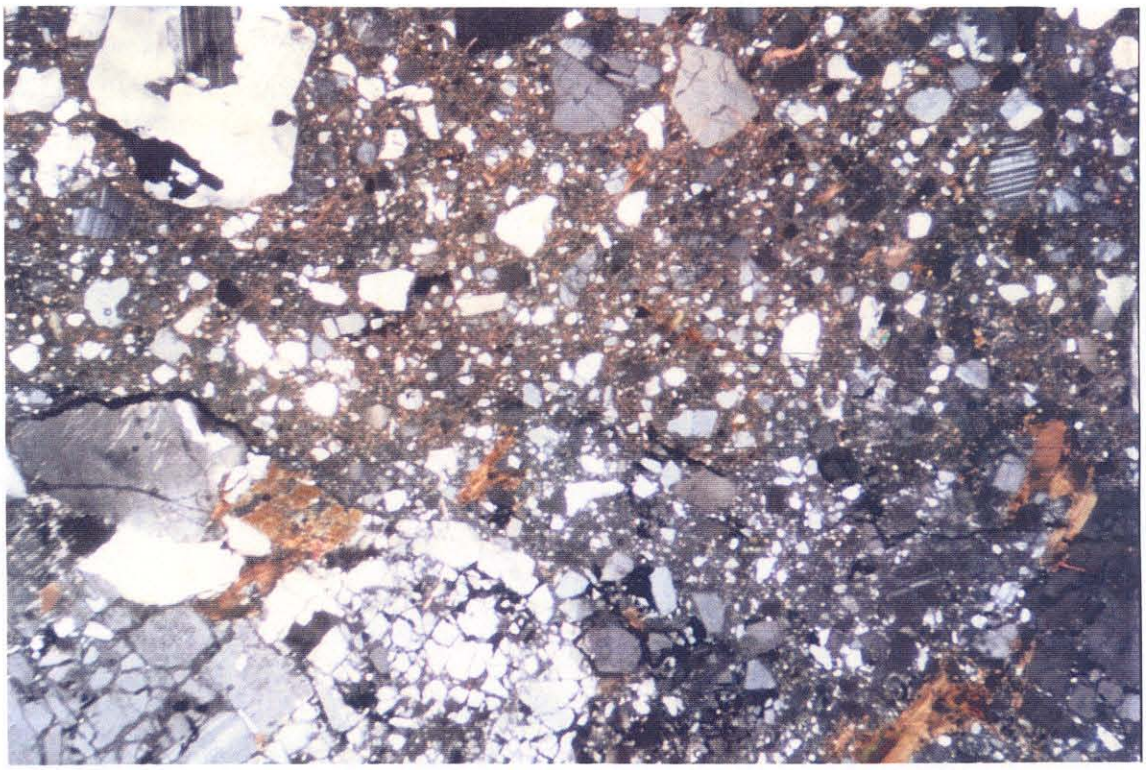

parts of the deposits, while coarser particles (greater than ~0.25 mm in diameter) had not. The fine grain size fraction in the Silver Reef landslide also appears to have exhibited excessive mobility at emplacement. The toe and basal parts of the carbonate landslide contain significant quantities of gold- and silver-bearing red hematite-stained gouge inherited from the lower part of slide block that formed the landslide (Dibblee, 1964; Shreve, 1968a). Part of the gouge was apparently transported at the leading edge of the landslide as it decended the slope, while some was smeared out along the basal contact (Figure 28). Shearing of the gouge mobilized the material sufficiently for it to form a red hematite-stained matrix in the limestone breccia. In fact, silver bromide, silver chloride and subordinate gold have been mined from the matrix of the landslide from open cuts and shallow adits (Dibblee, 1964).

The other everpresent feature of large landslides is their cohesive nature during movement. They typically exhibit very distinct margins beyond which little scattering of rock debris occurs. Along the margins of a fresh deposit, in fact, undamaged pastureland or a road may lie only one meter from the edge of a landslide that measures tens of meters in height (Heim, 1932). The cohesive nature of large landslides may relate to the presence of cohesive rock flour situated between the clasts in a large landslide (Figure 23b), formed by the interactions between constituent clasts during travel. The margins of large landslides typically stand at or below the angle of repose of loose, granular material, at about 25° to 35°.

The following **common** depositional characteristics apply to significant subsets of the landslides in Appendix A:

Terrain mantling: refers to the observation that, except for heavily confined deposits, large landslides commonly display sheet-like geometries and have a primarily depositional, rather than erosional, nature. With low thicknesses compared to their areal dimensions, with ratios commonly lying in the range of 1/100 to 1/1000, and with minimal erosivity, the landslides mantle the underlying surface and may reflect many of its original irregularities. This generality only fails in heavily confined landslides and in the proximal regions of very large landslides, where great thicknesses of material may completely bury the original topography.

Preserved stratigraphy: Large landslides encompassing multiple lithologies characteristically retain, in the final deposit, the relative geometric distribution of rock types present in the initial slidemasses prior to emplacement. Variations in the outcrop patterns of rock types in the headscarp lead to different distributions of lithologies in the final deposit (Table 10; Figure 24). Slidemasses containing multiple lithologies that intersect a slope at a high angle (Figure 24a) yield a landslide deposit composed of proximally- to distally-zoned breccia lithologies. The uppermost stratum on the slidemass comes to rest at the head of the landslide deposit, while the lowermost unit forms the toe of the slide. The Elm landslide provides an example of this behavior (Heim, 1932). Landslides derived from slope-parallel strata also maintain the stratigraphic relations of the headscarp, with the surficial layer on the slope generally forming the uppermost portion of the landslide deposit (Figure 24b). The El Capitan landslide provides the best example of this geometry (Krieger, 1977). Similarly, landslides formed from bedrock outcrops which vary in lithology across slope give rise to deposits lithologically zoned transverse to the movement direction (Figure 24c). The Tin Mountain landslide provides an example of this third type of geometry (Burchfiel, 1966). The slope-normal and slope-parallel preservation of stratigraphy illustrated in Figures 24a and 24b were previously recognized for the constraints these geometrical relationships placed on the kinematics of movement of large landslides (Shreve, 1968a; Krieger, 1977). The recognition here that cross-slope headscarp stratigraphy is also preserved gives these previous ideas much greater significance. These data together strongly illustrate that no large-scale mixing of landslide debris occurs in any dimension within large, dry, long-runout landslides. The stratigraphy of the final landslide deposit corresponds to the original three-dimensional stratigraphy of the in situ slidemass which has undergone extensive movement-parallel extension, minor transverse extension and significant thinning in the slope-normal dimension. Similar behavior is presumed to occur in most or all monolithologic landslides, but cannot be observed due to the lack of contrasting rock types.

Reverse grading: A number of partially eroded large landslide deposits expose an upward-coarsening texture at interior exposures. The manifestation

Figure 24. Illustration of different styles of preserved stratigraphy in large landslides.

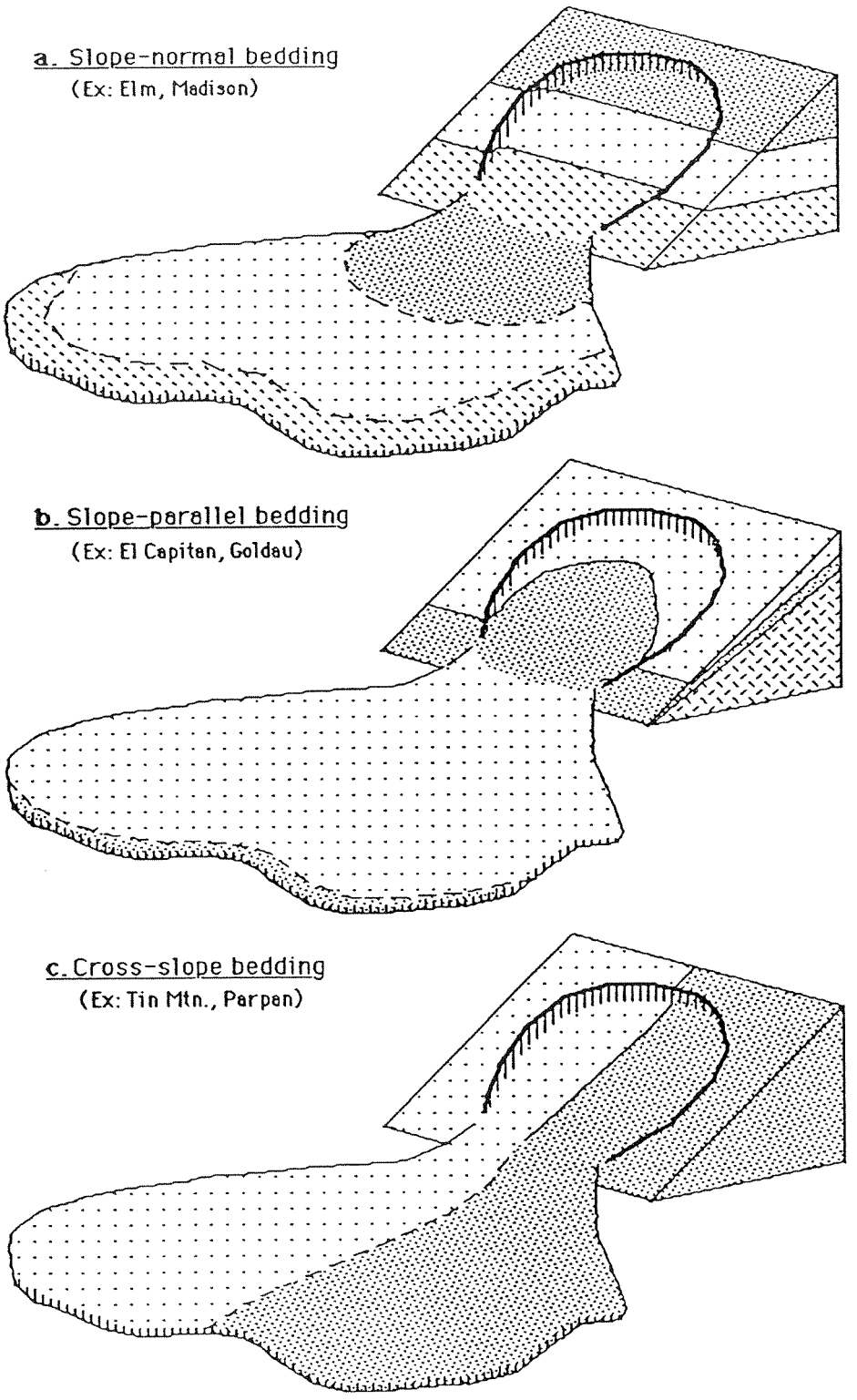
a. Slope-normal bedding
(Ex: Elm, Madison)
b. Slope-parallel bedding
(Ex: El Capitan, Goldau)
c. Cross-slope bedding
(Ex: Tin Mtn., Parpan)

of reverse grading varies somewhat between deposits and from area to area within individual deposits. Reverse grading appears to me to have two gradational endmembers. One endmember exhibits a continuous upward-coarsening texture from the base to the surface of the deposit, with rock flour concentrated at the base and large clasts or blocks situated on the surface of the deposit (Figure 25). The other endmember exposes fine-grained, ungraded breccia all the way from the base of the deposit to very near the surface, but also has larger clasts or blocks mantling the surface (Figure 26). In both cases a relatively sharp break in average grain size appears to occur between subsurface materials and the clasts or blocks littering the surface. In all cases I submit that the large surficial blocks originated at the surface of the initial slide block rather than having arrived there during emplacement as a result of upward migration from the interior. This is supported in part by evidence from landslides in slope-parallel strata (Figure 24b). In these landslides, the surface and basal strata of the in situ slidemass respectively form the top and base of the final landslide deposit. The large clasts surfacing these landslides fail to show the mixed lithologies that would be expected if large clasts migrated upwards from the basal strata during emplacement. In addition, I note that most of the blocks topping large landslides fail to show the degree of abrasion observed on clasts within the deposits (Figure 23), again suggesting to me that these large blocks do not originate below the surface.

Incorporated substrate material: Large landslides apparently may incorporate materials which they overrun in their downhill course. While most of the field evidence from these deposits suggests that they are non-erosive to moderately erosive, where they can be shown to erode their bed, strata below the depositional contact may be sliced off along a razor-sharp edge (Yarnold and Lombard, 1989). When the material picked up by a large landslide is relatively "inert," such as rock, alluvium or dry snow below the melting point, the debris appears to get trapped along the basal contact of the landslide, where it mixes slightly with landslide debris (Shreve, 1966; Bull and Marangunic, 1967; Yarnold and Lombard, 1989). It can also be partially mobilized to the extent that the material intrudes the landslide debris as small clastic dikes (see below). However, if the picked-up material is sufficiently mobile it can mix into the body of the landslide debris and transform the entire nature of the landslide (Plafker and Ericksen, 1978; Appendix B).

Figure 25. Photograph of interior exposure of the El Capitan landslide, Arizona, demonstrating the reverse-grading endmember behavior which exhibits a gradual grain size increase from the base upwards. The landslide breccia in this exposure is composed of Devonian dolomite. Sliding occurred in the Miocene (Krieger, 1977).

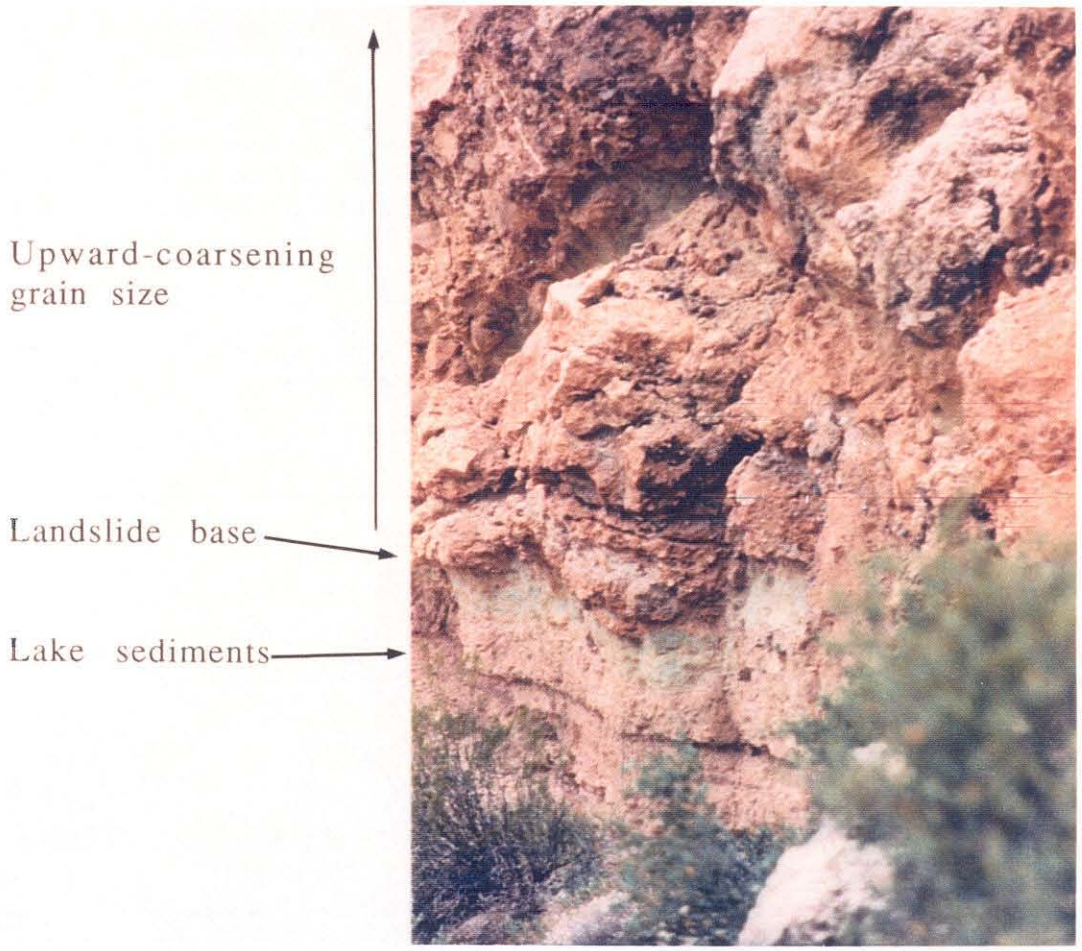
Upward-coarsening
grain size
Landslide base
Lake sediments

Figure 26. Exposure of the internal structure of the Martinez Mountain landslide, southern California. This portion of the landslide exhibits a surface layer of boulder gravel that overlies an ungraded region of pulverized granite gneiss.

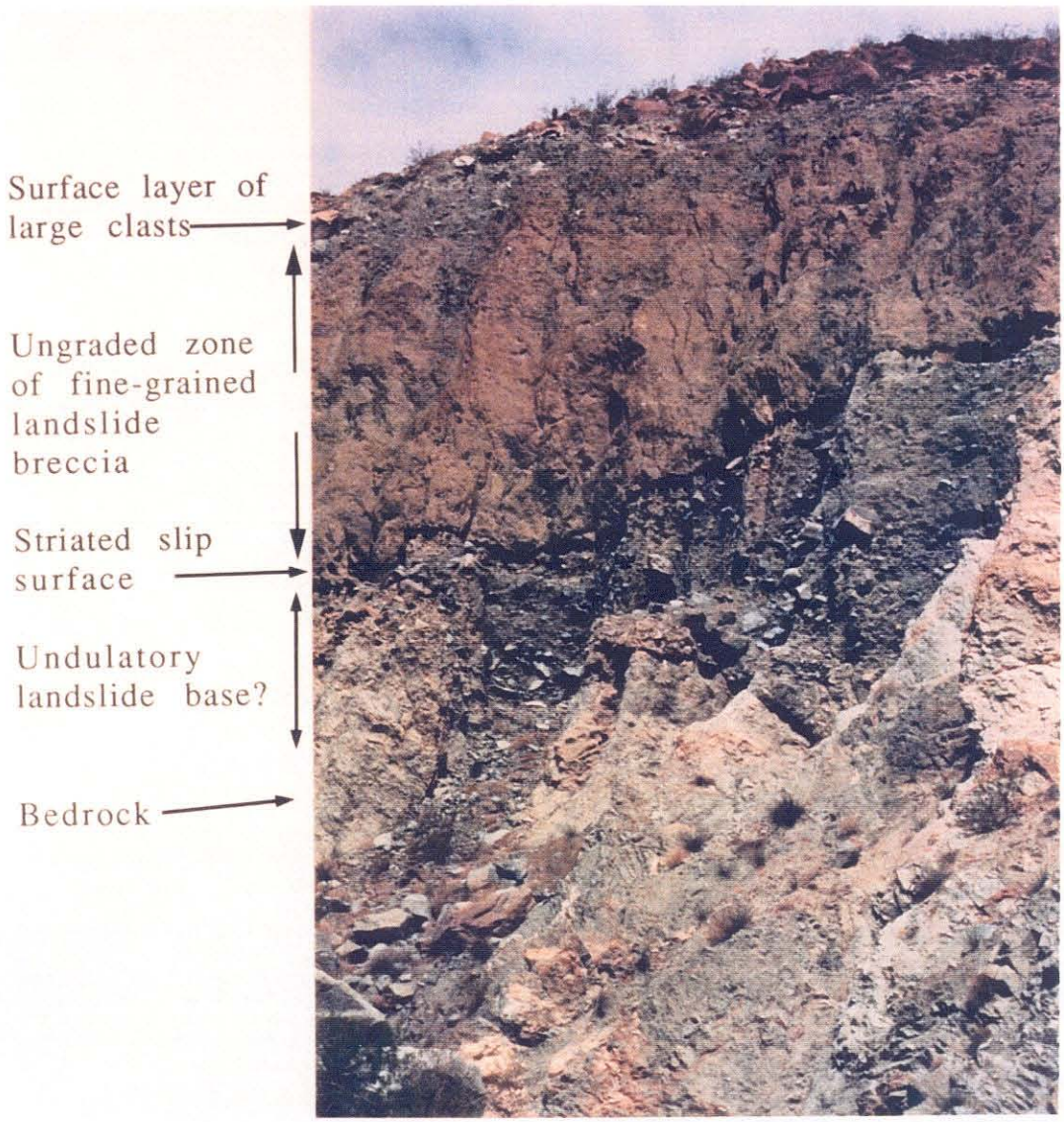
Surface layer of large clasts
Ungraded zone of fine-grained landslide breccia
Striated slip surface
Undulatory landslide base?
Bedrock

Examples of "mobile" materials include water, wet snow near the melting point, mud and moist sand.

Three-dimensional jigsaw puzzle breccia: The breccia composing large landslide deposits grades from large blocks, which may resemble in situ bedrock, down to pebbles and rock flour. One relatively common type of breccia consists of lenticular zones of variable size, in which the individual fragments are all apparently pieces of a pervasively shattered single source block. The individual fragments fit loosely together, sometimes separated by thin bands of matrix material, but exhibit little relative rotation, so that color bands and lithologic fabrics appear traceable and continuous throughout the zone. They may be "put together" as in a jigsaw puzzle (Shreve, 1987; Yarnold and Lombard, 1989). Fourteen large fresh and eroded landslides contain jigsaw-puzzle breccia, which generally occurs in, and may dominate, the upper reaches of a landslide deposit below the surface (Yarnold and Lombard, 1989). Shreve (1968a) and McSaveney (1978) believed that this material formed by the high-speed impact of landslide debris onto a depositional plain following a rockfall episode, after which the shattered fragments remained undispersed because of a lack of further relative movement internally as the landslide debris spread out and deposited. An alternative origin for the brecciation is that it forms because of rapid unloading of deeply buried rock during a rockfall episode (Albee, personal communication, 1991).

Spattering: Several large landslides spattered debris beyond their margins during emplacement, forming deposits that contrast sharply with the cohesive breccia landslide debris stream deposits. The spatter deposits consist of ice, rocks, soil and/or vegetative debris which discontinuously litter the surface surrounding the margin of a large landslide. The zone of spattering may extend up to a distinct margin, or it may become gradually less concentrated away from the landslide. The spatter deposits can only be recognized in fresh deposits. One, the Altels ice landslide, apparently left no lasting deposit; its characteristics were recorded just after the event. The spatter deposits vary greatly from deposit to deposit depending on the fall height and path regularity; the greater the fall height and path irregularity, the greater the spattering. The spatter deposits form from debris expelled from the cohesive debris stream, typically due to an irregularity in the travel path. This debris is

transported ballistically or is caught in an air blast and propelled to the spatter deposition zone. Spatter zones with distinct margins may extend several hundred meters from the edge of a landslide. In comparison, boulders ejected from the Huascaran 3 landslide, which had no distinct spatter-zone margin, traveled up to 4000 m from their ejection point (Plafker and Ericksen, 1978).

Proximal trough: Numerous large, heavily confined landslides exhibit a distinct proximal trough transverse to the movement direction of the slide. The trough occurs at the base of the steep initial portion of the fall path. In contrast to the normal expectation that the main mass of landslide debris should come to rest at the base of the slope from which it fell, these heavily confined landslides instead pile up on the opposite side of the valley, leaving the proximal trough behind as the lowest portion of the landslide surface (Figure 27). As a result, the new gorge of a valley blocked by a large landslide usually lies close to the break-away side, the rubble heap being on the opposite side covering the old course (Heim, 1932).

Dozed marginal ridges: Many large landslides apparently have the capacity to scour the surface over which they travel, removing anything in their path above the ground surface and sometimes excavating material from beneath the surface as well. Much of this material gets caught at the leading edges of the landslides, like scoured soil piled before the blade of a bulldozer. Proximally-thinning wedges of dozed material have been observed to form the leading edges of several historical landslides, and have been interpreted from prehistoric landslides on the basis of exposures of dozed substrate along and within the toes of these deposits (Figure 28; Shreve, 1966; 1968a; Eisbacher, 1979). The dozed material may mix somewhat with the trailing landslide debris. A remarkable array of detritus overrun by large historical landslides was later found in the moraine-like ridges surrounding them. Ridges surrounding the Elm, Goldau and Plurs landslides, for example, yielded fragments of destroyed houses, partially recognizable personal possessions and the dismembered and crushed remains of humans and animals all churned up with scoured soil. In addition, the marginal dike around the Elm landslide was found to contain utensils from the basement and attic of two overrun houses, a rope ladder, and a water pipe originally buried one meter below the surface that was carried

Figure 27. Diagram illustrating the proximal trough observed in numerous large, heavily confined landslides and the effects of this geometry on a drainage system blocked by a large landslide (Heim, 1932).

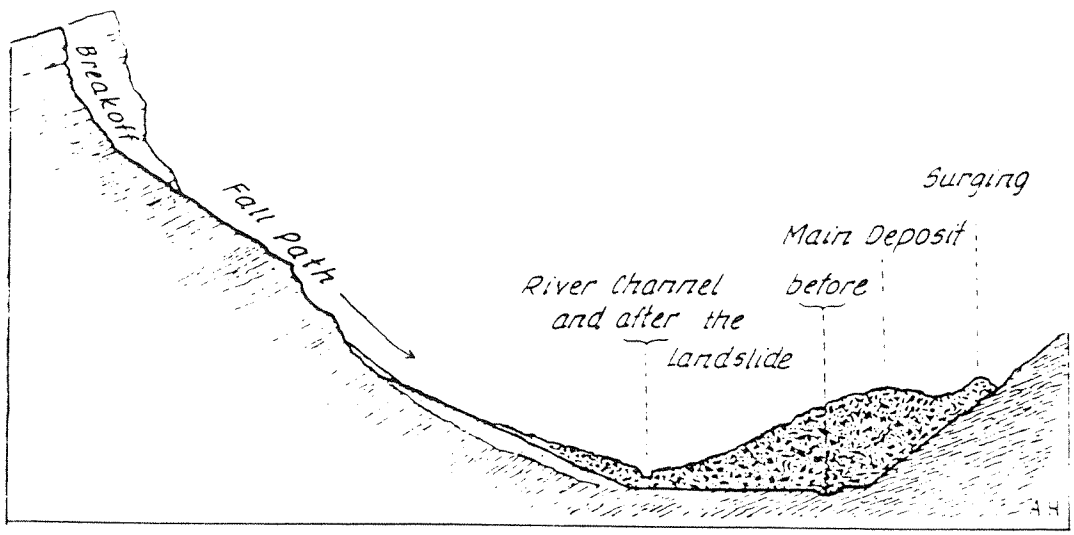
Breakoff
Fall Path
Surging
Main Deposit
before
River Channel
and after the
landslide

Figure 28. Bulldozed distal heap of material (stippled) at the toe of the Blackhawk landslide, southern California. Movement direction was from left to right. Hatched pattern indicates substrate material. The distal heap apparently came to rest first, forcing the trailing limestone breccia sheet to ramp up behind it and causing imbrication of the distal reaches of the landslide (modified from Shreve, 1968a).

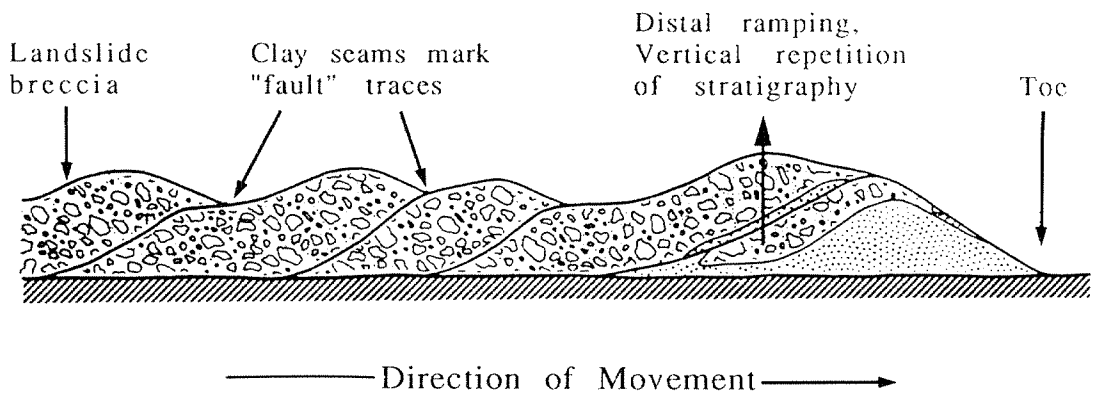
Landslide breccia
Clay seams mark "fault" traces
Distal ramping, Vertical repetition of stratigraphy
Toe
Direction of Movement

1400 m by the landslide (Heim, 1932). Likewise at Frank, a railroad tie from an overrun section of track occurred in the dozed dike surrounding the landslide, though the distal accumulation consisted primarily of mud rather than soil (Shreve, 1968a). Similarly, the distal margin of the Sherman landslide consisted of a mixture of landslide debris, snow ploughed from the surface of the Sherman glacier and wood fragments from a forested ridge overtopped by landslide debris (Shreve, 1966).

Proximal-to-distal size decrease: Large landslides may exhibit a proximal-to-distal decrease in average grain size, either by way of an increasing matrix-to-clast ratio or simply via a diminution of the average clast size between the headscarp and the toe. All of the landslides known to exhibit this characteristic formed in volcanic materials, though suggestions of this effect have been noted in some non-volcanic landslides as well (Heim, 1932; McSaveney, 1978). This observation does not include landslides or portions of landslides that transitioned into water-saturated debris flows in the course of movement, such as the Huascaran 2 and 3 landslides and portions of the Mt. St. Helens landslide. Two mechanisms appear responsible for this grain size decrease, debris milling and the incorporation of mobile, fine-grained substrate materials into a landslide during transport.

Oriented clasts: Several large landslides exhibit preferred orientations of larger surface clasts. The oriented clasts usually occur with their long axes nearly paralleling the local surficial topographic gradient, presumably the direction of landslide motion at those points (Figure 29; Eppler, et al., 1987). Although the long axes normally parallel the movement direction, some clasts on the Sherman landslide exhibited movement-normal orientations as well (McSaveney, 1978). The oriented surface clasts clearly indicate the transmission of basal and/or marginal stresses to the surfaces of these landslides during movement; the surficial debris did not travel as undeforming "rafts" of material. The strong fabric on the surfaces of these landslides presumably gives an indication of the stress regime that acted there during emplacement of the landslides. Apparently, the primary compressional stresses (minimum tensional stresses) acted normal to the movement direction, while minimum compression (maximum tension) acted in the travel direction.

Figure 29. This diagrams shows rose diagrams indicating the azimuths of surface clasts >0.5 m in diameter on the Chaos Jumbles I-III landslides, illustrating the dominant movement-parallel fabric of the surficial debris. The solid and dashed lines give the perimeters of the three overlapping landslides, the largest and oldest being deposit I. The landslides all originated at the lower right (southeast) in the progressive wasting of a dacite dome, and travelled to the upper left (northwest). Diagram modified from Eppler, et al. (1987).

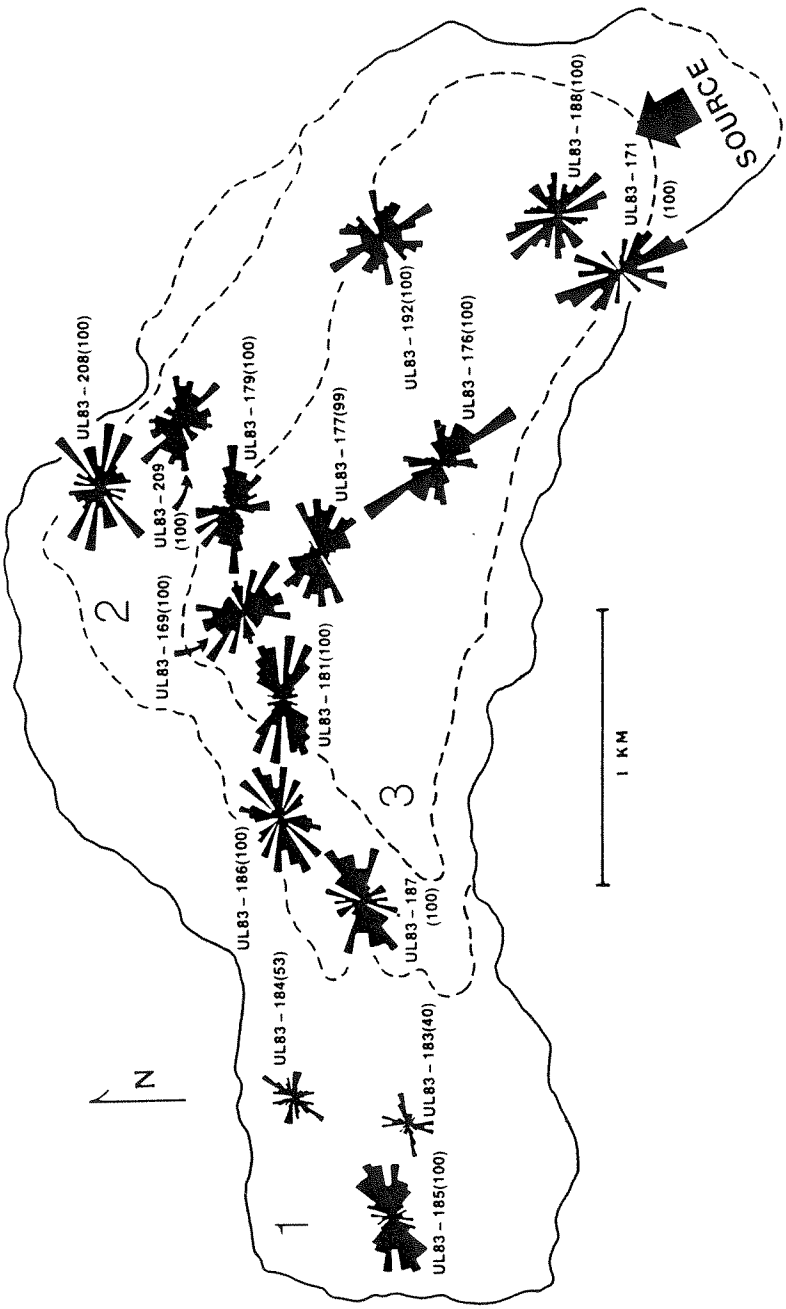
SOURCE
UL83 – 171 (100)
UL83 – 188(100)
UL83 – 192(100)
UL83 – 176(100)
UL83 – 177(99)
UL83 – 179(100)
UL83 – 209 (100)
UL83 – 208(100)
UL83 – 169(100)
UL83 – 181(100)
UL83 – 186(100)
UL83 – 187 (100)
UL83 – 184(53)
UL83 – 183(40)
UL83 – 185(100)
1
2
3
1 KM
N

Block bands: Several relatively fresh landslides exhibit bands of large boulders distributed on their surfaces in distinct radial or concentric patterns, most commonly the former. The boulders forming a band normally share a common lithology, and sometimes have a preferred orientation (see above). On the Carlson landslide, which exhibits a longitudinally ribbed morphology, the boulders usually occur in rows cresting the ribs and adjacent lateral levees, with few boulders lying in the intervening troughs (Appendix B).

Striations: A few partially eroded landslides display distinct striated textures along their bases. In some cases, boulders distributed near the base have striations etched into their surfaces at various orientations (Yarnold and Lombard, 1989). Elsewhere, such as in the Martinez Mountain landslide, a distinct, laterally continuous slide plane exists that is marked by downhill-parallel striations (Figure 30). The striations generally appear to form at the interface between the moving landslide debris and the substrate, but possibly they may also form along slide planes within a moving landslide. It appears that boulders may develop striae along a face while it is situated along a slide plane. Subsequently it may rotate relative to the slide plane and develop striations on another part of its surface, so that a boulder near the base may display a variety of striae orientations across its surface.

In addition to the common characteristics described above, a number of comparatively **rare** depositional forms mark small subsets of two or three large landslides each:

Rock-crested hummocks: This texture occurs on three large landslide deposits with volcanic compositions. The term describes a texture in which surface clasts preferentially occur at the crests of hummocks on a landslide surface and not in the intervening troughs. On the Carlson landslide, for example, the crests of many hummocks appear to be paved with stones, while other hummocks are peaked with piles of rocks and still others have no rocks at all (Appendix B). Ui, et al. (1986) and Crandell (1989) respectively interpreted all such hummocks on the Pungarehu and Mt. Shasta landslides as being the sites of large partially-buried boulders. One possible interpretation of this texture is that it forms as a result of a two-stage process, whereby a landslide is emplaced and then some of the moist, mobile matrix material drains away, leaving behind rock-cored hummocks standing in relief

Figure 30. Photograph of slip surface near the base of the Martinez Mountain landslide. Upper block moved from left to right relative to lower, coarser block. Note the movement-parallel striae on the base of the overhanging fine-grained block and the apparent comminuted zone in the center of the photo extending ~20 cm into the underlying material. For scale, typical cobbles in this view are about 10 cm in maximum dimension.

(Crandell, 1989). Conversely, the texture may form as a primary structure if boulders collect at the surface of a moist landslide during transport, as they appear to do on typical desert alluvial fan debris flows (Johnson, 1970).

Foliated texture: A few partially-eroded landslide deposits contain areas of foliation-like preferred orientations of platy mineral grains. The long axes of the grains are commonly aligned subparallel to the bases of the landslides. Usually this texture occurs near the base of a landslide lobe and does not continue laterally for great distances. Where this texture outcrops in the Adair Park megabreccia, for example, it is confined to the lower 5-25 cm of the breccia sheet in the distal portions of the landslide lobe (Yarnold and Lombard, 1989).

Clast rounding: Clast rounding has functioned to differing degrees in the two known occurrences of the phenomenon in large landslide deposits. The Altels long-runout ice landslide strongly exhibited this texture soon after its deposition in 1895. Heim (1932) described this deposit as a "spherical [ice] conglomerate, or rather, ice flour containing ice spheres." The other deposit exhibiting clast rounding was the Pungarehu landslide, composed of altered volcanic rocks, which displayed a slight proximal-to-distal increase in clast rounding. However, even in the most distal portion of this landslide, the clasts did not achieve spherical shapes as did the ice fragments in the Altels landslide (Ui, et al., 1986). Heim (1932) noted that while many large landslide deposits contain clasts that exhibit rounded corners and edges and jagged scars, none contained rock spheres comparable to the ice spheres found forming the Altels deposit. He attributed the difference to the fact that ice was more readily worked than rock in the mill-like interior of a large landslide.

Fused rock: Heuberger, et al. (1984) discussed the only known occurrences of fused rock found in association with large landslides. The fused rock occurs in two giant heavily confined landslides in crystalline rock: the Koefels, Austria and Langtang, Nepal deposits. The fused rock associated with the Austrian landslide has been named the "Koefels pumice," and is usually brown, though occasionally black, porous rock glass, corresponding chemically to the augengneiss and gneiss bedrock that compose the slide. The landslide slid into a valley on a well-defined basal slip surface and divided into two parts after impacting the opposite slope. The lower part of the slide was checked by the

opposite valley wall, while the upper section continued movement along a secondary slip surface. Because the bedrock had such great mechanical strength, the landslide did not disaggregate during movement into a rubble stream; rather, movement was largely constrained to the slip surfaces, though the bedrock in the landslide was indeed thoroughly fractured during transport. The fused glass occurred along both slip surfaces, though most of it has now been carried away for use as decorative stones. The Langtang landslide, also in gneiss, displays similar once-molten material along a primary slip surface well exposed by glacial erosion. The fused rock lies along the interface between solid bedrock below and well-fractured landslide breccia above. The glass has the appearance of hardened lubricating oil in outcrop. Again, because the bedrock had such great strength and did not disaggregate, movement of the landslide mass took place largely along a single slide plane. The presence of the fused rock indicates that the temperature of the rock along the slip surfaces in the two landslides must have approached 1000° C during emplacement.

Facies Model

The various depositional characteristics described in the preceding paragraphs do not occur randomly within the body of a large landslide lobe. Rather, specific regions of large landslides repeatedly show a sequence of depositional characteristics that varies with relative distance from the source region and with the nature of the substrate. Field studies of megabreccia deposits in the southern Basin and Range province by Yarnold and Lombard (1989), for example, suggest that a set of characteristic features is common to the deposits of long-runout landslides in arid climates. This set includes (from base to top): 1) undisturbed substrate 2) disturbed substrate; 3) a discontinuous zone of mixed substrate and landslide breccia; 4) a zone of matrix-rich breccia; 5) a region of matrix-poor breccia; and 6) a coarse boulder cap (Figure 31).

The landslide facies were also found to vary from proximal to distal exposures because of variations in proximal-to-distal substrate properties and because of internal trends related to the time evolution of the deposits themselves. Figure 31 illustrates the observation that in arid basins, the coarse, proximal substrate is much less apt to exhibit disruption than the finer-grained distal substrate (Krieger, 1977; Yarnold and Lombard, 1989). Also note the proximal-to-distal enlargement of the mixed and matrix-rich

Figure 31. Facies model of proximal and distal features of long-runout landslides in arid climates (exerpted from Yarnold and Lombard, 1989). The following list defines the various subfacies shown on the diagram and provides the depositional characteristics that occur in each region:

(6) Coarse boulder cap (oriented clasts, block bands, debris pyramids*);

(5) Matrix-poor breccia (three-dimensional jigsaw puzzle breccia, thrust faults and imbrication*);

(4) Matrix-rich breccia (striations, foliated texture, sub-horizontal slip surfaces*, clastic dikes [cd]);

(3) Mixed substrate and breccia, source region for clastic dikes (incorporated substrate material, load structures* [ls]);

(2) Disturbed substrate (basal strata disruption*, block scour*);

(1) Undisturbed substrate, coarse-grained alluvium proximally, fine-grained fluvial or lacustrine sediments distally.

Note the upward-coarsening textures displayed in the proximal, and especially in the distal landslide facies. Also note the absence of disturbed substrate in the proximal facies. Asterisk (*) indicates depositional features associated with stopping phase.

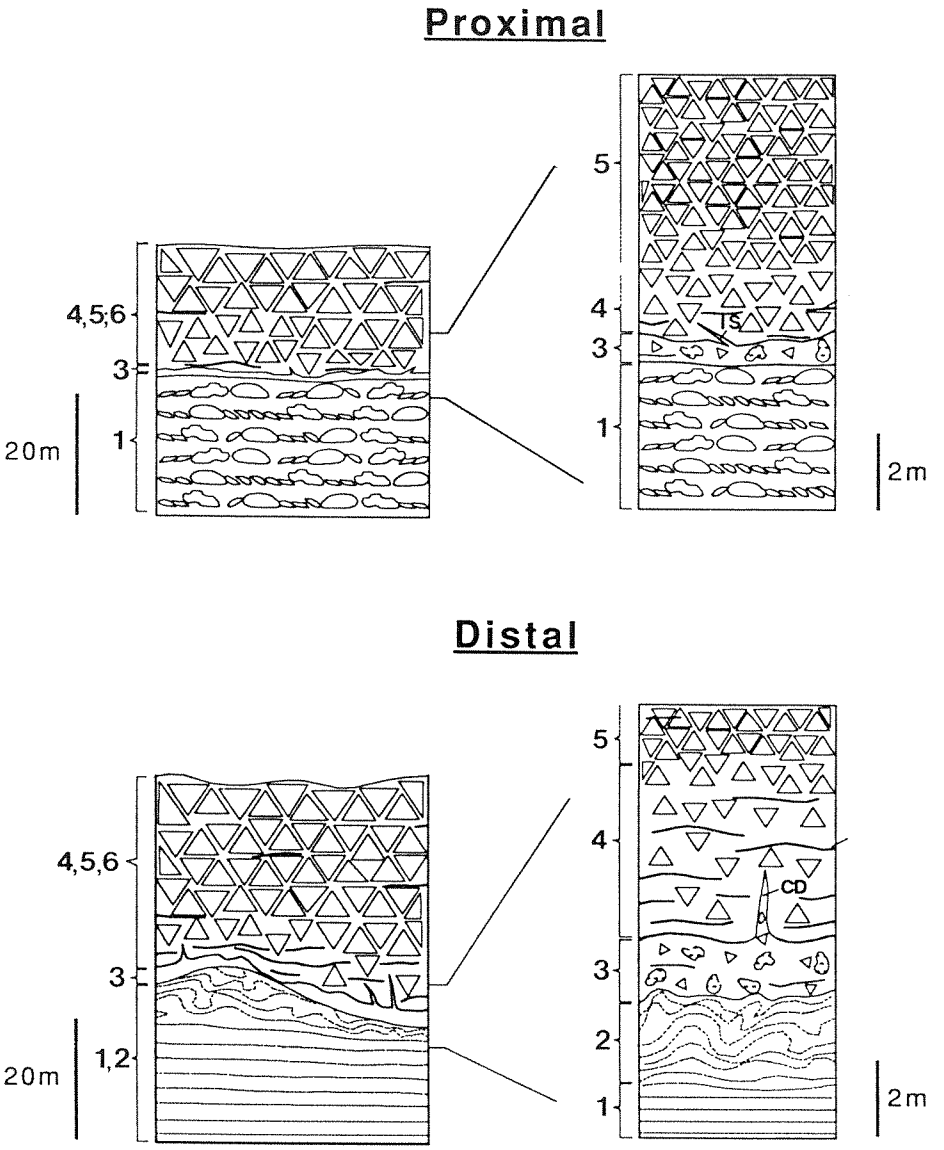
Proximal
4,5,6
3
1
20m
5
4
3
1
TS
2m
Distal
4,5,6
3
1,2
20m
5
4
3
2
1
CD
2m

zones near the base of a typical landslide sheet. Movement of the landslide over the substrate apparently has the effect of preferentially shearing and comminuting the basal material, producing rock flour that forms the matrix material in the mixed and matrix-rich zones.

In different environments, large landslide deposits may vary a good deal from the megabreccias described above. However, many of the basic facies relationships shown in Figure 31 seem to remain consistent despite significant changes in substrate properties. For example, descriptions of interior exposures of the Sherman landslide (Shreve, 1966), which fell upon the snow-covered Sherman glacier, correlate surprisingly well with the arid climate model. In the following it is submitted that the various sub-facies described by Shreve (1966) correlate with specific sub-facies of the arid climate facies model presented in Figure 31. Stratified snow, for example, formed the undisturbed substrate (1) of the Sherman slide. Above this layer was a discontinuous layer of clean, unstratified, disrupted snow (2), that graded upwards into snow containing a sparse admixture of sand and fine gravel (3). Above this level the snow merged with snow-free rock debris along a gradational contact a few centimeters thick (4). Above this contact stood matrix-poor debris (5,6) ranging from 1-3 m in thickness. The total thickness of entrained snow between the matrix-poor debris and the undisturbed, stratified snow measured 1-2 m. Apparently, snow formed about half the volume of the moving landslide (Bull and Marangunic, 1967). In the Sherman landslide, dry snow appears to have taken the place of the soft sediments beneath large, arid-climate landslides in the facies model. Despite these similarities, the Sherman landslide traveled with a thickness of only about 1/10 that of many of the megabreccias studied by Yarnold and Lombard (1989), indicating some fundamental differences in the behavior of these slides, perhaps related to differences in their substrate properties. Nevertheless, the data presented above support the conclusion that long-runout landslides consistently display certain facies relationships developed by their high-speed travel, during which time shear stresses concentrated near their bases preferentially comminute the basal material and disrupt the substrate. The degree of disruption of the substrate and the amount of substrate material entrained by a moving landslide depend on the relative strength or cohesion of the substrate. Soft materials such as dry snow become easily disrupted and

entrained, while tough, cemented alluvial gravels experience comparatively little disruption by the passage of a rapidly moving debris stream.

Eyewitness Accounts

The eyewitness accounts of large landslide movement presented here consist of observations of the actual kinematics of movement of the large landslide masses as well as descriptions of ancillary phenomena associated with their travel. The various observations made for each landslide are given in Table 11. Very few eyewitness accounts exist that document the actual **movement kinematics** of large landslides. Such detailed accounts only exist for the Altels, Elm, Goldau, Gros Ventre and Huascaran 2 and 3 landslides. The energetics of movement described below appear to vary mainly with the mode of initiation of the landslides. Large landslides beginning as rockfalls seem particularly violent.

The Goldau and Gros Ventre landslides, similar in volume and initial slidemass dimensions (Figures 21, 22; Table 9), also exhibited rather similar characteristics at emplacement according to eyewitness accounts. At Goldau (Figure 22), the landslide began movement as a slowly accelerating block glide. Some people on the slope at the time were even able to save themselves by jumping across the shearing lateral joint. The landslide block, covered by an upright forest, continued on for several hundred meters and lasted 15 to 30 seconds before accelerating and fragmenting into a mobile debris stream. Once the landslide fragmented, it moved extremely rapidly, in two places even leaping through the air, leaving the ground surface untouched. The landslide then rode out onto a saddle point and spread in fingers down each side. On one side the leading edge fell into Lake Lowerz, flooding the lakeshore (Heim, 1932).

Rather similar accounts document the emplacement of the Gros Ventre landslide. This landslide also began on a heavily forested slope, accompanied by dust and and a jerky motion reflected in the wild swaying motion of trees on the slope. The landslide continued sliding until it crossed the narrow Gros Ventre valley, at which time it impacted the opposite valley wall, piled up about 100 m, then partially slumped back and spread up and down the valley as flowing debris streams, filling in the valley for a length of approximately 2.5 km. Remarkably, many of the trees that rode the landslide down the hill survived the ordeal by at least twenty years, despite having come to rest at odd

Table 11. Observations of Runout Phase of Large Historical Witnessed Landslides

Name	Date	Observations	Reference
Bualtar 1-3, Pakistan	29-31 July 1986	dust	Hewitt, 1988
Huascaran 3, Peru	31 May 1970	spattering, slide kinematics, wind blast, dust, noise	Plafker and Ericksen, 1978
Huascaran 2, Peru	10 Jan. 1962	slide kinematics, wind blast	Plafker and Ericksen, 1978
Madison, MT	17 Aug. 1959	wind blast	Hadley, 1978
Khait, U.S.S.R.	10 July 1949	wind blast	Solonenko, 1977
Gros Ventre, WY	23 June 1925	slide kinematics, wind blast, dust, noise	Voight, 1978
Frank, Alberta	29 April 1903	wind blast, dust, noise, luminescence	Cruden and Hungr, 1986; Kent, 1966; Voight and Pariseau, 1978
Altels, Switz.	11 Sept. 1895	airborne leap, wind blast, spattering	Eisbacher and Clague, 1984
Gohna, India	6 Sept. 1893	dust, noise	Holland, 1894
Elm, Switz.	11 Sept. 1881	slide kinematics, airborne leap, wind blast, dust, noise, luminescence	Heim, 1882; 1932
Goldau, Switz.	2 Sept. 1806	slide kinematics, airborne leap, wind blast, dust, noise, luminescence	Heim, 1932
Diablerets 2, Switz.	23 June 1749	dust, luminescence	Heim, 1932
Plurs, Italy	4 Sept. 1618	dust, luminescence	Heim, 1932; Eisbacher and Clague, 1984

angles. However, only those trees less than 40 years old at the time of the landslide survived, either because the older trees were broken to pieces or their root systems were too damaged to support further growth (Voight, 1978).

The Elm landslide, the best observed historical landslide from start to finish, behaved quite differently from the Goldau and Gros Ventre landslides. This is primarily due to the fact that the Elm landslide began as a rockfall, rather than as a translational landslide. From eyewitness accounts, Heim (1882) divided the kinematics of the Elm landslide into three gradational phases: the fall, the airborne jump and the surge (Chapter II: Figure 6j). According to an eyewitness, the initiation of movement, like that of the Goldau and Gros Ventre landslides, began with a strong shuddering motion (Hsü, 1975): "When the falling rock began to slide, the forest moved like a herd of galloping sheep, and the pine swirled in confusion; then the whole mass suddenly sank." Unlike the Goldau and Gros Ventre landslides, however, the Elm slidemass did not remain in sliding contact with the mountain. Rather, the slidemass fell freely for a short distance, then impacted the underlying quarry floor and disintegrated. The disaggregated rubble then shot horizontally away from the mountain by deflecting off the quarry floor (Hsü, 1975):

> Then I saw the rockmass jump away from the ledge. The lower part of the block was squeezed by the pressure of the rapidly falling upper part, became disintegrated and burst forth into the air.
> ...The debris mass shot with unbelievable speed northward toward the hamlet of Untertal and over and above the creek, for I could see the alder forest by the creek under the stream of shooting debris.

Heim (1932) pictured this phase of the movement as akin to the behavior of a waterfall striking a protruding rock ledge. Like water pouring over a ledge, the underside of the landslide appeared smooth and well-defined as it arched through the air, allowing witnesses to observe houses, trees and fleeing people and cattle underneath. The upper boundary of the landslide was not well defined during the airborne leap, however; rocks in this zone moved chaotically and were accompanied by thick dust clouds (Heim, 1932; Hsü, 1975).

When the landslide debris hit the ground, it recombined into a cohesive, ground-hugging rock flow. The debris initially moved directly across a narrow valley (Chapter II: Figure 6j) and surged 110 to 115 m up the opposite valley wall. The leading debris stopped at this altitude, but the following

debris deflected to the left, side-stepped the hill and "flowed" another 1.5 km down a narrow U-shaped valley. Witnesses in the village of Müsli in the valley (Chapter II: Figure 6j) observed the oncoming landslide and described it as a "black rubble mass several meters high below the dust cloud driving out like a railway train." As the landslide surged across the mildly dipping valley floor, the central portion formed the highest and fastest moving part of the debris stream. During this phase, the debris stream ran into the lowest walls of buildings, pushing some houses for a while in front of it until they fell backwards onto the landslide, which quickly enveloped them. The rubble stream also ran under the abutment of an iron bridge across the Senft River, rolled the bridge over and dismembered it (Heim, 1932). A witness who barely escaped the onrushing landslide by running to the side described the close-up details of the landslide as follows (Hsü, 1975):

> The debris mass did not jump, did not skip, and did not fly in the air, but was pushed rapidly along the bottom like a torrential flood. The flow was a little higher at the front than in the rear, having a round and bulgy head, and the mass moved in a wave motion. All the debris within the stream moved confusedly as if it were boiling, and the whole mass reminded me of a boiling cornstew. The smoke and rumble was terrifying. I turned and ran, and a single jump saved me. When the [debris stream] drove past me like a speeding train, its outer edge was only a meter away. During my last jump, small stones were whirling around my legs, being stirred up by the wind. Otherwise I was not hurt by any fallen stones, nor did I feel any particularly strong air pressure.

Despite the violent phenomena surrounding emplacement of the Elm landslide, it was a relatively minor event in comparison with the later Huascaran 3 landslide (Plafker and Ericksen, 1978). This landslide, like Elm, originated as a large rockfall. The slidemass was composed of about 90% granodiorite and 10% glacier ice. The slidemass fell freely about 600 m before shattering in the subjacent drainage basin. Debris shot across a wet glacier, down the main drainage channel and divided into two lobes at a left-hand bend in the channel. The right-hand, or Yungay, lobe overtopped a ridge and ran directly into the city of Yungay. Survivors described the arrival of the Yungay lobe as a "terrifying roaring turbulent mass of rock, ice and mud." Initially, boulders came flying over the ridge, which bounced and rolled towards Yungay. This disgorging of loose boulders distinguishes the Huascaran 3 landslide from most other large landslides, observed and

prehistoric, few of which exhibit much evidence of boulder spatter far beyond the deposit margins. Some of the boulders ejected from this landslide had velocities on the order of 1000 km/hr, as estimated from the size of impact craters, and many flew up to 4 km on ballistic trajectories. A giant wave of wet debris arrived immediately after the boulders. It extended slightly beyond the limits of the initial wave and traveled in a "rolling," "wavelike," or "rolling confused motion," and as "a cresting wave ten stories high that broke over Cerro de Aira [the ridge where the lobes separated]." Simultaneously, the larger, left-hand, or Ranrahirca, lobe reportedly made a roaring noise and shook the ground as it passed observers. After passing the town this lobe shot perpendicularly across the Rio Santo, swept up the far valley wall and then fell back "like a wave on the shore." Residents noted that the surfaces of both debris lobes were covered with blocks of ice after the landslide (Plafker and Ericksen, 1978).

The earlier Huascaran 2 landslide followed much the same course as did the later and much larger Huascaran 3 event, except that the earlier landslide did not divide and send any debris into Yungay. The Huascaran 2 landslide also contained a rock and ice mixture, but closer to the proportions of 75% granodiorite and 25% ice. Huge ice blocks formed the leading edge of the landslide in its middle course, trailed by "a chaotic mass of rocks, chunks of ice and morainic detritus." Further downstream, where the landslide reached the upper end of the Ranrahirca alluvial fan, it spread out in the form of a 10- to 15-m-high wall which advanced "like a gigantic steamroller," that destroyed everything in its path and deposited a layer of ice, rocks and soil over the surface (Plafker and Ericksen, 1978).

Eyewitnesses of large landslides also report several **associated phenomena** commonly accompanying their emplacement (Table 11). These phenomena include wind blasts and other aerodynamic effects, noise, prodigious dust and various forms of lightning or some form of luminescence.

Wind blasts and other aerodynamic effects are commonly mentioned by witnesses of large landslides. These wind gusts vary in power from mild to hurricane strength. They often pick up massive objects and redeposit them elsewhere, including on the moving landslides themselves. The strongest winds occur directly in the path of the landslides, but the gusts do not seem to travel far beyond their lateral margins. At Elm, for example, strong winds generated in front of the landslide caused trees to bend and windows to rattle 4

km downvalley in the direction of movement of the slide. Close to the landslide, many people were lifted into the air in front of the rubble stream, carried and thrown by the gusts and then gently let down away from the landslide, alive but unconscious. More commonly, people picked up by the wind could be seen to whirl through the air and be dropped onto the landslide, where they usually disappeared without a trace. In several locations, wooden houses were also lifted into the air in front of the oncoming landslide and smashed on impact from the fall. However, many houses near the margin of the landslide standing only 100 m from those thrown by the wind remained fully intact (Heim, 1932).

Witnesses of wind gusts in the vicinity of other large landslides give similar accounts to the observations made at Elm. At Goldau, a herdsman and his goats, along with four children, were whirled into the air in front of the landslide and then fell back into the rubble stream. Also, house roofs were blown off or rolled ahead of the landslide (Heim, 1932). At Frank, the landslide was accompanied by a violent compressed-air blast which blew back into the coal mine near the base of the slope and strewed the valley with torn-off leaves and branches. Also, equipment, houses and in some cases people were carried many tens of feet without damage (Kent, 1966). Similarly, at Khait, a powerful air blast preceded the landslide which "broke constructions, uprooted trees and threw them down for hundreds of meters" (Solonenko, 1977). During the Gros Ventre landslide, a wind gust struck and blew away a bridge across the Gros Ventre river just upstream from the slide (Voight, 1978). At the Madison, Montana landslide, little unusual atmospheric activity was noted along its eastern edge, but a violent wind blast preceded the landslide along its western margin. Here, survivors reported that the wind gust overturned trailers and stripped off clothing. One eyewitness reported the wind strong enough to send a car tumbling over and over and to blow two members of her family bodily away. It also transported riverbed debris and fish at least 300 m onto the alluvial terrace south of the river and deposited a coat of fine sand and mud on the sides of trees (Hadley, 1959; 1978). The two historic Huascaran landslides were also associated with strong winds. The 1962 Huascaran 2 event exhibited a hurricane-like wind in its upper reaches, and a somewhat lesser wind lower in its course. The larger 1970 Huascaran 3 landslide had stronger associated wind-blast effects. As at Madison, a mud-laden wind blast preceded the landslide, which was strong enough to knock

people down and topple trees and abrasive enough to shred exposed flesh and strip trees of leaves. Based on the lengths of mud-free shadows behind obstructions of known heights, the muddy wind blast impinged on the ground at an angle ranging between 8° and 13° from the horizontal (Plafker and Ericksen, 1978). A rather similar situation accompanied the Altels ice landslide. A wind blast, this time laden with ice, carried ice blocks up to 1 km from the landslide. The blast "sanded" and felled trees, blew a small lake dry, toppled a stone wall and picked up and hurled cattle 500-1000 m horizontally and 250-350 m vertically (Eisbacher and Clague, 1984).

Prodigious dust clouds accompany large landslides just as commonly as wind gusts. Most of the dust apparently forms within the body of the landslide, rather than being kicked up from the ground surface ahead of a landslide as might be suggested by the preceding discussion. After interviewing many witnesses of large landslides, Heim (1932) developed the following understanding of the development of dust in large moving debris streams:

> The moving stream blows dense swirling dust clouds from vents, even in the worst wet weather, for repeatedly fresh dry breakage and frictional surfaces are formed....At every big rock avalanche these dust clouds are an unwelcome hindrance to observation. Over a wide periphery the surroundings are hidden in a dark dust cloud and covered with fallen dust from 1 to 10 cm thick. People, caught in the dust clouds of rubble streams, have often almost suffocated and have been plagued by throat and eye irritations that lasted many days (reports from Goldau and Elm). In closer proximity to larger rubble streams coarse dust falls like hail or sleet and from further away the wind driven dust clouds appear as dark smoke. After the rock avalanche of Goldau, a universal rain of dust extended over the whole region of Lake Zug [up to 15 km away], and Cham [15 km away] was covered with it. ...During a fall off the Diablerets the clear day was changed into dark night, and the surrounding pastures were so covered with rock dust that the cattle had to be driven away.

Similar reports exist from other large landslides. The small Plurs landslide, for example, with a volume of only 3-4 x 10^6 m^3, nevertheless sent dust as far as Chiavenna, 4 km away (Heim, 1932; Eisbacher and Clague, 1984). At Gohna, India, "Falling continued for three days with deafening noise and clouds of dust which darkened the neighbourhood and fell for miles around, whitening the ground and tree branches like snow" (Holland, 1894). Also at Frank, "Dust thrown up from the debris...settled like a pall over the valley" (Cruden and Hungr, 1986). Similarly, three dustfall episodes accompanied the emplacement

of the Bualtar 1-3 landslides over a three day period in 1986. The dust from these events was reported more than 25 km from the site of the rockfalls and was so dense in the vicinity of the landslides that the slide deposits were not observed until a rainstorm cleared the air of their dust (Hewett, 1988). In contrast, at the Gros Ventre and Huascaran 3 landslides dust clouds were only noted at the initiation of movement. At Gros Ventre a "brown mist" rose above the hillslope just prior to initiation (Voight, 1978), while at Huascaran 3, "within seconds after the [rock]fall an enormous dark cloud of dust rose from the base of the peak, rapidly obscuring it from view" (Plafker and Ericksen, 1978).

The movement of large landslides also generates considerable noise. Noises heard by eyewitnesses differ depending on their position with respect to a landslide and on the stage of movement of the landslide. At Huascaran 3, the initial rockfall movement phase produced a short, sharp noise, described as an "explosion," "cannon shot," "dynamite blast," or "sonic boom." Movement of the landslide itself was accompanied by a roaring noise (Plafker and Ericksen, 1978). A roar or rumble also accompanied the movement of the Gros Ventre landslide (Voight, 1978) and the initial phases of the Elm slide (Heim, 1932), while a "deafening noise" marked the emplacement of the Gohna landslide (Holland, 1894). Somewhat different noises were emitted by the Goldau and Frank landslides. The former produced a thunder-like rumble interrupted by hard, short bangs (Heim, 1932), while the Frank landslide generated a noise "resembling that of steam escaping under high pressure" (Kent, 1966). At Elm, the sound perceived in the ground surge stage differed from that of the earlier phases, either because of an actual change in the sound or because the landslide moved closer to the inhabitants of the valley and allowed them to hear some of the higher frequencies emitted by the slide. In either case, the ground surge moved with a "deafening crunching and scratching noise," joined by a "hollow, powerful bass accompaniment," akin to the sound of "a large wagon being pulled by galloping horses across a cobblestone road" (Heim, 1932).

Finally, five of the observed landslides listed in Table 11 were accompanied by some type of lightning-like flashes. It is unclear whether these landslides exhibited flashes from the moving landslide rubble per se, or from the thick accompanying dust clouds.

Analysis

A number of unique depositional characteristics accompany the runout phases of large landslides. Many of these unusual textural, structural and sedimentary features are associated with the debris streams that form in all but the most heavily confined large landslides. The debris streams exhibit remarkable fluid-like kinematic behavior. It is during their movement as debris streams that large landslides diverge from the behavior of most smaller mass movements, giving the large landslides their "long runout" character. The high-velocity travel of the debris streams themselves gives rise to an additional group of phenomena commonly associated with the emplacement of large landslides.

Large landslides always contain brecciated rock and behave in a cohesive manner. The stresses imposed by the high-velocity travel of a rock mass over its substrate apparently cause the brecciation, although the initial free-fall stage in rockfall-type landslides probably accounts for some of the clast disruption in these deposits. Brecciation of the rock in the landslides produces copious quantities of fine-grained rock flour, which fills the interstices between component clasts and probably causes the cohesive behavior of the debris streams. In most cases, the rock composing a large landslide becomes sufficiently disrupted that mobile debris streams can form, in which the constituent fragments can move with respect to one another to a limited degree, allowing the ground-hugging landslides to "flow" down channels and around obstructions, normally forming a terrain-mantling deposit that reflects the underlying topography. Only heavily confined landslides fail to exhibit streaming motion and terrain mantling; in extremely tough rock, movement can even be constrained to individual slip surfaces, leading to rock fusion in those areas. The limited nature of the relative motion of particles forming a debris stream is documented by the preservation of hillslope stratigraphy in the final deposit of most large landslides. Except perhaps for moist landslides, the material forming dry landslides has too much strength or "viscosity" to become mixed during transport in any direction. The reverse grading exhibited in many of these deposits, as well as the foliated texture occasionally observed suggests further that the stresses in a moving debris stream concentrate along the base, leading to preferred comminution and alignment of constituent grains in that area. The common occurrence of three-dimensional jigsaw puzzle breccia, and the occasional observations of

proximal-distal grain size decreases and clast rounding, however, pay tribute to the violent, mill-like activity present throughout the interiors of moving landslides. In addition, observations of incorporated substrate material, dozed marginal ridges and basal striations all document the fact that large mobile debris streams have significant interactions with their substrate. The degree of interaction apparently varies with the strength of the substrate, as coarse alluvium displays little modification, while lake sediments and especially dry snow exhibit major disruptions. Finally, the observations of rock spattering, proximal troughs, oriented clasts, block bands and rock-crested hummocks all indicate that the surfaces of moving debris streams, while apparently the sites of lowest energy in a large landslide, nevertheless experience considerable activity during transport, mostly due to variations and obstructions in the travel course.

The eyewitness accounts of large landslide travel and evolution provide additional data for an understanding of the long-runout phase of large landslide movement. All the eyewitness accounts point to the critical relationship between the development of a debris stream and the high velocities and low H/L values attained by large landslides. In translational-slip landslides, motion begins as a slowly accelerating slide. Ultimately, however, the slabs break up into mobile debris streams, at which time they accelerate wildly and their behavior changes from rigid sliding to something more akin to rafting of an extremely viscous fluid on a highly fluid, lubricated substrate. A similar transformation occurs in rockfall-type landslides. The impact of a large slab of rock following a free-fall of tens or hundreds of meters completely brecciates the rock mass and transforms its nature entirely. If it falls additional distance through the air it moves like a waterfall, and once it strikes the ground it forms a debris stream.

The movement of a ground-hugging debris stream produces a number of secondary phenomena commonly associated with large landslides: wind blasts, dust, noise and some sort of luminescence. The wind blasts result from the displacement of air by a moving landslide. The wind damage caused by moving landslides is concentrated in the primary movement direction, as the landslides spread and displace air only modestly in the transverse direction. The wind blast effects are probably concentrated when the landslides move down canyons, as they did at Elm, Gros Ventre, Khait, Madison and at both Huascaran events, with the landslide debris acting like a piston and the valley

walls like a cylinder. The dust clouds associated with the landslides apparently originate in the interiors of the landslides themselves due to the crushing of rock in their interiors, and not because of the wind blasts that precede them. The noises produced by large landslides apparently cover a wide spectrum of frequencies and may vary with time in the evolution of a landslide. The sounds heard by any particular observer will depend on his/her distance from the slide and/or upon the changing behavior of a moving landslide. The lightning or luminescence associated with many large landslides may have two different sources. Static electrical discharge in the clouds of dust thrown up by the moving debris streams might be one source, and the impact of piezoelectric minerals within a moving landslide could provide a second source.

4. *Stopping*

The stopping phase forms the third step in the chronology of a large landslide. The discussion of the stopping phase first considers a number of detailed descriptions of the common and rare depositional characteristics associated with this final phase of movement. Next, a number of relationships between the morphologies of large landslides and their depositional environments are noted for both martian and terrestrial landslides. Discussion of the stopping phase concludes with eyewitness accounts and instrumented observations of the cessation of motion of ground-hugging debris streams, with concentration on the issue of whether the termination of landslide motion occurs gradually, or abruptly, as suggested by many eyewitness accounts.

Depositional Characteristics

Nine depositional characteristics associated with the stopping phase are described below. These features most likely originated during the final stages of movement of large landslides, but some features may in part have been inherited from the earlier runout phase. These observations are subdivided into those characteristics common to many landslide deposits, and others shared by only two or three large landslide deposits.

Large landslide deposits exhibit seven **common** stopping-phase depositional characteristics. These characteristics are listed in Table 12 and described below:

Table 12: Depositional Characteristics of Stopping Phase of Large Landslides

I. Common (number and names of deposits with characteristic in parentheses):

A) Basal strata disruption (**11**: Adair Park mb, Ales mb, Artillery Mtns. mb, Black Canyon mb, Bonelli Peak mb, Buckskin Mtn. mb, Cross Hill mb, El Capitan, Panum, Split Mtn. mb, Vallecito Mtns. mb);

B) Sub-horizontal slip surfaces (**9**: Adair Park mb, Black Canyon mb, Blackhawk, Bonelli Peak mb, Buckskin Mtn. mb, Cross Hill mb, El Capitan, Martinez Mtn., Split Mtn. mb);

C) Clastic dike intrusion (**9**: Adair Park mb, Artillery Mtns. mb, Black Canyon mb, Blackhawk, Bonneville, Cross Hill mb, El Capitan, Mt. Shasta, Sherman);

D) Debris pyramids (**9**: Brazeau Lake, Elm, Frank, Hope, Mageik, Maligne Lake, Mt. Granier, Sherman, Stalk Lakes);

E) Thrust faults and imbrication, with primary compression parallel to the movement direction (**7**: Ales mb, Black Cyn. mb, Blackhawk, El Capitan, Split Mtn. mb, Vallecito Mtns. mb, Vesuvius 5);

F) Oblique imbricated ridges (**6**: Avalancha del Zarzo 1-2, Blackhawk, Loma de la Aspereza, NE Terra Cimmeria, Olympus Mons Caldera);

G) Multiple margins, two or more subparallel lateral margins, most strongly developed proximally (**5**: Blackhawk, Carlson, Goldau, Loma Redonda, Parpan).

II. Rare (number and names of deposits with characteristic in parentheses):

A) Load structures (**3**: Adair Park mb., Buckskin Mtn. mb, El Capitan);

B) Raised distal rim (**3**: Blackhawk, Frank, Silver Reef);

C) Block scour (**2**: Elm, Frank).

Basal strata disruption: Bedding in sedimentary strata immediately below the basal contact of large landslide deposits may exhibit significant disruption. The sediments exhibit folds, commonly verging in the landslide transport direction, as well as detachment surfaces, imbrication and general contortions. Deformation typically dies out 1-30 m below the basal contact of a landslide (Yarnold and Lombard, 1989). Lacustrine sediments, consisting of silts, sands and gypsiferous clays, form the most commonly disrupted substrate materials (Figure 25). However, disruption may also occur in fluvial sediments and alluvial fan deposits. Disrupted basal strata is most commonly encountered underlying the distal, rather than proximal, segments of large landslide deposits. Most likely this trend relates to the deposition of landslide debris on a proximally-to-distally fining sedimentary sequence; coarse sediments near the bedrock source area, decreasing to fine sands and silts a few kilometers away in a lake or playa. The weak, moist fine sediments encountered by the distal margin of a landslide would be more likely to be disrupted than coarse, dry alluvial fan sands and gravels encountered proximally (Krieger, 1977; Yarnold and Lombard, 1989). Alternatively, this trend may relate to peculiarities of the travel mechanism of large landslides (Krieger, 1977).

Sub-horizontal slip surfaces: Several substantially dissected large landslides and megabreccias display sub-horizontal slip surfaces in exposures near the bases of the deposits. The slip surfaces extend laterally up to tens of meters and commonly separate "units" within the breccia having contrasting lithologies and/or grain sizes (Figure 32). The slip surfaces themselves are planar, gently curved or undulatory and may be marked by thin gouge zones or by rock flour up to several centimeters thick. Sometimes the surfaces exhibit motion-parallel striations (Figure 30). Although joints, fractures and small faults pervade interior exposures of large landslide deposits, the sub-horizontal slip surfaces form the most continuous and well-developed of these structures (Yarnold and Lombard, 1989).

Clastic dike intrusion: Intrusive clastic dikes occur in several large landslide deposits. The dikes generally consist of some combination of crushed matrix material and incorporated substrate detritus, most typically well-sorted sandstone (Figure 33), though the Sherman landslide experienced intrusion by snow (Shreve, 1966). Usually the dikes can be traced to an origin just below

Figure 32. Sub-horizontal slip surfaces exposed in an unnamed megabreccia deposit in the northern Avawatz Mountains, California. Note that many tabular clasts are aligned with their long axes sub-parallel to the slip surfaces. Also note sub-horizontal fabric disruption by small boulder to the right of pencil in lower photograph. Slide movement direction probably from left to right and into the plane of the photographs.


Slip-surface
marked by
clay-rich
gouge


Gouge-rich
slip surfaces

Figure 33. A clastic dike intruding into the base of the El Capitan landslide, Arizona. The dike consists of well-sorted, structureless quartz sandstone as observed in field relations and in thin section. Inclusions of gravel appear to be derived from intrusion walls. The dike, which lies near the distal margin of the landslide intrudes about one meter upwards into the landslide breccia. Its symmetrical shape indicates that it was injected following cessation of movement of the landslide. Landslide motion was from left to right in this photo.

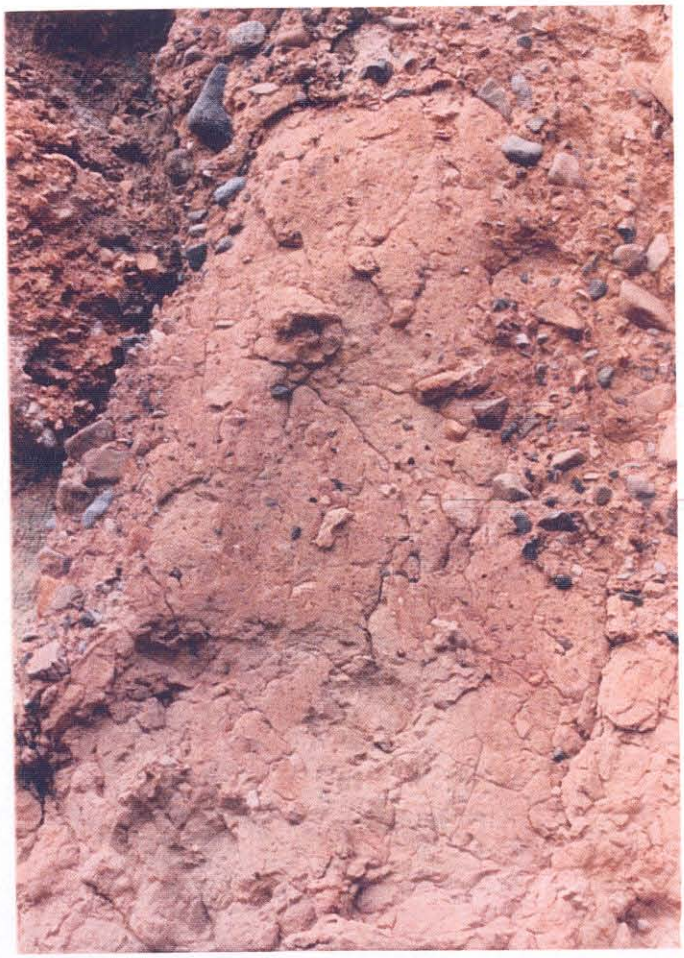

the base of a landslide sheet, and in some cases the intrusion can even reach the surface of the slide (Shreve, 1966). In addition to the primary materials, the dikes may incorporate minor quantities of landslide debris dislodged from the edges of the dike during injection. Although the dikes usually originate near the bases of the landslides, the Mt. Shasta landslide exhibited intrusion of sand-sized matrix material into large boulders floating in landslide debris (Crandell, et al., 1984). The dikes typically intrude subvertically up to 5 m and exhibit widths of a few centimeters to about a meter (Yarnold and Lombard, 1989). Their paths are straight, tortuous or stretched out in the movement direction of the landslide, suggesting intrusion may occur both prior to and after cessation of movement of a landslide; the symmetrical dikes probably formed after the end of movement, whereas the others probably occurred just prior to the end of movement and were accordingly stretched out in the movement direction. Had they occurred much earlier, the dikes would have been entirely separated from their source regions. As with the basal strata disruption, clastic dike intrusion is generally much better developed in distal regions of landslides than in proximal portions (Yarnold and Lombard, 1989). Clastic dikes are developed when loose, water-saturated sands are mobilized by rapid shearing, such that the sand becomes "quick" (Scott, 1963). Shearing of the substrate occurs either by the sliding motion of the breccia sheet over the substrate or simply by the rapid loading caused by the sudden deposition of several meters of rock. In either case, the fluid sand intrudes into the landslide either because it has a lower density than the overlying breccia or because it has developed a pore pressure in excess of the overburden pressure.

Debris pyramids: These features, also termed "molards," "debris mounds," or "debris cones" dot the surfaces of many fresh landslides; landslides older than about 200 years do not appear to retain them. The pyramids are composed of tightly packed, fine-grained debris piled at the angle of repose atop boulders on landslide surfaces. The fine-grained material resembles that normally found below the surfaces of large slides. The pyramids usually have the same lithology as the underlying boulder. This is particularly conspicuous when a boulder and debris pyramid having a common lithology occur in isolation in a zone of contrasting lithology on the surface of a landslide (Shreve, 1966). The pyramids always form atop boulders, though sometimes the boulders may not protrude above the general level of the landslide. They generally have the

shapes of glacial kames, but cross-sections lack the characteristic stratification patterns, water-worn pebbles and varied lithologies of the glacial features (Mollard, 1977). The pyramids typically occur in clusters toward the distal margins of large landslides. Specifically, they concentrate at sites of maximum spreading of the debris streams transverse to the movement direction of the landslides. The debris pyramids apparently represent samples of landslide interiors that get trapped atop boulders during spreading and thinning of a landslide (Heim, 1932; McSaveney, 1978). During dilation of the landslide, larger boulders below the surface must "run aground" and punch upwards towards the surface, carrying fine-grained debris on their surfaces. The occasional xenolithologic boulder-and-pyramid formations probably originate in zones of preserved stratigraphy beneath the surface.

Thrust faults and imbrication: A number of large landslides with good distal exposures provided by erosion or by quarrying activity expose low angle slip surfaces and structural imbrication, implying thrust faulting of the leading edges of these deposits (Figure 28). The imbrication causes a vertical repetition of the lower distal stratigraphy at the leading edge of a landslide. The thrust faulting at the leading edge of the landslides also leads to "distal ramping," a sudden reversal in the basal contact dip direction at the distal end of a landslide lobe (Yarnold and Lombard, 1989). These structures apparently reflect the overrunning of a relatively slowly moving distal margin of material by more rapidly moving material from behind.

Oblique imbricated ridges: This morphology surfaces certain large unconfined martian and terrestrial landslides. The landslides marked by this texture are characterized by a pair of lateral levees that extend from the source area to a distal heap of landslide debris. The levees, which form the lateral margins of the deposit, merge with the distal heap near the toe of the landslide (Figure 34). Headward of the distal heap, the levees stand above and bracket a relatively thin intervening layer of landslide debris. The oblique imbricated ridges mark this thin layer of debris from the base of the steep source scarp to the distal heap. The ridges are aligned in a downhill-divergent herringbone pattern, somewhat akin to marginal glacial crevasses, but extending all the way from the deposit margin to the centerline of the landslides. Distally this texture grades into a pattern of radial ridges on the

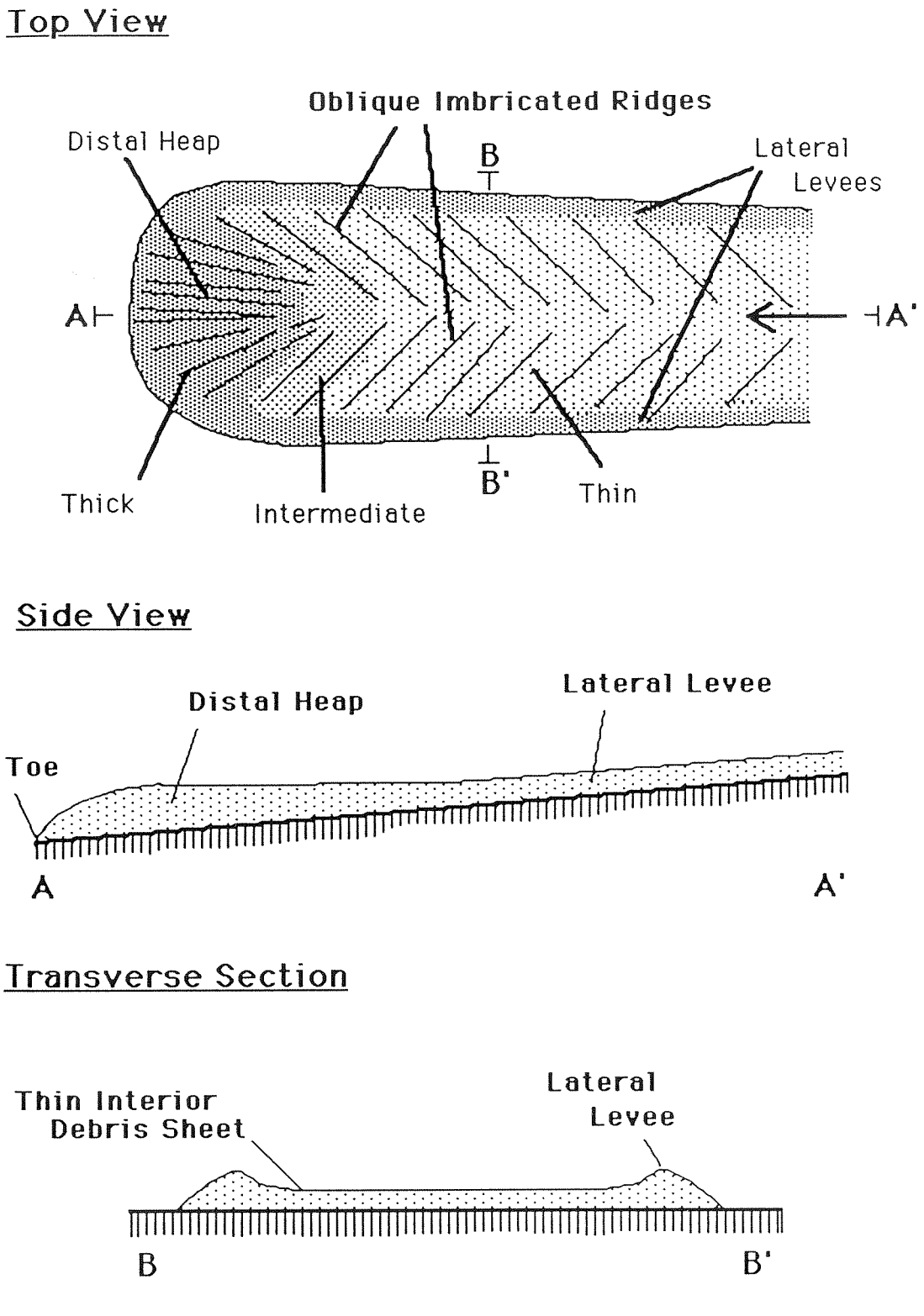

Figure 34. Schematic diagram illustrating the orientation of oblique imbricated ridges on the surfaces of large martian and terrestrial landslides marked by lateral levees and a distal breccia heap.

distal heap of several of the landslides. Fauque and Strecker (1988) believed this pattern to reflect progressive radial spreading of the landslides as they traveled down hill from the headscarp.

Multiple margins: Many large landslide deposits are bounded on their lateral margins by raised levees or dikes that stand higher than the level of the landslide debris bracketed by the levees (see Figure 34). Like the levees on the banks of a river or a lava flow, these structures must form along the margins of a large landslide when the debris between the levees stands at a level equal to or greater than the height of the top of the levees. The levees are left standing above the interior level of the landslide when the material towards the centerline of the landslide "recedes," presumably to move off down the slope. The levees are apparently left behind because the debris composing them falls below some critical velocity and is deposited. In a few instances, a primary dike, as described above, is joined outwards by a second marginal dike or by multiple marginal ridges. In these locations, the outermost dike had to form first. These normally occur in an en echelon pattern where a landslide moved downward and away from the location of the outermost dike. The Blackhawk landslide exhibits the best examples of multiple ridges; along the base of Hill 3747 the landslide formed and abandoned at least five marginal ridges as the slide moved around the hill (Shreve, 1968a; Johnson, 1978).

In addition to the common characteristics of the stopping phase described above, a number of comparatively **rare** depositional forms mark small subsets of two or three large landslides each:

Load Structures: Load structures mark the basal surfaces of three partially eroded large landslide deposits. Like the clastic dikes described earlier, load structures form when saturated sands are overrun and fluidized by shear stresses induced by the overriding breccia sheet. The shear forces are produced by the rapid loading of the substrate with the weight of the breccia sheet as well as by the sliding motion of the landslide. Unlike the clastic dikes, however, the fluidized sand only produces local substrate disturbances under the breccia sheets and does not intrude upwards into the sheet.

Raised Distal Rim: The Blackhawk, Silver Reef and parts of the Frank landslide exhibit raised distal rims. On the Blackhawk landslide, where this feature is best exposed, the distal 3 km of the landslide lobe is bounded by a

somewhat sinuous scarp about 15 m high, whose crest generally rises 2-3 m above the nearby landslide surface to form a definite distal rim (Shreve, 1987). Similar features occurred at the other two landslides, though in the Frank landslide a distal rim formed in only three places where the landslide debris ran up steep slopes and came to rest (Cruden and Hungr, 1986). Distal rims appear to form when the leading edge of a landslide banks up onto an obstacle and stops moving. The obstacle can either be a hill, as occurred in the Frank landslide, or it can be a landslide's own bulldozed distal debris heap (Figure 28).

Block Scour: This phenomenon took place in both the Elm and Frank landslides. At Elm, much of the thinner portion of the landslide was subsequently removed by the local inhabitants in an effort to reclaim pastureland overrun by the landslide. In this process, it was found that the leading edges of most of the larger blocks in these regions had ploughed up welts of soft, scoured earth in front of them. The same thing was found over a large area in the Frank landslide (Heim, 1932). These welts were probably the late-stage expression of the interaction of these landslides with their substrate. The welts probably formed because of the weakness of the soft soils overrun by the landslides. In comparison, erosional cross-sections in landslides in arid climates, where soft soils were absent, fail to show block scour.

Environmental Controls of Landslide Morphology

The debris aprons of large landslides exhibit a wide diversity of morphologies. They differ in plan view, in profile shape and in surface texture (Chapter II: Table 2; Figure 6). The morphologies observed on large landslide deposits primarily reflect the final conditions of the moving debris streams, because they evolve as they travel and thus preserve little information from their early movement stages (Heim, 1932). The origin of most of the morphologies observed on large landslides remains obscure. However, a small subset of features consistently relate to specific aspects of the depositional environments of the landslides. Three environmental factors appear to have some control on large landslide morphologies, including: depositional surface geometry, moist or icy substrate materials and the presence of an aqueous medium.

The planimetric forms and profile shapes of many large landslides appear to relate directly to their depositional surface geometries. For example, lobate landslides on Earth and Mars commonly form when landslide debris is forced to travel down a narrow channel that restricts its lateral motion (Appendix B). A lobate debris apron forms when the debris leaves the channel and moves out onto an unrestricted depositional surface. Apparently, during its channelized movement phase, the landslide debris develops a transverse velocity profile with material near the middle of the channel moving the fastest and debris near the edges moving more slowly. Upon reaching the depositional surface, the marginal material stops first, followed by the centerline material, leading to the bulbous final plan form (Appendix B). For unknown reasons, these landslides commonly exhibit either uniform or tapered profile shapes. Conversely, large martian and terrestrial landslides with blunt plan forms appear to develop only when their movement is entirely unconfined. These landslide deposits exhibit straight lateral margins because the landslide moves ahead at the same rate between the lateral margins; no transverse velocity profile exists to modify the form. Unlike lobate landslides, blunt plan-form landslides commonly have a distally raised profile shape. The nature of this behavior will be investigated in greater detail in Chapter IV. In places where landslide motion is strongly restricted by the depositional surface, landslides do not develop simple geometries. These heavily confined landslides commonly develop irregular plan view geometries and profile shapes.

Longitudinally ribbed landslides occur on Earth, Mars and the Moon. Longitudinal ribbing appears to develop in four primary environments. First, it occurs along the toes of many lobate landslides, despite significant differences in the composition of the deposits. They have been described from lobate terrestrial landslides in dry rock (Martinez Mountain deposit; Bock, 1977), in moist debris (Carlson landslide; Appendix B), and in ice (Altels; Heim, 1932), as well as from lobate martian landslides (Lucchitta, 1987a; Appendix B). Second, longitudinal ribbing occurs on many terrestrial landslides having ice or snow substrates. Examples include the Sherman (Shreve, 1966) and Fairweather (Bull and Marangunic, 1967) landslides. Third, many large landslides from terrestrial stratovolcanoes, such as Shiveluch (Lucchitta, 1979) and Socompa (Francis, et al., 1985) also exhibit marked longitudinal ribbing. Elsewhere, some large rotational landslides on Mars and the Moon also display the texture. Examples include the Mars 1 (Lucchitta, 1978a) and Tsiolkovsky

(El-Baz, 1972) deposits. There is no clear understanding of the origin of this texture or precisely how it may relate to the different settings in which the longitudinally ribbed landslides occur. Two possible origins of the texture have been forwarded. Where the ribbing terminates in a digitate pattern at the toe of a landslide lobe, it may form as a result of differential movement of the ridges along slip planes in the intervening swales (Shreve, 1966). Alternatively, where ribbing simply surfaces a landslide lobe and no digitate pattern appears at the toe of a landslide lobe, the pattern might result from non-continuous transverse extension of debris, like the necking of a steel rod under tension (Appendix B).

Two other debris apron textures, distal outrunner blocks and lobate terracing, observed on some attached debris apron landslides, also appear to form only in restricted environments. On Earth, these textures are only found on large subaqueous landslides. The distal outrunner blocks texture has at least two possible origins. One possibility is that it represents a segregation of matrix material from blocky material at the cessation of movement of a landslide per se, after which the matrix material separates from the landslide deposit and deposits elsewhere by way of turbidity flows (Lipman, et al., 1988). Gliding of discrete isolated blocks on a low-friction substrate in advance of the discrete leading edge of a landslide provides a second possibility (Prior, et al., 1984). The origin of the lobate-terraced texture remains obscure. Both textures occur on a small number of giant Valles Marineris landslides in addition to the subaqueous terrestrial examples. The significance of these martian examples will be discussed in Chapter IV.

Eyewitness Accounts

The mode of stopping of large landslides has considerable significance to several of the models proposed to explain the long-runout of large landslides. However, much of the evidence for the mode of stopping of these landslides comes from eyewitness accounts of only a very few large long-runout landslides. Newly available Soviet data on the kinematics of two artificially-triggered landslides provides new insight into this important phase of landslide movement.

The mobile debris streams formed in large landslide events commonly stop in two ways. One way is when the leading edge of a landslide runs headlong into a canyon wall, rebounds off and stops cold. The other, more interesting

mode occurs when a landslide stops moving on a relatively flat, unconfined surface. The best uninstrumented observations of the unconfined stopping phase of a mobile debris stream were made at the Elm landslide. Eyewitnesses of the event had just become aware of the catastrophic nature of the debris stream when "all of a sudden" the whole rock mass "froze as if touched by a magic wand." Eyewitnesses of the Goldau and Frank landslides reported that these landslides also came to sudden halts on flat ground (Heim, 1932; Shreve, 1987). These reports have led most researchers to believe that sudden halts from high speed characterize the final movement of large landslides. However, the only available instrumented data on the movement of large landslides (Figure 35), from two large artificial landslides triggered by the Soviets via underground nuclear(?) explosions (Adushkin, personal communication, 1990), indicate that slowing occurs gradually, not suddenly. The larger landslide decelerated from 25 m/s (56 mi/hr) to stop in 13 seconds, the smaller in only 9 seconds. These observations would seem to support the contention by Heim (1932) that the rapid stopping of large landslides described by eyewitnesses does not mean sudden "...in the mathematical sense but in the practical, every day sense of the word. It is 'sudden' to our sense and eye." Probably the fact that large areas of the moving debris streams came to rest at the same time gave observers the feeling that stopping was quite abrupt, though slowing and stopping may indeed have taken a few seconds.

In addition to these specific large landslide descriptions, a number of general remarks on the stopping of large landslides may be made from a synthesis of eyewitness accounts of the Elm, Goldau, Frank, Plurs and Diablerets 2 landslides (Heim, 1932). Heim (1932) states that long rubble streams surging over flat ground stop first at the rear, and that stopping propagates forward, with the front coming to a halt perhaps ten to thirty seconds after the rear. The last swirl of movement dominates the forms visible on a stationary deposit and obscures the forms exhibited at earlier phases of the movement. Finally, a large landslide exhibits significant interactions with the overrun depositional surface, typically dozing up the ground surface in front of it like a snowplow. This scoured material may surround a rubble stream like a moraine, and may hinder the forward motion of a landslide. Under such circumstances large landslides have been observed to overrun and roll over material hemmed in at the front, prematurely halting their motion.

Figure 35. Velocities and displacements of landslide leading edges for emplacement of two artificially-triggered Soviet landslides. The upper diagram plots the behavior of U.S.S.R. 1, which contained 80 x 10^6 m^3 of rock, while the lower diagram provides details of the 5 x 10^5 m^3 U.S.S.R. 5 landslide. Both landslides were derived from sedimentary rock sequences consisting of schistose claystone, sandstone and quartzite (Adushkin, personal communication, 1990).

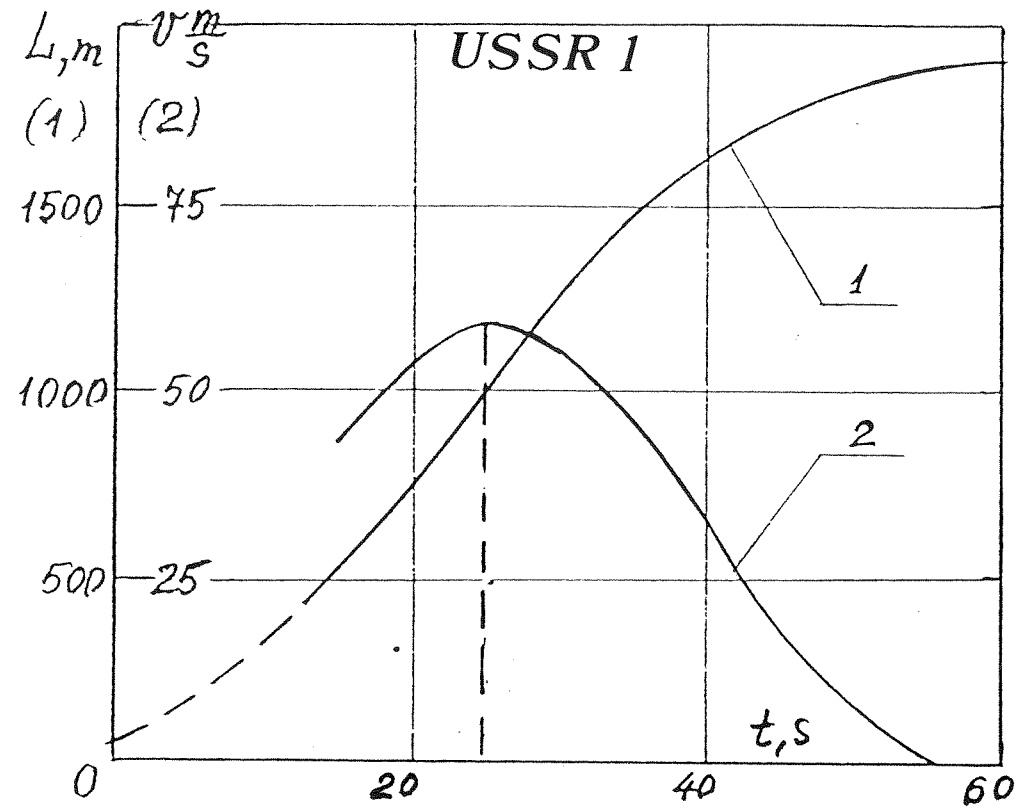
L, m
v, m/s
USSR 1
(1)
(2)
1500
75
1000
50
500
25
0
20
40
60
1
2
t, s

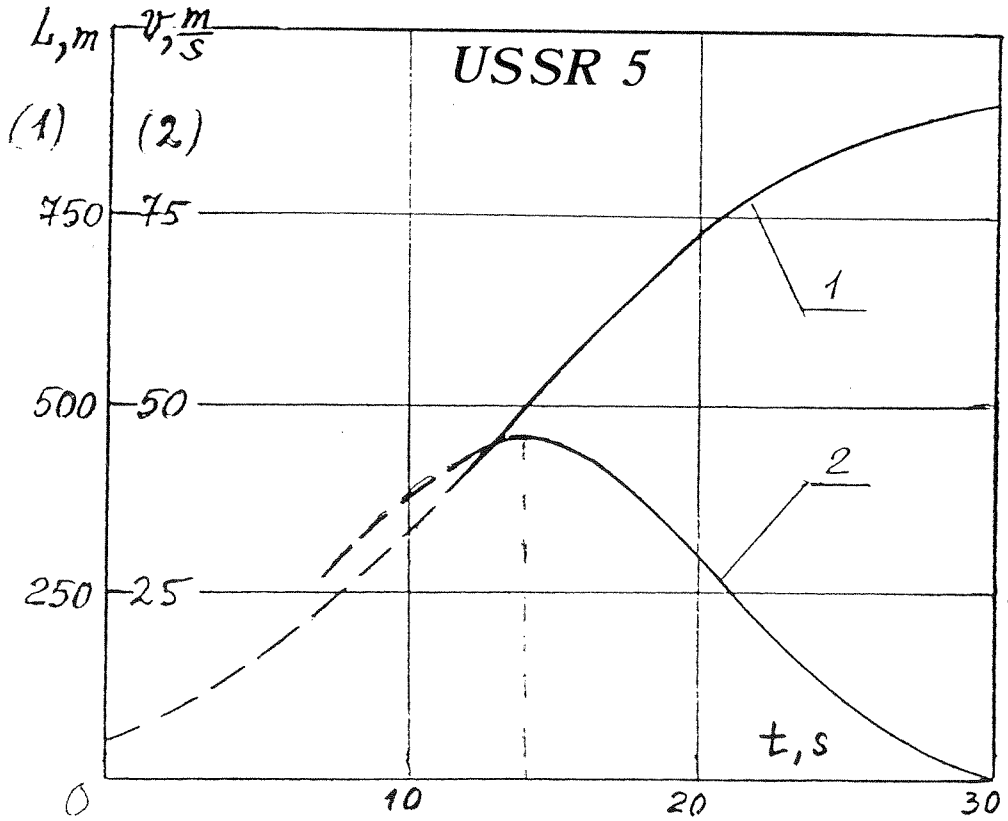
L, m
v, m/s
USSR 5
(1)
(2)
750
75
500
50
250
25
0
10
20
30
1
2
t, s

Analysis

The stopping phase is associated with a number of depositional characteristics related to the final movement stages of a debris stream. Two sedimentary features of large landslides, basal strata disruption and block scour, probably occur throughout the duration of a landslide event. However, most of the observed disruption occurs beneath the distal parts of the landslides and must have occurred late in the motion histories of the large landslides. Several of the depositional features that develop in the stopping phase are linked to the movement of one part of a landslide with respect to another part as stopping begins. These features include sub-horizontal slip surfaces, thrust faults and imbrication, and a raised distal rim. Two surficial structures, oblique imbricated ridges and multiple margins, are deposited by moving landslides in the course of their downhill travel. Other features form in the last gasp of movement of a large landslide. Debris pyramids and disrupted clastic dikes must form late in the chronology of a large landslide. This is because they appear to be the result of landslide motion, but significant activity subsequent to their formation would have reworked them entirely. Symmetrical clastic dikes and load structures probably date from the moment of cessation of movement, though they formed as a direct result of stresses imposed by the movement of the overriding debris streams.

Large landslides also develop a wide variety of large-scale morphologies in their final movement stages. The origins of most of the observed morphologies remain obscure, though a small number of features consistently relate to specific aspects of the depositional environments of the landslides. The geometries of landslide depositional surfaces often dictate the plan forms and profile shapes developed by large landslides, while certain surficial textures expressed on the surfaces of the deposits appear to relate to the geometry and nature of the depositional surface, or to the presence of an aqueous medium.

Comparison of eyewitness accounts with instrumented data of the stopping phase of large landslides appear at first to yield contradictory results. Eyewitnesses commonly described the stopping phases as occurring suddenly, while Soviet velocity data indicate that stopping takes place rapidly, but not instantaneously. The probable answer is that most large landslide debris streams slow down rapidly, not suddenly, but that the appearance of a large

body of rock coming to a rapid halt probably gives humans the feeling that stopping happens quite suddenly.

5. *Post Deposition*

The post-depositional period forms the final step in the chronology of a large landslide. During this stage a landslide deposit undergoes a variety of changes, some occurring directly upon the cessation of motion, others taking place in the long interval of time that often passes between emplacement and the study of a landslide in the field or from remote sensing images. The following discussion considers two depositional characteristics that are developed directly following the cessation of movement of a large landslide. In addition, the long-term effects of weathering and other processes on the degradation of large landslide deposits are considered.

Depositional Characteristics

Two depositional characteristics originate from the period of time directly following the emplacement of a large landslide, the intrusion of undisrupted clastic dikes and the formation of normal faults. Clastic dike intrusion (Figure 33) is thoroughly discussed in the preceding section. Reverse faults occur in two large landslide deposits, Blackhawk and Vesuvius 5. In both instances the normal faults post-date all the other structures and textures observed at interior exposures of the landslides (Johnson, personal communication, 1990; Hazlett, personal communication, 1990). At Blackhawk, the structures formed along the distal margin of the deposit in the same area thought to have experienced considerable compression in the final movement stages of the landslide (Figure 28). The normal faults in the Vesuvius 5 deposit, in contrast, formed throughout a significant length of the deposit (Hazlett, et al., in press). In both cases the structures appear to have formed after the cessation of movement of the landslides, as a sort of settling or relaxation phenomenon of the landslide breccia sheets (Johnson, personal communication, 1990).

Degradation

After a large landslide is deposited it may experience a variety of modes of degradation. Understanding the post-depositional degradation of a landslide deposit is critical to an interpretation of its surficial and interior textures. Most of the post-depositional modification of large landslide deposits is readily apparent. Often they experience erosion, but more often they become buried

by later sediments because they form in areas of net deposition. This includes terrestrial subaerial landslides deposited on alluvial fans and in glacial valleys, as well as most subaqueous landslides. Large landslides in three specific terrestrial settings warrant additional discussion, however: carbonate landslides in arid climates, large landslides emplaced on the surfaces of glaciers, and landslides deposited across active stream channels.

Large carbonate landslides deposited in arid environments form one of the primary sources of our information on long-runout landslides because they are common and relatively resistant to erosion in a dry climate. However, most of these landslides have nonetheless undergone significant post-depositional modification that is rarely documented in studies of the deposits. For late Pleistocene landslides such as Blackhawk, Saidmarreh and Silver Reef (Appendix A), much of the modification probably occurred under pluvial ice age conditions (Watson and Wright, 1969; Stout, 1977), though weathering has probably continued to a lesser degree through the Holocene. The primary effect of the weathering of these landslides is local dissolution and recementation of carbonate grains, especially the small grain size fraction, with resultant degradation of the original small-scale textures in the landslide interiors. The carbonate landslides can also exhibit large-scale modifications in surface texture due to the effects of solution on the landslide breccia. For example, the original surface texture of the Saidmarreh, Iran, landslide has been nearly effaced by solution. Small ridges and troughs a few meters deep and up to 100 m wide, as well as grabens as much as 3 km wide and 100 m deep, have formed extensively on the surface of the deposit due to cavernous weathering of the subsurface and subsequent collapse of the surficial layers of debris (Chapter II: Figure 6f). The major grabens trend roughly parallel and may be controlled by the structure of the underlying bedrock surface (Watson and Wright, 1969). The role of solution in altering the surficial textures of other carbonate landslides is unknown, but could be significant.

Large landslides deposited on glaciers also experience considerable post-depositional degradation. These landslides are modified by wastage of underlying ice, by preferential sublimation of surrounding ice and by movement of the underlying glacier. Landslides deposited on glacial ice that later wastes away may become degraded in a number of ways. The Pasayten landslide, for example, which fell onto a stagnant distributary of the Cordilleran ice sheet in late Pleistocene time, displays numerous kettles and

other ice-disintegration landforms. In addition, the original geometry of the deposit was disrupted by the disappearance of the underlying ice (Waitt, 1979). In recent times, landslides that fell onto glaciers in southern Alaska in the 1964 earthquake were also found to be degraded by the activity of the underlying ice sheets. One effect of landslide debris on active glaciers is that the presence of the debris prevents sublimation. The surrounding ice continues to sublimate as before, however, so that the landslide debris ends up on a pedestal of ice standing above the uncovered surface. An example of such behavior is provided by the Sioux landslide (Post, 1967). Ultimately, the margins of such debris-covered pedestals must experience mass wasting, so that textures in the landslide debris probably get disrupted entirely within a few years, depending on the sublimation rate of the glacier. Finally, relative motion between the center and margins of active valley glaciers can also break up the original structures and textures of large landslide deposits. Such disruption occurred quickly to the Bualtar 1-3 landslide deposits, for example, which fell upon the surging Bualtar glacier in the Karakoram Himalaya of Pakistan. In the year following their emplacement, the glacier had already moved 2 km down valley and had considerably disrupted the original outlines of the deposits (Hewett, 1988).

Large landslides falling into narrow canyons may cause the development of two types of landslide dams. Large landslides that travel down major drainage channels can block off side drainages, causing lakes to form along the lateral margins of a landslide. Examples where this has occurred include the Diablerets 2, Scima di Saoseo (Heim, 1932), Carlson (Appendix B) and Usoy landslides (Gaziev, 1984; Figure 16). Much more commonly, a large landslide will travel perpendicularly across a major drainage from a source on the slope above the channel, damming the primary stream. All of the landslide lakes described below formed in this manner.

Landslide dams vary considerably in their longevity. Some landslide dams remain stable for centuries or tens of centuries while others may fail in hours. Examples of large landslides that currently form stable dams include Poschaivo, Deyen, Obersee, Voralpsee (Heim, 1932), Angarakan (Solonenko, et al., 1984), Usoy (Gaziev, 1984), Mt. St. Helens and Madison (Costa and Schuster, 1988). Geologic evidence from ancient and now drained landslide lakes indicates that they are often stabilized by sand and mud carried into the dams by seepage of water through them. When a landslide dam is stable for a long

time, river waters pouring into the lake from upstream form a delta where the river enters the lake, the position of which migrates as the lake fills with water. Ultimately these lakes silt up entirely, forcing river waters to overtop and erode down through the dams (Heim, 1932). Examples of ancient, drained landslide lakes include those at Saidmarreh (Harrison and Falcon, 1938), Flims and Glärnisch-Guppen (Heim, 1932).

Other landslides fail before they have a chance to be silted-in and overtopped. Usually if a landslide dam is going to fail catastrophically, it does so shortly after it is impounded. Of 73 landslide-dam failures documented by Costa and Schuster (1988), 27% failed less than one day after formation, 41% failed within one week, about 50% failed within 10 days, 80% failed within 6 months and 85% failed within one year of formation. Examples include Disentis, which failed 3 hours after damming the Rhine on 29 June 1683 (Heim, 1932), Mayunmarca, which failed after 44 days (Kojan and Hutchinson, 1978), Gohna and Gros Ventre, which failed after more than a year (Heim, 1932; Costa and Schuster, 1988) and Biasca, which failed by overtopping twenty-one months after deposition of the landslide (Heim, 1932). Landslide dams fail by several mechanisms. Overtopping followed by downcutting is by far the most common means of failure, followed by seepage-related piping and by slope failure of an oversteepened downstream margin. In most documented cases of overtopping, the breach has resulted from headward fluvial erosion of the dammed downstream portion river into the base of the landslide (Costa and Schuster, 1988).

Many factors influence the stability of a landslide lake. Some important factors include the volume, size, shape and sorting of the landslide material; rates of seepage through the blockage; and rates of sediment and water flow into the newly formed lake. A landslide dam in its natural state differs from a constructed embankment dam in that it consists of a heterogeneous mass of unconsolidated or poorly consolidated earth material. It has no engineered water barrier or filter zones to prevent piping, nor drain zones to control pore pressures. It also has no channelized spillway or other protected outlet. Thus, landslide dams are susceptible to failure by a number of means not generally encountered in engineered dams. Often the amount of flow in a stream, and thus the rate at which a natural dam will fill, relates directly to the size of the upstream drainage area. Small landslides damming large drainage areas generally have very short life expectancies. Resistance to erosion forms the

most important characteristic in preventing erosion and failure of a landslide dam, either at the surface of the dam from surface-water runoff, or within the dam from piping and seepage (Costa and Schuster, 1988).

Summary

Large landslide deposits undergo a variety of modifications following deposition. Directly following the cessation of movement clastic dikes may intrude from liquified sands at the base and normal faults may develop due to relaxation and compaction within a breccia sheet. Over time, landslide deposits experience weathering, erosion and burial like other landforms. Large carbonate landslides in particular, even in arid climates, undergo significant modification in the post-depositional period. Dissolution and recementation affects all carbonate landslides and obscures interior textures. Where surface waters are plentiful, solution can even develop large-scale textures on the surfaces of the deposits. Landslides on advancing or receding glaciers experience particularly severe post-depositional degradation. They experience degradation due to wasting of underlying ice, sublimation of surrounding ice, and differential movements within advancing glaciers. Landslides that fall across active stream channels cause waters to pond upstream of the obstructions. Depending on the composition and geometry of a landslide, the amount of seepage through it, and the rate of delivery of water to the impounded lake, landslide dams may be short- or long-lived. When landslide dams fail, they usually do so by overtopping, often assisted by headward erosion into the landslide from the cut-off stream below. Landslide dams may also fail by seepage-induced piping and by slope failure.

D. Conclusions-Chapter III

This chapter has presented the systematics of the large landslide data collated in Appendix A. Specifically addressed were considerations of the log(volume) vs. H/L relationship in long-runout landslides as well as the systematics of the four-part chronology of large landslides: slope preparation and initiation, runout, stopping and post-depositional degradation. Collation of the information in this format has presented an improved portrait of the processes leading to large landslides and of the phenomena occurring during the travel of long-runout landslides.

The log(volume) vs. H/L behavior of large landslides provides insight into the nature of the long-runout mechanism that characterizes these deposits. All categories of large landslides exhibit a decrease in H/L with increasing volume. Long runout is actually the normal behavior for large landslides. The variation in H/L with increasing volume does, however, vary with different groupings of the large landslide data. Large terrestrial landslides from a variety of settings exhibit very similar overall log(volume) vs. H/L relations; non-volcanic, volcanic subaerial and subaqueous bedrock landslides follow similar trends on these plots. These trends contrast sharply with the log(volume) vs. H/L trend for martian landslides. Landslides on Mars compared to their terrestrial counterparts have shorter runout lengths for a given volume and fall height.

The plots of various subsets of large terrestrial landslide data on log(volume) vs. H/L diagrams provide important insights into the factors that influence the travel of long-runout landslides. These plots indicate that confinement, substrate properties and landslide composition all affect the log(volume) vs. H/L trends of large landslides. Among large landslides, distally-raised unconfined deposits and large landslides from coal mine tips exhibit the greatest runout lengths for a given volume and fall height. Heavily confined and deflected landslides, which behave about the same on log(volume) vs. H/L plots, exhibit the lowest runout lengths per unit fall height over the same range of volumes. Ice/rock landslides and landslides that traveled over icy substrates exhibit very similar behavior on log(volume) vs. H/L plots. This observation suggests that the nature of the material along the base of a landslide has a critical influence on its runout characteristics. The form of the headscarp, the morphology of landslide deposits and the presence or absence of seismic groundshaking generally has little influence on the log(volume) vs. H/L relations of large landslides aside from the effects already mentioned. The composition of a landslide, however, has considerable influence on the H/L value attained by a long-runout landslide. Two compositional characteristics profoundly influence the H/L values of large landslides: modal (most common) surface grain size and lithology. H/L values decrease with decreasing modal surface grain size, and, for a given modal surface clast size, H/L values decrease as lithology varies from metamorphic rocks to limestone to granite. The modal grain size of the clasts surfacing large landslide deposits derives mainly from the degree of jointing of the

preexisting slidemass and from the impact from free-fall in rockfall-type landslides; the grain sizes of these particles change little during the runout phase of the landslides. Extreme comminution of interior clasts occurs within the bodies of large landslides during transport, however. From this data, fine grain size seemingly bears a critical relation to the degree of runout traveled by large landslides. Landslides initially composed of smaller particles have lower average H/L values than those composed of larger clasts, while landslides composed of weaker rocks, which would fracture more easily into fine powder in the interiors of moving landslides, also experience decreased H/L values.

Slope preparation and slide initiation forms the initial stage in the chronology of a large landslide. Slopes are prepared for failure by a combination of factors, including the nature of the source rock, external processes that increase the shearing stresses on a rock mass and internal processes that act to decrease the shearing resistance of slope materials. Large translational and rockfall-type landslides form where source rock contains widely-spaced valley-dipping rock discontinuities. The 10^{10}-10^{11} m^3 upper volume limit for landslides with these forms of headscarp apparently relates of the strength and orientation of downhill-oriented discontinuities in large rock masses. Giant bedrock slumps, in contrast, form in the absence of such structures, usually when a potential slip surface can intersect a tectonic-scale plane of weakness in a slope. The bedrock lithologies of large rock masses also can have an important influence on the development of large landslides. In the terrestrial subaerial environment, carbonate rock masses are particularly susceptible to failure in catastrophically large events. Most of these large carbonate landslides are essentially monolithologic. Many formed at the termination of ice age climatic regimes in areas of mountain glaciation, when lateral support was removed by the wasting of large valley glaciers. Others formed in arid climates where limestone strata are relatively resistant to erosion.

In addition to source rock characteristics, a number of processes act to decrease the stability of slopes by increasing the shearing stresses applied to rock masses, such as the removal of lateral support, increased loading, seismic activity, volcanic activity and differential weathering. Rock masses can also be destabilized when the shearing resistance of slope material is decreased by pore pressure increases, weathering, fracture development, and, in particular,

long-term creep. On Earth, these processes have acted in many different environments over geologic time to set the stage for large landslides. However, systematic study of database information in this chapter has revealed that most of the known large terrestrial landslide deposits date from the Pleistocene epoch. This concentration of events can be linked in part to special circumstances caused by the onset, presence and termination of glacial regimes that increased the efficiency of several of the most common slope destabilizing processes. The onset of glacial conditions, for example, had the effect of lowering world-wide oceanic sea levels. Draw-down of the ocean apparently removed significant lateral support from the slopes of many oceanic islands, perhaps fast enough to trigger large-scale slope failures of whole quadrants of the islands. Full glacial conditions, in turn, had the effect of moderating the climates of many presently arid environments. Elevated rainfall during pluvial periods in such environments probably triggered a number of landslides of Pleistocene age by overloading slopes with excessive rain- or snowfall or by causing accelerated weathering and deterioration of discontinuities in large rock masses. Many large Pleistocene landslides date from the termination of glacial advances in mountainous terrain. Landslides were triggered by the removal of lateral support when mountain glaciers wasted away, especially in regions of carbonate bedrock where cold-weather erosional processes acted to decrease in situ rock strength with the greatest efficiency.

Seismic activity is sometimes important in the initiation of large landslides. However, seismic activity not only triggers the movement of large landslides; sometimes the motion of giant landslides can actually produce their own seismic emanations. Two large historical landslides corresponded with significant seismic events: the 1975 Kalapana, Hawaii slump and the 1980 Mt. St. Helens landslide. These events were modeled as "single-force" earthquakes, where the energy of the seismic waves originated directly in the movement of the landslide and coincident short-term decoupling of the landslides from their substrates. This characteristic of giant landslides leads me to hypothesize that these enormous events could conceivably provide a source of seismic energy for triggering other landslides. This is particularly true of the giant Valles Marineris and Hawaiian Ridge landslides that rapidly rotated through thousands of meters following initiation, probably giving rise to sustained moderate-intensity seismic events.

Systemization of eyewitness accounts of landslide initiation indicates that long-term creep plays a crucial role in the initiation of most observed large landslides. In general, a number of processes act on a slope to induce it to begin creeping. Once creep motion begins, it often accelerates with time, weakening a rock slope until it finally fails catastrophically. Large earthquakes sometimes accelerate the process, jarring loose already creep-weakened rock masses. In the absence of an earthquake trigger, the duration of creep preceding catastrophic failure may vary from a few days to tens of years. This time interval depends critically on the thickness of the slide block above the potential slide surface and upon the geometry of the latent detachment surface.

The runout phase comprises the most important step in the chronology of a large landslide because the unknown long-runout mechanism operates during this step. A number of unique depositional characteristics form on and within moving landslides during this phase. These features occur in specific regions on and within large landslide debris streams. They also retain characteristic relationships with one another, allowing the development of a generalized facies model for long-runout landslides.

Large landslides always contain brecciated rock, formed mainly near the base of a landslide during its high-velocity travel over its substrate. The finest component of this comminution process behaves in an extremely mobile, almost fluid manner in the highly sheared interiors of moving landslides. Powder smaller than intermediate sand may in fact mix throughout the mass of a moving landslide lobe from its source near the base of the landslide. This fine-grained component may account for the cohesive behavior of large landslides during their travel, and, as mentioned earlier, this material seems to play a critical role in the long runout of large landslide masses. In most cases, the breccia composing a large landslide is sufficiently disaggregated that the landslides move as thin, ground-hugging debris streams which may seem to flow down channels and around obstructions. The materials composing the debris streams remain quite structured during movement, however. In fact, the deposit of a typical large landslide appears to essentially form a brecciated counterpart of the original slidemass, one that has been elongated in the direction of transport, thinned parallel to the slope and extended slightly or not at all transverse to the transport direction. Thus, the relative three-

dimensional orientations of fragments in the original slidemass are retained in the final deposit, but not the relative spacing of those fragments.

The various depositional characteristics of long-runout landslides display consistent relationships that are repeated in many large landslide deposits. These relationships are particularly similar for landslides deposited in a common environment, but can be extended to landslide deposits in quite dissimilar environments. Yarnold and Lombard (1989) developed a facies model to explain the proximal and distal features of long-runout landslides in arid climates, which can be extended to describe facies relationships for landslides on icy substrates.

Eyewitness accounts suggest that long-runout landslides stop suddenly from high speed. However, while numerous structures develop in the latter stages of movement of long-runout landslides, few provide concrete evidence for a very rapid stopping phase. Newly available Soviet velocity data for the emplacement of two large artificially-triggered landslides suggests that large landslides decelerate gradually from high speed, not suddenly.

Finally, large landslides undergo several modifications following deposition. Just after stopping, they can be subject to clastic dike intrusion and normal faulting. Over time, they become weathered, eroded and buried. The surficial and interior features of carbonate landslides are especially susceptible to post-depositional degradation in most terrestrial environments. Large landslides emplaced on glaciers may experience rapid and severe degradation due to movement and ablation of the underlying ice sheet. Landslides deposited across active stream channels ultimately get breached by stream waters, but failure may occur on quite different time scales. Substantial dams in small drainage basins can last for centuries, but small dams across rivers draining large basins have substantially shorter life expectancies.

Chapter IV. Comparative Planetology of Large Long-Runout Landslides

A. Introduction: Importance of Interplanetary Comparisons

The comparison of large landslide deposits in varying planetary environments plays an important part in unraveling the role of liquid water on the surface of Mars subsequent to its very earliest history. Morphological comparisons between mass movement deposits on Earth and Mars indicate that the closest analogs of many Valles Marineris landslides are terrestrial deposits that were moist at emplacement. The terrestrial analogs include both giant subaqueous landslides as well as large subaerial landslides that incorporated water during travel and evolved into moist or water-saturated slides. Some of the moist-appearing Valles Marineris landslides seem to have inherited moisture from the source rock itself and thus appear gradational with martian outflow channels, while others might have derived water by falling into standing ice-covered bodies of water. Outside of Valles Marineris, martian landslides characteristically display morphologies reminiscent of dry terrestrial landslides.

The comparison of large landslide phenomena on Earth, Mars and the Moon also provides a powerful tool for understanding the motive processes operative in long-runout landslides. The observation, at least on Earth and Mars, of landslides having very similar morphologies (Chapter II) as well as analogous log(volume) vs. H/L relations (Chapter III: Figure 7; McEwen, 1989) strongly indicates that the process(es) responsible for producing long runout (H/L value less than 0.6) in terrestrial landslides also operates on the surface of Mars. Because of the significant atmospheric and gravitational differences between the surfaces of Earth and Mars, the morphology and log(volume) vs. H/L observations place stringent constraints on mechanisms proposed to explain long runout. Most importantly, the martian landslides provide strong evidence that atmospheric effects can play only a minor role in the runout of most large landslides and that mechanisms proposing a critical role for entrained or overridden air masses do not provide a general solution to the long-runout phenomenon.

This chapter first presents a discussion of the characteristics of terrestrial landslides that distinguish dry landslides from those that contain significant quantities of water. This set of observations provides the infrastructure from

which meaningful comparisons between martian and terrestrial landslides can be drawn to assess the role of water in influencing martian landslide phenomena. Following this section, comparisons of martian, lunar and terrestrial landslides are approached in the same structured format as followed in the preceding chapter on landslide systematics. As before, the analysis begins with comparisons of the slope preparation and slide initiation phase. This section includes a consideration of the comparative planetary distribution of landslides on Earth and Mars. The subsequent portion of the chapter compares various aspects of runout- and stopping-phase phenomena for landslides on Earth, Mars and the Moon. This includes a consideration of three groups of martian landslides that have debris apron morphologies suggestive of moist emplacement. Also, comparisons are drawn between a group of smaller martian landslides and their dry terrestrial analogs, a group that includes the Blackhawk landslide of southern California. This section also considers the characteristically greater thicknesses demonstrated by the martian landslides relative to their terrestrial counterparts and the possible causes of this behavior.

B. Wet vs. Dry Landslide Characteristics

Much of Chapter IV considers comparisons of large martian and terrestrial landslides with the intention of determining whether any martian landslides contained water during deposition. This approach first requires a clarification of what features distinguish dry (no perceptible pore water content) from moist (pore water present, but not water saturated) or wet (water saturated) landslides. In the following discussion, comparisons and contrasts are drawn between the characteristics of dry, moist and wet landslides to serve as a basis for assessing the martian landslides for possible water content. This discussion first covers general relationships between the landslides, followed by differences in their morphologies, in their depositional characteristics and in quantitative measures of their behavior.

In general, dry, moist and wet landslides exhibit gradational behavior. By adding water to a dry landslide to generate moist and wet deposits, certain characteristics change perceptibly while others remain largely unvaried. Specifically, some aspects of landslide morphology and depositional characteristics change markedly with increasing water content, while other, more quantitative, measures of landslide behavior change very little. The

primary changes in landslide behavior that accompany increases in water content result from changes in the behavior of the fine-grained component in a moving landslide, as water content does not materially alter the properties of macroscopic rock clasts in a moving landslide or debris flow (Johnson, 1970). No specific water content limits exist to precisely distinguish dry from moist from wet landslides. Based on laboratory reconstitutions of debris flow matrix material (Johnson, 1970; Shaller, unpublished data, 1986), as water is added to fine-grained material, it first has the effect of increasing the density of the material without materially changing its "viscosity" (ease of stirring). This appears to represent the effects of water adsorbing onto fine-grained mineral particles. At about 12-14% water by weight, the viscosity of the fine-grained material changes rapidly with increasing water content. In this realm of water content, all points where water could be adsorbed apparently are filled. Water therefore begins to fill the voidspaces between particles, markedly decreasing interparticle cohesion. During and after mixing this material retains the same grainy appearance. When left to dry, this material simply sets in place like cement. The term "moist" refers to this region of behavior and approximate water content. Above about 14% water content by weight, changes in viscosity become less variable with added increases in water content. At this stage of wetness, additional water appears simply to add to the porespace water content while the material is actively mixed. During mixing, the material takes on a very smooth, homogeneous appearance, but when stirring is halted, excess water is expelled from the mud, forming a water layer above the water-saturated sediment. In nature, debris flows containing this high of a water content presumably dewater when they cease moving. The water liberated from the debris could then cause so-called "clear-water" erosion and redeposition of landslide debris. Landslides interpreted to have contained water-saturated matrix materials are referred to here as "wet."

The morphologies of dry, moist and wet landslides differ from one another in a variety of ways, some distinct, some obscure. Because of the gradational effects of water content on morphology, only those characteristics most distinctive to separating dry from wet from moist landslides are discussed here.

Detailed field observations of many large terrestrial landslides indicate that they contained little or no pore water content during runout. These landslides exhibit many different large-scale morphologies. Six large unconfined landslides known to have been dry during runout from field observations,

however, exhibit a common, distinctive large-scale morphology that differs markedly from that of any known moist or wet landslides. These landslides have rockfall-type headscarps, detached debris aprons, a distally-raised profile shape, a blunt to slightly lobate plan form, distinctive marginal ridges or levees, and a surficial texture of oblique imbricated ridges (Chapter III: Figure 34). This distinct assemblage of features is not represented on any known moist or wet landslides, especially the distally-raised profile shape and the oblique imbricated ridge pattern. The six landslides exhibiting these characteristics consist of the Blackhawk and Silver Reef landslides of southern California (Shreve, 1968a), and the Loma Redonda, Loma de la Aspereza, Avalancha del Zarzo 1 and Avalancha del Zarzo 2 landslides of northwestern Argentina (Fauque and Strecker, 1988; Appendix A). Shreve (1968a) stated that all the field evidence at the Blackhawk and Silver Reef sites argued for dry emplacement of the landslides:

> Mechanical considerations show that the time-average velocity of the material in a wide, moving debris flow increases from zero at the bed to a maximum at the upper free surface; hence the surface material travels faster than the forward edge, eventually overtakes it, and is rolled under the advancing debris. Material found at the forward edge of a debris flow, therefore, necessarily arrived there by way of the upper surface. This means that, barring a remarkable coincidence, the Blackhawk landslide cannot have decended the alluvial slope simply as an unusually large debris flow, because the sandstone "breccia" at its distal edge is unaccompanied by similar material anywhere on its upper surface. Instead, it must have moved as a nearly undeforming sheet sliding on a relatively thin, easily sheared lubricating layer.

Also:

> A layer of water and mud...most probably was not present...under the Blackhawk and Silver Reef landslides, which traversed well-drained gravel-surfaced desert alluvial fans. Corroborating this conclusion is the fact that, in the few places where the base of the Blackhawk is exposed, it rests directly upon the underlying stratified gravel with no trace of a mud layer.

Similarly, Fauque and Strecker (1988) argued that the four Argentine "Blackhawk-like" landslides contained no water during deposition:

> Water is excluded as a lubricant and fluidizing agent for the avalanches at Sierra Aconquija because the avalanches have maintained their original morphology with sharply defined frontal lobes. The lobes are not disturbed by any outrunner blocks or protrusions of debris-flow-like material, as might be expected after a water/mud-based transport.

> Furthermore, for the involvement of a fluid component the fine material fraction of medium to fine sand and of silty sand appears too coarse to cause the buoyancy of larger particles as in a debris flow, for example.

Thus, the available evidence for these landslides suggests that the Blackhawk-like landslide morphology occurs only in dry, unconfined landslides.

A number of large terrestrial landslides display characteristics suggestive of moist deposition. These include lobate terrestrial subaerial deposits, such as the Carlson, Idaho landslide (Appendix B), as well as some subaqueous landslides off the Hawaiian Ridge (Lipman, et al., 1988) that do not appear to have been water saturated during emplacement.

The Carlson landslide of east-central Idaho exhibits field relations suggesting that it contained considerable pore water (i.e., moist) during runout. Its distinctive large-scale morphology distinguishes it from any known dry or wet landslides (Figure 36). The landslide has a complex rockfall-type headscarp, a detached debris apron, a tapered profile shape, a highly symmetrical lobate plan form, distinctive marginal ridges or levees, and a hummocky surficial texture marked medially by concentric ridges and troughs and distally by longitudinal ribbing (Appendix B). The morphology of the Carlson landslide differs from that of lobate dry rock landslides in having a much more symmetrical basal lobe than any known dry landslides, a much more regular pattern of longitudinal ribs, lower relief and a much smoother surficial texture (Figure 36). The fact that the landslide gives no indication of having dewatered after deposition suggests that it was moist during deposition, not water saturated. Exposures of the interior of the landslide show it to consist of unabraded basalt clasts supported in a fine-grained matrix of the same composition, a texture similar to that of common desert alluvial fan debris flows. The lack of abrasion and shattering of basalt clasts strongly distinguishes this deposit from common dry rock landslides, in which brecciation occurs at all scales (Chapter III: Figures 23a-23c).

The lobate-terraced texture forms a second morphology associated with moist deposition of landslide debris (Chapter II: Figure 6c). The lobate-terraced texture consists of large-scale rounded stair step-like overlapping lobes of landslide debris. On terrestrial subaqueous landslides, each rounded terrace, or stair step, may measure 1-5 km across, and rounded terrace risers may measure as much as 100-200 m high (Lipman, et al. 1988). Lipman, et al.

Figure 36. Illustration of the comparative morphologies of moist and dry lobate landslides. The upper diagram shows the moist Carlson landslide, Idaho, the lower diagram the dry Martinez Mountain rock avalanche of southern California (both photographs by J. S. Shelton). Both landslides measure approximately 1.6 km across at their widest parts. As compared with the dry Martinez Mountain slide, the Carlson landslide has much lower relief, a much more closely spaced, regular pattern of radial ridges along the toe and a far more symmetrical basal lobe plan form. In addition, the surface of the Carlson slide is dominated by gravel- and cobble-sized clasts in a fine-grained matrix whereas the Martinez Mountain landslide is mantled by an interlocking jumble of meter- and larger-sized boulders.

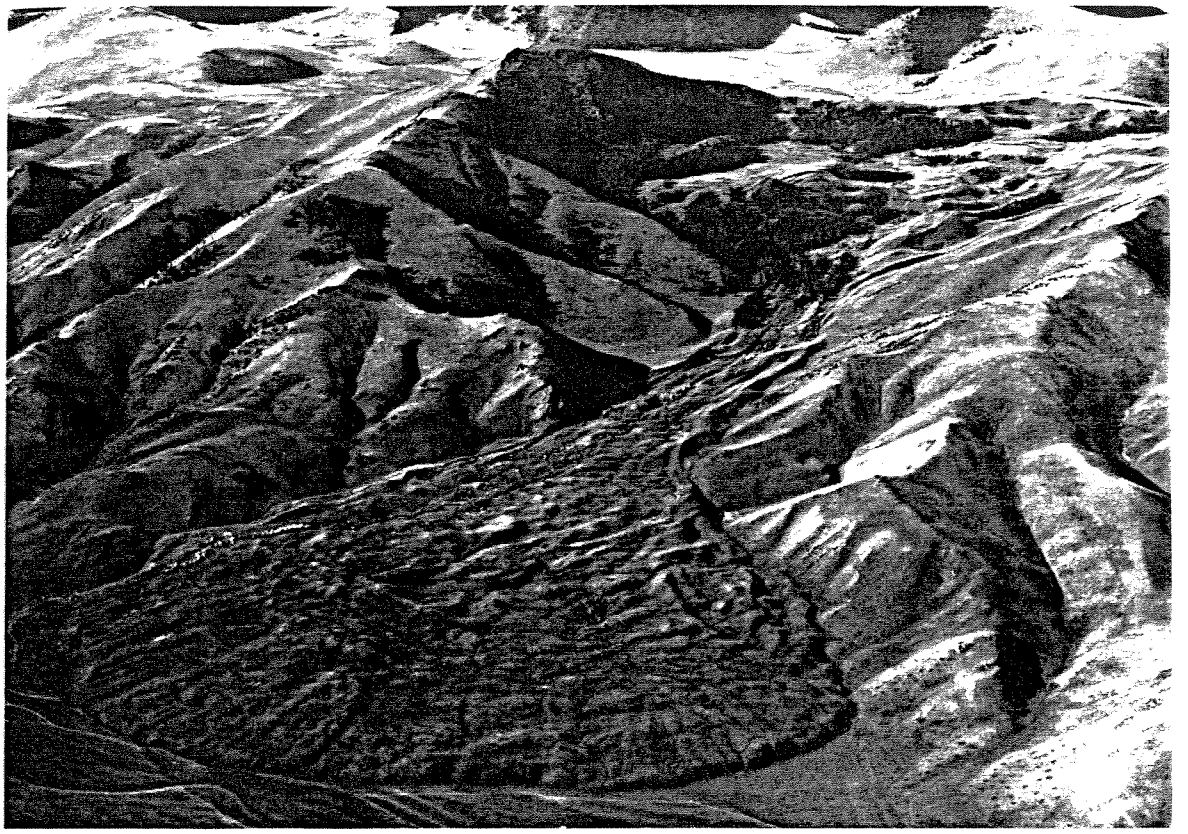

(1988) proposed that the lobate-terraced morphology observed in GLORIA side-scan sonar images probably developed by way of viscous flow of water-rich landslide debris, because of the morphologic similarity of this debris to silica-rich lava flows and to subaerial debris slides and mudflows. In all observed instances, this texture does not grade into water-dominated deposits, suggesting moist, rather than water-saturated deposition. Because lobate-terraced debris aprons occur from isolated Cretaceous seamounts adjacent to the Hawaiian Islands (Lipman, et al., 1988), they must form in predominantly fine-grained debris. Numerous terrestrial examples of the lobate-terraced texture occur on landslide debris aprons southwest of Hawaii Island (Chapter II: Figure 6b; Lipman, et al., 1988).

A number of large terrestrial landslides have morphologies indicative of water-saturated emplacement. Both water-saturated subaerial landslides, such as the Mt. Shasta (Crandell, 1989), Mt. St. Helens (Voight, et al., 1983) and Golungung (Siebert, 1984; Crandell, 1989) volcanic slides, as well as large subaqueous landslides, like the Alika 1 and 2 deposits (Lipman, et al., 1988), may exhibit these morphologies. A strong morphologic signpost for water-saturated deposition, both in the subaerial and subaqueous environments, is a combination of distinct and indistinct distal margins. Along indistinct margins, landslide debris often grades imperceptibly into water-dominated sedimentary deposits. As mentioned above, water-saturated matrix material may contain much more water in an agitated state than at rest. Thus, when a water-saturated landslide comes to rest, pore waters characteristically are expelled from the deposit which flow downslope and rework the surface, obscuring the original margin of the landslide. Because the clear waters expelled from the landslide winnow fines from the landslide, this process can generate mud or debris flows that can travel many kilometers from the original distal margin of a landslide. Numerous water-saturated subaerial and subaqueous landslides formed features of this sort. Subaerial examples include the Huascaran 2 and 3 (Plafker and Ericksen, 1978), Mt. St. Helens (Voight, et al., 1983), Pungarehu (Ui, et al., 1986) and Mt. Shasta (Crandell, 1989) landslides. Subaqueous examples include the Alika 1 (Lipman, et al., 1988) and Nuuanu landslides (Moore, et al., 1989). The deposits of these subaqueous Hawaiian Ridge landslides were documented by GLORIA side-scan sonar and, for the Nuuanu deposit, by a distal core sample (Lipman, et al., 1988; Moore, et al., 1989).

The distal outrunner blocks debris apron texture forms another morphology associated with moist or water-saturated emplacement. This texture generally occurs solely on subaqueous landslides, but it also appears to have begun to develop on a subaerial landslide that traveled into the shallow margin of a lake during runout. The distal glide blocks texture describes peripheral zones of scattered large mounds beyond the margins of massive landslide deposits (Chapter II: Figure 6b). Blocks observed fringing large terrestrial subaqueous landslides often measure several kilometers across and stand 100-200 m above the sea floor and may be separated from the main landslide mass by as much as 3-4 km of seemingly undisturbed sea floor sediment (Lipman, et al., 1988). Depending on the interpretation of the texture, it may represent either moist or water-saturated emplacement. Lipman, et al. (1988) theorized that the isolated glide blocks texture originated by way of segregation of matrix material from blocks after the culmination of movement of the landslides, implying water-saturated emplacement. Lipman, et al. (1988) postulated that fluids segregated from a landslide following deposition might erode away material along its toe to such an extent that only resistant blocks carried down in the landslide remained behind. An alternative origin for the glide blocks is that they originate outside the margins of large submarine landslides as associated slope failure products, and glide along ahead of the landslides along saturated, slippery substrate sediments (Prior, et al., 1984). A third possibility is that the blocks originate within the margins of a large landslide, then become separated from the landslide and glide along ahead of it atop a slippery substrate. This possibility is suggested by the Panum landslide, a subaerial landslide which slid out into the shallow margin of Mono Lake during runout (Sieh and Bursik, 1986; Sieh, personal communication, 1988). When the landslide slid out onto the shallow margin of the lake, it began to disaggregate into large cohesive blocks separated by mobile substrate material that intruded upwards between the blocks (Sieh, personal communication, 1988). Had the landslide traveled farther into the lake, it may have split off individual blocks, perhaps as occurred in the larger subaqueous landslides. The latter two interpretations do not require water-saturated conditions for a landslide mass, so that the distal glide blocks texture might instead represent moist deposition. Terrestrial landslides that exhibit the isolated glide blocks texture include the Alika 1 and

2 (Lipman, et al., 1988) deposits, as well as the South Kauai, Nuuanu, South Kona and perhaps other large Hawaiian Ridge landslides (Moore, et al., 1989).

Large moist and wet landslides differ from dry landslides on the basis of a number of additional depositional characteristics not outlined above. For example, the internal motions of moist and wet landslides appear rather less structured than those of dry landslides; unlike dry landslides, preserved headscarp stratigraphy has never been reported from moist or water-saturated landslides. The low internal friction afforded by moist matrix material appears responsible for this behavior. Moist and wet landslides can mix and overturn during runout, while dry landslides appear too viscous or rigid to do so. In addition, large moist and wet landslides fail to exhibit the reverse grading characteristic of dry long-runout landslides (Appendix B; Crandell, 1989). Enhanced internal mixing of moist and wet landslides during runout relative to dry deposits again appears responsible for this behavior. The preservation of slope-parallel stratigraphy in reverse-graded dry landslides such as El Capitan (Krieger, 1977; Chapter III), suggests that the clasts on the surfaces of large dry landslides begin and end motion there. In moist landslides, in contrast, vertical internal motions appear strong enough to homogenize the landslide debris during runout. Moist and water-saturated landslides also commonly exhibit a proximal-to-distal decrease in block-to-matrix ratio, corresponding to an overall fining of debris size with travel distance (Appendix B, Ui, et al., 1986; Crandell, 1989). Dry landslides do not exhibit this behavior per se. While dry long-runout landslides do develop an increasingly thick basal layer of fine, powdered debris with travel distance (Chapter III: Figure 31), this grain size diminution is not apparent on the surface of a large dry landslide. Apparently the homogenization of debris in moist and wet landslides mixes fines formed during runout throughout the body of a landslide, so that all parts of the landslides appear to decrease in average grain size and block-to-matrix ratio with distance traveled. The small-scale surface textures of large moist and wet landslides also differs considerably from that of dry landslides. The surfaces of dry landslides usually consist of a carpet of boulders relating to natural patterns of jointing in the host bedrock. The smoothest large dry rock landslides are composed of the small clast sizes; the surfaces of the Blackhawk and Silver Reef landslides of southern California (Shreve, 1968a), for example, consist almost entirely of ~3 cm limestone clasts. More commonly the rock fragment size measures from

meters to tens of meters in minimum dimension (Krieger, 1977; Bock, 1977; Yarnold and Lombard, 1989). The surfaces of moist and wet landslides, in contrast, appear to consist largely of fine-grained matrix material punctuated by occasional clasts and boulders of varying scale (Appendix B). Often the surfaces of these landslides are marked by large-scale hummocks. In water-saturated landslides, these generally represent large buried boulders that experienced partial exhumation during late-stage dewatering and mobilization of surface fines (Ui, et al., 1986; Crandell, 1989). Hummocks on the moist Carlson landslide are often crested by inset clasts having the appearance of paving stones set into the ground (Appendix B). These features may also represent buried boulders, but ones that escaped exhumation because of a lack of post-depositional dewatering.

The preceding discussion shows that certain qualitative differences in landslide morphology and depositional characteristics can be used to distinguish dry, moist and wet landslides. The observable qualitative differences between landslides of varying water content suggest that perhaps more quantitative measures of landslide properties might exist to provide less subjective estimates of the water content of large landslides. Three quantitative measures of landslide characteristics have been proposed to distinguish dry from water-bearing landslides (McEwen, 1989): log(volume) vs. H/L trends, apparent yield strength measurements and velocities. McEwen (1989) made these measures on a number of martian landslides in Valles Marineris and used the data to argue against a role for water in the martian deposits. These quantitative measures are evaluated below to ascertain their ability to distinguish landslides of varying water content.

Figure 37 compares the log(volume) vs. H/L trend of eight large moist and wet terrestrial landslides with that calculated for 163 other volcanic and non-volcanic terrestrial subaerial landslides. The moist and wet landslides plot well within log(volume) vs. H/L envelope for all terrestrial subaerial landslides, indicating that their overall runout geometries differ little from those of dry rock avalanches of similar volume. In addition, the RMA best-fit line through the moist and wet landslide datapoints (Chapter III) does not differ significantly in slope from the best-fit line through data for dry rock landslides having small modal (most common) grain sizes (Chapter III: Figure 12b). Thus, according to their log(volume) vs. H/L relations, moist and wet

Figure 37. Plot of log(volume) vs. H/L relations of moist and wet long-runout landslides as compared with the trend for all large terrestrial subaerial landslides.

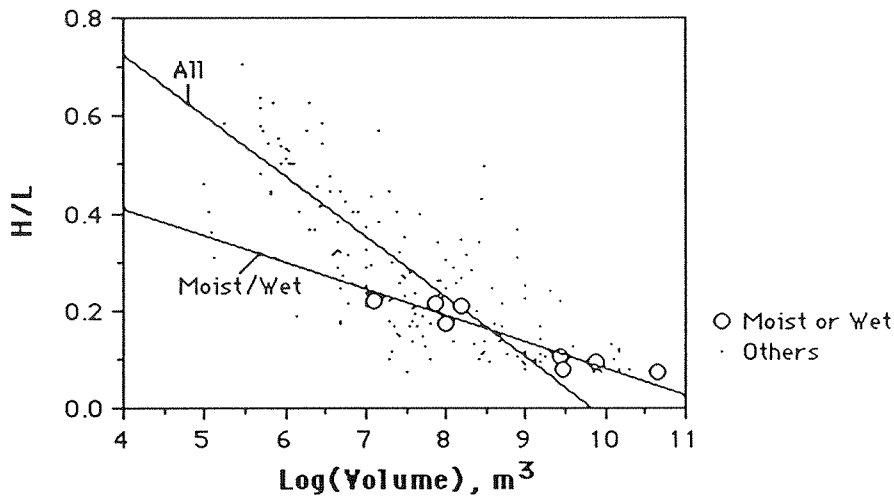

Moist/Wet: H/L = -0.0539 Log V + 0.622, R^2 = 0.874, se_s = 0.0676, se_i = 0.060

All: H/L = -0.124 Log V + 1.222, R^2 = 0.572, se_s = 0.00635, se_i = 0.0486

landslides behave essentially like fine-grained dry rock landslides during runout.

Many geological flow phenomena experience movement only when subjected to basal shear stresses beyond a certain "yield strength." As a first approximation to their material properties, such substances are often modeled in the geologic and engineering literature as Bingham plastics. Examples include the flow of muds, sludges and suspensions through pipes (Caldwell and Babbitt, 1941), the flow of glaciers (Nye, 1951), lava flows (Hulme, 1974), debris flows (Johnson, 1970; 1984), wet landslides (Voight, et al., 1983) and dry rock avalanches (Eppler, et al., 1987; McEwen, 1989). Two characteristics cited as indicative of large-scale plastic behavior are halting of motion on a slope and the presence of a parabolically-shaped distal profile, or "snout" along the toe of a deposit (Johnson, 1970). Equation 10 gives the basic yield strength formula, which assumes a Bingham rheology and steady flow conditions (Johnson, 1984):

$$k = \rho\, g\, D \sin \beta \tag{10}$$

where k is the yield strength in Pa, ρ is the density in kg/m^3, D is the deposit thickness in meters, g is the gravitational acceleration in m/s^2 and ß is the ground slope in degrees. The application of an equation describing the snout of a Bingham plastic glacier (Nye, 1951) provides a second method of estimating the yield strength. Assuming a small ground slope (Nye, 1967), Equation 11 gives the model snout profile:

$$x - A = (h/\alpha) + (h_o/\alpha^2) \ln| \alpha\, h - h_o | \tag{11}$$

with α the basal slope angle in rad, x horizontal distance (m), h the height (m) and A a constant. The variable h_o represents the ratio $k/\rho g$, where k, ρ and g are as above. Table 13 reports estimated yield strength values for two moist landslides and one dry rock landslide, together with estimated strength data from some other terrestrial mass movement deposits. Variations between these values are probably significant only for order-of-magnitude and greater strength differences. Table 13 shows that moist and wet terrestrial landslides exhibit about the same strength as the Chaos Jumbles dry rock avalanches, and greater strength than the Surprise Canyon debris flow and the Sherman landslide. Thus, moist and wet terrestrial landslides exhibit strength

Table 13. Yield Strength Estimates for Landslides and Debris Flows Assuming Simple Plastic Behavior

Name	Yield Strength (Pa)	Reference
Ice	100,000	Nye, 1951
Carlson ls	60,000-88,000[2]	Appendix B
Carlson ls	19,000[1]	Appendix B
Mt. St. Helens ls	2,000-20,000[1]	Voight et al., 1983
Chaos Jumbles ls	6,000-10,000[1]	Eppler et al., 1987
Surprise Cyn. df	2,000[1]	Johnson, 1984
Sherman ls	2,000[1]	McSaveney, 1978

Abbreviations: ls = landslide; df = debris flow
1 = Calculated using Equation 10, $k = \rho g D \sin \beta$.
2 = Calculated using Equation 11, profile method.

properties closer to dry rock landslides than to typical desert alluvial fan debris flows. Apparently, the matrix materials in the water-containing landslides contained sufficient moisture to flow, but little enough water to retain significant strength. This corresponds to an observation by Johnson (1970) that the strength of a fine-grained sample from a debris flow in Panamint Valley, California, increased over an order of magnitude when the debris lost only two percent water by weight. The comparatively low strength of the Sherman glacier landslide might have resulted from sliding and spreading of the landslide on a mobile low-strength cushion of snow (McSaveney, 1978). These results indicate that yield strength estimates alone can not be used to distinguish dry from moist or wet landslide deposits.

Runout velocity provides a third possible quantitative measure to distinguish dry from moist and/or wet landslides. For example, McEwen (1989) suggested that "High velocities (>50 m/s) are characteristic of large dry rock avalanches rather than water-saturated debris flows..." Table 14 reports velocity estimates for a number of large dry, moist and wet landslides. The data in the table distinctly show that moist and wet landslides do not travel at characteristically lower speeds than dry rock landslides. Rather, the moist and wet landslides tend to travel near the upper end of velocities reported for all large landslides. Thus, like the other quantitative measures tested, the overlapping velocity ranges of dry, moist and wet landslides rules out velocity as a method of distinguishing dry landslides from those having substantial water contents.

The failure of all the quantitative measures of landslide properties proposed by McEwen (1989) to separate dry from water-rich terrestrial landslides clearly invalidates the use of these measures to rule out the presence of moist or wet landslides on Mars. Later in this chapter, I show that the detailed morphological criteria that distinguish dry from moist or water-saturated landslides on Earth can be applied to the evaluation of martian landslide deposits. Based on morphology, a small number of martian landslides appear to have contained liquid water during runout.

C. Slope Preparation and Slide Initiation

The local and regional patterns of landslide initiation vary significantly between Earth, the Moon and Mars. The locations of large landslides on Earth coincide with three principal terrestrial environments (mountain ranges,

Table 14. Estimated Velocities of Terrestrial Subaerial Landslides

Name	Velocity (m/s)	Name	Velocity (m/s)
Rubble Creek	20	Tin Mtn.	56
Puget Peak	22	Koefels	56
Chibins 1	22	Chibins 17	58
Mageik	24	Scima di Saoseo	58
Vaiont	25	U.S.S.R. Artificial 1	58
Silver Reef	28	Bualtar 1	62
Khait	28	Stanley	62
Altdorf-Spiringen	31	Bormio	62
Twin Sildes 2	31	Mayunmarca	62
Black Canyon mb	33	Obersee	64
Ennetbühl	33	Blackhawk	65
North Nahanni	33	Glärnisch Guppen	67
Martinez Mtn.	36	North Arm	69
Tahoma Peak	39	Parpan	69
Goldau	39	**Mt. St. Helens***	**70**
Elm	42	Socompa Volcano	70
Biasca	44	Poschiavo	72
Corno di Dosde	44	Loma de la Aspereza	74
Madison	44	**Huascaran 3***	**78**
Voralpsee	44	Rockslide Pass	78
Hope	44	Chaos Jumbles 1	79
U-turn	44	Kandertal	83
U.S.S.R. Artificial 5	46	**Huascaran 1***	**87**
Gros Ventre	46	Chaos Jumbles 3	97
Huascaran 2*	**47**	Altels	100
Frank	49	Avalanche Lake	100
Sherman	51	Flims	100
Chaos Jumbles 2	55		
Disentis	56		
Triple	56		

*Moist and Wet Landslides in Bold Face Type

volcanoes, continental shelf margins) that commonly develop high, oversteepened topography. With certain exceptions, the proper conditions could develop at many sites on Earth at any time for triggering these events. In comparison, the circumstances of lunar landslide initiation all appear related to the impact processes that dominate the surface of the Moon. The process of landslide initiation on Mars, in turn, differs markedly from the lunar and terrestrial patterns. Landslides appear to have occurred on Mars in different high-relief locations at different times related to the geologic evolution of the planet. Landslides in Valles Marineris exhibit significantly different initiation styles than those occurring outside the equatorial chasma system.

In the following description of landslide characteristics on the Moon and Mars, much discussion centers around dating of surficial units using crater counts and upon the cratering history of the two planets. Much of the information available on the geologic histories of the Moon and Mars comes from the simple observation that older surfaces are more cratered than younger ones. According to Carr (1981), the rate of impact on planetary surfaces today is low and is strongly dependent on the size of the impacting object. For every ten-fold increase in size, the number of impacts decreases by a factor of about one hundred. On Earth, on which the flux of impacting bodies ranges within a factor of two or three of that on the other inner planets, a crater larger than 1 km forms on average only every two to three hundred thousand years in an area the size of the United States (10 million km^2; Carr, 1981). A crater larger than 10 km in diameter, in contrast, forms every ten to twenty million years and one larger than 100 km once every billion years. In addition Carr (1981) states that: "The rates of cratering on all planetary bodies are so low that if a surface appears cratered in a spacecraft image, it is almost certainly old compared with most features on the surface of the Earth. If several craters larger than 100 km in diameter are present on a planetary surface, then it almost certainly dates back to very early in the history of the planet, when impact rates were much higher than now."

Carr's latter statement comes as a direct outgrowth of radiometric age determinations made on lunar soil and rock samples returned by the Apollo missions. Most of the lunar samples dated at no more than about 4 billion years in age, indicating that a phase of global erosion, metamorphism and impact reworking reset the radiometric clocks in these samples over half a billion

years after the Moon first formed as a solid object. It is believed that this phase of geologic upheaval was caused by a massive bombardment of impacting objects that tailed off about 4 billion years ago, a phase termed "late heavy bombardment" (Murray, et al., 1981).

The heavily cratered terrain that forms much of the southern hemisphere of Mars has an appearance much like the lunar highlands, with clusters of large craters, multi-ringed impact basins and intercrater plains, and appears to record an ancient bombardment history similar to that deciphered for the Moon (Murray, et al., 1981). However, the ancient martian environment recorded in the heavily cratered terrain must have been dramatically different from the current martian environment and from the environment of the early Moon. This is because early Mars was dominated not only by impact, but probably by significant atmospheric erosion and volcanism as well. According to Murray, et al. (1981):

> The surface appears to have been continually modified during the period of heavy bombardment. Most of the large martian craters are clearly degraded (i.e., have "soft"-appearing rims; flat featureless floors; no secondaries; and few continuous deposits). They do, however, display a range of morphologies and degradation that implies modification during an extended period of crater formation. The paucity of smaller craters in some areas of Mars, compared with the Moon and Mercury, suggests that ancient depositional or erosional processes buried or destroyed small craters and subdued large craters *before* cessation of heavy bombardment.

After the cessation of heavy bombardment, the surface of Mars, like the Moon and Earth, appears to have been subject to a light bombardment flux that continues to the present (Carr, 1981).

On Earth, large landslides take place in a few principal environments. These include: 1) continental mountain ranges; 2) continental and oceanic volcanoes; and 3) continental shelf sedimentary sequences. Because each of these terrestrial environments has existed on Earth for most of its geologic history, large landslides have doubtless formed at many different times and places on the planet over time. Unlike Mars' one-way geologic evolution, the Earth repeatedly builds and rebuilds environments conducive to large landslide generation. Nevertheless, the current distribution of large landslides on Earth probably differs slightly from many earlier terrestrial distributions because of the effects of the geologically recent Pleistocene glacial advances. In particular, the Earth may exhibit more of these deposits at

present than at times in its geologic past because of special conditions related to the Pleistocene glacial advances (Chapter III). Examples include: 1) the triggering of giant landslides from oceanic volcanoes due to draw-down of oceanic sea levels at the onset of glacial conditions (Fairbridge, 1950); 2) the initiation of large continental landslides in currently arid climates due to heightened precipitation during glacial regimes (Stout, 1977); and 3) the triggering of creep and failure of large landslides in glacially-eroded valleys at the conclusion of glacial advances induced by the removal of lateral support when mountain glaciers wasted away (Heim, 1932).

On the Moon, large landslides occur in association with impact craters. In particular, they have been noted to occur within small bowl-shaped craters, in the ejecta blanket outside of the far-side crater Tsiolkovsky, and from a massif in the Taurus Mountains, part of the boundary of the Mare Serenitatis impact basin (Howard, 1973a). The two largest lunar landslides, the Tsiolkovsky and Apollo 17 deposits, appear to have formed as a direct result of impact-induced seismicity. The Tsiolkovsky landslide (Appendix A), for example, probably formed during or immediately after the impact that formed the crater (Howard, 1973a). The second-largest lunar landslide, the Apollo 17 "light mantle" deposit (Appendix A), in turn, appears to have been triggered when distant (~2250 km) secondaries from the Tycho cratering event impacted at the crest of the source slope for the landslide (Lucchitta, 1977). The Tsiolkovsky landslide appears to be a unique phenomenon in the solar system. Nothing like it has been observed elsewhere on the Moon or on Mars, where all the known landslides took place from the *interior* walls of impact craters, long after the actual impact events that formed the craters. The Tsiolkovsky deposit belongs to the Imbrian System of lunar stratigraphy and therefore dates from the first quarter of lunar history, between roughly 3.9 and 3.4 billion years ago (Murray, et al., 1981). The landslide thus may have formed as a result of some unusual property of the early lunar crust, or perhaps of the impactor; the origin of the deposit remains an open question. The Apollo 17 landslide, in contrast, was triggered by the impact of high-velocity secondaries from Tycho between 50 and 100 million years ago (Lucchitta, 1977). This type of landslide initiation probably has taken place at other times in other locations on the Moon, especially in the late heavy bombardment period. These older deposits probably cannot be recognized today, however, because of continual impact gardening and degradation of the surface over time.

As on Earth, and unlike the Moon, the distribution of landslides on Mars relates primarily to endogenic planetary processes. Landslides on Mars do not have a random distribution, but rather occupy certain preferred sites on the surface of the planet. The landslides are primarily restricted to equatorial regions of the planet and none appear to occur poleward of about 50° latitude (Figure 38). The absence of landslides in the polar regions may in part relate to the aeolian terrain-mantling deposits that cover and soften topography poleward of approximately 30° N and S latitudes (Figure 39; Carr, 1981). Although the martian surface north of about 30° latitude generally has low relief that would not favor the triggering of large landslides, much of the heavily cratered southern hemisphere south of 30° S exhibits considerable relief (Scott and Tanaka, 1986; Greely and Guest, 1987; Tanaka and Scott, 1987). This region contains many of the same units marked by landslides in equatorial regions of Mars (Figure 38). Thus, either landslides formed in the southern highlands and were subsequently buried and obscured by the aeolian mantle, or landslides never formed in the region. Only major features of relief appear through the aeolian mantle, which thickens poleward, suggesting that if landslides (40-80 m thick in occurrences in craters elsewhere on the planet) were blanketed by the mantle, they would not be visible today. Large landslides have apparently failed to form in the mantling material itself because of its gentle slopes and/or because the material is strongly cohesive. By far the greatest concentration of landslide deposits on Mars, 103 out of 161 total, or 64%, occurs in the Valles Marineris chasma system (boxed region in Figure 38; Figure 40). Outside of Valles Marineris (Figure 38) most of the large landslides occur in ancient cratered terrain (39/57, 68%), followed by landslides from the walls of outflow-cut channels (4/57, 7%) and by three landslides each in hummocky (fretted) terrain, from volcanic constructs, and from elevated regions in plains units. Two landslides each occur in the hummocky (chaotic) and hummocky (knobby) terrains, while only one deposit exists in the cratered plains unit.

Within Valles Marineris all of the landslides originated from the wall rock forming the perimeters of the chasmas; none originated in the layered deposits that floor the chasmas in places (unit *Hvl*, Figure 39), even though in many areas the layered terrain exhibits steeper slopes than the wall rock (McCauley, 1978; U. S. Geological Survey, 1986c). Most of the smaller landslides in Valles Marineris originated from steep bedrock outcrops cresting the

Figure 38. Distribution of martian landslides (red dots) outside of Valles Marineris chasma system plotted on map of martian physiographic provinces (Mutch, et al., 1976). Landslide distribution inside boxed area shown in Figure 40. Physiographic units as follows: *polar units* include *pi* (permanent ice), *ld* (layered deposits) and *ep* (etched plains); *volcanic units* include *v* (volcanic constructs), *pv* (volcanic plains), *pm* (moderately cratered plains), and *pc* (cratered plains); *modified units* include *hc* (hummocky terrain, chaotic), *hf* (hummocky terrain, fretted), *hk* (hummocky terrain, knobby), *c* (channel deposits), *p* (plains, undivided), and *g* (grooved terrain); *ancient units* include *cu* (cratered terrain, undivided) and *m* (mountainous terrain).

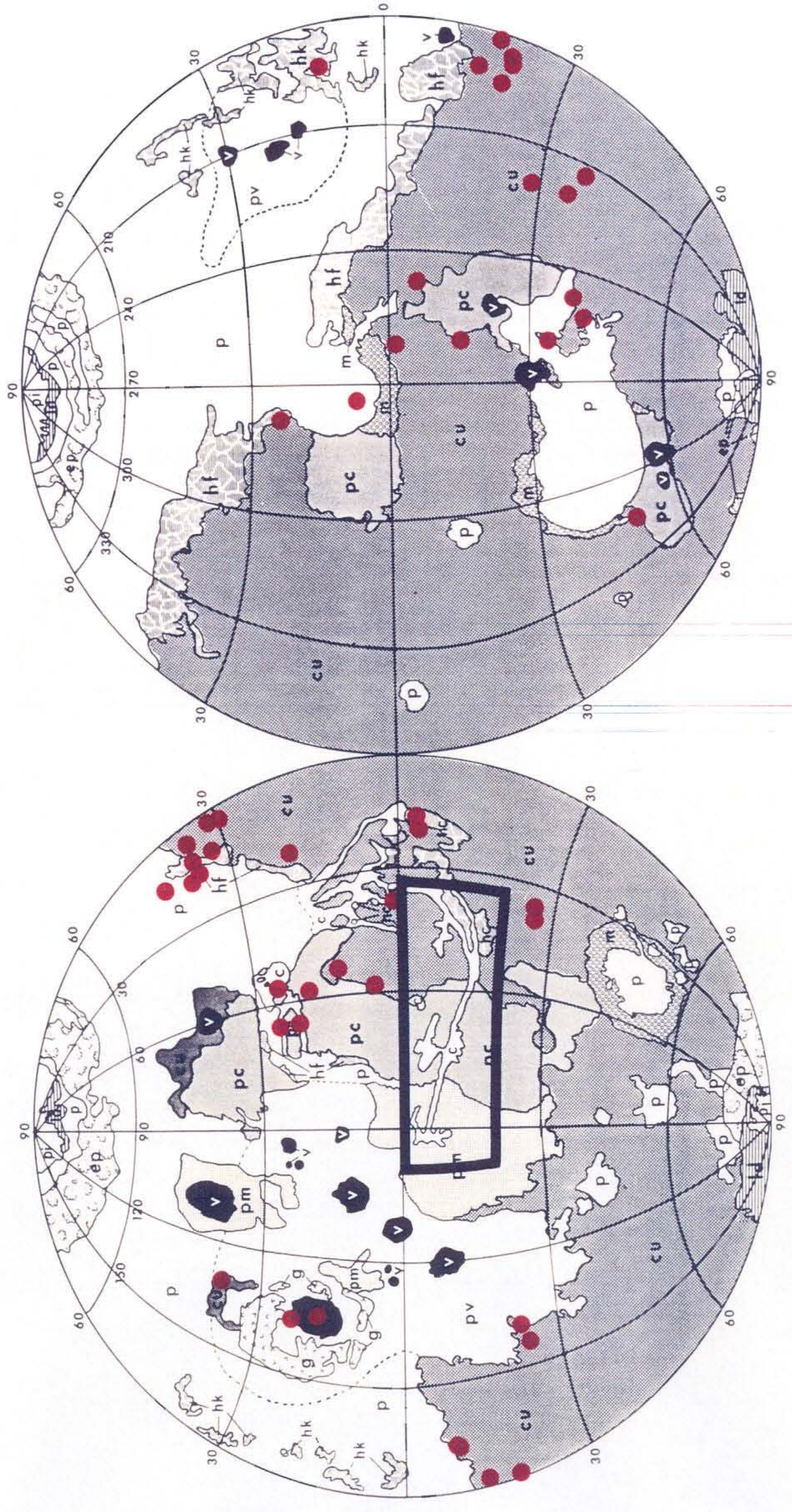

0
30
60
90
120
150
210
240
270
300
330
cu
pc
p
pv
pm
hf
hk
m
v
c
g
ep
ld

Figure 39. Latitudinal distribution of areas unmantled by aeolian sediments. Thickness of cover (shown unshaded) probably decreases from poles to a thin or nonexistent cover at ±30° latitude (Mutch, et al., 1976).

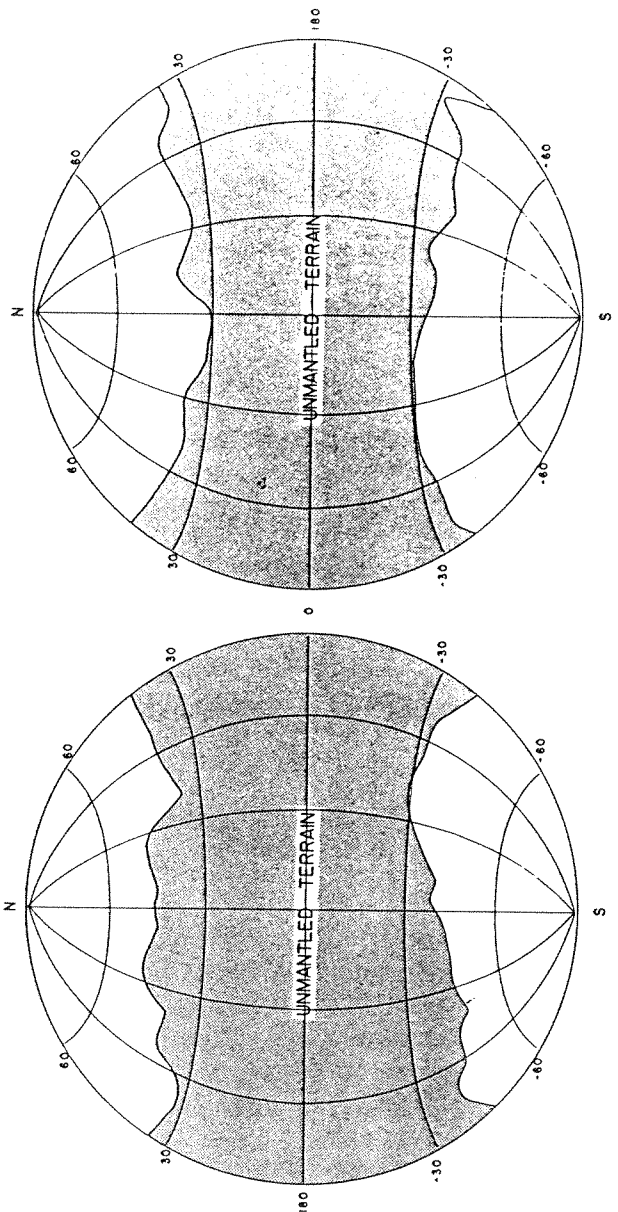
UNMANTLED TERRAIN
UNMANTLED TERRAIN
N
S
N
S
180
30
60
-30
-60
0

Figure 40. Distribution of martian landslides (red dots) in Valles Marineris chasma system plotted on geologic map of the western equatorial region of Mars (Scott and Tanaka, 1986). Heavy border marks area bounded by -20° latitude and equator, 35° and 100° west longitude, the same area boxed in Figure 38. Geologic units as follows: *channel-system materials* include *Hch* (older channel) and *Hcht* (chaotic materials); *western volcanic units* include At_5 (Tharsis volcanic unit #5), *Hsu* (upper member, Syria Planum Formation) and *Hsl* (lower member, Syria Planum Formation); *Valles Marineris* units include *As* (surficial deposits), *Avf* (Valles Marineris floor material) and *Hvl* (Valles Marineris layered material); *plateau sequence* units include Hpl_3 (smooth unit), Npl_2 (subdued cratered unit), Npl_1 (cratered unit), *Nplr* (ridged unit) and *Nplh* (hilly unit); *ridged plains material* is designated *Hr; highly deformed terrain material* includes *Hf* (younger fractured material) and *Nf* (older fractured material); other units include *Hnu* (undivided material), *v* (volcanic construct), *c* (impact crater rim and ejecta; yellow if superposed, brown if partly buried). Ball-on-bar symbol marks faults and grabens, diamond-on-bar symbol gives trend of mare-type wrinkle ridges.

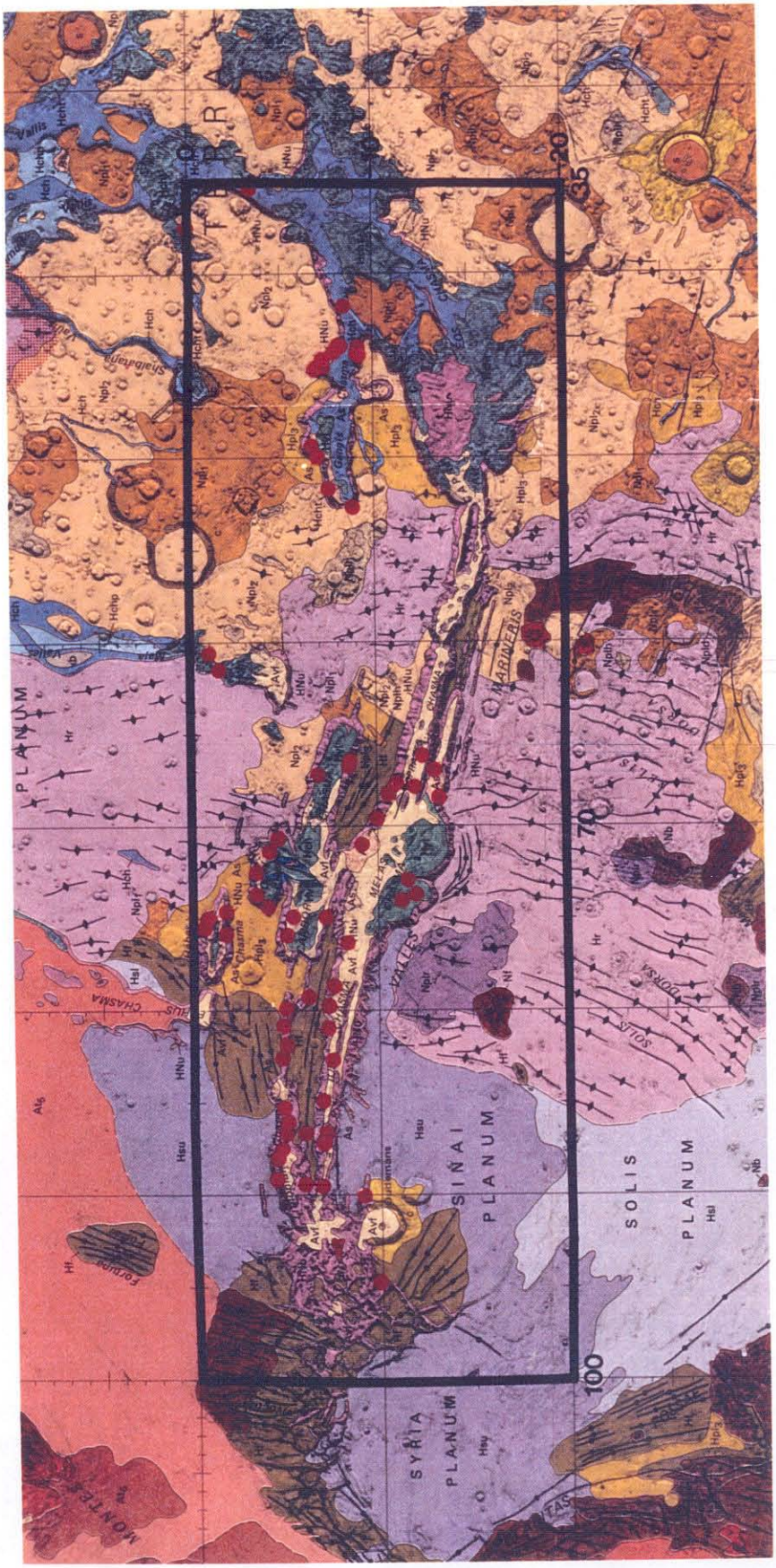
SOLIS PLANUM
SYRIA PLANUM
SINAI PLANUM
MARINERIS VALLES
SOLIS DORSA
20
35
70
100

margins of the chasmas (Chapter II: Figures 6h; Chapter III: Figure 17a). These bedrock outcrops commonly extend small distances above the large talus deposits that line the chasma walls in most locations (Lucchitta, 1978b). Like large terrestrial rockfalls, these landslides probably originated from bedrock outcrops containing chasma-dipping wall rock discontinuities, and may have fallen either as a result of long-term creep or due to impact- or fault-related seismic activity.

Unlike the rockfall landslides, the giant slumps that scallop the walls of the Valles Marineris do not exhibit such straightforward behavior. These landslides characteristically involve entire sections of chasma walls, from chasma floors up to plateau surfaces, including the buttressing talus deposits (Lucchitta, 1978a; 1979; McEwen, 1989). Fresh slumps always appear seated at about the same local elevation as the neighboring chasma floors. Fresh slumps are never observed to occur part way up the chasma walls; the family of smaller slumps that one might expect to occur on slopes neighboring the giant slumps do not exist. Some older(?) scalloped regions of chasma wall do indeed exist that form embayments part way up the chasma walls and sometimes are associated with landslide debris (U.S. Geological Survey, 1984a; 1986a). However, these features contain only hummocky terrain and never expose any clear exposures of back-rotated plateau surface materials. These features may represent old, partially eroded landslides that formed when "base level" in the chasmas was higher than at the time of formation of the fresh-appearing landslides (Lucchitta, personal communication, 1988), but if so, some remobilization of debris from these embayments has occurred since the fall in base level (U. S. Geological Survey, 1984a: between 9.5° and 11°S, 69° and 70°W).

The characteristic features of the giant Valles Marineris slumps described above provide some important insights into the nature of landslide initiation in the equatorial chasmas, as well as the nature of the slopes scalloped by the slumps. A number of means exist to initiate motion of large slump failures having non-oversteepened slopes, including: seismic activity (Terzaghi, 1950) or the presence of weak bedrock layers or structural discontinuities intersected by the slip surface of a slump (Reiche, 1937; Varnes, 1958). Where subsurface water is available, an increase in pore pressures along a potential slip surface can also help trigger movement (Terzaghi, 1950). Some of the giant Valles Marineris slumps may have been triggered by marsquakes

associated with tectonic activity along possible chasma-bounding faults (Carr, 1981), but most of the landslides appear to have post-dated surface faulting along chasma walls (Chapter III). As postulated by Carr (1981), increases in wall rock pore pressure might also have played a role in the triggering of the giant Valles Marineris slumps:

> Water or water-ice may have played a role in the formation of the landslides in Valles Marineris. The depths of the canyons considerably exceed the probable depths of the permafrost...Groundwater could therefore have existed beneath the permafrost behind the canyon walls, lowering the shear strength of the walls and making them susceptible to collapse, which may have been triggered by earthquakes along the longitudinal faults.

However, the absence of bedrock slumps less than a few hundred cubic kilometers in volume suggests that the slumps had strong structural control and were not triggered strictly by marsquakes or by pore water pressure increases. If the landslides were commonly triggered by seismic activity or by pore pressure changes, a whole family of bedrock landslides should exist, rather than just giant ones. These observations suggest that discontinuities exist(ed) within the Valles Marineris wall rock to cause the observed concentration of slumps in this region. Vertical structural discontinuities, such as grabens, parallel to chasma walls, seem to have provided some structural control for the slumps (Chapter III). However, the observation that all the giant slumps appear seated at the same local elevations as neighboring chasma floor units suggests an even more important role for the "base levels" represented by the chasma floors. If the horizontal surfaces expressed by the chasma floors represent erosional base levels caused by local discontinuities in crustal properties, these discontinuities may extend locally beneath the wall rock, causing the observed landslide initiation characteristics. The slip surfaces for the Valles Marineris landslides might have coincided with these surfaces much as the slip surface of the Hilina slump on Hawaii Island, responsible for the 1975 Kalapana earthquake, appears to have coincided with the volcanic pile-oceanic sediment interface (Eissler and Kanamori, 1987; Delaney, et al., 1990). Because the chasma floors neighboring the slumps vary considerably in depth and in elevation from one enclosed chasma to the next (U. S. Geological Survey, 1986c), the base levels represented by the chasma floors must relate to local, rather than to regional, changes in vertical crustal properties. If, as suggested by Sharp (1973) and Carr (1981) the depths of the

chasma floors relate at least in part to the removal of subsurface ice or other volatiles from the chasmas, the chasma floors could represent fossil volatile horizons. This origin could explain how the crustal discontinuity could extend locally beneath the chasma walls.

The landslides in Valles Marineris apparently formed relatively late in the geologic evolution of Mars. As a group, these landslides took place after the opening of the chasmas to their present configuration, after dissection of the wall rock into the typical spur-and-gulley erosional landform (Lucchitta, 1978b; see wall rock landforms neighboring Mars 24, 18, 84 and 85 deposits, Chapter II: Figures 6c, 6e and 6h) and after the deposition and partial erosion of chasma layered deposits, placing them relatively late in the ~3 billion year geologic history of Valles Marineris (Lucchitta, 1987a). Nevertheless, even the most recent landslides apparently occurred long ago by human standards, as most of these landslides, including all of the giant ones, are marked by impact craters ranging from <500 m up to about 4 km in diameter. Several of the giant landslides in Valles Marineris are marked by impact craters in the 4 km range, including the Mars 9, 11, 12, 13, and 25 deposits (Appendix A). Also, many of them are post-dated by aeolian landforms and by small mafic volcanic deposits which could date from as little as a few million years ago (Lucchitta, 1987a; b). While even the largest individual martian landslides are too small in areal extent to give statistically significant crater counts, the combined surfaces of giant landslide deposits in Tithonium and Ius Chasmas yield an average crater frequency of 570±130 craters ≥ 1 km diameter per 10^6 km^2 (Lucchitta, 1979). Plotted against the ages of other martian events, this value suggests that the morphologically distinct landslides were emplaced during the last quarter of martian geologic history, perhaps dating back to a maximum age of ~1 billion years, corresponding with late activities on the Tharsis volcanoes (Lucchitta, 1987a). The widely varying morphologic clarity and crater counts on the landslides suggest, however, that they took place over an extended period of time. The scalloped regions of wall rock containing hummocky material but usually not associated with debris apron deposits suggest that an earlier episode of landslide deposition and erosion may have occurred in Valles Marineris earlier in its development, prior to the deposition of the current generation of morphologically distinct deposits. Thus, while some Valles Marineris landslides appear quite young by martian standards, the geologic evidence suggests that the current distribution of landslide deposits in the

equatorial chasmas represents only the current snapshot of a very long term stochastic martian surficial process that might extend back to early martian history and perhaps continues today.

Outside of Valles Marineris, large landslides occur in both the oldest and the youngest terrains on the planet. Most of the large landslides on Mars not situated in Valles Marineris lie in the ancient cratered highlands (unit cu, Figure 38). However, they probably do not date from the origin of this terrain. This is because these landslides retain exquisitely preserved fine structures and textures on their surfaces, while the crater forms that date from the late heavy bombardment of Mars' early history are comparatively dull and degraded in appearance (Figures 45b-45f). Apparently, the landslides occurred after the intense atmosphere/surface interaction that continually modified the surface during that early period (Murray, et al., 1981). In addition, only a few of these landslides exhibit superposed impact craters, though the nearby surfaces may display numerous craters of all sizes. The delicate textures displayed on some of these landslides (Figures 45b-45f) in fact demonstrate that these deposits can not be covered by more than a few meters of dust, indicating that the landslides must date from a time when martian surface conditions were not greatly different than at present. Landslides having very similar morphologies to those occurring in the ancient cratered highlands occur on other parts of the planet as well, including some of the youngest terrains on the planet. One of these landslides actually lies in the summit caldera of Olympus Mons (Chapter II: Figure 6i) and therefore cannot have an age of more than a few hundred million years (Lucchitta, 1987a). This evidence suggests that, as in Valles Marineris, the landslides observed elsewhere on the planet are a very recent phenomenon relative to the terrains on which they occurred.

The Moon has an extremely small number of landslides on its surface relative to Mars. The Moon, with a surface area of ~3.8 X 10^7 km^2 (Resnick and Halliday, 1977), has only two long-runout landslides. Mars, in turn, with a surface area of ~1.5 X 10^8 km^2 (Resnick and Halliday, 1977), only 3.8 times greater than the surface area of the Moon, has nearly two hundred identifiable landslide deposits. The current distribution of martian landslides appears to represent the integrated sum of slides that have occurred infrequently on Mars over much of its geologic history after the late heavy bombardment period. Unlike Earth, the martian atmosphere is too thin and

cold to support substantial fluvial, glacial or aeolian erosion, and unlike the Moon the martian atmosphere is thick enough to prevent micrometeorites from bombarding the surface (Murray, et al., 1981). Therefore, once a landslide deposit forms, it remains essentially intact for a long time.

Notwithstanding the impact gardening of lunar features over time, the much higher concentration of landslides on Mars relative to the Moon probably relates more to internal factors than to external factors. For example, Mars has experienced much more tectonic activity than the Moon over geologic time, creating elevated source regions for landslide activity such as Valles Marineris and Olympus Mons. Because of the tectonic uplift and local erosion concentrated in these regions, both contain significant topographic relief and large areas of oversteepened slopes. They probably also provided source areas for shallow seismic impulses that could have triggered landslide initiation. The periodic presence of near-surface liquid water in wall rock in Valles Marineris might have provided an additional source of instability in that region. Water could have a direct effect on slope instability by developing high pore pressures behind wall rock outcrops (Carr, 1981), or an indirect effect, by causing the development of horizontal erosional discontinuities in the martian crust in the equatorial chasmas. On the Moon, in comparison, internal seismic activity is minor and deep-seated, and the crust has never contained significant water (Taylor, 1975).

Notably, the Moon exhibits relatively few landslides on its heavily cratered highlands relative to the numbers observed in Mars' ancient cratered terrain, despite the many geomorphic similarities between these units. One speculative cause for this difference is that the ancient cratered highlands on Mars formed when the planet retained its early, relatively heavy atmosphere. The cratered uplands formed during this interval may have experienced substantial physical and chemical weathering that did not occur on the Moon because it never supported a heavy atmosphere (Murray, et al., 1981). The current atmosphere of Mars is even capable of oxidative weathering of surficial materials, given the strong Fe^{+3} reflectance signature from martian surficial materials (Carr, 1981). Chyba, et al. (1989), for example, have calculated that the martian regolith is probably oxidized to a depth of at least 70 m, a value significant for at least the smaller martian slidemasses. Thus, the ancient martian highlands probably consist of more highly weathered rock

than the lunar highland impact breccias, or even than younger martian units which formed subsequent to Mars' early heavy-atmosphere period.

Weathering and degradation of ancient martian crustal materials in Mars' early history might also provide a partial cause for the landslides from wall rock in Valles Marineris. Below a capping of more recent mare-type basalts, most of the stratigraphy exposed in the walls of the equatorial chasmas on Mars is thought to consist of ancient highlands impact breccia (Lucchitta, 1978a), which formed early in martian history and was subsequently exhumed during the formation of the chasmas. Like the exposed ancient highlands materials elsewhere, these materials apparently experienced significant early weathering, which may have translated into preferred sites for landslide activity much later in martian history.

The lower lunar gravity, combined with significant cohesion in source rocks could provide another cause for the comparative deficit of large lunar landslides. However, this cause would not explain the observed diminishment of martian landslide frequency in rocks younger than the ancient cratered highlands.

D. Runout and Stopping

1. *Introduction*

The comparative planetology of the runout and stopping phases of large solar system landslides provides considerable evidence on the two primary problems under consideration in this work: the role of water in large martian landslides, and the nature of the long-runout mechanism(s) in large landslides. The problem of whether water was involved in the runout of any large martian landslides is addressed using three examples in this section. First, a large landslide complex at the north end of Ophir Chasma is investigated for evidence of a proposed high water content for this deposit (Lucchitta, 1987a). This geologically recent landslide exhibits considerable morphological evidence for wet emplacement. The landslide complex exhibits characteristics of both giant landslides and ancient martian outflow channels, suggesting that it may represent a unique hybrid of these features. Following this review, the morphologies of a small group of older giant Valles Marineris landslides are discussed. These landslides exhibit the lobate-terraced and isolated glide blocks debris apron morphologies characteristic of moist or

water-saturated deposition. Next, four large lobate martian landslides are investigated and their morphologies are compared with a moist terrestrial landslide of similar scale and morphology. Following this discussion, a comparison of "Blackhawk-like" landslides on Earth and Mars is developed that yields new insights into the mechanics of runout of dry rock landslides. This discussion considers the effects of the gravitational and atmospheric pressure differences between the two planets on the runout behavior of these deposits.

2. *Moist Landslides*

A unique **landslide complex** in Valles Marineris, Mars, originally described by Lucchitta (1987a), exhibits a variety of features strongly suggestive of wet emplacement. This landslide complex (Chapter III: Figure 17b, Figure 41) originates along the north wall of Ophir Chasma and consists of overlapping debris from three closely spaced landslides (Mars 35, 36 and 37; Appendix A). These landslides exhibit a variety of characteristics unique among martian landslides. For example, the proximal regions of all three landslides exhibit very similar, very subdued morphologies relative to similar portions of other martian landslides. Also, while the headscarps of these landslides have the characteristic scalloped appearance common to giant slumps in Valles Marineris, the proximal regions of the landslide deposits directly adjoining the headscarp scars lack any evidence of coherent back-rotated blocks of plateau surface material, as usually occurs in the proximal regions of Valles Marineris slumps (cf., Chapter II: Figures 6a, 6c, 6d, 6e). The proximal portion of Mars 37 is also surfaced by a number of interesting oval depressions that do not appear to be impact craters.

The most important morphologic aspect of these landslides, however, is that their debris aprons do not have entirely distinct distal margins. Rather, landslide debris grades distally in places into a low-relief, uniform, textured deposit that extends about 75 km from the distal reaches of the landslide debris aprons (U. S. Geological Survey, 1986c) down a pre-existing trough between two large areas of chasma layered terrain (McCauley, 1978). This trough dips southward along a gradient of approximately 4 m/km (Lucchitta, 1987a). All three landslides exhibit the gradational morphologic behavior, but it is best developed in the center landslide of the complex, Mars 36, in which landslide debris grades into the channelized deposit along its entire width. Debris from landslides Mars 35 and 36 appear to interfinger entirely, suggesting that the

Figure 41. Photomosaic of unique landslide deposits in Ophir and Candor Chasmas, Mars. Three large landslides, Mars 35-37 from east to west, fell from the north wall of Ophir Chasma and created an outwash plain and a channel extending 250 km from the source. Also note the level plain embaying mesas near the bottom of the scene and wall rock ridges in left and center of scene. Diagram from Lucchitta (1987a).

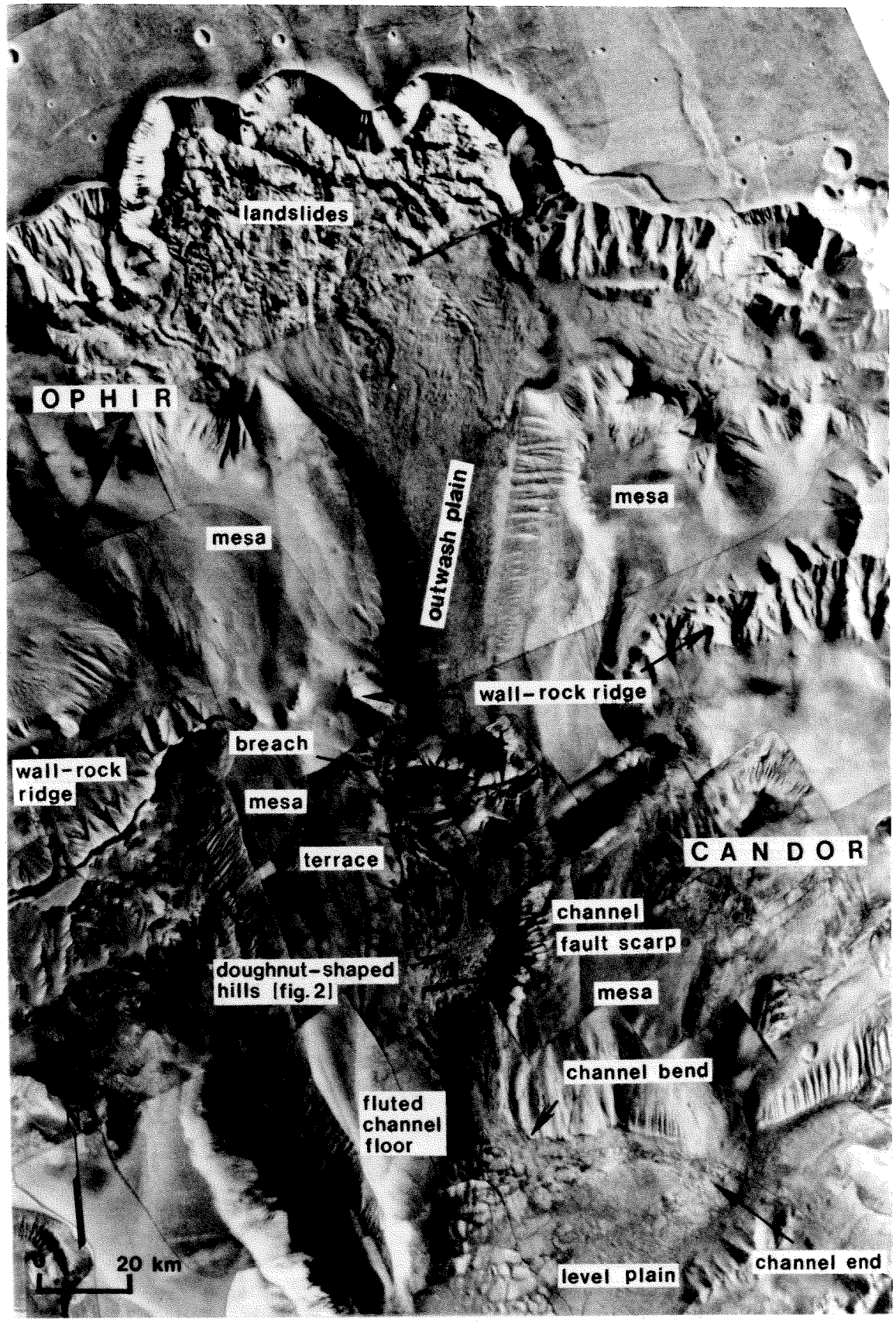
landslides
OPHIR
outwash plain
mesa
mesa
wall-rock ridge
breach
wall-rock ridge
mesa
terrace
CANDOR
channel
fault scarp
doughnut-shaped hills [fig. 2]
mesa
channel bend
fluted channel floor
20 km
level plain
channel end

two landslides occurred nearly simultaneously. Debris from Mars 37 overlies the western margin of Mars 36, and so must post-date the latter by a short time interval. Distally, however, debris from Mars 37 appears to merge with material from the previous events in the channelized reach, suggesting that Mars 37 fell in the same catastrophic episode in which the other two landslides occurred. In fact, fluidized material from Mars 37 appears to have overrun some sort of dark volcanic(?) material bordering the northeast margin of the layered deposits and carried it downstream, where it can be followed far to the south along the western margin of the channelized reach, suggesting that material from this landslide mixed with debris from the other two slides (Figure 41). An alternative possibility for this dark-appearing material is that it is an effect of shadowing, as suggested by the topographic contours in U. S. Geological Survey (1986c). However, this possibility would require that the channelized deposit be bowed up in the middle, a geometry that does not appear consistent with the apparent flow directions given by the texture of the channelized deposit.

The channelized debris continued southward until it reached a wall rock ridge extending directly across the trough, a ridge that separates Ophir and Candor Chasmas (U. S. Geological Survey, 1984c). A ~5 km-wide slot occurs in this ridge along its southwest margin. South of the gap, the broad trough separating the fluted layered terrain mesas continues to the south. Below the gap, the floor of the trough is marked by erosional and depositional landforms that differ greatly from the textured deposit south of the Ophir landslides. Here the trough contains a channel with a gradient of about 18 m/km (U. S. Geological Survey, 1986c) that exhibits a series of parallel, step-like incised terraces together with a hilly floor deposit. To the east of the terraces the main channel measures about 700 m deep, assuming a slope angle of 30° for the distinct western margin of the channel. Many of the small hills that dot the bottom of the channel and its terraced margin have elongated doughnut shapes. The doughnut-shaped hills vary considerably in scale, from < 500m to approximately 1500 m in maximum dimension.

Farther to the south along the east side of the channel, the hilly floor deposit first interfingers with, and then is obscured by fine, dark material that forms both wispy and dune-like landforms. To the south of this region the channel becomes less well defined, seemingly dividing into a number of parallel channels with the largest along the western margin of the trough.

The trough merges to the south with a low, level region in central Candor Chasma marked with a geometric pattern of low hills, extensive low mesas, and plateau regions etched by elongated furrows. The western and northern margins of this topographic basin (U. S. Geological Survey, 1986c) are very sharp and well defined.

Liquid water appears to have played a very important role in the development of the features described above. The Mars 35-37 deposits express strong morphologic evidence for having been water saturated during runout. By comparison with wet terrestrial landslides (see above), the gradational distal behavior of the landslide debris aprons from distinct lobate landslide debris to fine-grained, low-relief uniform deposits strongly suggests that the landslides contained large amounts of water during runout. When the landslides stopped moving, liquid water apparently escaped from the landslide material, reworked some of the marginal areas of the landslide lobes, and then apparently traveled on to the south as some sort of mudflow or debris flow.

Because even those portions of the debris apron adjoining the headscarp scars appear anomalously subdued in morphology, it appears that the wall rock involved in the landslides exhibited very low strength at failure and presumably provided the source of the water in the landslide debris. The water could have originated as permafrost ice in the giant slumps that became frictionally melted during travel of the landslides (Lucchitta, 1987a), or, more likely, by liquid pore water. Eyewitness accounts from large terrestrial landslides that contained glacial ice, for example, such as Huascaran 2 and 3 (Plafker and Ericksen, 1978) and Diablerets 2 (Heim, 1932) slides, indicate that ice behaves much like a rock when caught in a landslide. The ice blocks in these landslides remained largely intact during runout and did not become frictionally melted. In the much colder martian surface environment, entrained ice blocks would have even less tendency to melt. It appears possible to me that the oval depressions in the proximal reach of the Mars 37 deposit represent kettle-like depressions left by such ice blocks in the original deposit that wasted away after deposition (see below). The most likely source for the liquid water in these deposits, therefore, was probably not ice, but liquid water from a pressurized saline(?) wall-rock aquifer (c.f. Carr, 1981; 1986). The aquifer most likely occurred within about a kilometer of the ground surface along the northern edge of Ophir Chasma (Carr, 1981). At

failure, liquid water apparently became mixed with and saturated the landslide debris, ultimately escaping from the debris when the landslides came to rest.

After segregation from the landslide debris, the postulated mudflow material would have begun to freeze up rapidly upon contact with the low-pressure, low-pressure martian surface and atmosphere (Carr, 1981). Thus, advance of the mudflow down the channel would have occurred much like a lava flow on Earth, with a solid basal contact and a largely crusted-over ceiling. Presumably, much of the flow would have occurred through an interconnected series of roofed channels, like lava tubes.

Because the nature of the channelized deposits changes dramatically at the bedrock spur, it appears that another segregation process occurred when debris reached the spur. If the wet material remained dammed up at this site for a significant period of time, water and debris might have become segregated, leading to a temporary ice-covered lake of the type currently found in Antarctica (McKay, et al., 1985). Whether or not the material remained ponded for long at this site, segregation of debris and water at the wall rock ridge is supported by the fact that the flood(s) which ultimately spilled through the gap subsequently had a much different character than the channelized deposit headward of the alleged dam.

Draining down from the ridge, flood waters cut deeply into the bedrock below the gap, forming what appear to be a series of stepped cataracts spaced a kilometer or so apart. Downstream the flood(s) cut terraces into the layered terrain along the west side of the channel and deposited some material along the channel margin and floor. As hypothesized by Lucchitta (1987a), the doughnut-shaped hills forming portions of the channel floor deposits may have resulted from the deposition of ice blocks on the channel margins and floors. After the flood, these blocks sublimated away in place, forming large equivalents of terrestrial kettle holes. It appears noteworthy that the doughnut-shaped hills lying along the west-side terraces do not mark all of the terraces, only those two or more steps below the highest bank. This observation indicates that the first waters down the channel did not contain as many large chunks of ice as did later floods or episodes of the same flood. Perhaps flooding occurred in stages, as proposed for the Late Pleistocene Missoula floods (Baker and Bunker, 1985; Atwater, 1987), as water capped under a layer of ice at the wall rock ridge ultimately rose above the lip of the ridge. The first water down the hill would then not contain large chunks of ice,

while later the flood might contain large icebergs broken from the covering ice sheet. In all cases, however, the floodwaters must have been surfaced by ice because of the environmental conditions.

At the mouth of the channel, the ice-laden flood waters appear to have bifurcated to the east and southwest as they entered the level plain, cutting its pronounced northern margin and western margins. Once the icy floodwaters reached the plain, they apparently spread out across the basin and dumped their remaining charge of debris, forming the hummocky deposit flooring central Candor Chasma. After the end of the flooding events, fine, dark, sand-sized(?) material, perhaps carried down in the floods, was blown by winds to the east and southeast, so that some of the dark sand has moved up etched furrows along the western margin of the layered terrain that forms the east side of the channel. The dark dune forms along the bottom of the channel could have been deposited during a flood event, but it appears to me more likely that the dunes are largely aeolian in nature. This conclusion is drawn from the observation that the material clearly undergoes aeolian transport, as shown by the dark steaks of material to the east of the dunes, and that the dark sand dunes will remain dark in the dust-rich martian atmosphere only if the particles remain in constant motion (Lucchitta, 1987b).

As mentioned above, no other martian landslide deposits display the strong water-saturated signature of the Mars 35-37 deposits. However, the landslide complex does exhibit many similarities to ancient martian outflow channels and to the chaotic terrains from which they originate (Figure 42). Outflow channels are large erosional features apparently formed by catastrophic floods released from localized sources. They are often broadest and deepest at their heads and decrease in size distally. The outflow channels commonly originate in areas of chaotic terrain floored by haphazard jumbles of large angular blocks and bounded by arc-shaped slump blocks along the steep, marginal escarpments (Murray, et al., 1981; Figure 42). A number of mechanisms have been proposed to explain the source of these flood waters from the chaotic terrains, including: volcanic interaction with ground ice, geothermal melting of ground ice, geothermal decomposition of hydrated minerals, eruption of water under high pressures from confined aquifers and sudden releases of pooled water from ice-covered lakes (Carr, 1987; Robinson and Tanaka, 1990).

Figure 42. Ravi Valles outflow channel emerging from Aromatum Chaos (1° S, 43° W). This oblique view looks southward towards the source region of the flood which formed the outflow channel. The channel starts at full scale in a region of chaos enclosed by cliffs. Viking Orbiter photomosaic P-16983.

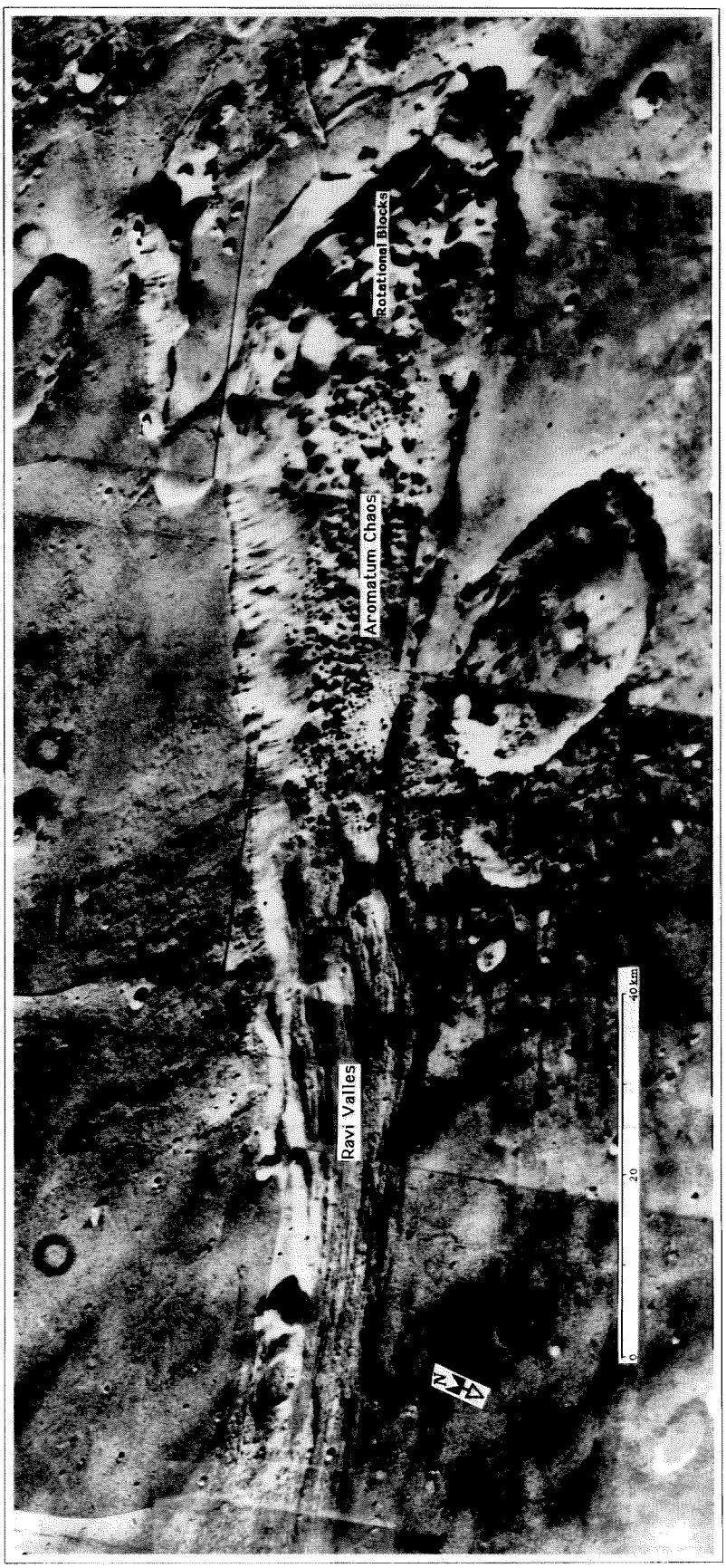
Rotational Blocks
Aromatum Chaos
Ravi Valles
A
A'
0
20
40 km

Comparison of the wet landslide complex in Figure 41 with the chaotic terrain and outflow channel complex shown in Figure 42 reveal many similarities between the two features, as well as a few noteworthy differences. First, both originate in regions of large slump blocks carved into old cratered plains. Downstream from the slump blocks, both features also exhibit large regions of hummocky material apparently deposited from debris-rich floodwaters, perhaps at points of reduced velocity along the paths of the floods. Beyond the hummocky deposits, the floods regained their erosive capability and scoured out terraces along channel margins and developed streamlined features along channel floors. Ultimately, the floodwaters from both sources debouched onto flat, wide basins, spread out and deposited their remaining loads of sediment. The floodwaters themselves presumably then froze solid, or, in deeper accumulations, crusted over with ice and formed temporary (saline?) lakes (McKay, et al., 1985). Subsequently, any ice exposed at the surface would have progressively sublimed away until all the water involved was ultimately transported away by the thin martian atmosphere.

The landslide complex and the chaotic terrain/outflow channel complex also exhibit a number of important differences. First, they are of somewhat different scales. The proximal region of chaotic terrain pictured in Figure 42, for example, measures only 35 km across, about half the width of the landslide complex at the north end of Ophir Chasma. The chaotic terrain also lacks any of the gradational debris flow deposits observed south of the Ophir landslide complex. The flood deposits that originated from the landslide complex began as landslide debris, then evolved into a debris flow deposit and then into a water-dominated flood. In comparison, the flood waters that originated in the chaos seem to have begun full-borne in the source region without passing through any of these gradational phases. Also, the hummocky terrain flooring Ravi Valles and other source regions of outflow channels do not appear to contain the doughnut-shaped hills characteristic of the Ophir landslide/outflow complex. Although some caution must be used in this conclusion because of the general lack of high-resolution imagery of the proximal outflow channels, it appears that the outflow channels did not contain the huge (500-1500 m) icebergs interpreted to have occurred in the Ophir event. This lends some weight to the speculative idea that the flood deposits south of the bedrock ridge between Ophir and Candor Chasmas may

have originated in an iced-over lake whose surficial ice cap provided the source of the large icebergs.

To me, the overall impression given by the Ophir landslide complex is of a feature intermediate in character between martian outflow channels and giant Valles Marineris slump-type landslides. Geomorphically, the landslide exhibits characteristics of both features. Proximally, the complex has the appearance of rather normal giant landslides, but distally the flood deposits evolved from the landslides have very much the same appearance and scale as the erosional and depositional features that characterize large outflow channels. The individual landslides making up the source region of the Ophir complex are all intermediate in scale for giant Valles Marineris landslides (Appendix A). In addition, the overall 70 km width of the complex lies between the upper and lower limits of width of the chaotic source regions for outflow channels. The landslide complex is wider than the Aromatum Chaos pictured in Figure 42, but has only about half the width of the headwalls of the larger Eus and Juventae Chasmas, source areas of the floods that cut Kasei Valles and Maja Valles, respectively. One of the most significant differences between the landslide complex and the outflow channels, however, is their disparate ages. The Ophir landslide complex has only a few superposed craters, all less than or equal to 500 m in diameter, indicating an extremely young age by martian standards (Lucchitta, 1987a). By comparison, all of the known martian outflow channels are older than the landslide complex, some much older. Outflow channels exhibit a range of crater numbers (the number of craters $\geq$ 1 km diameter per 10^6 km^2), from 5000 for the oldest portion of Kasei Valles, to 280 for Upper Tiu Valles, corresponding roughly in age from 3.6 billion years to 0.5 billion years (Baker, 1982). Of the eleven approximately dated outflow channels reported by Baker (1982), six formed between 3-4 billion years ago, three have ages of 2-3 billion years, and two have ages of less than 2 billion years. The absence of any kilometer- or larger-sized craters on the Ophir complex clearly suggests a more recent age than any of the outflow features. I infer that the landslide complex may represent a late stage equivalent of the outflow channels, one dominated more by rock debris and less by water than any of the previous outflow events. The decrease in the frequency of outflow events with time and their possible transition to a less water-dominated character represents a winding-down of the intermittent process responsible for their generation, whether it be geothermal, tectonic or volcanic activity.

Whatever the cause, the Ophir landslide complex demonstrates to me that liquid water was briefly available at the surface of Mars late in its geologic history, at least as recently as the most recent Valles Marineris landslides. The activity of surficial water on the planet clearly has been decreasing with time, but I infer that it has been available infrequently and in limited quantities locally in Valles Marineris and its environs throughout the entire period important to martian landslide emplacement.

Two older giant martian landslide deposits in Valles Marineris express morphologies that suggest that they too contained water at emplacement. These landslides, however, do not exhibit the landslide/mudflow transition described for wet landslides Mars 35-37 above, but rather express different signatures of moist to water-saturated emplacement. Specifically, these **older moist landslides** are surfaced by two debris apron morphologies which on Earth appear restricted to moist or water-saturated landslides: the lobate-terraced and the isolated glide blocks textures (Chapter II).

The lobate-terraced texture is well developed on landslide Mars 24, which lies in eastern Tithonium Chasma (Chapter II: Figure 6c). Individual terraces measure up to 5 km in length and 2 km in depth. Because of the rounded nature of the terraces, it is difficult to estimate the heights of each riser, but assuming an average slope angle of 20° (less than angle of repose of loose material), one arrives at a value of about 250 m for one characteristic lobe. These dimensions come very close to the dimensions of terraces on lobate-terraced debris aprons observed on terrestrial subaqueous landslides (see above). In addition, the Mars 24 landslide is also analogous in overall scale to the lobate-terraced debris-slide component of the Alika slide complex off the island of Hawaii, which, like Mars 24, probably originated as a giant slump (Lipman, et al., 1988; Chapter II: Figure 6b).

The second martian landslide displaying a moist, or perhaps water-saturated texture is the Mars 4 deposit (Figure 43), which lies in Ganges Chasma. The rather uniform, featureless debris apron of this landslide terminates along a digitate margin outside of which occur a number of isolated debris masses. These possible glide blocks measure roughly 2 km in maximum length and perhaps 150 m in maximum thickness. This makes the possible martian glide blocks very similar in size to those observed by the GLORIA imaging sonar system at the distal margins of several of the giant Hawaiian Ridge subaqueous landslides (Lipman, et al., 1988; Moore, et al., 1989).

Figure 43. Large landslide Mars 4 and overlapping deposit Mars 29 in Ganges Chasma, Mars. (7.1° S, 44.9° W), featuring possible distal glide blocks texture on the Mars 4 deposit. The movement directions of the two landslides are marked by arrows. East and northeastern margins of Mars 4 landslide fell into local basin during runout. An ice-covered lake might have filled this small basin at the time of the landslide, giving the landslide its isolated glide blocks texture. Viking Orbiter images 012A52, 012A54. The solar zenith angle measures approximately 63° for both halves of the image.

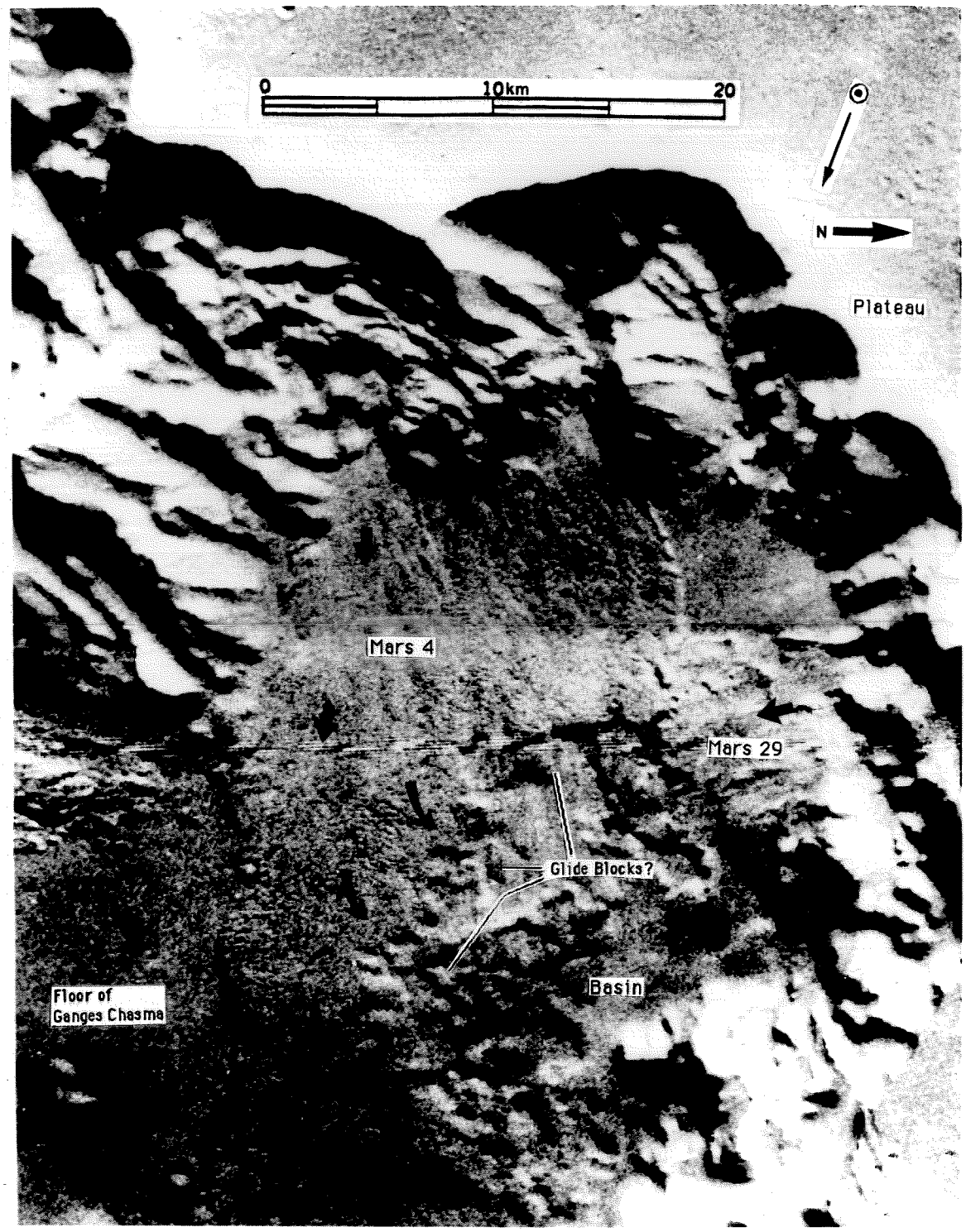
0
10km
20
N
Plateau
Mars 4
Mars 29
Glide Blocks?
Basin
Floor of
Ganges Chasma

Unfortunately, the resolution of the image in Figure 43 is too low to speculate on the specific origin of the distal glide blocks texture on the Mars 4 deposit, whether it might have occurred by separation of fines from a water-saturated landslide or by sliding on a moist substrate (see above). In addition to the size of the possible glide blocks, the overall dimensions of the Mars 4 landslide resemble those of the the Alika 1 slide off the southwest coast of Hawaii Island (Chapter II: Figure 6b). Thus, at the best available image resolution, the Mars 4 and Mars 24 landslides appear to express textures that on Earth occur only on moist or water-saturated landslides. The scale of the textural components is very similar on both planets.

Both the Mars 24 and Mars 4 deposits appear quite old in comparison with the Ophir landslide complex described above; both have rather degraded, subdued morphologies, and both exhibit at least two craters, a significant number for their comparatively small surface areas. Mars 24, for example, contains two 1.5 km-diameter craters, two 1 km-diameter craters and at least five ~500 m-diameter craters over a surface area of about 1500 km^2, whereas Mars 4 appears surfaced by two or three ≤500 m diameter impact craters over its roughly 500 km^2 surface area. In comparison, roughly six impact craters, all smaller than 500 m in diameter, pockmark the entire 10,000 km^2 Ophir landslide complex from the north end of Ophir to the flat plain in the center of Candor Chasma.

If Mars 4 and 24 were indeed moist at emplacement, their occurrence, together with that of the Ophir landslide complex, would suggest that water was periodically available within Valles Marineris throughout the time period associated with landsliding in the chasmas. Ice or saline(?) liquid water in the chasma wall rock provides the most likely source of water for the Mars 4 and 24 deposits, as suggested for the Ophir landslide complex (see above). Another speculative possibility is that the landslides fell into temporary ice-covered lakes during their runout phases, allowing the development of their moist or wet textures (Shaller, et al., 1989). This possibility is suggested by the fact that, unlike the Ophir complex, both the Mars 4 and 24 landslides apparently fell into shallow basins during emplacement (U. S. Geological Survey, 1980; Figure 43). If these depressions contained ice-covered liquid water when the landslides fell into them, the landslides might rapidly have developed their moist textures as they encountered the water and saturated substrate materials in the lakes, as began to occur in the subaerial Panum landslide as it entered

the shallow margin of Mono Lake during runout (Sieh and Bursik, 1986; Sieh, personal communication, 1988; see above). Nevertheless, the possibility that ice-covered lakes occurred even temporarily on Mars in the last billion years remains speculative because no other geologic evidence exists to support such late-stage pluvial episodes in Valles Marineris (Lucchitta, personal communication, 1989).

A third group of much smaller landslides occurs on Mars which also exhibit morphologies suggestive of moist emplacement. This group consists of a number of **lobate landslides**, four examples of which have been located on Mars: the Mars 84 and 85 deposits in Candor Chasma (Chapter II: Figure 6h), as well as two landslides lying near the base of Olympus Mons, the Mars 142 and 143 landslides (Baker, 1982; Appendix A). Lucchitta (1987a) believed that the morphologies of the two Candor Chasma landslides and of their source regions provided good evidence that these landslides contained considerable amounts of water during transport, and that the deposits must have flowed into place with much the same consistency as terrestrial mudflows:

> Smaller landslides emerging from large gullies on the Valles Marineris walls resemble mudflows on Earth; they form level, thin, spreading debris lobes... The absence of obvious break-away scars in many gullies indicates that the debris probably was derived from surficial material on the walls. Many mudflows on Earth also derive their material from unconsolidated material concentrated in valleys or on slopes and mobilized by floods...the similarity suggests that water was involved in the emplacement of small Martian slides.

More recently, McEwen (1989) countered this argument by discounting the morphological data and instead using log(volume) vs. H/L trends, yield strength estimates and velocity estimates of landslides in Valles Marineris as evidence that all the landslides observed in the chasmas were probably emplaced dry:

> Two critical questions about the Martian landslides have not been answered: were they water saturated, and what are their size-mobility relations? These questions are addressed in this paper with estimates of yield strength and and measurements of H/L vs. volume for landslides in Valles Marineris. These data show that the Valles Marineris landslides were probably dry (or unsaturated), and that they have a distinctive size-mobility trend that may be an important clue to the mechanism of transport.

As demonstrated previously in this chapter, however, these quantitative measures of landslide properties fail to provide useful means of separating dry from moist or wet landslides. Thus, morphology remains the only available means of distinguishing landslides of differing water content.

The lobate martian landslides all exhibit morphologies consistent with moist deposition as defined by the moist, lobate Carlson landslide (see above). The Carlson landslide and the lobate martian landslides all began motion as rockfalls in the upper reaches of wineglass-shaped canyons. In each case, landslide debris funneled through a narrow constriction in the channel below the headscarp to spread out and form a lobate, flattened, highly symmetrical, finely longitudinally ribbed debris apron. The lobate martian landslides differ from the Carlson landslide in not exhibiting the convex-downslope ridges and troughs texture observed on the Carlson and in having greater characteristic thicknesses than the terrestrial landslide (Table 15).

The debris apron morphologies exhibited by the lobate martian landslides make them much closer in morphology to the moist Carlson landslide than to any known terrestrial dry rock landslide (see above). Particularly significant on the martian landslides are the very smooth margins of their basal lobes and the fine spacing of their longitudinal ribs. While the lobate martian landslides differ from the Carlson landslide in not exhibiting the convex-downslope ridges and troughs texture, there are several reasonable explanations for this difference. One possibility is that the ridges and troughs exist on the lobes but cannot be resolved at the level of resolution of the Viking Orbiter images, which just barely reveal the presence of the distinct, linear longitudinal ribs. Conversely, even given the exact same materials for the martian landslides as for the Carlson landslide, the difference in gravity between the two planets might preclude development of the convex-downslope ridges and troughs texture on the martian landslides. On the Carlson landslide, this texture apparently formed due to compression between material at the toe of the landslide and faster, trailing material coming down the channel (Appendix B). On Mars, where deposit velocities must be lower due to the lower gravitational acceleration, the velocity differential might be significantly lower between material at the toe of a deposit and trailing material coming down the channel. In addition, the lobate martian landslides

Table 15. Critical Characteristics of Lobate Martian and Terrestrial Landslides

Name	Volume ($x10^6$ m^3)	Basal Lobe Width (km)	H/L	Thickness (m) Avg.	Max.
Carlson	100	1.8	0.17	30	70
Mars 143	NA	4	NA	NA	NA
Mars 84	1,500	5	0.2	60	100
Mars 85	1,500	5	0.2	60	100
Mars 142	26,000	14	0.1	160	160

characteristically have greater thicknesses than the Carlson landslide, also making compressional deformation more difficult.

The characteristically greater thicknesses of the lobate martian landslides with respect to the Carlson landslide appear to relate to the difference in gravity between the two planets, rather than to a difference in material properties. This conclusion is based on the fact that the lobate martian landslides have average and maximum thicknesses that average about 2.5 times the thickness of the Carlson landslide, a value roughly corresponding to the ratio in gravitational acceleration between Earth and Mars. Blackhawk-like landslides on the two planets (Table 16) of similar volume exhibit an analogous relationship. In general, the physical properties of the material at the base of a large landslide (Chapter III), together with the shear stresses applied to the basal material, appear to control the distances traveled by large landslides during runout; the basal material appears to behave as a sort of fluid under high shear stresses, which flows at a rate that increases with increasing shear stress. The lower gravity on Mars would cause the basal material of a martian landslide to be subject to less shear stresses than a landslide of similar thickness on Earth. This seems responsible for causing the terrestrial landslides to runout farther for a given volume and fall height than their martian counterparts, leading to thinner landslide deposits on Earth. This conceptual model of long-runout landslide behavior is described in full in Chapter VI.

The evidence presented above suggests that the lobate martian landslides were probably moist during deposition, like the Carlson landslide. Other evidence suggests that the Carlson landslide and its martian counterparts may have had rather similar lithologic compositions as well. This speculative argument is based on the fact that the Carlson landslide and a smaller, but morphologically similar deposit in the Columbia River valley in Washington State (45°45'N, 120°14'W), both originated in outcrops of weathered basalt (Appendix B; Anderson, personal communication, 1990). In addition, the Mars 142 and 143 landslides from Olympus Mons, a large shield volcano, probably also consist of some form of basalt, as may the two Candor Chasma landslides, Mars 84 and 85. The latter two landslides appear to have fallen from bedrock outcrops at the crest of the chasma, outcrops that have been interpreted as mare-type flood basalts (Scott and Tanaka, 1986). Because of the instability of water at the surface of Mars in the equatorial latitude range in which the four

Table 16. Critical Characteristics of Blackhawk-Like Martian and Terrestrial Landslides

Name	Volume ($x10^6$ m^3)	Fall Height (m)	H/L	Thickness (m) Avg.	Max.
Aval. del Zarz. 2	5	850	0.17	5	8-15
Loma de la Asp.	21	800	0.11	5	8-15
Aval. del Zarz. 1	37	900	0.14	5	8-15
Loma Redonda	65	700	0.10	5	8-15
Mars 118	150	2000	0.41	40	65
Mars 74	200	1100	0.23	40	60
Mars 141	200	2500	0.46	60	120
Silver Reef	230	900	0.13	20	30
Mars 108	250	900	0.16	45	70
Blackhawk	300	1200	0.13	16	30
Mars 101	500	1600	0.24	55	80
Mars 133	800	1900	0.19	30	50
Mars 109	1,500	1800	0.12	40	70

lobate martian landslides occur (Carr, 1981), they must have derived water from the subsurface. Fumarolic activity on Olympus Mons theoretically might have provided the water for the Mars 142 and 143 deposits, while the Candor Chasma landslide must have obtained water from high-pressure groundwater, as postulated for the Ophir landslide complex.

3. *Dry "Blackhawk-Like" Landslides*

One major group of large landslides I have identified on Earth, those with Blackhawk-like morphologies (Figure 44; Chapter III: Figure 34), in all cases exhibit field relations indicative of runout in a completely dry state (see above). I have found that these landslides also exhibit consistently low H/L values on log(volume) vs. H/L plots and only a minor trend towards decreasing H/L with increasing volume (Chapter III: Figure 7). I have located seven Blackhawk-like landslides on Mars which share nearly identical major and minor morphologies with their terrestrial counterparts (Chapter II: Figure 6i; Chapter III: Figure 17a; Figures 45a-45f). Four of these landslides, the Mars 101, 108, 109 and 133 deposits, occur in ancient cratered terrain; the remaining three, the Mars 74, 118 and 141 deposits, respectively lie in Valles Marineris, in chaotic terrain and in the summit caldera of Olympus Mons (Figure 46). Shreve (1968a) modeled the low-friction runout and morphological development of the Blackhawk and Silver Reef landslides by use of the air layer lubrication theory. He believed that these landslides captured and compressed air beneath them during air-launch episodes early in their movement phases and that the landslide debris subsequently slid and spread into place over this air cushion in a hovercraft-like fashion. The emplacement of the martian landslides under essentially modern martian atmospheric conditions, however, rules out air-layer lubrication as a cause of the low-friction runout and morphological development of Blackhawk-like landslides (Appendix D; E).

The Blackhawk-like landslides I discovered on Mars all exhibit morphologies consistent with dry deposition as defined by terrestrial Blackhawk-like landslides (see above). The martian and terrestrial Blackhawk-like landslides all began motion as rockfalls. All exhibited completely unconfined, unchanneled runout except for the Blackhawk (Figure 45a) and perhaps the Silver Reef landslides, which traveled short distances down channels in their proximal reaches. In each case, landslide

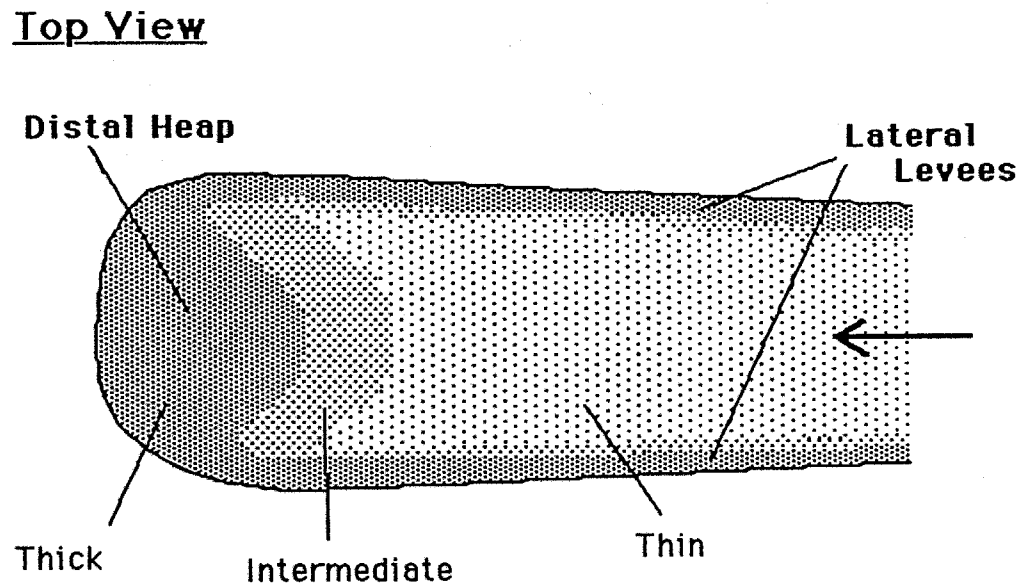

Figure 44. Generalized morphology of Blackhawk-like landslides on Earth and Mars.

Figure 45a. Aerial photograph of the Blackhawk landslide, southern California, illustrating several of the important characteristics of Blackhawk-like landslides.

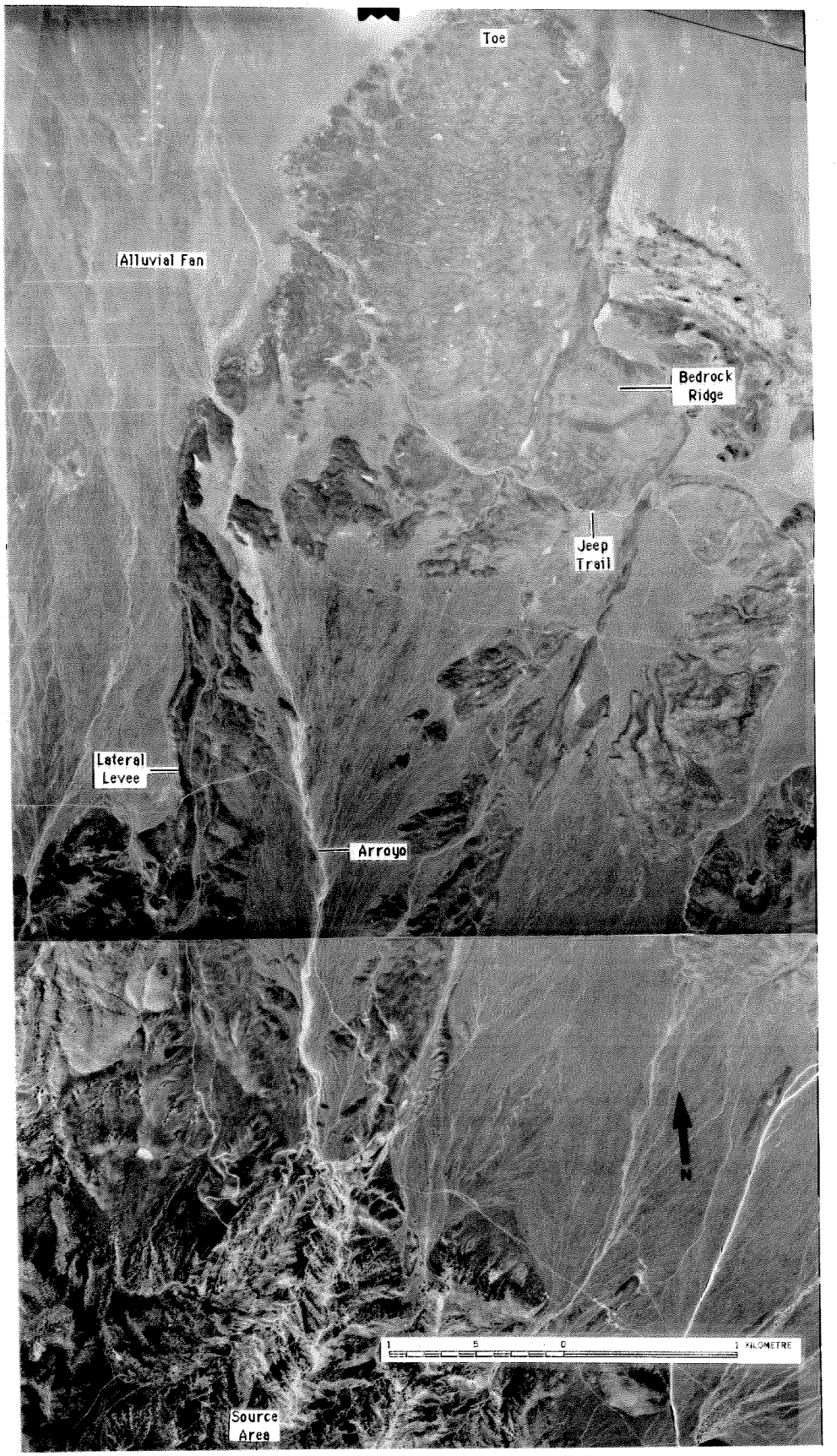
Toe
Alluvial Fan
Bedrock Ridge
Jeep Trail
Lateral Levee
Arroyo
N
1 5 0 1 KILOMETRE
Source Area

Figure 45b. Mars 101 Blackhawk-like deposit in Xanthe Terra, an ancient cratered upland region of Mars (15°40' N, 54°25' W). Viking Orbiter image 054A22. Solar zenith angle 37.54°.

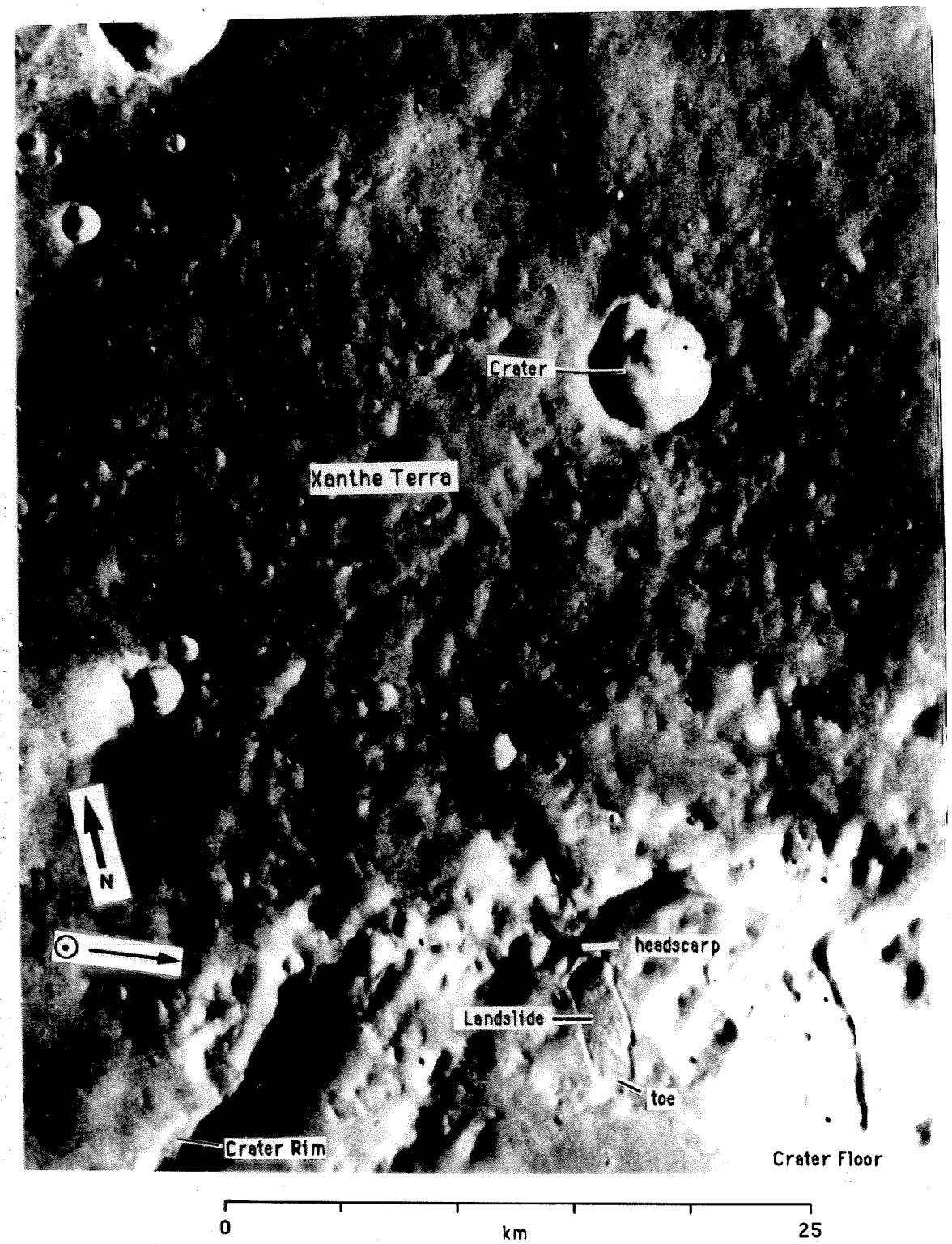
Crater
Xanthe Terra
N
headscarp
Landslide
toe
Crater Rim
Crater Floor
0
km
25

Figure 45c. Mars 108 Blackhawk-like deposit in Terra Sirenum region of Mars (14°36' S, 179°00' W). Viking Orbiter image 436S10. Solar zenith angle 68.07°.

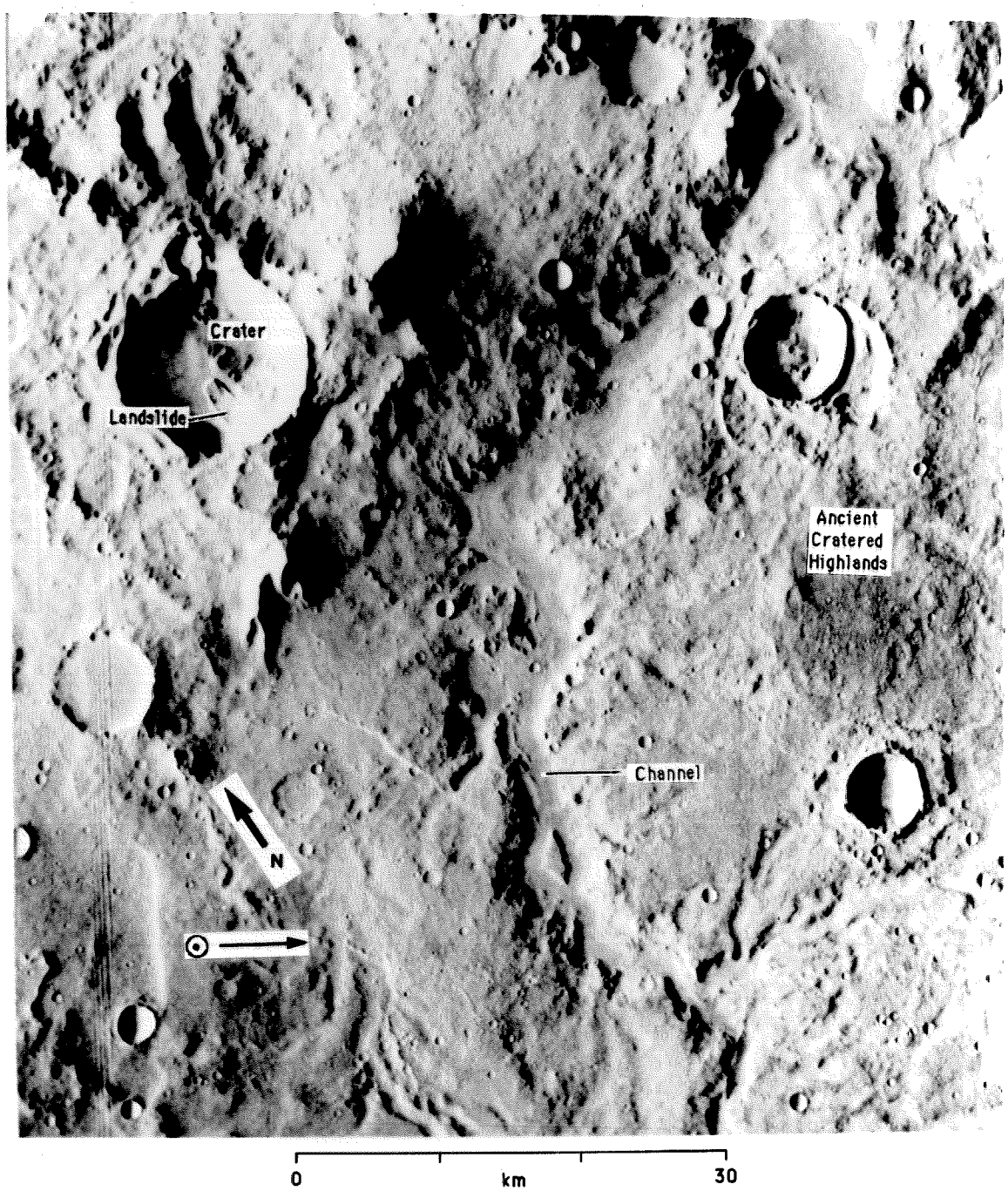
Crater
Landslide
Ancient
Cratered
Highlands
Channel
N
0
km
30

Figure 45d. Bi-lobate Mars 109 Blackhawk-like deposit in Ma'adim Valles region of Mars (19°03' S, 180°21' W). The flow-like feature on the crater floor to the west and southwest of the landslide appears to be a lava flow that poured into the crater along its south rim (U.S. Geological Survey, 1979). Viking Orbiter image 432S21. Solar zenith angle 75.68°.

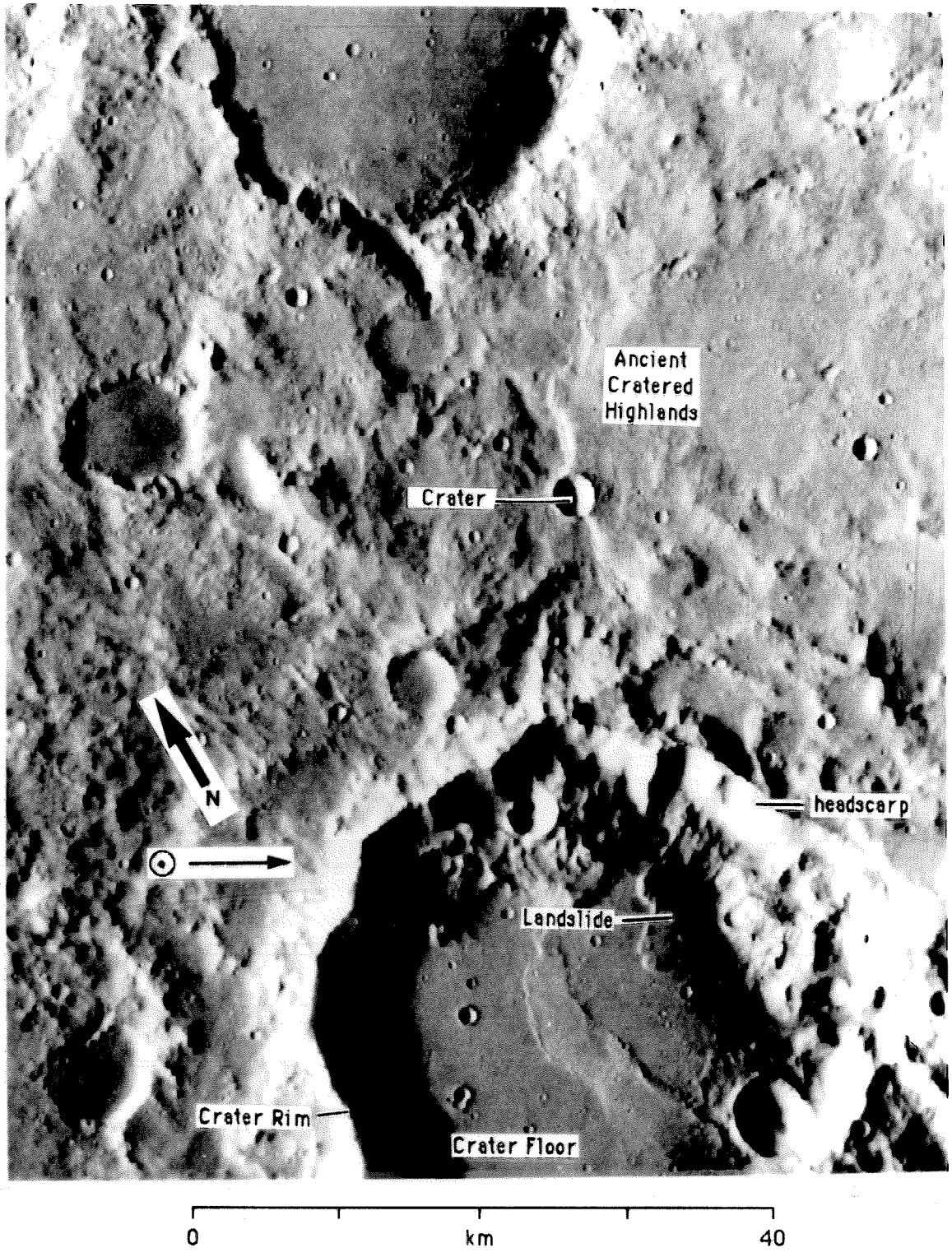
Ancient
Cratered
Highlands
Crater
N
headscarp
Landslide
Crater Rim
Crater Floor
0
km
40

Figure 45e. Mars 118 Blackhawk-like deposit in Iani Chaos region of Mars (4°55' S, 18°50' W). Viking Orbiter image 405B01. Solar zenith angle 61.88°.

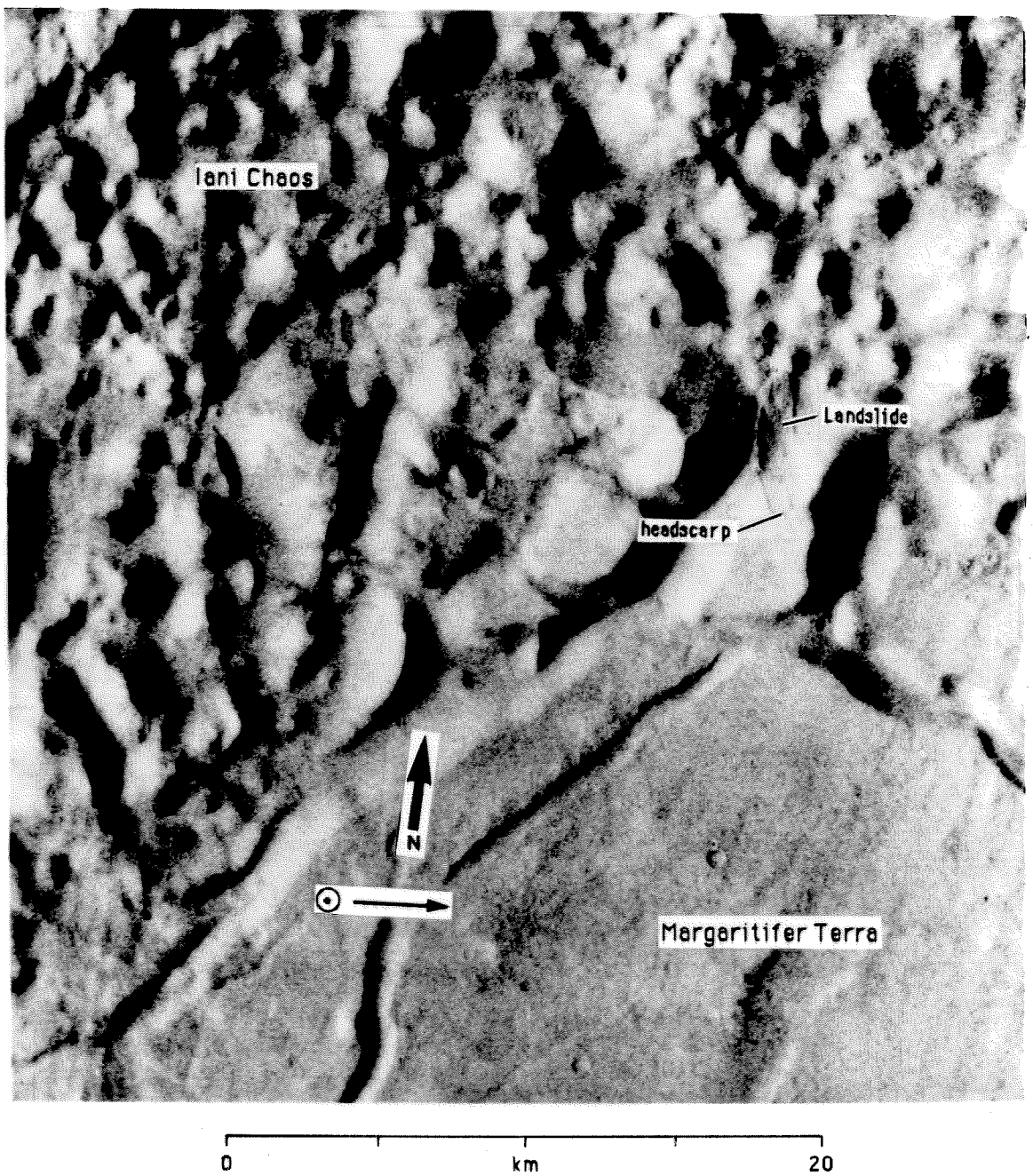
Iani Chaos
Landslide
headscarp
N
Margaritifer Terra
0
km
20

Figure 45f. Mars 133 Blackhawk-like deposit in the Ma'adim Valles region of Mars (22°33' S, 190°58' W). Viking Orbiter image 429S24. Solar zenith angle 77.21°.

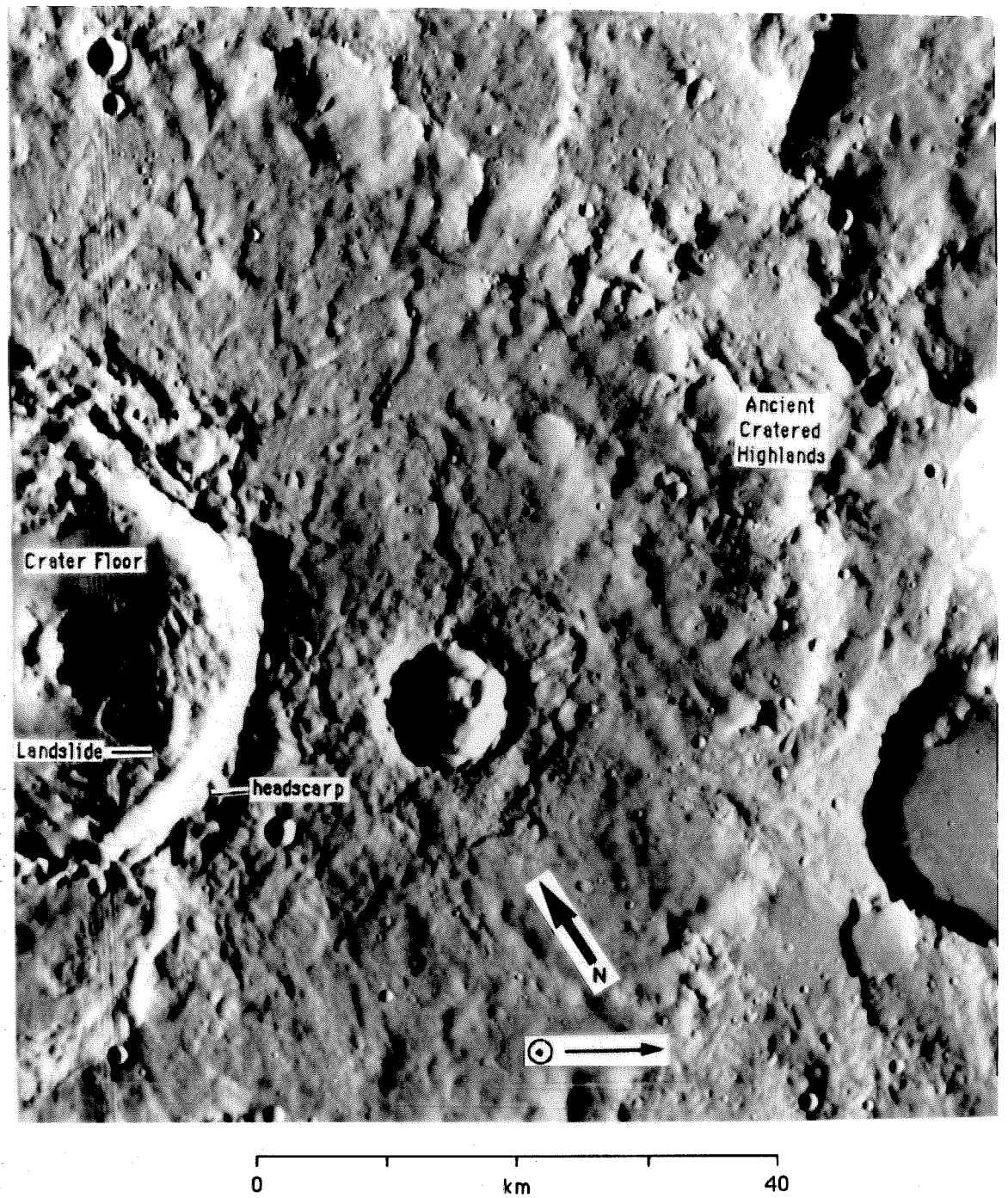
Ancient
Cratered
Highlands
Crater Floor
Landslide
headscarp
N
0
km
40

Figure 46. Distribution of Blackhawk-like martian landslides plotted on map of martian physiographic provinces (Mutch, et al., 1976). Physiographic units as follows: *polar units* include *pi* (permanent ice), *ld* (layered deposits) and *ep* (etched plains); *volcanic units* include *v* (volcanic constructs), *pv* (volcanic plains), *pm* (moderately cratered plains), and *pc* (cratered plains); *modified units* include *hc* (hummocky terrain, chaotic), *hf* (hummocky terrain, fretted), *hk* (hummocky terrain, knobby), *c* (channel deposits), *p* (plains, undivided), and *g* (grooved terrain); *ancient units* include *cu* (cratered terrain, undivided) and *m* (mountainous terrain).

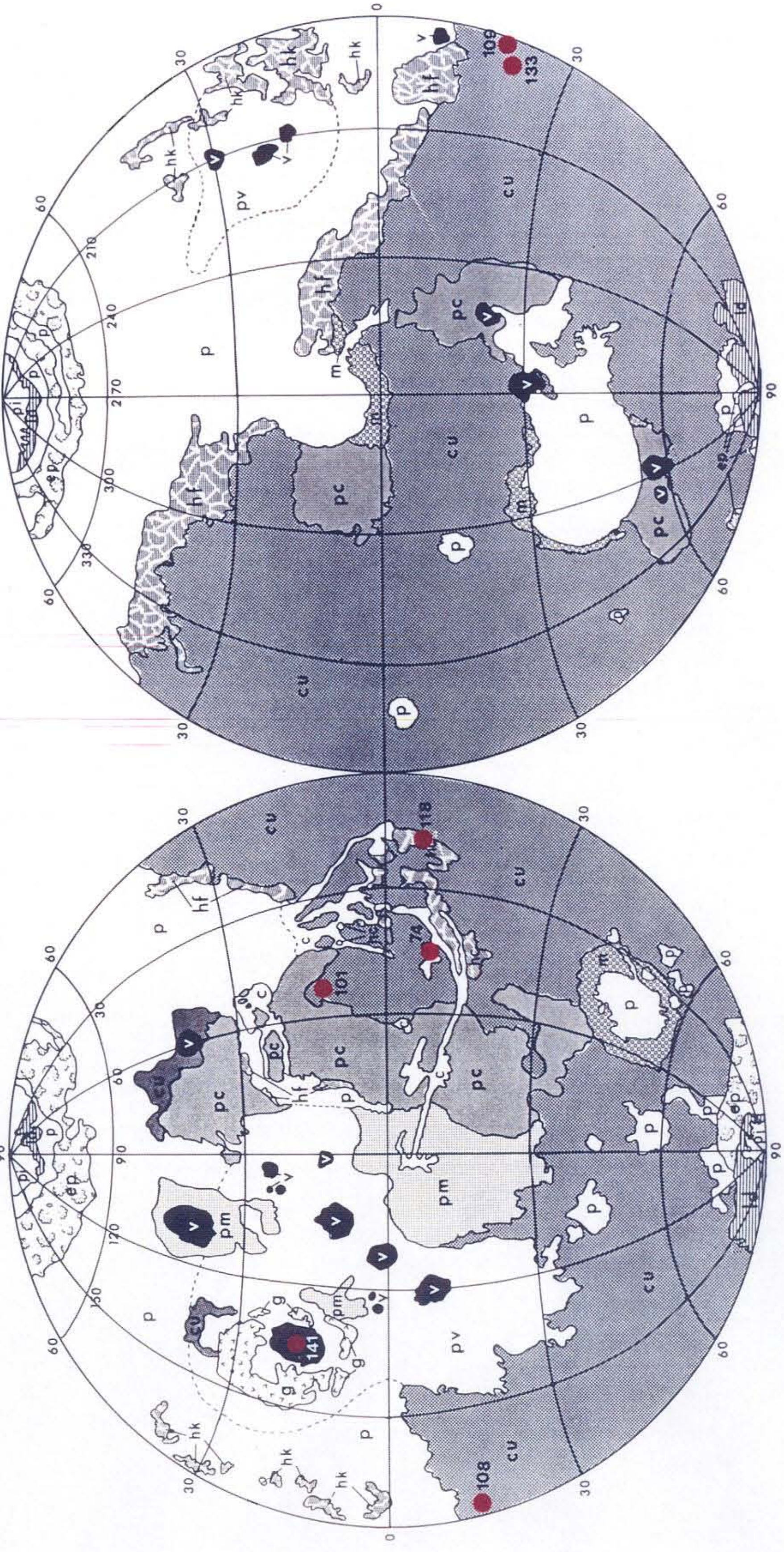
cu
pc
p
pv
pm
hf
hk
m
v
g
c
ep
pl
ld
109
133
108
141
101
74
118
0
30
60
90
120
150
210
240
270
300
330

debris deposited blunt-to-lobate, distally-raised debris aprons marked medially by a herringbone-like pattern of oblique imbricated ridges (Figure 34). In addition, all of the martian and terrestrial landslides except the Blackhawk and Silver Reef exhibit a subtle radial pattern of ridges and troughs on their distal heaps. The distal heaps of the Blackhawk (Figure 45a) and Silver Reef landslides are instead marked by a transverse pattern of ridges and troughs. Martian Blackhawk-like landslides differ principally from those on Earth in having characteristically greater thicknesses than their terrestrial counterparts.

The observation that terrestrial Blackhawk-like landslides exhibit consistently low H/L values on log(volume) vs. H/L plots and only a minor trend towards decreasing H/L with increasing volume (Chapter III: Figure 7) appears to relate to four important factors: their initiation style, confinement, lithologies and grain sizes. All the landslides were unconfined during runout, providing the opportunity for them to travel without any energy-consuming deflections. In addition, their compositions were conducive to support long runout. The four Argentine landslides consisted of granite, a material shown in Figure 12c (Chapter III) to correspond with consistently low H/L emplacement relative to landslides composed of limestone or metamorphic rocks. Apparently the granular nature of granite allows ready fragmentation of the material into fine powder in moving landslides, a substance apparently of critical significance to the development of long runout in large landslides (Chapter III). The limestone Blackhawk and Silver Reef landslides, in turn, seem to have fragmented into very small (~3 cm) average-sized clasts at the initiation of movement (Chapter III), another factor responsible for developing low H/L values in large landslides (Chapter III: Figure 12c).

The last important aspect of these landslides relating to the development of low H/L values is that the Blackhawk-like landslides appear to have traveled as thick pulses of debris during runout (Figure 47), leading to the final distally-raised profile shapes of the deposits. Perhaps this behavior resulted from initiation as coherent rockfalls in concert with their unconfined runout paths. Whatever the cause, the moving parts of these landslides must have traveled with much greater thicknesses than uniform or tapered landslides of equivalent volume. Because, as mentioned above for the lobate landslides, basal shear stresses appear critical to runout distances traveled, the Blackhawk-like landslides probably achieved low H/L values in part because

Figure 47. Interpretive kinematic model of the morphological development of a Blackhawk-like landslide. Steps 1-3 can be thought of as three progressive steps in the development of a Blackhawk-like landslide. As the landslide moves, it consumes material in the distal heap by depositing lateral levees and a thin veneer of debris between them. The morphologic development of a Blackhawk-like landslide can cease at any point in this evolution, depending on the initial kinetic energy and the volume of the landslide. Landslides containing a lot of debris relative to their kinetic energy content produce compact deposits like the Mars 141 landslide in the summit caldera of Olympus Mons (Step 1; Figure 6i). In contrast, landslides like the Avalancha del Zarzo 2 deposit (Fauque and Strecker, 1988), which start with much more energy per unit volume, may develop more elongated, moraine-like geometries.

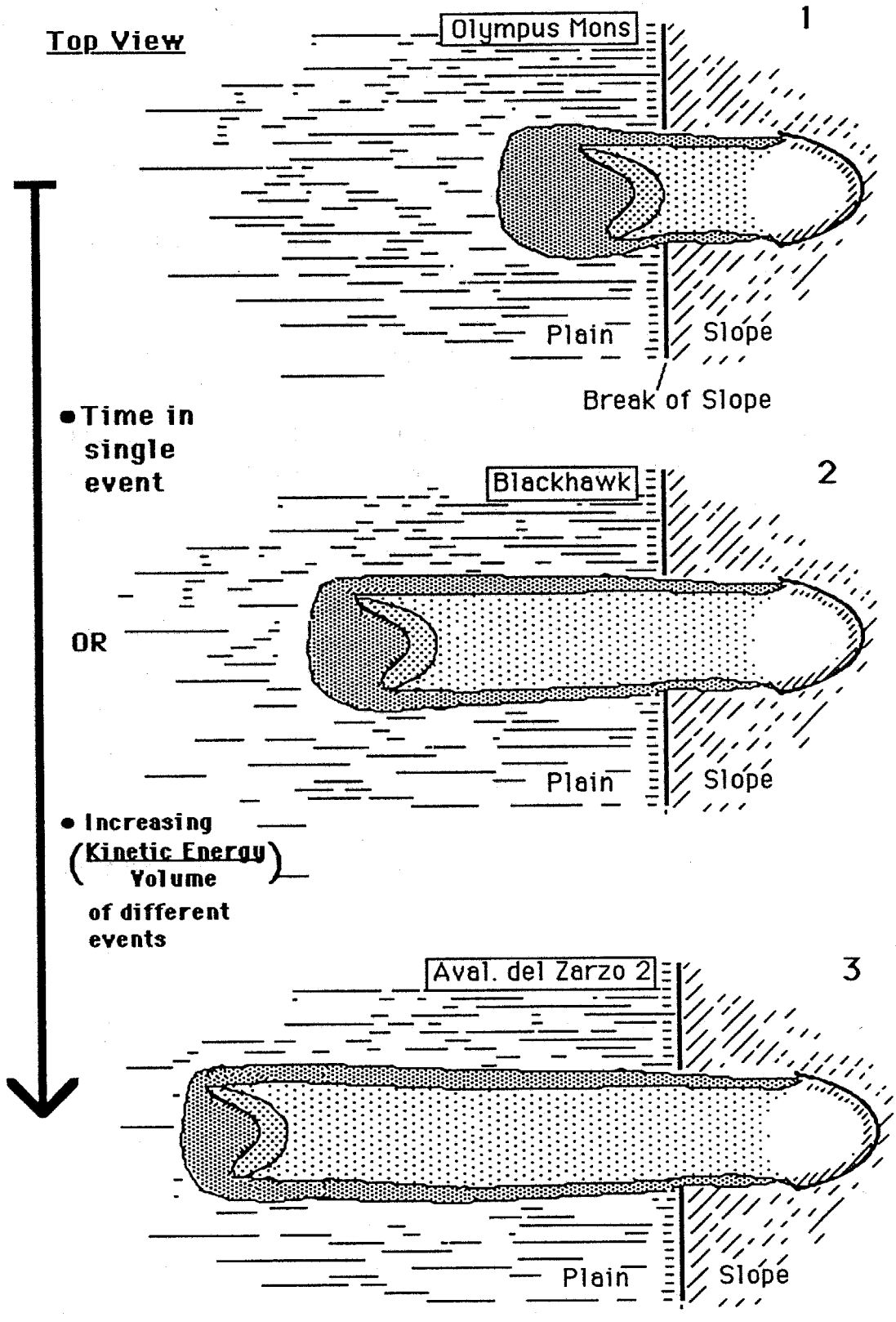
Top View
Olympus Mons
1
Plain
Slope
Break of Slope
• Time in single event
Blackhawk
2
OR
Plain
Slope
• Increasing (Kinetic Energy / Volume) of different events
Aval. del Zarzo 2
3
Plain
Slope

the shear stresses along the bases of the moving distal heaps remained high throughout transport. The lack of a strong decrease in H/L with increasing volume in these deposits seems also to relate to this behavior; data presented in Table 16 indicate that the thicknesses of the distal heaps vary little with increasing volume, unlike the behavior of other large landslides (Chapter V). Because the slides traveled with similar thicknesses over similar depositional surfaces, their basal shear stresses must have been quite similar during runout, leading to very similar H/L values. Thus, Blackhawk-like landslides form the low-H/L envelope of log(volume) vs. H/L behavior for large landslides because of a combination of favorable initiation characteristics, depositional geometries and grain sizes.

The primary morphologic differences between the martian and terrestrial Blackhawk-like landslides are the presence of transverse ridges and troughs on the terrestrial Blackhawk and Silver Reef landslides, and the consistently greater thicknesses of the martian deposits (Table 16). Because transverse ridges and troughs appear only on the Blackhawk and Silver Reef landslides, and not on all the terrestrial Blackhawk-like landslides, it appears likely that their occurrence relates either to the limestone composition of the Blackhawk and Silver Reef landslides (Appendix A) or to special circumstances of their deposition, and not to some special characteristics of the terrestrial environment. Because the Blackhawk and Silver Reef date from Late Pleistocene time, a pluvial period (Stout, 1977), it seems possible that the transverse ridges and troughs exposed on the landslides might have formed as post-depositional solution features (Chapter III), not as the primary features envisaged by Shreve (1968a). The surface of the Late Pleistocene Saidmarreh landslide, for example, another limestone landslide, is dominated by such solution features (Watson and Wright, 1969). All the other terrestrial Blackhawk-like slides, by comparison, consist of granitic breccia (Fauque and Strecker, 1988), and thus were not susceptible to post-depositional solution effects.

The other possibility is that the transverse ridges and troughs formed because the landslides bulldozed large distal heaps of debris ahead of them during runout (Shreve, 1968a). Based on eyewitness accounts of long-runout landslides, Heim (1932) stated that such ridges often formed during runout when landslides bulldozed material ahead of them that interrupted their free runout, causing the trailing material to pile up behind. Perhaps the

Blackhawk and Silver Reef were the only Blackhawk-like landslides to bulldoze large distal heaps because they were the only ones to experience channelized movement, and most of the debris bulldozed by the landslides originated in their source canyons (Shreve, 1968a).

The characteristically greater thicknesses of martian Blackhawk-like landslides relative to those on Earth (Table 16) probably reflect the difference in gravitational acceleration between the two planets. As in the case of the lobate landslides discussed earlier, this conclusion is based on the fact that the martian Blackhawk-like landslides have about 2.5 times the average and maximum thicknesses of their terrestrial counterparts of equivalent volume, a value roughly corresponding to the ratio in gravitational acceleration between Earth and Mars. As mentioned above, the shear stresses along the bases of these dry landslides appear to have an important effect on the runout distances achieved by the landslides during runout; the low-friction aspect of their high-velocity travel only occurs so long as the landslides maintain a critical minimum thickness. As described in detail in Chapter VI, I infer that the shear stresses must remain elevated during transport in order to allow the geological materials at the bases of large landslides to flow and act as basal lubricating agents, over which semi-rigid landslide debris slides and spreads into place. According to this concept, the basal lubricant has plastic properties; it flows at high shear stresses, but is rigid at low shear stresses. This concept contrasts with that proposed by McEwen (1989), who modeled landslide debris as having bulk-fluidized "Bingham plastic" properties (Chapter V; Appendix E). In his model, motion also occurs only above a critical threshold thickness, but above this "yield stress" flow can occur in the bulk of the deposit--it is not constrained to a basal lubricating layer. A basal lubricant, rather than bulk fluidization, is a requirement demanded by the geological relations of long-runout landslides outlined in Chapter III (Chapter V; Appendix E).

Like most other groups of martian landslides, the Blackhawk-like group does not have a random distribution on the surface of the planet. Considering that these landslides exhibit morphologies consistent with dry emplacement, it appears noteworthy that only a single Blackhawk-like landslide occurs in Valles Marineris, considering that over half the landslides on the planet lie within this region (Figures 38, 40). The concentration of these dry landslides outside of Valles Marineris thus contrasts sharply with the concentration of

moist-appearing landslides in the equatorial chasma system. This observation reiterates the probable role of water in influencing the distribution and morphologies of landslides in Valles Marineris.

Note also that the location of the martian Blackhawk-like landslides places them on some of the oldest and youngest geologic units on the planet (Figure 46). Because the Mars 141 and 118 landslides formed in relatively youthful terrains on the planet, in the summit caldera of Olympus Mons and in chaotic terrain, respectively, they clearly formed relatively late in martian geologic history, long after the dissipation of Mars' proposed early dense atmosphere (Murray, et al., 1981). However, even those deposits situated in the ancient cratered highlands do not appear of great age, because they exhibit few or no impact craters and have clear, unmodified morphologies relative to the surrounding landforms. All the martian Blackhawk-like landslides therefore probably occurred under essentially modern martian climatic conditions, long after the dissipation of Mars' early dense atmosphere.

Shreve (1968a) proposed that the low H/L values and characteristic morphologies of the Blackhawk and Silver Reef landslides could be attributed to air-layer lubrication of the landslides. By extension, the very similar morphologies of the martian landslides ought to be explicable by the same mechanism. However, the fact that all the Blackhawk-like landslides on Mars appear to have occurred under essentially current martian environmental conditions places into doubt the possibility that lubrication by compressed atmospheric gases played an important role in their emplacement.

For air-layer lubrication to operate, a landslide must capture and retain beneath it a pressure of gas equivalent to its weight (Shreve, 1968a; b). Following the method of Shreve (1968b), one may calculate that at the datum elevation on Mars (6.1 mbar pressure of CO_2 gas, ~200°K), a 65 m-thick breccia sheet (Table 16) with a density of 2000 kg/m^3 would have to trap a 60 m-high column of atmosphere per unit area of landslide to support a 0.3 m compressed gas cushion beneath the landslide (Appendix D). The range of environmental values described here corresponds roughly to the atmospheric density and temperature expected for most of the martian Blackhawk-like landslides (Carr, 1981). However, for the Blackhawk-like landslide Mars 141 (Chapter II: Figure 6i) in the summit caldera of Olympus Mons, 25 km above the datum elevation (0.3 mbar pressure of CO_2 gas, ~160°K; Carr, 1981), one calculates much different figures. For the same 2000 kg/m^3 density, the 120 m-thick landslide

(Table 16) would have to trap a 1340 m-column of atmosphere to support a 0.3 m compressed gas cushion beneath the landslide (Appendix D). Even given a suitable launching ramp, collecting the required volume of gas per unit area would prove impossible for any case on Mars, because most of the gas would escape from beneath a landslide dropping from a height of tens or hundreds of meters rather than being captured under the rubble. Furthermore, landslides Mars 74, 108, 118 and 141 do not show any apparent signs of a possible launching ramp (Chapter II: Figure 6i; Chapter III: Figure 17a; Figures 45c, 45e). For the Blackhawk landslide, in comparison, the 30 m-thick breccia sheet need only have captured a 0.8 m-thick column of air per unit area of landslide (Appendix D). Nonetheless, even to capture this comparatively small volume of air, Shreve (1968a) estimated that the landslide had to be deflected into the air at the launching ramp at an angle of between 29° and 39° and at a velocity of between 220 and 330 km/hr to capture the 1.4×10^7 m^3 of air necessary to provide the proper lubrication. Thus, even in Earth's comparatively thick atmosphere, collecting enough air to develop air lubrication for a landslide is not a trivial matter. The data from the martian landslides therefore provide good evidence that the morphologies and low H/L values demonstrated by Blackhawk-like landslides are not controlled by the air-layer lubrication mechanism as proposed by Shreve (1968a). Nonetheless, the geological evidence from the Blackhawk (Shreve, 1968) and from other long-runout landslides (Chapter III) indicate that these deposits did indeed slide into place over some type of basal lubricant. Captured and compressed atmospheric gases can not provide the general source of lubricant, however. Rather, I infer that weak substrate materials or crushed landslide debris forms the lubricating agent(s) in large landslides. This concept is described in detail in Chapter VI.

An interpretive kinematic model of the morphological development of martian and terrestrial Blackhawk-like landslides is presented in Figure 47. Immediately following the initial slope failure, the landslides take up a bulbous shape and begin to deposit behind them a thin sheet of rubble bracketed by sharp lateral levees. As motion continues, deposition of the thin sheet and levees proceeds from material in the distal heap, which decreases in thickness, length and sometimes in width with distance traveled. Given a sufficiently high ratio of fall height to volume, the process will continue until the distal heap is used up, resulting in a deposit consisting of an elongate

moraine-like ring of debris. Under less energetic starting conditions, the morphology of a Blackhawk-like landslide can "freeze" into place at some prior step in this progression.

E. Conclusions-Chapter IV

The comparison of large landslide phenomena on Earth, Mars and the Moon provides a powerful tool for understanding both the role of liquid water on the martian surface subsequent to its early heavy-atmosphere period. These comparisons also help clarify the nature of the processes responsible for long runout in large landslides.

Many dry, moist and wet landslides are separable on the basis of morphology and depositional characteristics but not on the basis of quantitative measures of landslide runout characteristics. Blackhawk-like landslides on Earth provide the one readily identifiable landslide morphology that always appears to represent dry emplacement. Several different morphologies give proof of moist runout. One of these is the symmetrical lobate morphology characterized by the Carlson landslide, Idaho. A lobate-terraced debris apron morphology and perhaps also the distal glide blocks texture also represent moist emplacement, though the latter texture might instead be representative of water-saturated deposition. Landslides that contain so much water that the water segregates from them at the cessation of movement are termed water-saturated or wet landslides. These landslides have very distinctive morphologies. In the six known terrestrial subaerial and subaqueous wet landslides, each deposit is marked by a lack of distinct distal margins and by a proximal-to-distal gradation from landslide debris into debris flows or mudflow deposits. Because the addition of water to a landslide apparently strongly reduces the effective viscosity of their fine-grained component, moist and wet landslides experience bulk fluidization during transport, negating preserved stratigraphy and reverse grading in these deposits. Several quantitative measures of landslide moisture content were proposed by McEwen (1989), including: log(volume) vs H/L trends, estimated yield strengths and velocities. All these measures fail to separate dry from wet from moist landslides, however. This observation indicates to me that the runout mechanism in moist, wet and dry landslides must essentially be the same despite some of their differences in depositional characteristics. Particularly interesting is the observation that wet and moist landslides and

dry fine-grained landslides exhibit very similar log(volume) vs. H/L trends. Thus, the fine-grained component of these landslides, not their water content, appears critical to the H/L relations achieved by large landslides during runout.

I have found that martian landslides do not have a random distribution, but rather occupy certain preferred sites on the surface of the planet. I infer that, like Earth and unlike the Moon, the distribution of martian landslides relates to endogenic processes in the martian crust and not to impact processes. Almost all martian landslides lie between 30° N and S latitudes. The lack of landslides outside of this equatorial belt appears to me to relate to the aeolian terrain-mantling deposits that cover and soften topography poleward of approximately 30° N and S latitudes. In the unmantled region, approximately two-thirds of the 161 landslide deposits found on Mars lie in Valles Marineris. Many rockfalls formed in Valles Marineris from bedrock outcrops cresting the chasmas because of oversteepening and failure of bedrock along chasma-dipping discontinuities. In contrast, the giant slumps in Valles Marineris originate from chasma walls bounded by large talus piles, even though these slopes should exhibit considerable gravitational stability. Although many of these slumps may have formed because of marsquakes or pore water pressure increases, I infer that most are controlled by vertical structural discontinuities in plateau rock and horizontal discontinuities in wall rock. The latter appear to coincide with the erosional base level horizons represented by the neighboring chasma floor surfaces. These horizontal discontinuities might represent fossil ice-water horizons within the equatorial chasma system. The Valles Marineris landslides all appear to date from the later half of Mars' geologic evolution. The presence of landslides with widely varying morphological freshness, as well as some scalloped regions of chasma wall that generally are not accompanied by landslide debris, suggests that the present distribution of Valles Marineris landslides may represent just the current stage of a very long-term process of landslide deposition and erosion in the equatorial chasmas. Outside of Valles Marineris, most of the large landslides deposits occur in ancient cratered terrain, the oldest exposed surfaces on the planet. These landslides probably do not date from the origin of these surfaces, however, because the slides retain fine surficial textures while the surrounding cratered landforms are comparatively dull and

degraded in appearance. As in Valles Marineris, these landslides are a recent phenomenon relative to the surfaces on which they are deposited.

A number of factors are probably responsible for the contrasting numbers of large landslides on Mars and the Moon. Primarily, Mars has experienced a variety of geologic processes over time not matched by events on the Moon. Tectonic activity on Mars, for example, has created many important sites for landslide initiation such as Valles Marineris and Olympus Mons. Rift-like tectonics in Valles Marineris and the development of large volcanic constructs on Mars have provided both the topographic relief and the oversteepened slopes necessary to initiate large landslides. They probably also provided source areas for shallow seismic impulses that could have triggered their initiation. In contrast, internal lunar seismic activity has probably been comparatively miniscule and deep-seated over most of the Moon's geologic history. Another factor in the high concentration of landslides on Mars relative to the Moon is the role of water behind wall rock in Valles Marineris. High pore pressures in these areas might have been responsible for some of the highly concentrated landslide deposits in this region, but the possible role of fossil horizontal ice-water discontinuities in the martian crust might provide a much more important effect. Also, Mars apparently underwent an early cycle of aqueous erosion ending with the cessation of the late heavy bombardment of the solar system. During this period, surficial materials could have experienced considerable weathering that later provided preferred sites for large landslide initiation. In comparison, the Moon does not support any subsurface liquid water today, nor is there any evidence that it ever contained any free water. The unweathered lunar surficial materials therefore might be stronger and more cohesive than much of the ancient surficial highlands material on Mars. Once formed, martian landslides tend to remain intact for very long periods because of a lack of processes, such as impact gardening (Murray, et al., 1981), to erode or bury them. Continual impact gardening of lunar surface features, in contrast, forms a comparatively efficient means of eroding and burying landslides on the Moon. The Moon may therefore in part expose less landslides than Mars because many early lunar landslide deposits have been completely reworked by these processes over geologic time.

I have found considerable morphological evidence to support the concept that liquid water played an important role in the runout of some large martian landslides. This conclusion contrasts markedly with that of McEwen (1989),

who stated that all the Valles Marineris landslides "were probably dry" at emplacement. The presence of liquid water is suggested by moist and wet landslide morphologies on deposits in Valles Marineris and from Olympus Mons. Three groups of landslide phenomena in Valles Marineris provide evidence of moist or wet emplacement. The largest and clearest example is provided by a large triple-reentrant landslide complex in Ophir Chasma. These landslides exhibit indistinct distal margins that grade into low-relief textured deposits that appear to represent water-saturated mudflows or debris flows. If so, these water-rich flows must have traveled like lava flows on Earth because of the cold surface temperatures and very low surface pressure on Mars. Downstream, the debris flow deposits transition into water-dominated flow(s). The water-dominated flows probably formed by segregation of water from the debris flows to form an ice-covered lake. Overfilling of this ice-covered lake led to catastrophic Missoula flood-like erosion and deposition below the postulated location of the fossil lake. The Ophir landslide complex appears to me to represent a deposit intermediate in character between common giant slumps and martian outflow channels. The scale, headscarp relations and distal water-dominated flood features displayed by the complex closely resemble martian outflow channel characteristics. However, the intermediate debris flow reach of the landslide complex does not appear to be represented in any known outflow channel phenomena. The Ophir landslide complex may therefore represent a late-stage equivalent of martian outflow channels, one dominated more by rock debris and less by water than any previous events.

Morphological evidence also exists to support a role for water in some older Valles Marineris slumps. Two of these landslides, the Mars 4 and 24 deposits, express morphologies that on Earth correspond only to moist and/or wet deposition: the lobate-terraced and isolated glide blocks textures. These textures occur on the Mars 4 and 24 deposits at scales equivalent to similar features observed on subaqueous landslides on Earth. The source of water in these slumps could have been water or ice in chasma wall rocks, as postulated for the Ophir landslide complex, or perhaps they derived water from ice-covered lakes that the landslides encountered during runout.

Lobate landslides form a third group of much smaller landslides on Mars that exhibit morphologies suggestive of moist emplacement. This group consists of lobate landslides that fell from the flanks of Olympus Mons and from chasma walls in Valles Marineris. Their highly symmetrical shapes and

the even spacing of their longitudinal ribs suggest that they traveled with the same characteristics as the moist Carlson landslide. The characteristically greater thicknesses of the martian landslides apparently relate to the difference in gravitational acceleration between the two planets. This behavior, together with the depositional characteristics of large landslides summarized in the preceding chapter, suggest that basal shear stresses play a strong role in the movement of large landslides. The fine material concentrated near their bases acts in a fluid fashion and flows in response to high applied shear stresses.

Landslides with dry, Blackhawk-like morphologies occur on both Earth and Mars. The unusually low H/L values characteristically observed on terrestrial members relative to other landslides on Earth appear to relate to their unconfined geometries, to favorable compositions and to the fact that the landslides traveled in thick heaps during deposition. The pulse-like deposition of the landslides kept basal shear stresses elevated during runout relative to landslides that tapered off in thickness, assisting in the development of the characteristically low H/L values of the Blackhawk-like slides. The martian and terrestrial members of this morphology class exhibit remarkable similarities in primary and secondary morphologic characteristics, with the exception that the Blackhawk and Silver Reef landslides exhibit a pattern of transverse ridges and troughs not represented on any of the other members of the class. These anomalous features appear to have formed either as a result of post-depositional modification or due to the bulldozing of material during runout. Perhaps the most significant physical differences between martian and terrestrial Blackhawk-like landslides are the much greater thicknesses of the martian deposits. This characteristic probably results from the difference in gravity between the two planets, with the terrestrial landslides spreading out over their fluid, fine-grained basal layers to a greater degree than their martian counterparts in response to Earth's greater gravitational acceleration. Like most other martian landslides, the seven deposits in the Blackhawk-like group do not have a random distribution on the surface of the planet. Rather, they occur on some of the oldest and youngest terrains on the planet. Even those landslides situated in the ancient cratered highlands do not appear to be of great age, however, because of their unmodified morphologies and their lack of impact craters relative to the surrounding landforms. All the Blackhawk-like landslides on Mars therefore probably occurred under

essentially modern martian climatic conditions, long after the dissipation of Mars' early dense atmosphere. Because martian Blackhawk-like landslides traveled under very low atmospheric pressures, the air-layer lubrication theory of Shreve (1968a) cannot provide a general solution to the morphological development and low H/L values achieved by these landslides. The martian landslides simply cannot capture a significant quantity of gas beneath them during runout to allow the development of a basal layer of compressed gas on which the landslides could slide into place. Thus, differences in gravitational acceleration between Earth and Mars appear to have a recognizable influence on the runout behavior of large landslides, but differences in atmospheric pressure have no identifiable effect.

Chapter V. Critical Evaluation of Proposed Mechanisms for Long Runout

A. Introduction

Scientists and engineers have struggled to understand how and why large falling masses of rock exhibit their remarkable suite of characteristics ever since Heim (1882) first recognized the unusually great runout lengths of large landslides. Over the decades since Heim conducted his pioneering studies of the Elm landslide and of a whole population of older and larger landslides in the Alps, researchers have repeatedly revisited the problem using a wide variety of approaches. These efforts have yielded no less than twenty imaginative mechanical models for explaining long runout ($H/L < 0.6$) in high-volume rapid landslides (Appendix E: Tables 1-3). These modeling efforts can be subdivided into two groups: the majority, which attempt to explain long runout by way of a single unifying theory, and others that attempt to explain the phenomenon on a case-by-case basis. Modelers seeking a unified theory for long runout are supported by the fact that long runout occurs as the rule in large landslides, rather than the exception. Unfortunately, no worker has yet successfully integrated the full spectrum of field observations into a unified theory, so that all suffer from one or more serious flaws in fully explaining the wide variety of features that characterize long-runout landslides. These unsuccessful efforts have resulted primarily from a common failure in the approach to the problem. In nearly every case, these models have been developed to explain the characteristics of individual landslides or of a small subset of landslides, such as historically observed occurrences, and then have been advanced as general solutions to the problem. The primary object of the current research was therefore to first fully collate all the available information on long-runout landslides, to use this information to evaluate existing proposed models of long runout, and then to propose a new theory if the existing models came up short.

B. Description and Evaluation of Proposed Models for Long Runout in Large Landslides (Appendix E)

Appendix E begins with a discussion of a simple block-on-inclined-plane model to explain landslide travel, to provide a basic understanding of the anomalous nature of long-runout landslides. Following this discussion, four separate categories of theories are discussed and evaluated for their ability to

explain the variety of unusual phenomena associated with long-runout landslides. These categories include: 1) bulk fluidization and flow of landslide debris; 2) basal lubrication, i.e., special forms of lubrication along the base of the slides; 3) mass-loss mechanisms coupled with normal frictional sliding; and 4) individual-case mechanisms. The first three categories include descriptions of mechanisms proposed as unifying theories of long runout, applicable to many or all large landslides. The fourth category consists of mechanisms proposed to explain long runout on a case-by-case basis. The theories presented in the fourth category do not assume to explain long runout as a universal property of large landslides, but rather attempt to explain the phenomenon based on local effects of the depositional environment. The various theories composing these groups approach the subject with varying degrees of depth, ranging from qualitative, kinematic arguments to highly quantitative mathematical modeling efforts.

C. Synopsis

The following synopsis summarizes the arguments for and against the mechanical models of long runout proposed in the literature. This synopsis is based on the detailed description and evaluation of each proposed mechanical model of long runout contained in Appendix E, which makes use of the systemized landslide data presented in Chapters III and IV.

A conceptual model of a sliding block on an inclined plane provides the most basic model of landslide runout. This model is most useful in highlighting the difference between "normal" frictional behavior and the character of long-runout landslides. For a rigid block sliding down an inclined plane with a constant basal coefficient of sliding friction, one finds that the center of gravity of such a block will always end movement when the fall height to runout length ratio of the center of mass equals the coefficient of sliding friction of the block over its substrate. In this model, the mass of the sliding block and the acceleration of gravity in the experimental setting have no influence on the H/L ratio traveled by the block at emplacement. Nearly all large landslides vary from this model in some respects, however. For example, most do not remain rigid blocks during emplacement. Also, some can experience anomalously low or variable coefficients of sliding friction during runout. The results of these departures from the sliding block model are that both volume (~mass) and gravitational acceleration become important factors

in determining the distance a large landslide will travel during runout for a given value of fall height. The complex models outlined in Appendix E each made use of one or two of these departures from the sliding block model to explain long runout in large landslides.

The treatment of large landslides in the scientific and engineering literature has often considered these mass movements as traveling by means of a common, but obscure, mechanism. Heim (1932) appears to have been the first individual to make this implicit assumption after his study of numerous large Alpine landslides. At least thirteen different mechanical theories have been proposed to explain long runout as a group phenomenon. These theories consist of bulk fluidization models (Heim, 1932; Kent, 1966; Hsü, 1975; Davies, 1982; Melosh, 1983; Krumdieck, 1984; Trunk, et al., 1986; Campbell, 1989; McEwen, 1989; Potapov and Ivanov, 1991), basal lubrication models (Shreve, 1968a; Erismann, 1979) and one mass-loss "rocket" model (Van Gassen and Cruden, 1989). Most of these theories have been proposed to explain a few critical characteristics of large landslides, such as their long runout and high velocities. None of the general theories proposed to date, however, have proven capable of explaining the critical characteristics of long-runout landslides common to most deposits (Table 17).

Most of the theories proposed to explain long runout in large landslides call on some mode of fluidization to account for the low apparent frictional coefficients achieved in these deposits during runout. Although these models all can explain the low apparent friction and high velocities of long-runout landslides, they generally fail to account for many of the other common characteristics of these deposits. All but Campbell (1989) can account for the general fluid appearance of large landslides and the sheet-like geometries of the non-heavily confined deposits (Table 17). However, few can successfully explain the internal structures of long-runout landslide deposits. The preservation of stratigraphy and the appearance of fragile three-dimensional jigsaw puzzle breccia (Chapter III), for example, indicate that the large landslides can experience only minor internal shear during runout. Turbulent flow, and even significant laminar flow, would prevent the retention of headscarp stratigraphy and jigsaw-puzzle breccia in the final deposit. These two characteristics alone rule out half of the fluidization theories as general explanations of the long-runout phenomenon (Table 17). The remaining five models (Davies, 1982; Campbell, 1989; McEwen, 1989;

Table 17. Proposed General Theories for Long Runout vs. Critical Characteristics of Large Landslides

Theory Name & Author	High Speed	Fluid Form	Sheet-like Geometry	Pres. Strat.	Reverse Grading	Volume Effect	Onset Volume	3D Jigsaw Breccia	Sudden Halt	Mars/ Moon?	Dist. Raised
Bulk Fluidization Models											
Kinematic flow (Heim, 1932)	√	√	√	X	?	√	?	X	√	?	?
Air fluidization (Kent, 1966)	√	√	√	X	X	?	?	X	?	X	?
Air fluidization + aerodynamic lift (Krumdieck, 1984)	√	√	√	X	X	?	?	X	?	X	√
Grain flow in fluid medium (Hsü, 1975)	√	√	√	X	?	?	X	X	X	√	?
Grain flow w/out fluid medium (Davies, 1982)	√	√	√	?	√	√	X	√	√	√	?
Computer simulation of grain flow (Campbell, 1989)	√	?	?	√	?	?	?	√	√	√	?
Acoustic fluidization (Melosh, 1983)	√	√	√	?	?	?	√	?	√	√	?

√ = theory accounts for observation; X = theory cannot account for observation; ? = observation not addressed or unclear in theory

Table 17, con't.

Theory Name & Author	High Speed	Fluid Form	Sheet-like Geometry	Pres. Strat.	Reverse Grading	Volume Effect	Onset Volume	3D Jigsaw Breccia	Sudden Halt	Mars/ Moon?	Dist. Raised
Computer-simulated flow, bi-viscous rheology (Trunk, et al., 1986)	√	√	√	X	?	?	?	?	?	?	?
Computer-simulated flow, power-law rheology (Potapov & Ivanov, 1991)	√	√	√	?	?	?	?	?	?	√	?
Bingham plastic rheology (McEwen, 1989)	√	√	√	X	?	√	X	?	X	√	?
Basal Lubrication Models											
Air-layer lubrication (Shreve, 1968a)	√	√	√	√	X	?	?	√	√	X	√
Dissociated rock & melted rock lubrication (Erismann, 1979)	√	?	?	√	?	√	?	?	?	?	?
Low-Velocity Mass-Loss Model											
Low-velocity mass-loss (Van Gassen & Cruden, 1989)	√	?	√	?	?	X	X	?	?	√	X

√ = theory accounts for observation; X = theory cannot account for observation; ? = observation not addressed or unclear in theory

Melosh, 1983; and Potapov and Ivanov, 1991) all assert that these internal structures in long-runout landslides can be preserved if most of the flow remains constrained to near the base of the landslides (Chapter III; Appendix E). However, the mechanisms by which flow remains constrained to a basal layer cannot be proven for any of these models. Davies (1982) used doubtful mechanical simulations of dispersive grain flow to support his model. Melosh (personal communications, 1990; 1991) cannot prove that acoustic fluidization works at all, and his computer simulations further suggest that if it does operate it should produce a flow regime that extends upwards throughout the moving landslide and does not remain constrained to near the base as predicted in Melosh (1983; 1986; 1987). The model by Campbell (1989) has many question marks because of its bare-bones nature. The computer simulations give some interesting results, but they do not really mimic the internal behavior of large landslides. Primarily, they fail to consider the brecciation of component clasts and the likely possibility that the fine powder that accumulates along the bases of large landslides would interfere strongly with the interparticle collisions concentrated in this zone. It appears likely that the boundary conditions of computer grain-flow models using undeforming disks to represent clasts should break down early in the runout of actual large landslides. The last two models, those of Potapov and Ivanov (1991) and McEwen (1989) model landslide runout in essentially the same way, as substances that flow at high strain rates but that flow only very slowly or not at all at lòw strain rates. One problem with both theories is that both fail to model the long-runout phenomenon on the level of clasts in the landslides. Instead, both models view the landslides as homogeneous substances subject to flow when sufficiently sheared. Thus, zones of flowing material may extend to varying distances from the base of a slidemass depending on the thickness and velocity of the landslide. Large dry landslides actually display a significant degree of heterogeneity in their material properties upwards from their basal regions. While flow may indeed occur in fine material near the base of a large landslide, flow does not appear readily capable of migrating upwards in a large dry landslide. Perhaps a Bingham or power-law viscosity can explain the flow behavior of the fine-grained basal material in dry landslides, or even of the entire bodies of large moist or wet landslides (Appendix B). However, these models have not yet achieved the degree of sophistication necessary to describe the runout behavior of large dry landslides.

Lubrication models generally provide a better explanation of the geological relations observed in long-runout landslides than the fluidization models. However, they have problems identifying a universal lubricant for all long-runout landslides. Despite its success in explaining the long runout and morphological development of the Blackhawk landslide, the air-layer lubrication model by Shreve (1959; 1968a) cannot be shown to operate universally for large landslides on Earth because many large landslides fail to exhibit launch ramps, as well as the morphological features deemed critical to the model by Shreve (1968a). The model also has great problems in explaining the long runout of martian landslides, together with the reverse grading observed in many terrestrial landslides (Table 17). In an effort to obtain a more universal lubricant for large landslides, Erismann (1979) suggested that melted rock concentrated along the bases of large landslides or gas from dissociated limestone might provide likely lubricating agents. However, melted rock occurs only very infrequently in large landslides (Chapter III), and few rocks other than limestone appear capable of dissociating into a convenient gas for lubricating purposes. Thus this model also fails to explain long-runout via basal lubrication because of its failure to explain the nature of a universal lubricant.

The low-velocity mass-loss model of landslide runout forwarded by Van Gassen and Cruden (1989) approaches the explanation from a completely different angle than the lubrication and fluidization theories. It can explain several phenomena not properly accounted for by any of the other theories, but it has just as many failings as the other theories. The model primarily fails because of its prediction that landslides should exhibit a degree of long runout related to their profile shapes. Tapered landslides should have the lowest H/L values and distally raised the largest, in contradiction to the characteristically low observed H/L values of distally-raised slides. The model also fails to explain any of the volume-dependent characteristics of large landslides (Table 17).

An alternative means to view the travel of large landslides is to consider their behavior on an individual-case basis. Using this outlook, one may consider the long runout of large landslides as an opportunistic phenomenon that occurs under various different conditions for different reasons. Proposals have been made in the literature that individual large landslides have exhibited long runout because of various bulk fluidization or basal

lubrication mechanisms. These mechanisms include earthquake fluidization (Solonenko, 1972; Hazlett, et al., in press), sliding on a vaporized pore fluid gas cushion (Habib, 1975; Goguel, 1978), sliding on a weak stratum in the landslide debris (Watson and Wright, 1969; Johnson, 1978), or sliding over snow (McSaveney, 1978), mud (Evans, personal communication, 1990), or moist soil (Heim, 1932) in the substrate. For some of the landslides, the proposed operative mechanism probably doesn't work, such as earthquake fluidization in the Vesuvius 1-7 deposits. For most of the other landslides described by these theories, however, the proposed mechanism provides a viable explanation for the long runout and other characteristics of these deposits. For example, basal pore fluid vaporization provides a viable explanation for the travel of large coherent landslides, and basal lubrication by mud or snow seems reasonable for landslides that travel down river channels or across snow-covered glaciers, respectively. Nevertheless, the data compiled in this thesis suggests that these phenomena all simply comprise variants on a common theme; most of the valid individual-case theories propose one form or other of a basal lubricant over which the landslide debris runs out. Because long runout occurs in brecciated debris streams even in the absence of micaceous material, mud or snow along the basal contact, some universal lubricant must be available even when these other lubricants are absent. Brecciated rock concentrated along the basal surfaces of large landslides appears to me the likely candidate material for this universal lubricating agent. The interaction of a large landslide with its substrate during runout appears responsible for most of the observed characteristics of these features. Where a weak substrate material occurs, the landslide debris slides and spreads into thin sheets over the substrate. Where the substrate is firmly cemented, breakdown of rock into powder in the landslide debris itself forms a poorer lubricant over which the debris slides in thick sheets. This conceptual model is presented in detail in the following chapter.

Chapter VI. Distributed Deposition and Basal Lubrication Concept for Long Runout of Large Landslides

A. Description of Concept

In the following chapter I describe how and why I think large landslides commonly experience long runout. I submit that they do so because of their brecciated nature and because of the limited strength of the geological materials overrun by the landslides during their travel. Brecciation allows these landslides to come to rest piecemeal, with the slowest, trailing particles that can lose energy the fastest coming to rest first. The ultimate strength of geologic materials, in turn, appears to be overcome at the bases of larger long-runout landslides, due to a combination of high shear rates and large basal shear stresses. Once the basal materials fail, they experience flow. Where the landslide debris is dry, the overriding landslide breccia rafts into place over this failed material. If the material is moist or water-saturated, flow appears to begin near the base, but it can migrate upwards to encompass the entire thickness of a large landslide. Based on these concepts, the runout distance achieved by a landslide will specifically depend upon its initiation style, travel thickness, confinement, substrate properties, and debris properties, as well as on the gravitational acceleration of its planetary environment.

I infer that the long runout process begins when a landslide mass becomes brecciated in its early movement stages. Unlike a cohesive sliding block, the clasts making up a brecciated landslide are not constrained to all come to rest at the same instant of time. Like all other natural processes, the material composing a large landslide will lose its excess energy to the environment as quickly as possible; in a brecciated landslide, those particles which can lose their energy the fastest get deposited first, while higher-energy material continues to move. I term this concept distributed deposition. The geologic data and eyewitness accounts suggest to me that the material at the tail end of a moving slide loses energy the fastest and thus deposits first, while the rest of the material continues sliding down slope. The final result of this process, without any other factors involved, is a landslide deposit longitudinally extended in the direction of sliding relative to the dimensions of the initial slidemass. Compared to a cohesive sliding block model (Appendix E), some material is deposited earlier than if the landslide had traveled cohesively, while some travels beyond the limit reached by the downslope end of a

cohesive sliding block (Figure 48). I infer that the center of gravity of a brecciated landslide undergoing distributed deposition should travel about the same distance as a landslide which slid cohesively into place (Figure 48).

Given the distributed deposition concept as a starting point, I feel that a second, equally important, compositional effect comes into play in large landslides: natural basal lubrication. This process appears to function in both water-rich and dry landslides. In moist and water-saturated landslides, wet matrix material forms a natural low-strength lubricant over which a landslide can travel; in these landslides a combination of bulk flow and basal slip appears to occur (Appendix B), with most of the deformation constrained to near the base. Computer modeling studies of the flow a bi-linear viscous fluid by Potapov and Ivanov (1991) appear to closely mimic the inferred behavior of large moist landslides (Appendix E). Basal lubrication of large dry landslides appears to have a rather different character. I infer that at the high shear stresses and strain rates applied by the overriding landslide debris, the materials near the bases of large dry landslides also fail and flow, but that the region of flow does not propagate upwards into the bulk of the landslide as it does in moist and wet landslides. Dry long-runout landslides therefore appear to raft into position over thin layers (~10cm-5m) of fluidized basal material (Figure 49a, 49b).

The geologic evidence indicates to me that both the moist and dry basal lubricants behave in a plastic manner; at low shear stresses they behave rigidly, while at high shear stresses they flow with a material-dependent viscosity. I infer that large landslides stop moving when they thin sufficiently that the basal shear stresses drop below the yield stress of the lubricant, forcing the landslide debris to slide to a halt. The runout distance of a large landslide with a basal lubricant will depend on the nature of the lubricant, which will differ from slide to slide. Moist and wet landslides and rapid dry landslides which travel over weak substrate materials, such as snow, mud or soil, will continue to slide and spread until they form very thin sheets of debris (Figure 49a). However, landslides which move over strong substrates, such as bedrock, appear to develop their own basal lubricant during runout; during travel, these landslides develop a basal layer of comminuted debris over which the landslide debris slides and spreads. I infer that the dry rock powder that forms the lubricant for these landslides has greater strength at high rates of shear than snow or mud, causing dry

Figure 48. Cartoon showing distributed deposition concept for a large landslide. Top diagram shows initiation of a rockfall-type landslide from a horizontally-stratified source slope. During the runout phase, the unloading of deep-seated rock, together with a changing path geometry and the impact of the slidemass on the ground surface brecciate the landslide (clear arrow). The tail end of the landslide mass comes to rest first, while the rest of the deposit slides down slope with a coefficient of sliding friction close to 0.6. The landslide comes to rest with some debris deposited prematurely relative to a cohesive sliding block, while some material gets deposited farther than calculated from the sliding block model.

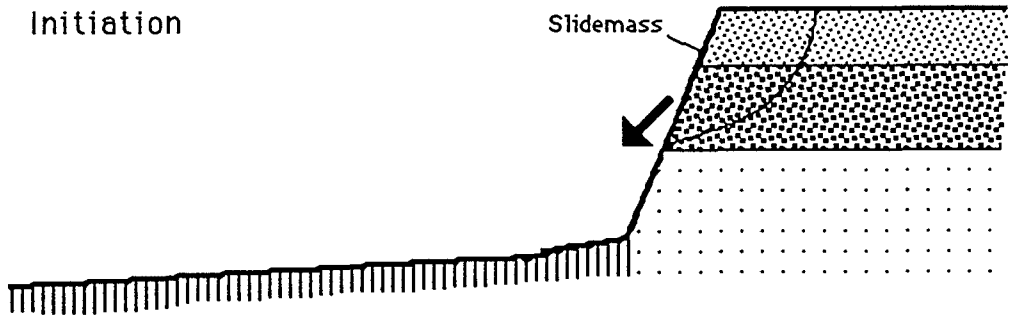
Initiation
Slidemass

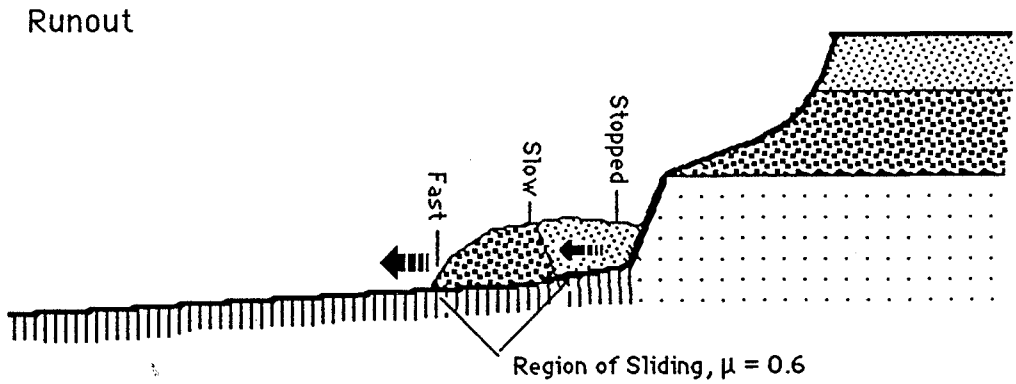
Runout
Fast
Slow
Stopped
Region of Sliding, μ = 0.6

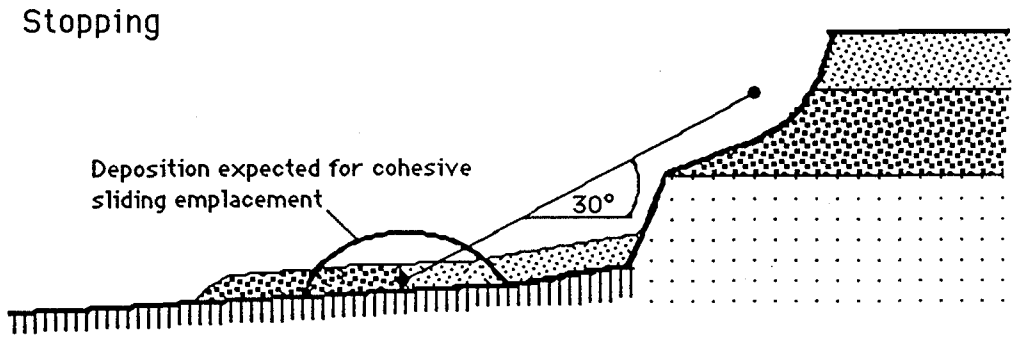
Stopping
Deposition expected for cohesive sliding emplacement
30°

Figure 49a. Cartoon showing basal lubrication concept for a large landslide traveling over a weak substrate. The landslide begins the runout phase in a brecciated condition, due to unloading, impact and changes in slope geometry. The landslide travels onto a low-strength substrate, such as soil, mud or snow. The shear stress at base of the landslide overcomes the yield strength of the substrate, which begins to flow beneath the landslide. The landslide slips forward and spreads out over the fluidized basal lubricant in the middle of the runout phase. The landslide comes to rest when the landslide thins sufficiently that the shear stresses along its base fall below the yield strength of the lubricant, causing the landslide to rapidly skid to a halt. On the weak substrate the landslide debris only ceases motion once it has spread out into a thin sheet with large areal dimensions.

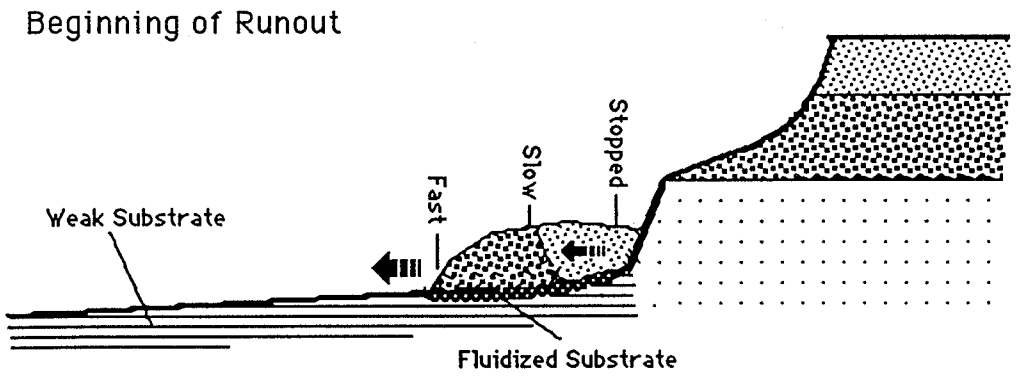
Beginning of Runout
Stopped
Slow
Fast
Weak Substrate
Fluidized Substrate

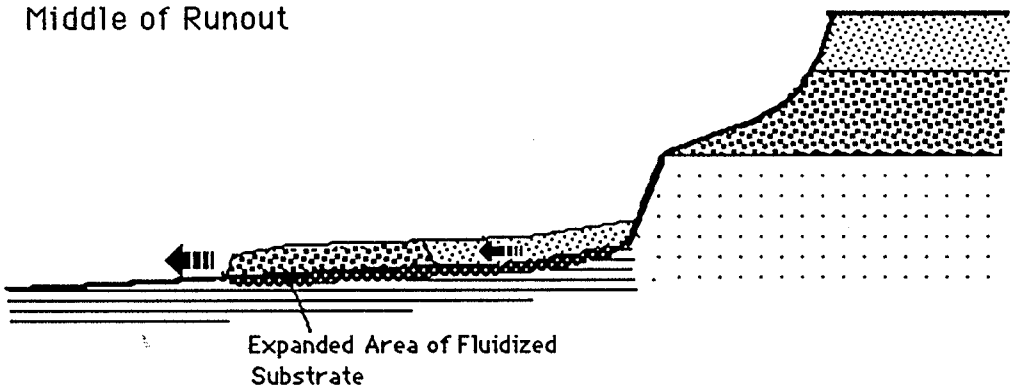
Middle of Runout
Expanded Area of Fluidized
Substrate

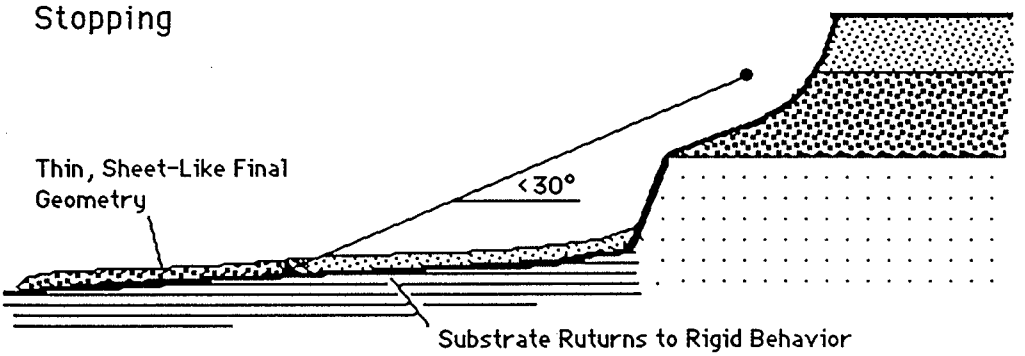
Stopping
Thin, Sheet-Like Final
Geometry
< 30°
Substrate Ruturns to Rigid Behavior

Figure 49b. Cartoon showing basal lubrication concept for a large landslide traveling over a strong substrate, such as bedrock or strongly cemented alluvium. The landslide begins the runout phase in a brecciated condition, due to unloading, impact and changes in slope geometry. The landslide begins to spread due to distributed deposition, and rock flour begins to concentrate along the base of the moving portion of the slide, in response to frictional sliding-induced comminution of the landslide breccia. As rock flour forms along the base, it is exposed to shear stresses beyond the yield strength of the powdered rock. The landslide slips forward and spreads out over the fluidized rock flour lubricant in the middle of the runout phase. The landslide comes to rest when the landslide thins sufficiently that the shear stresses along its base fall below the yield strength of the lubricant, and the landslide rapidly skids to a halt. Over the moderately strong rock flour lubricant, landslide debris comes to rest in much thicker sheets than landslides which traveled over weak substrate materials.

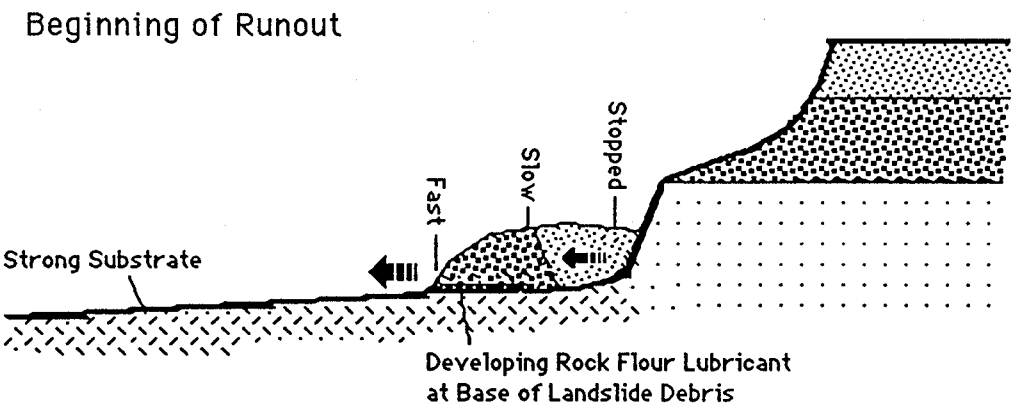
Beginning of Runout
Fast
Slow
Stopped
Strong Substrate
Developing Rock Flour Lubricant
at Base of Landslide Debris

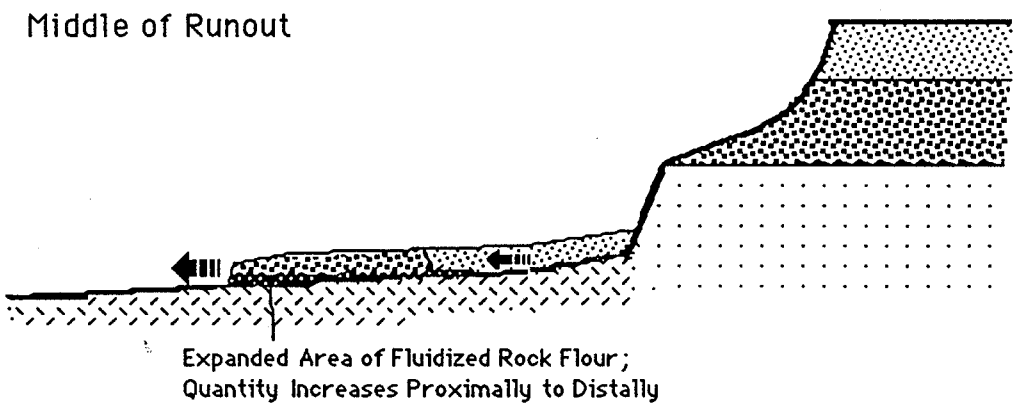
Middle of Runout
Expanded Area of Fluidized Rock Flour;
Quantity Increases Proximally to Distally

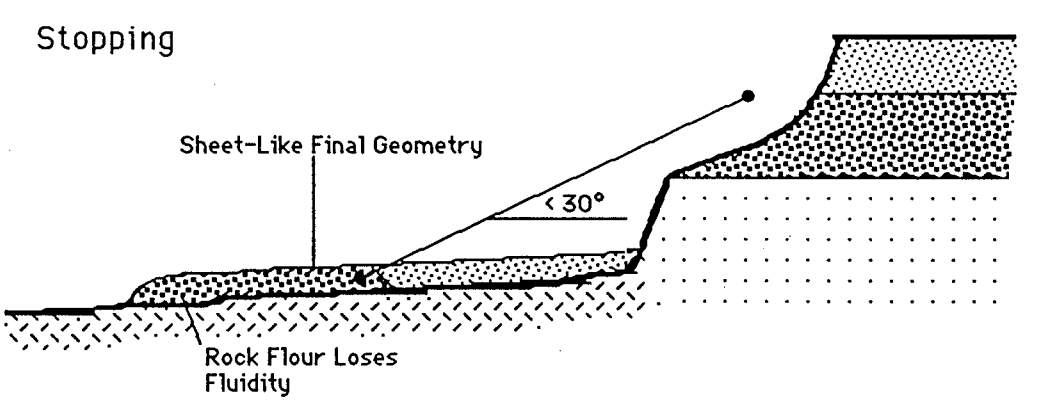
Stopping
Sheet-Like Final Geometry
< 30°
Rock Flour Loses
Fluidity

landslides moving over bedrock to stop moving at much greater thicknesses than those lubricated by weak substrate materials (Figure 49b).

These concepts differs from previous theories in one very basic way: based on the geologic evidence, I submit that long runout is actually the normal behavior of large landslides, and is an inevitable result of the brecciated nature of these slides and of the ultimate strength of the non-indurated natural geological materials overrun by the landslides. I show in this chapter that the distributed deposition and basal lubrication (DDBL) concept provides a good explanation of the geologic and eyewitness observations of long-runout landslides. I also show that it explains the gradational behavior of dry to moist landslides and the characteristic variations in thicknesses observed between morphologically similar martian and terrestrial long-runout landslides. I then show that the geological materials proposed in the concept to act as basal lubricants exhibit the necessary rheological properties required by the concept.

I have shown (Chapter V) that the numerous general theories previously forwarded to explain long runout in large dry landslides (Heim, 1932; Kent, 1966; Shreve, 1968a; Hsü, 1975; Erismann, 1979; Davies, 1982; Melosh, 1983; Krumdieck, 1984; Trunk, et al., 1986; Campbell, 1989; McEwen, 1989; Van Gassen and Cruden, 1989; Potapov and Ivanov, 1991) all fail as published to fully explain *the wide variety of critical geological relations expressed by long-*runout landslides. Other theories have been forwarded to explain the long runout of individual landslides on a case-by-case basis. These include proposals that long runout has occurred as a result of earthquake fluidization (Solonenko, 1972; Hazlett, et al., in press; McSaveney, 1978) or because of basal lubrication by various agents, such as vaporized pore fluids (Habib, 1975; Goguel, 1978), overridden snow (McSaveney, 1978), overridden mud (Evans, personal communication, 1990), or by a weak stratum in the landslide debris itself (Watson and Wright, 1969; Johnson, 1978). Where the geological relations of the individual landslides are described, the lubrication theories often give good explanations for the observed features (Chapter V). I therefore based my DDBL concept upon ideas developed in the basal lubrication theories of Shreve (1968a), Watson and Wright (1969), Johnson (1978) and McSaveney (1978). My concept also incorporates some aspects of the Van Gassen and Cruden (1989) momentum-transfer model.

I submit that the first critical step in the evolution of long-runout landslides occurs at the moment of initiation, or in the early stages of runout, when a large, cohesively moving landslide disaggregates into a rapidly moving mass of brecciated rock having little intergranular cohesion. All long-runout landslides consist of breccia and in almost all cases the breccia is disaggregated to the degree that minor relative motions can occur between neighboring clasts (Chapter III).

I infer that brecciation of landslide debris occurs in different ways for landslides having different initiation mechanisms. For example, cohesive rockfalls may become brecciated due to impact from free fall (Jeffreys, 1923; Shreve, 1968a), or perhaps at initiation of movement in the headscarp region due to the rapid unloading of highly stressed rock (Albee, personal communication, 1990; Appendix B). In slumps, brecciation principally occurs in the concentrated area of shearing centered along the rotational slip surface (Varnes, 1958); as motion continues, the zone of brecciation appears to widen and the rotational movement is taken up by distributed shear of breccia rather than by slip on discrete slide planes (Eissler and Kanamori, 1987). I infer that planar slides may become brecciated in much the same manner; debris along the initial slide surface becomes sheared beyond its brittle strength and brecciates, after which movement is taken up primarily by distributed shear of breccia rather than by slip on discrete slide planes (Yarnold and Lombard, 1989). In addition, I infer that the travel of a planar slidemass over an irregular surface may flex the brittle rock and cause it to fail in tension. The initial sizes of the breccia fragments in a rockfall landslide, which experiences a comparatively uniform initial stress regime, may not vary much from one point to another in the slidemass and will depend on the natural pattern of discontinuities in the in situ slidemass; dense rock with few discontinuities will generate a mass of house-sized or larger boulders (Chapter III: Figure 23a), whereas initially highly brecciated rock will generate a mass of small clasts (Johnson, 1978).

After brecciation of a slidemass, the next critical step in the evolution of large moist, wet and dry landslides appears to occur when the brecciated landslide debris encounters slopes angled at less than the angle of repose of loose rock fragments. At this stage, the first of the two important mechanisms at work in long-runout landslides can begin to take effect: distributed

deposition. The distributed deposition concepts described below are based on, but extend considerably, the ideas of Van Gassen and Cruden (1989; 1990).

Once a landslide mass has disaggregated, its leading and trailing portions no longer travel as a cohesive block; those portions of the landslide which can come to rest will be deposited, while other portions will continue to move down slope. This sort of behavior must occur in all large disaggregated landslides because the landslide deposits are always extended in the direction of travel relative to the initial dimensions of their slideblocks (Chapter III). Indeed, eyewitness accounts (Heim, 1932) indicate that long-runout landslides often cease motion from head to toe; longitudinal extension occurs because the rear stops moving while the toe continues traveling down slope. Notably, long-runout landslides that bulldoze large ridges of material ahead of them during runout may not come to rest strictly in this fashion (Chapter III); sometimes, such as at Elm and Blackhawk, the bulldozed ridge can arrest motion of the toe of a slide prematurely, causing a piling up of trailing material behind the toe in the distal portions of a slide (Heim, 1932; Shreve, 1968a). However, this behavior appears to distort only the last moments of motion of large slides, which, for the most part, come to rest from head to toe.

Based on normal frictional models, however, distributed deposition should not occur. For example, if two touching blocks of the same material slide down an inclined plane in tandem, they will both accelerate down the slope at the same rate and will reach the bottom of the slope in contact at the same velocity. Beyond the base of the slope on a level depositional surface, the leading block would wish to decelerate relative to the trailing block on the slope, but because they remain in contact they interact, with the leading block pushed ahead by the trailing block and the trailing block held back by the leading block. They will therefore end motion in contact in the same locations as if they had moved as a single rigid block.

In actual large landslides in frictional contact with the ground, however, I submit that two factors enter into play that are not considered in the sliding block model: 1) random vibrations of individual clasts; and 2) impulses traveling through landslide debris from slope changes or other obstacles encountered by the landslide. While random vibrations of particles should occur in landslides of all scales, I infer that impulses propagating through landslide debris should only hold significance for landslides of large dimensions. This is because long-runout landslides commonly travel at

velocities between about 10 and 100 m/s (Appendix C); within one second, a 10-100 m length of landslide debris will therefore encounter any change in slope or obstacle to motion. The velocity of compressional waves through landslide breccia, in comparison, probably ranges between about 400 and 2000 m/s, based on the range of seismic velocities for alluvium and unsaturated glacial till (Press, 1966). Thus, the trailing portion of a moving several-hundred-meter-long landslide should feel the effects of a change in slope before it physically reaches that site. I submit that the collective effects of impulses arising elsewhere in the landslide debris and of the vibrations of individual grains should be to allow material at the rear end of a moving landslide to slow relative to the velocity of fragments toward its leading edge. This is because the most proximal moving fragments are completely free to slow down relative to the rest of the debris sheet, so that every rearward-directed force applied to a tail-end fragment relative to leading fragments should cause relative slowing of the trailing clasts. The summation of rearward-directed forces ultimately causes the rear-end debris to come to rest, while material toward the toe remains in motion. The distributed deposition concept is detailed in Figure 50.

Distributed deposition allows the explanation of several important characteristics of long-runout landslides in addition to the longitudinal extension and head-to-tail stopping phenomena. The degree of brecciation, for example, appears to have a very strong influence on both the onset volume of long runout (Chapter III: Figure 8b) and upon the degree of long runout a landslide experiences (Chapter III: Figure 12c). When the source material of a landslide is initially highly comminuted, such as the debris in a coal tip or the weathered grus mantling a slope, long runout can occur at volumes as low as 10,000-25,000 m^3 (Heim, 1932; Campbell and Shaw, 1978). In comparison, landslides in bedrock only begin to exhibit long runout when their volumes exceed about 10^6 m^3 (Appendix A). Also, long-runout landslides appear to exhibit a distinct trend towards decreasing H/L with decreasing average clast size (Chapter III: Figure 12c). These observations suggest that distributed deposition may operate with greater efficiency for landslides composed of smaller clast sizes. I infer that as the average clast size diminishes, the vibration or impulse necessary to halt the trailing particles in a large landslide also diminishes, causing the observed increase in efficiency.

Figure 50. Simplified concept of distributed deposition at the tail end of a brecciated landslide. The landslide debris is assumed to exhibit little tensile strength as it travels down slope with angle ß to the horizontal. Step A shows that two types of forces other than friction act on the moving landslide debris: random vibrations of individual particles due to local path irregularities (vibrations shown only for tail-end blocks) and impulses originating elsewhere in the landslide that propagate back through the landslide debris (F_A, F_B). The free-body diagram shows the summation of forces acting on the tail-end block; because it cannot transmit extraneous rearward-directed impulses to any other blocks, the last block slows relative to those leading it down slope. The process is repeated in Step B. In nature, this discrete process occurs in a continuous fashion, so that the slidemass experiences longitudinal extension during runout, and stopping that begins at the tail end.

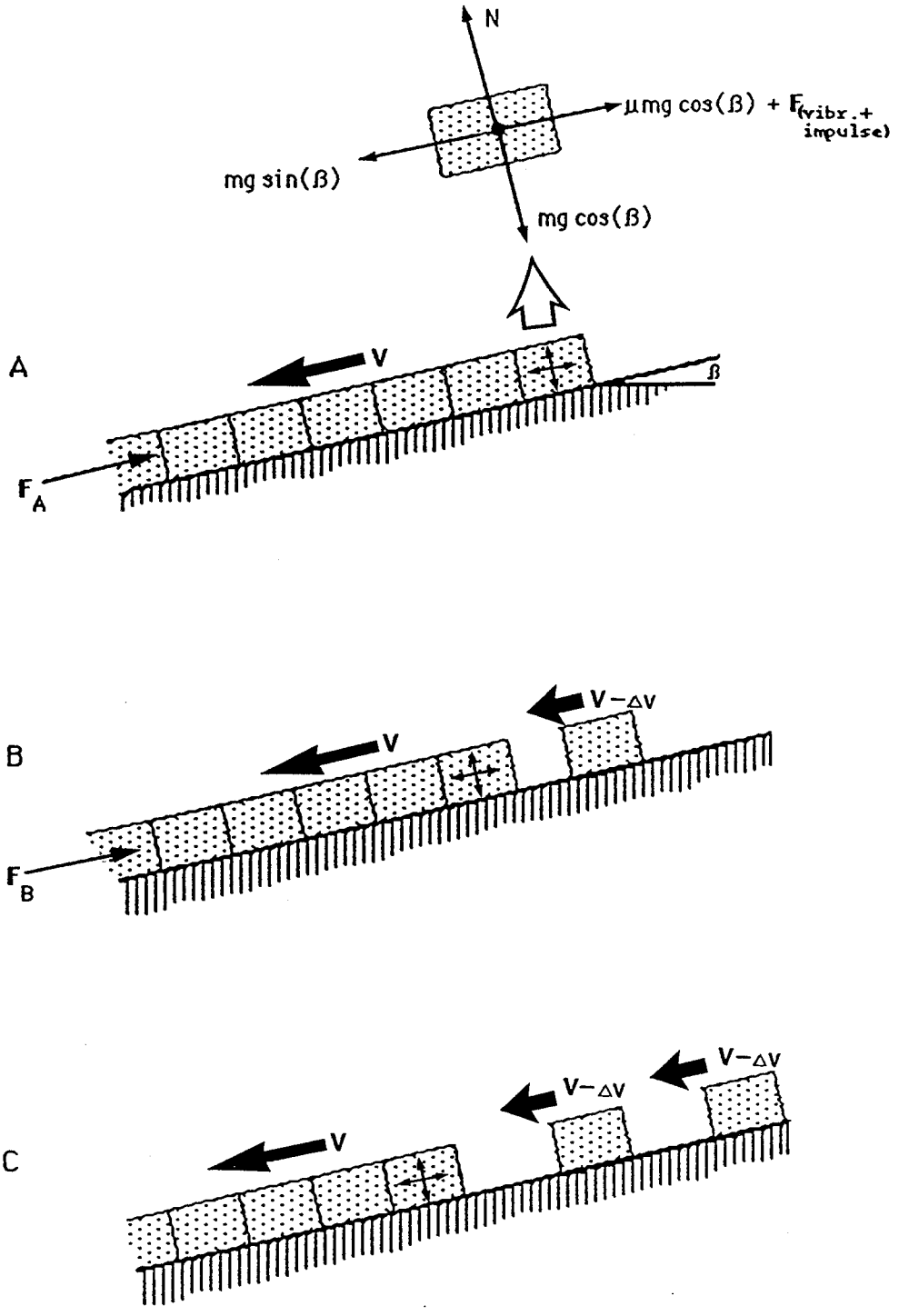
N
μmg cos(ß) + F(vibr.+ impulse)
mg sin(ß)
mg cos(ß)
A
V
ß
F A
B
V−ΔV
V
F B
C
V−ΔV
V−ΔV
V

Also, because the distributed deposition concept predicts that the debris in a large moving landslide will exhibit a spectrum of velocities, from slowest at the rear to most rapid at the toe, the materials at the toe couldpotentially achieve greater velocities than predicted from simple conservation of energy calculations; i.e., a boulder at the toe of a large landslide could travel faster as part of the landslide than if it experienced free fall from the same height. This observation appears capable of explaining such remarkable circumstances as the boulders ejected from the Huascaran 3 landslide at velocities of up to 1000 km/hr, speeds much greater than they could have obtained strictly from free-fall from the headscarp region of the landslide (Plafker and Ericksen, 1978).

With no other factors involved, I feel that the cumulative effects of these random influences on a large brecciated landslide should be to distribute the deposition of landslide debris over an extended distance, but not to have any significant impact on the distance traveled by the center of mass of the landslide. This is because the energy of the fall is simply redistributed though a moving landslide, so that the toe travels farther than it would have in a cohesive sliding block, and the tail end not as far, with all energy still lost from the system by way of frictional interactions with the substrate (c.f. Hungr, 1990). Nevertheless, I feel that this effect influences the H/L values reported of many large landslides, and probably fully explains the runout behavior of small-end long-runout landslides. However, the real depression of center of gravity slopes traveled by larger landslides to values below 30° (Chapter II: Table 1) cannot be explained strictly by this phenomenon, nor can many other critical characteristics of long-runout landslides.

When landslide volumes reach a few million or tens of millions of cubic meters, I submit that another mechanism besides distributed deposition comes into play; the geologic materials along the basal surfaces of these large landslides no longer act in a rigid manner. It appears to me that these larger long-runout landslides begin to deposit debris like the smaller slides, with tail-end material coming to rest first, and the rest of the debris continuing down slope (Figures 49a, 49b). However, the basal materials beneath these larger slides experience shear stresses and/or strain rates that exceed their strength, causing the basal materials to experience plastic flow. Where the basal material consists of dry granular matter, a combination of high strain rates as well as high shear stresses appear necessary to cause fluidization, because

such materials remain rigid in significant thicknesses under static load conditions. In contrast, where the material is moist or wet, flow appears to occur so long as the basal shear stresses alone remain high. The highly symmetrical nature of moist lobate landslides such as the Carlson slide (Appendix B), for example, suggest that large landslides with a significant water content can continue to travel and spread even at low velocities, whereas large dry landslides always appear to travel at high average speeds (Chapter III: Figure 35). The shear stress applied by a large landslide on its base is given by Equation 12 (Johnson, 1970):

$$\sigma_b = \rho g D \sin(ß) \qquad (12)$$

where σ_b is the shear stress in Pa, ρ is the density of rock debris in kg/m^3, D is the thickness of the debris sheet in meters and ß is the slope angle. Once basal materials have failed and begun to flow, the runout of a landslide is no longer controlled by distributed deposition. Rather, it is controlled by the plastic rheology of failed basal material (yield strength and viscosity), as well as by the initial conditions of the slide, its depositional geometry, its thickness and the gravitational acceleration of the environment. Equation 12 shows, for example, that for a given density of landslide breccia and slope angle, a landslide will have to travel with a greater thickness on Mars ($g = 3.72\ m/s^2$) than on the Earth ($g = 9.80\ m/s^2$) to generate the same basal shear stress. Thus, a large landslide on Mars having the same basal lubricant as one on Earth would have to travel with 2.6 times the thickness of its terrestrial counterpart to exert the same basal shear stress. This thickness difference is characteristic of morphologically similar landslide deposits on the two planets (Chapter IV) and supports the concept that larger long-runout landslides on both Earth and Mars travel over a plastically-deforming basal lubricants.

In large dry landslides, I infer that the low tensile-strength landslide breccia spreads into place over the deforming basal material in a manner quite similar to that first advocated by Shreve (1968a) for the Blackhawk landslide, except that he proposed air as the basal lubricant. The dry landslide breccia experiences extension over the flowing lubricant, but generally little other internal deformation, because nearly all the deformation and flow takes place in the lubricant. Two factors appear responsible for constraining flow to near the base of large dry landslides. One factor is that the high strain rates

apparently necessary to fluidize the dry basal materials drop off away from the basal contact of a large dry slide, causing the landslide debris a short distance above the basal contact to remain in a non-fluid condition. Such characteristics of flowing masses of grains are revealed in recent computer simulations of grain flow (c.f. Campbell, 1989). A second factor is that the basal materials that experience flow have sand-sized and finer grain sizes. This material comes from the comminution of clasts near the bases of large landslides and from material incorporated from the substrate. Clast sizes generally increase away from the base, producing the reverse grading common to large dry landslides (Chapter III). Because the high shear-rate and shear stress-induced fluidization only appears to involve this fine material, it suggests to me that fluidization is materially constrained to the fine material near the base and cannot propagate upwards into the overlying coarser interlocked breccia. This factor provides a second possible explanation for why large landslides exhibit lower H/L values with lower average surficial clast sizes and with weaker lithologies (Chapter III: Figure 12c). Both factors would act to allow greater production of fines near the bases of large landslides, thus making basal lubrication more efficient.

The geological evidence from long-runout landslides thus suggests that high stain rates and basal shear stresses act to fluidize the debris lying along the bases of large landslides. I do not offer a precise microscopic mechanism by which flow occurs in dry materials, however; I just describe the macroscopic rheology. Indeed, depending on the nature of the substrate and of the landslide debris, it is possible that the lubricant might sometimes flow by way of mechanical grain flow (Bagnold, 1954; 1956; Hsü, 1975; Davies, 1982; Savage, 1984; Hanes and Inman, 1986; Hui and Haff, 1986; Campbell, 1989; Drake, 1990), by cataclastic flow (Borg, et al., 1960; Paterson, 1978; Hirth, 1989) or perhaps by thixotropic flow of clay-rich or micaceous materials where this material is available (Scott, 1963; Johnson, 1978).

I submit that two endmember behaviors exist in the development of a basal lubricant for large dry landslides. Where a landslide moves over a weak substrate, such as snow, mud or soil, the substrate material shears beneath the weight of the landslide debris, which may then spread out into a thin sheet over the lubricant. Because these materials have so much less strength at high shear rates than dry landslide rubble, the substrate material completely controls the travel behavior of these slides. However, where a landslide

travels over bedrock or over a strongly-cemented substrate, I infer that comminuted material from the landslide itself (Chapter III: Figure 23c) concentrates along the base and acts as the lubricant. This occurs only when the substrate material has greater strength than the powdered breccia. According to the observations of arid-terrain megabreccias by Yarnold and Lombard (1989), the rock flour develops as a function of time during travel in these landslides, with little available in the early stages of travel. I therefore suggest that the proximal reaches of arid long-runout landslides are deposited according to distributed deposition, but later the behavior grades into basal lubrication as the landslides build up a basal layer of rock flour, after which they may slide and spread into place.

Between the two endmember behaviors described above lies an important class of landslides which seem to be self-lubricated from the outset of motion. I refer to large planar landslides which initiate motion by sliding frictionally along a preferred weak stratum in a layered sedimentary sequence, then suddenly accelerate, brecciate, and continue down hill at very high speed (Heim, 1932). Most of the landslides of this type consist of limestone that traveled over weak marl layers (Heim, 1932; Watson and Wright, 1969), while other landslides took place in clastic sedimentary sequences and appear to have moved over inclined weak siltstone beds (Voight, 1978; Kojan and Hutchinson, 1978). I infer that in landslides of this type, the initial frictional sliding soon fluidizes the weak substrate material, so that the landslide transitions quickly from sliding over its base to being rafted downslope over its fluidized basal materials.

I show in the following paragraphs that the DDBL concept can explain much of the variability observed between large dry landslides. Especially important are those features outlined in Table 17 (Chapter V), as well as the other common characteristics of large landslides listed in Tables 10, 11 and 12 and in Figure 31 (Chapter III).

The ubiquitous *high speed* runout of long-runout landslides (Appendix E: Figure 4) originates in the initial failure of the slope, as a slump, planar slide or rockfall. It may remain relatively high along the toe during runout due to the effects of distributed deposition and of the basal lubricant that shears readily at high shear stresses.

The *cohesive nature, preserved stratigraphy, three-dimensional jigsaw puzzle breccia* and *basal striations* (Chapter III: Table 10) occur because the

landslides slide over the substrate and do not exhibit bulk fluidization. Clasts near the surface ride down slope without much interparticle interaction, preventing a spattering of rocks from the landslide, disaggregation of jigsaw-puzzle blocks or mixing of the headscarp stratigraphy (Chapter III: Figure 24).

The *volume effect*, in which H/L values decrease with increasing volume, I infer results from a complex interplay of processes. Because of the downslope-oriented direction of momentum of the landslides, they generally spread out into elongate sheets at deposition. According to the DDBL concept, the sheet-like geometries of the landslides will depend upon the following factors: 1) the initial volume of a landslide; 2) the average thickness of the final deposit, which will depend on the confinement, the nature of the basal lubricant, the acceleration of gravity, and to some degree the initial geometry; and 3) the degree of elongation of the resultant deposit, a factor which will depend upon the initiation style and the confinement. The larger the volume of a landslide, the larger the area that will be covered by the resulting deposit, all other factors being equal. This fact accounts for the general decrease in H/L values and center of gravity slopes experienced by all large landslides with increasing volume (Chapter III). The variability in the H/L vs. log(volume) trends comes from variations in landslide composition, substrate properties, confinement, initiation style and gravitational acceleration, which modify the dimensions of the final sheet-like landslide deposits.

The *sheet-like* or *terrain-mantling* geometries of unconfined landslides (Chapter III) occurs, I submit, as a result of distributed deposition in small-end long-runout landslides, but in larger slides occurs mostly due to spreading and flowing of a basal lubricant. Because the landslide debris overlying the basal lubricant is brecciated, it has very low tensile strength, so that spreading of the basal layer thins the overriding breccia in the direction of flow. Where runout is not complicated by confinement effects, I submit that the thickness of the final debris sheet will vary primarily with the nature of the basal lubricant. For example, landslides with volumes ranging from 3-30 x 10^6 m^3 that fell onto snow-covered glaciers all spread out into very thin 2-10 m-thick sheets (Appendix A; Shreve, 1966; Post, 1967). Landslides in arid climates, in contrast, tend to be deposited in much thicker sheets (Yarnold and Lombard, 1989), I presume because of the greater strength of their highly sheared basal lubricants.

It appears to me that the *threshold volume* of the long runout phenomenon comes about for several reasons. First, for the distributed deposition concept to work, the landslide has to have an orderly arrangement of debris with a significant thickness. If the landslide is only a few clast-diameters thick, interactions of the clasts directly with the substrate will overwhelm any of the other effects described, and the landslide will come to rest due to frictional sliding and non-elastic impacts of landslide debris with each other and with the substrate. The basal lubrication concept also clearly contains an implicit volume threshold because the substrate materials must be subject to high shear stresses during runout, as well as high shear rates, in order to exhibit fluid behavior. This can only occur beneath landslides moving in sheets thick enough to produce adequate basal shear stresses.

Reverse grading, *incorporated substrate material* and *basal strata disruption* are readily explained in my DDBL concept, because material at the landslide/substrate interface experiences significant shearing due to frictional interactions between the landslide and the substrate. The texture within a landslide coarsens upwards and the degree of substrate deformation decreases downwards (Chapter III: Figures 25, 26; Sieh and Bursik, 1986; Cruden and Hungr, 1986; Yarnold and Lombard, 1989) because the shear stresses decrease away from the sliding basal contact of the landslide. The geologic relations of several large landslides (Chapter III; Krieger, 1977) suggest to me that the material at the top of a large landslide begins and ends movement there; this material experiences the lowest energy environment during emplacement and retains clast sizes derived from the initial brecciation of the landslide mass.

The moraine-like *dozed marginal ridges* (Chapter III: Figure 28) form because the front edges of fast-moving landslides scrape the surfaces off in front of them as they move (Heim, 1932). Heim (1932) described the development of these features as follows:

> As a snowplow dozes up the snow in front of it, so the debris stream wants to scour up what it can from the ground. This scoured material surrounds the rubble stream like the huge lateral moraine of a glacier. It can even hinder the stream, until the pursuing rubble overruns and rolls over that hemmed in at the front. In the last moments of motion some such rolling movements at the frontal brow of rubble streams have been observed, or have been recognized in the structure of the front.

It appears to me that the size of a marginal ridge depends largely on the nature of the substrate; a soft substrate yields a large dozed ridge (Heim, 1932), whereas a hard-pan substrate allows little scraping up of material (Watson and Wright, 1969). Material pushed forward by the toe of a landslide may form an important source of basal lubricant, as suggested by Johnson (1978) for the Blackhawk landslide. The Blackhawk apparently overran and ploughed up weathered micaceous Old Woman Sandstone from Blackhawk Canyon and carried it the full length of the landslide. Some of this material crops out locally along the base of the landslide sheet (Johnson, 1978), where it could have helped lubricate the slide.

As related by Heim (1932) above, the *thrust faults and imbrication* observed along the leading margins of some large landslides (Shreve, 1968a; Kerr, 1984; Yarnold and Lombard, 1989; Chapter III: Figure 28) appear related to the ploughing of marginal ridges. When sufficient debris is bulldozed ahead of a large landslide it impairs the forward motion of the sliding sheet, causing the leading edge of a slide to ramp up on the distal ridge and perhaps come to rest. Depending on the thickness of the sliding sheet, trailing material might then be thrown into folds and/or exhibit thrust faulting and imbrication (Chapter III: Figure 28).

The *sudden halt* reported by eyewitnesses of some large landslides (Heim, 1932; Shreve, 1968a) may or may not actually occur in nature (Chapter III: Figure 35). Notwithstanding this observation, the basal lubrication concept does predict that a basally-lubricated landslide should experience a sudden halt when its thickness drops below the critical "yield" value for the material properties of its basal lubricant. Once this occurs, I infer that the landslide debris should slide frictionally to a halt over the "solidified" lubricant.

Distally raised or "Blackhawk-like" landslides (Chapter IV) exhibit lower H/L values on average than other long-runout landslides (Chapter III: Figure 7), a relationship which I submit can be explained by use of the basal lubrication concept, together with a hypothesis concerning the initial conditions of the distally-raised landslides. Six distally-raised long-runout landslides are definitely known on Earth, two in southern California (Shreve, 1968a) and four in Argentina (Fauque and Strecker, 1988). Each of these landslides began as rockfalls and each traveled in an unconfined manner down the surfaces of piedmont alluvial fans (Shreve, 1968a; Fauque and

Strecker, 1988). I conclude that each of these landslides must have begun motion in a very coherent state, such that in each case the landslides entered their depositional zones as thick uniformly-moving debris heaps with relatively small areal dimensions. Rather then spreading out in a sheet-like fashion during deposition, the landslides remained relatively thick as they traveled down slope (Chapter IV: Figure 46), thus traveling farther before thinning out to their critical thickness than they would have under different starting conditions. They therefore exhibit lower H/L values as a group than landslides of equivalent volume that spread out as sheets of uniform thickness or those that were tapered in profile.

The *fluid appearance* and *oriented clasts* of some dry long-runout landslides can be explained in various ways. I submit that the ability of landslides to seemingly flow down channels and around obstacles relates to the fluid behavior of the basal lubricant. The lava flow- or glacier-like appearance of convex-downslope ridge and trough "flow" structures observed on the surfaces of some channeled landslides (Heim, 1932; Chapter II: Figure 2) seems to occur because of the differing velocities of material traveling down the center of a channel relative to that moving along its margins. If a landslide must maintain a critical thickness to allow flow of a basal lubricant, as predicted in the concept, then material at the thin edges will become stranded and cease moving while material toward the center of the channel will continue to move over its fluidized base. Shear stresses will therefore develop between the center of a channeled landslide and its margins. If a landslide is already folded due to differential velocities between leading and trailing debris, these folds will be bent into arcuate shapes by the transverse velocity profile. I feel that the preferred orientation of clasts on the surfaces of some large landslides (McSaveney, 1978; Eppler, et al., 1987; Appendix B) probably also relates to the shear stresses acting along their surfaces, because the clasts generally appear to align with their long axes parallel to the axes of minimum compression/maximum extension acting along the surfaces of the slides (Appendix B). I also infer that the longitudinal debris trains that occur on some channeled landslides (Kojan and Hutchinson, 1978; Appendix B) occur because of the development of a transverse velocity profile in these landslides. The development of such a profile can apparently cause the moving landslide to physically divide into parallel longitudinal cells of debris, with the fastest debris trains moving down the center of a channel, and with relative

velocities between the trains being taken up along their margins (Appendix B: Figure 9).

Rock *spattering* beyond the margins of a landslide occurred on a few landslides that made sharp turns during their runout (Plafker and Ericksen, 1978; Kojan and Hutchinson, 1978; Eisbacher, 1979; Chapter III). I infer that such fast changes in geometry cause rapid compression of parts of a moving landslide, throwing some of the loose cobbles on the surface into the air, and ejecting some cobbles or boulders entirely (Kojan and Hutchinson, 1978). Sometimes fine-grained landslide debris spatters evenly around the distal margins of large landslides (Post, 1967; Eisbacher and Clague, 1984). I imagine that this debris is probably material entrained in the disturbed air mass surrounding a large landslide that settles out of suspension after the landslide has stopped moving.

I submit that the *proximal trough* associated with many large heavily confined landslides (Heim, 1932; Solonenko, 1984; Gaziev, 1984) relates to the distributed deposition mechanism of large brecciated landslides. Large disaggregated landslides can begin depositing trailing material while still on a slope (Heim, 1932; Chapter III: Figure 27). Most of the landslide, however, continues on down slope and either encounters a soft substrate lubricant or begins to flow over its own evolving basal rubble layer. However, when a large landslide is heavily confined, the portion of the landslide that is not deposited on the source slope impacts the opposite wall of the canyon and comes to rest. Because heavily confined landslides generally have not traveled far enough to develop a basal lubricant and may not encounter any weak substrate materials in a bedrock canyon, they cannot flow away after hitting the opposite wall, despite retaining a significant thickness. In other cases where a basal lubricant exists, I infer that the landslides may rebound off the opposite wall and continue to travel down canyon. Examples of landslides that exhibited the latter behavior include the Gros Ventre (Voight, 1978), Mayunmarca (Kojan and Hutchinson, 1978) and Flims (Heim, 1932) landslides.

I feel that the radial *block bands* that occasionally litter the surfaces of large landslides (Heim, 1932; Shreve, 1966; Mathews and McTaggart, 1969; Appendix B) represent the effects of the longitudinal extension that dominates the deformation of long-runout landslides. A large fractured section of bedrock initially closely spaced on the surface of a landslide in its proximal reach will, I submit, become strewn out in the down-flow direction as the

landslide spreads out over its basal lubricant. This will result in a chain of boulders longitudinally distributed on the final deposit. The single situation where a radial block band was observed (Hewett, 1988) occurred on a lobate landslide and probably formed in an analogous manner; I conclude the band resulted from concentric spreading of the slide's basal lobe, which extended the boulders from a single source into a swath across the toe of the deposit.

I suggest that the *sub-horizontal slip surfaces* that occur near the bases of many large landslides (Yarnold and Lombard, 1989; Chapter III: Figures 26, 32) probably form in the last stages of movement of a large landslide, when the basal shear stresses fall below the yield stress of the basal lubricant. Because a landslide may yet have considerable momentum when the lubricant loses its fluidity, the shear stresses cause the resolidified material to fail in a brittle fashion. The landslide then comes to rest rapidly by frictional sliding along the slip surfaces. Depending on the geometry of the landslide, the homogeneity of the lubricant, etc., the slip surfaces may extend broadly (Chapter III: Figure 26), or they may only occur locally (Chapter III: Figure 32), where one part of the lubricant fails in a brittle fashion while another part remains fluid.

Clastic dike intrusion occurs commonly at the bases of large landslides (Shreve, 1966; Crandell, 1989; Yarnold and Lombard, 1989), both during runout and after the cessation of motion, because of the strong interaction of the landslide with its substrate. I submit that asymmetric dikes were intruded into moving landslides during runout and provide direct evidence that fluidized material existed along the bases of these landslides while they were in motion. Sometimes fluidized basal material remains available after the cessation of motion of large landslides. This material may then intrude upwards into the halted debris masses, forming symmetrical dikes (Chapter III: Figure 33).

I infer that the *debris pyramids* which occur on the surfaces of some landslides (Heim, 1932; Shreve, 1966; Mollard, 1977) relate to the spreading and thinning of the landslide breccia sheets during runout. Based on the basal lubrication concept, a landslide will spread and thin until its thickness drops the basal shear stress below the yield strength of the substrate. This final thickness may be less than the minimum dimensions of some of the large blocks rafted down within a large landslide. If so, the boulders will "touch bottom" at some point and get punched upwards through the debris sheet. Smaller debris encountered by the boulder as it moves upwards through the

sheet would get trapped on top and slough off at the angle of repose of the granular material at the surface of the slide, forming a debris pyramid. Probably only those debris cones formed just before the cessation of motion remain preserved after motion has ceased; others would probably be destroyed by vibration or rotation of the underlying boulder while motion continued. One might easily imagine that a landslide composed of different slope-parallel lithologies (Chapter III: Figure 24) could result in a situation where a substrate boulder and its debris cone originated in the basal layer and contrasted lithologically with the surficial material, a situation observed by Shreve (1966) on the Sherman landslide.

Oblique imbricated ridges form on the surfaces of Blackhawk-like landslides on both Earth and Mars (Fauque and Strecker, 1988; Chapter IV: Figure 34). They occur on the thin parts of these landslides proximal to their distal debris heaps. I submit that these regions reflect landslide debris deposited during runout of the landslides prior to the cessation of motion of their distal heaps (Chapter IV). According to the idea of differential deposition, the trailing end of a distal heap should move slower than the leading edge, causing the heap to thin and lengthen in the downhill direction during runout. The trailing material ultimately thins and slows sufficiently that it no longer shears the basal lubricant sufficiently to flow, so this material comes to rest. This does not seem to be a perfectly continuous process, however, and material gets deposited in a wave-like or pulsate fashion along the trailing margin of the distal heap. I conclude that the radial orientation of the ridges reflects the geometry of the trailing end of a distal heap as it descends a slope (Chapter IV: Figure 46).

Multiple margins form a special form of lateral levee on a number of large landslides (Heim, 1932; Johnson, 1978; Appendix B). Lateral levees form at the margins of landslides with distal heaps and those that move through channels. In both cases they form where landslide debris travels in a pulse-like fashion; tapered landslides and those moving as sheets of uniform thickness do not form them. According to my DDBL concept, they form along the edge of channels where landslide debris ramps up onto the channel walls and thins to below the critical thickness for flow of the substrate (Appendix B). When the pulse of moving debris wanes in the channel, movement occurs between the perched levees, where the debris remains thick enough to cause flow of the basal lubricant. It appears likely to me that they form at the margins of

distally-raised landslides for much the same reasons. The debris in a moving distal heap spreads outwards during runout over the basal lubricant. At the lateral edge, the thickness must drop to zero, so the material forming the lateral margins of the distal heap are continuously deposited during runout. However, the material a short distance from the edge retains the critical thickness and keeps sliding downhill over the substrate, perhaps separated from the stopped levees by a shear zone (c.f. Shreve, 1968a). The only debris remaining between the levees is that deposited from the thin rear end of the distal heap. Multiple en echelon lateral levees form when a landslide encounters a rapidly changing slope (Appendix B). Rather than thickening and flowing around an obstacle to form a single sinuous levee, the landslide just retains its thickness and sheds off imbricated levees until the slope moderates.

The prodigious quantities of *dust* that always accompany the runout of large landslides (Holland, 1893; Heim, 1932; Hewett, 1988), I infer, forms due to the high shear stresses concentrated near the bases of the landslides as they travel. This fine material is very mobile. Most of it remains near the base, where it forms the lubricant for many dry landslides. However, the dust also infiltrates upwards through the entire debris mass (Dibblee, 1964; Hewett, 1988) and pours out of gaps in the surface of the landslide (Heim, 1932), becoming entrained in the disturbed air mass surrounding the rapidly moving landslides.

The *wind blasts* that often precede large rapidly moving landslides (Heim, 1932; Plafker and Ericksen, 1978; Hadley, 1978) are very likely the result of the air displaced from in front of an onrushing mass as it slides along the ground. The air that slips upwards over the leading edge of these landslides is capable of picking up people and buildings not firmly planted on the ground and throwing them onto the surface of the onrushing landslide (Heim, 1932; Fahnestock, 1978). Those items with firmer ties to the ground get overrun by the landslides (Heim, 1932).

The *luminescence* associated with large moving landslides can occur in two ways. I conclude that the primary source is probably static electrical discharges in the dust clouds emitted by the landslides. Impacting of certain minerals within a landslide mass might also give off sparks visible to an observer.

The *airborne leap* observed of some large landslides appears to me to be a result simply of the ballistics of a landslide traveling at high speed. Where a landslide encounters an abrupt increase in slope along its travel path, it may briefly leave the ground along a ballistic path until it again hits the ground and continues sliding. I submit that any air captured in this process probably leaks out though the top of the breccia sheet (as does the dust) as the landslide moves on down slope.

Despite the many geological characteristics that I can explain with the DDBL concept, however, some relations remain unclear. For example, I have mentioned that I infer that small-end long-runout landslides and the early stages of larger landslide emplacement are dominated by distributed deposition. However, the precise kinematics of deposition of the slow material at the rear end of a moving landslide by this mechanism remain unclear. The vibrations and rearward-directed impulses called upon to slow and then stop the tail-end clasts (Figure 50) would probably not act in the same way on clasts of different sizes; small clasts might be readily slowed by these effects, but not larger ones. I would think that this effect might cause some confusion of the stratigraphy in the small-end slides and in the proximal reaches of larger landslides. A second unclear aspect is precisely how a large landslide that flows over its own comminuted debris would act along its leading edge. Along its toe, a self-lubricated landslide would continually be outrunning its lubricant and traveling over the bare substrate. Perhaps the toe would have to be pushed from behind by trailing material that traveled atop the lubricant.

Geologic relations exhibited by moist and water-saturated terrestrial subaerial landslides indicates to me that their behavior is gradational with that of dry long-runout landslides. Moist and water-saturated landslides exhibit many of the same characteristics as dry long-runout landslides, including the *high speed, fluid form, sheet-like geometry, three-dimensional jigsaw puzzle breccia* and *volume effect*. They differ from dry landslides, however, in not exhibiting *preserved stratigraphy* or *reverse grading* (Plafker and Ericksen, 1978; Voight, et al., 1983; Crandell, 1989; Appendix B). Field relations at the Carlson landslide (Appendix B) and at the site of a Tertiary megabreccia deposit which traveled into a lake (Yarnold, personal communication, 1991), show that large dry slides may transition rapidly into moist or water-saturated landslides when they incorporate water. These observations suggest that the water enters the fine-grained component of these landslides and modifies them from

clast-supported breccia sheets overlying a fine-grained basal layer to matrix-supported debris flows. Despite the sedimentological differences between dry and moist or water-saturated landslides, however, their log(volume) vs. H/L trends (Chapter IV: Figure 36) and apparent plastic yield strengths overlap (Chapter IV: Table 13). Of particular interest is the similarity in the log(volume) vs. H/L trends of landslides with a small modal grain size (Chapter III: Figure 12b) and those in a moist or water-saturated state (Chapter IV: Figure 36). This observation suggests to me that the more fine-grained material a dry long-runout landslide contains, the more it travels like a moist or wet landslide, a fact that emphasizes the importance of fine-grained material in controlling the long-runout process of dry, moist and wet slides.

The group of observations outlined above suggests to me that dry and moist landslides travel in much the same way; by the flow of a plastic basal layer. In dry landslides, this layer is constrained along the base of the landslide. When water is added to this material, the yield strength does not appear to change radically (both dry and moist landslides travel in sheets 5-100 m thick; Appendix A), but the viscosity of the basal rock flour must drop considerably; this viscosity decrease allows the moist rock flour to invade the overlying breccia as a matrix, allowing bulk mixing of the landslides. Nevertheless, most of the shear strain seems to remain concentrated near the base of a moist landslide. This is suggested by the retention of jigsaw-puzzle blocks on the surfaces of large moist landslides (Ui, et al., 1986; Appendix B). It is also suggested by the theoretical work of Johnson (1984), who showed that most of the flow in a plastic debris flow should remain constrained near the base, and by the computer modeling efforts of Potapov and Ivanov (1991), who show that the active layer in a landslide with a two-parameter viscous flow rheology (Appendix E: Figure 10a) will remain within the lower reaches of a landslide during runout. The basal lubrication concept thus appears consistent with the gradational relationship between dry and moist landslides.

Some laboratory data exist to support my idea that large landslides commonly slide into place over fluidized substrate materials, such as soil, mud, snow and rock flour. Johnson (1970), for example, found that the fine-grained component of debris flow deposits from the Panamint Mountains, California, exhibited plastic behavior with yield strengths that ranged from 80 Pa for a water content of 16% by weight, up to 270 Pa for a water content of 14%. This material may provide a reasonable analog for many moist soils. In

comparison, the basal shear stress for a 30 m-thick brecciated limestone landslide (ρ = 2500 kg/m^3) moving down a 5° alluvial slope would measure ~60,000 Pa (Equation 12), far greater than necessary to overcome the yield strength of the moist soil. This suggests to me that moist soils should usually provide an adequate basal lubricant for large landslides, as postulated for the Elm slide by Heim (1932).

Many large landslides have fallen onto snow-covered glaciers during runout and spread into thin sheets (Shreve, 1966; Post, 1967). Data from Yosida (1963) indicates that compacted snow exhibits a plastic rheology, with a distinct yield stress that varies with the degree of compaction of the snow (Figure 51). Lightly compacted snow (ρ = 230 kg/m^3), as might be expected to occur near the surfaces of glaciers (Mellor, 1963), exhibits a yield strength of about 20,000 Pa (Figure 51; Yosida, 1963). The Sherman landslide, which traveled over a snow-covered glacier, came to rest on a 5° slope with a thickness of 3-6 m (Shreve, 1966). With an assumed density of 2700 kg/m^3 (McSaveney, 1978), the basal shear stress of the Sherman landslide varied between about 7,000 and 14,000 Pa at the time it came to rest (Equation 12). These observations are consistent with the concept that the landslide slid and spread into place over viscously flowing snow until the thickness of the debris sheet and the surface slope declined sufficiently to drop the basal shear stress below the yield strength of the snow, at which time the landslide slid frictionally to a halt.

Limited laboratory data also support the concept that the fine-grained rock flour commonly found along the basal contacts of long-runout landslides can provide a source of lubricant. Figure 52 shows the shear stress-strain relations of a dry sand under a normal load of 10^5 Pa (Brown and Richards, 1970); the rate of shear developed in the triaxial tests was not reported. For densely packed sand-sized material, as observed near the bases of the Martinez Mountain (Chapter III: Figure 30) and El Capitan (Chapter III: Figure 25) landslides, the dry sand would yield at a stress of a little over 10^5 Pa, after which it would flow at an unknown rate under a stress of ~70,000 Pa. For a landslide like Blackhawk, traveling down a 5° alluvial slope and having a breccia density of about 2500 kg/m^3, the landslide could flow over this substrate material as long as it retained a thickness of over ~33 m (Equation 12). This value is very close to the maximum thickness of the distal heap of the landslide (Shreve, 1968a). I presume that the landslide would readily have

Figure 51. Shear stress versus strain relations for snow under different degrees of compaction, showing marked bi-linear relations and yield stresses. Curve "A" gives best approximation to near-surface snow conditions (Mellor, 1963). Diagram from Yosida (1963).

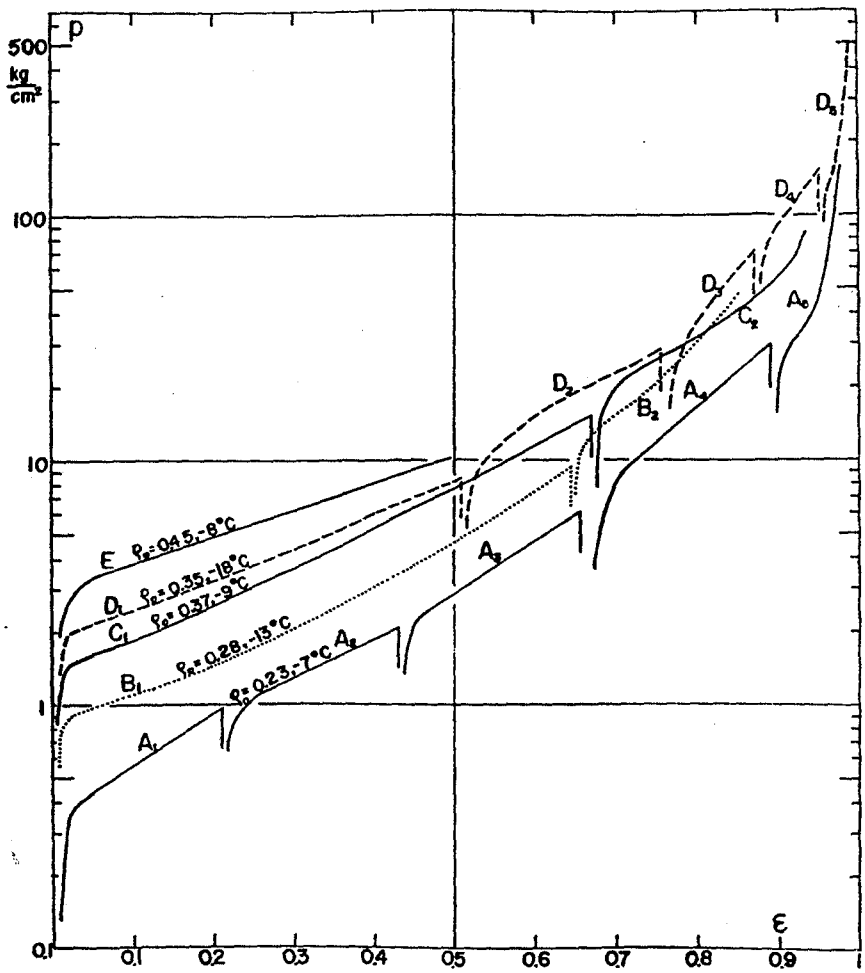
p
500
kg/cm²
100
10
1
0.1
0.1
0.2
0.3
0.4
0.5
0.6
0.7
0.8
0.9
ε
E ρ₀=0.45,-9°C
D₁ ρ₀=0.35,-18°C
C₁ ρ₀=0.37,-9°C
B₁ ρ₀=0.28,-15°C
A₂ ρ₀=0.23,-7°C
A₁
A₃
D₂
B₂
A₄
D₃
C₂
A₅
D₄
D₅

Figure 52. Shear stress versus strain relations for dry sand with different packings under a normal load of 10^5 Pa (Brown and Richards, 1970).

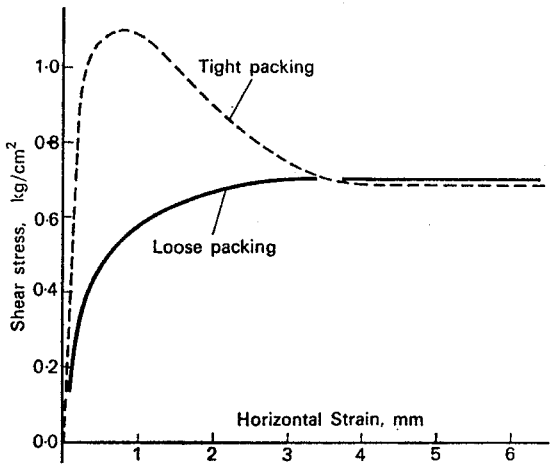
Tight packing
Loose packing
Shear stress, kg/cm²
1·0
0·8
0·6
0·4
0·2
0·0
Horizontal Strain, mm
1
2
3
4
5
6

exceeded the critical ~10^5 Pa basal shear stress earlier in its movement history as it traversed steeper parts of its travel path with a greater thickness. Given similar basal material on Mars, a thickness of ~86 m would be required to cause the sand to flow (Equation 12), a value close to that observed on some of the martian Blackhawk-like landslides (Chapter IV: Table 16). The available laboratory data therefore supports the basal lubrication concept for explaining the long runout of large landslides.

B. Proposed Tests of the Distributed Deposition and Basal Lubrication Concept

I feel that several different types of complimentary studies are necessary to fully evaluate the DDBL concept for long-runout landslides. These future studies include: detailed field work on partially-eroded long-runout landslides; geotechnical centrifuge studies; in-depth studies of the rheological properties of potential basal lubricants under the pressure, shear stress, and shear rate conditions anticipated at the bases of large landslides; detailed computer simulations of landslide runout; and the potential study of a large artificially-triggered dam-construction landslide planned by the Soviets for 1997. Table 18 lists the future studies to be conducted and summarizes the motivations for each study.

Future field studies of large landslides aimed at evaluating the DDBL concept should concentrate on partially eroded landslides with good basal exposures, whose overall dimensions remain reasonably well distinguishable. Although this presents a difficult set of criteria, a number of landslides of this type have been investigated previously, including the El Capitan (Krieger, 1977), Black Mountain (Longwell, 1951), Martinez Mountain (Bock, 1977; Baldwin, 1986) and Blackhawk (Shreve, 1968a) deposits. For comparison with other landslides, all aspects of the deposits must be considered in an analysis of the model behavior, including their initiation styles, fall heights, runout lengths, detailed morphologies, degrees of confinement, lithologies, clast sizes and the nature of their substrate materials.

To test the distributed deposition concept, the sedimentary textures and the basal contact relations of small-end long-runout landslides should be studied and compared with those of larger deposits. This process could also be investigated by studying in detail the proximal to distal variations in depositional characteristics of larger landslides, especially variations in

Table 18. Summary of Proposed Tests of the Distributed Deposition/Basal Lubrication Concept

General Test	Specific Tests/Observations	Motivation
I. Field studies of large, partially-eroded slides	A. Basic Properties 1. Initiation Style 2. Dimensions 3. Morphology 4. Confinement 5. Breccia Lithology, Clast Sizes 6. Substrate Properties	•Full characterization of landslide properties necessary for drawing comparisons between different landslide deposits
	B. Compare Characteristics of Larger and Smaller Long-Runout Slides 1. Sedimentary Textures 2. Basal Contact Relations	•Evaluation of distributed deposition concept, gradation between dist. deposition and basal lubrication
	C. Map Development of Candidate Basal Lubricating Materials 1. Sedimentology 2. Petrographic Studies 3. Geochemical Signatures	•Determine source locations and source materials for basal lubricants, test microscopic processes active in the lubricant, long-runout mechanisms
	D. Map Internal Structures of Large Landslides 1. Distal Ramping, Imbrication 2. Bulldozed Distal Wedge	•Specific tests of concept against other theories, such as air-layer lubrication
II. Geotechnical Centrifuge Studies	A. Model Runout of Large Landslides 1. Proper Size Scaling 2. Color-Coded Stratigraphy	•Observe whether long runout can be reproduced in the laboratory with characteristics akin to real slides
	B. Variable Properties 1. Initiation Style 2. Substrate 3. Slide Composition	•Test tenets of distributed deposition/basal lubrication concept, effects of gravitational acceleration, confinement

Table 18. con't.

	4. Confinement 5. Gravity	
III. Triaxial Compression Tests of Candidate Basal Lubricants	A. Weak Substrate Materials 1. Snow 2. Soil 3. Mud 4. Gypsum?	•Determine rheologies of weak substrate materials under representative pressure conditions
	B. Rock Flour	•Determine whether rock flour has the rheologic properties necessary for basal lubricating action
IV. Computer Models	A. Microscopic Approach 1. Rectilinear Grains 2. Fragmentation Effects 3. Initiation to Stopping	•Ground-up approach would allow modeling of long runout from basic physical principles of flowing grains
	B. Macroscopic Approach 1. Moist Landslide Simulation 2. Dry Landslide Simulation	•Top-down approach takes field relations and attempts to use assumptions of material rheological properties and initial conditions to model landslide runout
V. Large Artificially-Triggered Kambarata I Landslide, Kirghizia, U.S.S.R.	A. Kinematics of Travel 1. Behavior of surface 2. Behavior of interior	•Test competing concepts of long runout
	B. Activity of a Basal Lubricant 1. Evolution of Rock Flour 2. Excavation of Weak Substrate Materials	

characteristics arising at the point where a basal lubricant first appears in their basal outcrops. One prediction of this study is that the sliding surface should exhibit considerable erosion under a landslide moving by distributed deposition, where frictional interactions with the substrate should be important. Such erosion should diminish where basal lubrication occurs. This degree of erosion anticipated would be much more profound than any erosion anticipated from a bulk fluidized landslide, which should be a largely depositional process, not an erosional one. I have also predicted (see above) that distributed deposition should be sensitive to grain size variations. One should detect that finer-grained portions of an individual slide deposit in thicker accumulations than coarser accumulations, all factors being equal.

Another important step would be to map out the development of the basal lubricant in large slides, as Johnson (1978) did for the Blackhawk landslide. Sedimentary relations, petrographic studies and geochemical signatures should be used to provide data on the source materials and locations of the lubricant, as well as on the microscopic processes active in the lubricating layer. The development of the lubricant with travel distance should be mapped out, as well as the relationship of the landslide breccia to its lubricant. This data should, for example, determine conclusively whether large landslides traveled in contact with their substrates for the duration of motion, as I propose, or whether they coasted into position on an air layer as proposed by Shreve (1968a). In the latter case, the basal layers of large landslides should consist of material derived locally when the debris impacted the ground and stopped abruptly after their air layer lubricant drained away. This type of study could be done on landslides such as Martinez Mountain and El Capitan, where large portions of the basal contact are exposed, as well as on Tertiary megabreccia deposits, such as those described by Yarnold and Lombard (1989) in Arizona.

In addition to these studies, I have given evidence that the ramping and imbrication of the leading edges of landslides like Blackhawk probably occur because of bulldozing of material by the landslides during runout. This interpretation differs markedly from that of Shreve (1968a), who postulated that the ramping and imbrication occurred in large landslides when their basal air lubricant ran out, causing their distal margins to touch ground and rapidly grind to a halt, with resultant piling up of trailing debris. Therefore, where imbricated landslide debris occurs in the field, such as in the Vallecito

Mountains of southern California (Kerr, 1984), evidence should be sought to determine whether it is always associated with a distal wedge of bulldozed material. This should provide another test of the DDBL concept versus the air layer lubrication theory of Shreve (1968a).

Geotechnical centrifuge studies proposed by R.F. Scott (personal communication, 1991) provide a more controllable procedure for ascertaining the nature of long runout in large landslides. A centrifuge capable of handling approximately 0.125 m^3 of material and able to generate a centripetal acceleration of 100g would be capable of simulating a landslide with a volume of 0.125×10^6 m^3, a value at the low end of the volume realm of long-runout landslides. The use of a centrifuge would provide a ready means of testing the basal lubrication concept. Different substrate materials could be placed along the track of the landslide to see how a model landslide might interact with its substrate. A simulated slide on ice, snow or wet sediment, for example, would be predicted to spread out more and travel farther from the headscarp than dry material moving over a dry substrate. Also, one could test the concept of whether material that becomes fragmented into fine powder during runout could act as a lubricant. The travel path of debris in the centrifuge could be manipulated to mimic natural conditions, such as heavy confinement, differing initiation conditions or even the effects of a launching ramp. Also, the grains composing the simulated landslides could be colored to discern where the debris travels during runout. High-speed films of model landslides could help elucidate their travel kinematics. One could also test the role of grain size, grading and grain material properties on landslide runout, or the effects of adding water to the mix. To test the effects of martian environmental conditions, it may prove possible to compare the behavior of landslides of the same volume run under simulated terrestrial and martian conditions. For the simulated martian run, the centrifuge would be run at a lower spin rate, to simulate the lower martian gravity, and the test chamber could be partially evacuated to examine any changes caused by the near-absence of air (Scott, personal communication, 1990).

A critical test for the basal lubrication concept is a study of the rheological properties of many potential basal lubricants under the pressure (~2-100 bars) and shear stress conditions anticipated at the bases of large landslides. Materials which should be tested include snow, mud, soil and rock flour of differing compositions. The rock flour should be generated in a rock mill of

some type using intact rock specimens from the surfaces of long-runout landslides, to allow comparison of the rheological data with the observed behavior of the landslide. Unfortunately, the strain rates necessary cannot be achieved in normal triaxial devices, requiring the development of special equipment and procedures to study the deformation of these materials (Scott, personal communication, 1991) under these conditions.

Another approach to the study of the DDBL concept is to develop computer models of long-runout landslides based on the critical observations and ideas presented in this thesis. There are two basic approaches to the computer modeling of long-runout slides, microscopic and macroscopic. In the microscopic approach, the trajectories of individual interacting particles in a granular mass are calculated based on microscopic conditions (Scott, personal communication, 1990). The modeling effort by Campbell (1989) is an example of such a study. Two concepts could be studied using the microscopic approach: 1) modeling of granular flow between a rigid crust and substrate to test the basal lubrication concept for a dry, granular lubricant; and 2) modeling of entire granular avalanches to test the distributed deposition concept. To be of value as a predictive tool, such future computer studies of the DDBL concept should incorporate many grains with a variety of *rectilinear* shapes (to allow interlocking behavior), followed from initiation to deposition, allowing them to fragment into smaller pieces when they encounter high shear stresses. Unfortunately, however, aside from the difficulty in programming such a simulation and the extensive computer time it would require to run, this approach would suffer from a lack of knowledge on how exactly to model the interactions of the fine-grained component. Presumably, interparticle cohesion should increase relative to frictional factors as particle size diminishes, and some model of this behavior would have to be assumed for the fine material.

A second computer modeling approach involves assuming that certain broad macroscopic laws govern the runout behavior of large landslides, based on field observations of the deposits. The computer simulation would set up the source geometry and would track the behavior of a landslide from initiation to the cessation of its movement. The computer model of Potapov and Ivanov (1991) is an example of such an approach. They model the behavior of large landslides as viscous fluids with a bi-viscous power-law rheology. This rheology approaches the behavior of moist landslides like the Carlson

(Appendix B). However, a macroscopic model designed to test the basal lubrication concept for dry landslides should include a plastic basal layer overridden by a rigid crust having little tensile strength. This model could be tested using different headscarp forms and marker beds in the in situ slidemass to see how the final calculated appearance matches observed field relations. Running the model with varying physical parameters could be used to test changes in the properties of the basal lubricant on the predicted runout behavior.

The U.S.S.R is planning to trigger a giant landslide of approximately 100 x 10^6 m^3 volume in 1997 for a dam construction project. This landslide provides a potential test-bed for the DDBL concept, as the opportunity exists for American and other non-Soviet scientists to monitor the emplacement of this giant landslide in a joint study with scientists and engineers at the Schmidt Institute of the Physics of the Earth, Moscow (Adushkin, personal communication, 1991). The landslide will be initiated by detonation of 1/4 megaton of chemical explosives. Triggering of the main slide will be preceded by the emplacement of two much smaller bracketing landslide dams to check the lateral motion of the primary. The landslide will be deposited across a steep-sided valley, so it will be a highly confined one that is anticipated to fill the valley to a maximum depth of 250 m (Adushkin, personal communication, 1991). This landslide could be monitored at all its important stages: prior to and at initiation, during travel and stopping, and after emplacement.

Although the landslide will be heavily confined and thus will not have an opportunity to strongly display long runout, the study of this slide should nevertheless illuminate the early stages of development of long-runout landslides. For example, large heavily confined landslides such as the Madison (Hadley, 1978) and Usoy (Preobrazhensky, 1920) slides, like other large landslides, exhibit preserved stratigraphy. Understanding the development of this characteristic feature even in a highly confined slide should prove to be of great significance. The DDBL concept, for example, predicts that all the translational motion should be constrained to the lower few meters of the slidemass. Bulk fluidization models, in contrast, predict some overturn of the leading edge of large slides during runout (Trunk, et al., 1986; Potapov, personal communication, 1991). These competing concepts could be tested on the Soviet slide.

The preservation of stratigraphy in the Soviet slide, could be tested by determining the three-dimensional kinematics of the landslide during runout. One way to achieve this goal would be to determine the pre- and post-emplacement locations of many points initially on the surface of the in situ slidemass. I would wish to begin this project by making a detailed geologic map of the in situ slope. A similar map made of the final disposition of the landslide debris would provide a very important starting point for understanding the kinematics of the landslide. Painting large stripes of different colors on the slidemass prior to runout would provide another way to track the surficial movement of the landslide. The stripes could be optically tracked during runout using high-speed cameras, at least until the mass became obscured with dust. The stripes could be augmented by shallowly buried transmitting devices in hardened containers placed at various points prior to initiation (perhaps at intersections of painted lines), to track the displacement histories of these points during runout. I infer that most of the material that begins motion at the surface of a large landslide also finishes motion there (another testable hypothesis), so that some remnant of the stripes and the transmitters will probably remain after emplacement of the slide to ascertain their final locations. Doppler radar devices could also be aimed at different points on the surface to obtain velocity data during runout which should work even through prodigious dust clouds.

To obtain some idea of the kinematics in the third dimension, tough artificial clasts could be placed into the slidemass prior to initiation which could be tracked down after the event. The artificial clasts should outwardly seem to have rock-like density and elastic properties, so that they would not behave differently from other rocks in the landslide; some sort of ceramic exterior might prove a good choice. However, the artificial clasts could each be given a core of a dense metal so that they could be tracked down with sensitive magnetometers after emplacement. Perhaps the metal cores could be given precise sizes and disparate shapes such that the magnetic profiles above them could be used for identification and depth estimation (Dobrin, 1976) without resorting to excavation. In addition, accelerometers with multiple degrees of freedom buried in the slidemass prior to initiation could telemeter data to recording stations on the vibrations and impulses traveling though the landslide debris during runout, to determine whether landslide cobbles indeed come to rest because of the action of these random forces.

Finally, according to the DDBL concept, a landslide should interact with its base for the duration of its travel, in contrast to bulk fluidization models, where landslide debris simply flows onto and buries the surface, or air-layer lubrication, where the landslide debris only contacts the surface at the end of the runout phase. Thus, the interactions of the slide with its substrate should be tested over the duration of its emplacement. One method of testing the interaction of the slide with its substrate would be to plant transmitters at various depths within the stream channel before the slide, that were hard-wired to monitoring stations. Those surviving the landslide could give an estimate of the degree of erosion accomplished by the landslide as it passed over the channel, and thus an indication of the degree of interaction of the slide with the substrate.

The degree of interaction of the slide with its substrate could also be estimated by sampling the rock flour expelled by the landslides during runout. The rock flour generated in large landslides appears to form near their bases during runout due to the mechanical breakdown of clasts in this region. Because a subset of this material gets blown out of the landslides during runout to form the dust clouds associated with these slides, the nature of the dust should give an indirect measure of the source of the rock flour produced in the landslide during runout. Chemical tracers placed in the substrate prior to the landslide could be tested for in the dust to determine the how much of the dust originated as scraped-up substrate. Direct checks of the basal surface of the landslides after emplacement would be difficult, but might be achieved along the margins of the slide by tunneling in from the side through any soft substrate materials overrun by the landslide.

Appendix A: Database of Giant Landslides

1. Rank 2. Name	3. Volume 4. Area	5. Thickness a. Avg b. Max	6. Drop 7. Velocity	8. Length: a. Straight b. Curved	9. Fahr-böschung 10. Type	11. Location 12. Lat./Long.	13. Confinement 14. Age	15. Composition
1	3	5a	6	8a	9	11	13	15
2	4	5b	7	8b	10	12a / 12b	14	

References: - - -

Moisture: - - - Notes:

Substrate: - - -

Unit Designation:

-	cu. km	m	m	m	-	-	-	-
-	sq. km	m	km/hr	m	-	deg / deg	-	

References: - - -

Moisture: - - - Notes:

Substrate: - - -

1. Rank 2. Name	3. Volume 4. Area	5. Thickness a. Avg b. Max	6. Drop 7. Velocity	8. Length: a. Straight b. Curved	9. Fahr-böschung 10. Type	11. Location 12. Lat./Long.	13. Confinement 14. Age	15. Composition
M 1	17880	3791	7000	119000	0.06	Ius Chasma	deflected	NA
Mars 19	4716	NA	300	119000	IB4,3	-6.4 / 87	NA	

References: Lucchitta, 1979; 1987a; McEwen, 1989

Moisture: NA Notes: The landslide originated at the intersection of graben-bounding faults with wall rock in Valles Marineris. The largest known martian landslide. Best picno: 057A42; Best photomosaics: I-1207, I-1294. Landslide #19 from Lucchitta, 1979.

Substrate: NA

M 2	5800	NA	7000	117000	0.06	Ius Chasma	NA	NA
Mars 15 (Ius Labes)	NA	NA	250	NA	IB4,2,3	-8 / 78.5	NA	

References: Lucchitta, 1979; 1987a; U.S.G.S., 1986b

Moisture: NA Notes: The landslide originated at the intersection of graben-bounding faults with wall rock in Valles Marineris. Several small craters (1-3 km) dot the surface, indicating substantial age. Southernmost part of apron seems composed of thin stacked longitudinally ribbed sheets. Elsewhere border is unclear, craters appear through thin parts of the debris apron. Best picno: 058A77; Best photomosaics: I-1841, I-1842. Landslide #15 from Lucchitta, 1979.

Substrate: NA

M 3	4880	4153	7000	70000	0.10	Ophir Chasma	NA	NA
Mars 35	1175	NA	NA	NA	IB2,4	-3.4 / 70.7	NA	

References: Lucchitta, 1987a; McEwen, 1989

Moisture: wet? Notes: The landslide originated at the intersection of wrinkle ridges and graben-bounding faults with wall rock in Valles Marineris. Part of triple-reentrant wet(?) landslide complex at the northernmost part of Ophir Chasma. Best picno: 913A09; Best photomosaic: I-1592.

Substrate: NA

---

1. Rank 2. Name	3. Volume 4. Area	5. Thickness: a. Avg b. Max	6. Drop 7. Velocity	8. Length: a. Straight b. Curved	9. Fahrböschung 10. Type	11. Location 12. Lat./Long.	13. Confinement 14. Age	15. Composition
M 4	4183	3363	8400	82500	0.10	Ophir Chasma	NA	NA
Mars 36	1244	NA	NA	NA	IB2,4	-3.2 / 71.2	NA	

References: Lucchitta, 1987a; McEwen, 1989

Moisture: wet? Notes: The landslide originated at the intersection of graben-bounding faults with wall rock in Valles Marineris. Part of triple-reentrant wet(?) landslide complex at the northernmost part of Ophir Chasma. Best picno: 913A10; Best photomosaic: I-1592.

Substrate: NA

M 5	4047	1840	6800	95000	0.07	Ius Chasma	NA	NA
Mars 18	2200	NA	300	NA	IB4,3	-6.4 / 85.2	NA	

References: Lucchitta, 1979; 1987a; McEwen, 1989

Moisture: NA Notes: The landslide originated at the intersection of graben-bounding faults with wall rock in Valles Marineris. Morphologically similar to landslides from Oahu and Molokai islands on Earth. Debris apron appears only slightly fluidized compared with other, similar volume landslides. Best picno: 064A12; Best photomosaic: I-1207. Landslide #18 in Lucchitta, 1979.

Substrate: NA

M 6	3267	2538	7200	76000	0.09	Ophir Chasma	NA	NA
Mars 33	1287	NA	NA	NA	IB4	-3.1 / 73.9	NA	

References: McEwen, 1989

Moisture: NA Notes: The landslide originated from wall rock in Valles Marineris. Distinct black continuous horizontal band occurs in headscarp wall. Debris apron flows over and around etched layered terrain. No obvious etching or superposed craters. Best picno: 915A09; Best photomosaic: I-1592.

Substrate: NA

---

1. Rank 2. Name	3. Volume 4. Area	5. Thickness: a. Avg b. Max	6. Drop 7. Velocity	8. Length: a. Straight b. Curved	9. Fahr-böschung 10. Type	11. Location 12. Lat./Long.	13. Confinement 14. Age	15. Composition
M 7	2960	1767	8000	64000	0.13	Ophir Chasma	NA	NA
Mars 37	1675	NA	NA	NA	IB2,4	-3.1 / 71.6	NA	

References: Lucchitta, 1987a; McEwen, 1989

Moisture: wet? Notes: The landslide originated at the intersection of a sill(?) and graben-bounding faults with wall rock in Valles Marineris. Part of triple-reentrant wet(?) landslide complex at the northernmost part of Ophir Chasma. Black material is strung out downstream from two point sources in debris flow-like debris apron. Best picno: 913A10; Best photomosaic: I-1592.

Substrate: NA

M 8	2761	2413	6800	63000	0.11	Tithonium Chasma	NA	NA
Mars 26	1144	NA	NA	NA	IB4,2	-5.2 / 86.2	NA	

References: Lucchitta, 1979; McEwen, 1989

Moisture: NA Notes: The landslide originated at the intersection of graben-bounding faults with wall rock in Valles Marineris. It is old, marked by large craters. Its debris apron appears to have fluidized when it impacted the opposite wall; the apron then traveled west, downvalley. Best picno: 063A69; Best photomosaic: I-1207. Landslide #26 in Lucchitta, 1979.

Substrate: NA

E(u) 1	1600	200	5267	180000	0.03	Hawaii, U.S.A.	unconfined	basalt volcanics
Nuuanu	8000	2000	NA	180000	IB4	22 / 157	Pleistocene	

References: Lipman, et. al., 1988; Moore, et al., 1989

Moisture: NA Notes: Landslide documented only by depth contours. Striking, giant transverse ridges, very analogous to many martian landslides in western Valles Marineris. Age uncertain. Probably will be investigated further by GLORIA device sometime soon.

Substrate: NA

---

1. Rank 2. Name	3. Volume 4. Area	5. Thickness: a. Avg b. Max	6. Drop 7. Velocity	8. Length: a. Straight b. Curved	9. Fahr- böschung 10. Type	11. Location 12. Lat./Long.	13. Confinement 14. Age	15. Composition
M 9	1282	1031	8200	63000	0.13	Ophir Chasma	NA	NA
Mars 34	1244	NA	NA	NA	IB4,2	-3.1 / 72.6	NA	

References: McEwen, 1989

Moisture: NA Notes: The landslide originated at the intersection of a sill(?) with wall rock in Valles Marineris. The landslide scar exhibits a broad black horizontal scar, suggesting that the landslide dissected a sill. Banding from this feature can be recognized in coherent blocks near the source. Best picno: 914A10; Best photomosaic: I-1592.

Substrate: NA

L 1	1200	NA	4500	NA	NA	Tsiolkovsky Crater	NA	NA
Tsiolkovsky	NA	NA	NA	80000	IB2	-22 / -128	Imbrian	

References: El-Baz, 1972; Howard, 1973b

Moisture: NA Notes: NA

Substrate: NA

E(u) 2	1100	275	5572	125000	0.04	Hawaii, U.S.A.	unconfined	basalt volcanics
Wailau	4000	2000	NA	125000	IB4	21.5 / 157	Pleistocene	

References: Lipman, et. al., 1988; Moore, et al., 1989

Moisture: NA Notes: A rift zone apparently formed a detachment surface for the upper end of the headscarp. Apparently somewhat older than the overlapping Oahu slide from its more subdued character. Landslide documented only by depth contours. Striking, giant transverse ridges, very analagous to many martian landslides in western Valles Marineris. Age uncertain. Probobly will be investigated further by GLORIA device sometime soon.

Substrate: NA

---

1. Rank / 2. Name	3. Volume / 4. Area	5. Thickness: a. Avg / b. Max	6. Drop / 7. Velocity	8. Length: a. Straight / b. Curved	9. Fahrböschung / 10. Type	11. Location / 12. Lat./Long.	13. Confinement / 14. Age	15. Composition
M 1 0	833	775	5400	56000	0.10	Tithonium Chasma	NA	NA
Mars 24	1075	NA	NA	NA	IB1,6	-3.9 / 87.6	NA	

References: Lucchitta, 1979; McEwen, 1989

Moisture: moist? Notes: The landslide originated from wall rock in Valles Marineris. The landslide has a morphology suggestive of wet(?) emplacement. It has a large superposed crater suggestive of considerable age. Linear truncation of the southernmost part of the landslide might be fault controlled. Overrides layered terrain to the west and southwest. Best picno: 063A67; Best photomosaic: I-1207. Landslide #24 in Lucchitta, 1979.

Substrate: NA

M 1 1	688	775	3600	45000	0.08	Tithonium Chasma	NA	NA
Mars 30	888	NA	300	NA	IB4,1	-4.7 / 79.7	NA	

References: Lucchitta, 1979; 1987a; McEwen, 1989

Moisture: NA Notes: The landslide originated at the intersection of graben-bounding faults with wall rock in Valles Marineris. Part of the deposit spilled off to the west in a small discrete lobe. Best picno: 921A09; Best photomosaic: I-1841. Landslide #30 from Lucchitta, 1979.

Substrate: NA

M 1 2	668	1018	4400	31000	0.14	Tithonium Chasma	NA	NA
Mars 25	656	NA	NA	NA	IB1	-4.3 / 86.8	NA	

References: Lucchitta, 1979; McEwen, 1989

Moisture: NA Notes: The landslide originated from wall rock in Valles Marineris. The landslide is extremely old, given two large superposed craters. The larger one impacted in the direct center of the debris apron, perhaps obscuring slide textures. The landslide is postdated by small later slumps from the north wall and by Mars 26 to the east. Best picno: 063A67; Best photomosaic: I-1207. Landslide #25 in Lucchitta, 1979.

Substrate: NA

---

1. Rank 2. Name	3. Volume 4. Area	5. Thickness: a. Avg b. Max	6. Drop 7. Velocity	8. Length: a. Straight b. Curved	9. Fahr-böschung 10. Type	11. Location 12. Lat./Long.	13. Confinement 14. Age	15. Composition
M 1 3	655	1394	7600	54000	0.14	Ophir Chasma	NA	NA
Mars 38	470	NA	NA	NA	IB3	-4.4 / 70	NA	

References: McEwen, 1989

Moisture: NA Notes: The landslide originated at the intersection of a small crater, graben-bounding faults, a wrinkle ridge and a sill(?) with wall rock in Valles Marineris. Only one observed small impact crater occurs on the deposit. Best picno: 913A11; Best photomosaic: I-1592.

Substrate: NA

E(u) 3	400	100	5700	92000	0.06	Hawaii, U.S.A.	unconfined	basalt volcanics
Alika 1	4000	200	120	92000	IB4	19.25 / 156.25	~100,000 yrs	

References: Lipman, et. al., 1988

Moisture: NA Notes: Lobe 1 of 2-lobed flow. May have generated huge tidal wave deposit on nearby islands at ~100,000 before present. Mapped by GLORIA at 50m resolution with additional small regions covered by seaMARCII sonar device.

Substrate: NA

E(u)	272	25	2470	NA	NA	Senegal, Africa	NA	sediment
West Africa #1	10928	NA	NA	NA	NA	15.75 / 19	100,000+ yrs	

References: Jacobi, 1976

Moisture: NA Notes: NA

Substrate: NA

---

1. Rank 2. Name	3. Volume 4. Area	5. Thickness: a. Avg b. Max	6. Drop 7. Velocity	8. Length: a. Straight b. Curved	9. Fahr-böschung 10. Type	11. Location 12. Lat./Long.	13. Confinement 14. Age	15. Composition
E(u) 4	200	100	4800	90000	0.05	Hawaii, U.S.A.	Slight	basalt volcanics
Alika 2	2000	200	120	95000	IB4	19.25 / 156.25	~100,000 yrs	

References: Lipman, et. al., 1988

Moisture: NA Notes: Lobe 1 of 2-lobed flow. Might have generated huge tidal wave deposit on nearby islands at ~100,000 before present. Mapped by GLORIA at 50m resolution with additional small regions covered by seaMARCII sonar device.

Substrate: NA

M 1 4	200	100	2000	60000	0.03	Gangis Chasma	unconfined	NA
Mars 1	2000	NA	100	60000	IB2	-8.75 / 44.6	NA	

References: Lucchitta, 1978a; 1979

Moisture: NA Notes: The landslide originated at the intersection of a 20 km-diameter crater with wall rock in Valles Marineris. The first well-described martian landslide. It overlies two adjacent landslides. Best picno: 014A30; Best photomosaic: I-1381. Landslide #1 in Lucchitta, 1979.

Substrate: NA

M 1 5	157	483	2800	33000	0.08	Tithonium Chasma	NA	NA
Mars 28	325	NA	NA	NA	IB4	-4.78 / 82.86	NA	

References: Lucchitta, 1979; McEwen, 1989

Moisture: NA Notes: The landslide originated from the intersection of a crater with wall rock in Valles Marineris. Best picno: 064A25; Best photomosaic: I-1207. Landslide #28 from Lucchitta, 1979.

Substrate: NA

---

1. Rank 2. Name	3. Volume 4. Area	5. Thickness: a. Avg b. Max	6. Drop 7. Velocity	8. Length: a. Straight b. Curved	9. Fahr- böschung 10. Type	11. Location 12. Lat./Long.	13. Confinement 14. Age	15. Composition
E 5	45	67	3550	49000	0.07	northern California	unconfined(CH)	andesite
Mt. Shasta	675	76	NA	49000	-B1,4	41.5 / 122.5	300,000-380,000 B.P.	

References: Siebert, 1984; Crandell, 1988

Moisture: wet Notes: Elevation drop above an estimate, the actual scar has been covered up by later volcanics. This is the largest known terrestrial subaerial landslide deposit. The landslide exhibits clastic dikes, a proximal to distal size decrease and rock-crested hummocks.

Substrate: alluvium

E(u) 6	40	50	5200	65000	0.08	Hawaii, U.S.A.	channeled	basalt volcanics
Ka Lae-E	800	200	NA	72500	IB4	18.75 / 155.87	Pleistocene	

References: Lipman, et. al., 1988; Moore, et al., 1989

Moisture: NA Notes: A channelized landslide which originated on the south shore of Hawaii Island and flowed down the channel between two (constructive) rift zones.

Substrate: NA

E(u) 7	39	321	1350	24400	0.06	Hawaii, U.S.A.	unconfined	basalt volcanics
Papa'u	121.6	1100	NA	26600	IIICcba	19.08 / 155.2	3500+ yrs	

References: Fornari, et. al., 1979

Moisture: NA Notes: Deposit formed from collapse of fragmental mass of lava rock and sand erupted into the ocean from Kilauea volcano. The velocity is unclear, but if rapid it should have produced a large tsunami. Only age constraint is that collapse scar has been partially refilled with debris which is estimated to have taken 3500 years at minimum.

Substrate: NA

---

1. Rank 2. Name	3. Volume 4. Area	5. Thickness: a. Avg b. Max	6. Drop 7. Velocity	8. Length: a. Straight b. Curved	9. Fahr- böschung 10. Type	11. Location 12. Lat./Long.	13. Confinement 14. Age	15. Composition
M 1 6	32	256	3600	29000	0.12	Tithonium Chasma	NA	NA
Mars 65	125	NA	NA	NA	NA	-8.2 / 85.1	NA	

References: McEwen, 1989

Moisture: NA Notes: NA

Substrate: NA

M 1 7	29	83	4000	20000	0.20	Ophir Chasma	NA	NA
Mars 97	350	NA	NA	NA	IIICcaa	-4.3 / 74.4	NA	

References: Lucchitta, 1987a; McEwen, 1989

Moisture: NA Notes: The landslide originated at the intersection of a 20 km-diameter crater with wall rock in Valles Marineris. Mentioned as a possible moist landslide or debris flow in Lucchitta, 1987. Best picno: 915A10; Best photomosaic: I-1592.

Substrate: NA

M 1 8	26	160	4000	41000	0.10	Olympus Mons Flank	unconfined(CH)	basalt?
Mars 142	162.5	160	NA	NA	IIICbab	23.7 / 136.1	NA	

References: This paper

Moisture: moist? Notes: Possibly two-pulse deposit, but probably two separate events. One superposed crater. Fell from NW corner of Olympus Mons. Best picno: 047B37

Substrate: NA

---

1. Rank / 2. Name	3. Volume / 4. Area	5. Thickness: a. Avg / b. Max	6. Drop / 7. Velocity	8. Length: a. Straight / b. Curved	9. Fahrböschung / 10. Type	11. Location / 12. Lat./Long.	13. Confinement / 14. Age	15. Composition
E8	20	120	1200	15000	0.08	western Iran	partial	limestone
Saidmarreh	166	NA	NA	15000	IICdda	33 / -47.5	early Holocene	

References: Harrison and Falcon, 1938

Moisture: dry Notes: A bedding-plane failure initiated movement of this landslide. The largest non-volcanic terrestrial subaerial landslide. Caused by collapse of one limb of an anticline whose base was eroded by a river. The landslide exhibits preserved slope-parallel stratigraphy and reverse grading. Surface grain size; maximum: 10 m.

Substrate: bedrock, alluvium

E9	15	1000	3400	30000	0.11	central Nepal	heavy	migmatite, gneiss
Langtang	15	NA	NA	NA	IIA	28.5 / -85	25000 B.P.	

References: Heuberger, et. al., 1984

Moisture: NA Notes: The sliding surface is visible in profile in a stream cut. At the interface, a layer of fused rock (hyalomylonite) occurs that has the appearance of hardened lubricating oil. Rocks are fractured to breccia near the sliding surface, less so upwards. A temperature of 1000° C was required to melt the rock.

Substrate: NA

E10	15	11	3900	50000	0.08	Tanzania	NA	NA
Meru Volcano	1400	NA	NA	NA	NA	NA / NA	7200 B. P.	

References: Siebert, 1984

Moisture: NA Notes: NA

Substrate: NA

---

1. Rank / 2. Name	3. Volume / 4. Area	5. Thickness: a. Avg / b. Max	6. Drop / 7. Velocity	8. Length: a. Straight / b. Curved	9. Fahrböschung / 10. Type	11. Location / 12. Lat./Long.	13. Confinement / 14. Age	15. Composition
E 1 1	15	31	3000	25200	0.12	northern Chile	moderate	dacite
Socompa Volcano	490	50	252	35000	IB1,2	-24.38 / 68.25	500-10000 B.P.	

References: Francis, et. al., 1985

Moisture: NA Notes: Utilized remote sensing data in preliminary survey. The landslide incorporated material from beneath the volcano; the failure surface cut down through the volcanic edifice into the subvolcanic basement. Probable that emplacement was volcanic blast driven.

Substrate: NA

M 1 9	14	80	2000	18000	0.11	Tithonium Chasma	NA	NA
Mars 22	175	NA	NA	NA	IIICbab	-5.6 / 87.6	NA	

References: McEwen, 1989

Moisture: NA Notes: The landslide originated at the intersection of a crater with wall rock in Valles Marineris. Best picno: 928A02; Best photomosaic: I-1207. Landslide #22 in Lucchitta, 1979.

Substrate: NA

E 1 2	12.5	14	4000	40000	0.10	Mexico	NA	NA
Colima Volcano	900	NA	NA	NA	NA	NA / NA	4028 B. P.	

References: Siebert, 1984

Moisture: NA Notes: NA

Substrate: NA

---

1. Rank 2. Name	3. Volume 4. Area	5. Thickness: a. Avg b. Max	6. Drop 7. Velocity	8. Length: a. Straight b. Curved	9. Fahr-böschung 10. Type	11. Location 12. Lat./Long.	13. Confinement 14. Age	15. Composition
E13	12	300	2120	16000	0.13	Graübunden, Switz.	heavy	limestone
Flims	40	720	360	24000	IICdca	46.883 / -9.25	interglacial	

References: Heim, 1932

Moisture: NA Notes: A bedding-plane failure initiated movement of this landslide. Monolithologic, largest Alpine landslide.

Substrate: NA

M20	11	250	1200	8000	0.15	Tithonium Chasma	NA	NA
Mars 64	44	NA	NA	NA	NA	-4.9 / 82.6	NA	

References: Lucchitta, 1979; McEwen, 1989

Moisture: NA Notes: Part of landslide #28 in Lucchitta, 1979.

Substrate: NA

E(u)14	10.5	11	1650	80950	0.02	California, U.S.A.	Channeled	turbidite fan sediment
Sur	1000	75	NA	80950	IIC	36 / 122.75	late Holocene	

References: Normark and Gutmacher, 1988

Moisture: NA Notes: NA

Substrate: NA

---

1. Rank / 2. Name	3. Volume / 4. Area	5. Thickness: a. Avg / b. Max	6. Drop / 7. Velocity	8. Length: a. Straight / b. Curved	9. Fahr-böschung / 10. Type	11. Location / 12. Lat./Long.	13. Confinement / 14. Age	15. Composition
E15	9	NA	2400	32000	0.08	Japan	NA	NA
Yatsugatake-A Volcano	NA	NA	NA	NA	NA	NA / NA	NA	

References: Ui, 1983

Moisture: NA Notes: NA

Substrate: NA

E16	7.5	30	2600	31000	0.08	New Zealand	NA	NA
Egmont Volcano-A	250	NA	NA	NA	NA	NA / NA	23000 B. P.	

References: Siebert, 1984

Moisture: NA Notes: NA

Substrate: NA

E17	7.5	30	2600	27000	0.10	New Zealand	NA	volcanics
Pungarehu	250	35	NA	27000	NA	-39.3 / -173.8	22100+-600 B.P.	

References: Ui, et. al., 1986

Moisture: NA Notes: The landslide exhibits three-dimensional jigsaw puzzle breccia, a proximal-distal average size decrease, rock-crested hummocks and clast rounding.

Substrate: NA

---

1. Rank 2. Name	3. Volume 4. Area	5. Thickness: a. Avg b. Max	6. Drop 7. Velocity	8. Length: a. Straight b. Curved	9. Fahr- böschung 10. Type	11. Location 12. Lat./Long.	13. Confinement 14. Age	15. Composition
E 1 8	7.1	6	4500	60000	0.08		NA	volcanic
Mawenzi Volcano	1150	NA	NA	NA	NA	NA / NA	Pleistocene	

References: Siebert, 1984

Moisture: NA Notes: NA

Substrate: NA

M 2 1	5.5	65	6400	21000	0.30	Tithonium Chasma	NA	NA
Mars 66	84	NA	NA	NA	NA	-4.4 / 85.8	NA	

References: McEwen, 1989

Moisture: NA Notes: NA

Substrate: NA

M 2 2	5.3	65	6200	20000	0.31	Tithonium Chasma	NA	NA
Mars 67	81	NA	NA	NA	NA	-4.4 / 85.4	NA	

References: McEwen, 1989

Moisture: NA Notes: NA

Substrate: NA

---

1. Rank 2. Name	3. Volume 4. Area	5. Thickness: a. Avg b. Max	6. Drop 7. Velocity	8. Length: a. Straight b. Curved	9. Fahr- böschung 10. Type	11. Location 12. Lat./Long.	13. Confinement 14. Age	15. Composition
M 2 3	4.3	65	6200	19000	0.33	Tithonium Chasma	NA	NA
Mars 68	66	NA	NA	NA	NA	-4.4 / 85.6	NA	

References: McEwen, 1989

Moisture: NA Notes: NA

Substrate: NA

E 1 9	4	NA	2400	19000	0.13	Japan	NA	NA
Akagi Volcano	NA	NA	NA	NA	NA	NA / NA	Pleistocene	

References: Siebert, 1984

Moisture: NA Notes: NA

Substrate: NA

M 2 4	3.3	66	5000	16000	0.31	Ius Chasma	NA	NA
Mars 69	50	NA	NA	NA	NA	-7.8 / 84.4	NA	

References: McEwen, 1989

Moisture: NA Notes: NA

Substrate: NA

---

1. Rank 2. Name	3. Volume 4. Area	5. Thickness: a. Avg b. Max	6. Drop 7. Velocity	8. Length: a. Straight b. Curved	9. Fahr-böschung 10. Type	11. Location 12. Lat./Long.	13. Confinement 14. Age	15. Composition
E20	3	222	600	5364	0.11	Austria	heavy	augengneiss
Koefels	13.5	500	200	5364	IIB	47.09 / -10.9	8700 B.P.	

References: Heuberger, et. al., 1984

Moisture: NA Notes: The landslide exhibits a proximal trough. It divided into two parts after impacting the opposite river bank; the lower section was checked by the bank while the upper section overrode the bank and flowed an additional few hundred meters along a secondary slip-surface. Much material slid coherently, with much appearing to be unaltered bedrock. Fused rock formed at slip surfaces which then intruded into the slidemass (Koefels pumice).

Substrate: NA

E21	2.9	17	1900	25000	0.08	Indonesia	NA	NA
Galunggung Volcano	175	NA	NA	NA	NA	NA / NA	NA	

References: Siebert, 1984

Moisture: wet Notes: NA

Substrate: NA

E22	2.8	47	2550	24000	0.11	Washington, U.S.A.	deflected (CH)	volcanics
Mt. St. Helens	60	195	252	26000	IBdca	NA / NA	May, 1980	

References: Voight, et al., 1983; Siebert, 1984

Moisture: moist, wet Notes: The collapse immediately followed a magnitude- 5.2 earthquake beneath the volcano. Because of excess water in the debris avalanche, its surficial part remobilized to form distructive lahars that extended 95 km farther downstream along the Toutle, Cowlitz and Columbia Rivers. The deposit exhibits a proximal-distal size decrease.

Substrate: alluvium

---

1. Rank / 2. Name	3. Volume / 4. Area	5. Thickness: a. Avg / b. Max	6. Drop / 7. Velocity	8. Length: a. Straight / b. Curved	9. Fahr-böschung / 10. Type	11. Location / 12. Lat./Long.	13. Confinement / 14. Age	15. Composition
E 2 3	2.75	NA	1650	7500	0.22	Switzerland	heavy	limestone
Engelberg	NA	NA	NA	NA	IIC	NA / NA	interglacial	

References: Heim, 1932

Moisture: NA Notes: Monolithologic

Substrate: NA

E 2 4	2	22	2250	20000	0.11	Japan	NA	NA
Asama Volcano	90	NA	NA	NA	NA	NA / NA	NA	

References: Siebert, 1984

Moisture: NA Notes: NA

Substrate: NA

E 2 5	2	200	1650	6800	0.24	Tadzhikistan, USSR	heavy	shale + carbonates
Usoy	10	NA	NA	NA	IIICdda	NA / NA	18 Feb. 1911	

References: Preobrajensky, 1920; Gaziev, 1984

Moisture: NA Notes: A fault plane formed a detachment surface for the upper end of the headscarp. Apparently triggered by large earthquake. Initiated debate on whether landslide fall itself was source of earthquake. Exhibits preserved stratigraphy and a proximal trough.

Substrate: NA

---

1. Rank 2. Name	3. Volume 4. Area	5. Thickness: a. Avg b. Max	6. Drop 7. Velocity	8. Length: a. Straight b. Curved	9. Fahr- böschung 10. Type	11. Location 12. Lat./Long.	13. Confinement 14. Age	15. Composition
E26	1.8	124	620	5900	0.11	California, U.S.A.	partial	carbonate
Tin Mtn.	14.5	150	200	5900	IICdda	36.83 / 117.53	late Pleistocene	

References: Burchfiel, 1966

Moisture: NA Notes: Motion was initiated along a valley-dipping bedding-parallel fault plane. The landslide exhibits preserved cross-slope stratigraphy and three-dimensional jigsaw puzzle breccia. Surface grain size; modal: 10 cm; maximum: 2.5 m.

Substrate: NA

M27	1.5	43	1800	15000	0.12	Crater Aj	unconfined	NA
Mars 109	35	70	NA	15000	IIICcbd, b	-19.05 / 180.35	NA	

References: This paper

Moisture: dry Notes: One superposed crater, ~500 m diameter. Bilobate, toe of larger lobe cut off in image. Smaller lobe toe seems digitate. Looks like a version of the Silver Reef that traveled relatively far, thinning out the "head." Best picno: 432S21. Mosaic #: 1215

Substrate: NA

E27	1.5	23	1050	11000	0.10	Philippines	NA	NA
Iriga Volcano	65	NA	NA	NA	NA	NA / NA	1628 A. D.	

References: Siebert, 1984

Moisture: NA Notes: NA

Substrate: NA

---

1. Rank 2. Name	3. Volume 4. Area	5. Thickness: a. Avg b. Max	6. Drop 7. Velocity	8. Length: a. Straight b. Curved	9. Fahr-böschung 10. Type	11. Location 12. Lat./Long.	13. Confinement 14. Age	15. Composition
E 2 8	1.5	44	1200	11000	0.11	Honshu, Japan	NA	NA
Bandai Volcano	34	NA	NA	NA	NA	NA / NA	1888 A.D.	

References: Schuster and Crandell, 1984; Siebert, 1984

Moisture: NA Notes: The avalanche rushed down the slopes of the volcano into streams at its base, forming lahars that travelled along the stream valleys, destroying villages and farmlands and killing 461 people. The debris only mixed in water at its margins, where the lahars were formed. The landslide exhibited a proximal to distal size decrease.

Substrate: NA

M 2 6	1.5	60	3400	16500	0.21	Candor Chasma	unconfined(CH)	basalt?
Mars 84	25	100	NA	NA	IIICbab	-8.31 / 66.48	NA	

References: This paper

Moisture: moist? Notes: Landslide mentioned Ref. 3, Lucchitta. Similar volume and morphology to Carlson Landslide, Idaho. Best picno: 910A15. Mosaic #: 1591

Substrate: NA

E 2 9	1.5	NA	2450	17500	0.14	Switzerland	NA	NA
Siders	NA	NA	NA	NA	NA	NA / NA	NA	

References: Lucchitta, 1978a

Moisture: NA Notes: NA

Substrate: NA

---

1. Rank 2. Name	3. Volume 4. Area	5. Thickness: a. Avg b. Max	6. Drop 7. Velocity	8. Length: a. Straight b. Curved	9. Fahr- böschung 10. Type	11. Location 12. Lat./Long.	13. Confinement 14. Age	15. Composition
E 3 0	1.5	15	2000	12000	0.17	Kamchatka, U.S.S.R.	NA	NA
Shiveluch Volcano	98	NA	NA	NA	NA	NA / NA	1964 A. D.	

References: Siebert, 1984

Moisture: NA Notes: NA

Substrate: NA

M 2 5	1.5	60	3500	15200	0.23	Candor Chasma	unconfined(CH)	basalt?
Mars 85	25	100	NA	NA	IIICbab	-8.28 / 66.29	NA	

References: This paper

Moisture: moist? Notes: Landslide mentioned in Ref. 3, Lucchitta. Similar volume and morphology to Carlson landslide, Idaho. Best picno: 910A15. Mosaic #: 1591

Substrate: NA

M 2 8	1.4	64	6200	17000	0.36	Tithonium Chasma	NA	NA
Mars 70	22	NA	NA	NA	NA	-4.4 / 85.7	NA	

References: McEwen, 1989

Moisture: NA Notes: NA

Substrate: NA

---

1. Rank 2. Name	3. Volume 4. Area	5. Thickness: a. Avg b. Max	6. Drop 7. Velocity	8. Length: a. Straight b. Curved	9. Fahr-böschung 10. Type	11. Location 12. Lat./Long.	13. Confinement 14. Age	15. Composition
E 3 1	1.3	NA	1500	15000	0.10	Japan	NA	NA
Iwaki Volcano	NA	NA	NA	NA	NA	NA / NA	NA	

References: Ui, 1983

Moisture: NA Notes: NA

Substrate: NA

E 3 2	1.3	NA	1280	13500	0.09	Switzerland	NA	NA
Tamins	NA	NA	NA	NA	NA	NA / NA	NA	

References: Lucchitta, 1978a

Moisture: NA Notes: A bedding-plane failure initiated movement of this landslide.

Substrate: NA

E 3 3	1	NA	2400	21000	0.11	New Zealand	NA	NA
Egmont Volcano-B	NA	NA	NA	NA	NA	NA / NA	12-14000 B.P.	

References: Siebert, 1984

Moisture: NA Notes: NA

Substrate: NA

---

1. Rank / 2. Name	3. Volume / 4. Area	5. Thickness: a. Avg / b. Max	6. Drop / 7. Velocity	8. Length: a. Straight / b. Curved	9. Fahrböschung / 10. Type	11. Location / 12. Lat./Long.	13. Confinement / 14. Age	15. Composition
E34	1	NA	2700	23000	0.12	U.S.S.R.	NA	NA
Camen	NA	NA	NA	NA	NA	NA / NA	prehistoric	

References: Adushkin, personal communication, 1990

Moisture: NA Notes: NA

Substrate: NA

E35	1	NA	2200	28000	0.08	Kamchatka, U.S.S.R.	NA	NA
Bezymianny Volcano	NA	NA	NA	NA	NA	NA / NA	1956	

References: Ui, 1983

Moisture: NA Notes: NA

Substrate: NA

E36	1	NA	1400	15500	0.09	Austria	Channeled	NA
Fernpass	NA	NA	NA	NA	NA	NA / NA	NA	

References: Lucchitta, 1978a

Moisture: NA Notes: NA

Substrate: NA

---

1. Rank / 2. Name	3. Volume / 4. Area	5. Thickness: a. Avg / b. Max	6. Drop / 7. Velocity	8. Length: a. Straight / b. Curved	9. Fahr-böschung / 10. Type	11. Location / 12. Lat./Long.	13. Confinement / 14. Age	15. Composition
E37	1	22	1300	12000	0.11	Nicaragua	NA	NA
Mombacho Volcano	45	NA	NA	NA	NA	NA / NA	NA	

References: Siebert, 1984

Moisture: NA Notes: NA

Substrate: NA

E38	1	NA	1870	8250	0.23	Peru	deflected-90°,90°(CH,DI-18	sandstone
Mayunmarca	NA	NA	225	NA	IIICdab,c	-12.63 / 74.68	0°) 25 Apr. 1974	

References: Kojan and Hutchinson, 1978

Moisture: NA Notes: Preceeded by four years of creep motions marked by small slumps in the source area. The landslide spattered rock debris where it struck a ridge aligned transverse to the movement direction. Surface grain size; maximum: 10 m.

Substrate: NA

E39	1	NA	1000	4000	0.25	U.S.S.R.	NA	NA
Ircht	NA	NA	NA	NA	NA	NA / NA	NA	

References: Adushkin, personal communication, 1990

Moisture: NA Notes: NA

Substrate: NA

---

1. Rank 2. Name	3. Volume 4. Area	5. Thickness: a. Avg b. Max	6. Drop 7. Velocity	8. Length: a. Straight b. Curved	9. Fahr- böschung 10. Type	11. Location 12. Lat./Long.	13. Confinement 14. Age	15. Composition
M 2 9	0.9	69	2200	7000	0.31	Tithonium Chasma	NA	NA
Mars 71	13	NA	NA	NA	NA	-5.1 / 81.2	NA	

References: McEwen, 1989

Moisture: NA Notes: NA

Substrate: NA

E 4 0	0.9	15	1150	12000	0.10	Indonesia	NA	NA
Papandajan Volcano	60	NA	NA	NA	NA	NA / NA	1772 A. D.	

References: Siebert, 1984

Moisture: NA Notes: NA

Substrate: NA

E 4 1	0.8	NA	1920	5275	0.36	Glarus, Switz.	deflected(CH)	NA
Glarnisch Guppen	NA	270	240	7500	IIIC	47 / -9	interglacial	

References: Heim, 1932

Moisture: NA Notes: NA

Substrate: NA

---

1. Rank / 2. Name	3. Volume / 4. Area	5. Thickness: a. Avg / b. Max	6. Drop / 7. Velocity	8. Length: a. Straight / b. Curved	9. Fahrböschung / 10. Type	11. Location / 12. Lat./Long.	13. Confinement / 14. Age	15. Composition
M 3 0	0.8	32	1900	10000	0.19	NE Terra Cimmeria	unconfined	NA
Mars 133	25	50	NA	10000	IIICcbd	-22.2 / 190.96	Fresh	

References: This paper

Moisture: dry Notes: Lies in 30 km diameter crater with central peak. A "Blackhawk-type" landslide. The landslide exhibits oblique imbricated ridges. Best picnos: 429S24, 429S26.

Substrate: NA

E 4 2	0.8	NA	2000	19000	0.11	Japan	NA	NA
Myoko Volcano-A	NA	NA	NA	NA	NA	NA / NA	19600 B. P.	

References: Siebert, 1984

Moisture: NA Notes: NA

Substrate: NA

E 4 3	0.77	NA	2460	8000	0.31	Glarus, Switz.	deflected(CH)	limestone
Glarnisch Gleiter	NA	350	NA	NA	IIIC	47.1 / -9	interglacial	

References: Heim, 1932

Moisture: NA Notes: Monolithologic

Substrate: NA

---

1. Rank 2. Name	3. Volume 4. Area	5. Thickness: a. Avg b. Max	6. Drop 7. Velocity	8. Length: a. Straight b. Curved	9. Fahr- böschung 10. Type	11. Location 12. Lat./Long.	13. Confinement 14. Age	15. Composition
E 4 4	0.6	NA	740	6600	0.11	Switzerland	NA	NA
Deyen	NA	NA	NA	NA	II	NA / NA	NA	

References: Hsü, 1975

Moisture: NA Notes: NA

Substrate: NA

M 3 1	0.5	56	1600	6600	0.24	Xanthe Terra	unconfined	NA
Mars 101	9	80	NA	6600	IIICcbd	15.67 / 54.15	NA	

References: This paper

Moisture: dry Notes: Blackhawk-like landslide from crater rim, towards inside of crater. Best picno: 054A22. Mosaic #: 1721

Substrate: NA

E 4 5	0.5	29	1600	7500	0.21	France	unconfined	NA
Mt. Granier	17.5	NA	NA	NA	NA	45.5 / -6	NA	

References: Eisbacher and Clague, 1984

Moisture: NA Notes: A bedding-plane failure initiated movement of this landslide. The surface of the landslide is marked by debris pyramids.

Substrate: NA

---

1. Rank 2. Name	3. Volume 4. Area	5. Thickness: a. Avg b. Max	6. Drop 7. Velocity	8. Length: a. Straight b. Curved	9. Fahr-böschung 10. Type	11. Location 12. Lat./Long.	13. Confinement 14. Age	15. Composition
E46	0.5	20	1350	9500	0.14	Guadeloupe Island	NA	NA
Soufriere Volcano	25	NA	NA	NA	NA	NA / NA	3000 B. P.	

References: Siebert, 1984

Moisture: NA Notes: NA

Substrate: NA

E47	0.498	107	920	5470	0.17	Alberta, Canada	partial	siltstone, chert, limestone
Maligne Lake	4.66	170	NA	5470	IICdc-	52.7 / 117.6	Holocene	

References: Cruden, 1976

Moisture: NA Notes: A bedding-plane failure initiated movement of this landslide. The landslide exhibits debris pyramids.

Substrate: NA

E48	0.48	40	850	5700	0.15	Japan	NA	NA
Unzen Volcano	12	NA	NA	NA	NA	NA / NA	1792 A. D.	

References: Siebert, 1984

Moisture: NA Notes: NA

Substrate: NA

---

1. Rank / 2. Name	3. Volume / 4. Area	5. Thickness: a. Avg / b. Max	6. Drop / 7. Velocity	8. Length: a. Straight / b. Curved	9. Fahrböschung / 10. Type	11. Location / 12. Lat./Long.	13. Confinement / 14. Age	15. Composition
E49	0.45	NA	750	5500	0.14	Nwst. Terr., Canada	Deflected-90°-40°(CH)	carbonate, siltstone
Rockslide Pass	NA	NA	280	6100	IICdca	63.33 / 127.75	Holocene	

References: Eisbacher, 1979

Moisture: NA Notes: A bedding-plane failure initiated movement of this landslide. The landslide exhibits preserved slope-parallel stratigraphy, with basal siltstones coming to rest at the toe of the slide.

Substrate: NA

E50	0.4	NA	800	4600	0.17	Nwst. Terr., Canada	deflected-20°, 55°(CH, DI-30°)	carbonates
Avalanche Lake	NA	140	360	NA	IICdda	62.25 / 127.25	about 200 B. P.	

References: Eisbacher, 1979

Moisture: NA Notes: A bedding-plane failure initiated movement of this landslide. Monolithology, rock spattering and dozed distal material mark the landslide. The slide slammed against a wall and threw material 500 m up the opposite valley wall.

Substrate: NA

E51	0.4	37	1500	8700	0.17	Tadzhikistan, U.S.S.R.	deflected-90°(CH,DI-70°)	crystalline rock
Khait	10.7	NA	100	10500	IIICa-a	39.16 / -70.85	10 July 1949	

References: Seed, 1968; Solonenko, 1972; 1977

Moisture: NA Notes: Triggered by 7.5-magnitude earthquake, associated wind blast. Wiped out the villages of Khait and Khisarak.

Substrate: NA

---

1. Rank 2. Name	3. Volume 4. Area	5. Thickness: a. Avg b. Max	6. Drop 7. Velocity	8. Length: a. Straight b. Curved	9. Fahr-böschung 10. Type	11. Location 12. Lat./Long.	13. Confinement 14. Age	15. Composition
E 5 2	0.37	NA	910	3700	0.25	Montana, U.S.A.	unconfined	carbonate
Sawtooth 1	NA	NA	NA	NA	IIIC	47.54 / 112.65	late Pleistocene	

References: Mudge, 1965

Moisture: NA Notes: The landslide fell from the oversteepened hanging wall of a thrust fault. Monolithologic. Surface grain size; modal: 8 cm; maximum: 3 m.

Substrate: NA

E 5 3	0.35	3	2500	27000	0.09	New Zealand	NA	NA
Egmont Volcano-C	120	NA	NA	NA	NA	NA / NA	6570 B. P.	

References: Siebert, 1984

Moisture: NA Notes: NA

Substrate: NA

E 5 4	0.3	21	1200	9000	0.13	California, U.S.A.	unconfined(CH)	limestone
Blackhawk	14	30	235	9000	IIICbbd,a	34.42 / 116.78	17,400(+or-550) B.P.	

References: Shreve, 1968a; Johnson, 1978

Moisture: dry Notes: Originated from hanging wall of a thrust fault. It exhibits reverse grading, incorporated substrate material, three-dimensional jigsaw puzzle breccia, sub-horizontal slip surfaces, clastic dike intrusions, thrust faults and imbrication, a dozed marginal dike, oblique imbricated ridges, multiple margins, especially along the northeast margin, a raised distal rim, a foliated internal texture and normal faults. Type locality for "air layer lubricated" landslides. Surface grain size; modal: 2.5 cm; maximum: 11 m.

Substrate: alluvium

---

1. Rank 2. Name	3. Volume 4. Area	5. Thickness: a. Avg b. Max	6. Drop 7. Velocity	8. Length: a. Straight b. Curved	9. Fahr-böschung 10. Type	11. Location 12. Lat./Long.	13. Confinement 14. Age	15. Composition
M 3 2	0.3	75	2200	6000	0.37	Tithonium Chasma	NA	NA
Mars 72	4	NA	NA	NA	NA	-5.1 / 81.1	NA	

References: McEwen, 1989

Moisture: NA Notes: NA

Substrate: NA

E 5 5	0.3	NA	750	6500	0.12	Japan	NA	NA
Usu Volcano	NA	NA	NA	NA	NA	NA / NA	7-8000 B. P.	

References: Siebert, 1984

Moisture: NA Notes: NA

Substrate: NA

E 5 6	0.29	171	1520	3050	0.50	India	heavy	carbonates
Gohna	1.7	260	NA	NA	IIICdda	NA / NA	6 Sept. 1893	

References: Holland, 1894

Moisture: NA Notes: The landslide was triggered by heavy rainfall. It was associated with concentrated dust fallout and loud noises. The landslide displays a proximal trough.

Substrate: NA

---

1. Rank 2. Name	3. Volume 4. Area	5. Thickness: a. Avg b. Max	6. Drop 7. Velocity	8. Length: a. Straight b. Curved	9. Fahr-böschung 10. Type	11. Location 12. Lat./Long.	13. Confinement 14. Age	15. Composition
E57	0.275	NA	670	1570	0.43	Montana, U.S.A.	unconfined	carbonate
Sawtooth 2	NA	85	NA	NA	IIICdd-	47.54 / 112.65	late Pleistocene	

References: Mudge, 1965

Moisture: NA Notes: The landslide fell from the oversteepened hanging wall of a thrust fault. Monolithologic and exhibits oriented clasts.

Substrate: NA

E58	0.27	NA	1400	12500	0.11	Japan	NA	NA
Yatsugatake-B Volcano	NA	NA	NA	NA	NA	NA / NA	Pleistocene	

References: Siebert, 1984

Moisture: NA Notes: NA

Substrate: NA

M33	0.25	45	900	5700	0.16	Terra Sirenum	unconfined	NA
Mars 108	5.5	70	NA	5700	IIICcbd	-14.6 / 179	NA	

References: This paper

Moisture: dry Notes: Lies in 15 km crater. Very "Blackhawk-like," ~7 km by ~ 2 km. Best picno: 436S10. Mosaic #: 1186

Substrate: NA

---

1. Rank 2. Name	3. Volume 4. Area	5. Thickness: a. Avg b. Max	6. Drop 7. Velocity	8. Length: a. Straight b. Curved	9. Fahr- böschung 10. Type	11. Location 12. Lat./Long.	13. Confinement 14. Age	15. Composition
E59	0.25	NA	1200	12000	0.10	Japan	NA	NA
Komagatake Volcano	NA	NA	NA	NA	NA	NA / NA	1640 A. D.	

References: Siebert, 1984

Moisture: NA Notes: NA

Substrate: NA

E60	0.25	NA	540	1600	0.34	Italy	heavy	limestone
Vaiont	NA	250	90	NA	IICdda	46.3 / -12.4	9 Oct. 1963	

References: Mueller, 1964; 1968

Moisture: NA Notes: Preceeded by 3 years of pre-landslide creep associated with dam filling. A bedding-plane failure initiated movement of the landslide. Collapse into full reservoir displaced water that killed thousands.

Substrate: NA

E	0.25	19	NA	NA	NA	Austria	NA	NA
Tschirgant	13.2	NA	NA	NA	NA	NA / NA	NA	

References: Heuberger, et. al., 1984

Moisture: NA Notes: NA

Substrate: NA

---

1. Rank 2. Name	3. Volume 4. Area	5. Thickness: a. Avg b. Max	6. Drop 7. Velocity	8. Length: a. Straight b. Curved	9. Fahr-böschung 10. Type	11. Location 12. Lat./Long.	13. Confinement 14. Age	15. Composition
E	0.246	NA	NA	NA	NA	Kirghizia, U.S.S.R.	NA	NA
Karasu	NA	NA	NA	NA	NA	NA / NA	NA	

References: This paper

Moisture: NA Notes: NA

Substrate: NA

E 6 1	0.24	23	1555	7900	0.20	California, U.S.A.	deflected-40°(CH)	granitic gneiss
Martinez Mtn.	10.36	120	128	9000	IIICbdd,b	33.58 / 116.28	late Pleistocene	

References: Bock, 1977; Baldwin, 1986

Moisture: dry Notes: Downslope-oriented foliation planes and perhaps subjacent detachment fault planes directed the initial movement. The slide is monolithologic, reverse graded and has sub-horizontal slip surfaces with movement-parallel striations. Arcuate transverse ridges defining lobate features near the toe suggest that landsliding occurred in several surges. Surface grain size; modal: 300 cm; maximum: 15 m.

Substrate: bedrock, alluvium

E 6 2	0.23	23	1400	8000	0.18	Japan	NA	NA
Myoko Volcano-B	10	NA	NA	NA	NA	NA / NA	7780 B. P.	

References: Siebert, 1984

Moisture: NA Notes: NA

Substrate: NA

---

1. Rank 2. Name	3. Volume 4. Area	5. Thickness: a. Avg b. Max	6. Drop 7. Velocity	8. Length: a. Straight b. Curved	9. Fahrböschung 10. Type	11. Location 12. Lat./Long.	13. Confinement 14. Age	15. Composition
E 6 3	0.23	NA	900	7000	0.13	California, U.S.A.	unconfined(DI-20°)	limestone
Silver Reef	NA	NA	100	7000	IIICbbd	34.36 / 116.78	Pleistocene	

References: Shreve, 1968a

Moisture: dry Notes: The landslide fell from the oversteepened hanging wall of a thrust fault. The landslide exposes preserved slope-normal stratigraphy, three-dimensional jigsaw puzzle breccia, a dozed marginal dike and a raised distal rim. Borders the Blackhawk landslide. Surface grain size; modal: 2.5 cm; maximum: 11 m.

Substrate: alluvium

M 3 4	0.2	67	2500	5500	0.45	Olympus Mons Caldera	unconfined	NA
Mars 141	3	120	NA	5500	IIICcbd	18.08 / 133.54	NA	

References: This paper

Moisture: dry Notes: Headscarp on inner wall of Olympus Mons caldera, SW caldera. Best picno: 474S22

Substrate: NA

L 2	0.2	10	1900	9000	0.21	Taurus-Littrow Valley	unconfined	impact breccia
Apollo 17	21	20	NA	9000	IIICdca	20.2 / -30.8	50-100 m.y.	

References: Howard, 1973a;b; Lucchitta, 1977

Moisture: NA Notes: Probably initiated by impact of secondaries from Tycho at top of massif.

Substrate: NA

---

1. Rank 2. Name	3. Volume 4. Area	5. Thickness: a. Avg b. Max	6. Drop 7. Velocity	8. Length: a. Straight b. Curved	9. Fahr-böschung 10. Type	11. Location 12. Lat./Long.	13. Confinement 14. Age	15. Composition
E64	0.2	43	675	2400	0.28	U.S.S.R.	NA	NA
Rarz	4.6	NA	NA	NA	NA	NA / NA	NA	

References: Gregorian, et al., 1983

Moisture: NA Notes: NA

Substrate: NA

M33	0.2	36	1100	4800	0.23	Gangis Chasma	unconfined	NA
Mars 74	5.5	60	NA	4800	IIICcbd	-7.65 / 44	NA	

References: This paper

Moisture: dry Notes: "Blackhawk like." Best picno: 014A31. Mosaic #:1381

Substrate: NA

E65	0.18	30	1620	5140	0.32	Italy	deflected-75°,15°(CH,DI-90°)	dolomite
Bormio	6	NA	225	NA	IIICd--	46.5 / -10.4	prehistoric	

References: Heim, 1932

Moisture: NA Notes: Monolithologic

Substrate: NA

---

1. Rank 2. Name	3. Volume 4. Area	5. Thickness: a. Avg b. Max	6. Drop 7. Velocity	8. Length: a. Straight b. Curved	9. Fahr- böschung 10. Type	11. Location 12. Lat./Long.	13. Confinement 14. Age	15. Composition
M 3 6	0.15	43	2000	4900	0.41	Iani Chaos	deflected (CH)	NA
Mars 118	3.5	65	NA	5000	IIICcbd,b	-4.91 / 18.83	NA	

References: This paper

Moisture: dry Notes: A very nice example of a IIICcbd, falling at a slight diagonal from a plateau into some jumbled terrain; 5 km long, 1 km wide. Best picno: 405B01. Mosaic #: 1382

Substrate: NA

E 6 6	0.15	5	4200	20000	0.21	Peru	deflected-multiple(CH)	granodiorite
Huascaran 1	30	NA	315	NA	IIIC	-9 / 77.5	pre-Columbian	

References: Hsü, 1975; Plafker and Erickson, 1978

Moisture: wet Notes: NA

Substrate: snow, alluvium

E 6 7	0.15	NA	1500	4350	0.34	Graubünden, Switz.	heavy	crystalline
Poschiavo	NA	270	260	NA	IIICdda	46.3 / -10	postglacial	

References: Heim, 1932

Moisture: NA Notes: The landslide is marked by a proximal trough.

Substrate: NA

---

1. Rank 2. Name	3. Volume 4. Area	5. Thickness: a. Avg b. Max	6. Drop 7. Velocity	8. Length: a. Straight b. Curved	9. Fahr- böschung 10. Type	11. Location 12. Lat./Long.	13. Confinement 14. Age	15. Composition
E68	0.15	NA	1560	5800	0.27	Graubünden, Switz.	deflected-90°,90°(CH,DI-18	dolomite +
Parpan	NA	NA	250	NA	IIICdda	46.8 / -9.5	0°) postglacial	crystalline

References: Heim, 1932

Moisture: NA Notes: The landslide exhibits preserved cross-slope stratigraphy, a proximal trough and multiple margins.

Substrate: NA

E69	0.14	NA	2210	11000	0.20	Bern, Switz.	deflected-35°(CH)	limestone
Kandertal	NA	NA	300	NA	IIC	46.5 / -7.67	postglacial	

References: Heim, 1932

Moisture: NA Notes: A bedding-plane failure initiated movement of this landslide. Monolithologic and exhibits a marginal trough.

Substrate: NA

E70	0.13	NA	650	2560	0.25	Alberta, Canada	unconfined	limestone
Upper Kananaskis	NA	NA	NA	2560	IICaa-	50.63 / 115.17	postglacial	

References: Locat and Cruden, 1977

Moisture: NA Notes: A bedding-plane failure initiated movement of this landslide.

Substrate: NA

---

1. Rank / 2. Name	3. Volume / 4. Area	5. Thickness: a. Avg / b. Max	6. Drop / 7. Velocity	8. Length: a. Straight / b. Curved	9. Fahrböschung / 10. Type	11. Location / 12. Lat./Long.	13. Confinement / 14. Age	15. Composition
E71	0.12	NA	800	6000	0.13	Japan	NA	NA
Kurohime Volcano	NA	NA	NA	NA	NA	NA / NA	Pleistocene	

References: Siebert, 1984

Moisture: NA Notes: NA

Substrate: NA

E72	0.12	NA	1840	6350	0.29	Glarus, Switz.	deflected-98°,74°(CH,DI)	limestone
Obersee	NA	NA	230	NA	IIC	47.1 / -9.1	postglacial	

References: Heim, 1932

Moisture: NA Notes: NA

Substrate: NA

E75	0.1	19	750	4400	0.17	Idaho, U.S.A.	unconfined(CH)	basalt
Carlson	5.2	75	NA	4700	IIICbab,d	44.28 / 113.73	Holocene	

References: Shaller, in press

Moisture: moist Notes: The crown of the headscarp intersected an anticlinal fold axis, suggesting that joints along the axis acted as detachment planes for the slidemass. A monolithologic landslide, which incorporated wet basaltic alluvium from the substrate during movement and generated a moist landslide with debris flow-like properties. The landslide also exhibits rare radial block bands with radially oriented blocks, a proximal to distal average grain size decrease, a short double margin and many rock-crested hummocks.

Substrate: alluvium

---

1. Rank 2. Name	3. Volume 4. Area	5. Thickness: a. Avg b. Max	6. Drop 7. Velocity	8. Length: a. Straight b. Curved	9. Fahr- böschung 10. Type	11. Location 12. Lat./Long.	13. Confinement 14. Age	15. Composition
E74	0.1	42	725	2970	0.24	U.S.S.R.	NA	NA
Ainy	2.4	NA	NA	NA	NA	NA / NA	NA	

References: Adushkin, personal communication, 1990

Moisture: NA Notes: NA

Substrate: NA

M37	0.1	33	4200	7500	0.56	Tithonium Chasma	NA	NA
Mars 73	3	NA	NA	NA	NA	-4.9 / 84.8	NA	

References: McEwen, 1989

Moisture: NA Notes: NA

Substrate: NA

E73	0.1	43	708	2340	0.30	U.S.S.R.	NA	NA
Magian	2.3	NA	NA	NA	NA	NA / NA	prehistoric	

References: Gregorian, et al., 1983

Moisture: NA Notes: NA

Substrate: NA

1. Rank 2. Name	3. Volume 4. Area	5. Thickness: a. Avg b. Max	6. Drop 7. Velocity	8. Length: a. Straight b. Curved	9. Fahr-böschung 10. Type	11. Location 12. Lat./Long.	13. Confinement 14. Age	15. Composition
E	0.086	NA	NA	NA	NA	U.S.S.R.	NA	NA
Kapkatash	NA	NA	NA	NA	NA	NA / NA	NA	

References: This paper

Moisture: NA Notes: NA

Substrate: NA

E76	0.086	55	320	1220	0.26	Alberta, Canada	unconfined	limestone, dolomite
Medicine Lake	1.55	250	NA	NA	IICcbd	52.88 / 117.84	Holocene	

References: Cruden, 1976

Moisture: NA Notes: A bedding-plane failure initiated movement of this landslide. The landslide is marked by a proximal trough.

Substrate: NA

E77	0.08	NA	1450	5500	0.26	Graubünden, Switz.	deflected-110°-75°(CH)	crystalline
Scima di Saoseo	NA	NA	210	NA	IIIC	46.4 / -10.1	postglacial	

References: Heim, 1932

Moisture: NA Notes: Originated on opposite side of mountain peak which shed the Corno di Dosde landslide.

Substrate: NA

---

1. Rank / 2. Name	3. Volume / 4. Area	5. Thickness: a. Avg / b. Max	6. Drop / 7. Velocity	8. Length: a. Straight / b. Curved	9. Fahrböschung / 10. Type	11. Location / 12. Lat./Long.	13. Confinement / 14. Age	15. Composition
E78	0.08	23	750	2200	0.34	Novaya	unconfined	NA
U.S.S.R. Artificial 1	3.5	NA	210	2200	NA	72 / -55	late 20th century	

References: Adushkin, personal communication, 1990

Moisture: NA Notes: Triggered by an underground nuclear(?) explosion approximately 1 km underground.

Substrate: NA

E79	0.075	3	4000	18600	0.22	Peru	deflected-multiple(CH,DI-35°)	granodiorite
Huascaran 3	22.5	NA	280	NA	IIIC	-9 / 77.5	31 May 1970	

References: Plafker and Erickson, 1978

Moisture: wet Notes: The landslide occurred from a peak whose support was removed by the 1962 landslide. Triggered by an earthquake, the slide overran Yungay (18,000 inhabitants) as a "10-story breaking wave." Accompanied by dust, mud-charged wind blasts, rumbling and a spattering of boulders hundreds of meters from the landslide. The landslide incorporated wet snow during its descent over a glacier, transforming it into a giant mudflow. The landslide spattered out boulders at a velocity of up to 1000 km/hr.

Substrate: snow, alluvium

E80	0.065	12	700	7000	0.10	NW Argentina	unconfined(CH)	granite
Loma Redonda	5.52	15	NA	7000	IIICbbd	-27.22 / 66.22	middle Pleistocene	

References: Fauque and Strecker, 1988

Moisture: dry Notes: The landslide fell from the oversteepened hanging wall of a reverse fault. A monolithologic landslide which exhibits reverse grading. Surface grain size; modal: 200 cm; maximum: 20 m.

Substrate: alluvium

---

1. Rank 2. Name	3. Volume 4. Area	5. Thickness: a. Avg b. Max	6. Drop 7. Velocity	8. Length: a. Straight b. Curved	9. Fahr-böschung 10. Type	11. Location 12. Lat./Long.	13. Confinement 14. Age	15. Composition
E 8 1	0.065	NA	550	3200	0.17	Nwst Terr., Canada	deflected-100°(CH)	carbonate
U-turn	NA	NA	160	4300	IICdda	65 / 131.5	Holocene	

References: Eisbacher, 1979

Moisture: NA Notes: A bedding-plane failure initiated movement of this landslide. Monolithologic, displays widening and narrowing in channeled portion and abrupt changes in thickness.

Substrate: NA

E(u)	0.055	8	NA	NA	NA	British Columbia,	NA	Deltaic sediments
Kitimat	6.8	NA	NA	NA	NA	53.98 / 128.68	1975 A.D.	

References: This paper

Moisture: NA Notes: NA

Substrate: NA

E 8 2	0.054	9	800	6500	0.12	Alaska, U.S.A.	unconfined(CH)	basalt
Mageik	5.8	NA	88	8500	IIICbca	58.13 / 155.25	1912 A.D.	

References: Griggs, 1922

Moisture: NA Notes: The landslide was shed from a large cirque-like headscarp. This landslide coincided with the 1912 eruption of Katmai volcano, 20 km from the site of the slide. It was monolithologic, might have incorporated mobile substrate materials, displayed debris pyramids and a proximal to distal grain size decrease. Surface grain size; modal: 3 m; maximum: 23 m.

Substrate: NA

---

1. Rank 2. Name	3. Volume 4. Area	5. Thickness: a. Avg b. Max	6. Drop 7. Velocity	8. Length: a. Straight b. Curved	9. Fahr-böschung 10. Type	11. Location 12. Lat./Long.	13. Confinement 14. Age	15. Composition
E83	0.05	11	651	3476	0.19	California, U.S.A.	deflected-50°(CH)	dacite
Chaos Jumbles 2	4.4	16	198	3660	IIICbac	40.53 / 121.55	1540-1620 A.D.	

References: Eppler, et. al., 1987

Moisture: NA Notes: Second of three overlapping landslide deposits at Chaos Crags. Monolithologic with downhill-oriented clasts. Surface grain size; modal: 5 cm; maximum: 1 m.

Substrate: NA

E84	0.05	NA	850	5800	0.15	Nwst. Terr., Canada	deflected-90°(CH)	carbonate
Nozzle	NA	NA	NA	6900	IICaca	65.03 / 131.97	Holocene	

References: Eisbacher, 1979

Moisture: NA Notes: A bedding-plane failure initiated movement of this landslide. Rock spattering zone, monolithologic.

Substrate: NA

E85	0.05	NA	300	1350	0.22	China	NA	loess
Sale Mountain	NA	NA	NA	NA	IA-d-	NA / NA	March 1983	

References: Gongxian and Bangdong, 1984

Moisture: NA Notes: Damaged 4 villages.

Substrate: NA

---

1. Rank / 2. Name	3. Volume / 4. Area	5. Thickness: a. Avg / b. Max	6. Drop / 7. Velocity	8. Length: a. Straight / b. Curved	9. Fahrböschung / 10. Type	11. Location / 12. Lat./Long.	13. Confinement / 14. Age	15. Composition
E86	0.047	18	1220	3080	0.40	British Columbia, Can.	heavy	metavolcanics
Hope	2.65	79	160	3080	IICddc,a	NA / NA	9 Jan. 1965	

References: Mathews and McTaggart, 1969

Moisture: NA Notes: A prior prehistoric landslide removed underlying support from the slope. Downslope-oriented foliation planes directed the initial movement. The landslide exhibits preserved slope-parallel stratigraphy, debris pyramids, a proximal trough and radial block bands. Minor seismic activity occurred at about the time of the landslide, of magnitude 3.1 and 3.2, but the exact time of landsliding is not known relative to these events. Surface grain size; modal: 60 cm; maximum: 24 m.

Substrate: NA

---

1. Rank / 2. Name	3. Volume / 4. Area	5. Thickness: a. Avg / b. Max	6. Drop / 7. Velocity	8. Length: a. Straight / b. Curved	9. Fahrböschung / 10. Type	11. Location / 12. Lat./Long.	13. Confinement / 14. Age	15. Composition
E87	0.044	7	770	4550	0.17	California, U.S.A.	deflected-50°(CH)	dacite
Chaos Jumbles 1	6.4706	9.5	284	5040	IIICbac	40.53 / 121.55	1540-1620 A.D.	

References: Eppler, et. al., 1987

Moisture: NA Notes: Largest and oldest of three overlapping deposits. Monolithologic, with downhill-oriented clasts. Surface grain size; modal: 5 cm; maximum: 1 m.

Substrate: NA

---

1. Rank / 2. Name	3. Volume / 4. Area	5. Thickness: a. Avg / b. Max	6. Drop / 7. Velocity	8. Length: a. Straight / b. Curved	9. Fahrböschung / 10. Type	11. Location / 12. Lat./Long.	13. Confinement / 14. Age	15. Composition
E88	0.04	14	1300	6800	0.19	Arizona, U.S.A.	unconfined(DI-20°)	dolomite
El Capitan	2.8	35	NA	6800	IIC	33.17 / 110.78	Late Miocene	

References: Krieger, 1977; Yarnold and Lombard, 1989

Moisture: NA Notes: A bedding-plane failure probably initiated movement of this landslide. This partially eroded landslide exhibits preserved slope parallel stratigraphy, reverse grading, incorporated inert substrate material, three-dimensional jigsaw puzzle breccia, basal strata disruption, sub-horizontal slip surfaces, clastic dike intrusion, thrust faults and imbrication and load structures.

Substrate: NA

---

1. Rank 2. Name	3. Volume 4. Area	5. Thickness: a. Avg b. Max	6. Drop 7. Velocity	8. Length: a. Straight b. Curved	9. Fahrböschung 10. Type	11. Location 12. Lat./Long.	13. Confinement 14. Age	15. Composition
E89	0.04	NA	700	3000	0.23	British Columbia, Can.	unconfined	shale, graywacke, conglomerate
Stalk Lakes	NA	NA	NA	3000	IICb-b	57.2 / 127.6	postglacial	

References: Eisbacher, 1971; Mollard, 1977

Moisture: NA Notes: A bedding-plane failure initiated movement of this landslide. Surfaced by debris cones.

Substrate: NA

E90	0.0391	11	660	3220	0.20	Alberta, Canada	partial	carbonates
Mount Kitchener	3.63	100	NA	NA	IICdd-	52.22 / 117.27	Holocene	

References: Cruden, 1976

Moisture: NA Notes: A bedding-plane failure initiated movement of this landslide. Monolithologic.

Substrate: NA

E91	0.038	NA	610	3400	0.18	Wyoming, U.S.A.	deflected-90°,90°(CH,DI-18 0°)	sandstone, siltstone
Gros Ventre	NA	70	165	NA	IICdda	NA / NA	23 June 1925	

References: Alden, 1928; Voight, 1983

Moisture: NA Notes: The landslide was predicted from subsurface noises five years before initiation. A bedding-plane failure initiated its movement. The landslide was observed to slide into a river valley, accompanied by dust, noise and, in places, a wind blast. It exhibits indications of reverse grading and preserved slope-parallel stratigraphy.

Substrate: NA

---

1. Rank 2. Name	3. Volume 4. Area	5. Thickness: a. Avg b. Max	6. Drop 7. Velocity	8. Length: a. Straight b. Curved	9. Fahr- böschung 10. Type	11. Location 12. Lat./Long.	13. Confinement 14. Age	15. Composition
E92	0.037	5	900	6500	0.14	NW Argentina	unconfined	granite
Avalancha del Zarzo 1	7.53	15	NA	6500	IIICbbd	-27.2 / 66.22	middle Pleistocene	

References: Fauque and Strecker, 1988

Moisture: dry Notes: The landslide fell from the oversteepened hanging wall of a reverse fault. Monolithologic, with a distinct moraine-like morphology and inverse grading. The northern levee displays obliquely trending imbricated ridges that point uphill and into the center of the slide and the frontal lobe shows radial outward ridging. The flow was greatest and moved farthest in the axial parts of the slide. Surface grain size; modal: 200 cm; maximum: 20 m.

Substrate: alluvium

E93	0.0365	14	830	3000	0.28	Alberta, Canada	partial	limestone
Frank	2.67	14	175	3000	IIICaac	49.6 / 114.4	29 April 1903	

References: Daly, et al., 1912; Cruden and Hungr, 1986

Moisture: dry Notes: The slide was preceeded by 7 months of rock bursts in a coal mine at the base of the slope. The crown intersected an anticlinal fold axis. It was accompanied by a wind blast, thick dust, a hissing noise and lightning. It is monolithologic, exhibits reverse grading, incorporated some overrun material from the Crowsnest River, has debris pyramids, a proximal trough, a raised distal rim, block scour and dozed wet material up in front of it. Surface grain size; modal: 100 cm; maximum: 11 m.

Substrate: alluvium, mud

E94	0.035	NA	1100	5175	0.21	Glarus, Switzerland	unconfined(CH)	conglomerate + marl
Goldau	NA	100	140	7620	IICada	47.1 / -8.6	2 September 1806	

References: Heim, 1932

Moisture: NA Notes: The slide was preceeded by noises and surficial cracks. A bedding-plane failure initiated movement of the landslide. It began by slowly sliding but rapidly built up speed and broke up. Dust, a wind blast, noise and luminescence accompanied the slide, which milled up obstacles in its path. The landslide contains preserved slope-parallel stratigraphy, reverse grading and multiple margins.

Substrate: NA

1. Rank 2. Name	3. Volume 4. Area	5. Thickness: a. Avg b. Max	6. Drop 7. Velocity	8. Length: a. Straight b. Curved	9. Fahr- böschung 10. Type	11. Location 12. Lat./Long.	13. Confinement 14. Age	15. Composition
E95	0.035	NA	450	2660	0.17	Yukon Terr., Canada	deflected-35°-15°	carbonate
Triple	NA	NA	200	2770	IICa-a	64.62 / 132.73	Holocene	

References: Eisbacher, 1979

Moisture: NA Notes: A bedding-plane failure initiated movement of this landslide. Monolithologic, apparently shed a side lobe of 10 million cubic meters volume that had about the same mobility as the main mass. The landslide spattered rock beyond its margin during emplacement.

Substrate: NA

E96	0.033	9	183	2515	0.07	eastern California	unconfined	rhyolitic ash, blocks
Panum	3.5	15	NA	2515	IIICaab	37.95 / 119.05	1345+-20 A.D.	

References: Sieh and Bursik, 1986

Moisture: dry Notes: Monolithologic, with extreme basal strata deformation. Coarseness and sorting decrease away from the source. Paleomagnetic analysis suggests emplacement temperatures greater than 600°C. Formed from collapse of a partially molten rhyolite dome.

Substrate: mud

E98	0.03	NA	950	4100	0.23	Nwst. Terr., Canada	deflected-35°,125°(CH,DI-1 90°)	carbonate
North Arm	NA	NA	250	4600	IICdda	62.25 / 127.25	about 200 B. P.	

References: Eisbacher, 1979

Moisture: NA Notes: Monolithologic

Substrate: NA

---

1. Rank 2. Name	3. Volume 4. Area	5. Thickness: a. Avg b. Max	6. Drop 7. Velocity	8. Length: a. Straight b. Curved	9. Fahr-böschung 10. Type	11. Location 12. Lat./Long.	13. Confinement 14. Age	15. Composition
E98	0.03	NA	1900	5450	0.35	Wallis, Switz.	deflected-65°-50°(CH)	limestone + ice
Diablerets 2	NA	NA	NA	5500	IIICdcc	46.3 / -7.2	23 July 1749	

References: Heim, 1932; Eisbacher and Clague, 1984

Moisture: dry Notes: The slide was preceeded by noises from the slidemass. The base of the headscarp intersected a fold axis, suggesting that joints along the axis acted as detachment planes for the slidemass. Strongly channeled, with two substantial impacts from valley walls.

Substrate: rock, soil The slide was accompanied by thick dust and luminescence. It completely covered the smaller 1714 deposit.

E99	0.03	NA	1050	3900	0.27	St. Gallen, Switz.	deflected(CH)	limestone
Voralpsee	NA	NA	160	NA	IIIC	47.15 / -9.4	prehistoric	

References: Heim, 1932

Moisture: NA Notes: NA

Substrate: NA

E100	0.03	4	1100	5000	0.22	Alaska, U.S.A.	unconfined	sandstone, siltstone + snow
Sherman	8.25	6	185	NA	IIICaab	60.55 / 145.17	27 March 1964	

References: Shreve, 1966; McSaveney, 1978

Moisture: NA Notes: A bedding-plane failure initiated this landslide. Probably triggered by the 1964 Alaska earthquake. The slide fell onto the Sherman glacier. It exhibited preserved slope-parallel stratigraphy, reverse grading, incorporated substrate material (dry snow), three-dimensional jigsaw puzzle breccia, clastic dike intrusion (again, dry snow), debris pyramids, a dozed marginal dike, oriented clasts and radial block bands. Surface grain size; modal: 30 cm; maximum: 17 m.

Substrate: NA

---

1. Rank / 2. Name	3. Volume / 4. Area	5. Thickness: a. Avg / b. Max	6. Drop / 7. Velocity	8. Length: a. Straight / b. Curved	9. Fahrböschung / 10. Type	11. Location / 12. Lat./Long.	13. Confinement / 14. Age	15. Composition
E101	0.028	NA	425	1550	0.27	Montana, U.S.A.	heavy	dolomite, gneiss, schist
Madison	NA	67	160	1550	IIICdda	44.83 / 111.42	17 Aug. 1959	

References: Hadley, 1960; 1978

Moisture: NA Notes: Landslide was triggered by Hebgen Lake earthquake and was associated with mud splattering and a very strong wind blast. The landslide exhibits preserved slope-normal bedding, reverse grading and a proximal trough. Surface grain size; modal: 30 cm; maximum: 10 m.

Substrate: NA

E102	0.027	3	1550	6100	0.25	Alaska, U.S.A.	unconfined	NA
Schwan	9	NA	NA	6100	IIICba-	60.88 / 145.18	27 March 1964	

References: Post, 1967

Moisture: NA Notes: This deposit was probably triggered by the 1964 Alaska earthquake, though it was not observed at emplacement. The landslide deposit fell across a snow-covered glacier. It was surrounded by a discontinuous dust layer 30 m or more in width.

Substrate: snow

E103	0.026	11	430	2910	0.15	California, U.S.A.	deflected-50°(CH)	dacite
Chaos Jumbles 3	2.43	15	350	3010	IIICbac	40.53 / 121.55	1540-1620 A.D.	

References: Eppler, et. al., 1987

Moisture: NA Notes: Last and smallest of three rockfall avalanche deposits from the Chaos Crags in the time period 1540-1620 A.D.. Monolithologic, with downhill-oriented clasts. Surface grain size; modal: 15 cm; maximum: 5 m.

Substrate: NA

---

1. Rank 2. Name	3. Volume 4. Area	5. Thickness: a. Avg b. Max	6. Drop 7. Velocity	8. Length: a. Straight b. Curved	9. Fahr- böschung 10. Type	11. Location 12. Lat./Long.	13. Confinement 14. Age	15. Composition
E104	0.026	3	3350	10500	0.32	Alaska, U.S.A.	deflected-45°-60°-35°(CH)	NA
Fairweather	8.5	NA	NA	NA	IIICaab	58.88 / 137.67	1965 A.D.	

References: Post, 1967

Moisture: NA Notes: Emplaced on a snow-covered glacier.

Substrate: snow

E105	0.025	NA	400	1000	0.40	Alberta, Canada	NA	sedimentary
Cadomin	NA	NA	NA	NA	IIC	52.97 / 117.34	postglacial	

References: Locat and Cruden, 1977

Moisture: NA Notes: NA

Substrate: NA

E106	0.025	NA	1035	6900	0.15	Brit. Columbia, Canada	deflected-20°-50°-60°(CH)	dacite
Rubble Creek	NA	100	72	NA	IIICbaa	49.96 / 123.13	1855 or 1856	

References: Moore and Mathews, 1978

Moisture: NA Notes: Monolithologic. Surface grain size; maximum: 5 m.

Substrate: NA

---

1. Rank 2. Name	3. Volume 4. Area	5. Thickness: a. Avg b. Max	6. Drop 7. Velocity	8. Length: a. Straight b. Curved	9. Fahr-böschung 10. Type	11. Location 12. Lat./Long.	13. Confinement 14. Age	15. Composition
E107	0.023	3	1300	7700	0.17	Alaska, U.S.A.	unconfined(CH)	NA
Allen 4	7.5	NA	NA	NA	IIICbab	60.78 / 144.93	1965 A.D.	

References: Post, 1967

Moisture: NA Notes: The landslide deposit fell across a snow-covered glacier. The deposit was surrounded by a discontinuous dust layer 30 m or more in width around its margin.

Substrate: snow

E108	0.021	5	800	7000	0.11	NW Argentina	unconfined	granite
Loma de la Aspereza	4.25	15	266	7000	IIICcbd	-27.13 / 66.2	middle Pleistocene	

References: Fauque and Strecker, 1988

Moisture: dry Notes: The landslide fell from the oversteepened hanging wall of a reverse fault. A monolithologic landslide which exhibits reverse grading and oblique imbricated surface ridges. Surface grain size; modal: 200 cm; maximum: 20 m.

Substrate: alluvium

E109	0.021	70	800	2666	0.30	S. island, New Zealand	heavy	indurated conglomerate
Stanley	0.3	140	225	2666	NA	-41.01 / -172.61	17 June1929	

References: Adams, 1981

Moisture: NA Notes: Formed during 1929 Buller earthquake. Impounded stream runoff to form Lake Stanley.

Substrate: NA

---

1. Rank / 2. Name	3. Volume / 4. Area	5. Thickness: a. Avg / b. Max	6. Drop / 7. Velocity	8. Length: a. Straight / b. Curved	9. Fahrböschung / 10. Type	11. Location / 12. Lat./Long.	13. Confinement / 14. Age	15. Composition
E110	0.02	NA	290	2850	0.10	Yukon Terr., Canada	deflected-30°-30°-20°(CH)	carbonate
Damocles	NA	NA	NA	3050	IICdca	64.28 / 131.13	Holocene	

References: Eisbacher, 1979

Moisture: NA Notes: A bedding-plane failure initiated movement of this landslide. Monolithologic, continuous zone of spattered rock occurs along one lateral margin of the deposit. Surface grain size; maximum: 9 m.

Substrate: NA

E	0.02	3	NA	NA	NA	Arizona, U.S.A.	NA	granodiorite, sed. rocks
Cross Hill	6	50	NA	NA	NA	32 / 110.75	Oligocene-Miocene	

References: Yarnold and Lombard, 1989

Moisture: NA Notes: This megabreccia deposit exhibits reverse grading, inert incorporated substrate material, three-dimensional jigsaw puzzle breccia, basal strata disruption, sub-horizontal slip surfaces and intruded clastic dikes.

Substrate: NA

E111	0.02	NA	1190	2670	0.45	Italy/Switz.	deflected-70°(CH)	NA
Corno di Dosde	NA	NA	160	3750	IIIC	46.55 / -10.3	postglacial	

References: Heim, 1932

Moisture: NA Notes: On opposite face of mountain peak from which Scima di Saoaeo landslide originated.

Substrate: NA

---

1. Rank 2. Name	3. Volume 4. Area	5. Thickness: a. Avg b. Max	6. Drop 7. Velocity	8. Length: a. Straight b. Curved	9. Fahr-böschung 10. Type	11. Location 12. Lat./Long.	13. Confinement 14. Age	15. Composition
E112	0.02	3	1200	6700	0.18	Alaska, U.S.A.	unconfined(DI-30°)	NA
Steller	7.5	NA	NA	NA	IIICba-	60.58 / 143.28	27 March 1964	

References: Post, 1967

Moisture: NA Notes: Probably triggered by great 1964 Alaska earthquake, though not observed at emplacement. Deposited on snow-covered glacier.

Substrate: snow

E113	0.02	NA	790	3600	0.22	Washington, U.S.A.	deflected-40°(CH)	arkose
Pasayten	NA	240	NA	NA	IICdda	48.83 / 120.7	11-13000 B.P.	

References: Waitt, 1979

Moisture: NA Notes: A bedding-plane failure initiated movement of this landslide. Dispersed on wasting Cordilleran glacier. Essentially monolithologic. Surface grain size; maximum: 5 m.

Substrate: snow

E	0.02	NA	NA	NA	NA	Wallis, Switz.	NA	limestone + ice
Diablerets 1	NA	NA	NA	NA	NA	46.4 / -7.3	23 June 1714	

References: Heim, 1932; Eisbacher and Clague, 1984

Moisture: NA Notes: The base of the headscarp intersected a fold axis, suggesting that joints along the axis acted as detachment planes for the slidemass. First of two landslides in this area, this one later being covered over by Diablerets 2. 15 killed. Landslide preceeded by noises from the mountain. Story of one survivor told in "Derborence" by C. F. Ramuz.

Substrate: NA

---

1. Rank 2. Name	3. Volume 4. Area	5. Thickness: a. Avg b. Max	6. Drop 7. Velocity	8. Length: a. Straight b. Curved	9. Fahr- böschung 10. Type	11. Location 12. Lat./Long.	13. Confinement 14. Age	15. Composition
E114	0.015	NA	1900	3333	0.57	Switzerland	heavy	gneiss
Biasca	NA	NA	160	4042	IIICdda	46.4 / -9.1	30 Sept. 1513	

References: Eisbacher and Clague, 1984

Moisture: NA Notes: Dammed a river, forming a lake that later broke through, killing 600.

Substrate: NA

E115	0.015	NA	740	1950	0.38	Graubünden, Switz.	heavy	schist
Disentis	NA	NA	200	2000	IIICdda	46.7 / -8.8	29 June 1683	

References: Heim, 1932

Moisture: NA Notes: The landslide exhibits a proximal trough.

Substrate: NA

E	0.015	NA	600	NA	NA	New Zealand	NA	sandstone
Matiri	NA	NA	NA	NA	NA	-41.66 / -172.3	290 B.P.	

References: Adams, 1981

Moisture: NA Notes: Landslide dammed a river forming Lake Matiri. Overtopping of the landslide caused a large mudflow.

Substrate: NA

---

1. Rank 2. Name	3. Volume 4. Area	5. Thickness: a. Avg b. Max	6. Drop 7. Velocity	8. Length: a. Straight b. Curved	9. Fahr-böschung 10. Type	11. Location 12. Lat./Long.	13. Confinement 14. Age	15. Composition
E116	0.013	2	4200	19000	0.22	Peru	deflected-50°-70°(CH)	granodiorite
Huascaran 2	6	NA	170	NA	IIIC	-9 / 77.5	10 January 1962	

References: Plafker and Erickson, 1978

Moisture: wet Notes: Landslide was observed to began with a rockfall, followed by rapid "bobsled-like" down-valley transport banking up on outsides of bends. Strong associated wind blast. The landslide incorporated wet snow during its descent over a glacier, transforming it into a giant mudflow.

Substrate: snow, alluvium

E117	0.012	120	500	1700	0.29	Siberia, U.S.S.R.	heavy	cataclased granite
Angarakan	0.1	70	NA	NA	IIICdda	56.3 / -113	250-300 B. P.	

References: Solonenko, et. al., 1984

Moisture: NA Notes: The landslide exhibits a proximal trough. Surface grain size; maximum: 10 m.

Substrate: NA

E118	0.012	NA	1600	3704	0.43	Italy	deflected-80°(CH)	gneiss
Antronapiana	NA	NA	NA	4167	IIICba-	46.1 / -8.2	27 July 1642	

References: Eisbacher and Clague, 1984

Moisture: NA Notes: Killed 93 people.

Substrate: NA

---

1. Rank 2. Name	3. Volume 4. Area	5. Thickness: a. Avg b. Max	6. Drop 7. Velocity	8. Length: a. Straight b. Curved	9. Fahr-böschung 10. Type	11. Location 12. Lat./Long.	13. Confinement 14. Age	15. Composition
E119	0.0102	5	920	2490	0.37	Alberta, Canada	unconfined	quartzite
Jonas Creek South	2.06	5	NA	NA	IIC-a-	52.43 / 117.41	Holocene	

References: Cruden, 1976

Moisture: NA Notes: A bedding-plane failure initiated movement of this landslide. Monolithologic.

Substrate: NA

E120	0.01	NA	800	3400	0.24	Switzerland	unconfined(CH)	Glacial debris, breccia
Corbeyrier-Yvorne	NA	NA	NA	3400	IICdd-	46.4 / -7	4 March 1584	

References: Eisbacher and Clague, 1984

Moisture: NA Notes: The slide was preceeded by ground cracking and noises. Its velocity was so great that the front locally became airborne as it cleared slight elevations in the track, jumping over several plots and grape stands without doing any damage. Killed 328 people.

Substrate: NA

E121	0.01	2	1490	4560	0.33	Karakoram, Pakistan	deflected-35°(CH)	schist and marble
Bualtar 1	4.1	10	223	4800	IICdaa	37 / -72	29 July 1986	

References: Hewett, 1988

Moisture: NA Notes: The landslide exhibits preserved slope-parallel bedding and reverse grading. It occurred during melting of heavy snowpack and rains. Meltwater from diurnal freeze-thaw triggered the failures on successive days late in the day. Beneath the surface 15-35% fines but only 5% or less clay. Particles finer than intermediate sand dispersed through the mass during emplacement. Surface grain size; modal: 200 cm; maximum: 44 m.

Substrate: snow

---

1. Rank / 2. Name	3. Volume / 4. Area	5. Thickness: a. Avg / b. Max	6. Drop / 7. Velocity	8. Length: a. Straight / b. Curved	9. Fahr-böschung / 10. Type	11. Location / 12. Lat./Long.	13. Confinement / 14. Age	15. Composition
E122	0.01	NA	610	2130	0.29	Glarus, Switz.	deflected-50°(CH)	slate
Elm	NA	50	150	2375	IIICdcc	46.9 / -9.2	11 Sept. 1881	

References: Buss and Heim, 1881; Heim, 1932

Moisture: dry Notes: The best witnessed large landslide. Triggered by slate mining activities. Preceeded by loud creaking. It was emplaced via an air launch and was associated with dust, a localized wind blast, deep rattling noise, milling of overrun objects and luminescence. It was observed to come to an abrupt halt. When fresh, the slide exhibited preserved slope-normal stratigraphy, rock spattering, debris pyramids, a proximal trough, a dozed marginal dike, radial block bands and block scour.

Substrate: soil

E123	0.01	NA	950	4500	0.21	Yukon Terr., Canada	deflected-45°(CH)	carbonate
Twin Slides 1	NA	NA	NA	4800	IICdca	65.27 / 133.23	Holocene	

References: Eisbacher, 1979

Moisture: NA Notes: Forms left branch of two simultaneous landslides down different drainage channels originating in single rockfall. Monolithologic. Widening and narrowing of debris lobe suggests pulse-like motion.

Substrate: NA

E124	0.01	NA	900	3600	0.25	Yukon Terr., Canada	deflected-50°(CH)	carbonate
Twin Sildes 2	NA	NA	110	4200	IICdca	65.27 / 133.23	Holocene	

References: Eisbacher, 1979

Moisture: NA Notes: A bedding-plane failure initiated movement of this landslide. Right-hand branch of twin landslides produced by same rockfall which travelled down separate channels. Monolithologic. Widening and narrowing of debris lobe suggests pulse-like motion.

Substrate: NA

---

1. Rank 2. Name	3. Volume 4. Area	5. Thickness: a. Avg b. Max	6. Drop 7. Velocity	8. Length: a. Straight b. Curved	9. Fahr-böschung 10. Type	11. Location 12. Lat./Long.	13. Confinement 14. Age	15. Composition
E	0.008	NA	1400	NA	NA	Italy	NA	carbonate
Bocca di Brenta	NA	NA	NA	NA	NA	46.2/ -10.9	May 1882	

References: Eisbacher and Clague, 1984

Moisture: NA Notes: NA

Substrate: NA

E125	0.008	17	600	1500	0.40	Novaya	unconfined	NA
U.S.S.R. Artificial 2	0.48	NA	NA	1500	NA	72/ -55	late 20th century	

References: Adushkin, personal communication, 1990

Moisture: NA Notes: Triggered by an underground nuclear(?) explosion approximately 1 km underground.

Substrate: NA

E126	0.007	2	1430	3550	0.40	Karakorum, Pakistan	deflected-35°(CH)	schist and marble
Bualtar 2	3.3	10	NA	3700	IICbab	37/ -72	30 July 1986	

References: Hewett, 1988

Moisture: NA Notes: The landslide exhibits preserved slope-parallel bedding and reverse grading. It occurred during melting of heavy snowpack and rains. Meltwater from diurnal freeze-thaw triggered the failures on successive days late in the day. Beneath the surface 15-35% fines but only 5% or less clay. Particles finer than intermediate sand dispersed through the mass during emplacement. Surface grain size; modal: 200 cm; maximum: 44 m.

Substrate: snow

---

1. Rank 2. Name	3. Volume 4. Area	5. Thickness: a. Avg b. Max	6. Drop 7. Velocity	8. Length: a. Straight b. Curved	9. Fahr-böschung 10. Type	11. Location 12. Lat./Long.	13. Confinement 14. Age	15. Composition
E127	0.007	15	400	1550	0.26	N. W. T., Canada	deflected-90°(CH)	limestone
North Nahanni	0.47	NA	120	1850	IICdda	62.27 / 124.18	5 Oct. 1985	

References: Evans, et. al., 1987

Moisture: NA Notes: A fault formed a detachment surface for the upper end of the headscarp. Triggered by the Oct. 1985 North Nahanni earthquake (M = 6.6). Preserved slope-parallel stratigraphy suggested by variation in the weathered color and modal size of blocks in the deposit. Also exhibits a proximal to distal clast size decrease. At the distal margin and along lateral margins spruce trees were toppled with their tops pointing into the slide mass. Suggests no air blast.

Substrate: NA

E128	0.006	NA	650	3000	0.22	Kola Peninsula,	deflected-75°-55°(CH)	ice + mine tailings
Chibins 9	NA	NA	NA	NA	NA	68 / -37	late 20th century	

References: Adushkin, personal communication, 1990

Moisture: NA Notes: Failure of mine dump due to oversteepening of slope.

Substrate: NA

E129	0.006	2	1400	4500	0.31	Alaska, U.S.A.	deflected-40°(DI-5°)	NA
Sioux	3	NA	NA	NA	IIICda-	60.53 / 144.32	27 March 1964	

References: Post, 1967

Moisture: NA Notes: Landslide probably triggered by 1964 Alaska earthquake. Landslide was emplaced on snow.

Substrate: snow

---

1. Rank / 2. Name	3. Volume / 4. Area	5. Thickness: a. Avg / b. Max	6. Drop / 7. Velocity	8. Length: a. Straight / b. Curved	9. Fahrböschung / 10. Type	11. Location / 12. Lat./Long.	13. Confinement / 14. Age	15. Composition
E130	0.0055	NA	590	1400	0.42	Switzerland	NA	NA
Wengen 2	NA	NA	NA	NA	NA	NA / NA	NA	

References: Hsü, 1975

Moisture: NA Notes: NA

Substrate: NA

E131	0.0054	5	880	3250	0.27	Alberta, Canada	partial	quartzite
Jonas Creek North	1.08	NA	NA	NA	IICda-	52.43 / 117.41	Holocene	

References: Cruden, 1976

Moisture: NA Notes: Monolithologic

Substrate: NA

E132	0.005	5	850	5000	0.17	NW Argentina	unconfined	granite
Avalancha del Zarzo 2	1	8	NA	5000	IIICcbd	-27.22 / 66.22	middle Pleistocene	

References: Fauque and Strecker, 1988

Moisture: dry Notes: The landslide fell from the oversteepened hanging wall of a reverse fault. Monolithologic, with a distinct moraine-like morphology and inverse grading. The northern levee displays obliquely trending imbricated ridges that point uphill and into the center of the slide and the frontal lobe shows radial outward ridging. The flow was greatest and moved farthest in the axial parts of the slide. Surface grain size; modal: 200 cm; maximum: 20 m.

Substrate: alluvium

---

1. Rank 2. Name	3. Volume 4. Area	5. Thickness: a. Avg b. Max	6. Drop 7. Velocity	8. Length: a. Straight b. Curved	9. Fahr-böschung 10. Type	11. Location 12. Lat./Long.	13. Confinement 14. Age	15. Composition
E133	0.005	NA	750	2350	0.32	Italy	unconfined	carbonate
Antelao	NA	NA	NA	2400	IICb--	46.5 / -12.3	21 April 1814	

References: Eisbacher and Clague, 1984

Moisture: NA Notes: 300 killed. New houses are being built on the rubble of this slide.

Substrate: NA

E134	0.005	NA	2300	5200	0.44	Wallis, Switz.	partial	gneiss, ice
Simplon	NA	NA	NA	5400	IIICaaa	46.3 / -8.1	19 Mar. 1901	

References: Eisbacher and Clague, 1984

Moisture: NA Notes: Incorporated substrate material (ice) from overrun glacier.

Substrate: NA

E135	0.005	NA	300	1700	0.18	Switzerland	NA	conglomerate, marl
Ennetbühl	NA	NA	120	NA	IIC	NA / NA	postglacial	

References: Heim, 1932

Moisture: NA Notes: NA

Substrate: NA

---

1. Rank 2. Name	3. Volume 4. Area	5. Thickness: a. Avg b. Max	6. Drop 7. Velocity	8. Length: a. Straight b. Curved	9. Fahr-böschung 10. Type	11. Location 12. Lat./Long.	13. Confinement 14. Age	15. Composition
E136	0.00482	16	300	1220	0.25	Alberta, Canada	partial	limestone
Beaver Flats South	0.3	65	NA	NA	IIC-ba	50.9 / 115	Holocene	

References: Cruden, 1976

Moisture: NA Notes: Motion was initiated along a valley-dipping bedding-parallel fault plane. Monolithologic, proximal trough.

Substrate: NA

E137	0.0046	45	427	1113	0.38	California, U.S.A.	deflected-30°(CH)	sandstone
Beatty	0.10117	300	NA	1151	IIICc	37 / 122	18 April 1906	

References: Hector, 1989

Moisture: NA Notes: This deposit is located 2 km from the San Andreas Fault, and fell during the 1906 San Francisco earthquake. A tributary canyon added debris to the landslide "much as confluent glaciers do." The mass of soil debris crushed the Hoffman shingle mill in its path. Surface grain size; maximum: 10 m.

Substrate: NA

E138	0.0045	NA	1100	3850	0.29	Switzerland	unconfined(CH)	ice
Altels	NA	7	360	3850	IIICbab	46.5 / -7.7	11 Sept. 1895	

References: Heim, 1932; Eisbacher and Clague, 1984

Moisture: NA Notes: Powerful airblast, tossed cattle 500-1000m horizontally and 250-350m vertically. Formed a compact 'ice conglomerate,' with well-rounded pieces of ice embedded in a turbid matrix of ice powder. Monolithologic. Spattering of ice and rock accompanied air blast.

Substrate: NA

---

1. Rank 2. Name	3. Volume 4. Area	5. Thickness: a. Avg b. Max	6. Drop 7. Velocity	8. Length: a. Straight b. Curved	9. Fahr-böschung 10. Type	11. Location 12. Lat./Long.	13. Confinement 14. Age	15. Composition
E139	0.0045	5	884	2720	0.33	Alberta, Canada	unconfined	carbonates, shale
Brazeau Lake	0.9	NA	NA	2720	IICdda	52.4 / 117.08	early July, 1933	

References: Cruden, 1982

Moisture: NA Notes: A bedding-plane failure initiated movement of this landslide. Two processes that might have been important to slide triggering include: 1) presence of soft, weathered shale; and 2) the decay of high-level permafrost, permitting infiltration of surface water and the buildup of pore-water pressures. A monolithologic landslide with plentiful debris cones on its surface, right-circular cones 6-8 m high with rounded tops and sides at the angle of repose.

Substrate: NA

E140	0.00413	14	350	1100	0.32	Alberta, Canada	partial	limestone
Beaver Flats North	0.3	60	NA	NA	IICd-a	50.9 / 115	Holocene	

References: Cruden, 1976

Moisture: NA Notes: A bedding-plane failure initiated movement of this landslide. Monolithologic.

Substrate: NA

E141	0.004	NA	500	1600	0.31	Kola Peninsula,	deflected-90°	ice + mine tailings
Chibins 17	NA	NA	210	NA	NA	68 / -37	late 20th century	

References: Adushkin, personal communication, 1990

Moisture: NA Notes: Failure of mine dump due to oversteepening of slope.

Substrate: NA

---

1. Rank 2. Name	3. Volume 4. Area	5. Thickness: a. Avg b. Max	6. Drop 7. Velocity	8. Length: a. Straight b. Curved	9. Fahr-böschung 10. Type	11. Location 12. Lat./Long.	13. Confinement 14. Age	15. Composition
E142	0.0036	30	500	1125	0.44	Ecuador	NA	NA
Pisque River	0.12	NA	NA	NA	NA	NA / NA	NA	

References: Plaza-Nieto, et al., 1990

Moisture: NA Notes: NA

Substrate: NA

E143	0.0035	NA	950	2000	0.48	Lombardy, Italy	unconfined	granite gneiss
Plurs	NA	NA	NA	2000	IIICdda	46.4 / -9.4	4 Sept. 1618	

References: Heim, 1932; Eisbacher and Clague, 1984

Moisture: NA Notes: Noises and creep preceded the landslide, which was accompanied by dust and luminescence. The landslide mass is monolithologic and the deposit was surrounded by a dozed marginal dike.

Substrate: NA

E144	0.003	3	1300	2400	0.54	Karakoram, Pakistan	unconfined(DI-110°)	schist and marble
Bualtar 3	1.2	10	NA	2400	IICbab	37 / -72	31 July 1986	

References: Hewett, 1988

Moisture: NA Notes: The landslide exhibits preserved slope-parallel bedding and reverse grading. It occurred during melting of heavy snowpack and rains. Meltwater from diurnal freeze-thaw triggered the failures on successive days late in the day. Beneath the surface 15-35% fines but only 5% or less clay. Particles finer than intermediate sand dispersed through the mass during emplacement. Surface grain size; modal: 200 cm; maximum: 44 m.

Substrate: snow

---

1. Rank 2. Name	3. Volume 4. Area	5. Thickness: a. Avg b. Max	6. Drop 7. Velocity	8. Length: a. Straight b. Curved	9. Fahr-böschung 10. Type	11. Location 12. Lat./Long.	13. Confinement 14. Age	15. Composition
E145	0.003	NA	700	1200	0.58	France	unconfined	gneiss, quartzite
Clavans	NA	NA	NA	1200	IIICbaa	45.1 / -6.2	1418 A. D.	

References: Eisbacher and Clague, 1984

Moisture: NA Notes: Still clearly visible.

Substrate: NA

E146	0.0026	NA	370	900	0.41	Kola Peninsula,	unconfined	ice + mine tailings
Chibins 8	NA	NA	NA	NA	NA	68 / -37	late 20th century	

References: Adushkin, personal communication, 1990

Moisture: NA Notes: Failure of mine dump due to oversteepening of slope.

Substrate: NA

E147	0.0025	NA	500	1100	0.45	Switzerland	NA	NA
Wengen 1	NA	NA	NA	NA	NA	NA / NA	NA	

References: Hsü, 1975

Moisture: NA Notes: NA

Substrate: NA

---

1. Rank 2. Name	3. Volume 4. Area	5. Thickness: a. Avg b. Max	6. Drop 7. Velocity	8. Length: a. Straight b. Curved	9. Fahr-böschung 10. Type	11. Location 12. Lat./Long.	13. Confinement 14. Age	15. Composition
E148	0.0024	NA	400	1100	0.36	Kola Peninsula,	partial	ice + mine tailings
Chibins 6	NA	NA	NA	NA	NA	68/ -37	late 20th century	

References: Adushkin, personal communication, 1990

Moisture: NA Notes: Failure of mine dump due to oversteepening of slope.

Substrate: NA

E149	0.002	NA	400	1100	0.36	Kola Peninsula,	partial	ice + mine tailings
Chibins 1	NA	NA	80	1100	NA	68/ -37	late 20th century	

References: Adushkin, personal communication, 1990

Moisture: NA Notes: Failure of mine dump due to oversteepening of slope.

Substrate: NA

E150	0.002	10	500	800	0.63	Novaya	unconfined	NA
U.S.S.R. Artificial 4	0.2	NA	NA	800	NA	72/ -55	late 20th century	

References: Adushkin, personal communication, 1990

Moisture: NA Notes: Triggered by an underground nuclear(?) explosion approximately 1 km underground.

Substrate: NA

---

1. Rank 2. Name	3. Volume 4. Area	5. Thickness: a. Avg b. Max	6. Drop 7. Velocity	8. Length: a. Straight b. Curved	9. Fahr-böschung 10. Type	11. Location 12. Lat./Long.	13. Confinement 14. Age	15. Composition
E151 Puget Peak	0.0018 0.5	4 6	1215 80	2130 2130	0.57 IIICbab	Alaska, U.S.A. 60.03 / 148.55	unconfined(CH) 27 March 1964	argillite, graywacke + snow

References: Hoyer, 1971

Moisture: NA Notes: The avalanche was triggered by the1964 Alaska earthquake. Three joint sets were discerned in the headwall. The landslide exhibited incorporated substrate material and rock spattering. Many areas were underlain by undisturbed stratified snow.

Substrate: NA Surface grain size; modal: 90 cm; maximum: 6 m.

E152 Chibins 4	0.0015 NA	NA NA	400 NA	1000 NA	0.40 NA	Kola Peninsula, 68 / -37	deflected-90°(CH) late 20th century	ice + mine tailings

References: Adushkin, personal communication, 1990

Moisture: NA Notes: Failure of mine dump due to oversteepening of slope.

Substrate: NA

E153 Kootenay 1	0.0014 NA	NA NA	300 NA	1600 NA	0.19 NA	British Columbia, Can. NA / NA	NA NA	coal mine tailings

References: Campbell and Shaw, 1978

Moisture: NA Notes: Adit 29

Substrate: NA

---

1. Rank 2. Name	3. Volume 4. Area	5. Thickness: a. Avg b. Max	6. Drop 7. Velocity	8. Length: a. Straight b. Curved	9. Fahr- böschung 10. Type	11. Location 12. Lat./Long.	13. Confinement 14. Age	15. Composition
E154 Chibins 5	0.0013 NA	NA NA	250 NA	500 NA	0.50 NA	Kola Peninsula, 68/ -37	unconfined late 20th century	ice + mine tailings

References: Adushkin, personal communication, 1990

Moisture: NA Notes: Failure of mine dump due to oversteepening of slope.

Substrate: NA

E155 Vesuvius 7	0.0012 0.1456	8 NA	410 NA	820 NA	0.50 IICba-	Italy 40.8/ -14.45	unconfined 1944 A.D.	volcanic ash, agglutinate

References: Hazlett, et al., in press

Moisture: NA Notes: The landslide exhibits preserved slope-parallel stratigraphy. Triggered by eruption-related earthquake activity.

Substrate: NA

E156 Chibins 3	0.0011 NA	NA NA	350 NA	700 NA	0.50 NA	Kola Peninsula, 68/ -37	unconfined (CH) late 20th century	ice + mine tailings

References: Adushkin, personal communication, 1990

Moisture: NA Notes: Failure of mine dump due to oversteepening of slope.

Substrate: NA

---

1. Rank 2. Name	3. Volume 4. Area	5. Thickness: a. Avg b. Max	6. Drop 7. Velocity	8. Length: a. Straight b. Curved	9. Fahr- böschung 10. Type	11. Location 12. Lat./Long.	13. Confinement 14. Age	15. Composition
E157	0.0011	8	360	680	0.53	Italy	unconfined(DI-125°)	volcanic ash, blocks, spatter
Vesuvius 6	0.136	NA	NA	NA	IICdac,d	40.8 / -14.45	1944 A.D.	

References: Hazlett, et al., in press

Moisture: NA Notes: The landslide exhibits preserved slope-parallel stratigraphy. Triggered by eruption-related earthquake activity.

Substrate: NA

E158	0.001	NA	750	1400	0.54	Novaya	unconfined	NA
U.S.S.R. Artificial 3	NA	NA	NA	1400	NA	72 / -55	late 20th century	

References: Adushkin, personal communication, 1990

Moisture: NA Notes: Triggered by an underground nuclear(?) explosion approximately 1 km underground.

Substrate: NA

E159	0.001	8	636	1240	0.51	Italy	unconfined(DI-40°)	volcanic ash, blocks + spatter
Vesuvius 5	0.1264	NA	NA	NA	IICba-	40.8 / -14.45	1944 A.D.	

References: Hazlett, et al., in press

Moisture: NA Notes: The landslide exhibits preserved slope-parallel stratigraphy, thrust faults and imbrication and normal faults. Triggered by eruption-related earthquake activity.

Substrate: NA

---

1. Rank / 2. Name	3. Volume / 4. Area	5. Thickness: a. Avg / b. Max	6. Drop / 7. Velocity	8. Length: a. Straight / b. Curved	9. Fahrböschung / 10. Type	11. Location / 12. Lat./Long.	13. Confinement / 14. Age	15. Composition
E160	9E-4	NA	200	400	0.50	Kola Peninsula,	unconfined	ice + mine tailings
Chibins 14	NA	NA	NA	NA	NA	68 / -37	late 20th century	

References: Adushkin, personal communication, 1990

Moisture: NA Notes: Failure of mine dump due to oversteepening of slope.

Substrate: NA

E161	9E-4	8	505	940	0.54	Italy	unconfined(DI-50°)	volcanic ash, blocks + spatter
Vesuvius 2	0.1128	NA	NA	NA	IICba-	40.8 / -14.45	1944 A.D.	

References: Hazlett, et al., in press

Moisture: NA Notes: The landslide exhibits preserved slope-parallel stratigraphy. Triggered by eruption-related earthquake activity.

Substrate: NA

E162	8E-4	NA	250	450	0.56	Kola Peninsula,	unconfined	ice + mine tailings
Chibins 10	NA	NA	NA	NA	NA	68 / -37	late 20th century	

References: Adushkin, personal communication, 1990

Moisture: NA Notes: Failure of mine dump due to oversteepening of slope.

Substrate: NA

---

1. Rank 2. Name	3. Volume 4. Area	5. Thickness: a. Avg b. Max	6. Drop 7. Velocity	8. Length: a. Straight b. Curved	9. Fahr-böschung 10. Type	11. Location 12. Lat./Long.	13. Confinement 14. Age	15. Composition
E163	7.9E-4	8	470	960	0.49	Italy	unconfined(DI-40°)	volcanic ash, agglutinate
Vesuvius 4	0.0992	NA	NA	960	IICba-	40.8 / -14.45	1944 A.D.	

References: Hazlett, et al., in press

Moisture: NA Notes: The landslide exhibits preserved slope-parallel stratigraphy. Triggered by eruption-related earthquake activity.

Substrate: NA

E164	7.5E-4	NA	400	1300	0.31	Graubünden, Switz.	unconfined	gneiss, carbonate
Monbiel	NA	NA	NA	1300	IIICb--	46.9 / -9.9	17 June 1770	

References: Heim, 1932; Eisbacher and Clague, 1984

Moisture: NA Notes: NA

Substrate: NA

E165	7E-4	NA	250	400	0.63	Kola Peninsula,	unconfined	ice + mine tailings
Chibins 2	NA	NA	NA	400	NA	68 / -37	late 20th century	

References: Adushkin, personal communication, 1990

Moisture: NA Notes: Failure of mine dump due to oversteepening of slope.

Substrate: NA

---

1. Rank 2. Name	3. Volume 4. Area	5. Thickness: a. Avg b. Max	6. Drop 7. Velocity	8. Length: a. Straight b. Curved	9. Fahr-böschung 10. Type	11. Location 12. Lat./Long.	13. Confinement 14. Age	15. Composition
E166	6.5E-4	NA	1050	2400	0.44		NA	NA
Val Lagone	NA	NA	NA	NA	NA	NA / NA	NA	

References: Hsü, 1975

Moisture: NA Notes: NA

Substrate: NA

E167	6.5E-4	4	1200	2700	0.44	Graubünden, Switz.	unconfined(CH)	amphibolite gneiss
Zarera	0.15	NA	NA	2750	IIICb-a	46.4 / -10.1	13 June 1486	

References: Eisbacher and Clague, 1984

Moisture: NA Notes: 300 killed

Substrate: NA

E168	6E-4	NA	300	550	0.55	Kola Peninsula,	unconfined (DI-30°)	ice + mine tailings
Chibins 13	NA	NA	NA	550	NA	68 / -37	late 20th century	

References: Adushkin, personal communication, 1990

Moisture: NA Notes: Failure of mine dump due to oversteepening of slope.

Substrate: NA

1. Rank 2. Name	3. Volume 4. Area	5. Thickness: a. Avg b. Max	6. Drop 7. Velocity	8. Length: a. Straight b. Curved	9. Fahr- böschung 10. Type	11. Location 12. Lat./Long.	13. Confinement 14. Age	15. Composition
E169	5.5E-4	8	285	500	0.57	Italy	unconfined(DI-40°)	volcanic blocks, ash, spatter
Vesuvius 3	0.0688	NA	NA	NA	IICba-	40.8 / -14.45	1944 A.D.	

References: Hazlett, et al., in press

Moisture: NA Notes: The landslide exhibits preserved slope-parallel stratigraphy. Triggered by eruption-related earthquake activity.

Substrate: NA

E170	5E-4	NA	1300	2100	0.62	Switzerland	deflected-80°(CH)	flysh
Altdorf-Spiringen	NA	NA	110	2500	IIICd--	46.8 / -8.7	29 May 1887	

References: Eisbacher and Clague, 1984

Moisture: NA Notes: Possibly triggered by snowmelt infiltration. Surged 50 m up opposite slope, killed 7.

Substrate: NA

E171	5E-4	NA	820	1290	0.64	Switzerland	unconfined	gneiss, schists
Airolo	NA	NA	NA	NA	IIIC	46.6 / -8.7	28 Sept 1898	

References: Heim, 1932; Eisbacher and Clague, 1984

Moisture: NA Notes: The slope is 40 degrees; the gneiss substrate dip 50 degrees into the slope. Cut through a forest, killed 3.

Substrate: NA

---

1. Rank / 2. Name	3. Volume / 4. Area	5. Thickness: a. Avg / b. Max	6. Drop / 7. Velocity	8. Length: a. Straight / b. Curved	9. Fahrböschung / 10. Type	11. Location / 12. Lat./Long.	13. Confinement / 14. Age	15. Composition
E172	5E-4	NA	1800	3100	0.58		NA	NA
Schachental	NA	NA	NA	NA	NA	NA / NA	NA	

References: Hsü, 1975

Moisture: NA Notes: NA

Substrate: NA

E173	5E-4	NA	240	500	0.48	Kola Peninsula,	unconfined	ice + mine tailings
Chibins 7	NA	NA	NA	500	NA	68 / -37	late 20th century	

References: Adushkin, personal communication, 1990

Moisture: NA Notes: Failure of mine dump due to oversteepening of slope.

Substrate: NA

E174	3E-4	NA	170	240	0.71	Kola Peninsula,	unconfined	ice + mine tailings
Chibins 15	NA	NA	NA	240	NA	68 / -37	late 20th century	

References: Adushkin, personal communication, 1990

Moisture: NA Notes: Failure of mine dump due to oversteepening of slope.

Substrate: NA

---

1. Rank / 2. Name	3. Volume / 4. Area	5. Thickness: a. Avg / b. Max	6. Drop / 7. Velocity	8. Length: a. Straight / b. Curved	9. Fahrböschung / 10. Type	11. Location / 12. Lat./Long.	13. Confinement / 14. Age	15. Composition
E175	2.5E-4	0	745	5800	0.13	Nevada, U.S.A.	NA	volcanics
Summit Lake	8.2	NA	NA	NA	NA	41.5 / 119	NA	

References: Curry and Melhorn, 1990

Moisture: NA Notes: NA

Substrate: NA

E176	1.8E-4	8	375	640	0.59	Italy	unconfined	volcanic ash, agglutinate
Vesuvius 1	0.0224	NA	NA	640	IICba-	40.8 / -14.45	1944 A. D.	

References: Hazlett, et al., in press

Moisture: NA Notes: The landslide exhibits preserved slope-parallel stratigraphy. Triggered by eruption-related earthquake activity.

Substrate: NA

E177	1.3E-4	NA	213	700	0.30	British Columbia, Can.	NA	coal mine tailings
Kootenay 2	NA	NA	NA	NA	NA	NA / NA	8 Nov. 1974	

References: Campbell and Shaw, 1978

Moisture: NA Notes: NA

Substrate: NA

---

1. Rank 2. Name	3. Volume 4. Area	5. Thickness: a. Avg b. Max	6. Drop 7. Velocity	8. Length: a. Straight b. Curved	9. Fahr-böschung 10. Type	11. Location 12. Lat./Long.	13. Confinement 14. Age	15. Composition
E178	1.2E-4	NA	190	530	0.36	British Columbia, Can.	NA	coal mine tailings
Kootenay 3	NA	NA	NA	NA	NA	NA / NA	NA	

References: Campbell and Shaw, 1978

Moisture: NA Notes: NA

Substrate: NA

E179	1.1E-4	NA	125	310	0.40	British Columbia, Can.	NA	coal mine tailings
Kootenay 4	NA	NA	NA	NA	NA	NA / NA	May, 1972	

References: Campbell and Shaw, 1978

Moisture: NA Notes: NA

Substrate: NA

E180	1E-4	3	425	925	0.46	Novaya	unconfined	NA
U.S.S.R. Artificial 5	0.04	NA	165	925	NA	72 / -55	late 20th century	

References: Adushkin, personal communication, 1990

Moisture: NA Notes: Triggered by an underground nuclear(?) explosion approximately 1 km underground.

Substrate: NA

---

1. Rank 2. Name	3. Volume 4. Area	5. Thickness a. Avg b. Max	6. Drop 7. Velocity	8. Length: a. Straight b. Curved	9. Fahr-böschung 10. Type	11. Location 12. Lat./Long.	13. Confinement 14. Age	15. Composition
M	NA	NA	NA	NA	NA	Terra Tyrrhena	NA	NA
Mars 59	NA	NA	NA	NA	-B4	-18.82 / 261	NA	

References: This paper

Moisture: NA Notes: Deposit lies within a 40 km-diameter crater. Smooth reentrant. Best picno: 445A313

Substrate: NA

M	NA	NA	NA	NA	NA	Arabia Terra	NA	NA
Mars 58	NA	NA	NA	NA	IB1	32.55 / 2.44	NA	

References: This paper

Moisture: NA Notes: Slump with debris apron inside crater rim. Best picno: 212S06

Substrate: NA

M	NA	NA	NA	NA	NA	Orcus Patera region	NA	NA
Mars 60	NA	NA	NA	NA	-B1	9.08 / 190	NA	

References: This paper

Moisture: NA Notes: Small, tri-lobate deposit, 2 km across, 2 long from headscarp. Best picno: 727A31

Substrate: NA

---

1. Rank 2. Name	3. Volume 4. Area	5. Thickness: a. Avg b. Max	6. Drop 7. Velocity	8. Length: a. Straight b. Curved	9. Fahr- böschung 10. Type	11. Location 12. Lat./Long.	13. Confinement 14. Age	15. Composition
M	NA	NA	NA	NA	NA	Capri Chasma	NA	NA
Mars 6	NA	NA	NA	NA	IIICcbd	-8.84 / 41.64	NA	

References: This paper

Moisture: NA Notes: Headscarp lies on shallowly dipping chasma wall. Best picno: 14A38

Substrate: NA

M	NA	NA	NA	NA	NA	Crater Mvd	NA	NA
Mars 57	NA	NA	NA	NA	IB-	-6.78 / 22.64	NA	

References: This paper

Moisture: NA Notes: Very hazy image of slide in small enclosed basin~15 km in diameter. Best picno: 378B08

Substrate: NA

M	NA	NA	NA	NA	NA	Coprates Chasma	NA	NA
Mars 54	NA	NA	NA	NA	-B-	-13.3 / 66	NA	

References: This paper

Moisture: NA Notes: Emanates from the same spur as A6 (L9), but to the east and on the opposite side, falling into a parallel subsidiary graben. Best picno: 338A07

Substrate: NA

---

1. Rank 2. Name	3. Volume 4. Area	5. Thickness: a. Avg b. Max	6. Drop 7. Velocity	8. Length: a. Straight b. Curved	9. Fahr- böschung 10. Type	11. Location 12. Lat./Long.	13. Confinement 14. Age	15. Composition
M	NA	NA	NA	NA	NA	Coprates Chasma	NA	NA
Mars 53	NA	NA	NA	NA	IB1	-13.3 / 68.7	NA	

References: This paper

Moisture: NA Notes: Just south of A6 (L9), at the west end of a large complex of landslides all in a row. Resolution is too low to single out the others. Best picno: 338A07

Substrate: NA

M	NA	NA	NA	NA	NA	Memnonia	NA	NA
Mars 56	NA	NA	NA	NA	-B1	-27.5 / 144.15	NA	

References: This paper

Moisture: NA Notes: Collapse of scarp at intersection with a small crater. The entire base of the scarp in this area seems to have shed a small debris blanket, the wall material seems very weak here. Best picno: 457A27

Substrate: NA

M	NA	NA	NA	NA	NA	Terra Sirenum	NA	NA
Mars 55	NA	NA	NA	NA	IB2	-12.2 / 173	NA	

References: This paper

Moisture: NA Notes: Occurs inside a 50 km-diameter crater. 2 km superposed crater, several smaller ones. Distal edge digitate. Perhaps related to impact that generated neighboring splash crater or to nearby volcanic crater. Best picno: 439509

Substrate: NA

---

1. Rank 2. Name	3. Volume 4. Area	5. Thickness: a. Avg b. Max	6. Drop 7. Velocity	8. Length: a. Straight b. Curved	9. Fahr-böschung 10. Type	11. Location 12. Lat./Long.	13. Confinement 14. Age	15. Composition
M	NA	NA	NA	NA	NA	Maadim Valles region	NA	NA
Mars 61	NA	NA	NA	NA	IB2,3	-17.5 / 182.08	NA	

References: This paper

Moisture: NA Notes: Occurs at intersection between rims of overlapping 35+ km craters. Best picno: 434S16

Substrate: NA

M	NA	NA	NA	NA	NA	Coprates Chasma	NA	NA
Mars 78	NA	NA	NA	NA	IIICbaa	-11.3 / 67.28	NA	

References: This paper

Moisture: NA Notes: Dark material partially mantles surface. Best picno: 80A01. Mosaic #: 1591

Substrate: NA

M	NA	NA	NA	NA	NA	Gangis Chasma	NA	NA
Mars 77	NA	NA	NA	NA	IIICbbd	-7.7 / 44.32	NA	

References: This paper

Moisture: NA Notes: Very low-viscosity flow. Note that in D1-D5 a linear feature "dike" runs through and connects all five headscarps. Best picno: 014A31. Mosaic #: 1381

Substrate: NA

---

1. Rank 2. Name	3. Volume 4. Area	5. Thickness: a. Avg b. Max	6. Drop 7. Velocity	8. Length: a. Straight b. Curved	9. Fahr- böschung 10. Type	11. Location 12. Lat./Long.	13. Confinement 14. Age	15. Composition
M	NA	NA	NA	NA	NA	Capri Chasma	NA	NA
Mars 8	NA	NA	NA	NA	IIICbab	-8.46 / 41.45	NA	

References: This paper

Moisture: NA Notes: Overlaps Mars 7, which protruded up enough to be visible. Best picno: 14A38

Substrate: NA

M	NA	NA	NA	NA	NA	Melas Chasma	NA	NA
Mars 79	NA	NA	NA	NA	IIICcbd	-12 / 72.8	NA	

References: This paper

Moisture: NA Notes: Travel distance seems short with respect to apparent fall height. Best picno: 91A05. Mosaic #: 1593

Substrate: NA

M	NA	NA	NA	NA	NA	Gangis Chasma	NA	NA
Mars 76	NA	NA	NA	NA	IIICbbd	-7.61 / 44.34	NA	

References: This paper

Moisture: NA Notes: Very low-viscosity flow with distinct levees. Best picno: 014A31. Mosaic #: 1381

Substrate: NA

---

1. Rank 2. Name	3. Volume 4. Area	5. Thickness: a. Avg b. Max	6. Drop 7. Velocity	8. Length: a. Straight b. Curved	9. Fahr-böschung 10. Type	11. Location 12. Lat./Long.	13. Confinement 14. Age	15. Composition
M	NA	NA	NA	NA	NA	Hebes Chasma	NA	NA
Mars 63	NA	NA	NA	NA	IB2	-1.83 / 76.1	NA	

References: This paper

Moisture: NA Notes: Collapse of chasma wall sent debris apron into Hebes Chasma moat. Extremely rough terrain. Best picno: 738A72

Substrate: NA

M	NA	NA	NA	NA	NA	Maadim Valles region	NA	NA
Mars 62	NA	NA	NA	NA	-B2	-21.25 / 186.35	NA	

References: This paper

Moisture: NA Notes: Occurs in 35-km diameter crater. Best picno: 430S27

Substrate: NA

M	NA	NA	NA	NA	NA	Gangis Chasma	NA	NA
Mars 75	NA	NA	NA	NA	IIICaab	-7.7 / 44.17	NA	

References: This paper

Moisture: NA Notes: Small coherent caprock slide. Best picno: 014A31. Mosaic # 1381

Substrate: NA

---

1. Rank 2. Name	3. Volume 4. Area	5. Thickness: a. Avg b. Max	6. Drop 7. Velocity	8. Length: a. Straight b. Curved	9. Fahr-böschung 10. Type	11. Location 12. Lat./Long.	13. Confinement 14. Age	15. Composition
M	NA	NA	NA	NA	NA	Capri Chasma	NA	NA
Mars 7	NA	NA	NA	NA	IIICbaa	-8.66 / 41.44	NA	

References: This paper

Moisture: NA Notes: Headscarp not imaged. Very irregular lobe. "Old;" subdued in appearance. Two to five superposed craters. Possible longitudinal ribs distally. Best picno: 14A38

Substrate: NA

M	NA	NA	NA	NA	NA	Hydraotes Chaos	NA	NA
Mars 52	NA	NA	NA	NA	-B-	0.15 / 37.49	NA	

References: This paper

Moisture: NA Notes: Landslide lies in chaotic terrain, most large nearby craters dissected. Best picno: 897A89

Substrate: NA

M	NA	NA	NA	NA	NA	Hebes Chasma	NA	NA
Mars 40	NA	NA	NA	NA	-B1,4	-0.7 / 74.9	NA	

References: This paper

Moisture: NA Notes: The landslide occurred from the intersection of graben-bounding faults and a chasma wall. Headscarp collapse features run perpendicular to slope, suggesting than a failure mechanism other than a slump might have been in operation. Debris apron fades out away from the headscarp, obscuring dimensions. Best picno: 917A03; mosaic #I-1840, I-1599.

Substrate: NA

---

1. Rank 2. Name	3. Volume 4. Area	5. Thickness: a. Avg b. Max	6. Drop 7. Velocity	8. Length: a. Straight b. Curved	9. Fahr-böschung 10. Type	11. Location 12. Lat./Long.	13. Confinement 14. Age	15. Composition
M	NA	NA	NA	NA	NA	Gangis Chasma	unconfined	NA
Mars 4	NA	NA	NA	NA	IB1,5	-7.13 / 44.9	NA	

References: Lucchitta, 1979

Moisture: NA Notes: The landslide occurred from a chasma wall. Best picnos: 012A52, 012A54; mosaic #I-1381. Landslide #4 in Lucchitta, 1979.

Substrate: NA

M	NA	NA	NA	NA	NA	Uzboi Valles	NA	NA
Mars 42	NA	NA	NA	NA	IB2	-27.51 / 37.3	NA	

References: This paper

Moisture: NA Notes: Quadrant failure of impact crater inner wall. Best picno: 467A15; mosaic#: I-1209.

Substrate: NA

M	NA	NA	NA	NA	NA	Noctis Labyrinthus	NA	NA
Mars 41	NA	NA	NA	NA	II?B4	-8.8 / 90	NA	

References: This paper

Moisture: NA Notes: Landslide occurs where splash crater nearly overrides a graben. Best picno: 064A09; mosaic #: I-1206.

Substrate: NA

---

1. Rank 2. Name	3. Volume 4. Area	5. Thickness: a. Avg b. Max	6. Drop 7. Velocity	8. Length: a. Straight b. Curved	9. Fahr-böschung 10. Type	11. Location 12. Lat./Long.	13. Confinement 14. Age	15. Composition
M	NA	NA	NA	NA	NA	Hebes Chasma	NA	NA
Mars 39	NA	NA	NA	NA	-B1	-0.5 / 75.68	NA	

References: This paper

Moisture: NA Notes: The landslide occurred from the intersection of a plateau crater and a chasma wall. Only the upper portion of the landslide is coherent, the lower reaches are extremely etched in appearance. This could be wind erosion, though the headscarp region and a nearby slide seem unaffected. Perhaps the material was etched and redistributed by water liberated at the time of collapse. Best picno: 917A04; mosaic #I-1840.

Substrate: NA

M	NA	NA	NA	NA	NA	Gangis Chasma	unconfined	NA
Mars 3	NA	NA	NA	NA	IB2	-8.89 / 44.2	NA	

References: Lucchitta, 1979

Moisture: NA Notes: The landslide occurred at the intersection of a crater and a chasma wall. The landslide underlies the Mars 1 deposit. Best picno: 014A32; mosaic #I-1381. Landslide #3 in Lucchitta, 1979.

Substrate: NA

M	NA	NA	NA	NA	NA	Gangis Chasma	NA	NA
Mars 29	NA	NA	NA	NA	IB2,5	-6.83 / 44.83	NA	

References: This paper

Moisture: NA Notes: The landslide occurred from a chasma wall. Best picno: 012A54; mosaic #I-1381.

Substrate: NA

---

1. Rank 2. Name	3. Volume 4. Area	5. Thickness: a. Avg b. Max	6. Drop 7. Velocity	8. Length: a. Straight b. Curved	9. Fahr-böschung 10. Type	11. Location 12. Lat./Long.	13. Confinement 14. Age	15. Composition
M	NA	NA	NA	NA	NA	Melas Chasma	NA	NA
Mars 32	NA	NA	NA	NA	-B2,3	-10/ 69.5	NA	

References: This paper

Moisture: NA Notes: The landslide occurred from a chasma wall. Unusual headscarp area shows no obvious rotational blocks. Instead, the whole slideblock appears to have fluidized. The debris apron was very fluid; debris flows out between remnants/outliers of layered terrain. Best picnos: 912A17, 912A20; mosaic #I-1591.

Substrate: NA

M	NA	NA	NA	NA	NA	E. Tithonium Chasma	unconfined	NA
Mars 31	NA	NA	300	NA	IB1	-4.5/ 79.5	NA	

References: Lucchitta, 1979;1987

Moisture: NA Notes: The landslide originated from wall rock in Valles Marineris. Best picno: 920A10. Landslide #31 from Lucchitta, 1979.

Substrate: NA

M	NA	NA	NA	NA	NA	Uzboi Valles	NA	NA
Mars 43	NA	NA	NA	NA	IB2	-27.51/ 37.52	NA	

References: This paper

Moisture: NA Notes: Smaller landslide adjacent to Mars 42. Large ridge between the two debris aprons suggests that emplacement was not synchronous. Best picno: 467A17; mosaic#: I-1209.

Substrate: NA

---

1. Rank 2. Name	3. Volume 4. Area	5. Thickness: a. Avg b. Max	6. Drop 7. Velocity	8. Length: a. Straight b. Curved	9. Fahr- böschung 10. Type	11. Location 12. Lat./Long.	13. Confinement 14. Age	15. Composition
M	NA	NA	NA	NA	NA	Gangis Chasma	NA	NA
Mars 5	NA	NA	NA	NA	IIICaab	-7.76 / 44.26	NA	

References: This paper

Moisture: NA Notes: Very fresh. Sand dunes in wind shadow. Coherent caprock slab should be studied in greater detail. Landslide #5 in Lucchitta, 1979. Best picno: 014A31. Mosaic #: 1381

Substrate: NA

M	NA	NA	NA	NA	NA	Gangis Chasma	NA	NA
Mars 49	NA	NA	NA	NA	-B	-7.35 / 50.64	NA	

References: This paper

Moisture: NA Notes: Post layered-terrain landslide; apron extends into chasma. Best picno: 897A11

Substrate: NA

M	NA	NA	NA	NA	NA	Gangis Chasma	NA	NA
Mars 51	NA	NA	NA	NA	-B-	-8.5 / 52.71	NA	

References: This paper

Moisture: NA Notes: Enlargement of the chasma seems to occur via landsliding here. Collapse-type headscarp, but debris apron inconspicuous. Best picno: 897A13

Substrate: NA

---

1. Rank 2. Name	3. Volume 4. Area	5. Thickness: a. Avg b. Max	6. Drop 7. Velocity	8. Length: a. Straight b. Curved	9. Fahr- böschung 10. Type	11. Location 12. Lat./Long.	13. Confinement 14. Age	15. Composition
M	NA	NA	NA	NA	NA	Gangis Chasma	NA	NA
Mars 50	NA	NA	NA	NA	IB-	-7.76 / 51.97	NA	

References: This paper

Moisture: NA Notes: Adjacent to high-albedo chasma floor material. Best picno: M9168A165

Substrate: NA

M	NA	NA	NA	NA	NA	Gangis Chasma	NA	NA
Mars 48	NA	NA	NA	NA	-B1	-6.17 / 49.52	NA	

References: This paper

Moisture: NA Notes: Post layered-terrain landslide. Large superposed crater. Best picnos: 897A38,40

Substrate: NA

M	NA	NA	NA	NA	NA	Kasei Valles	NA	NA
Mars 45	NA	NA	NA	NA	IB1	28.57 / 56.6	NA	

References: This paper

Moisture: NA Notes: Smaller, older deposit overrun by Mars 44. Best picno: 667A36; mosaic#: I-1305.

Substrate: NA

---

1. Rank 2. Name	3. Volume 4. Area	5. Thickness: a. Avg b. Max	6. Drop 7. Velocity	8. Length: a. Straight b. Curved	9. Fahr-böschung 10. Type	11. Location 12. Lat./Long.	13. Confinement 14. Age	15. Composition
M	NA	NA	NA	NA	NA	Kasei Valles	NA	NA
Mars 44	NA	NA	NA	NA	IB2	28.57 / 56.6	NA	

References: This paper

Moisture: NA Notes: Symmetrical debris apron pitted with small craters. Best picno: 667A34; mosaic#: I-1305.

Substrate: NA

M	NA	NA	NA	NA	NA	Promethei Terra	NA	NA
Mars 47	NA	NA	NA	NA	-B2	-34.74 / 258	NA	

References: This paper

Moisture: NA Notes: Failure of impact crater inner wall. Deposit lies within crater in area of "rock glaciers." Deposit has distinct circuate headscarp, slump blocks at head. Best picno: 411S10; mosaic#: I-1451.

Substrate: NA

M	NA	NA	NA	NA	NA	Nili Fossae	NA	NA
Mars 46	NA	NA	NA	NA	IB1	25.44 / 282.13	NA	

References: This paper

Moisture: NA Notes: Small slump and debris apron at the intersection of a plateau crater and an outwash-cut cliff. Best picno: 216A17; mosaic#: I-1414.

Substrate: NA

---

1. Rank 2. Name	3. Volume 4. Area	5. Thickness: a. Avg b. Max	6. Drop 7. Velocity	8. Length: a. Straight b. Curved	9. Fahrböschung 10. Type	11. Location 12. Lat./Long.	13. Confinement 14. Age	15. Composition
E	NA	NA	549	NA	NA	Utah, U.S.A.	NA	claystone, siltstone
Thistle	NA	100	NA	2440	Slow	NA / NA	NA	

References: Pack, et. al., 1984

Moisture: NA Notes: Reactivated in April 1983. Entrenchment of the Spanish Fork River in the late Pleistocene could have undercut beds of shaley siltstone that dip at 50 degrees into the canyon. At its maximum extent about 15000 B.P., Lake Bonneville would have submerged the toe of the slope at Thistle by about 40 meters. Catastrophic dropping of lake level about 14000 years ago might have created a rapid drawdown that contributed to the initial failure.

Substrate: NA

E	NA	NA	1890	6920	0.27	Washington, U.S.A.	deflected(CH)	andesite
Tahoma Peak	NA	NA	140	NA	IIIC	46.9 / 121.7	14 Dec. 1963	

References: Crandell and Fahnestock, 1965

Moisture: NA Notes: A total volume of 11 million cubic meters is estimated for the event, the integrated volume of seven separate slides. The landslide exhibited incorporated substrate material (snow).

Substrate: NA

E(u)	NA	0	NA	50000	0.00	Hawaii, U.S.A.	unconfined	basalt
Waianae	6100	NA	NA	50000	IIA	NA / NA	NA	

References: Moore, et al., 1989

Moisture: NA Notes: NA

Substrate: NA

---

1. Rank 2. Name	3. Volume 4. Area	5. Thickness: a. Avg b. Max	6. Drop 7. Velocity	8. Length: a. Straight b. Curved	9. Fahr-böschung 10. Type	11. Location 12. Lat./Long.	13. Confinement 14. Age	15. Composition
E	NA	NA	NA	5200	0.00	California, U.S.A.	NA	quartz diorite
Vallecito Mtns. mb	NA	45	NA	NA	NA	NA / NA	Miocene	

References: Kerr, D. R., 1984

Moisture: NA Notes: Bedding in the subjacent strata is disrupted. Three dimensional jigsaw puzzle fractures and low-angle thrust planes and imbrication mark the breccia. The basal contact is sharp, undulatory and in places striated. Ran up on a basement hill.

Substrate: NA

E	NA	NA	NA	NA	NA	California, U.S.A.	NA	quartz diorite, schist
Split Mtn. mb	NA	180	NA	NA	NA	NA / NA	Miocene	

References: Kerr, 1984

Moisture: NA Notes: The megabreccia deposit exhibits three-dimensional jigsaw puzzle breccia, sub-horizontal slip surfaces and thrust faults and imbrication. Bedding in the subjacent strata is disrupted. The basal contact is sharp, undulatory and in places striated.

Substrate: NA

E	NA	0	NA	NA	NA	California, U.S.A.	unconfined	carbonates
Saline Valley	25	NA	NA	NA	NA	36.89 / 117.92	NA	

References: Stout, 1986

Moisture: NA Notes: Several prospect pits dug on surface, mine shaft drilled into main body of deposit. Deposit lies at the mouth of lead canyon and has an alluvial filled pull-away separating the Bonanza King and other Cambrian formations. No slip surface is exposed, although numerous "fault" scarps are in the alluvial filled pull-away.

Substrate: NA

---

1. Rank 2. Name	3. Volume 4. Area	5. Thickness: a. Avg b. Max	6. Drop 7. Velocity	8. Length: a. Straight b. Curved	9. Fahr- böschung 10. Type	11. Location 12. Lat./Long.	13. Confinement 14. Age	15. Composition
E(u)	NA	0	NA	235000	0.00	Hawaii, U.S.A.	unconfined	basalt
Nuuanu	23000	NA	NA	235000	NA	NA / NA	NA	

References: Moore, et al., 1989

Moisture: NA Notes: A rift zone apparently formed a detachment surface for the upper end of the headscarp.

Substrate: NA

E(u)	NA	0	4500	100000	0.05	Hawaii, U.S.A.	unconfined	basalt
South Kauai	6800	NA	NA	100000	IB	21.5 / 159.5	5,000,000 yrs	

References: Moore, et al., 1989

Moisture: NA Notes: Apparently is composed of debris avalanches from both the south flank of Kauai volcano and the east flank of Niihau volcano on the west. The axis of the landslide is marked by a broad longitudinal ridge that crosses the axis of the Hawaiian Deep and forms a low welt separating two basins. Most blocks 500 m to 2 km in size and stand 50-100 m above the general surface. 25 m sediment cover is observed, the thickest of all in the Hawaiian islands, suggesting the greatest age.

Substrate: NA

E	NA	NA	NA	1500	0.00	Nevada, U.S.A.	NA	limestone
Snowdrift megabreccia	NA	NA	NA	NA	NA	NA / NA	L. Cretac./E. Tertiary	

References: Rowland, et. al., 1985

Moisture: NA Notes: Largest block is 400m X 150m X 40 m. Distal portion well preserved with a distinct snout. Medial and proximal portions overlie nonresistant redbeds. Using the snout height (16.5 m), the slope angle (3 degrees), and the density (2.55 g/cc), a yield strength of 140,000 Newtons/sq. meter. The distal portion is matrix-supported, though matrix material is only a small overall component. Flow was dry and subaerial.

Substrate: NA

---

1. Rank 2. Name	3. Volume 4. Area	5. Thickness: a. Avg b. Max	6. Drop 7. Velocity	8. Length: a. Straight b. Curved	9. Fahr- böschung 10. Type	11. Location 12. Lat./Long.	13. Confinement 14. Age	15. Composition
E(u)	NA	0	NA	NA	NA	Hawaii, U.S.A.	NA	NA
Wailau	13000	NA	NA	NA	NA	NA / NA	NA	

References: Moore, et al., 1989

Moisture: NA Notes: NA

Substrate: NA

E	0.015	NA	600	NA	NA	New Zealand	NA	sandstone
Matiri	NA	NA	NA	NA	NA	-41.66 / -172.3	290 B.P.	

References: Adams, 1981

Moisture: NA Notes: Landslide dammed a river forming Lake Matiri. Overtopping of the landslide caused a large mudflow.

Substrate: NA

E	0.02	3	NA	NA	NA	Arizona, U.S.A.	NA	granodiorite, sed. rocks
Cross Hill	6	50	NA	NA	NA	32 / 110.75	Oligocene-Miocene	

References: Yarnold and Lombard, 1989

Moisture: NA Notes: This megabreccia deposit exhibits reverse grading, inert incorporated substrate material, three-dimensional jigsaw puzzle breccia, basal strata disruption, sub-horizontal slip surfaces and intruded clastic dikes.

Substrate: NA

---

1. Rank 2. Name	3. Volume 4. Area	5. Thickness: a. Avg b. Max	6. Drop 7. Velocity	8. Length: a. Straight b. Curved	9. Fahr- böschung 10. Type	11. Location 12. Lat./Long.	13. Confinement 14. Age	15. Composition
E(u)	272	25	2470	NA	NA	Senegal, Africa	NA	sediment
West Africa #1	10928	NA	NA	NA	NA	15.75 / 19	100,000+ yrs	

References: Jacobi, 1976

Moisture: NA Notes: NA

Substrate: NA

E	0.008	NA	1400	NA	NA	Italy	NA	carbonate
Bocca di Brenta	NA	NA	NA	NA	NA	46.2 / -10.9	May 1882	

References: Eisbacher and Clague, 1984

Moisture: NA Notes: NA

Substrate: NA

E	0.02	NA	NA	NA	NA	Wallis, Switz.	NA	limestone + ice
Diablerets 1	NA	NA	NA	NA	NA	46.4 / -7.3	23 June 1714	

References: Heim, 1932; Eisbacher and Clague, 1984

Moisture: NA Notes: The base of the headscarp intersected a fold axis, suggesting that joints along the axis acted as detachment planes for the slidemass. First of two landslides in this area, this one later being covered over by Diablerets 2. 15 killed. Landslide preceeded by noises from the mountain. Story of one survivor told in "Derborence" by C. F. Ramuz.

Substrate: NA

---

1. Rank 2. Name	3. Volume 4. Area	5. Thickness: a. Avg b. Max	6. Drop 7. Velocity	8. Length: a. Straight b. Curved	9. Fahr-böschung 10. Type	11. Location 12. Lat./Long.	13. Confinement 14. Age	15. Composition
E	0.246	NA	NA	NA	NA	Kirghizia, U.S.S.R.	NA	NA
Karasu	NA	NA	NA	NA	NA	NA / NA	NA	

References: This paper

Moisture: NA Notes: NA

Substrate: NA

E	0.25	19	NA	NA	NA	Austria	NA	NA
Tschirgant	13.2	NA	NA	NA	NA	NA / NA	NA	

References: Heuberger, et. al., 1984

Moisture: NA Notes: NA

Substrate: NA

E(u)	0.055	8	NA	NA	NA	British Columbia,	NA	Deltaic sediments
Kitimat	6.8	NA	NA	NA	NA	53.98 / 128.68	1975 A.D.	

References: This paper

Moisture: NA Notes: NA

Substrate: NA

---

1. Rank 2. Name	3. Volume 4. Area	5. Thickness: a. Avg b. Max	6. Drop 7. Velocity	8. Length: a. Straight b. Curved	9. Fahr-böschung 10. Type	11. Location 12. Lat./Long.	13. Confinement 14. Age	15. Composition
E	0.086	NA	NA	NA	NA	U.S.S.R.	NA	NA
Kapkatash	NA	NA	NA	NA	NA	NA / NA	NA	

References: This paper

Moisture: NA Notes: NA

Substrate: NA

E(u)	NA	0	4600	140000	0.03	Hawaii, U.S.A.	unconfined	basalt
North Kauai	14000	NA	NA	140000	IB	22.5 / 159.5	5,000,000 yrs	

References: Moore, et al., 1989

Moisture: NA Notes: Triple-reentrant headscarp. Hummocky or blocky surface texture. Slope failure took place when the island stood at least 900 m above its present level (from a submerged terrace at this depth) and was about twice as large. Therefore, subaerial parts of the island were involved in the failures.

Substrate: NA

M	NA	NA	NA	NA	NA	Candor Chasma	NA	NA
Mars 88	NA	NA	NA	NA	IIIBbab	-6.75 / 67.12	NA	

References: This paper

Moisture: NA Notes: Seems to have traveled a great distance when compared to the landslide fall height. Slide appears to overrun some chaotic terrain, though this is not fully clear and chaos may be later. The slide lies right at the boundary between the valley floor and the mountains, possibly along a fault scarp. Mountain front 20 km SE is very straight for 75 km, strongly suggesting fault bounded range front in this area. Best picno: 911A11. Mosaic #: 1590

Substrate: NA

---

1. Rank 2. Name	3. Volume 4. Area	5. Thickness: a. Avg b. Max	6. Drop 7. Velocity	8. Length: a. Straight b. Curved	9. Fahr- böschung 10. Type	11. Location 12. Lat./Long.	13. Confinement 14. Age	15. Composition
M	NA	NA	NA	NA	NA	Candor Chasma	NA	NA
Mars 87	NA	NA	NA	NA	ICbab	-6.25 / 68.42	NA	

References: This paper

Moisture: NA Notes: Appears similar in form to Mars 84, Mars 85 with addition that a coherent rotational slide block remains in the headscarp area. The distal edge might be overriden by material shed off of the opposite slope. Best picno: 911A12. Mosaic #: 1590

Substrate: NA

M	NA	NA	NA	NA	NA	Coprates Chasma	NA	NA
Mars 9 (Coprates	NA	NA	NA	NA	IB2	-11.75 / 67.6	NA	

References: Lucchitta, 1979; U. S. Geol. Surv., 1984a

Moisture: NA Notes: The landslide originated from a partially eroded spur of wall rock in Valles Marineris. Headscarp area very poorly imaged. Two large craters lie at distal end of the debris apron, but the morphology is very fresh. Best picno: 080A01; Best photomosaic: I-1591. Landslide #9 from Lucchitta, 1979.

Substrate: NA

M	NA	NA	NA	NA	NA	Tithonium Chasma	NA	NA
Mars 89	NA	NA	NA	NA	IIICcbd	-4.16 / 87.07	NA	

References: This paper

Moisture: NA Notes: May be one component of a larger landslide deposit that abuts the headscarp region. Best picno: 063A67. Mosaic #: 1207

Substrate: NA

---

1. Rank 2. Name	3. Volume 4. Area	5. Thickness: a. Avg b. Max	6. Drop 7. Velocity	8. Length: a. Straight b. Curved	9. Fahr-böschung 10. Type	11. Location 12. Lat./Long.	13. Confinement 14. Age	15. Composition
M	NA	NA	NA	NA	NA	Candor Chasma	NA	NA
Mars 86	NA	NA	NA	NA	IIICcbd	-8.44 / 66.73	NA	

References: This paper

Moisture: NA Notes: Landslide appears to have travelled downvalley, not directly downslope. Best picno: 910A16. Mosaic #: 1591

Substrate: NA

M	NA	NA	NA	NA	NA	Melas Chasma	NA	NA
Mars 81	NA	NA	NA	NA	IIICcbd	-8.17 / 76.64	NA	

References: This paper

Moisture: NA Notes: South-most edge poorly imaged. Source area unclear. Best picno: 66A17. Mosaic #: 1842

Substrate: NA

M	NA	NA	NA	NA	NA	Melas Chasma	NA	NA
Mars 80	NA	NA	NA	NA	IIICcaa	-11.85 / 74.49	NA	

References: This paper

Moisture: NA Notes: Atypical morphology—perhaps eroded. Best picno: 915A24. Mosaic #: 1593.

Substrate: NA

---

1. Rank 2. Name	3. Volume 4. Area	5. Thickness: a. Avg b. Max	6. Drop 7. Velocity	8. Length: a. Straight b. Curved	9. Fahr- böschung 10. Type	11. Location 12. Lat./Long.	13. Confinement 14. Age	15. Composition
M	NA	NA	NA	NA	NA	Melas Chasma	NA	NA
Mars 83	NA	NA	NA	NA	IIICcbd	-8.15 / 75.19	NA	

References: This paper

Moisture: NA Notes: A small, rather sinuous landslide. Best picno: 917A18. Mosaic #: 1842

Substrate: NA

M	NA	NA	NA	NA	NA	Melas Chasma	NA	NA
Mars 82	NA	NA	NA	NA	IIICcbd	-8.11 / 76.64	NA	

References: This paper

Moisture: NA Notes: South-most edge poorly imaged. Source area unclear. Best picno: 66A17. Mosaic #: 1842

Substrate: NA

M	NA	NA	NA	NA	NA	Tithonium Chasma	NA	NA
Mars 90	NA	NA	NA	NA	IIICaab	-4.87 / 82	NA	

References: This paper

Moisture: NA Notes: Landslide apron movement at 90° to direction of initial collapse. Best picno: 064A27. Mosaic #: 1207

Substrate: NA

---

1. Rank 2. Name	3. Volume 4. Area	5. Thickness: a. Avg b. Max	6. Drop 7. Velocity	8. Length: a. Straight b. Curved	9. Fahr- böschung 10. Type	11. Location 12. Lat./Long.	13. Confinement 14. Age	15. Composition
M	NA	NA	NA	NA	NA	Ophir Chasma	NA	NA
Mars 97	NA	NA	NA	NA	IIICcaa	-4.1 / 74.47	NA	

References: This paper

Moisture: NA Notes: Discussed in Lucchitta's #3 reference as a "debris flow." Best picno: 915A10. Mosaic #: 1592

Substrate: NA

M	NA	NA	NA	NA	NA	Ophir Chasma	NA	NA
Mars 96	NA	NA	NA	NA	IIICcbd	-4.27 / 74.33	NA	

References: This paper

Moisture: NA Notes: Very long and narrow compared with most landslides. Best picno: 915A10. Mosaic #: 1592

Substrate: NA

M	NA	NA	NA	NA	NA	Capri Chasma	NA	NA
Mars 99	NA	NA	NA	NA	IIICbaa	-3.43 / 35.19	NA	

References: This paper

Moisture: NA Notes: Headscarp formed at the intersection of a crater and chasma wall. Distal end appears finely digitate. Best picno: 014A55.

Substrate: NA

---

1. Rank 2. Name	3. Volume 4. Area	5. Thickness: a. Avg b. Max	6. Drop 7. Velocity	8. Length: a. Straight b. Curved	9. Fahr-böschung 10. Type	11. Location 12. Lat./Long.	13. Confinement 14. Age	15. Composition
M	NA	NA	NA	NA	NA	Capri Chasma	NA	NA
Mars 98	NA	NA	NA	NA	IIICbaa	-3.25 / 35.09	NA	

References: This paper

Moisture: NA Notes: Headscarp formed at the intersection of a crater and chasma wall. Located together with Mars 99, Mars 100 in outflow-cut channel. Distal end appears finely digitate, so may be longitudinally ribbed at a fine scale. Source area in shadow. Best picno: 014A55.

Substrate: NA

M	NA	NA	NA	NA	NA	Tithonium Chasma	NA	NA
Mars 95	NA	NA	NA	NA	IIICaab	-4.41 / 89.2	NA	

References: This paper

Moisture: NA Notes: Highly irregular distal and lateral margins evident. Best picno: 063A66. Mosaic #: 1207

Substrate: NA

M	NA	NA	NA	NA	NA	Tithonium Chasma	NA	NA
Mars 92	NA	NA	NA	NA	IIICbab	-4.68 / 84.32	NA	

References: This paper

Moisture: NA Notes: "Martinez Mountain-like," the toe of this landslide displays fine digitations and thin longitudinal ribbing. Best picno: 926A04. Mosaic #: 1207

Substrate: NA

---

1. Rank 2. Name	3. Volume 4. Area	5. Thickness: a. Avg b. Max	6. Drop 7. Velocity	8. Length: a. Straight b. Curved	9. Fahr- böschung 10. Type	11. Location 12. Lat./Long.	13. Confinement 14. Age	15. Composition
M	NA	NA	NA	NA	NA	Tithonium Chasma	NA	NA
Mars 91	NA	NA	NA	NA	IIICaad	-6.05 / 79.67	NA	

References: This paper

Moisture: NA Notes: Fall height very great for distance traveled, but the deposit spread out more than usual, maybe because of the high energy of fall. Best picno: 920A12. Mosaic #: 1841

Substrate: NA

M	NA	NA	NA	NA	NA	Tithonium Chasma	NA	NA
Mars 94	NA	NA	NA	NA	IIICcbd	-6.05 / 79.67	NA	

References: This paper

Moisture: NA Notes: A secondary slide atop Mars 91, with more distinct morphology. Best picno: 920A12. Mosaic #: 1841

Substrate: NA

M	NA	NA	NA	NA	NA	Tithonium Chasma	NA	NA
Mars 93	NA	NA	NA	NA	IIICcba	-4.68 / 84.29	NA	

References: This paper

Moisture: NA Notes: This slide predates Mars 92, since it is diverted by this slide. Texture appears featureless, at least at this resolution. Best picno: 926A04. Mosaic #: 1207

Substrate: NA

---

1. Rank 2. Name	3. Volume 4. Area	5. Thickness: a. Avg b. Max	6. Drop 7. Velocity	8. Length: a. Straight b. Curved	9. Fahr-böschung 10. Type	11. Location 12. Lat./Long.	13. Confinement 14. Age	15. Composition
M	NA	NA	NA	NA	NA	Cydonia Mensae	NA	NA
Mars 115	NA	NA	NA	NA	IIICbab	35.03 / 12.95	NA	

References: This paper

Moisture: NA Notes: Small lobe extending from erosional remnant mountain. Best picno: 218S08. Mosaic #: 1351

Substrate: NA

M	NA	NA	NA	NA	NA	Cydonia Mensae	NA	NA
Mars 114	NA	NA	NA	NA	IIICcbd	33.65 / 15.7	NA	

References: This paper

Moisture: NA Notes: Very small landslide in 7 km diameter crater; 1 km long, 350 m wide. Best picno: 219S11. Mosaic #: 1351

Substrate: NA

M	NA	NA	NA	NA	NA	Crater Curie	NA	NA
Mars 117	NA	NA	NA	NA	IIICcbd	29.65 / 4.85	NA	

References: This paper

Moisture: NA Notes: Collapse into large crater, possibly a bilobed deposit. Best picno: 206A18. Mosaic #: 1344

Substrate: NA

---

1. Rank / 2. Name	3. Volume / 4. Area	5. Thickness: a. Avg / b. Max	6. Drop / 7. Velocity	8. Length: a. Straight / b. Curved	9. Fahrböschung / 10. Type	11. Location / 12. Lat./Long.	13. Confinement / 14. Age	15. Composition
M	NA	NA	NA	NA	NA	Arabia Terra	NA	NA
Mars 116	NA	NA	NA	NA	IIICcbd,b	35.13 / 6.67	NA	

References: This paper

Moisture: NA Notes: A landslide of substantial size in image; 7 km long by 3 km wide, lying in a 30 km wide crater. Headscarp and apron morphologies very clear. Best picno: 216S13. Mosaic #: 1351

Substrate: NA

M	NA	NA	NA	NA	NA	Acidalia Planitia	NA	NA
Mars 113	NA	NA	NA	NA	IIICcbd	38.7 / 18.1	NA	

References: This paper

Moisture: NA Notes: Small landslide in 25 km diameter crater; 1.8 km long, 0.9 km wide. Best picno: 225S19. Mosaic #: 1351

Substrate: NA

M	NA	NA	NA	NA	NA	Sirenum Fossae	NA	NA
Mars 110	NA	NA	NA	NA	IIICcbd	-26.49 / 139.91	NA	

References: This paper

Moisture: NA Notes: Landslide toe clear, but medial portion subdued. Alcove which could be headscarp is evident. Landslide occurs on floor of a small flat-floored basin, ~35 km across, with very steep walls. Best picno: 457A06. Mosaic #: 1187

Substrate: NA

---

1. Rank 2. Name	3. Volume 4. Area	5. Thickness: a. Avg b. Max	6. Drop 7. Velocity	8. Length: a. Straight b. Curved	9. Fahrböschung 10. Type	11. Location 12. Lat./Long.	13. Confinement 14. Age	15. Composition
M	NA	NA	NA	NA	NA	Melas Chasma	unconfined	NA
Mars 11 (Melas Labes)	NA	NA	450	NA	IB2,5	-8.5 / 71.5	NA	

References: Lucchitta, 1979; 1987; U. S. Geol. Surv., 1984b

Moisture: NA Notes: The landslide originated from the intersection of a graben-bounding fault with wall rock in Valles Marineris. Abuts possible ancient lake of Lucchitta, 1987. Best picnos: 091A08, 913A57; Best photomosaic: I-1593. Landslide #11 from Lucchitta, 1979.

Substrate: NA

M	NA	NA	NA	NA	NA	Arabia Terra	NA	NA
Mars 112	NA	NA	NA	NA	IIICcbd	32.2 / 12.45	NA	

References: This paper

Moisture: NA Notes: A small landslide, 1 km wide by 3.2 km long, similar to "Blackhawk type," but somewhat misshapen by irregular topography. Best picno: 227S17. Mosaic #: 1351

Substrate: NA

M	NA	NA	NA	NA	NA	Arabia Terra	NA	NA
Mars 111	NA	NA	NA	NA	IIICcbd	23 / 21.65	NA	

References: This paper

Moisture: NA Notes: A small landslide, 1.2 km wide by 2.5 km long. Headscarp intersects small crater. Landslide fell into a large crater. Best picno: 670A48. Mosaic #: 1344

Substrate: NA

---

1. Rank / 2. Name	3. Volume / 4. Area	5. Thickness: a. Avg / b. Max	6. Drop / 7. Velocity	8. Length: a. Straight / b. Curved	9. Fahr-böschung / 10. Type	11. Location / 12. Lat./Long.	13. Confinement / 14. Age	15. Composition
M	NA	NA	NA	NA	NA	Acidalia Planitia	NA	NA
Mars 119	NA	NA	NA	NA	IIICcbd	43.09 / 14.3	NA	

References: This paper

Moisture: NA Notes: Deposit lies in splash crater with large central peak, 20 km diameter. Best picno: 032A30

Substrate: NA

M	NA	NA	NA	NA	NA	Terra Cimmeria	NA	NA
Mars 125	NA	NA	NA	NA	IIICcbd	-35.67 / 213.54	NA	

References: This paper

Moisture: NA Notes: Simple slide in 40-km diameter crater. Best picno: 425S40

Substrate: NA

M	NA	NA	NA	NA	NA	Terra Cimmeria	NA	NA
Mars 124	NA	NA	NA	NA	IIICbba	-29.4 / 223.4	NA	

References: This paper

Moisture: NA Notes: Moderate-sized deposit in 40 km-diameter crater. Best picno: 424S06, 08

Substrate: NA

---

1. Rank 2. Name	3. Volume 4. Area	5. Thickness: a. Avg b. Max	6. Drop 7. Velocity	8. Length: a. Straight b. Curved	9. Fahr- böschung 10. Type	11. Location 12. Lat./Long.	13. Confinement 14. Age	15. Composition
M	NA	NA	NA	NA	NA	Terra Cimmeria	NA	NA
Mars 127	NA	NA	NA	NA	IIICbab	-36.72 / 212.65	NA	

References: This paper

Moisture: NA Notes: Occurs in 40 km-diameter crater with Mars 126. Distinct light/dark longitudinal banding. Best picno: 425S42

Substrate: NA

M	NA	NA	NA	NA	NA	Terra Cimmeria	NA	NA
Mars 126	NA	NA	NA	NA	IIICbab	-36.72 / 212.65	NA	

References: This paper

Moisture: NA Notes: Occurs in 40 km-diameter crater with Mars 127. Distinct light/dark longitudinal banding. Best picno: 425S42

Substrate: NA

M	NA	NA	NA	NA	NA	Terra Cimmeria	NA	NA
Mars 123	NA	NA	NA	NA	IIICcba	-33.7 / 223.5	NA	

References: This paper

Moisture: NA Notes: Overlaps deposit Mars 122, suggesting different ages. Source areas near small crater at edge of larger crater. Small crater simple bowl. Best picno: 422S14

Substrate: NA

---

1. Rank / 2. Name	3. Volume / 4. Area	5. Thickness: a. Avg / b. Max	6. Drop / 7. Velocity	8. Length: a. Straight / b. Curved	9. Fahrböschung / 10. Type	11. Location / 12. Lat./Long.	13. Confinement / 14. Age	15. Composition
M	NA	NA	NA	NA	NA	Isidis Planitia	NA	NA
Mars 120	NA	NA	NA	NA	IIICcbd	5.38 / 272.15	NA	

References: This paper

Moisture: NA Notes: Deposit lies in 10 km diameter crater. Best picno: 718A29, 31

Substrate: NA

M	NA	NA	NA	NA	NA	Melas Chasma	unconfined	NA
Mars 12	NA	NA	NA	NA	IB4	-12.6 / 73.6	NA	

References: Lucchitta, 1979

Moisture: NA Notes: The landslide occurred from the intersection of graben-bounding faults and a chasma wall. Double-reentrant headscarp. Complex apron, seemingly very fluid. Substantial age suggested by superposed craters, indistinct distal and lateral margins.

Substrate: NA Close to chasma floor layered terrain. Best picno: 091A03; mosaic #I-1593. Landslide #12 in Lucchitta, 1979.

M	NA	NA	NA	NA	NA	Terra Cimmeria	NA	NA
Mars 122	NA	NA	NA	NA	IIICcba	-33.7 / 223.5	NA	

References: This paper

Moisture: NA Notes: Overlaps deposit Mars 123, suggesting different ages. Source areas near small crater at edge of larger crater. Small crater simple bowl. Best picno: 422S14

Substrate: NA

---

1. Rank / 2. Name	3. Volume / 4. Area	5. Thickness: a. Avg / b. Max	6. Drop / 7. Velocity	8. Length: a. Straight / b. Curved	9. Fahrböschung / 10. Type	11. Location / 12. Lat./Long.	13. Confinement / 14. Age	15. Composition
M	NA	NA	NA	NA	NA	Terra Tyrrhena	NA	NA
Mars 121	NA	NA	NA	NA	IIICbab	-1.4 / 258	NA	

References: This paper

Moisture: NA Notes: 4 km broad headscarp area partially encircles 4.5 km-diameter bowl-shaped crater. Stratigraphy visible. 12 m resolution. One crater, ~150 m diameter. Could be related to the impact but none of the rest of ejecta blanket is similar. Best picno: 129S03-5

Substrate: NA

M	NA	NA	NA	NA	NA	Terra Sirenum	NA	NA
Mars 107	NA	NA	NA	NA	IIICcbd	-11.75 / 172.79	NA	

References: This paper

Moisture: NA Notes: Headscarp indeterminate—too much slope glare. Two or more small (~100+ m) craters. Best picno: 439S09. Mosaic #: 1186

Substrate: NA

E	NA	0	NA	NA	NA	Washington, U.S.A.	NA	basalt
Bonneville	14	NA	NA	NA	NA	NA / NA	700 B.P.	

References: Palmer, 1977

Moisture: NA Notes: The distal margin of the deposit was intruded by clastic dikes.

Substrate: NA

---

1. Rank 2. Name	3. Volume 4. Area	5. Thickness: a. Avg b. Max	6. Drop 7. Velocity	8. Length: a. Straight b. Curved	9. Fahr-böschung 10. Type	11. Location 12. Lat./Long.	13. Confinement 14. Age	15. Composition
E	NA	NA	NA	8000	0.00	Nevada, U.S.A.	NA	gneiss, schist and granite
Bonelli Peak mb	NA	120	NA	NA	NA	NA / NA	Miocene	

References: Longwell, 1951; Yarnold and Lombard, 1989

Moisture: NA Notes: This megabreccia deposit exhibits basal strata disruption, sub-horizontal slip surfaces and a foliated texture locally. Outcrops are now drowned by waters in Lake Mead.

Substrate: NA

E(u)	NA	NA	NA	NA	NA	East Indes	unconfined	volcanics
Goenoeng Api	NA	NA	NA	NA	NA	-6.68 / -126.68	late Pleistocene	

References: Fairbridge, 1950

Moisture: NA Notes: Possibly triggered by Pleistocene sea level drop and resultant removal of support from a large portion of the volcanic cone.

Substrate: NA

E	NA	NA	NA	NA	NA	Arizona, U.S.A.	NA	blue quartzite
Buckskin Mtn. mb	NA	20	NA	NA	NA	NA / NA	Miocene	

References: Yarnold and Lombard, 1989

Moisture: NA Notes: This megabreccia deposit exhibits incorporated substrate material, three-dimensional jigsaw puzzle breccia, basal strata disruption, sub-horizontal slip surfaces and load structures.

Substrate: NA

---

1. Rank 2. Name	3. Volume 4. Area	5. Thickness: a. Avg b. Max	6. Drop 7. Velocity	8. Length: a. Straight b. Curved	9. Fahr-böschung 10. Type	11. Location 12. Lat./Long.	13. Confinement 14. Age	15. Composition
E	NA	0	600	8000	0.08	Arizona, U.S.A.	unconfined	gneiss,
Black Canyon mb	24	180	120	NA	IIIC	35.92 / 114.68	Miocene	schist, granite

References: Longwell, 1951; Yarnold and Lombard, 1989

Moisture: NA Notes: This eroded landslide deposit exhibits reverse grading, incorporated inert substrate material, three-dimensional jigsaw puzzle breccia, basal strata disruption, sub-horizontal slip surfaces, clastic dike intrusions, thrust faults and imbrication and basal striations.

Substrate: NA

E	NA	NA	NA	NA	NA	France	unconfined	carbonate
Ales mb	NA	NA	NA	NA	NA	NA / NA	Tertiary	

References: Koop, 1952

Moisture: NA Notes: This deposit exhibits preserved slope-parallel stratigraphy, basal strata disruption, internal thrust faults and imbrication and striations on clasts.

Substrate: NA

E	NA	NA	NA	NA	NA	Arizona, U.S.A.	NA	granite
Adair Park mb	NA	100	NA	NA	NA	32.78 / 114.43	L. Oligocene-E. Miocene	

References: Yarnold and Lombard, 1989

Moisture: NA Notes: Monolithologic, displaying reverse grading, boulders with 3-dimensional jigsaw puzzle fractures, incorporated substrate material, disruption of underlying strata, sub-horizontal internal slip surfaces, clastic dike intrusion, basal striations, load structures and a foliated texture.

Substrate: NA

---

1. Rank 2. Name	3. Volume 4. Area	5. Thickness: a. Avg b. Max	6. Drop 7. Velocity	8. Length: a. Straight b. Curved	9. Fahr-böschung 10. Type	11. Location 12. Lat./Long.	13. Confinement 14. Age	15. Composition
E	NA	NA	NA	NA	NA	California, U.S.A.	NA	metavolcanics
Avawatz Mtns. mb	NA	10	NA	NA	NA	35.65 / 116.49	early Quaternary	

References: Brady, 1984.

Moisture: NA Notes: Monolithologic breccia. Several distinct sheets are evident in vicinity, aggregating over 100 m in thickness. Internally chaotic and devoid of matrix. The eroded landslide also displays three-dimensional jigsaw puzzle breccia.

Substrate: NA

E	NA	NA	NA	5000	0.00	Arizona, U.S.A.	NA	NA
Artillery Mtns. mb	NA	170	NA	NA	NA	NA / NA	NA	

References: Yarnold and Lombard, 1989

Moisture: NA Notes: This megabreccia deposit exhibits inert incorporated substrate material, three-dimensional jigsaw puzzle breccia, basal strata disruption and intruded clastic dikes.

Substrate: NA

E	NA	NA	4085	NA	NA		channeled	NA
Greenwater mb	NA	NA	NA	54000	NA	NA / NA	NA	

References: Schuster and Crandell, 1984.

Moisture: NA Notes: NA

Substrate: NA

---

1. Rank / 2. Name	3. Volume / 4. Area	5. Thickness: a. Avg / b. Max	6. Drop / 7. Velocity	8. Length: a. Straight / b. Curved	9. Fahrböschung / 10. Type	11. Location / 12. Lat./Long.	13. Confinement / 14. Age	15. Composition
M	NA	NA	NA	NA	NA	Prometheii Terra	NA	NA
Mars 104	NA	NA	NA	NA	IIICcbd	-37.8 / 248.7	NA	

References: This paper

Moisture: NA Notes: Landslide extending from a small peak, possibly volcanic (?). This slide simply shows as an outline, a raised rim. Inside the rim it is featureless. Half of peak shaded; crest has two pits or craters. Best picno: 585B24. Mosaic #: 1451

Substrate: NA

M	NA	NA	NA	NA	NA	Hellespontus Montes	NA	NA
Mars 103	NA	NA	NA	NA	IIICbaa	-50.82 / 317.05	NA	

References: This paper

Moisture: NA Notes: Very poorly imaged; only visible as a lighter area than the surrounding surface; headscarp region evident, however. Best picno: 577B45. Mosaic #: 1586

Substrate: NA

M	NA	NA	NA	NA	NA	Prometheii Terra	NA	NA
Mars 106	NA	NA	NA	NA	IIICbaa	-41.61 / 251.4	NA	

References: This paper

Moisture: NA Notes: Best picno: 411S22. Mosaic #: 1451

Substrate: NA

---

1. Rank 2. Name	3. Volume 4. Area	5. Thickness: a. Avg b. Max	6. Drop 7. Velocity	8. Length: a. Straight b. Curved	9. Fahr-böschung 10. Type	11. Location 12. Lat./Long.	13. Confinement 14. Age	15. Composition
M	NA	NA	NA	NA	NA	Prometheii Terra	NA	NA
Mars 105	NA	NA	NA	NA	IIICcbd	-37.8 / 248.7	NA	

References: This paper

Moisture: NA Notes: Same description as Mars 104. Best picno: 585B24. Mosaic #: 1451

Substrate: NA

M	NA	NA	NA	NA	NA	Tithonium Chasma	NA	NA
Mars 102	NA	NA	NA	NA	IIICaab	-5.49 / 89.35	NA	

References: This paper

Moisture: NA Notes: Deposit appears to be a thick debris apron, though source area is unclear. Best picno: 063A63. Mosaic #: 1207

Substrate: NA

E	NA	0	NA	NA	NA	California, U.S.A.	NA	Topanga Formation
Las Tunas Beach	0.777	NA	NA	NA	IIA, Slow	NA / NA	modern	

References: McNamera and Rodine, 1987

Moisture: NA Notes: Heavy winter rains in 1978 and 1980 reactivated 50% of an ancient slide mass. Maximum movement rate was 1 foot per year in early 1984.

Substrate: NA

---

1. Rank 2. Name	3. Volume 4. Area	5. Thickness: a. Avg b. Max	6. Drop 7. Velocity	8. Length: a. Straight b. Curved	9. Fahr-böschung 10. Type	11. Location 12. Lat./Long.	13. Confinement 14. Age	15. Composition
E(u)	NA	0	3500	80000	0.04	Hawaii, U.S.A.	unconfined	basalt
Kaena	3900	NA	NA	80000	IB	22 / 158.25	NA	

References: Moore, et al., 1989

Moisture: NA Notes: NA

Substrate: NA

M	NA	NA	NA	NA	NA	Capri Chasma	NA	NA
Mars 100	NA	NA	NA	NA	IIICbaa	-3.17 / 35.09	NA	

References: This paper

Moisture: NA Notes: Headscarp formed at the intersection of a crater and chasma wall. Very narrow for its length. No other structures visible. Best picno: 014A55.

Substrate: NA

M	NA	NA	NA	NA	NA	Coprates Chasma	unconfined	NA
Mars 10 (Ophir Labes)	NA	NA	NA	NA	-B2,4	-11 / 68.2	NA	

References: Lucchitta, 1979; U. S. Geol. Surv., 1984a

Moisture: NA Notes: Unusual headscarp region. The landslide originated from wall rock in Valles Marineris. Black material covers much of the surface and is concentrated in longitudinal streaks. Best picno: 080A02; Best photomosaic: I-1591. Landslide #10 from Lucchitta, 1979.

Substrate: NA

---

1. Rank 2. Name	3. Volume 4. Area	5. Thickness: a. Avg b. Max	6. Drop 7. Velocity	8. Length: a. Straight b. Curved	9. Fahr-böschung 10. Type	11. Location 12. Lat./Long.	13. Confinement 14. Age	15. Composition
M	NA	NA	NA	NA	NA	Gangis Chasma	NA	NA
Mars 155	NA	NA	NA	NA	IA	-7.4 / 45.4	NA	

References: This paper

Moisture: NA Notes: Large slump blocks present, but no real headscarp area. Region of etched terrain beyond slide toe is very peculiar. Best picno: 12A52. Mosaic #: 1381

Substrate: NA

M	NA	NA	NA	NA	NA	Gangis Chasma	NA	NA
Mars 154	NA	NA	NA	NA	IA	-7 / 44.4	NA	

References: This paper

Moisture: NA Notes: Best picno: 12A54. Mosaic #: 1381

Substrate: NA

M	NA	NA	NA	NA	NA	Juventae Chasma	NA	NA
Mars 157	NA	NA	NA	NA	IA	-1.2 / 61.53	NA	

References: This paper

Moisture: NA Notes: Slump block is capped by dark bumpy layer. Probable superposed crater. Best picno: 81A22. Mosaic #: 1677

Substrate: NA

---

1. Rank 2. Name	3. Volume 4. Area	5. Thickness: a. Avg b. Max	6. Drop 7. Velocity	8. Length: a. Straight b. Curved	9. Fahr-böschung 10. Type	11. Location 12. Lat./Long.	13. Confinement 14. Age	15. Composition
M	NA	NA	NA	NA	NA	Kasei Valles	NA	NA
Mars 156	NA	NA	NA	NA	IA	23.3 / 59.9	NA	

References: This paper

Moisture: NA Notes: Best picno: 226A49. Mosaic #: 1870

Substrate: NA

M	NA	NA	NA	NA	NA	Juventae Chasma	NA	NA
Mars 153	NA	NA	NA	NA	IIICbba	-0.83 / 60.65	NA	

References: This paper

Moisture: NA Notes: Post-outflow landslide in chaotic terrain. Best picno: 905A02

Substrate: NA

M	NA	NA	NA	NA	NA	Kasei Valles	NA	NA
Mars 150	NA	NA	NA	NA	IIICcbd	25.56 / 64.44	NA	

References: This paper

Moisture: NA Notes: Source is in small canyon that connects large, lower basin to an upper, enclosed graben. Distal end of the deposit is cut off at an escarpment. Either downfaulted or eroded at this contact. Best picno: 226A05

Substrate: NA

---

1. Rank 2. Name	3. Volume 4. Area	5. Thickness: a. Avg b. Max	6. Drop 7. Velocity	8. Length: a. Straight b. Curved	9. Fahr- böschung 10. Type	11. Location 12. Lat./Long.	13. Confinement 14. Age	15. Composition
M	NA	NA	NA	NA	NA	Kasei Valles	NA	NA
Mars 149	NA	NA	NA	NA	IIICcbd	22.5 / 63.98	NA	

References: This paper

Moisture: NA Notes: Small slide originates at intersection of plateau and outflow channel, where small crater was undercut. Best picno: 226A43

Substrate: NA

M	NA	NA	NA	NA	NA	Juventae Chasma	NA	NA
Mars 152	NA	NA	NA	NA	IIICcbd	-0.8 / 60.7	NA	

References: This paper

Moisture: NA Notes: Pos-outflow landslide in chaotic terrain. Best picno: 905A02

Substrate: NA

M	NA	NA	NA	NA	NA	Xanthe Terra	NA	NA
Mars 151	NA	NA	NA	NA	IIICcbd	4.92 / 59.53	NA	

References: This paper

Moisture: NA Notes: Deposit lies within 30 km diameter crater. The exterior of the crater was eroded by water at some point. Best picno: 79A64

Substrate: NA

---

1. Rank 2. Name	3. Volume 4. Area	5. Thickness: a. Avg b. Max	6. Drop 7. Velocity	8. Length: a. Straight b. Curved	9. Fahr- böschung 10. Type	11. Location 12. Lat./Long.	13. Confinement 14. Age	15. Composition
M	NA	NA	NA	NA	NA	Gangis Chasma	NA	NA
Mars 158	NA	NA	NA	NA	IA	-7.12 / 50.1	NA	

References: This paper

Moisture: NA Notes: Best picno: 897A40

Substrate: NA

M	NA	NA	NA	NA	NA	Ius Chasma	NA	NA
Mars 21	NA	NA	NA	NA	IB4	-7.04 / 89.58	NA	

References: Lucchitta, 1979

Moisture: NA Notes: The landslide occurred from the intersection of graben-bounding faults and a chasma wall. Best picno: 064A12; mosaic #I-1207. Landslide #21 in Lucchitta, 1979.

Substrate: NA

M	NA	NA	NA	NA	NA	Ius Chasma	NA	NA
Mars 20	NA	NA	NA	NA	- A	-6.69 / 88.29	NA	

References: This paper

Moisture: NA Notes: Lucchitta's slide #20. No debris apron apparent. Best picno: 929A02. Mosaic #: 1207

Substrate: NA

---

1. Rank 2. Name	3. Volume 4. Area	5. Thickness: a. Avg b. Max	6. Drop 7. Velocity	8. Length: a. Straight b. Curved	9. Fahr-böschung 10. Type	11. Location 12. Lat./Long.	13. Confinement 14. Age	15. Composition
M	NA	NA	NA	NA	NA	Tithonium Chasma	NA	NA
Mars 27	NA	NA	250	NA	NA	-4.33 / 85.5	NA	

References: Lucchitta, 1979; 1987

Moisture: NA Notes: The landslide originated from wall rock in Valles Marineris. Local geology extremely complex, with many overlapping landslide units. The boundaries of the deposit are rather uncertain. Best picno: 064A22. Landslide #27 from Lucchitta, 1979.

Substrate: NA

M	NA	NA	NA	NA	NA	Tithonium Chasma	NA	NA
Mars 23	NA	NA	NA	NA	IIICabd	-3.9 / 89.44	NA	

References: This paper

Moisture: NA Notes: Landslide #23 in Lucchitta, 1979. Best picno: 063A68. Mosaic #: 1207

Substrate: NA

M	NA	NA	NA	NA	NA	Gangis Chasma	unconfined	NA
Mars 2	NA	NA	NA	NA	IB2	-8.89 / 45	NA	

References: Lucchitta, 1979

Moisture: NA Notes: The landslide occurred at the intersection of a crater and a chasma wall. The landslide underlies the Mars 1 deposit. Best picno: 014A29; mosaic #I-1381. Landslide #2 in Lucchitta, 1979.

Substrate: NA

---

1. Rank 2. Name	3. Volume 4. Area	5. Thickness: a. Avg b. Max	6. Drop 7. Velocity	8. Length: a. Straight b. Curved	9. Fahr- böschung 10. Type	11. Location 12. Lat./Long.	13. Confinement 14. Age	15. Composition
M	NA	NA	NA	NA	NA	Ius Chasma	NA	NA
Mars 16	NA	NA	NA	NA	IB2	-7.16 / 79.45	NA	

References: Lucchitta, 1979

Moisture: NA Notes: The landslide occurred from the intersection of graben-bounding faults and a chasma wall. Very subdued debris apron texture. Additional downdropping of chasma floor might have occurred subsequent to deposition. Several superposed craters suggest considerable age, and Mars 15 deposit seems to overlie this deposit. Best picno: 066A12; mosaic #I-1841. Landslide #16 in Lucchitta, 1979.

Substrate: NA

M	NA	NA	NA	NA	NA	Acheron Fossae	NA	NA
Mars 159	NA	NA	NA	NA	IA	37.61 / 131.29	NA	

References: This paper

Moisture: NA Notes: Slump from a horst into a graben filled with a smooth-to-ridged material that displays flow features, including arcuate ridges and flow streamline forms. Best picno: 129A46

Substrate: NA

M	NA	NA	NA	NA	NA	Ius Chasma	NA	NA
Mars 17	NA	NA	NA	NA	-B4	-7.17 / 80.67	NA	

References: Lucchitta, 1979

Moisture: NA Notes: The landslide occurred from the intersection of small plateau craters and a chasma wall. An irregular heap of debris, perhaps reworked by some process? Best picnos: 063A40; mosaic #I-1207. Landslide #17 in Lucchitta, 1979.

Substrate: NA

---

1. Rank 2. Name	3. Volume 4. Area	5. Thickness: a. Avg b. Max	6. Drop 7. Velocity	8. Length: a. Straight b. Curved	9. Fahr- böschung 10. Type	11. Location 12. Lat./Long.	13. Confinement 14. Age	15. Composition
M	NA	NA	NA	NA	NA	Argyre Planitia	NA	NA
Mars 160	NA	NA	NA	NA	IIA?	-54.69 / 41.71	NA	

References: This paper

Moisture: NA Notes: Small mountain displays a scar and slide-mass of same dimensions, in shape of very flat half ellipse. Only distal end slightly disrupted, the rest seems to have slid as an intact mass. Best picno: 567B34

Substrate: NA

M	NA	NA	NA	NA	NA	Hebes Chasma	NA	NA
Mars 148	NA	NA	NA	NA	IIICaab	-1.73 / 74.32	NA	

References: This paper

Moisture: NA Notes: Small slide from chasma wall. Headscarp shows some stratification. One superposed crater. Best picno: 915A06

Substrate: NA

M	NA	NA	NA	NA	NA	Maadim Valles region	NA	NA
Mars 134	NA	NA	NA	NA	IIICbaa	-22.85 / 189.37	NA	

References: This paper

Moisture: NA Notes: Lobate with rough upper surface. In 25 km-diameter crater. Best picno: 429S28

Substrate: NA

---

1. Rank 2. Name	3. Volume 4. Area	5. Thickness: a. Avg b. Max	6. Drop 7. Velocity	8. Length: a. Straight b. Curved	9. Fahr- böschung 10. Type	11. Location 12. Lat./Long.	13. Confinement 14. Age	15. Composition
M	NA	NA	NA	NA	NA	Maadim Valles region	NA	NA
Mars 132	NA	NA	NA	NA	IIICcbd	-13 / 190	NA	

References: This paper

Moisture: NA Notes: This slide is deposited downhill from small bowl crater. Best picno: 432S01

Substrate: NA

M	NA	NA	NA	NA	NA	Capri Chasma	NA	NA
Mars 136	NA	NA	NA	NA	IIICcbd	-8.52 / 41.7	NA	

References: This paper

Moisture: NA Notes: Headscarp occurs at the intersection of an impact crater with a chasma wall. Debris flowed over scarp. Large superposed crater. Best picno: 14A38

Substrate: NA

M	NA	NA	NA	NA	NA	Capri Chasma	NA	NA
Mars 135	NA	NA	NA	NA	IIICcbd	-8.52 / 41.72	NA	

References: This paper

Moisture: NA Notes: Headscarp occurs at the intersection of an impact crater with a chasma wall. Debris flowed over a fault (?) scarp of moderate height and then on over the chasma floor. Overlaps Mars136. Best picno: 14A38

Substrate: NA

---

1. Rank 2. Name	3. Volume 4. Area	5. Thickness: a. Avg b. Max	6. Drop 7. Velocity	8. Length: a. Straight b. Curved	9. Fahr- böschung 10. Type	11. Location 12. Lat./Long.	13. Confinement 14. Age	15. Composition
M	NA	NA	NA	NA	NA	Maadim Valles region	NA	NA
Mars 131	NA	NA	NA	NA	IIICbba	-20.96 / 185.57	NA	

References: This paper

Moisture: NA Notes: Collapse into a 35 km-diameter crater. Best picno: 431S22

Substrate: NA

M	NA	NA	NA	NA	NA	Maadim Valles region	NA	NA
Mars 129	NA	NA	NA	NA	IIICcbb,d	-13.25 / 187.16	NA	

References: This paper

Moisture: NA Notes: Moderate-scale deposit in 50 km-diameter crater. Has Martinez-Mtn.-like combination of lateral ridges and broadly digitate basal portion. Best picno: 434S03

Substrate: NA

M	NA	NA	NA	NA	NA	Orcus Patera region	NA	NA
Mars 128	NA	NA	NA	NA	IIICcbd	9.55 / 189.5	NA	

References: This paper

Moisture: NA Notes: Very small deposit, ~1.5 km in length, ~.8 km wide. Shed from a mountain ~5 km across. Best picno: 727A23

Substrate: NA

---

1. Rank 2. Name	3. Volume 4. Area	5. Thickness: a. Avg b. Max	6. Drop 7. Velocity	8. Length: a. Straight b. Curved	9. Fahr- böschung 10. Type	11. Location 12. Lat./Long.	13. Confinement 14. Age	15. Composition
M	NA	NA	NA	NA	NA	Maadim Valles region	NA	NA
Mars 130	NA	NA	NA	NA	IIICbbb	-20/ 186.8	NA	

References: This paper

Moisture: NA Notes: Irregular depositional pattern produced by irregular terrain. Collapse was into a 50 km-diameter crater. Best picno: 431S18

Substrate: NA

M	NA	NA	NA	NA	NA	Candor Chasma	NA	NA
Mars 13 (E. Candor	NA	NA	400	NA	IB4	-4.75/ 75.33	NA	

References: Lucchitta, 1979;1987; U. S. Geol. Surv., 1986a

Moisture: NA Notes: The landslide originated from the intersection of a graben-bounding fault with wall rock in Valles Marineris. The landslide lies just north of an extremely complex region of etched layered terrain. Dark material mantles lower slopes in a band across the lower part of the debris apron. The distal edge is unclear, perhaps eroded. Considerable age suggested by subdued morphology, superposed craters. Best picno: 066A24; Best photomosaic: I-1841. Landslide #13 from Lucchitta, 1979.

Substrate: NA

M	NA	NA	NA	NA	NA	Capri Chasma	NA	NA
Mars 137	NA	NA	NA	NA	IIICcbd	-8.5/ 41.66	NA	

References: This paper

Moisture: NA Notes: Source on shadowed chasma wall. One superposed crater. Best picno: 14A38

Substrate: NA

---

1. Rank 2. Name	3. Volume 4. Area	5. Thickness: a. Avg b. Max	6. Drop 7. Velocity	8. Length: a. Straight b. Curved	9. Fahr-böschung 10. Type	11. Location 12. Lat./Long.	13. Confinement 14. Age	15. Composition
M	NA	NA	NA	NA	NA	Candor Chasma	NA	NA
Mars 14 (W. Candor	NA	NA	NA	NA	IB3	-4.7 / 76.2	NA	

References: Lucchitta, 1979; U. S. Geol. Surv., 1986a

Moisture: NA Notes: The landslide originated from wall rock in Valles Marineris. Local geology extremely complex, with high-contrast surface units. The debris apron appears to lap up against layered terrain. The boundaries of the deposit are rather uncertain. The base of the debris apron has been significantly obscured by overlapping dark material. Best picno: 065A27; Best photomosaic: I-1841. Landslide #14 from Lucchitta, 1979.

Substrate: NA

M	NA	NA	NA	NA	NA	Noctis Labyrinthus	NA	NA
Mars 144	NA	NA	NA	NA	IIICaab	-10 / 95	NA	

References: This paper

Moisture: NA Notes: Fan-shaped deposit in closed basin in Noctis Labyrinthus. Dark/black material lies along basal scarp of graben below headscarp. Volcanic material from late stage? Best picno: 064A02

Substrate: NA

M	NA	NA	NA	NA	NA	Olympus Mons Flank	NA	NA
Mars 143	NA	NA	NA	NA	IIICcbd	23.7 / 136.1	NA	

References: This paper

Moisture: NA Notes: Moderate-sized deposit from NW basal scarp of Olympus Mons. Not very well imaged. Best picno: 047B37

Substrate: NA

---

1. Rank 2. Name	3. Volume 4. Area	5. Thickness: a. Avg b. Max	6. Drop 7. Velocity	8. Length: a. Straight b. Curved	9. Fahr-böschung 10. Type	11. Location 12. Lat./Long.	13. Confinement 14. Age	15. Composition
M	NA	NA	NA	NA	NA	NEMare Tyrrhenum	NA	NA
Mars 140	NA	NA	NA	NA	IIICbbb	-4.68 / 246.95	NA	

References: This paper

Moisture: NA Notes: Very high resolution image exists of slide, which originates from inner crater wall. Headscarp may dissect small crater on large crater rim. Best picno: 123S01

Substrate: NA

M	NA	NA	NA	NA	NA	Capri Chasma	NA	NA
Mars 139	NA	NA	NA	NA	IICcbd	-8.72 / 41.51	NA	

References: This paper

Moisture: NA Notes: Source on chasma wall. Best picno: 14A38

Substrate: NA

M	NA	NA	NA	NA	NA	Louros Valles	NA	NA
Mars 146	NA	NA	NA	NA	IIICcbd	-7.24 / 82.78	NA	

References: This paper

Moisture: NA Notes: Larger and earlier of two superposed deposits. Stratification visible in slide scar. Best picno: 923A12

Substrate: NA

---

1. Rank 2. Name	3. Volume 4. Area	5. Thickness: a. Avg b. Max	6. Drop 7. Velocity	8. Length: a. Straight b. Curved	9. Fahrböschung 10. Type	11. Location 12. Lat./Long.	13. Confinement 14. Age	15. Composition
M	NA	NA	NA	NA	NA	Louros Valles	NA	NA
Mars 147	NA	NA	NA	NA	IIICcbd	-7.3 / 82.78	NA	

References: This paper

Moisture: NA Notes: Smaller and later of two superposed deposits. Stratification visible in slide scar. Best picno: 923A12

Substrate: NA

M	NA	NA	NA	NA	NA	Capri Chasma	NA	NA
Mars 138	NA	NA	NA	NA	IIICcaa	-8.78 / 41.57	NA	

References: This paper

Moisture: NA Notes: Source on chasma wall. Best picno: 14A38

Substrate: NA

M	NA	NA	NA	NA	NA	Louros Valles	NA	NA
Mars 145	NA	NA	NA	NA	IIICaab	-8 / 83	NA	

References: This paper

Moisture: NA Notes: Probable multiple-event slide. Origin in deeply incised canyon in chasma wall. Best picno: 924A11

Substrate: NA

Appendix B

Analysis of a Large Moist Landslide, Lost River Range, Idaho, U.S.A.

Philip J. Shaller
California Institute of Technology
Division of Geological & Planetary Sciences
Mail Stop 170-25
Pasadena, CA, USA 91125
(818) 356-6143

Canadian Geotechnical Journal
Volume 48, August 1991

This paper describes the regional geology, dimensions, morphology, sedimentology and age relations of the Holocene "Carlson landslide," a large moist landslide composed of basalt breccia located on the eastern margin of the Lost River Range, Idaho. These data are combined to deduce the factors that prompted the slope failure, the kinematics of initiation, travel and stopping of the landslide, as well as its post-emplacement degradation. The landslide is compared to other terrestrial mass movements on the basis of morphology, sedimentology, log(volume) vs. fall height/runout length relations and estimated Bingham plastic yield strength. Morphology and sedimentology distinguish dry landslides from moist and water-saturated deposits. However, moist and water-saturated landslides plot well within the log(volume) vs. H/L envelope for dry terrestrial landslides, and exhibit overlapping ranges of estimated Bingham plastic yield strength values with dry landslides, indicating that moist and water-saturated landslides must travel much like dry rock avalanches of similar volume. Thus the mechanism(s) responsible for causing anomalous runout in large dry landslides could operate in moist and water-saturated landslides as well. Morphological comparison of the Carlson landslide with lobate martian landslides suggests a role for water in the martian landslides.

Key words: landslides, debris flows, long runout, morphology, water, Mars.

Introduction

A large landslide of Holocene age lies in the upper Pahsimeroi River valley of east-central Idaho, 12 km northeast of Doublespring Pass, at 44°17' N, 113°44' W (Figure 1). The landslide originated in Tertiary basalts just north of Spring Hill mountain, at the eastern edge of the Lost River Range, and traveled rapidly eastward down a preexisting drainage channel, finishing movement as a giant debris

flow. The name "Carlson landslide" is suggested for the deposit because Carlson Lake occupies part of its headscarp. Shelton (1966) published an aerial photograph and brief analysis of the deposit, but no previous field studies have focused on the landslide.

This landslide was investigated as part of a larger study (Shaller 1991) of large (>10^6 m^3) martian and terrestrial landslides aimed at determining the role of water in the initiation and travel of large landslides on Mars, and the travel mechanics of "long-runout" landslides. Hsü (1975) defined long-runout landslides as those having fall height (vertical distance from crown to toe) to travel length (horizontal distance between crown and toe) ratios of less than 0.6. Hsü (1975) defined this ratio as the "fahrböschung" after Heim (1932); in this paper Hsü's terminology is shortened to H/L. This particular landslide (Figure 2) was investigated because of its similarity in scale and morphology to a pair of landslides in Mars' Candor Chasma (Figure 3; Shaller 1991). Past arguments for and against water in the martian landslides have used morphologies, log(volume) vs. H/L relations, Bingham plastic yield strength estimates, and velocities to compare martian landslides to terrestrial mass movements (Lucchitta 1978; 1987; McEwen 1989). These studies have led to contradictory conclusions concerning the nature of martian landslides. Are they analogous to dry rock avalanches on Earth or did they travel in a moist (wet, but not water saturated) or water-saturated condition? The Carlson landslide was studied in an effort to evaluate these arguments, specifically how the presence of water influences the qualitative and quantitative behavior of large bedrock landslides. Study of the Carlson landslide also provides insight into the elusive mechanism responsible for long runout in large landslides.

Regional Geology

The Carlson landslide appears on the 1:125,000-scale Borah Peak Quadrangle map of Ross (1947), and a portion of its headscarp occurs on the 1:62,500-scale Doublespring Quadrangle map by Mapel *et al.* (1965). The landslide lies at the eastern edge of the northwest-striking Lost River Range, which parallels the Lemhi and Beaverhead Ranges to the east. Together these ranges comprise an area of basin-and-range structure north of the Snake River Plain. The western margins of each range are bounded by normal faults displaying latest-Quaternary activity (Scott *et al.* 1985). The Lost River fault broke most recently in the 1983 (M_S = 7.3) Borah Peak earthquake. The Lemhi fault has experienced no historic activity, but does exhibit Holocene displacement (Haller 1988). The eastern borders of the Lemhi and Lost River Ranges display no Quaternary faulting. The active west-side faulting and lack of east-side faulting together suggest progressive eastward tilting of the three ranges through the Quaternary (Scott *et al.* 1985).

Limestone of Mississippian to Pennsylvanian age underlies most of the central Lost River Range, except on the east where Tertiary Challis Volcanics, consisting of basalt, tuff and agglomerate deposits, overlie the Limestone unit. Repeated folding of the core of the range has produced a broad anticlinal form with an axis paralleling the range. The bedrock geology in Figure 1, borrowed from Mapel *et al.* (1965), shows that the Carlson landslide originated along the folded contact between the Limestone unit and the Challis Volcanics. The conspicuous terraced river channels near the toe of the Carlson landslide (Figure 2) were probably cut by late-Pleistocene flood waters enhanced by melting headwater glaciers at the close of the Pleistocene (Ross 1947).

Physical Properties of the Carlson Landslide

Dimensions

The Carlson landslide measures 4400 m in length from the crown of the headscarp bowl to the tip of the toe. As determined from the movement-parallel surface lineations, the landslide traveled a total distance of 4700 m between these points, associated with a crown to toe elevation drop of 750 meters. For comparison with other deposits, these values give the landslide an H/L of 0.17 for the straight-line length and 0.16 for the movement-parallel trajectory.

The headscarp bowl, the area of the landslide above the 8000' elevation contour, measures 1.88 km across at the lip of the bowl at the 8560' contour. Upon collapse of the pre-existing slope, debris streamed downhill through a bottleneck only 280 m wide at its narrowest point between 8000' and 7280'. Below 7280' the debris piled up, forming a basal lobe 1.8 km in width. The Carlson landslide has an area of 5.2 km^2; 3.1 km^2 in the primary depositional region downslope of the 8000' elevation contour (Figure 7), and 2.1 km^2 in the headscarp bowl, the source region for the landslide.

The marginal thickness of the deposit was estimated at three locations, at one point in the neck and at two sites along the toe of the landslide. The thickness of the south-side levee in the neck is estimated at ~16 m (Figure 4) from field measurements of the outer slope of the levee, in combination with the reconstructed pre-landslide profile across the drainage basin. Figure 1 shows the location of the profile in Figure 4. Topographic contours in Figure 6 allow comparison of the present topography of the landslide with the estimated pre-landslide geometry of the buried channel. Profiles of the toe of the Carlson landslide were ascertained by use a variable-length staff (7-12') and attached inclinometer by placing the staff on the ground parallel to the surface and measuring the length and inclination of consecutive segments of the slope. Taking into

consideration the 3.5° slope of the underlying alluvial surface, these measurements indicate that the toe of the landslide thickens to 16 m at points 80-90 m from the edge of the deposit (Figure 5). Figure 1 shows the locations of the profiles along the southeastern margin of the basal lobe.

The volume of the Carlson landslide below the 8000' elevation contour is estimated at 100 x 10^6 m^3. This value is derived from Figure 6, an isopach map of the landslide developed from the present and reconstructed pre-landslide topography of the drainage basin. Longitudinal and transverse channel profiles and piedmont slopes of neighboring drainages in the Challis Volcanics, together with the marginal and distal thickness profiles shown in Figures 4 and 5 allowed reconstruction of the pre-landslide topography. Reconstruction of the failed slope made by extension of present slopes into the headscarp bowl gave a compatible estimate for the missing volume, ranging from 50 to 150 x 10^6 m^3 depending on the degree of gullying of the original slope.

Morphology

The Carlson landslide displays several gradational surficial textures in its headscarp bowl, neck and basal lobe (Figures 7, 8). Three gradational morphologies occur from northwest to southeast across the headscarp bowl. These areas are labeled in Figure 7 as follows: (1) a region of high-amplitude downstream-aligned ridges and troughs; (2) a pattern of curved ridges and troughs arranged concentrically about Carlson Lake; and (3) an area of low relief southeast of Carlson Lake. Ridges and troughs in the northwestern portion of the bowl display amplitudes of 20-30 m, the highest relief textures on the Carlson landslide.

Headscarp bowl textures grade downhill into movement-parallel ridges and troughs in the neck, labeled "4" in Figure 7, that vary in

spacing and amplitude with lateral and downslope position. The neck ridges and troughs generally consist of straight, parallel, rounded ridges that meet in v-shaped hollows except where the hollows are filled by alluvium. The spacing of ridges averages about 50 m, decreasing slightly from the upper to lower neck. Individual ridges generally stand 25 to 100 m apart and typically rise 5-10 m above neighboring hollows. In the upper neck (7600'-8000'), the ridges originating from the northern half of the headscarp bowl (Figure 7: texture 1) have much greater relief than those coming from the southern part of the bowl (Figure 2). These differences in relief decrease downslope; below ~7600' (Figure 7) the ridges have a uniform appearance across the deposit. The ridges are of variable length, with none extending the entire length of the neck. Ridges formed by division, with one ridge separating into two crests separated by a trough. They disappeared either when two ridges merged to form a single wider ridge or when the outside pair of three parallel ridges moved together and squeezed out an intermediate ridge and trough. Both processes formed dead-end troughs on the landslide surface that pond water (Figure 7). Transverse sections at several locations in the neck consistently show seven troughs and six ridges between the lateral levees, indicating a balance in the development and demise of ridges on the landslide in its waning movement stages (Figure 9).

Marginal levees of variable dimensions bound the Carlson landslide from the lower headscarp bowl to the basal lobe. The north-side levee originates in the headscarp bowl, where it is composed of a series of en echelon ridge segments that step inward and downward until the levee becomes continuous at about 7600' (Figure 7). Below 7600' the north-side levee generally displays higher relief than the south-side levee. At points where the landslide encounters side drainages, the north-side levee passes the depressions without deviation, while the south-side levee extends some distance up the

channels (Figures 1, 2, 8). In the upper neck, the outer slope of the north-side levee measures 25-30°, much steeper than the 5° outer slope of the south-side levee. The outer slope of the south-side levee steepens downhill, to 5-10° at the first major side drainage, 12° at the second side channel, and finally to 25° along the edge of the basal lobe. The outer slope of the north-side levee, in contrast, remains about 25° along its entire length. The inner scarps of the levees both consistently measure about 32° along their entire length. In the neck they stand well above the interior level of the landslide. The maximum relief observed between crest of the lateral levees and the interior is about 15 m.

Below 7520', the movement-parallel ridges that dominate the neck between the levees give way to a different set of textures (Figure 7). Below the neck the movement-parallel ridges grade into a hummocky region dominated by closed depressions and a convex-downslope pattern of concentric ridges and troughs, labeled "5" in Figure 7. The major concentric ridges and troughs in this region exhibit amplitudes of 5-15 m and an average spacing of 80 m, varying between 30 and 110 m. At the distal portion of the basal lobe, this region grades into a radial pattern of about 85 ridges and troughs along the toe of the landslide, labeled "6" in Figure 7. Like the movement-parallel features in the neck, the toe exhibits rounded ridges and v-shaped troughs except where alluvium fills the troughs. However, the radial ridges are of lower amplitude (2-5 m) and are more closely spaced (30 m) on average than those in the neck. At the leading edge of the landslide the ridges form promontories, and the troughs embayments when observed in plan view.

Sedimentology

The Carlson landslide consists primarily of a very poorly sorted mixture of basaltic rock fragments in a fine-grained matrix of basaltic

composition. The matrix is here defined as silt to very coarse sand (1/256 to 2 mm); the material in this size range generally supports and separates clasts of larger dimensions. Powder x-ray diffraction of the matrix did not resolve a clay signature, indicating a clay content below 5-10% by volume (A. L. Albee, personal communication, 1989). In addition to the basaltic materials, trace quantities of limestone, agglomerate and quartz rock fragments also occur in the landslide. The rock fragments typically have angular to sub-angular shapes.

The sedimentology of the landslide varies proximally to distally. In the headscarp bowl, the landslide consists primarily of medium to coarse pebble gravel (8-32 mm) of basaltic composition, with few cobbles or boulders and very little matrix. Limestone rock fragments occur mixed with the basalt breccia within about 200 m of the headscarp. Between the headscarp bowl and the basal lobe the deposit grades into a mixture of larger rock fragments and matrix, in the process changing from a clast-supported to a matrix-supported texture. Rock fragment sizes in the basal lobe vary considerably, with very coarse pebble gravel (32-64 mm) quite common, and some fragments of cobble (64-256 mm) and boulder gravel (>256 mm) also evident. A few boulders ranging up to 6 m in length occur on the basal lobe, often lying with their major horizontal axes aligned with the local movement direction.

The matrix-supported texture of the debris in the basal lobe together with the observation that the matrix material takes on a malleable, plastic consistency when wetted suggests that in its final movement stages the Carlson landslide probably traveled as a moist debris flow. Unlike water-saturated landslides such as Mt. St. Helens (Voight *et al.* 1983) and Mt. Shasta (Crandell 1989), the Carlson landslide apparently did not dewater at the termination of movement, suggesting a lower water content for the Carlson landslide. Unlike the

large water-saturated landslides, the moist Carlson landslide appears simply to have dried in place after the cessation of movement.

Age

The Carlson landslide overlies fluvial terraces interpreted by Ross (1947) as marking the terminal melting of ice-age glaciers. An upward-fining fluvial sequence exposed beneath the toe of the landslide also characterizes the late Pleistocene-Holocene transition (Pierce and Scott 1982). These observations suggest a Holocene age for the landslide. A conventional radiocarbon age of 2420 ± 130 B. P. (M. Stuiver, personal communication, 1990) was obtained from a sample of carbonized peat removed from a small playa atop the basal lobe of the landslide, yielding a minimum age of 420 B. C. (Stuiver and Becker 1986) for the landslide deposit. The peat occurred 56 cm below the surface of the playa, which had a total depth of at least 86 cm in massive, fine-grained sediments. Assuming a constant sedimentation rate, this gives an estimated minimum age of about 3,700 B. P., suggesting an early to middle Holocene age for the landslide.

Discussion

Discussion of the Carlson landslide is conveniently separated into five stages: slope preparation, initiation, travel, stopping and degradation.

Slope Preparation

A series of factors played a role in preparing the slope failure that formed the Carlson landslide. The development of steep topography and the progressive eastward Quaternary tilting of the Lost River Range began the destabilization of the slope. Tilting of the Challis Volcanics-Limestone unit contact and daylighting of the contact at the crown of the headscarp probably provided an avenue for the migration of surface waters into the hillslope, promoting weathering

along the contact. Stratigraphy exposed in the headscarp together with rock fragments in the landslide indicate that the original slope consisted of a series of highly jointed lava flows separated in places by thin lenses of volcaniclastic rock. The observation that very few clasts as large as cobbles or boulders occur in the landslide attests to the pervasiveness of the jointing in the failed slope; at failure, the slope disaggregated primarily into very coarse pebble gravel (32-64 mm) and smaller-sized material along these joints. The location of the headscarp at the elevation of nearby Pleistocene valley glaciers (Mapel *et al.* 1965) suggests that ice wedging and freeze-thaw processes may have played an important role in widening and loosening the joints and fractures in the slidemass. Considerable in situ chemical weathering had probably also taken place along the joints prior to failure, as evidenced by a red silt weathering residuum found sandwiched between the loose rock fragments forming a large basalt boulder on the landslide surface. Headward erosion of the now-buried drainage channel probably provided the critical factor in the destabilization of the slope by removing lateral support from the base of the slidemass in the direction of dip of the bedrock stratigraphy.

Initiation

The slope failure which produced the Carlson landslide apparently began at the lower end of the present headscarp bowl, between 8000' and 8160' (Figure 7), at a point where the original drainage basin reached its steepest gradients. The scarp failure reached headward from this point back to the resistant limestone bedrock at the rear of the present headscarp bowl. Movement of the wedge-shaped mass of Challis Volcanics may have begun along its eastward-sloping contact with the underlying Limestone unit (Section A-A', Figure 1). However, once movement had begun, the landslide mass must have rapidly disaggregated into rock fragments because no material exists

on the landslide which appears to have simply translated or rotated into position. Rather than beginning motion as a coherent slide or slump which fragmented during runout, the initial motion of the landslide appears to have involved disaggregation of the slidemass.

Because the Carlson landslide took place in a region of Holocene seismic activity, the possibility exists that an earthquake triggered initiation of the landslide. The central Lost River fault experienced a spasm of Holocene activity, producing three scarp-forming earthquakes between about 5,500 and 8,000 B.P. These earthquakes occurred on the Warm Springs, Thousand Springs and Mackay segments of the fault, all within 30 km of the Carlson landslide. Before this interval, surface faulting on the Lost River had not occurred since about 12 ka (Schwartz and Crone 1988). Holocene faulting also occurred on the Mahogany Creek segment of the Lemhi fault around this same time, approximately 40 km east of the landslide (Stickney and Bartholomew 1987). The offset produced by the 1983 (M_S = 7.3) Borah Peak earthquake closely mimicked the prehistoric offset on the Thousand Springs segment of the Lost River fault (Salyards 1985), suggesting an equally large magnitude for the prehistoric event. Despite this possible link to seismic activity, no positive evidence exists to link initiation of the landslide to an earthquake. Based on eyewitness accounts of the initiation of large historical landslides, few appear to actually coincide with earthquake shocks (Shaller 1991). More likely the landslide simply failed after a prolonged period of creep initiated by the removal of lateral support from the base of the slope caused by headward erosion of the old stream channel.

Travel

The Carlson landslide exhibited complex, changing behavior during its travel from the headscarp to the alluvial plain. All the available evidence is consistent with the landslide having been a

rapid event, emplaced over a period of a few minutes. The primary observations consistent with rapid emplacement are superelevation of the landslide on the south side of its channel in the upper neck, and the highly symmetrical plan form of the landslide's basal lobe on the north-dipping alluvial fan surface (Figure 7). Because the landslide did not clearly run up onto any obstacles that halted its movement, no direct measurement of its velocity is available.

As outlined above, the slidemass appears to have disaggregated into a sliding or flowing jumble of basalt rock fragments soon after initiation. As the landslide moved down slope, its content of moist matrix material appears to have steadily increased until this viscous/plastic material dictated the movement of the landslide in its latter movement stages. At least two possibilities exist to explain the source of moist matrix in the landslide. The most likely possibility is that the in situ fractured and jointed slidemass contained a considerable quantity of water along these bedrock discontinuities at the moment of the slope failure. The underlying limestone bedrock, believed by Meinzer (1924) to exhibit cavernous weathering in the nearby Double Springs drainage basin, might have provided a supplementary source of water. Comminution of the basalt rock fragments in the landslide during movement provides the most likely source of sand and silt in the matrix, into which the available water mixed during transport. Brecciation of rock into fine grain sizes is a common process in large landslides, and occurs either because of mechanical grinding in the landslides or due to the shattering of component rock fragments caused by the sudden release of overburden pressure on highly loaded rock (Shaller 1991). Another possibility is that the landslide began as a dry mass of rock fragments which eroded moist sands and silts from its bed as it traveled. Such bed erosion is observed in the geologic relations of large partially-eroded rock avalanches in the western United States (Yarnold and Lombard

1989). Also, the Huascaran 2 and 3 landslides are believed to have transitioned from dry rock avalanches to water-saturated debris flows in this manner by traveling over and incorporating wet snow early in their travel phases (Plafker and Ericksen 1978). Because the Carlson landslide traveled down a channel whose drainage basin encompassed only Challis Volcanics, sediments incorporated into the landslide from the channel would predominantly have had the observed basaltic composition.

Both the processes described above may explain the observed proximal-to-distal increase in matrix content of the landslide, and indeed both may have occurred during emplacement of the landslide. However, morphological evidence from headscarp bowl and upper neck structures supports the concept that, while the sand and silt in the landslide may have originated either in the substrate or in brecciation of landslide clasts, the water probably originated in the slidemass. At initiation, disaggregated basaltic breccia traveled into the upper neck region between 8000' and 7600', where debris from disparate sources in the headscarp mixed together (Figure 7). The differing relief of the longitudinal ridges in the upper neck suggest that the material issuing from the headscarp differed somewhat in mechanical properties between different sources in the bowl. Low-relief ridges issuing from the subdued southeast portion of the headscarp bowl (Figure 7: texture 3), contrast with the high-relief ridges forming the northwestern part of the upper neck. These ridges continue from similar high-relief structures in the northwestern segment of the headscarp bowl (Figure 7: texture 1). A variation in the initial water content of the slidemass across the headscarp bowl provides the most likely cause for these morphological differences; a higher water content in the southeastern debris source gave this material a more fluid character than the debris originating elsewhere in the headscarp bowl. Below

about 7600', however, the landslide debris between the marginal levees becomes quite homogeneous in appearance. Homogenization of the debris seems to have occurred rapidly through this area, probably because the debris moved at its greatest rate as it funneled down the upper neck and through the 280 m-wide narrows near 7680' (Figure 7). A cross-section through the landslide at this point (Section B-B', Figure 1) indicates that the south-side levee may have been superelevated as much as 25 m above the north-side levee at the height of the event. This superelevation, together with the discontinuous downward- and inward- stepping north-side levee indicates that material evacuating the headscarp initially had a strong component of northwest to southeast momentum.

Below 7600', landslide debris slid or flowed through the neck, filling the channel to the height of the lateral levees at the moment of maximum mass flux. Figure 9a gives the estimated appearance of the cross-section of the landslide at maximum flux for the channel geometry at the site of Figure 4 (see Figure 1 for location). The variation in inclination between the outer slopes of the lateral levees in the neck, 5-12° along the south side of the channel, 25° along the north, appears related to the contrasting fluidity between the landslide debris originating from the different ends of the headscarp bowl. The more fluid debris from the southeast portion of the bowl gave the south-side levee its lower slope, while less fluid material from the northwestern portion of the bowl formed the north-side levee. Thus, in contrast to the bulk of the landslide, the material along its margins apparently did not mix well as it moved down slope. The lobate form of the basal portion of the landslide suggests that as landslide debris passed through the channel it developed a transverse velocity profile, with the fastest material moving down the centerline of the channel, grading to stopped material along the margins (Figure 9a). As the major pulse of debris waned in the channel, the level of

moving debris receded between the halted lateral levees of the landslide. The removal of lateral support from the inner walls of the levees caused them to erode back at an angle of ~32°, the angle of repose of loose granular material (Figure 9b). Because this angle is consistently steeper than the outer margins of the lateral levees, it appears that the material forming the levees exhibited lower shear strengths when moving than when halted; the debris thus appears to have exhibited thrixotropic behavior. The level of moving debris continued to wane in the channel, with recession of the inner banks of the levees, until the debris in the channel came to a halt (Figures 9c, 9d).

The movement-parallel ridges and troughs in neck (Figure 7: texture 4) probably formed due to shearing between rapidly moving material at the center of the channel and slower material at its edges (Figure 9a-9c). The furrows likely formed as high-energy shear zones between the ridges, as inferred for some longitudinal structures of similar geometry observed on the Sherman (Shreve 1966) and Mayunmarca (Kojan and Hutchinson 1978) landslides. The observation that the troughs separated ridges of contrasting lithology in these landslides demonstrated that displacement of the ridges had occurred along the longitudinal grooves. Unfortunately, the monolithologic nature of the Carlson landslide precludes such a demonstration. An alternative explanation for the movement-parallel neck ridges is that they formed from discrete sources of rubble in the headscarp, akin to the formation of longitudinal ridges on rock glaciers (Wahrhaftig and Cox 1959), and became aligned as the rubble mass passed into the narrows below. The primary drawback to this idea is that the ridges are not continuous through the neck region, but rather die out in places and reappear elsewhere, remaining constant in number across the landslide. This observation suggests that their formation was an ongoing, dynamic process as the landslide

passed through the neck, possibly related to the relationship between the shear strength and the transverse velocity profile of the moving debris.

At the base of the neck, the landslide slowed, thinned and spread out where the channel widened and the slope decreased. Because material reached the rear of the basal lobe more rapidly than the flow front advanced, debris backed up into the neck near the end of movement. The concentric ridge and trough pattern (Figure 7: texture 5) probably formed due to compression between material at the toe of the landslide and faster, trailing material moving down the channel.

The toe of the landslide displays a radial pattern of ridges and troughs (Figure 7: texture 6) that bears many similarities to the parallel pattern of ridges in the neck. Like the neck ridges and troughs, those at the toe may also have formed as the result of differential movement, as ridges closer to the mid-line of the basal lobe slipped slightly further than their neighbors towards the left or right margins. Instead of advancing along a smooth front, the landslide appears to have advanced as a series of tightly spaced fingers. Due to spreading of the lobe, these ridges apparently formed under conditions of longitudinal compression and radial tension. Non-continuous thinning of the toe, like the necking of a steel rod under tension, may therefore also have played a role in the development of these features.

Stopping

The morphology of the Carlson landslide suggests that it gradually slowed to a halt. This interpretation comes from the observation that the concentric basal lobe ridges indicative of longitudinal compression are rather subdued in comparison with the pronounced pattern of radial ridges and troughs at toe of the landslide. In its final

movement stages, therefore, the landslide seems to have been much more strongly influenced by spreading of the basal lobe than by longitudinal compression caused by a rapid halt. This character contrasts markedly with the pronounced transverse ridging observed on dry rock avalanches observed or inferred to have come to an abrupt halt, such as the Elm (Heim 1932) and Blackhawk (Shreve 1968) landslides.

Degradation

The Carlson landslide has undergone only minor post-depositional degradation. Alluvium has been deposited along the margins of the landslide where it blocked off side drainages and has also collected in enclosed basins on the landslide surface (Figure 1). Also, Carlson Lake has apparently risen at least once, and perhaps several times above the level of the sill at the northeastern margin of the headscarp bowl. Waters that have overtopped the sill have incised a ~3 m-deep channel into the steep slope below the edge of the bowl. Slope wash and raveling has degraded the toe of the landslide to a small degree, and one of the radial troughs along the toe of the landslide has experienced minor fluvial incision accompanied by the deposition of a small alluvial cone at the toe of the landslide.

Comparison of the Carlson Landslide with Other Terrestrial Mass Movement Deposits

In the following, the Carlson landslide is compared with other mass movement deposits on the basis of morphology, sedimentology, and on the basis of several quantitative measures of landslide properties. The combined data are then used to access the mechanical behavior of the landslide during runout.

Morphology

The morphology of the Carlson landslide shares some significant similarities and differences with other geologic flow phenomena. For

example, detailed similarities exist between the morphologies of the Carlson landslide and a small piedmont glacier photographed on Ellesmere Island (Sharp 1988). Like the Carlson landslide, the glacier funneled through a narrow mountain-front gap and spread out to form a symmetrical basal lobe upon reaching a nearly flat piedmont slope. In addition, surface textures on the glacier closely mimic those on the landslide, including lateral levees in the neck, concentric ridges and troughs on the upper basal lobe and even a radial pattern of ridges along the toe! Some terrestrial mass movements involving rocky materials also mimic the morphology of the Carlson landslide. A particularly similar, though smaller deposit lies on the north bank of the Columbia River directly opposite Arlington, Oregon (J. L. Anderson, personal communication, 1990). This landslide occurred in lava flows of the Columbia River Basalt and volcaniclastic sediments of the Ellensburg Formation. Like the Carlson landslide, the "Arlington" landslide funneled through a narrow constriction where it deposited a pair of levees. It also built a symmetrical basal lobe at the base of slope featuring both concentric and radial ridges. Unfortunately, the site has not been visited, so it is unknown whether, like the Carlson, this landslide contained a significant water content at emplacement. The closest known dry rock analog to the Carlson landslide is the Martinez Mountain rock avalanche, which lies along the western margin of the Salton Trough in southern California and contains 380 x 10^6 m^3 of brecciated gneiss (Shelton 1966; Bock 1977). Like the Carlson landslide, the rock avalanche travelled down a channel and debouched onto a nearly level alluvial fan. It displays paired levees in the channeled portion and a small number of radial ridges on its basal lobe. Unlike the Carlson landslide, however, the Martinez Mountain deposit lacks concentric basal lobe ridges, has a much less symmetrical basal lobe and exhibits a much more broadly and irregularly spaced pattern of radial ribs on its basal lobe.

The principle connection between the lobate geologic flow phenomena described above is that all experienced channelized transport for significant distances before being discharged onto low-gradient piedmont slopes. In each case, channelized transport apparently gave the moving material a distribution of velocities, from slow at the margins, resulting in the deposition of lateral levees, to a maximum along the center line. The rates of downslope travel of the mass movements relative to their spreading rates controlled the detailed forms of their basal lobes. The Carlson and Arlington landslides and the piedmont glacier all moved down slope and spread at about the same rate, yielding their symmetrical plan forms. The Martinez Mountain dry rock avalanche spread much less rapidly relative to its downhill speed upon leaving its channeled reach, producing a less regular plan form.

Sedimentology

The Carlson landslide exhibits sedimentary characteristics akin to other large moist and water-saturated landslides and distinct from dry rock landslides. Together with other large moist and water-saturated landslides (Ui *et al.* 1986; Crandell 1989), the Carlson landslide fails to exhibit reverse grading, a common characteristic of large dry landslides (Cruden and Hungr 1986; Yarnold and Lombard 1989). The surficial textures of large moist and water-saturated landslides also differ considerably from that of dry landslides. Large dry landslides are commonly surfaced by a carpet of cobbles or boulders (Krieger 1977; Bock 1977; Yarnold and Lombard 1989), whereas the surfaces of the Carlson and other moist and water-saturated landslides generally consist of fine-grained matrix punctuated by occasional clasts and boulders of varying scale (Plafker and Ericksen 1978; Crandell 1989). The low internal friction afforded by moist matrix material appears responsible for this behavior. Moist and wet landslides can mix and

overturn during runout, while dry landslides appear too viscous or rigid to do so (Shreve 1968; Shaller 1991). Moist and water-saturated landslides, including the Carlson, also commonly exhibit a proximal to distal decrease in rock fragment to matrix ratio, corresponding to an overall fining of debris size with travel distance (Ui *et al.* 1986; Crandell 1989). Dry landslides do not generally exhibit this behavior (Heim 1932). While dry long-runout landslides do develop an increasingly thick basal layer of fine, powdered debris with travel distance, this grain size diminution is not apparent on the surface of a large dry landslide (Yarnold and Lombard 1989). Perhaps homogenization of debris in moist and wet landslides mixes the fine-grained component formed during runout throughout the body of a landslide, so that all parts of the landslides appear to decrease in average grain size and block to matrix ratio with distance traveled. The surfaces of moist and water-saturated landslides are also often marked by large-scale hummocks. In water-saturated landslides, these generally represent large buried boulders that experienced partial exhumation during late-stage dewatering and remobilization of surface fines (Ui *et al.* 1986; Crandell 1989). Hummocks on the moist Carlson landslide are often crested by inset clasts having the appearance of paving stones set into the ground. These features may also represent buried boulders, but ones which escaped exhumation because of a lack of post-depositional dewatering.

Quantitative Measures of Landslide Properties

The preceding discussion shows that certain qualitative differences in landslide morphology and depositional characteristics distinguish dry from moist and water-saturated landslides. However, two common quantitative measures of large landslide travel behavior, log(volume) vs. H/L trends and apparent Bingham plastic yield

strength measurements, do not distinguish between landslides of differing water content.

Observational data for large rapid landslides containing over 10^6 m^3 of rock indicate that as their masses increase beyond this threshold volume, the landslides exhibit a rough log-normal group tendency towards decreasing H/L with increasing volume (Scheller 1971; Scheidegger 1973; Hsü 1975; Ui 1983; Shaller 1991). Figure 10 compares the log(volume) vs. H/L trends of eight large moist and water-saturated terrestrial landslides (Table 1) with that of 163 dry volcanic and non-volcanic terrestrial subaerial landslides (Shaller 1991). The moist and water-saturated landslides plot well within the log(volume) vs. H/L envelope for dry terrestrial subaerial landslides, indicating that the travel behavior of the moist landslides apparently differs little from that of dry rock avalanches of similar volume. Thus the mechanism(s) responsible for causing anomalous runout in large dry landslides seem(s) to operate in moist and water-saturated landslides as well.

Many geological flow phenomena experience movement only when subjected to basal shear stresses beyond a certain "yield stress." As a first approximation to their material properties, such substances are often modeled in the geologic and engineering literature as Bingham plastics. Examples include the flow of muds, sludges and suspensions through pipes (Caldwell and Babbitt 1941), the flow of glaciers (Nye 1951), lava flows (Hulme 1974), debris flows (Johnson 1970; 1984), water-saturated landslides (Voight *et al.* 1983) and dry rock avalanches (Eppler *et al.* 1987; McEwen 1989). Two characteristics cited as indicative of large-scale plastic behavior are halting of motion on a slope and the presence of a parabolically-shaped distal profile, or "snout" along the toe of a deposit (Johnson 1970), both features expressed on the Carlson landslide. Equation 1

gives the basic Bingham plastic yield strength formula, which assumes steady flow conditions (Johnson 1984):

$$[1] \qquad k = \rho\, g\, D \sin \beta$$

where k is the Bingham plastic yield strength in Pa, ρ is the density in kg/m^3, D is the deposit thickness in meters, g is the gravitational acceleration in m/s^2 and ß is the ground slope in degrees. Table 2 reports estimated Bingham plastic yield strength values for several moist and dry landslide deposits. Table 2 shows that moist and water-saturated terrestrial landslides exhibit about the same estimated Bingham plastic yield strength as the Chaos Jumbles dry rock avalanches, and greater strength than the Surprise Canyon debris flow and the Sherman landslide. Thus, moist and water-saturated terrestrial landslides exhibit Bingham plastic yield strength properties closer to dry rock landslides than to typical desert alluvial fan debris flows.

Comparison of the Carlson Landslide with Lobate Martian Landslides

Four large lobate landslides have been located on Mars: two in Candor Chasma (Figure 3), and two near the base of Olympus Mons (Baker 1983). Lucchitta (1987) believed that the morphologies of the two Candor Chasma landslides and of their source regions provided good evidence that these landslides contained considerable amounts of water during transport, and that the deposits must have flowed into place with much the same consistency as terrestrial mudflows. More recently, McEwen (1989) countered this argument by discounting the morphological data and instead using log(volume) vs. H/L trends, yield strength estimates and velocity estimates of landslides in Valles Marineris (from overtopped obstacle heights) as evidence that all the landslides observed in the chasmas were probably emplaced dry. However, as demonstrated above, log(volume) vs. H/L trends and yield

strength estimates fail to provide useful means of separating dry from moist or wet landslides. In addition, dry and water-saturated landslides on Earth exhibit an overlapping range of velocities (Shaller 1991), thus also ruling out velocity estimates as a method of distinguishing dry landslides from those having significant water contents. Thus, morphology remains the only available means of distinguishing landslides of differing water content.

The lobate martian landslides all exhibit morphologies consistent with moist deposition as defined by the lobate Carlson landslide. The Carlson landslide and the lobate martian landslides all began motion as rockfalls and funneled through a narrow constriction in the channel below the headscarp to spread out and form a lobate, flattened, highly symmetrical, finely longitudinally ribbed debris apron. The lobate martian landslides differ from the Carlson landslide in not exhibiting the convex-downslope ridges and troughs texture observed on the Carlson and in having greater characteristic thicknesses than the terrestrial landslide (Table 3; Shaller 1991).

The debris apron morphologies exhibited by the lobate martian landslides make them much closer in morphology to the moist Carlson landslide than to any known terrestrial dry rock landslide. Particularly significant on the martian landslides are the very smooth margins of their basal lobes and the fine spacing of their longitudinal ribs. While the lobate martian landslides differ from the Carlson landslide in not exhibiting the convex-downslope ridges and troughs texture, there are several reasonable explanations for this difference. One possibility is that the ridges and troughs exist on the lobes but cannot be resolved in the Viking Orbiter images. Conversely, even given the exact same materials for the martian landslides as for the Carlson landslide, the difference in gravity between the two planets might preclude development of the convex-downslope ridges and troughs texture on the martian landslides. On the Carlson landslide,

this texture apparently formed due to compression between material at the toe of the landslide and faster, trailing material coming down the channel. On Mars, where deposit velocities must be lower due to the lower gravitational acceleration, the velocity differential might be significantly lower between material at the toe of a deposit and trailing material coming down the channel. In addition, the lobate martian landslides characteristically have greater thicknesses than the Carlson landslide, also making compressional deformation more difficult. The characteristically greater thicknesses of the lobate martian landslides relative to the Carlson landslide probably relate to the difference in gravity between the two planets, rather than to a difference in material properties. This conclusion is based on the fact that the lobate martian landslides have average and maximum thicknesses that average about 2.5 times the thickness of the Carlson landslide (Table 3), a value roughly corresponding to the ratio in gravitational acceleration between Earth (9.8 m/s^2) and Mars (3.72 m/s^2). Other groups of landslides on the two planets of similar volume exhibit an analogous relationship; apparently the shear stresses applied at the base of a large landslide control their travel distances during runout (Shaller 1991).

The evidence presented above suggests that the lobate martian landslides were probably moist during deposition, like the Carlson landslide. Other evidence suggests that the Carlson landslide and its martian counterparts may have had rather similar lithologic compositions as well. This speculative argument is based on the fact that the Carlson landslide and a smaller, but morphologically similar deposit in the Columbia River valley in Washington State (45°45'N, 120°14'W), both originated in outcrops of weathered basalt (J. L. Anderson, personal communication, 1990). In addition, the landslides from Olympus Mons, a large shield volcano, probably also consist of some form of basalt, as may the two Candor Chasma landslides. The

latter two landslides appear to have fallen from bedrock outcrops at the crest of the chasma, outcrops which have been interpreted as mare-type flood basalts (Scott and Tanaka 1986). Because of the instability of water at the surface of Mars in the equatorial latitude range in which the four lobate martian landslides occur (Carr 1981), they must have derived water from the subsurface. Fumarolic activity on Olympus Mons theoretically might have provided the water for two of the deposits, while the Candor Chasma landslides most likely obtained water from the high-pressure groundwater aquifers postulated by Carr (1981).

Travel Mechanism(s)

The Carlson landslide comprises a composite mass movement deposit, with morphological and sedimentary properties akin to both large dry long-runout landslides and to much smaller desert alluvial fan debris flow deposits. With regard to log(volume) vs. H/L relations and estimated Bingham plastic yield strength properties, however, the Carlson and other moist landslides exhibit behavior compatible with dry rock avalanches and distinct from debris flows. These facts, together with the observation that large dry-rock landslides such as Carlson and the Huascaran landslides (Plafker and Ericksen 1978) transformed gradationally into debris flows during travel, suggests that the processes involved in long-runout landslides and debris flows must be gradational in nature.

Many different theories have been proposed to explain long runout in large rock avalanches. Some have attempted to explain long runout on a case-by-case basis (Habib 1975; Goguel 1978; Johnson 1978; McSaveney 1978; Solonenko 1984), while others have approached long runout as a mechanism underlying the behavior of all large landslides. Models proposed to explain long runout as a general property include bulk fluidization theories (Heim 1932; Kent 1966; Hsü

1975; Davies 1982; Krumdieck 1984; Savage 1984; Trunk *et al.* 1986; Melosh 1987; Campbell 1989; Potapov and Ivanov 1991), lubrication theories (Shreve 1968; Erismann 1979) and a mass-loss theory (Van Gassen and Cruden 1989). The process(es) responsible for long runout apparently operate on Mars (McEwen 1989; Shaller 1991) and perhaps on the Moon (Howard 1973), as well as on Earth.

Debris flows of the type commonly associated with desert alluvial fan flood processes have also been described by a variety of mechanical models. These include behavior as a Newtonian fluid (Sharp and Nobles 1953), as a Bingham plastic (Johnson 1970), and as a Coulomb-viscous substance (Johnson 1970; 1984).

Most of the mechanisms proposed to explain both long-runout landslides and debris flows could apply to the Carlson landslide if its behavior is viewed individually. Exceptions include behavior as a Newtonian fluid, air fluidization and air-layer lubrication. A Newtonian fluid rheology (Sharp and Nobles 1953) can be ruled out because the landslide halted motion on a slope, has a significant thickness and does not give any indication of exhibiting slow viscous motion at present. Air fluidization (Kent 1966; Krumdieck 1984) also fails because this process generates normal grading (Brown and Richards 1970), whereas the Carlson landslide exhibits a lack of grading, and perhaps some indications of reverse grading as suggested by the smattering of large boulders on its surface. Air-layer lubrication (Shreve 1968) probably also can be ruled out for the Carlson landslide because the landslide does not appear to have experienced the airborne leap necessary for trapping an air cushion. The weak transverse ridge-and-trough texture on the landslide and its failure to exhibit a raised distal margin provide additional evidence against air-layer lubrication.

Based on comparisons with other large landslides and with debris flows, the Carlson landslide appears to have traveled by means of the

flow of its fine-grained matrix material. The homogeneous morphology and sedimentology of the basal lobe of the landslide suggests that in its final movement stages the landslide experienced bulk fluidization and traveled as a giant debris flow whose behavior depended upon the nature of its moist matrix material, perhaps flowing with a Bingham plastic or Coulomb-viscous rheology (Johnson 1970; 1984). Such rheological properties could, in fact, explain the observed greater thicknesses of the martian landslides relative to the Carlson; for the same material properties, a landslide with either rheology should flow 0.38 times as thick on Earth as on Mars (Equation 1; Johnson 1984). The evidence of bulk flow of the Carlson landslide becomes less apparent proximally, however. If the landslide began movement by sliding, it probably developed a basal layer of comminuted debris, as often occurs along the basal contacts of large dry landslides (Yarnold and Lombard 1989). Addition of water to this basal material might have led to its mobilization throughout the body of the landslide. Perhaps the gradational behavior between dry rock avalanches, moist landslides and debris flows results from fine-grained material playing the critical role in each form of mass transport. Sliding of large landslides into place on thin lenses of flowing, comminuted substrate material could explain many of the characteristics of dry long-runout landslides (Shaller 1991). Addition of water to the material might give it considerably different properties, including reduced viscosity, allowing the matrix to mix upwards into the bulk of the landslide, ultimately causing the observed apparent bulk fluidization of the landslide debris. Unfortunately, this model remains speculative because of a lack of information on the viscous properties of powdered dry rock subject to high shear stresses at moderate overburden pressures. Nevertheless, it provides a conceptual model for landslide behavior that is amenable to testing in the laboratory.

Conclusions

The early to middle Holocene Carlson landslide began movement as a dry rock landslide and ended movement as a giant debris flow. Headward erosion of the now buried drainage basin, in combination with eastward tilting of stratigraphy, lava flow jointing, steep topography and in situ weathering of the basaltic bedrock all helped prepare the original slope for failure. The basalt slidemass initially contained a considerable quantity of water along its joints and fractures, especially in its southeast quadrant. At initiation this water became free to mix with fine rock debris generated during movement of the landslide, material which originated either in comminution of the rock debris in the landslide and/or by incorporation of underlying sediments. The morphologies of the lateral levees reflect the different fluidities of the debris spilling out of the headscarp bowl and provide evidence that the landslide debris had more fluid behavior when halted than when moving. Longitudinal ribs in the neck and at the toe apparently formed by shear between debris trains moving at different speeds, whereas the concentric ridge and trough pattern formed by differential velocities between the toe and neck of the landslide. The landslide came to a gradual halt starting at the toe, after which it dried and set like concrete. Since then the landslide has undergone only minor degradation.

The moist Carlson landslide shares its basic lobate geometry with glaciers and with other large landslides. In all cases this lobate geometry appears to result from channelized movement. The Carlson landslide differs in detail with lobate dry rock avalanches because of the relatively greater ability of the moist debris to spread out upon leaving its channel than the dry debris. However, while the morphologies and sedimentologies of large dry and moist landslides

differ in detail, their log(volume) vs. H/L and apparent Bingham plastic yield strengths do not differ significantly.

The morphologies of lobate martian landslides suggest their emplacement as moist landslides. Detailed differences in deposit thickness and morphology between these deposits and the Carlson landslide probably result from the difference in gravitational acceleration between the two planets. Thus, a limited role for water on the martian surface is supported by the lobate martian landslides.

The geometry and sedimentology of the Carlson landslide rule out Newtonian fluid flow, air fluidization and air-layer lubrication as likely mechanisms in the travel of the landslide. Rather, the landslide appears to have flowed as a Bingham plastic or a Coulomb-viscous substance late in its travel history. However, its apparent transition from dry sliding to moist flow and the observed quantitative similarities between moist, water-saturated and dry landslides suggests that the flow of fine-grained material plays the critical role in each form of mass movement. The flow of basal dry rock powder appears to control the runout of dry rock avalanches, whereas moist fine-grained material controls the travel of water-rich landslides.

Acknowledgements

Support for this project was provided by NASA grant #NAGW-1373. I am indebted to John Shelton for encouragement and background information on the Carlson landslide and for the use of his aerial photo of the landslide in this manuscript. Many thanks to A. L. Albee, Ron Scott, Bob Sharp and Bruce Murray for their time and help in interpreting the landslide and improving this manuscript, and to Murray for unflagging support of this venture. Thanks also to Tom Rockwell for use of the "Livingston corer" and to Danny Hagens for tutorial on same, and to Doane Western Co. for permission to cross the old Carlson Ranch property. Finally, I owe overwhelming gratitude to

Ann Shaller for field assistance above and beyond the call of duty despite sleet and charging antelopes.

BAKER, V. R., 1983. The Channels of Mars. University of Texas Press, Austin, pp 1-198.

BOCK, C. G. 1977. Martinez Mountain rock avalanche. *In* Landslides. *Edited by* D. R. Coates. Reviews in Engineering Geology, **3**: 155-168.

BROWN, R. L. and RICHARDS, J. C., 1970. Principles of Powder Mechanics. Pergamon Press, Oxford, UK, pp. 1-223.

CALDWELL, D. H. and BABBITT, H. E. 1941. Flow of muds, sludges and suspensions in circular pipe. Industrial and Engineering Chemistry, **33**: 249-256.

CAMPBELL, C. S. 1989. Self-lubrication for long runout landslides. Journal of Geology, **97**: 653-665.

CARR, M. H., 1981. The Surface of Mars. Yale University Press, New Haven, CT, pp. 1-232.

CRANDELL, D. R., 1989. Gigantic debris avalanche of Pleistocene age from ancestral Mount Shasta volcano, California, and debris-avalanche hazard zonation. United States Geological Survey Bulletin 1861, pp. 1-32.

CRUDEN, D. M. and HUNGR, O., 1986. The debris of the Frank slide and theories of rockslide-avalanche mobility. Canadian Journal of Earth Sciences, **23**: 425-432.

DAVIES, T. R. H., 1982. Spreading of rock avalanche debris by mechanical fluidization. Rock Mechanics, **15**: 9-24.

EPPLER, D. B., FINK, J. and FLETCHER, R. 1987. Rheologic properties and kinematics of emplacement of the Chaos Jumbles rockfall avalanche, Lassen Volcanic National Park, California. Journal of Geophysical Research, **92**: 3623-3633.

ERISMANN, T. H. 1979. Mechanisms of large landslides. Rock Mechanics, **12**: 15-46.

FAUQUE, L. and STRECKER, M. R., 1988. Large rock avalanche deposits (Sturzströme, sturzstroms) at Sierra Aconquija, northern Sierras Pameanas, Argentina. Eclogae Geologicae Helvetia, **81**: 579-592.

GOGUEL, J. 1978. Scale-dependent rockslide mechanisms, with emphasis on the role of pore fluid vaporization. *In* Rockslides and Avalanches, 1; natural phenomena. *Edited by* B. Voight. Elsevier, New York, NY, pp. 693-706.

HABIB, P., 1975. Production of gaseous pore pressure during rock slides. Rock Mechanics, **7**: 193-197.

HALLER, K. M. 1988. Proposed segmentation of the Lemhi and Beaverhead faults, Idaho, and Red Rock fault, Montana--Evidence from studies of fault-scarp morphology. Geological Society of America, Abstracts with Programs, **20**: 418-419.

HEIM, A. 1932. Bergsturz und Menschenleben. Fretz & Wasmuth Verlag A. G., Zürich, pp 1-217. (English translation by N. A. Skermer, BiTech Publishers, Vancouver, B. C.)

HOWARD, K. A. 1973. Avalanche mode of motion: Implications from lunar examples. Science, **180**: 1052-1055.

HSÜ, K. J. 1975. Catastrophic debris streams (sturzstroms) generated by rockfalls. Geological Society of America Bulletin, **86**: 129-140.

HULME, G. 1974. The interpretation of lava flow morphology. Geophysical Journal of the Royal Astronomical Society, **39**: 361-383.

JOHNSON, A. M. 1970. Physical Processes in Geology. Freeman, Cooper & Co., San Francisco, pp. 433-459.

JOHNSON, A. M. 1984. Debris flow. *In* Slope Instability. *Edited by* D. Brunsden and D. B. Prior. John Wiley & Sons, New York, NY, pp. 257-361.

JOHNSON, B. 1978. Blackhawk landslide, California, U.S.A. *In* Rockslides and Avalanches, 1; natural phenomena. *Edited by* B. Voight. Elsevier, New York, NY, pp. 481-504.

KENT, P. E. 1966. The transport mechanism in catastrophic rock falls. Journal of Geology, **74**: 79-83.

KOJAN, E. and HUTCHINSON, J. N. 1978. Mayunmarca rockslide and debris flow. *In* Rockslides and Avalanches, 1; natural phenomena. *Edited by* B. Voight. Elsevier, New York, NY, pp. 315-361.

KRIEGER, M. H. 1977. Large landslides, composed of megabreccia, interbedded in Miocene basin deposits, southeastern Arizona. United States Geological Survey, Professional Paper 1008, pp. 1-25.

KRUMDIECK, M. A. 1984. On the mechanics of large landslides. 4th International Symposium on Landslides, Toronto, vol. 1, pp. 539-544.

LUCCHITTA, B. K. 1978. A large landslide on Mars. Geological Society of America Bulletin, **89**: 1601-1609.

LUCCHITTA, B. K. 1987. Valles Marineris, Mars: Wet debris flows and ground ice. Icarus, **72**: 411-429.

MAPEL, W. J., READ, W. H. and SMITH, R. K. 1965. Geologic map and sections of the Doublespring Quadrangle, Custer and Lemhi Counties, Idaho. United States Geological Survey General Quadrangle Map GQ-464, scale 1:62500.

MCEWEN, A. S. 1989. Mobility of large rock avalanches: Evidence from Valles Marineris, Mars. Geology, **17**: 1111-1114 .

MCSAVENEY, M. J. 1978. Sherman Glacier rock avalanche, Alaska, U.S.A. *In* Rockslides and Avalanches, 1; natural phenomena. *Edited by* B. Voight. Elsevier, New York, NY, pp. 197-258.

MEINZER, O. E., 1924. Ground water in Pahsimeroi Valley, Idaho. Idaho Bureau of Mines and Geology, Pamphlet No. 9, 36 pp.

MELOSH, H. J. 1987. The mechanics of large rock avalanches. Geological Society of America, Reviews in Engineering Geology, **7**: 41-49.

NYE, J. F. 1951. The flow of glaciers and ice-sheets as a problem in plasticity. Royal Society of London, Proceedings, Series A, **207**: 554-572.

PIERCE, K. L. and SCOTT, W. E. 1982. Pleistocene episodes of alluvial-gravel deposition, southeastern Idaho. *In* Cenozoic Geology of Idaho. *Edited by* B. Bonnichsen and R. M. Breckenridge. Idaho Bureau of Mines and Geology Bulletin 26, pp. 685-702.

PLAFKER, G. and ERICKSEN, G. E. 1978. Nevados Huascarán avalanches, Peru, *In* Rockslides and Avalanches, 1; natural phenomena. *Edited by* B. Voight. Elsevier, New York, NY, pp. 197-258.

POTAPOV, A. V. and IVANOV, B. A., 1991. Landslide motion: Numerical simulation for Earth and Mars. 22nd Lunar and Planetary Science Conf., in press.

ROSS, C. P. 1947. Geology of the Borah Peak quadrangle, Idaho. Geological Society of America Bulletin, **58**: 1085-1160.

SALYARDS, S. L. 1985. Patterns of offset associated with the 1983 Borah Peak, Idaho, earthquake and previous events. *In* Proceedings of Workshop 28 on the Borah Peak, Idaho, Earthquake. *Edited by* R. S. Stein and R. C. Bucknam. United States Geological Survey Open File Report 85-290, pp. 59-75.

SAVAGE, S. B., 1984. The mechanics of rapid granular flows. Advances in Applied Mechanics, **24**: 289-366.

SCHELLER, E., 1971. Beitrag zum Bewegungsverhalten grosser Bergstürze. Eclogae Geologicae Helvetiae, **64**: 195-202.

SCHEIDEGGER, A. E., 1973. On the prediction and reach of catastrophic landslides. Rock Mechanics, **5**: 231-236.

SCHWARTZ, D. P. and CRONE, A. J. 1988. Paleoseismicity of the Lost River fault zone, Idaho: Earthquake recurrence and segmentation. Geological Society of America, Abstracts with Programs, **20**: 228.

SCOTT, D. H. and TANAKA, K. L., 1986. Geologic map of the western equatorial region of Mars. United States Geological Survey

Miscellaneous Investigations Series Map I-1802-A, scale 1:15,000,000.

SCOTT, W. E., PIERCE, K. L. and HAIT, M. H. 1985. Quaternary tectonic setting of the 1983 Borah Peak earthquake, central Idaho. Bulletin of the Seismological Society of America, **75**: 1053-1066.

SHALLER, P. J. 1991. Analysis and Implications of large martian and terrestrial landslides, Ph.D. Thesis, California Institute of Technology.

SHARP, R. P. 1988. Living Ice: Understanding Glaciers and Glaciation. Cambridge University Press, New York, NY, p 25.

SHARP, R. P. and NOBLES, L. H., 1953. Mudflow of 1941 at Wrightwood, southern California. Geological Society of America Bulletin, **64**: 547-560.

SHELTON, J. S. 1966. Geology Illustrated. W. H. Freeman and Company, San Francisco, pp 124-125, 381.

SHREVE, R. L. 1966. Sherman landslide, Alaska. Science, **154**: 1639-1643.

SHREVE, R. L. 1968. The Blackhawk landslide. Geological Society of America, Special Paper 108, pp. 1-47.

SIEBERT, L., 1984. Large volcanic debris avalanches: Characteristics of source areas, deposits, and associated eruptions. Journal of Volcanology and Geothermal Research, **22**: 163-197.

SOLONENKO, V. P., DEM'YANOVICH, M. G. and AVDEEV, V. A., 1984. The engineering seismogeology of the northern Muya Interrift Commissure (Baikal Rift Zone). International Association of Engineering Geologists, IV International Congress: 1-13.

STICKNEY, M. C. and BARTHOLOMEW, M. J. 1987. Seismicity and late Quaternary faulting of the northern Basin and Range Province, Montana and Idaho. Bulletin of the Seismological Society of America, **77**: 1602-1625.

STUIVER, M. and BECKER, B. 1986. High-precision decadal calibration of the radiocarbon time scale, AD 1950-2500 BC. Radiocarbon, **28**: 863-910.

TRUNK, F. J., DENT, J. D. and LANG, T. E., 1986. Computer modeling of large rock slides. Journal of Geotechnical Engineering, **112**: 348-360.

UI, T., 1983. Volcanic dry avalanche deposits- Identification and comparison with nonvolcanic debris stream deposits. Journal of Volcanology and Geothermal Research, **18**: 135-150.

UI, T., KAWACHI, S. and NEALL, V. E. 1986. Fragmentation of debris avalanche material during flowage -- Evidence from the Pungarehu Formation, New Zealand. Journal of Volcanology and Geothermal Research, **27**: 255-264.

VAN GASSEN, W. and CRUDEN, D. M. 1989. Momentum transfer and friction in the debris of rock avalanches. Canadian Geotechnical Journal, **26**: 623-628.

VOIGHT, B., JANDA, R. J., GLICKEN, H. and DOUGLASS, P. M. 1983. Nature and mechanics of the Mount St. Helens rockslide-avalanche of 18 May 1980. Geotechnique, **33**: 243-273.

WAHRHAFTIG, C. and COX, A. 1959. Rock glaciers in the Alaska Range, Geological Society of America Bulletin, **70**: 383-436.

YARNOLD, J. C. and LOMBARD, J. P. 1989. A facies model for large rock-avalanche deposits formed in dry climates, *In* Conglomerates in Basin Analysis: A symposium Dedicated to A. O. Woodford. *Edited by* I. P. Colburn, P. L. Abbott and J. Minch, Pacific Section S.E.P.M., pp. 9-31.

TABLE 1. CRITICAL CHARACTERISTICS OF LARGE MOIST AND WATER-SATURATED TERRESTRIAL LANDSLIDES

Name	Volume (x 10^6 m^3)	H/L	Reference
Mt. Shasta	45,000	0.07	Crandell 1989
Mt. St. Helens	25,000	0.11	Voight *et al.* 1983
Pungarehu	7,500	0.10	Ui *et al.* 1983
Galunggung	2,900	0.08	Siebert 1984; Crandell 1989
Huascaran 1	150	0.21	Plafker and Ericksen 1978
Carlson	100	0.17	this paper
Huascaran 3	50-100	0.22	Plafker and Ericksen 1978
Huascaran 2	13	0.22	Plafker and Ericksen 1978

TABLE 2. BINGHAM PLASTIC YIELD STRENGTHS OF LANDSLIDES AND DEBRIS FLOWS

Name	Bingham Plastic Yield Strength (Pa)	Reference
Ice	100,000	Nye 1951
Carlson ls	19,000*	this paper
Mt. St. Helens ls	2,000-20,000*	Voight *et al.* 1983
Chaos Jumbles ls	6,000-10,000*	Eppler *et al.* 1987
Surprise Cyn. df	2,000*	Johnson 1984
Sherman ls	2,000*	McSaveney 1978

Abbreviations: ls = landslide; df = debris flow
* = Calculated using Equation 1, $k = p\ g\ D \sin ß$.

TABLE 3. CRITICAL CHARACTERISTICS OF LOBATE MARTIAN AND TERRESTRIAL LANDSLIDES

Name	Volume ($x10^6$ m^3)	Basal Lobe Width (km)	H/L	Thickness (m) Avg.	Max.
Carlson	100	1.8	0.17	30	70
Mars 143	NA	4	NA	NA	NA
Mars 84	1,500	5	0.2	60	100
Mars 85	1,500	5	0.2	60	100
Mars 142	26,000	14	0.1	160	160

FIG 1. Geologic map and sections of the Carlson landslide, Idaho.

FIG 2. Vertical aerial photograph of the Carlson landslide.

FIG 3. Viking Orbiter image 909A12 of two martian landslides in Candor Chasma, part of the Valles Marineris canyon system.

FIG 4. Calculation of thickness of south-side levee. Location shown in Figure 1.

FIG 5. Profiles of two promontories or digitations at the toe of the Carlson landslide. See Figure 1 for location.

FIG 6. Isopach map of the Carlson landslide showing present topography and reconstructed pre-landslide channel geometry. Reconstruction based on comparisons with neighboring drainage basins in Challis Volcanics, together with distal and marginal thickness calculations. Elevation contours in feet.

FIG 7. Generalized morphology of the Carlson landslide.

FIG 8. Oblique aerial photograph of the Carlson landslide (photo courtesy of J. S. Shelton).

FIG 9. Conceptualized appearance of cross-section through the Carlson landslide at four different times in its evolution. View is upstream with debris approaching viewer. Channel geometry drawn in true scale from channel dimensions at site of Figure 4 (see Figure 1 for location). Size of "+" mark is proportional to debris velocity; darker pattern represents stopped material. Diagram A shows maximum flux conditions. Figure B shows subdivision of landslide into parallel ribs moving at different velocities; lowering level of debris in the channel oversteepens inner banks of levees. Waning movement continues in Figure C, and Figure D shows stopped condition.

FIG 10. Plot of log(volume) vs. H/L for the Carlson landslide and the seven other moist and water-saturated landslides listed in Table 1 vs. 163 dry terrestrial subaerial landslides (Shaller 1991).

Figure 1. Geologic Map and Sections of the Carlson Landslide, Idaho

Figure 1. Shaller, 1990.

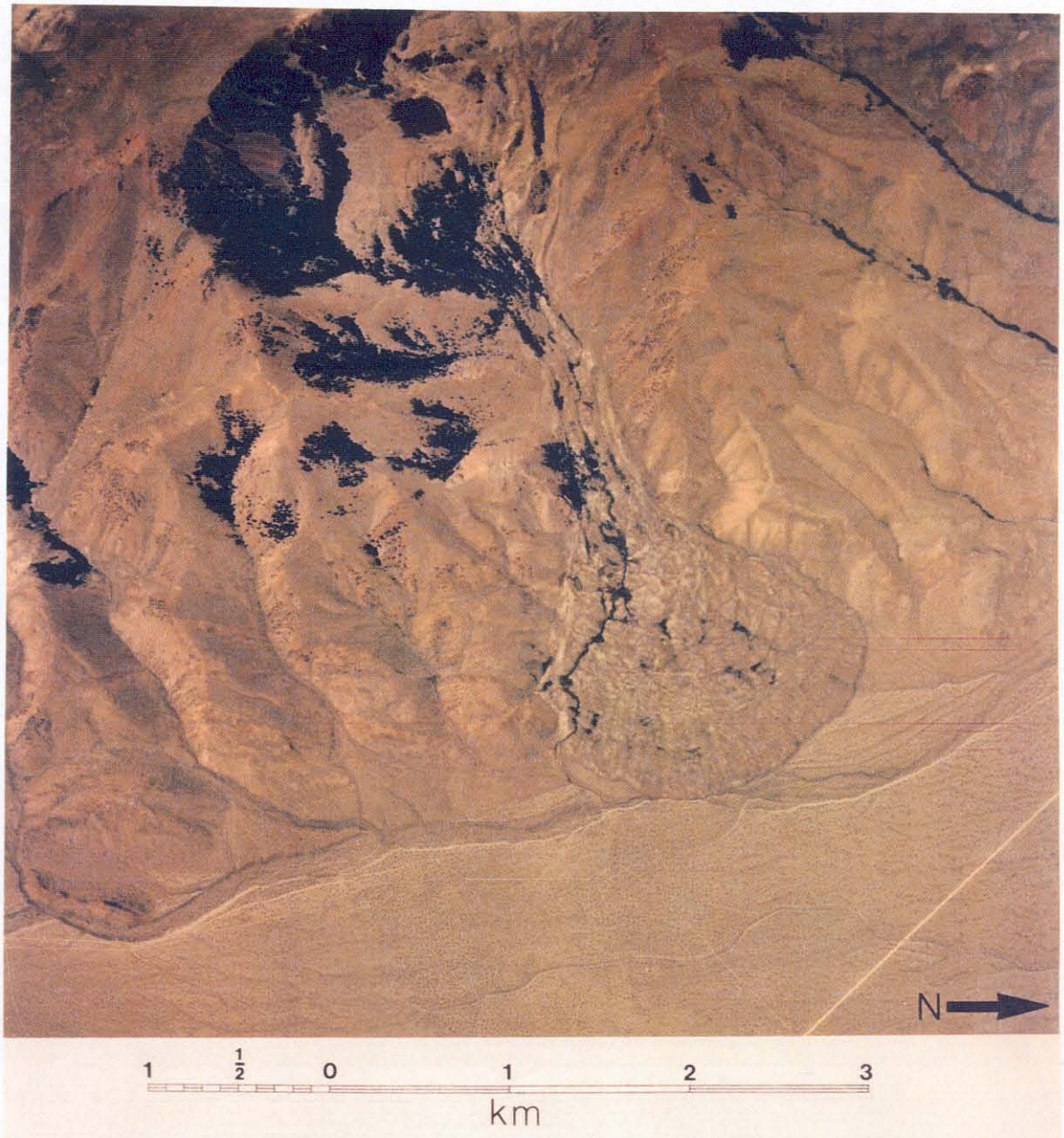

Figure 2. Shaller, 1990.

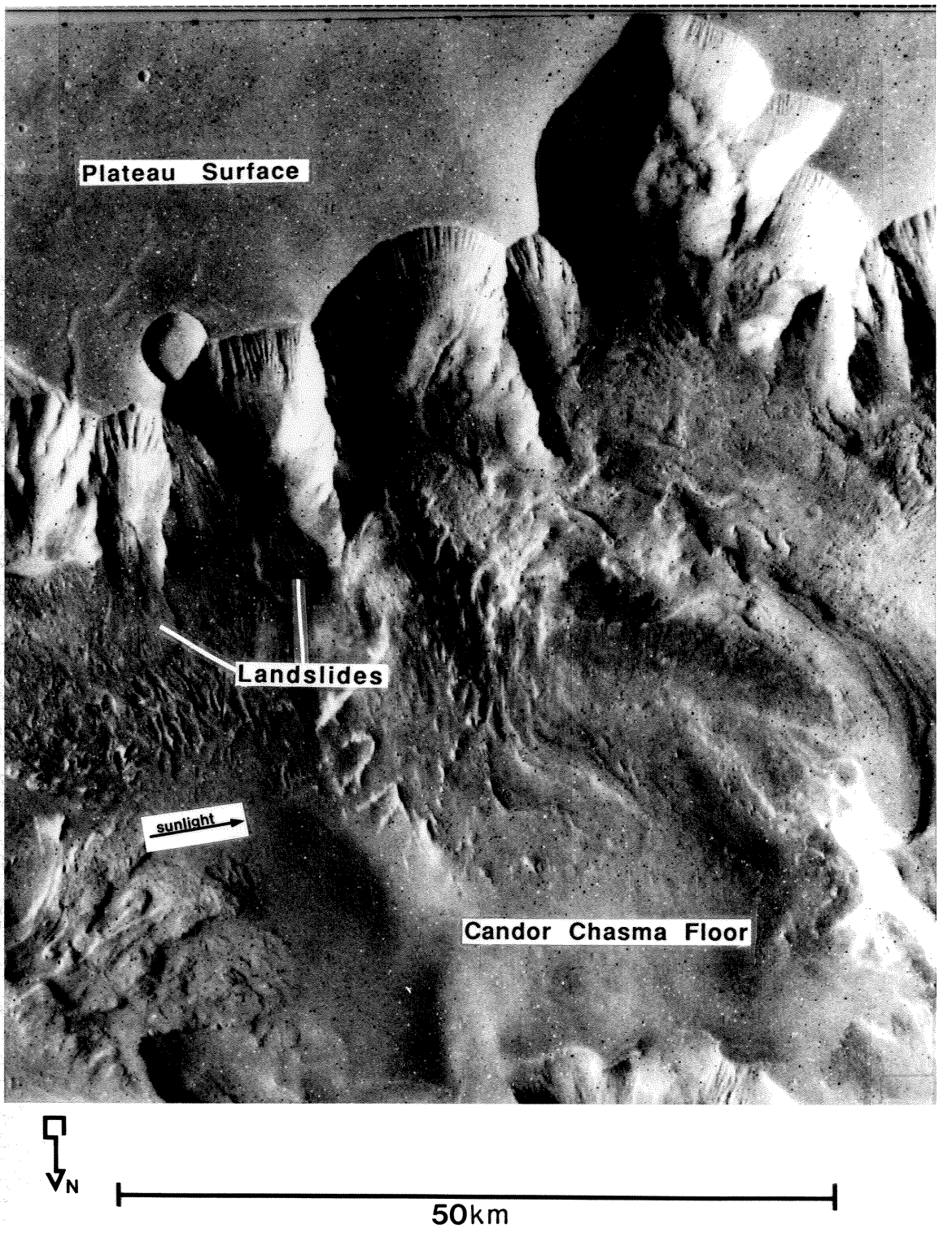

Figure 3. Shaller, 1990.

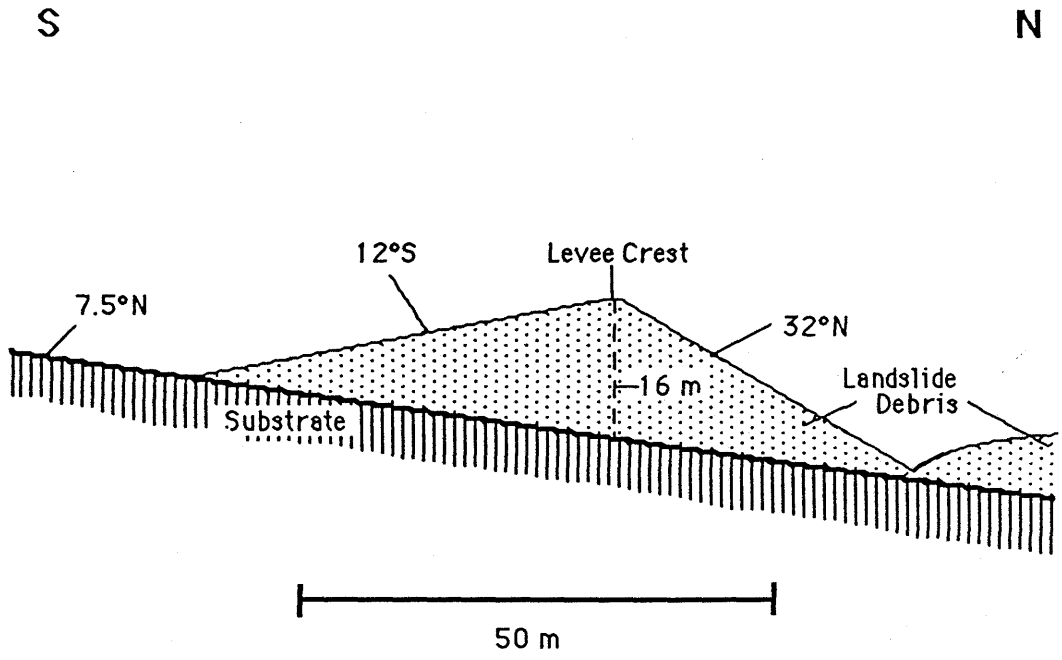

Figure 4. Shaller 1991. Analysis of a large moist landslide...

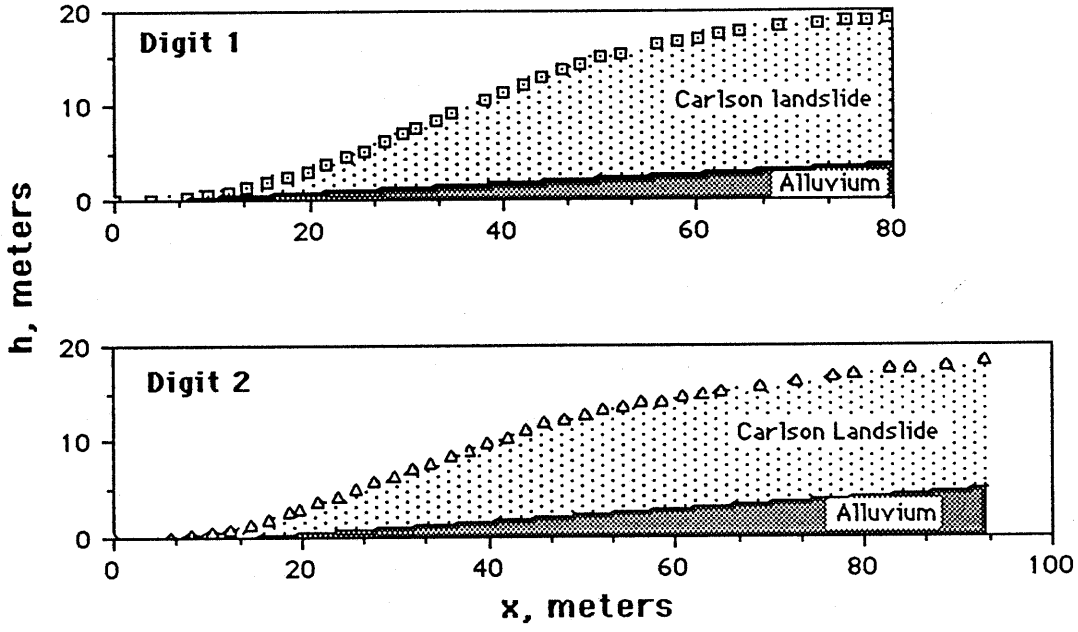

Figure 5. Shaller 1991. Analysis of a large moist landslide...

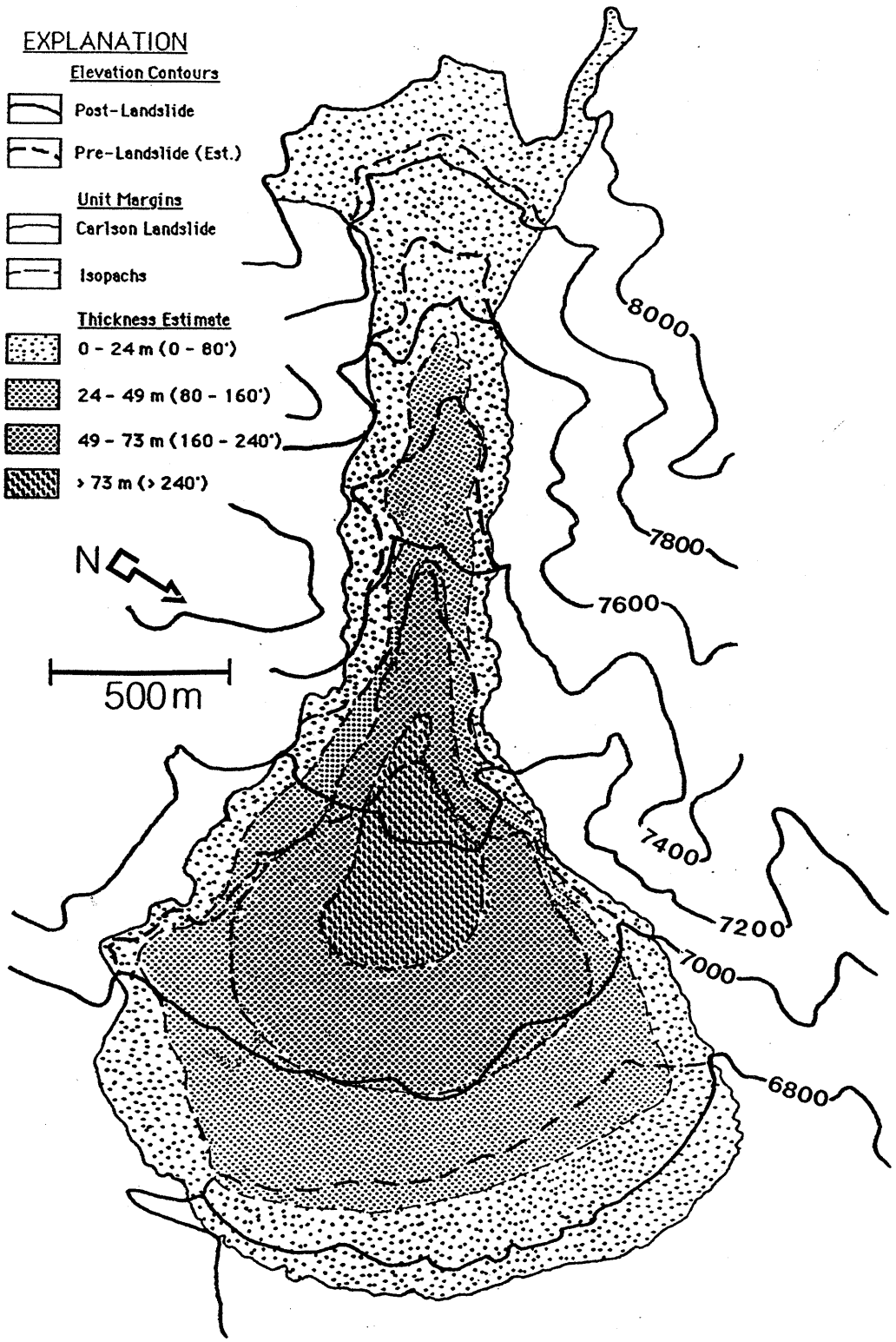

Figure 6. Shaller, 1990.

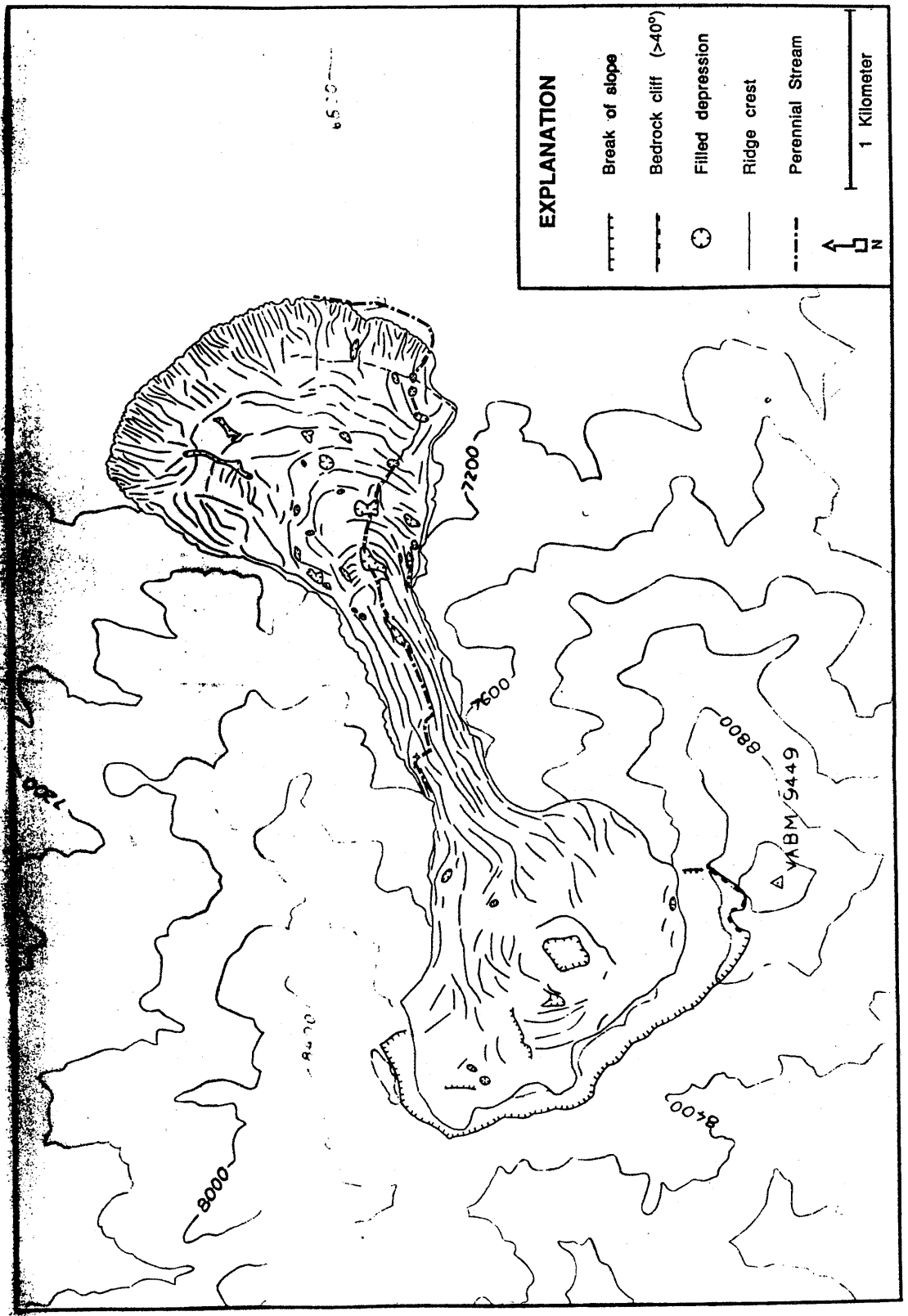

Figure 7. Shaller, 1990.

Figure 8. Shaller, 1990.

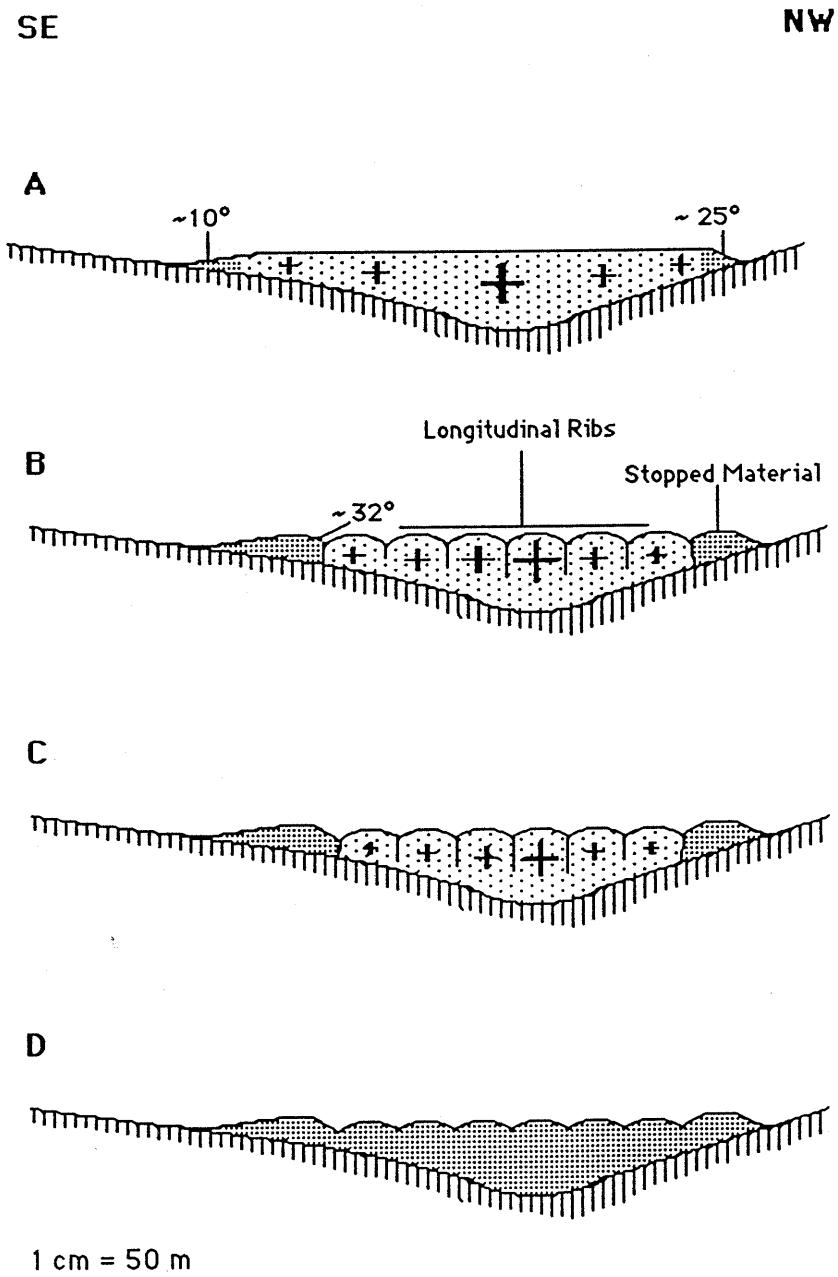

Figure 9. Shaller 1991. Analysis of a large moist landslide...

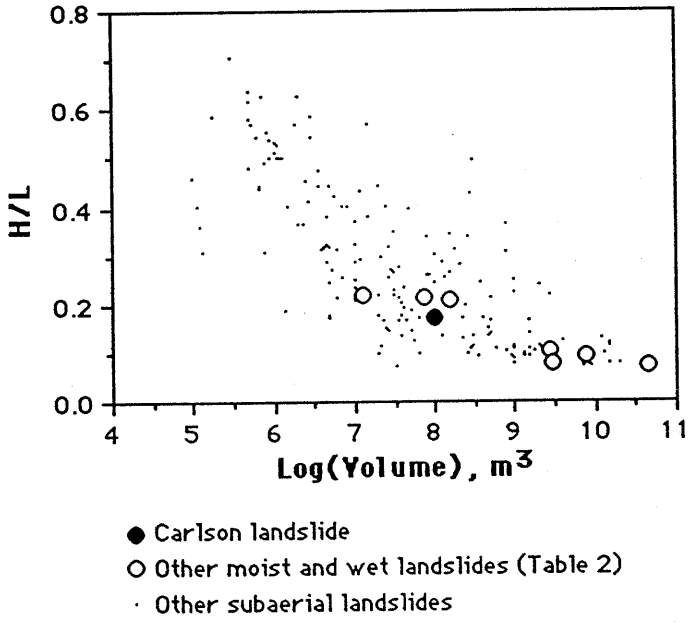

Figure 10. Shaller 1991. Analysis of a large moist landslide...

Appendix C: Velocity Estimation Techniques

The high velocities traveled by long-runout landslides is one of their most remarkable properties. Many different methods have been used in the literature to estimate the velocities attained by large landslides during runout. The most common method derives velocities from the heights of obstacles climbed by landslide debris (Chapter II), but several other methods also exist for estimating this property of large landslides. These include eyewitness accounts, superelevation of channeled debris, spattering of individual boulders and use of the average estimated friction coefficient.

Velocity estimates based on eyewitness accounts provide the average speed of a landslide based on its length and estimated duration. Understandably, however, few people close enough to observe giant landslides have had the composure to time the events. The best observed and described giant landslide occurred at Elm, Switzerland on 11 September 1881. Though many qualitative descriptions of the velocity were recorded, such as "faster than the railway," the best estimate was made from the following account (Heim, 1932):

> Several eyewitnesses of rockfalls can state how far they were able to run at top speed, from the moment when they recognized the danger, to the moment when the rubble stream passed by them, or until this or that house was hit. The most precise and coherent statement of this kind was made from the youngest witness questioned at Elm, the very intelligent boy, Fridolin Rhyner, then eleven years old. He had fled the Untertal and stopped for a moment at the right abutment of the Sernft bridge and looked back towards the Tschingelberg. That was when he saw the entire top of the Plattenberg break loose. Terrified, he fled with four more boys across the bridge to the highway. He heard houses and the bridge behind him being crushed. At the uphill corner of the house of the school-master Wyss, he stopped and looked back. The rock stream had just completed its act of destruction and stood frozen and still. The path covered by Fridolin, one third going east downhill, and two-thirds uphill going south with a change of direction of 90°, measured 190 m (according to a report to me by surveyor Wild). It takes an agile boy 38 to 40 seconds to run this distance. Let's add another 5 seconds for the recognition of the danger and to think about starting. This then gives us 45 seconds for the entire duration of the rock avalanche. The rubble masses completed the run of 2500 m in 45 to 50 seconds from the uppermost scarp to standstill, yielding an average velocity of 50 m per second.

Heim (1932) also attempted to understand something of the movement history of the Elm landslide from the eyewitness accounts, and assessed the error of the velocity estimates:

> From different sources we arrive at one half minute for the plunge of the bulk of the masses at Elm and for the spreading out from the Düniberg to standstill, another half minute. This would give 45 m per second as an average velocity. The maximum velocity certainly exceeded 100 m per second.
>
> These estimates however can be 50 percent incorrect. Movement of between 50 to 150 m per second by mountain plunges seems to be the rule.

Velocity estimates for other large witnessed landslides give mostly comparable speed and error estimates (Table 1). Further, Table 2 shows that the average velocity estimates from the eyewitness data are consistent within broad error bars of those derived from obstacle height calculations using Equations 2a and 2b. These data support the use of the two equations as rough estimators of landslide speed and back up Heim's assertion that large landslides commonly travel at or above 50 m/s (180 km/hr, 113 mi/hr) at emplacement.

Three other little-used devices have been devised to derive velocity estimates for large landslides. These methods provide landslide velocities where no overtopped obstacles or eyewitness accounts exist.

Plafker and Ericksen (1978) used a quantitative relation derived for determining the velocity of banked debris flows in sinuous channels, to estimate the velocity of the moist 1970 Huascaran landslide where it passed through a gentle curve. Equation 1 gives the velocity of moving debris from the estimated superelevation of the landslide and the radius of curvature of the bend:

$$v = \sqrt{rg(\tan\beta)} \qquad (1)$$

where v gives the velocity in m/s, r the radius of curvature of the channel in m, g the acceleration of gravity in m/s^2 and ß the inferred tilt of the slide, in degrees. ß is obtained from the slope between the unequal heights of the inner and outer lateral levees of the landslide in the curve. This method yielded a velocity estimate of 47 m/s for the Huascaran landslide, somewhat lower than estimates of 75-100 m/s from eyewitness accounts and >67m/s from overtopped obstacles. The derivation of Equation 1 makes some fairly stringent

Table 1. Average Speed Estimates for Giant Witnessed Landslides

Name	Estimated Duration(sec)	Travel Length(m)	Velocity (m/s)	References
Elm 11 Sept. 1881	25 - 75	2500	33 - 100	Heim,1932
Frank 29 April 1903	20 - 120	1900	16 - 95	Cruden and Krahn,1978
Gros Ventre 23 June 1925	90 - 270	3500	13 - 38	Alden,1928; Voight,1978
Huascaran 3 31 May 1970	90 - 120	9000	75 - 100	Plafker and Ericksen,1978
Madison 17 Aug. 1959	<60	1500	>25	Hadley,1959; 1978
Mayunmarca 25 April 1974	≈180	8300	≈ 46	Kojan and Hutchinson,1978

Table 2. Comparison of Speed Estimates for Giant Witnessed Landslides

Name	Surge Height(m)	Velocity(m/s) Equation 2 (local estimate)	Velocity(m/s) Witnesses (average)	References
Elm	114	47	33 - 100	Heim,1932
Frank	139	52	16 - 95	Cruden and Krahn,1978
Gros Ventre	100	44	13 - 38	Alden,1928; Voight,1978
Huascaran 3	>230	>67	75 - 100	Plafker and Ericksen,1978
Madison	120	48	>25	Hadley,1959; 1978
Mayunmarca	200	63	≈ 46	Kojan and Hutchinson,1978

assumptions, including: 1) the channel has a gradient of less than 15°; 2) the debris surface in cross-section lies normal to the acceleration direction of the debris; and 3) the debris behaves as a perfect fluid (Johnson, 1984). The assumption of perfect fluid behavior along with the low velocity estimate calculated for the Huascaran landslide indicates that this method gives only approximate, apparently conservative, estimates of landslide velocities.

Another velocity estimation technique originated and has found use only in the study of the 1970 Huascaran landslide. A remarkable phenomenon associated with this landslide was that large boulders were ejected from the landslide during movement at colossally high velocities, ranging between 125 and 278 m/s, or 450 to 1000 km/hr (Plafker and Ericksen, 1978)! To date, no other known landslide has demonstrated rock spattering on this scale. These numbers were derived by assuming that the boulders flew on ballistic trajectories from inferred sites of origin in the landslide, and are in excess of what would be expected for a purely gravitational fall. Somehow, perhaps by the differential deposition mechanism (Chapter VI), the boulders became preferentially accelerated by the landslide. Velocity estimates made from spattering rocks clearly give a large overestimate of landslide velocities.

The last known technique for landslide velocity estimation makes use of the geometry and estimated friction coefficient, or "fahrböschung," of a landslide to estimate its acceleration, velocity and elapsed time of emplacement. The fahrböschung is the tangent of the slope of the line connecting the crown of the headscarp with the toe of a landslide deposit, and has been used as a proxy for the much more difficult to obtain true average friction coefficient of a landslide deposit (Heim, 1932; Chapter II). For the Chaos Jumbles landslides, Eppler, et al. (1987) used the fahrböschung, together with the angles of the slopes traversed by the landslides and the constraints that their initial and final velocities had to equal zero to estimate the accelerations of the landslides during emplacement. The relationship of the fahrböschung to the slope along which the landslides moved determined whether the landslides accelerated or decelerated; slope angles greater than the fahrböschung meant the landslides accelerated, while angles smaller than the fahrböschung forced the landslides to decelerate.

Three overlapping landslide deposits make up the Chaos Jumbles (Eppler, et al., 1987). Each landslide deposit was separated into three travel segments of consistent slope and direction. At the end of Segment 2, the oldest and largest

landslide, Chaos Jumbles #1, made a large turn after ramping up at least 110 m (360') onto Table Mountain. The fahrböschung technique gave a velocity estimate of 68 m/s for this landslide at the end of Segment 2, compared to an estimate of 46 m/s using the runup height in Equation 2a. Under nearly the same depositional geometry, the smaller Chaos Jumbles #2 deposit ran about 25 m (90') up Table Mountain. For this deposit, the fahrböschung technique yielded a final Segment 2 velocity of 23 m/s, compared to a runup height speed estimate of 22 m/s. This method thus appears to give velocity estimates within 50% of those obtained from runup heights, making this an acceptable alternate method for estimating landslide velocities.

Appendix D: Application of Air-Layer Lubrication to Martian Landslides

The calculations presented below are based on the mathematical theory of air-layer lubrication presented by Shreve (1968b). Numbered equations correspond to equations in Shreve (1968b). All calculations are made in SI units (International System of Units).

1) Calculate the thickness of the column of martian (present-day) atmosphere required to provide a 0.3 m (~1 ft) cushion of compressed gas beneath a 65 m-thick landslide.

•First, calculate the pressure required at the base of the breccia sheet using Equation 1a from Shreve (1968b):

$$P_b = P_t + \sigma_a g s \qquad (1a)$$

in which P_b is the pressure in the air layer, P_t is the pressure of the atmosphere at the top of the debris layer, g is the gravitational acceleration, s is the thickness of the debris layer and σ_a is its arithmetic mean bulk density. For a 65 m-thick martian landslide, the following values are assumed for the variables in Equation 1a: P_t = 608 Pa (at 6.1 mbar datum elevation; Carr, 1981), σ_a = 2000 kg/m^3, g = 3.72 m/s^2, s = 65 m. This gives a value for $\underline{P_b = 484208 \text{ Pa}}$.

•Second, calculate the temperature of the compressed gas layer under the breccia sheet using Equation 2d from Shreve (1968b), which assumes isentropic compression:

$$T_t/T_b = (P_t/P_b)^{(\gamma - 1)/\gamma} \qquad (2d)$$

in which T_t is the atmospheric temperature, T_b is the temperature of the gas in the cushion beneath the breccia layer and γ is the ratio of the heat capacities of CO_2 gas (95.32% of martian atmosphere; Carr, 1981) at constant pressure and at constant volume. The following values are assumed for the variables in Equation 2d: P_t = 608 Pa, P_b = 484208 Pa, T_t = 200°K (Carr, 1981), γ = 0.263 (JANAF, 1971; Moore, 1972). This gives a value for $\underline{T_b = 690°K}$.

•Third, calculate the number of moles of gas in the compressed gas layer under the breccia sheet for a unit area of the sheet (1 m^2) using the ideal gas equation (Shreve, 1968b):

$$P_bV_b = nRT_b$$

$$n = P_bV_b/RT_b$$

in which n is the number of moles in the calculated volume, V_b equals the volume of gas trapped between the landslide and the ground surface for a unit area (1 m^2) of the surface and R is the gas constant. The following values are assumed in the preceding equation: P_b = 484208 Pa, V_b = 0.3 m^3, R = 8.314 Pa·m^3/°K·mole, and T_b = 690°K. This gives a value for n = 22.99 moles.

•Fourth, calculate the original (uncompressed) volume of the gas, V_t, trapped in the compressed gas layer under the breccia sheet for a unit area of the sheet (1 m^2) using the ideal gas equation (Shreve, 1968b):

$$P_tV_t = nRT_t$$

$$V_t = nRT_t/P_t$$

For values of n = 22.99 moles, R = 8.314 Pa·m^3/°K·mole, T_t = 200°K, and P_t= 608 Pa, V_t = 62.87 m^3.

Therefore, in order for a 65 m-thick martian landslide to be supported by a 0.3 m-thick gas layer compressed from the atmosphere, the landslide would have to trap a 62.87 m-high column of air *per unit area* of the landslide.

2) For the sake of comparison, calculate the thickness of the column of atmosphere required to provide a 0.3 m (~1 ft) cushion of compressed gas beneath the Blackhawk landslide.

•First, calculate the pressure required at the base of the breccia sheet using Equation 1a from Shreve (1968b). For the 30 m-thick Blackhawk landslide, the following values are assumed for the variables in Equation 1a: P_t = 101325 Pa, σ_a = 2000 kg/m^3, g = 9.80 m/s^2, s = 30 m. This gives a value for P_b = 400029 Pa.

•Second, calculate the temperature of the compressed gas layer under the breccia sheet using Equation 2d from Shreve (1968b). The following values are assumed for the variables in Equation 2d: P_t = 101325 Pa, P_b = 400029 Pa, T_t = 293°K, γ = 1.4 (Shreve, 1968b). This gives a value for T_b = 434°K.

•Third, calculate the number of moles of gas in the compressed gas layer under the breccia sheet for a unit area of the sheet (1 m^2) using the ideal gas equation (Shreve, 1968b). For the following assumed values, P_b = 400029 Pa, V_b = 0.3 m^3, R = 8.314 Pa·m^3/°K·mole, and T_b = 434°K, one calculates a value for n = 33.83 moles.

•Fourth, calculate the original (uncompressed) volume of the gas, V_t, trapped in the compressed gas layer under the breccia sheet for a unit area of the sheet (1 m^2) using the ideal gas equation (Shreve, 1968b). For values of n = 33.83 moles, R = 8.314 Pa·m^3/°K·mole, T_t = 293°K, and P_t= 101325 Pa, we obtain a value for **V_t = 0.813 m^3.**

Therefore, in order for the 30 m-thick Blackhawk landslide to be supported by a 0.3 m-thick gas layer compressed from the atmosphere, the landslide only has to trap a 0.813 m-high column of air per unit area of the landslide, almost two orders of magnitude less volume than required for the martian landslide.

3) Calculate the column of gas that landslide Mars 141, which lies in the summit caldera of Olympus Mons, would have to capture in order to be lubricated by a compressed gas cushion.

•First, calculate the pressure required at the base of the breccia sheet using Equation 1a from Shreve (1968b). For the 120 m-thick Mars 141 landslide, the following values are assumed for the variables in Equation 1a: P_t = 29 Pa (Carr, 1981), σ_a = 2000 kg/m^3, g = 3.72 m/s^2, s = 120 m. This gives a value for P_b = 892829 Pa.

•Second, calculate the temperature of the compressed gas layer under the breccia sheet using Equation 2d from Shreve (1968b). The following values are assumed for the variables in Equation 2d: P_t = 29 Pa, P_b = 892829 Pa, T_t =

160°K (Carr, 1981), γ = 1.23 (JANAF, 1971; Moore, 1972). This gives a value for T_b = 1105°K.

•Third, calculate the number of moles of gas in the compressed gas layer under the breccia sheet for a unit area of the sheet (1 m^2) using the ideal gas equation (Shreve, 1968b). For the following assumed values, P_b = 892829 Pa, V_b = 0.3 m^3, R = 8.314 Pa·m^3/°K·mole, and T_b = 1105°K, one calculates a value for n = 29.16 moles.

•Fourth, calculate the original (uncompressed) volume of the gas, V_t, trapped in the compressed gas layer under the breccia sheet for a unit area of the sheet (1 m^2) using the ideal gas equation (Shreve, 1968b). For values of n = 29.16 moles, R = 8.314 Pa·m^3/°K·mole, T_t = 160°K, and P_t= 29 Pa, we obtain a value for **V_t = 1337 m^3.**

Therefore, in order for the 120 m-thick Mars 141 landslide to be supported by a 0.3 m-thick gas layer compressed from the atmosphere, the landslide would have to trap a 1337 m-high column of air *per unit area* of the landslide. This would prove impossible because the entire vertical fall height of the landslide is only 2500 m and the landslide had no launching ramp.

Appendix E: Description and Evaluation of Proposed Models for Long Runout in Large Landslides

A. Introduction

Appendix E begins with a discussion of a simple block-on-inclined-plane model for landslide travel, to provide a basic understanding of the anomalous nature of long-runout landslides. The model predicts, for example, that for the same materials and starting geometries, landslides on Earth, Mars and the Moon should all finish movement in the same configuration, though the rates of the process would vary considerably between the three planets. Following this analysis, four separate categories of theories are discussed and evaluated for their ability to explain the variety of unusual phenomena associated with long-runout landslides. These categories include: 1) fluidization and flow of landslide debris; 2) special forms of lubrication along the base of the slides; 3) mass-loss mechanisms coupled with normal frictional sliding; and 4) individual-case mechanisms. The first three categories include descriptions of mechanisms proposed as unifying theories of long runout, applicable to all large landslides. The fourth category consists of mechanisms proposed to explain long runout on a case-by-case basis. These theories do not assume to explain long runout as a universal property of large landslides, but rather attempt to explain the phenomenon based on local effects of the depositional environment. The various theories composing these groups approach the subject with varying degrees of depth, ranging from qualitative, kinematic arguments to highly quantitative mathematical modelling efforts. In the analysis of each theory below, the models are appraised primarily on the basis of their ability to explain the observed geologic relations of the individual deposits for which they were developed, as well as for long-runout landslides as a group.

B. Block-on-Inclined-Plane Model

One simplistic yet informative method of modeling the travel of large landslides is to view the moving landslide as a block of constant mass and proportions that slides down a slope and onto a flat depositional surface with a constant coefficient of sliding friction. Figure 1 illustrates the geometry of this model. In this model, a block of mass m lies on a slope with an angle ß to the horizontal. At rest, the landslide block has a static coefficient of friction,

Figure 1. Diagram illustrating the block-on-inclined-plane model of landslide runout described in the text. Primary diagram provides the geometry of the model. Underlying two illustrations provide free-body diagrams of the block at rest on the slope, when accelerating down the slope and when decelerating on the level depositional surface. See text for discussion.

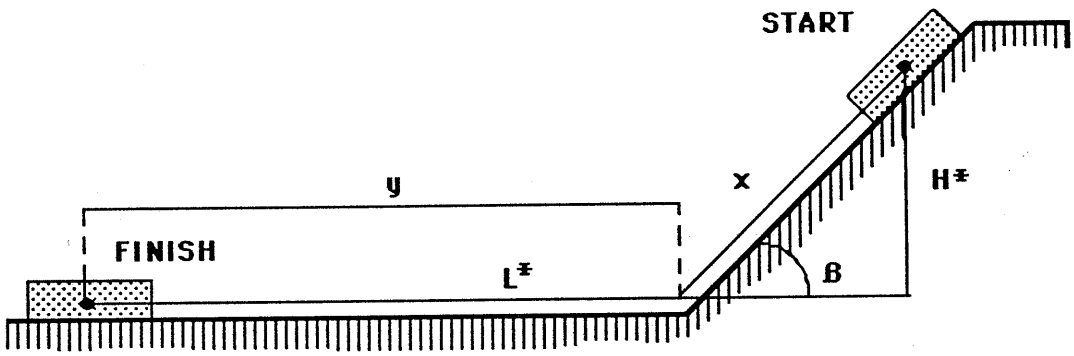
START
y
x
H±
FINISH
L±
β

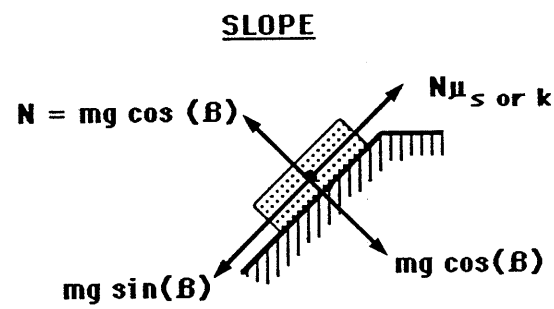
SLOPE
N = mg cos (β)
Nμs or k
mg sin(β)
mg cos(β)

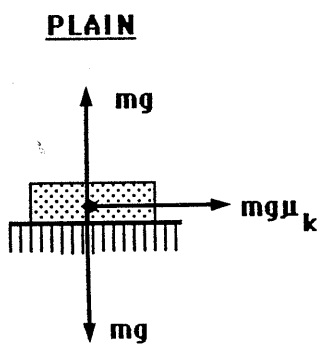
PLAIN
mg
mgμk
mg

μ_s. Referring to the free-body diagram labeled "slope," the block initially rests in a static condition, just in equilibrium against sliding. Under these conditions, μ_s can easily be shown to equal tan(ß) (Appendix EE). Rockfalls and planar landslides on Earth, Mars and the Moon take place along discontinuities in rock masses that range in inclination from 20° to 65° (Chapter III: Table 9), which in this purely frictional model would correspond to static coefficients of friction ranging from 0.36 to 2.15. A commonly sited intermediate value for the static friction coefficient in rock is 0.6, corresponding to an average internal friction angle of about 31° (Hsü, 1975).

If this static condition is disrupted, for example by an earthquake, the block will begin to slide down the slope, because under normal circumstances μ_k, the coefficient of sliding friction, is always less than μ_s (Resnick and Halliday, 1977). Referring again to Figure 1, the block begins to slide down the slope at this time and accelerates all the way down the slope of length x. The acceleration of the block and its velocity at the base of the slope will vary with the gravitational acceleration. For starting conditions where H = 500 m, ß = 30° and μ_k = 0.5, if g is allowed to vary according to differences in gravitational acceleration between Earth (9.8 m/s^2), Mars (3.72 m/s^2) and the Moon (1.67 m/s^2)(Resnick and Halliday, 1977), the velocities of the block at the base of the slope will range from 36.2 m/s on Earth to 22.3 m/s on Mars to 15.0 m/s under lunar gravitational acceleration (Appendix EE).

Assuming the frictional coefficient remains constant between the slope and the depositional plain, one can calculate the distance the blocks travel from the break in slope given the velocities calculated above and applying the forces on the block depicted under the term "plain" in Figure 1. In each case, the blocks move 133.7 m from the break in slope before coming to rest. This calculation illustrates that, despite the variations in gravity between the three bodies, landslides travelling under conditions of coherent frictional sliding will always end up in the same configuration for the same starting conditions. Under terrestrial gravity a sliding block will accelerate faster coming down slope than an identical block on Mars or the Moon. However, the frictional restraining forces in the deceleration phase are also proportional to the gravitational acceleration and therefore will decelerate the block much more rapidly on Earth than on the Moon or on Mars. These effects balance out in the model, giving the same stopping points for the blocks in all three cases.

Note that the rates of the process vary markedly between the three planets, however.

Using the results derived above, one can calculate the ratio of the vertical drop, H*, to the horizontal distance, L*, traveled by the block in each experiment (Figure 1). In each case the vertical fall height measures 500 m and the total horizontal distance traveled by each block amounts to exactly 1000 m (Appendix EE). The H*/L* ratio for the block in this model therefore equals 0.5, precisely the coefficient of sliding friction for the block over the substrate. Note also that mass drops out of every calculation made in Appendix EE. This means that the initial mass of the block has no influence whatsoever on the ultimate distance traveled by the block in this model.

The results of this simple sliding block model contrast markedly with some of the basic observations of long-runout landslides made in the preceding chapters. For example, unlike large landslides on both Earth and Mars, the model predicts no influence of increasing block mass on the predicted fall height to runout length ratio of a landslide. With a rigid slide block, this ratio should vary only with the coefficient of sliding friction between the block and the ground. Secondly, the model does not predict any influence of gravity on the fall height to runout length ratio of a sliding block, whereas the available evidence suggests that for a given volume of landslide debris, a landslide on Earth will travel further, and thus exhibit a lower ratio than a comparable landslide on Mars (Chapter III: Figure 7; McEwen, 1989).

Part of the discrepancy between the sliding block model and the actual observed behavior of large rock landslides comes from the method of calculation of H/L values for large landslide deposits. In order to facilitate estimation of H/L, H and L are commonly measured between the toe of a landslide and crown of its headscarp (Chapter II). While the general lack of information on the initial dimensions of a failed slope necessitates this estimation for most landslides, this procedure can result in considerable underestimation of the true kinetic friction experienced by a landslide during runout. Figure 2 compares the true (marked with asterisk) and estimated H and L measurements for the simple sliding block model, and relates these values for the case of negligible slide block thickness. For normal values of ß (25°-45°), L/L* will always be larger than H/H*, requiring that H/L < H*/L* for this geometry. The magnitude of the problem increases with the dimensions of the slide block. For example, in the previously described case

Figure 2. Diagram illustrating the observation that the normal method used to report H/L ratios for long-runout landslides will provide artificially low values of the actual ratio experienced by a large landslide simply due to the non-negligible dimensions of the slide block.

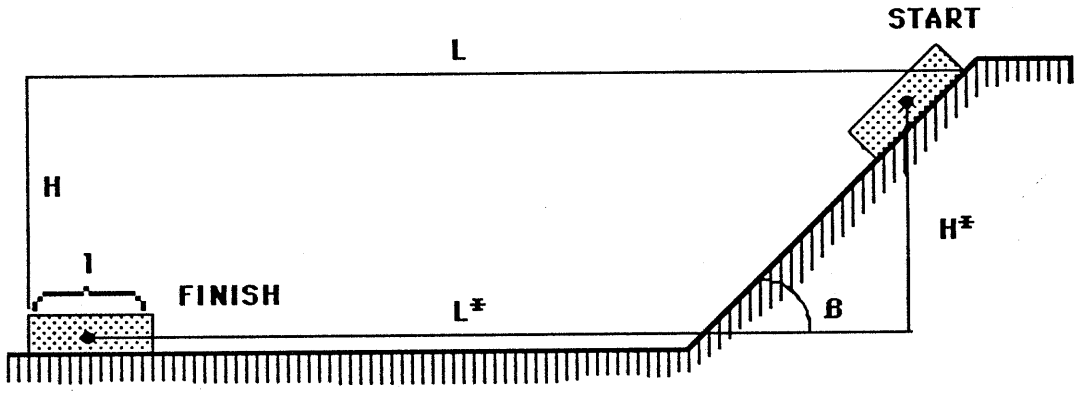

Assuming negligible slide block thickness:

$$H = H^* + 1/2 \sin(\beta)$$

$$L = L^* + 1/2 + 1/2 \cos(\beta)$$

Therefore, for a given value of H^* and L^*:

$$\frac{H}{L} < \frac{H^*}{L^*}$$

where μ_K = 0.5, H* = 500 m, L = 1000 m, ß = 30°, giving a true value of H*/L* = 0.5, one arrives at an H/L estimate of 0.49 for a landslide block 50 m in length, and a value of 0.46 for a slidemass 250 m long. The degree of underestimation of true H/L values appears even more significant when one considers the unusual geometries of actual long-runout landslide deposits. In real landslides, the initial slide blocks do not remain intact, but rather fragment during transport, forming breccia deposits with much greater areal dimensions than the slide blocks from which they originated. This problem forms the object of further discussion in Chapter VI.

C. Complex Models

1. *Bulk Fluidization Models*

Bulk fluidization theories form the first large group of models proposed to explain the long-runout of large landslides (Table 1). These models suggest that clasts forming large landslides move with respect to each other during runout throughout the body of a landslide, like molecules in a dense gas or a fluid, and therefore give a large moving landslide the appearance of flowing during runout. Fluidization of landslide debris has been suggested to occur by various means, including by upward injection of air into overriding rock masses, by energy from the fall, by self-generated acoustic energy and by energy added from external sources, such as an earthquake.

Albert Heim provided the first analysis of the nature of long runout in large landslides. After field study of many old, large Alpine landslides and extensive interviews with numerous survivors of the Elm landslide of 1881, Heim (1932) concluded that large landslides experience some sort of bulk flow, perhaps akin to the behavior of glaciers and lava flows:

> When we look out over a large, inanimate, rock rubble stream from a favorable vantage point...we are quite often seized by the impression of streaming - as much as, or even more than, by looking at a glacier or a lava stream!...It is remarkable that the form and the fluid structure of our debris stream roaring down in one to three minutes at the most, shows such surprisingly similar development to that originating through slow movement [of glaciers and lava flows].

In addition to conceptualizing the large-scale properties of long-runout landslides as fluid-like, Heim (1932) also attempted to understand the phenomenon on the scale of the individual clasts within a moving landslide,

Table 1. Bulk Fluidization Theories Proposed to Explain Long Runout in Large Landslides

The following list gives the major reference and title of the principle bulk fluidization models proposed to explain the long runout of large landslides. They appear in the order of appearance in the text:

1. Heim, 1932: Kinematic bulk fluidization;

2. Kent, 1966: Air fluidization;

3. Krumdieck, 1984: Air fluidization with aerodynamic lift;

4. Hsü, 1975: Mechanical fluidization: Bagnoldian flow of grains in a dense, low-viscosity fluid;

5. Davies, 1982: Mechanical fluidization: Dispersive grain flow;

6. Campbell, 1989: Computer simulations of mechanically fluidized grains;

7. Melosh, 1983: Acoustic fluidization;

8. Trunk, et al., 1986: Computer modeling of large landslides using Navier-Stokes equations of fluid flow;

9. Ivanov and Potapov, 1991: Computer modeling of large landslides using Navier-Stokes equations of fluid flow and a power-law rheology;

10. McEwen, 1989: Bulk Bingham plastic flow of large landslides.

which he conceptualized as being analogous to the molecules in a flowing liquid:

> The bigger the mass of rock that breaks away simultaneously, the more prominent the stream form becomes, and the more clearly the motion has the appearance of **flowing**. The larger the falling mass, the smaller in relation to it is the single rock, which plays the same role in the rubble stream as a water molecule does in a river. One restriction exists in the stream of rock debris, and that is the greater friction of the particles between each other, and the resistance to displacement within the rubble...the rocks are still much too big compared with molecules in a real liquid. This is partly compensated for by the greater specific weight and the far greater accumulation of "live" kinetic energy from the fall.

Interviews of Elm survivors by Heim (1882; 1932) led him to believe that the stopping phase of large landslides differs in a fundamental sense from the behavior of smaller mass movements. In small mass movements, such as a sand flow down an embankment at the beach, material at the lower edge of the failure area starts moving first, and the failure works its way back up the slope. Because the leading edge material begins first and with lower potential energy than trailing material, it comes to rest first at the base of the slope where the gradient flattens out. Trailing material which started movement a little later, and with a little additional initial potential energy, follows the leading material down slope and piles into the stopped leading edge at the base of the slope. Stopping therefore normally should begin at the front of a mass movement and progress toward the rear. Heim (1932) noted, however, that large landslides behaved in a quite different fashion:

> From the spot where the gradient flattens off the entire length of the rubble stream becomes the region of deposition. The rear parts exhaust themselves soon because of transmission of their kinetic energy to the front part and they therefore come to rest sooner. As a rule, one observes in a rubble stream that has come to a halt the thickness is greatest at the beginning of the deposit, and from here towards the lower end it thins out with noticeable regularity...The deepest rubble stops first; the upper still rolls and travels quickly...The further forward a block lies in a rubble stream, the more it has been subjected to pushing and buffeting forces from behind. The further back it lies in the stream, the sooner the replenishment of energy by pushing from behind has ceased so that it could come to rest. A long rubble stream on flat ground comes to rest first at the rear.

In addition to the unusual back-to-front nature of the stopping of large landslides, Heim also believed that stopping of the debris streams took place

rapidly (Chapter III). Although he apparently recognized that stopping did not occur instantaneously from high speed as suggested by observers of the Elm, Goldau and other large historical landslides in the Alps, he nevertheless believed that some anomalous slow-down did occur. This observation led him to the conclusion that large moving landslides exhibit velocity-dependent sliding friction coefficients, which decrease with increasing velocity. This behavior would explain both the high velocities experienced by the landslides during their runout, as well as their apparent rapid slow-downs from high speed. Because the frictional coefficient would dramatically increase with decreasing velocity, stopping would experience a positive-feedback effect, with the rate of slowing increasing as the velocity dropped from high speed, yielding a very rapid slow-down phase.

The mechanical behavior of long-runout landslides conceptualized by Heim appear to originate primarily in his investigations of several comparatively small, historically witnessed landslides: Diablerets 1 and 2, Goldau, Plurs and especially Elm. For example, he discusses the observation that many large landslides exhibit morphologies that give the impression of glacier or lava-like streaming. One important fact not addressed by Heim is that all the landslides displaying such behavior traveled down channels. Channelized landslides may give the appearance of mountain glaciers and lava flows, but unconfined landslides like Blackhawk or Saidmarreh experience much different morphological development (Chapter IV: Figure 44a). Heim also suggests that long-runout landslides do not exhibit much interclast cohesion. This appears true of smaller long-runout landslides such as Elm (Heim, 1932) and Diablerets 1 (Ramuz, 1947), which seem to have consisted entirely of cobbles and boulders, but field data from larger landslides indicates that the copious quantities of fines produced in these events could have given these landslides considerable interclast cohesion during transport (Chapter III).

Heim attempted in a variety of ways to conceptualize the movement of long-runout landslides as some sort of bulk fluid flow, both at a large scale and at the scale of individual clasts, the "molecules" in a moving debris stream. As mentioned above, the surface textures of some long-runout landslides indeed give the impression of flow. However, the relations exposed in the interiors of large landslides rule out bulk flow in long-runout landslides. This is required by the fact that headscarp stratigraphy is preserved in all dry multiple-lithology landslides (Chapter III: Figure 24), an observation that places strict

limits on the amount of internal motion a large landslide might experience. Turbulent mixing of landslide debris would clearly cause disruption of stratigraphy throughout a landslide mass and must be dismissed. However, bulk laminar flow too would cause the disruption of stratigraphy, because material at the leading edge of a laminar flow would by necessity roll over and mix (Figure 3). *This problem is the principle drawback to all proposed mechanisms of long runout which attempt to describe the phenomenon by means of a bulk flow process.* The possibility does exist, however, that the basal layer of a long-runout landslide might experience laminar flow during runout. Such behavior might in fact help explain the observations of horizontal slip surfaces and foliation in basal exposures of some long-runout landslides (Chapter III). Heim's observation that the blocks on the central ridge of a channelized debris stream move faster than those along the margins certainly suggest a flow phenomenon, but bulk flow need not occur to develop this appearance. Because Heim (1932) noted the flow structures primarily only on channelized landslides, the likelihood exists that the landslides developed transverse velocity profiles, with material along the centerline moving faster than material along the edges of a channel. However, rather than occurring by way of bulk flow, this velocity distribution probably occurred in a more discontinuous fashion (Appendix B), such as along vertical slip planes. The streaming or shooting behavior suggested by Heim, however, cannot hold for most landslides because both imply turbulent flow, which would thoroughly mix the debris in the landslides during transport (Daugherty, 1937). By conceptualizing long-runout landslides as fluids, Heim was also able to hypothesize why the behavior of large landslides should change with increasing volume. Increasing the volume of a landslide would have the effect of reducing the effective sizes and therefore the importance of individual clasts within the moving debris. This concept jibes to some extent with the observation made in Chapter III that grain size has a critical effect on the H/L ratios exhibited by large landslides (Chapter III: Figure 12c). Smaller clast sizes were found to correlate with lower H/L ratios independently of volume. The precise mechanism by which small clasts modify the behavior of large landslides remains unresolved. This problem is addressed further in Chapter VI.

The stopping phase of long-runout landslides appears to have given Heim considerable pause. His interviews of Elm survivors seem to have convinced

Figure 3. Schematic diagram showing progressive destruction of preserved stratigraphy along the toe of a large landslide exhibiting laminar flow. Step 1 shows landslide early in movement phase moving from right to left across page. In Step 2, laminar flow has oversteepened the leading edge of the landslide, forcing it to break off at about the angle of repose of loose material. The material that breaks off immediately is bulldozed by the landslide, mixing the debris and plastering it on the front of the moving landslide (Step 3). Flow continues in Step 4, again leading to oversteepening of the toe, repeating the process. At the end of the first two steps of this process, mixed material forms the toe of the landslide and occurs along the bottom of its leading edge.

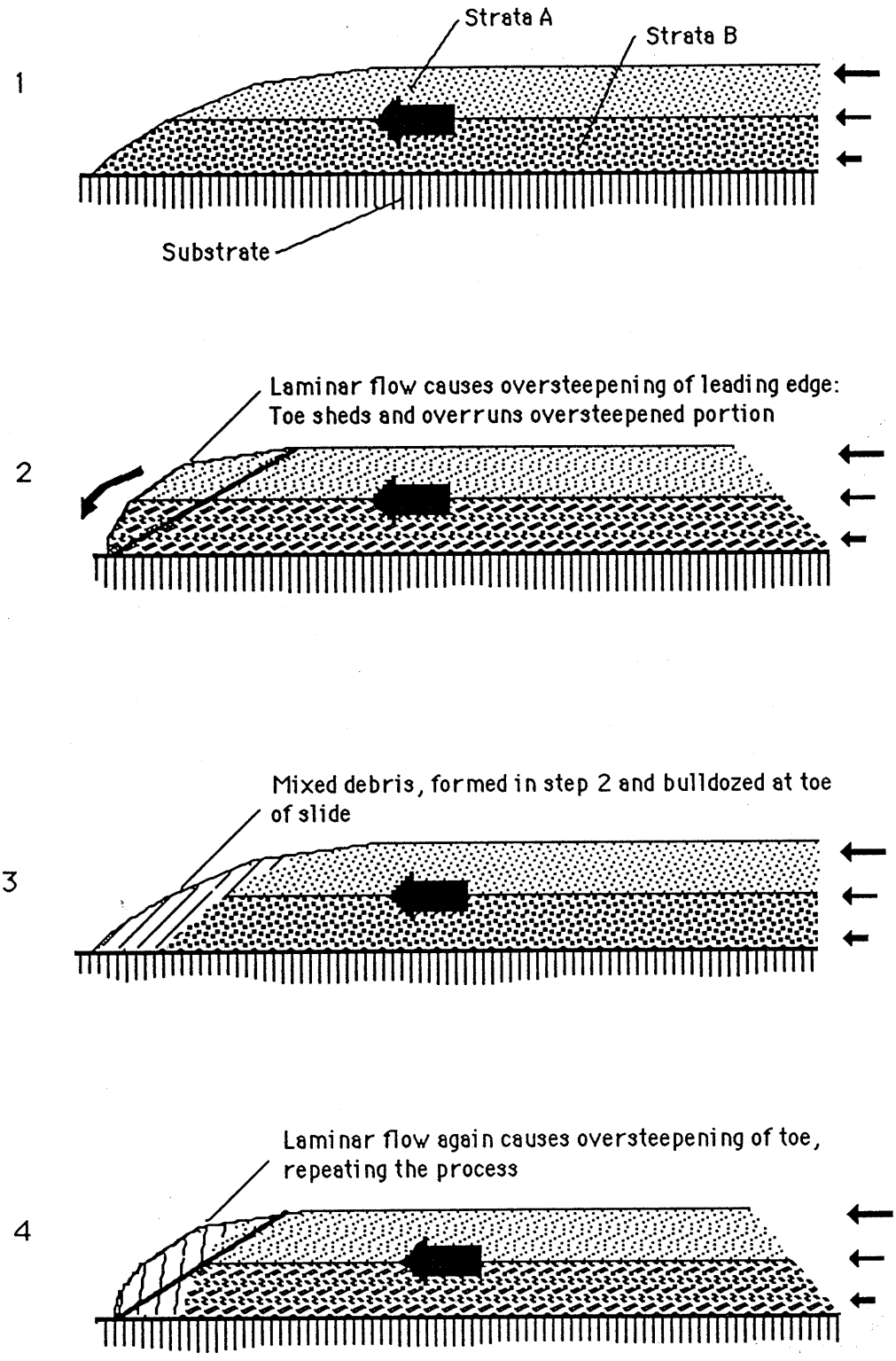
1
Strata A
Strata B
Substrate
2
Laminar flow causes oversteepening of leading edge:
Toe sheds and overruns oversteepened portion
3
Mixed debris, formed in step 2 and bulldozed at toe
of slide
4
Laminar flow again causes oversteepening of toe,
repeating the process

him that large landslides stop with remarkable abruptness, leading him to conceive of a velocity-dependent frictional coefficient. In reality, little evidence exists to support this model. For example, the data on terrestrial long-runout landslides do not show any clear correlation between emplacement velocity (principally derived from the heights of overtopped obstacles; Chapter II), and H/L (Figure 4). Also, velocity data from two Soviet artificially-triggered landslides that exhibited long runout (Appendix A; Chapter III: Figure 35) do not support the idea that landslides stop suddenly from high speed, as suggested by eyewitnesses of the Elm landslide (Heim, 1932). Thus, a velocity-dependent frictional coefficient does not appear necessary, nor is it capable of explaining these critical observations.

The second of these models proposed **air fluidization** to explain the long-runout of large landslides (Kent, 1966). Kent based his theory on geologic relations of the Saidmarreh, Frank and Madison landslides, as well as on eyewitness accounts of the emplacement of Frank and Madison. Referring specifically to Frank, but meaning to apply the idea also to the other two deposits, Kent stated:

> ...it seems highly probable that the high speed and high fluidity of the landslip, with its ability to flow uphill without hindrance from normal friction, was due to fluidization with air -- the air entrapped during the first few hundred feet of fall being "entangled" in the rock for long enough to permit the rock to flow as a liquid. As the air escaped, the angular blocks locked together to form the present mass, as incapable of flowing as could well be imagined, but certainly far too thin in relation to its area to transmit thrust pressures through more than a few hundred feet.

Kent's strong belief in an important role for air in the mobilization of these large landslides was strongly influenced by eyewitness accounts from the Frank and Madison landslides of strong air blasts accompanying passage of the debris (Chapter III). Kent (1966) used several lines of evidence to support his theory, including: the fan-like spreading of the landslides, the fact that they ended movement in thin sheets relative to their aerial dimensions, that they traveled at high speeds, exhibited a high degree of fluidity during runout, and were deposited as a chaotic assortment of blocks without gravity sorting. Kent did not single out any of the above characteristics for explanation by entrapped air fluidization. Rather, he simply stated that: "Fluidization by entrapped air appears to be the only mechanism capable of

Figure 4. Plot of H/L values versus maximum velocities for terrestrial long-runout landslides, illustrating that little correlation exists between the two parameters.

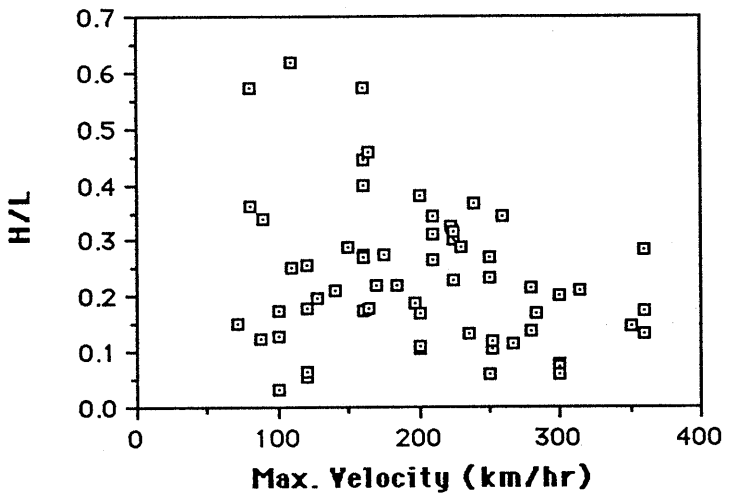
0.7
0.6
0.5
0.4
0.3
0.2
0.1
0.0
H/L
0
100
200
300
400
Max. Velocity (km/hr)

explaining the observed features, and major landslides of sheetlike form thus present a special and perhaps unique case of geomorphological transport."

Although the air fluidization theory of Kent (1966) explains the high speed emplacement and sheet-like geometries of the Frank, Saidmarreh and Madison landslides, it has difficulty in explaining other important geologic relations in these and other long-runout landslides. One drawback of air fluidization is that it fails to explain the preserved stratigraphy observed in these three landslides (Appendix A). These observations suggest that the landslides did not experience turbulent flow throughout their interiors during emplacement as expected with fluidization by escaping air (Brown and Richards, 1970). Instead, the landslides all give the appearance of sliding or flowing into place along a weak, easily sheared basal surface (Chapter III). Another problem with air fluidization is that in industrial use it gives rise to normally-graded bedding when a distribution of clast sizes exist (Brown and Richards, 1970). This distribution results because air expelled from beneath a landslide should carry smaller particles more readily than larger ones. When the air finally gives out, the larger clasts fall out of suspension first, followed by smaller fragments, leading to a gradation of clast sizes from large at the bottom to small on top. In contrast, each of the landslides mentioned by Kent as having experienced air fluidization exhibit reverse grading, with the largest clasts on top (Appendix A). Other long-runout landslides either reverse grading or no grading at all; none have graded bedding (Appendix A; Chapter III). In addition, Cruden and Hungr (1986) have calculated that given the fall height and dimensions of the Frank landslide and a dry frictional coefficient for the landslide debris of 0.6, the pore pressures developed in the landslide should only have been sufficient to fluidize a 5 m-thick debris sheet. This value falls well below the 14 m average depth of the Frank landslide (Appendix A). Fluidization by air would also prove quite difficult on Mars, and impossible on the Moon. The composite evidence therefore suggests that air fluidization does not provide a reasonable method for achieving long runout in any known large landslides.

Krumdieck (1984) also presented a model of long runout based on air fluidization, but with an added twist; he proposed that the geometries of certain landslides enabled them to develop aerodynamic lift during runout that reduced the frictional force at the bases of the landslides. Krumdieck (1984) stated that:

> A mass of granular material or rock debris sliding down a mountain will develop a front head with diminishing thickness toward the tail; in other words, it will develop a roughly aerodynamic profile. The movement of the mass downhill will alter the air current, similar to the way in which the profile of an airplane wing does, by creating a narrowing zone of air circulation on the back of the wing...Due to high pressure below the moving mass and low pressure above, air is entrained at the underside and fluidization (liquifaction) results.

The Krumdieck model has a great many substantial problems. Those inconsistencies applicable to air fluidization of landslide debris are outlined above. The aerodynamic lift mechanism has an equal number of problems. For example, it only applies to distally raised landslides. It also fails to take into account that the moving body consists of brecciated rock, so that any lift that might develop would simply pluck the rocks off the surface of the landslide and would not lift the entire moving landslide. Also, the mechanism would have great difficulty explaining the long runout of large landslides on Mars or the Moon. Further, while a moving landslide might appear to have a wing-like profile shape at the macroscopic level, it will have an extremely rough surface at the small scale important to air flow over the surface. Air could therefore not move smoothly over the landslide "wing." Drag should therefore form the only atmospheric effect on a rapidly moving landslide (Daugherty, 1937).

Several theories that succeeded the air fluidization model of Kent (1966) instead invoked **mechanical fluidization** to explain the long runout of large landslides. These models include the mechanical fluidization theories of Hsü (1975) and Davies (1982), mechanical models in which fluidization concentrates along the base of a moving landslide (i.e., Campbell, 1989), and a variant of the latter in which basal fluidization occurs in concert with deposition of slow-moving debris from the base of a moving landslide (Savage, personal communication, 1990).

Hsü (1975) in essence restated Heim's conceptual model of flow in long-runout landslides in quantitative terms based on the cohesionless grain flow theory of Bagnold (1954; 1956). This theory describes the turbulent flow of a dispersion of cohesionless grains in a fluid medium (Hsü, 1975). Hsü (1975) pointed out that the flow of mixtures of solid grains and fluid involves a fluid-transmitted stress, t, and a grain-transmitted stress, T; the total stress, TS, is the sum of the two. In an ideally fluidized bed, as envisioned by Kent (1966), t would provide the dominant component of the total stress, being produced by a

rising current of air, and T would ideally equal zero. Hsü (1975) considered this method a highly improbable means of suspending landslide debris, especially for landslides on the airless Moon. He believed, on the contrary, that the flow motion of the debris of large landslides was propelled principally by the stress transmitted by grains, T, as a result of grain collisions. In this type of flow, kinetic energy transfers through grain collisions, and dissipates by friction during such impacts. The mathematical derivation of "Bagnoldian" grainflow is quite involved and will not be pursued here. It might prove useful to view the final products of the derivation, however:

(1) the gravitational stress, S_g, which drives the movement of a landslide is given by:

$$S_g = [p_f + (p_s - p_f)C] \cdot dg \sin(ß) \qquad (1a)$$

where d is the slide thickness, C is the volume concentration of the flowing rock, p_s and p_f are the densities of the solid and fluid, respectively, g is the gravitational acceleration and ß is the slope angle of the bed.

(2) the shearing resistance to grain flow, caused principally by grain collisions, is given by:

$$TS = (p_s - p_f) \cdot Cdg \cos(ß) \tan(∂) \qquad (1b)$$

where ∂ gives the coefficient of kinetic friction between grains in the moving mass.

(3) the initiation of a grain flow therefore requires that:

$$S_g \geq TS \qquad (1c)$$

These equations indicate that flowing grain masses can move down gentle slopes in the presence of an interstitial fluid that reduces the effective normal pressure on grains and consequently reduces the frictional resistance. For wet landslides like Huascaran 3 (Appendix A), Hsü (1975) proposed that mud could form the fluid component between clasts, giving rise to the observed fluid-like flow of these landslides. In the case of large dry landslides, in turn, Hsü postulated that fine dust might act as the interstitial fluid. Using Elm as an example, for assumed variables of $∂ = 17°$, $C = 0.5$ and $p_S = 2.4$, he obtained an

estimate of 0.8 for the density of the fluid phase, which he concluded to consist of a mixture of 1/3 dust and 2/3 air or vacuum by volume. Hsü therefore considered this model valid for the description of long-runout in large landslides, even on the surface of the Moon.

The mechanical fluidization model proposed by Hsü takes as a given the kinematic descriptions of long-runout landslide movement by Heim (1932), namely that these landslides flow into place like some sort of viscous fluid. This type of behavior applies to wet landslides like Huascaran 2 and 3 (Chapter IV), which appear to have traveled as large, turbulent debris flows during emplacement. However, the cohesionless grain flow model fails to explain the observation of preserved stratigraphy in dry long-runout landslides because the theory presupposes turbulent flowing motion throughout a landslide mass. In addition, Melosh (1983) objected to Hsü's model on conceptual grounds, arguing first that dust suspension in dry rock landslides could not act as the type of interstitial fluid required by Bagnold's theory. He also points out that:

> ...keeping the rock mass fluidized by this method requires too much energy.
> Consider an example based on the Blackhawk landslide of southern California. The slide is 30 m thick, which would have required a pressure of 6 bars near its base to support it as it moved. Suppose that collisions among rock fragments 1 cm in diameter, which form most of the observable breccia layer, were responsible for fluidizing the flow, and that their average density while flowing was half the collapsed density of the slide. The mean random velocity of the rocks must then have been 14 m/sec and there must have been 7 collisions/sec in each cubic centimeter of the slide. This would mean that the kinetic-energy density was 1.5 X 10^6 erg/cm^3 (each rock fragment occupies roughly 2 cm^3, and would have carried an average of 3 X 10^6 erg). Making the rather optimistic assumption that only 50% of the kinetic energy of the fragments was lost in each collision, the rate of energy dissipation would have been 5 X 10^6 erg/cm^3/sec. Thus, after only 1/3 sec the entire initial kinetic energy of the rock fragments was lost in inelastic collisions, and more energy had to be supplied from somewhere to keep the slide going. The only possible source of new energy is the gravitational potential energy of the rock mass. If it traveled at a velocity of 50 m/sec, the slide would have to have moved down a slope steeper than 34° to make good the energy lost by collisions of the rock fragments, assuming perfectly efficient conversion of potential energy to kinetic energy of the fragments. Obviously, this mechanism cannot account for the observed ability of long-runout landslides to move down slopes as gradual as 5°. Indeed, the computed 34° is nearly the same as the static angle of repose.

Data in Chapter III, however, present the possibility that the fine material concentrated along the base of a long-runout landslide might have an important impact on the effective friction experienced by a large landslide during runout. The sometimes structureless, sometimes horizontally textured nature of this basal material suggests that it might have flowed during runout and the overlying debris may have ridden downhill on top of this mobile carpet. However, if this basal material did indeed flow, it probably did not do so because of mechanical fluidization (Melosh, 1983):

> If the size of the rock fragments is decreased (the bottommost layer of the Blackhawk slide, for instance, is probably composed of sand), the average rock velocity and energy density to support the slide are unchanged, but the number of collisions per second in a given volume increases, thus increasing the rate of energy dissipation and making the mechanism still less plausible.

Furthermore, nothing in the cohesionless grain flow model can account for the volume dependence of H/L exhibited by long-runout landslides, and there is no reason for this mechanism to work only for the large ($>10^6$ m^3) landslides that exhibit long-runout.

Davies (1982) also believed that mechanical fluidization of the brecciated rock in a moving landslide causes the long runout of large landslides. Davies (1982) based his model on the grain-flow theory of Bagnold (1954) and extended upon the mechanical fluidization theory of Hsü (1975). Davies (1982) states that:

> The present study investigates the hypotheses that:
>
> (a) the debris deposits of sturzstroms are formed by fluidlike spreading of the debris under the action of gravity, and
>
> (b) that this spreading occurs due to fluidisation of the debris caused by high basal shear rates as it moves rapidly across the ground-- a process called mechanical fluidisation..
>
> The essence of mechanical fluidisation is the concept that a high energy input to a mass of granular material causes high impulsive contact pressures between individual grains, so that they become statistically separated and the mass dilates. The internal resistance to shear stress is thereby reduced...and the mass may flow under gravity when dilated. The high relative velocity between the base of a highspeed debris mass and the stationary underlying material seems to be a likely source of energy, since Bagnold [1954] has shown that dilation results when a grain mass is subject to unidirectional shear. The mechanism envisaged is thus as follows:

(i) a debris mass achieves a high velocity by virtue of its fall from a mountain;

(ii) upon reaching relatively level ground, if the forward velocity is sufficient, shear at the base of the debris causes dilation and reduction of internal friction;

(iii) the debris mass becomes fluidised and spreads out under gravity, retaining forward motion;

(iv) when the forward velocity decreases so that the basal shear is no longer sufficient to maintain the dilation the internal friction increases, the mass becomes rigid and it slides quickly to a halt.

In an effort to better understand the effects of mechanical fluidization on a flowing mass of grains, Davies (1982) modeled the process in the laboratory using a quantity of coarse sand in a plastic tray that was surfaced with a coating of glued-on coarse sand, and which could be made to oscillate at frequencies between 4 and 30 Hz. Davies (1982) found that at frequencies greater than about 10 Hz the inertia of the main grain mass held it stationary while the tray floor and sides oscillated relative to it. Other results of the test were summarized as follows:

(i) Some dilation of the entire grain mass occurred at sufficiently high oscillation velocities; however, it was evident that the degree of dilation was locally much greater close to the sides of the tray than at its centre. It seems probable that a similar locally high dilation occurred at the base of the grain mass although this was, of course, unobservable.

(ii) Grains much larger than the mean grain diameter accumulated at the surface of the sand during vibration.

(iii) By slightly tilting the apparatus the entire grain mass could be made to flow under gravity when the mean velocity of oscillation was sufficiently high (about 25 Hz with an amplitude of 5 mm, giving a mean velocity of 0.25 ms^{-1}). It is deduced that basal shear in a sturzstrom may be capable of causing dilation in the basal region, and that this may be sufficient to allow fluid spreading of the debris mass.

Davies (1982) combined the results of the flowing grain experiment described above with the mathematical theory of grain flow of Bagnold (1954) and with the H/L vs. log(volume) relations of 26 long-runout landslides on Earth, Mars and the Moon to attempt to understand the origin of several common characteristics of long-runout landslides. These features include: the size effect (decrease in H/L with increasing volume), the observation of preserved stratigraphy, three-dimensional jigsaw-puzzle breccia and inverse grading in landslide debris, the reported sudden stops of large landslides from high speed and the occurrence of extraterrestrial long-runout landslides

(Chapter III, Chapter IV). Davies (1982) viewed the size effect as the result of "fluid-like" spreading of long-runout landslides during runout into thin sheets; the larger the volume, the larger the area covered by debris, and the longer the runout length for a given fall height. He attributed the preservation of stratigraphy to the observation in the experimental study that the relative motion between a moving mass of grains and the substrate was concentrated near the base, over which unsheared material moved with little disruption. To explain the observation of three-dimensional jigsaw-puzzle breccia and inverse grading, he hypothesized the following:

> Since the main region of shearing is postulated to be close to the base of a sturzstrom, it follows that rocks shattered during the original fall from the mountain, or subsequently, may be carried for long distances at the surface of the flow without their constitutive pieces becoming widely separated. A related problem, that of the accumulation of large boulders at the surface of the deposit, may be explained by [a tenet of dispersive grain flow which states that] the dispersive pressure on a clast increases with clast size, hence large clasts will tend to be preferentially forced into the region of lowest shear at the surface...

Davies (1982) attempted to explain the sudden stops of long-runout landslides reported by eyewitnesses in Heim (1932) as follows:

> As a dilated, flowing sturzstrom slows down, a critical velocity seems likely to occur at which the degree of dilation begins to reduce appreciably. This will accordingly cause the internal friction of the shearing layers to increase, and the velocity of flow will thus decrease more rapidly. The result may be to cause the distal edges of the flow to become, quite suddenly, solidified, and to slide to a halt quite rapidly under "normal" frictional effects.

Finally, Davies (1982) provided an analysis of the observation of long-runout landslides on Mars and the Moon:

> The mechanisms proposed herein do not in any way depend on the presence of an intergranular fluid; they may thus operate under any atmospheric conditions in which grain shearing is inertial.
> Since the angle of repose of granular materials is substantially independent of the density of the grains, there is no reason to expect that the geometry of sturzstrom deposits will vary under different gravitational conditions. The processes described above may thus operate in similar fashion on Earth, on the Moon and on Mars.

While Davies (1982) addresses many of the most important properties of long-runout landslides in his analysis, his proposed model of basal shear-induced mechanical fluidization is based on a number of flawed assumptions

and observations which place the model into considerable doubt. First, the experimental apparatus used to support his theory modeled a large landslide as a mass of coarse sand moving over a sand-surfaced vibrating table. This experiment lacked any consideration of scaling laws for forces or material strengths; rather, the sand grains in this apparatus experienced only minor shear stresses relative to clasts near the base of an actual large landslide moving at high velocity with a thickness of tens or hundreds of meters. In addition, the experiment provided a source of vibrational energy to fluidize the grains in the mass, much as is done to sink piers into well-sorted sand in engineering projects (Scott, 1963); the fluidization of the basal materials in the moving sand body therefore did not result from movement-induced shear of the mass of sand along its base as Davies (1982) suggested, but rather originated from the external energy added to the system. Together this evidence indicates that the experimental apparatus fails to give any positive evidence that the base of a large landslide could be fluidized by its own movement over the substrate. Therefore, while his observations of the nature of the scale effect and three-dimensional jigsaw-puzzle effect appear qualitatively correct in assuming that these features originate in some sort of basal flow phenomenon over which the landslide debris may spead out, the experimental results he used as evidence fail to support mechanical fluidization as the mode of flow.

In addition to difficulties arising from the lack of a proper experimental procedure, Davies' proposed model also fails to properly explain some important geological relations associated with long-runout landslides. One problem arises when he attempts to explain the inverse grading of large landslide deposits as resulting from the migration of large clasts upwards through a moving breccia mass during transport. Although this mechanism clearly operates in vibrated granular beds containing a variety of clast sizes, the preservation of stratigraphy observed in field relations of long-runout landslides suggests that this phenomenon does not occur in these deposits (Chapter III: Table 10). Instead, material that begins motion near the base remains near the base for the duration of movement and becomes well sheared during transport, while material beginning near the surface stays near the surface throughout movement. Examples of landslides exhibiting this behavior include El Capitan (Krieger, 1977), Goldau (Heim, 1932) and Martinez Mountain (Chapter III). Another aspect of the Davies (1982) model is that it

predicts a sudden stop for large landslides, related to the collapse of shear-induced dilation of the flowing breccia during slowing of the landslides. However, as shown in Figure 35 (Chapter III), Soviet data for two long-runout landslides fail to show any evidence of sudden stopping, suggesting that collapse of a flowing dilated mass of debris probably does not account for the stopping of long-runout landslides. Third, Davies (1982) predicts that the phenomenon of long runout should not differ significantly between Earth, Mars and the Moon if the landslides are mobilized by mechanically fluidized basal grains. This prediction is not supported by the comparative planetology data in Chapter IV, however, which demonstrate that martian long-runout landslides characteristically travel with greater thicknesses for shorter distances than their terrestrial counterparts.

Several workers are currently investigating more sophisticated fluidization models of long-runout for giant landslides. These workers make use of computer models of flowing circular grains to evaluate the possibility of mechanical self-fluidization of large landslides (Campbell, 1989; Jenkens, personal communication, 1990; Savage, personal communication, 1990). In the published model of Campbell (1989):

> Each particle was a two-dimensional disc, free to translate and rotate, but whose motion was confined to the x-y plane. The particles interact with one another by collision during which energy is dissipated through a coefficient of restitution...and through surface friction. Both linear and angular momentum are conserved in the collision equations...The flow is driven by a gravitational acceleration vector inclined at an angle [theta] with respect to the vertical to simulate the slope of the channel. The control volume was bounded on the bottom by a solid surface, and was unbounded on the top to simulate a free surface. In the direction of flow, the control volume is bounded by "periodic boundaries." As the particle leaves the downstream periodic boundary, it reenters the upstream boundary with exactly the same velocity and position relative to the bottom boundary.

In this model, particle and bed properties can be manipulated in the program to develop a low-density basal layer of rapidly moving particles that supports an overriding high-density, low-mobility debris "plug" during runout. When set up with the proper initial conditions, this model can yield apparent frictional coefficients of less than 0.1 for the moving mass. This approach seems useful, but the plug-flow behavior only works for very limited pre-set conditions. Drake (1990), for example, was not able to

reproduce these results using a mechanical model of grain flow involving small plastic spheres:

> The low apparent friction characteristic of certain rare, massive landslides that travelled great distances over nearly level ground...has been ascribed by some workers to the existence of a low-bulk-density collisional region, or 'grain-gas' layer, at the base of the landslide. However, in the nearly steady, small-scale flows studied, there is no experimental evidence that such a layer can exist beneath a nondeforming quasi-static zone: in every experiment the bulk density decreased monotonically with distance from the bed.

In addition, instead of following the flowing grains from initiation to stopping to really test for long runout, the grains in Campbell's model are simply given an initial velocity and followed until they cease moving. This method also ignores the mechanics associated with the initiation and break-up of the original slide mass and fails to take into account the effects of brecciation on component clasts. The appearance in a real landslide of large quantities of fine material along the base of a moving breccia sheet would break down the initial boundary conditions of the computation, a factor not considered in the model. Computer models of grain flow in large landslides provide an excellent new approach to the problem of long-runout, but most of the models fail to consider any geologic evidence on these deposits other than their low apparent frictional coefficients (Campbell, 1989; Jenkins, personal communication, 1990). Successful computer grain flow modeling of long runout will require following non-circular fragments from the beginning to end of movement, allowing fragmentation of the individual clasts to occur during transport, and possibly allowing the properties (i.e., cohesion) of the fragments to vary with grain size.

The **acoustic fluidization** theory of Melosh (1979; 1983; 1986; 1987) presents yet another approach to modeling long runout as a flow phenomenon. Melosh has proposed the theory as a more geologically and energetically acceptable version of fluidization than the dispersive grain flow model of Hsü (1975). As opposed to Hsü's model, where the fluidization energy is derived directly from the kinetic energy of a falling rock mass via inter-clast collisions, Melosh proposes that acoustic fluidization is produced by the propagation of strong sound waves of just the right frequency through a flowing breccia stream. The concept behind acoustic fluidization is that if an applied sound field is strong enough, it could relieve the immobilizing

overburden pressure in a debris stream and allow separation of the debris fragments for the duration of a sound wave rarefaction, over a region comparable in size to half the pulse wavelength. As illustrated in Figure 5, the actual magnitude of the pressure fluctuations in a random sound, or acoustic, field follows a probability distribution; only occasionally does the pressure fluctuation exceed the overburden pressure and allow local failure to occur within the mass of rock. Nevertheless, when the amplitude of the pressure fluctuations approaches the overburden pressure, such failures become frequent enough to permit the mass of debris to experience relative internal motions under relatively low applied shear stresses. While at rest, a landslide deposit might form an interlocked aggregate of high strength, but with enough acoustic energy applied, the individual fragments vibrate around, lowering the shear strength of the mass sufficiently to permit flow under the high shear conditions normally encountered in long-runout landslides. The acoustic energy for fluidization is thought to be broad-band white noise (hissing) generated by the movement of a landslide as it falls down slope; the acoustic energy, therefore, is generated at the expense of the gravitational potential energy of the debris.

Acoustic fluidization requires much less energy than mechanical fluidization, making fluidization by sound a much more energetically attractive alternative for the mobilization of long-runout landslides than dispersive grain flow. Melosh (1983) states that:

> The elastic modulus K of the rock debris enters the energy balance because the overburden pressure σ_{zz} is supported by elastic waves rather than by the impact of rock against rock that characterizes dispersive grain flow. The energy density thus required in the acoustic field is a factor of σ_{zz}/K less than that associated with the random motion of individual rocks. In the case of the Blackhawk landslide, σ_{zz} is about 6 bars, while K is about 6000 bars, giving acoustic fluidization a 1000 to 1 energy advantage over dispersive grain flow.

In theory, at very high sound intensities, acoustically fluidized debris should behave like a Newtonian fluid of viscosity η, where $\eta = \rho\lambda\alpha$. In this equation, ρ is the density of the rock debris, λ is the wavelength of the sound field and α is the speed of sound. At lower sound intensities, flow still occurs, but the debris behaves like a non-Newtonian fluid with a viscosity that is a function of the applied stress.

Figure 5. This schematic diagram compares static rock fragments (left) to acoustically fluidized rock debris (center) and debris moving in accordance with the theory of dispersive grain flow (right). The rock fragments are idealized as spheres of equal size. At the left, the pressure at some point in the interior of a landslide, averaged over a region that is large compared to a rock fragment but small compared to the mass of debris, is constant in time and equal to the overburden pressure. In the middle, sound waves propagate through the debris, causing the pressure to fluctuate about the overburden pressure, represented by the dashed line, and slightly displacing the rock fragments. At the right, the overburden pressure is supported by collisions among the rock fragments, in analogy to the molecules in a gas. The kinetic energy required for this explanation of fluid-like rock flow is much larger than that needed by acoustic fluidization (Melosh, 1983).

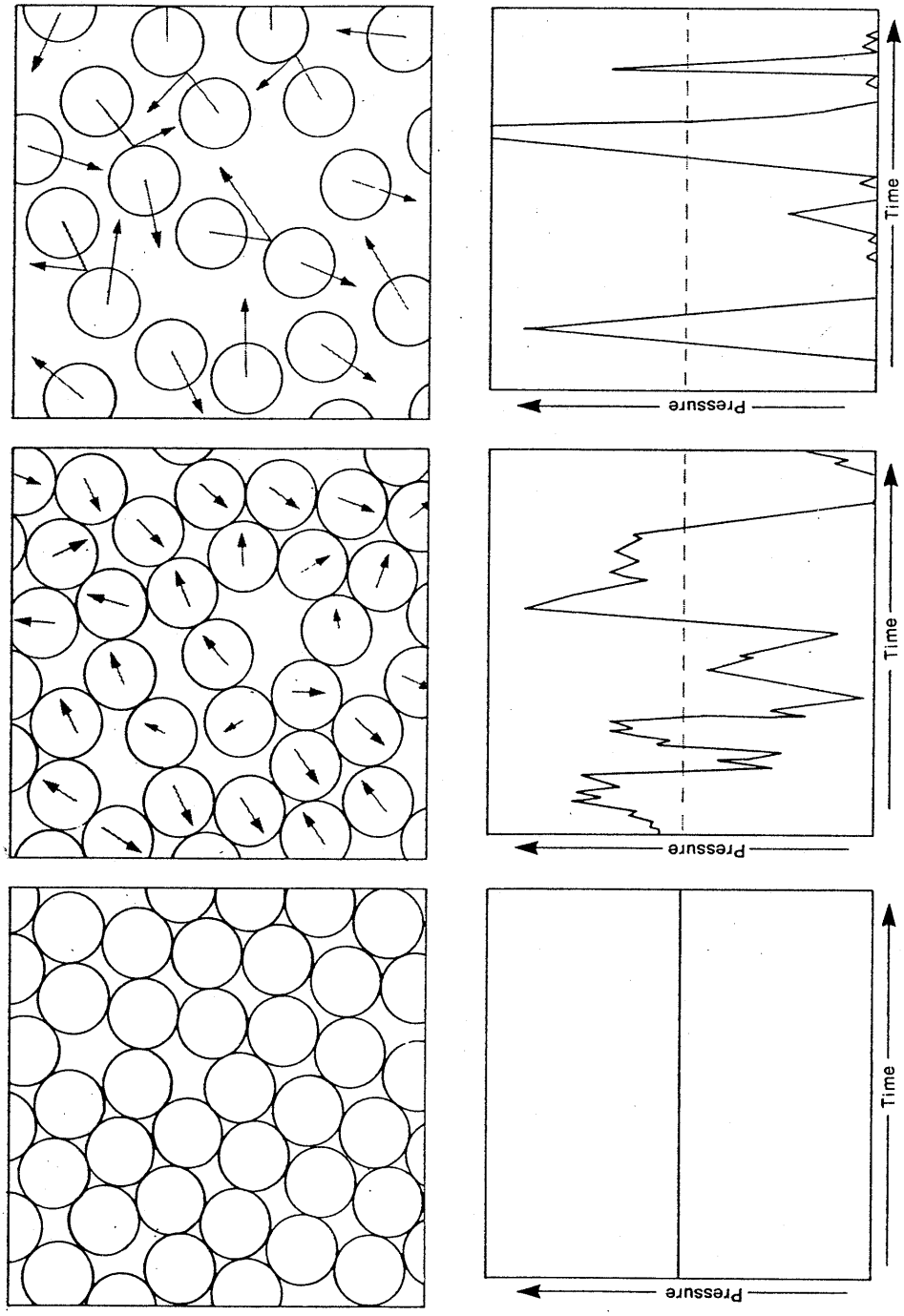
Time
Pressure
Time
Pressure
Time
Pressure

In addition to the energetic advantages of acoustic fluidization, Melosh (1983) also suggested that some of the unusual geologic aspects of long-runout landslides could be explained with the theory. Early experimental tests, for example, suggested that when a fluid of this sort flows down a slope, most of the shear strain remains confined to a narrow zone along the bottom boundary (Melosh, 1983). This would support the geologic relations described in Chapter III, which indicate that most of the shear strain in a landslide lobe is concentrated near its base during transport. However, a more recent model of the process (Melosh, personal communication, 1990) suggests that an acoustically fluidized flow should exhibit flow through most of its interior, not just in a confined zone near the base (Figure 6), a result that might negate the earlier finding. As discussed earlier, bulk flow, whether turbulent or laminar (Figure 3), is not consistent with the presentation of stratigraphy in dry long-runout landslides. Melosh (1983) also noted that acoustic fluidization is critically subject to radiative energy losses, but that radiation losses should become smaller as the ratio of a slide's volume to its surface area increases. Melosh (1983) therefore proposed that if the volume to area ratios of large landslides increase with increasing volume, this could provide an answer for the "volume effect" (decreasing H/L with increasing volume) in long-runout landslides. However, data from Appendix A place this assumption into some doubt. Specifically, Figure 7 indicates that the volume to area ratios of large landslides increase only slightly with increasing volume, and that most of the high values of volume/area correspond to heavily confined landslides which could not easily spread out during emplacement. Thus, instead of exhibiting a strong trend towards increasing volume/area with increasing volume, the aspect ratios of long-runout landslides tend to remain about the same for most large landslides, regardless of volume. In addition, Figure 8 illustrates that H/L values do not vary in any consistent way with the volume to area ratios of terrestrial subaerial long-runout landslides. This observation invalidates the idea that an increase in volume/area for large landslides should decrease their H/L values, a correspondence that would be anticipated if acoustic fluidization controlled the runout of these deposits.

In summary, acoustic fluidization provides a mechanism by which granular materials can flow with only a small input of energy from self-produced sound waves. This theory provides a much more energetically favorable means of fluidizing granular materials than dispersive grain flow.

Figure 6. Plot of the results of a recent computer simulation of acoustically fluidized grain flow, showing predicted kinetic energy and velocity distributions in the flowing material. For this simulation, r is the "regeneration factor," a modified version of the seismological quality factor, Q; gamma is the ratio of scattering length to slide depth, and alpha is the Coulomb friction factor. Energy at the surface is set at zero. This plot indicates that, while the energy in an acoustically fluidized landslide is concentrated near the base, a distribution of velocities occurs upwards through the mass of debris, suggesting that debris along the front of such a flow should roll over during movement (Melosh, personal communication, 1990). This type of velocity distribution does not appear representative of most large landslide deposits (see text).

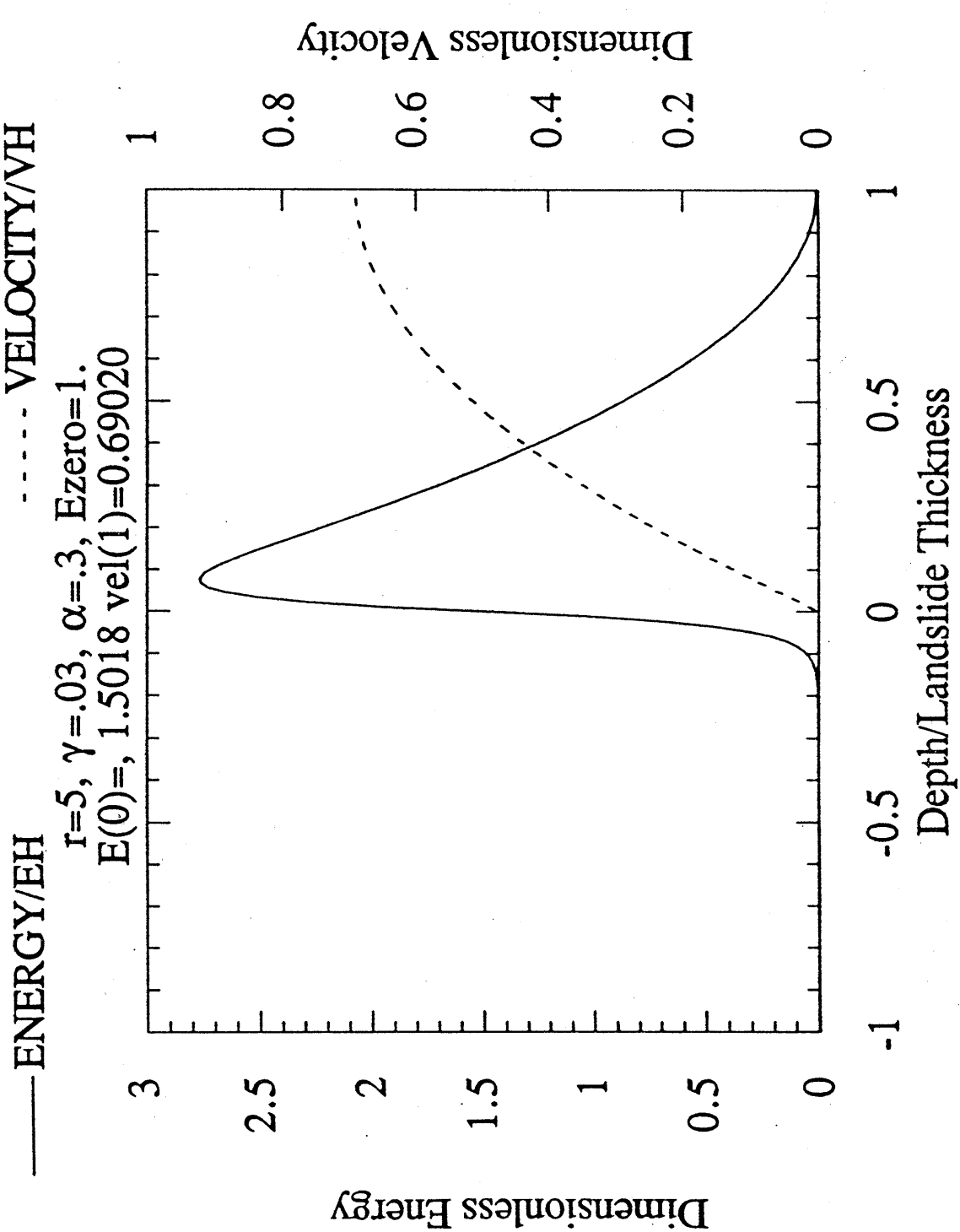
——ENERGY/EH
- - - - - VELOCITY/VH
r=5, γ=.03, α=.3, Ezero=1.
E(0)=, 1.5018 vel(1)=0.69020
Dimensionless Energy
Dimensionless Velocity
Depth/Landslide Thickness
3
2.5
2
1.5
1
0.5
0
1
0.8
0.6
0.4
0.2
0
-1
-0.5
0
0.5
1

Figure 7. Plot of log(volume) vs. volume/area for terrestrial subaerial landslides. Upper diagram gives data for all terrestrial subaerial landslides, with heavily confined landslides highlighted. Lower diagram shows all but heavily confined landslides. Both plots show a weak tendency towards increasing V/A with volume, but heavy confinement strongly influences the observed trends.

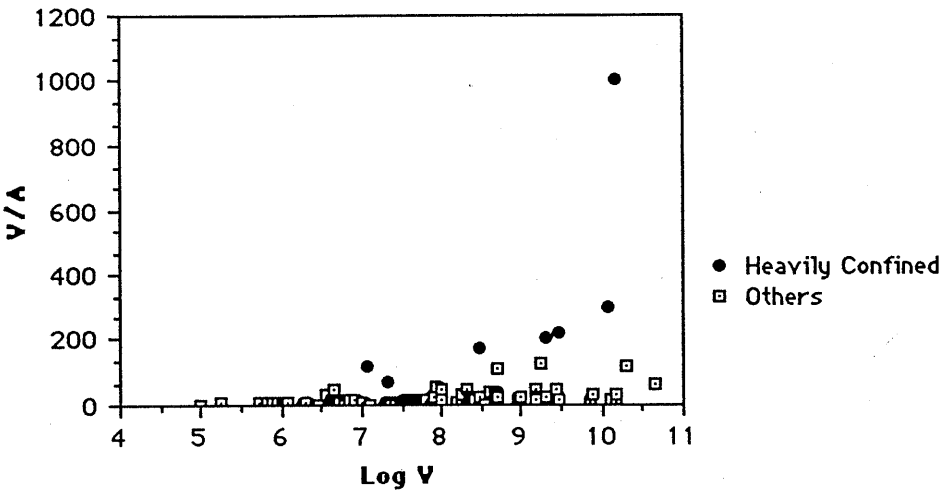
1200
1000
800
600
400
200
0
V/A
4
5
6
7
8
9
10
11
Log V
Heavily Confined
Others

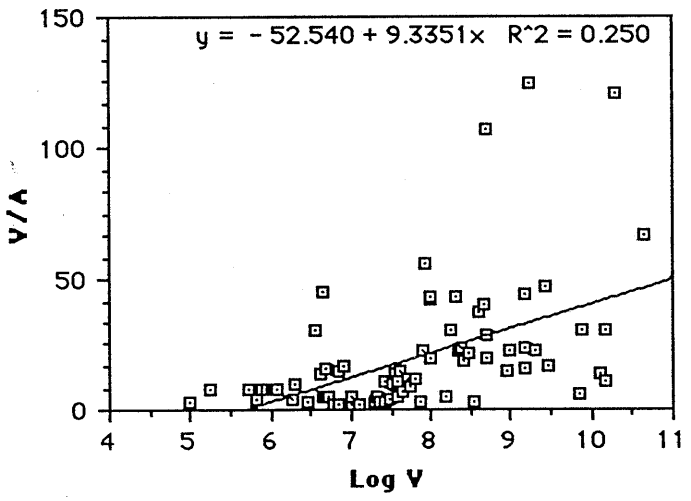
y = - 52.540 + 9.3351x R^2 = 0.250
150
100
50
0
V/A
4
5
6
7
8
9
10
11
Log V

Figure 8. Plot of log(volume/area) versus H/L for terrestrial subaerial landslides illustrating that H/L does not vary characteristically with the volume to area ratio.

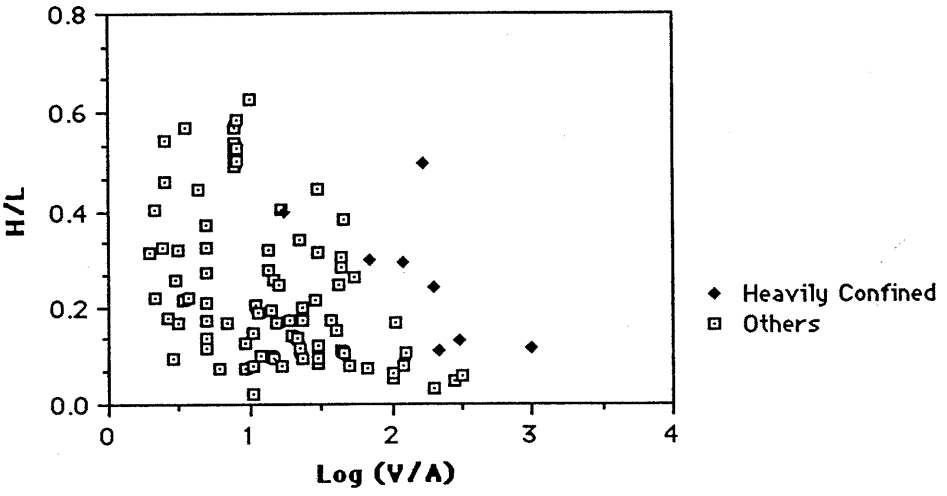
0.8
0.6
0.4
0.2
0.0
H/L
0
1
2
3
4
Log (V/A)
Heavily Confined
Others

However, the dimensional and geologic relations of large landslides fail to support the mechanism, as currently understood, to explain the observed long runout in these deposits.

Two related bulk fluidization theories, those of Trunk, et al. (1986) and Potapov and Ivanov (1991), applied **numerical methods** in an effort to model the behavior of several large landslides. Both efforts used a computer algorithm of the Navier-Stokes equations in two dimensions to model large landslides as incompressible fluids of varying rheology. Both Trunk, et al. (1986) and Potapov and Ivanov (1991) used a computer algorithm termed "SMAC," or "Simplified Marker and Cell" (Trunk, et al., 1986) to simulate the behavior of large landslides. The Navier-Stokes equations can be solved using a variety of assumed relationships between applied stresses and velocity gradients. Initial efforts in using the SMAC computer simulation by Trunk, et al. (1986) modeled the runout of the Madison landslide (Appendix A) in two dimensions using both linear (Newtonian) and bi-linear (pseudo-plastic) viscosity relations. In setting up the problem, Trunk, et al. (1986) chose a profile down the approximate center of the mass of the slide along the apparent direction of flow of the landslide and programmed the fluid in the program to have the same initial configuration as the in situ slide block. A dolomite marker bed in the slidemass was labeled specifically to observe how accurately the model could account for the preservation of stratigraphy between the headscarp and the final deposit. Upon initiation, the entire mass was assumed to begin moving together. Trunk, et al. (1986) modeled the runout of the Madison landslide according to three cases. Case I assumed a Newtonian viscosity with zero friction between the fluid and the bed and used a close numerical simulation of the initial mountain profile to model the runout. Case II also used a Newtonian viscosity, but this time included a frictional coefficient of 0.2 between the fluid and the bed and used a modified version of SMAC in which the slope profile was considered flat and smooth and the gravitational force was varied with each vertical column of cells to correspond to the actual slope profile. Case III was modeled exactly as in Case II, but used a bi-linear viscosity instead of a Newtonian viscosity. Figure 9 shows the results of the three computer simulations relative to the actual profile of the Madison landslide. In each case, the reported computer fit to the physical data was obtained iteratively by varying viscosity (all cases), friction (Cases II and III) and yield stress (Case III only) until the runout distance and final debris

Figure 9. Diagram from Trunk, et al. (1986) showing results of the SMAC computer simulation of the Madison landslide. The upper diagram shows the actual pre- and post-event topography of the Madison landslide as measured along a longitudinal profile of the deposit, and includes the distribution of dolomite in the source region prior to movement and after deposition. The lower diagram illustrates the results of the three computer simulations of the landslide.

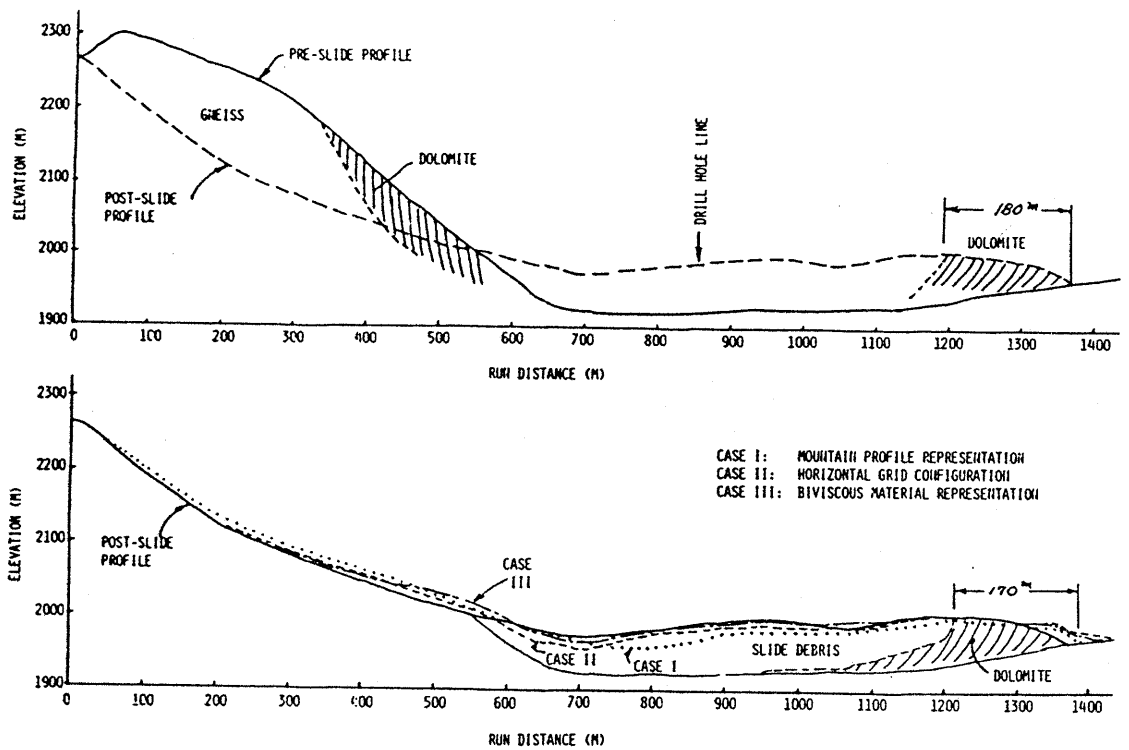
PRE-SLIDE PROFILE
GNEISS
DOLOMITE
POST-SLIDE PROFILE
DRILL HOLE LINE
180 m
DOLOMITE
ELEVATION (M)
RUN DISTANCE (M)
CASE I: MOUNTAIN PROFILE REPRESENTATION
CASE II: HORIZONTAL GRID CONFIGURATION
CASE III: BIVISCOUS MATERIAL REPRESENTATION
POST-SLIDE PROFILE
CASE III
CASE II
CASE I
SLIDE DEBRIS
170 m
DOLOMITE
ELEVATION (M)
RUN DISTANCE (M)

distribution were nominally approximated by the model. According to Trunk, et al. (1986): "Although coupling existed between the parameters the dominant effect was that friction controlled runout distance and viscosity controlled the distribution of the debris."

Trunk, et al. (1986) viewed the three numerical simulations as representing, "three levels of approximation in representing the nominal motion of the slide." Case III, which modeled the landslide using a pseudo-plastic rheology, allowed the closest approximation to the actual slide profile (Figure 9). The authors therefore believed that this model corroborated the theory of McSaveney (1978), that large landslides flow according to a Bingham viscosity, by way of "a mechanism of an active high-shear-stress layer in the basal zone of the flowing material." Trunk, et al. (1986) also pointed out some drawbacks in their simulations:

> During the flow of a granular material such as a landslide, dilatation, or volume, expansion occurs, and any expansion in volume results in a change in the values of the model material parameters. Increases in volume as a result of the shearing motion will result in corresponding decreases in model viscosity. Thus, the model parameters are likely to be site specific...For slides of smaller thickness with lighter overburden pressures, dilatation would likely be more extensive, requiring significant reduction in one or both of the model parameters, [yield strength] or [viscosity], with additional changes in travel distance as flow depth changes...

The numerical simulation of the Madison landslide by Trunk, et al. (1986) provides little useful information on the runout mechanism of large landslides. The principle problem with the approach is that it models long runout landslides as fluids. As described previously, dry long-runout landslides cannot exhibit bulk fluidization because of the incompatibility of this behavior with the preservation of stratigraphy in these deposits. Note that the dolomite at the leading edge of the model Madison landslide in Figure 9 rolls under the landslide because of laminar flow just as illustrated in Figure 3. This behavior counters the observational data on the preservation of stratigraphy in dry long-runout landslides (Chapter III). The model also attempts to model a three-dimensional process by way of a two-dimensional model, a method that underestimates the true degrees of freedom of movement of the material. The computer model simply contained sufficient freedom of variability that it allowed the operators to rather closely approximate the final disposition of the landslide debris. The fact that all three cases of the model

allowed for good approximations of the landslide profile suggest that the supposedly significant differences in the rheologies assumed for each case really had almost no impact on the predicted runout of the landslide debris. Case III probably came closest to approximating the true profile because this version of the model contained the greatest number of variable functions, not because the assumed rheology came closest to the real behavior of the landslide. The most basic problem with the model is that it has no capability to predict the possible runout behavior of large landslides from first principles.

Potapov and Ivanov (1991) also used the SMAC method to simulate the runout behavior of large landslides. In their modeling efforts, however, Potapov and Ivanov (1991) used a power-law shear stress-strain rate rheology in place of the linear and bi-linear relationships assumed by Trunk, et al. (1986). They state that: "This law has been chosen partially due to the impossibility of using the same two-viscous model parameters [Trunk, et al., 1986] for different avalanches and partially due to the results of the Melosh [1983] theory." The power-law relationship used by Potapov and Ivanov (1991) has the form:

$$\tau = A\, p\, \dot{\varepsilon}^{\alpha} \qquad (2)$$

where τ is shear stress, p is density and $\dot{\varepsilon}$ is shear strain rate. At low values of shear strain, a straight line $\tau/p\dot{\varepsilon} = 300\ m^2/s$ replaced the power law because the algorithm could not model the infinite viscosity at zero strain rate given by Equation 2 (Figure 10a). These viscosity relations were used in the SMAC program to model the runout of three terrestrial long-runout landslides: Madison, Usoy and U.S.S.R. Artificial #1 (Appendix A). For all three landslides, Potapov and Ivanov (1991) found best-fit values of $A = 144$ and $\alpha = 0.28$ in Equation 2, with units in SI (International System of Units) dimensions. The result of the model experiment for the Usoy slide is shown in Figure 10b, in which the model behavior is compared to the actual post-event topography of the landslide. Using these values, Potapov and Ivanov (1991) also modeled the comparative runout behavior of large martian and terrestrial landslides (Figure 10c). In the latter experiment, the computer simulation was run for a given landslide volume and headscarp geometry, by varying the gravitational acceleration between the terrestrial and martian simulations.

Figure 10a. Diagram from Potopov and Ivanov (1991) showing the power-law shear stress vs. strain rate relation calculated to best fit the depositional geometries of the Madison, Usoy and U.S.S.R. #1 landslides.

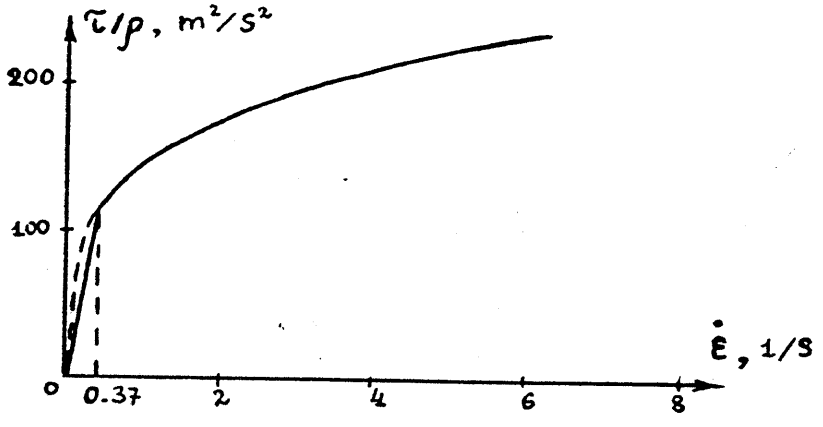
τ/ρ, m²/s²
200
100
0
0.37
2
4
6
8
ε̇, 1/s

Figure 10b. Diagram from Potopov and Ivanov (1991) showing results of the SMAC computer simulation of the Usoy landslide. The upper diagram shows the pre-event topography of the Usoy landslide as measured along a longitudinal profile of the deposit. The lower diagram illustrates the results of the computer simulation of the landslide (dashed) relative to the actual geometry of the Usoy landslide deposit (solid).

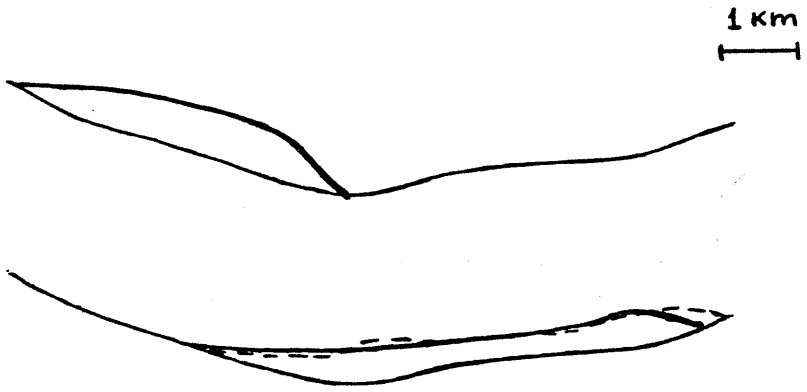
1 km

Figure 10c. Diagram from Potopov and Ivanov (1991) showing comparative results of a SMAC computer simulation of a large landslide of given volume and headscarp geometry deposited under terrestrial (9.8 m/s^2) and martian (3.72 m/s^2) gravitational acceleration. The upper diagram shows the pre-event topography of the landslides. The lower diagram gives the results of the simulations, illustrating that martian landslides are calculated to travel at greater thicknesses for shorter distances than their terrestrial counterparts.

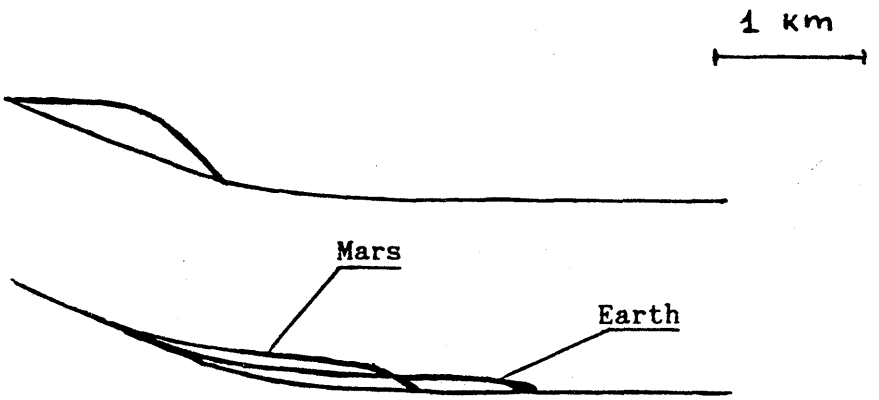
1 km
Mars
Earth

The power-law rheology chosen to model large landslides by Potapov and Ivanov (1991) carries the use of the SMAC program a step farther than accomplished by Trunk, et al. (1986). The power-law model apparently allows for a good estimation of the post-event topography of all three tested terrestrial landslides. Potapov and Ivanov (1991) state that: "For all three considered avalanches the discrepancy between the observed and simulated profiles is small. Part of the difference can be ascribed to the lateral spreading of the avalanches which is not simulated by our two-dimensional model." The model also successfully mimics the characteristically shorter runout distances of large martian landslides relative to their terrestrial counterparts (Chapter IV).

While the modeling efforts of Potapov and Ivanov (1991) appear more widely applicable than the earlier efforts of Trunk, et al. (1986), the model actually suffers all the same basic problems as the Trunk, et al. model. The paramount difficulty with the approach is that it makes use of a model that assumes bulk fluidization of the landslide mass. As with the other bulk fluidization theories presented above, this assumption generates major difficulties in attempting to explain the preservation of stratigraphy in long-runout landslide deposits. In addition, while the power-law model appears capable of modeling the runout behavior of multiple landslides according to the same power-law constants, a capability which surpasses that achieved by Trunk, et al. (1986), this capability may simply relate to the fact that all three landslides chosen had rather similar emplacement geometries. While differing significantly in volume, both Madison (Chapter II: Figure 6k) and Usoy (Chapter III: Figure 16) were heavily confined in deep canyons which allowed for little lateral spreading of debris. The depositional geometry of the U.S.S.R. #1 deposit is less well known, but it also appears to have been emplaced across a rather narrow valley, causing runup of debris on the far wall of the canyon (Adushkin, personal communication, 1990). Therefore, while the model parameters used by Potapov and Ivanov (1991) appear capable of modeling heavily confined landslides with similar depositional geometries, it is doubtful that this model can predict the behavior of deflected or unconfined landslides. The capability of the model in qualitatively predicting the shorter runout distances of the martian landslides, however, lends some support to the concept that large landslides exhibit some fluid character during runout.

The last bulk fluidization theory to be considered in this chapter is the Bingham plastic flow model proposed by McEwen (1989). McEwen (1989) did not explain this choice of rheology, but used the Bingham model to show that martian landslides exhibit yield strengths on the same order of magnitude as terrestrial dry rock avalanches, which he interpreted to mean that the martian landslides probably traveled in a dry condition. Though not stated in McEwen (1989), he apparently based this choice of model on the quantitative ease of calculation of yield strengths using this method (McEwen, personal communication, 1990) and upon the work of earlier researchers who calculated yield strength estimates using the Bingham model for dry rock landslides (McSaveney, 1978; Eppler, et al., 1987), for the moist to wet Mt St. Helens landslide (Voight, et al., 1983) and for common desert alluvial fan debris flows (Johnson, 1984). Table 13 (Chapter IV) summarizes the yield strength values estimated for these various mass movements.

As demonstrated in Chapter IV, the assumption of a Bingham plastic model for large landslides gives equivalent yield strength estimates for dry, moist and wet landslides. But how applicable is the Bingham plastic rheology to the approximation of the behavior of long-runout landslides? Johnson (1970) apparently pioneered the use of the Bingham rheology to approximate the behavior of mass movement deposits, specifically desert alluvial fan debris flows. Referring to debris flows, Johnson (1970) stated:

> Debris has been considered to behave much as water by several investigators, who attribute the different flow rates of debris and water to their markedly different viscosities...Such estimates of viscosities do give us some concept of the sluggishness of debris flows, but they may be misleading in several respects...A striking feature not explainable in terms of simple viscous behavior is the characteristically blunt terminations or steep outer margins of debris deposits and debris flows...[which are] strikingly similar to the profile of the meniscus at the edge of a drop of water on a flat, dry surface...the meniscus at the edge of a water drop and the blunt termination of a debris flow are results of imperfections of the viscosities of the two substances. The meniscus is attributed to surface tension of the water and the blunt termination is attributed to finite strength of slurries...

Johnson (1970) also stated that the finite strength and high densities of debris flows gave them the capability to raft boulders downstream, as observed in many flood events. He also stated that field observations of debris flows suggested that "the flow is primarily laminar." Johnson (1970) applied a Bingham plastic model to the debris flows he studied as a first approximation to

their behavior. Using the Bingham rheological model (Chapter IV: Equation 10), Johnson (1970; 1984) developed the idea of "plug flow," in which regions of flowing debris would move rigidly if the shear stresses applied to those areas dropped below a critical level, the so-called yield strength.

The primary drawback with the use of the Bingham plastic bulk fluidization model to explain dry rock landslides is its assumption of laminar flow. As shown on numerous occasions in this section, laminar flow is not compatible with the preservation of stratigraphy in large dry landslides (Figure 3). Although one might call upon the concept of plug flow to explain the preservation of stratigraphy in rigidly rafted portions of a Bingham flow, the shear stress in such a fluid (the rate of change of the velocity profile) will vary with the velocity of the fluid, its viscosity, and, if flowing through a channel, the distance flowed down the channel relative to its width (Daugherty, 1937). Thus, the velocity profile in a moving Bingham plastic flow will vary continuously during its travel, often changing the size of any rigid plug, making it highly unlikely that large dry landslides could travel by this mechanism without significant distortion of the headscarp stratigraphy.

Another possibility, quite distinct from the bulk fluidization model, is that the fine-grained material concentrated along the basal portions of dry long-runout landslides approach Bingham plastic behavior. At high shear stresses this material might flow quite readily, allowing high-velocity runout and spreading of landslide debris. Spreading would occur until the debris thinned sufficiently to reduce the shear stress at the base below a critical level, at which time the material would cease flowing and the landslide would come to a halt. This mechanism appears capable of explaining the gradational behavior of moist and dry landslides, the greater thicknesses of martian landslides and many of the other unique characteristics of long-runout landslides. While this proposed model explains many of the fluid properties of long-runout landslides, it actually has more in common with many of the basal lubrication theories discussed below. This proposed model behavior is developed in depth in Chapter VI.

2. *Basal Lubrication Models*

Several theories proposed to explain long runout in large landslides invoke super-lubrication along the bases of slidemasses at emplacement (Table 2).

Table 2. Basal Lubrication Theories Proposed to Explain Long Runout in Large Landslides

The following list gives the major reference and title of the two principle lubrication models proposed as general explanations of long runout in large landslides. They appear in the order of appearance in the text:

1. Shreve, 1968a: Air-layer lubrication;

2. Erismann, 1979: Dissociated or melted rock lubrication.

The first and most durable of these theories is the **air-layer lubrication** mechanism proposed by Shreve (1959; 1966; 1968a; b; 1987), who argued that the low H/L ratios of some long-runout landslides, as well as certain aspects of their morphologies and internal structures, could be explained by the hovercraft-like sliding of landslide breccia on a layer of compressed air captured under the debris after being launched from a rock ledge. Shreve (1959) developed the theory to explain the long runout and unusual sedimentological and morphological features of the Blackhawk landslide, and later applied the theory to the Sherman, Alaska landslide (1966) as well as to other well-known landslides such as Elm, Frank and Saidmarreh (1968a), which he termed "Blackhawk type" landslides. Shreve (1968a) stated his theory as follows:

> According to this idea a landslide of the Blackhawk type starts as a huge rockfall which acquires such high speed in its descent that at a projecting shelf of rock or sudden steepening of slope it leaves the ground, overriding and trapping a cushion of compressed air upon which it traverses the gentler slopes below with little friction, much as the slipper in a thrust bearing slides on a cushion of oil with no metal-to-metal contact. The distance and direction travelled after launching depends upon the initial velocity, the gradient and the smoothness of the land surface, and the amount, redistribution and leakage of the trapped air.

Shreve (1968a) turned to the idea of air-layer lubrication because he recognized the failure of bulk flow to explain the preserved stratigraphy in the Blackhawk and Silver Reef landslides:

> Mechanical considerations show that the time-average velocity of the material in a wide, moving debris flow increases from zero at the bed to a maximum at the upper free surface; hence the surface material travels faster than the forward edge, eventually overtakes it, and is rolled under the advancing debris. Material found at the forward edge of a debris flow, therefore, necessarily arrived there by way of the upper surface [Figure 3]. This means that, barring a remarkable coincidence, the Blackhawk landslide cannot have descended the alluvial slope simply as an unusually large debris flow, because the sandstone "breccia" at its distal edge is unaccompanied by similar material anywhere on its upper surface. Instead, it must have moved as a nearly undeforming sheet sliding on a relatively thin, easily sheared lubricating layer.

Several characteristics of the Blackhawk and Blackhawk-type landslides were cited by Shreve (1968a) as support for an air-layer lubrication mechanism, including: preserved stratigraphy (Chapter III: Figure 24), dozed

distal ridges (Chapter III: Figure 28), low H/L values, dust clouds, debris pyramids, high-speed emplacement, three-dimensional jigsaw-puzzle breccia, raised distal rims (Chapter III), lateral levees, and transverse ridges and troughs (Chapter IV: Figure 43). Shreve (1966, 1968a) speculated that the abnormally low H/L values provided a measure of the volume of air trapped beneath a large landslide; the larger the fallen mass, the more air was trapped to lubricate the sliding process. Shreve (1968a) used air-layer lubrication to explain the other features as follows:

> The *high speed, local lithological homogeneity* [preserved stratigraphy], and *distal wedge of transported debris* [dozed distal ridges] of these landslides result because the air layer, having low density and viscosity and relatively great thickness, is easily sheared, so that the mass of debris slides rather than flows.
> The *extensive dust cloud* is generated by the escape of compressed air through the sliding sheet of breccia.
> The *lateral ridges* [lateral levees] form where leakage at the sides allows the lateral edges of the thicker forward portion of the sliding mass to fall and stop, forming dikes which stand higher than the thinner rearward portion of the breccia sheet [Figure 11a]. They would not form where the velocity at the edge has a significant lateral component...
> Some of the *debris cones* [debris pyramids] may form by the accumulation, in such protected places as the tops of large boulders, of smaller debris thrown upward by the air escaping where the breccia is highly permeable, as where it undergoes marked dilation. Others, however, such as the xenolithologic debris cones of the Sherman landslide...must form by an entirely different mechanism as yet unknown.
> The *sudden stop* occurs and the *distal rim and scarp* [raised distal rim] form when the leading edge of the advancing breccia hits the ground and very rapidly loses its forward momentum, causing the breccia to pile up behind [Figure 11b].
> The *surface pattern of transverse ridges and soil streaks* reflects an imbricate internal structure which forms as the zone of impact travels like a wave back up the length of the breccia lobe [Figure 11b]. Both this surface pattern and the distal rim and scarp would be absent where the zone of impact travels forward from an initial point of contact beneath the landslide, as perhaps occurred in the Sherman landslide...and in the southern part of the Frank landslide.
> The *three-dimensional jigsaw puzzle effect* results from the pervasive fracturing of large blocks by the impact [of the initial rockfall], the shattered fragments remaining undispersed because of the lack of further [relative] movement.

The air-layer lubrication theory explains a number of the morphological and sedimentological characteristics common to long-runout landslides, more so than any other published theory to date. The theory is particularly thorough in addressing many of the characteristics observed on and within

Figure 11a. Formation of lateral levees on long-runout landslides according to the air-layer lubrication theory of Shreve (1968a). Air escapes from under the lateral edge, allowing it to settle and stop. If rearward portion of breccia sheet is thinner, then a prominent lateral levee is formed.

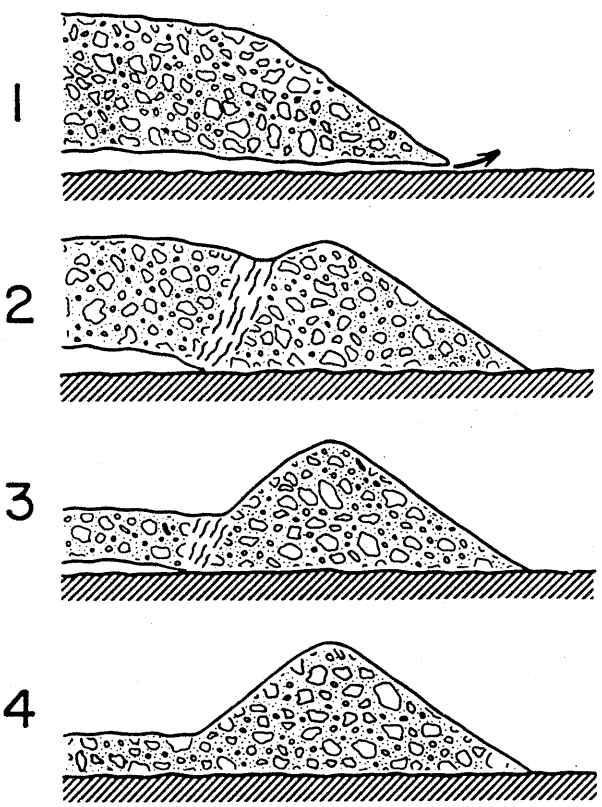
1
2
3
4

Figure 11b. Termination of movement on long-runout landslides according to the air-layer lubrication theory of Shreve (1968a). The initial impact occurs at the distal edge, resulting in the formation of a raised distal rim, transverse ridges and an imbricate internal structure.

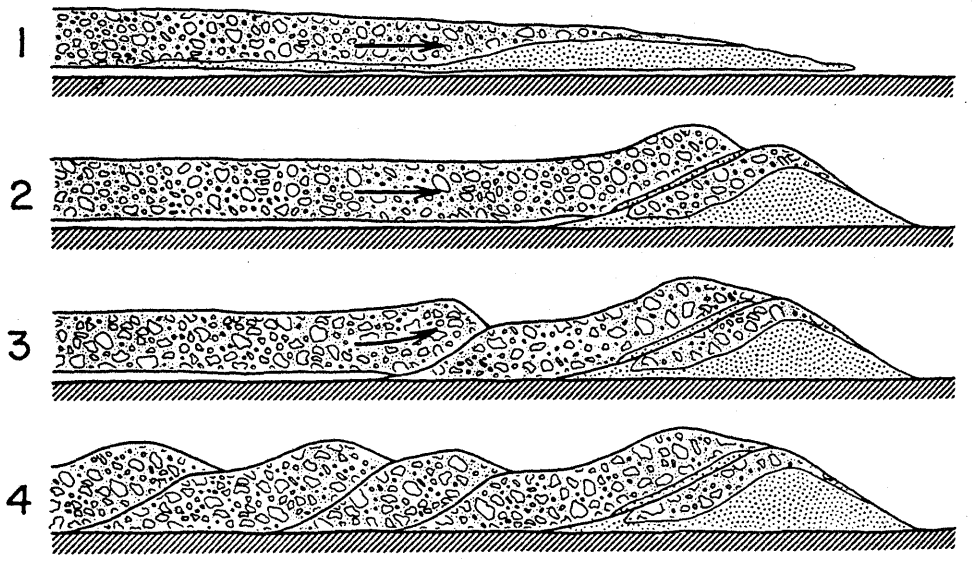
1
2
3
4

the Blackhawk landslide, for which the theory was developed (Shreve, 1959). However, the air-layer lubrication theory cannot provide a universal explanation for long runout, because it fails to explain several significant facts regarding long-runout landslides, such as the low H/L values experienced by many terrestrial landslides which did not experience an air-launch episode, or those that lack depositional characteristics key to air lubrication, or the majority of landslides on Mars, which must have occurred under essentially modern martian environmental conditions (Chapter IV). In addition, while the air lubrication theory provides explanations for many characteristics of the Blackhawk landslide, these features can in most cases be explained by other mechanisms that do not require basal lubrication by air.

Shreve (personal communication, 1990) has stated that not all long-runout landslides are postulated to travel by means of air-layer lubrication, only those exhibiting certain special features characteristic of Blackhawk type landslides. Other than Blackhawk, he lists Elm, Frank, Saidmarreh and Sherman among probable air-layer lubrication landslides (Shreve, 1966; 1968a). However, these landslides all fail to exhibit one or more of the primary geologic relations deemed critical to the air-layer lubrication mechanism. For example, the Elm landslide (Heim, 1932) experienced an airborne launch and exhibits a pattern of ridges and troughs on its surface. However, it lacks a raised distal rim and has no lateral levees, although the latter observation may reflect the fact that the landslide thinned as it moved (Shreve, 1968a). Cruden and Hungr (1986) also used morphological evidence to argue against air-layer lubrication for the Frank landslide; Frank lacks lateral ridges or levees, has only very poorly developed transverse ridges, and exhibits a raised distal rim in only three short areas along the slide margin. The Saidmarreh landslide too lacks a number of geologic relations deemed critical by Shreve for air-layer lubrication. Watson and Wright (1969) tested the Saidmarreh landslide point-by-point to assess the probability that the landslide experienced air-layer lubrication. They found that Saidmarreh lacks a launching platform, a wedge of bulldozed debris, lateral levees, a raised distal rim, an original transverse ridges and troughs morphology (one later developed by erosion), and three-dimensional jigsaw puzzle blocks. The single feature of Saidmarreh consistent with Shreve's model is preservation of stratigraphy between the headscarp and the debris apron. On the basis of this evidence, Watson and Wright (1969) concluded that little positive evidence exits to support the idea that the

landslide moved on a cushion of air. For the Sherman landslide, Shreve (1966) himself had some difficulty in applying air-layer lubrication. For example, the landslide exhibited an air launch, a low H/L value, lateral ridges and a raised distal rim (argued against by McSaveney, 1978), but lacked the transverse ridges and troughs expected if the toe of the landslide had stopped rapidly from high speed when air at the leading edge gave out. He ended by reasoning that in the case of the Sherman landslide, stopping must have begun at the rear and progressed forward, in contrast to his interpretation of stopping of Blackhawk. In summary, terrestrial landslides designated as of the "Blackhawk type" by Shreve (1968a) mostly fail to exhibit the morphological criteria put forward to explain this phenomenon in Blackhawk.

A number of landslides on Mars (Figures 6i, 17a, 43a-f) exhibit morphologies much more reminiscent of the Blackhawk than Elm, Frank, Saidmarreh or Sherman. The only significant morphological differences between the martian landslides and the Blackhawk are the characteristically greater thicknesses and a lack of transverse ridges and troughs on the surfaces of the martian deposits. The fact that all the Blackhawk-*like* landslides on Mars appear to have occurred under essentially current martian environmental conditions places into doubt the possibility that basal lubrication by compressed atmospheric gases played an important role in their emplacement (Chapter IV; Appendix D).

Other characteristics of Blackhawk-like landslides are also difficult to reconcile with the air-layer lubrication theory. One factor is that the martian deposits and the terrestrial examples reported from Argentina (Fauque and Strecker, 1988) fail to exhibit transverse ridges, which Shreve (1968a) attributed to catastrophic slowing of air-lubricated landslides when the air layer leaks out. Of Blackhawk-like landslides, only the neighboring Blackhawk and Silver Reef landslides of southern California exhibit this surficial morphology. Two alternative explanations for the source of this pattern can be conceived of in addition to that offered by Shreve (1968a). First, the pattern may represent a piling up of landslide debris behind a growing bulldozed heap of substrate along the leading edge of a landslide. As a landslide traveled and scraped up the terrain ahead of it, the bulldozed heap would become ever larger and harder to push. Ultimately, the landslide debris right behind the distal heap might ramp up on it and stop moving, forcing the trailing material to pile up likewise. Heim (1932) stated that the leading edge

of the Elm landslide exhibited such behavior, which perhaps led to its transverse pattern of ridges and troughs. Alternatively, the surficial ridges and troughs may be strictly erosional in nature, as observed on the Saidmarreh landslide (Watson and Wright, 1969). The Blackhawk, Silver Reef and Saidmarreh all consist primarily of limestone and all experienced exposure to pluvial Pleistocene environmental conditions (Stout, 1977; Watson and Wright, 1969), so that the three might be expected to erode in a like fashion. All the other Blackhawk-like landslides on Earth consist of granite breccia and do not exhibit the ridge and trough pattern.

The evidence provided above leads to the conclusion that air-layer lubrication does not explain long runout for most landslides, including those proposed by Shreve (1968a) as best representing the phenomenon. Evidence from martian landslides with Blackhawk-like morphologies indicate that most of the features deemed diagnostic of air lubrication cannot result from this mechanism. Also, data from other terrestrial landslides place into doubt the mechanism proposed by Shreve to account for the distinguishing ridges and troughs pattern on the surface of the Blackhawk and Silver Reef landslides. In general, the mechanism does not seem to have much importance in mobilizing long-runout landslides.

One other lubricated sliding theory has been proposed to explain the critical characteristics of long-runout landslides as a group, especially their high velocities, low H/L values and the observation of preserved stratigraphy in these deposits. This model, proposed by Erismann (1979), advocates low-friction sliding on **dissociated or melted rock** confined along a hypothesized basal slide plane to explain the characteristics of long-runout landslides. Erismann (1979) states:

> ...it is obvious that a working hypothesis must fulfill certain conditions in order to be in agreement with the wide spectrum of available evidence:
>
> (a) It must account for a high energy concentration in the vicinity of the gliding surfaces, even in case of advanced disintegration of the material.
>
> (b) It must explain the size effect independently from the material involved.
>
> (c) It can hardly be imagined without a lubricating effect.
>
> (d) It must account for enormous quantities of lubricant.
>
> In such instances it is nothing but natural to consider the possibility of the mass itself generating the material required for lubrication. The

> lubricant cannot, however, consist of untransformed pulverized rock. On the contrary, it must have acquired the properties of an effective lubricant.
> The postulated high energy concentration suggests the transformation by the high temperature reigning in the critical zone near the gliding surfaces. Owing to the bad heat conductivity this zone must be very thin...Thus the size effect finds an explanation, the heating energy being approximately proportional to the thickness of the mass. In other terms: The high economy in the locomotion of a large landslide is explained as a consequence of size-dependent lubrication.

Erismann (1979) believed that self lubrication could occur in at least two different materials: limestone and gneiss. For large limestone landslides, i.e., Flims (Appendix A), he believed that high temperatures developed along a discrete slip surface would continuously dissociate the carbonate rock into a mixture of lime (CaO) and CO_2 gas during travel. As in the vaporized fluid model described previously, the carbon dioxide gas would provide a lubricant along a basal slip surface. For large landslides in gneiss such as Koefels, he reckoned that slide-induced heating could melt the crystalline rock locally, generating a fluid lubricant. Erismann realized that the principle drawback to this mechanism was the rapid escape of the gaseous or fluid lubricant away from the slide plane faster than it could be replaced by transformed rock material. In the absence of any data on the temperature/pressure relations along the base, on the permeability or density of the moving debris, or on the viscosities of the proposed lubricants, Erismann (1979) concluded that self-lubrication by such means is "plausible," but that additional work was required to address these unknown parameters.

Some geologic evidence exists to support Erismann's model, but the theory also has a number of significant drawbacks. Field evidence indeed exists to support Erismann's contention that melted rock and calcined rock can form in large landslides. For example, Hewett (1988) reported the probable presence of CaO intermixed in the debris of the carbonate-containing Bualtar 1-3 deposits, and Heuberger, et al. (1984) reported amorphous glass along slip surfaces in the Koefels and Langtang landslides (Appendix A; Chapter III). However, Hewett (1988) believed that the calcined rock in the Bualtar deposits probably formed along the bases of the translational slides during the early stages of their sliding motion, and then became mixed into the debris as the landslides disintegrated into brecciated debris streams further down slope. This observation contrasts with Erismann's proposal that lubrication of the base of

a limestone landslide could occur by way of carbonate dissociation throughout the duration of its emplacement, even in the brecciated state. However, once a rock mass brecciates, the base of the landslide no longer exhibits distinct slip surfaces of any great extent (Chapter III), so that vapor production would slow or stop, and any vapor constrained along the slip plane might escape upwards into or through the breccia, turning off the process. Thus, limestone disssociation might provide a functional mechanism for large coherent slide blocks, allowing them to develop high velocities. Once these landslides reached high speeds, however, even minor disruption of the slide blocks due to movement-related stresses could provide a natural breaking mechanism by stopping the production of gas and allowing accumulated vapor to leak out.

The data on melted rock in large landslides from Heuberger et al. (1984) also fail to support Erismann's theory; the melted rock only occurred along discrete slip surfaces in the Koefels and Langtang landslides. Had the landslide dissociated into loose rubble, slipping would no longer have followed a single plane and melt production would presumably have ceased. In addition, no information exists on the rheologic properties of the melt rock to suggest that it would indeed have acted like a lubricant during movement; the viscous fluid might even have hindered slip.

Erismann (1979) based many of the concepts for his model on the assumption that the size effect for large landslides occurred because landslide thickness scales with volume and that the heating energy at the base should increase with the thickness of the mass. Thus, landslides with greater volumes should travel with greater thicknesses, generate more heat and, by extension, more molten or dissociated rock, and therefore should experience lower H/L values. However, data from Appendix A fail to support this contention, as H/L values fail to show any characteristic decrease with increasing average or maximum thicknesses for terrestrial long-runout landslides (Figure 12).

Finally, the mechanism fails to deal with the question of lithologies other than gneiss and limestone. Heating of sandstone, granite and quartzite, for example, would generate vapors or melts under widely different pressure/temperature regimes. H/L vs. log(volume) relations should therefore differ markedly between various lithologies, but this observation is not supported by such relations compared in Figure 12a (Chapter III).

Figure 12. Plot of H/L values versus average and maximum thicknesses of terrestrial long-runout landslides, illustrating a lack of correlation between H/L and deposit thickness values.

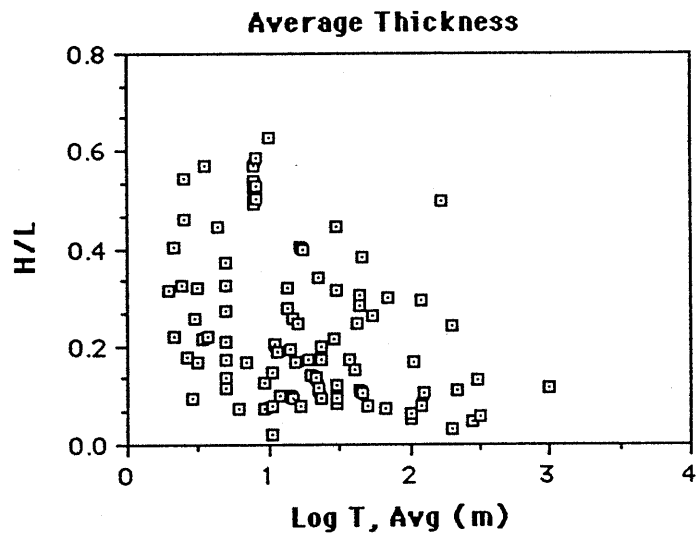
Average Thickness
H/L
0.8
0.6
0.4
0.2
0.0
0
1
2
3
4
Log T, Avg (m)

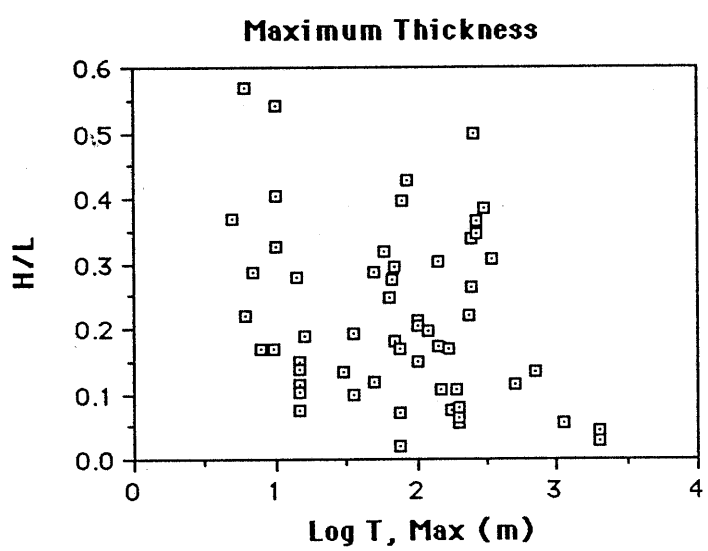
Maximum Thickness
H/L
0.6
0.5
0.4
0.3
0.2
0.1
0.0
0
1
2
3
4
Log T, Max (m)

3. *Mass-Loss ("Rocket-Stage") Models*

Mass-loss models form a third set of mechanisms forwarded to explain long runout in large landslides. These models propose that the low H/L values achieved by large landslides occur because they selectively drop off low-velocity material during movement (Van Gassen and Cruden, 1989; Savage, personal communication, 1990), in a mechanism analogous to a rocket shedding burned-out stages during its ascent. The ultimate runout length of a large landslide travelling by such a mechanism would depend on the rate and timing of the mass loss; the more low-velocity mass lost early in the process, the farther the ultimate runout of the toe of the slide (Van Gassen and Cruden, 1989).

Van Gassen and Cruden (1989) propose a model for long runout in large landslides in which the travel distance of the center of gravity of a mass of loose, dry, purely frictional material depends upon momentum transfer within the mass. In this model, landslide debris deposits gradually from a sliding mass of breccia. The breccia is presumed to maintain a constant angle of sliding friction of 30° throughout the course of movement. Van Gassen and Cruden (1989) outline the model as follows:

> Consider a slide of loose material entering its accumulation zone with a velocity v_0. Friction slows particles at the slide toe to a velocity $v_0 - \Delta v$ after a short time, whereas the material behind is still entering the runout zone at a velocity v_0. So the material at the toe and the back interact. The leading particles are propelled forward, while the material behind is slowed down and some of it is deposited. This process continues throughout the accumulation zone. The properties of the material and the geometry of the accumulation zone determine the shape of the resulting deposit. Here some simple shapes of the final deposit are assumed and the corresponding runout is calculated.

The model therefore varies the rate of deposition according to the thickness profile of the landslide being modeled. Landslides of uniform thickness are modeled by a linear depositional profile, in which the mass of the still-moving portion of the landslide decreases directly with the distance traveled, while tapered landslides, which decrease in thickness proximally to distally, are modeled by an exponential mass-loss profile.

The model proposed by Van Gassen and Cruden (1989) makes the assumption that the clasts composing a large landslide slow by friction, but come to rest strictly by means of momentum transfer, and that the moving part of the

landslide experiences a "normal" coefficient of sliding friction along its base equal to about 0.6. Rocks are only deposited in this model after they give up their momentum to other moving rocks in the mass; they lose no momentum to the ground in the moment they stop, though they can lose momentum to the ground while in motion through friction along the base. Once a landslide mass reaches a depositional area (slope angle below 30°), material at the trailing end of the moving landslide begins to deposit by transferring its energy forward to the moving part of the landslide. The toe of the landslide continues to slide down slope propelled by the input of momentum from stopped trailing clasts until the wave of stopping catches up with the toe, when stopping is complete. The authors propose that this mechanism allows the center of gravity of a landslide to travel farther from its starting point than would occur for a simple sliding block. Equations 3a-c give the travel distances for the center of mass of a landslide upon entering the zone of accumulation, assuming a sliding block model, linear deposition and exponential deposition, respectively:

$$L = -\frac{v_o^2}{2g(\sin\beta - \mu_k\cos\beta)} \qquad (3a)$$

$$L = -\frac{3}{2}\frac{v_o^2}{2g(\sin\beta - \mu_k\cos\beta)} \qquad (3b)$$

$$L = -1.93\frac{v_o^2}{2g(\sin\beta - \mu_k\cos\beta)} \qquad (3c)$$

In each equation, L is the slope-parallel distance, in m, traveled by the center of gravity of a landslide in the accumulation zone, v_o is the velocity of the landslide, in m/s, upon entering the accumulation zone, g is the gravitational acceleration in m/s^2, ß is the slope angle, in degrees, of the accumulation zone and μ_k is the coefficient of sliding friction of the debris over the substrate. This model predicts that the center of mass of a landslide with a tapered profile should travel somewhat farther during deposition than one with uniform thickness, which in turn should travel about 1.5 times farther than a landslide

sliding as a rigid block. The model also predicts that landslide velocity profiles should vary depending on the mode of deposition (Figure 13). It is noteworthy that even under optimal conditions this model is only capable of increasing the runout length of the center of gravity *in the accumulation zone* by a factor of two (Equations 3a, 3c). Using the block-on-inclined plane model presented earlier in this chapter as an example, in which the fall height measured 500 m down a 30° slope followed by runout onto a flat surface, the exponential mass-loss model could only reduce the coefficient of sliding friction of the center of mass to 0.44 from the 0.5 assumed in the sliding block model. The primary importance of this model is therefore not in its ability to increase the travel distance of the center of gravity of a landslide, but rather in its ability to produce a region of extended deposition that allows the toe of a landslide to travel much farther down slope than otherwise would be achieved by a sliding rigid-block landslide. This is because the travel distances commonly reported in H/L plots refer to the horizontal length between the crown of a headscarp and the toe of a landslide, not the distance traveled by a landslide's center of mass.

The Van Gassen and Cruden (1989) momentum transfer model has mixed success in attempting to explain some of the critical characteristics of long-runout landslides. The model explains some features of large landslides quite well, but other aspects rather poorly. Some questions have also been raised in the literature as to the theoretical validity of the model.

The momentum transfer model can explain a number of important aspects of long-runout landslides: the cause of stopping from head to toe; the extension of landslide deposits relative to their original slide block dimensions; some aspects of the facies model of long-runout landslides; the development of low H/L values; and the characteristically high velocities attained by large landslides during runout. One of the most useful outcomes of this model is its explanation of the longitudinal extension experienced by long-runout landslides during runout. The degree of extension can be quite substantial in some instances, measuring, for example, about 400% in the El Capitan landslide (Krieger, 1977). This extension should naturally occur if a landslide stops in the gradual manner prescribed by Van Gassen and Cruden (1989). The back-to-front mode of stopping required by the model also agrees with the observations made of many large landslides by Heim (1932). In addition, the

Figure 13. Plot from Van Gassen and Cruden (1989) showing predicted velocity profiles for the leading edges of landslides deposited as sliding blocks, and by linear and exponential distributed deposition. On the diagram, v_o equals the velocity of a landslide upon entering the accumulation zone, and L_o equals the characteristic length traveled by the center of mass of a landslide according to the exponential mass-change model.

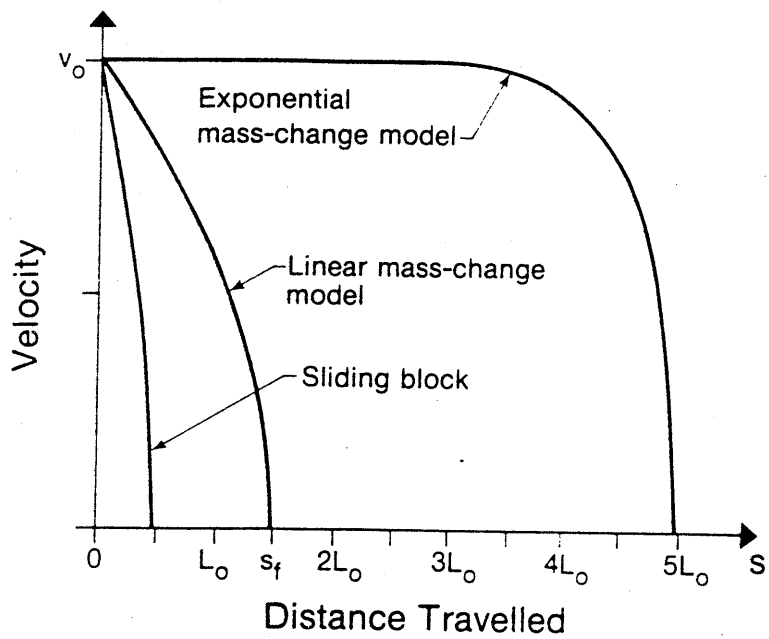
v_o
Exponential
mass-change model
Linear mass-change
model
Sliding block
Velocity
0
L_o
s_f
$2L_o$
$3L_o$
$4L_o$
$5L_o$
S
Distance Travelled

momentum transfer model can also explain many aspects of the landslide facies model of Yarnold and Lombard (1989) discussed in Chapter III (Figure 31). Material near the head of a landslide would stop rapidly according to the model, preventing much interaction between the landslide breccia and the substrate. Material along the toe of the landslide, however, which obtains momentum from trailing clasts, should experience much greater internal shear and interactions with the substrate because of its much greater travel time, in concert with the observations of Yarnold and Lombard (1989). The model also provides an explanation of the low H/L values achieved by many large landslides, their consistently high runout velocities and the fact that the landslides should come to rest gradually, as supported by Soviet landslide velocity data (Figure 35), rather than abruptly as suggested by Shreve (1968a) and Davies (1982).

Despite the variety of characteristics correctly predicted by the momentum transfer model, the theory fails to account for a number of equally important features of long-runout landslides. For example, the model cannot explain the characteristic trend of decreasing H/L with increasing volume observed for large landslides. Total landslide mass does not even enter the equations for the travel distances of landslide centers of gravity (Equations 3a-3c). Rather, the theory holds that the H/L of a landslide should vary with the profile shape of a landslide. Tapered landslides should, according to the model, experience the lowest H/L values, followed by landslides of uniform thickness, and then by those having distally raised profiles. Figure 14 provides convincing evidence that this assumption does not hold. In fact, distally raised landslides consistently have among the lowest H/L values of all long-runout landslides. The theory also fails to explain why long runout should only occur in landslides having volumes in excess of $\sim 10^6$ m^3. Presumably, this mechanism ought to work for small granular slides as well. The momentum transfer mechanism also does not readily reveal how changes in lithology and clast size could modify the H/L values experienced by large landslides (Chapter III) and it fails to explain why martian landslides should not travel as far as their terrestrial counterparts for a given volume and fall height (Chapter IV). Changes in gravitational acceleration cancel out in their model because both the gravitational acceleration, g, and the velocity at the beginning of the accumulation zone, v_o, factor into Equations 3a-3c, and v_o^2 scales with g (see section B of this appendix). The theory also specifically anticipates that the

Figure 14. Histogram showing frequency distribution of landslide profile shapes plotted against ranges of H/L values for terrestrial subaerial long-runout landslides.

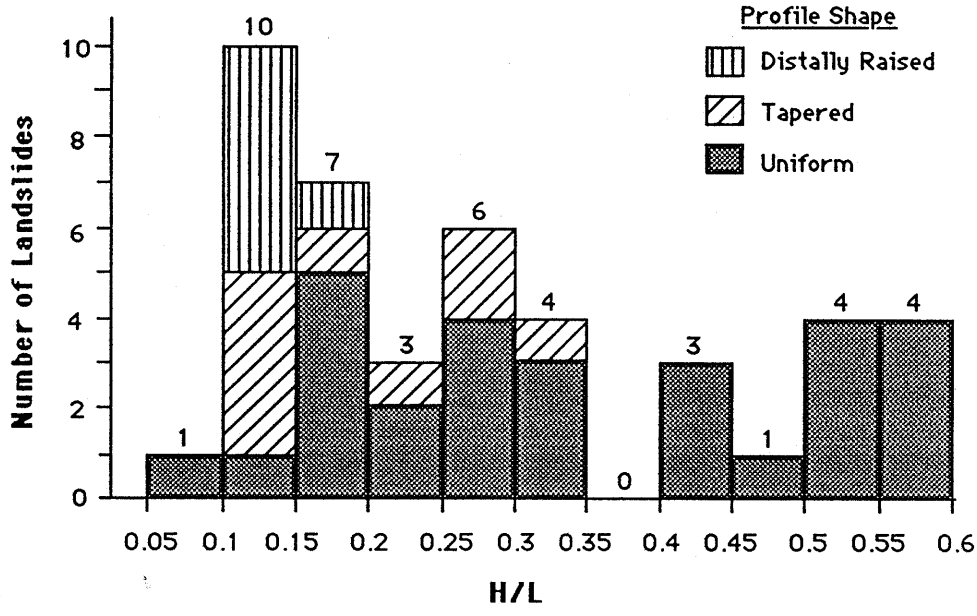
Profile Shape
Distally Raised
Tapered
Uniform
Number of Landslides
H/L
0
2
4
6
8
10
0.05
0.1
0.15
0.2
0.25
0.3
0.35
0.4
0.45
0.5
0.55
0.6
1
10
7
3
6
4
0
3
1
4
4

most distal fragment along the toe of a landslide should be the last to stop moving, as stopping propagates from the head to the toe. In general large landslides exhibit this behavior, but in detail rather large regions of moving landslides appear to come to rest at the same time (Chapter III). In addition, the mass-loss theory fails to explain the preservation of stratigraphy in large dry landslides. Because the theory does not explain *kinematically* how mass is lost from a moving landslide, it is unclear whether or not stratigraphy might be preserved during runout.

In addition to the difficulties the momentum transfer model has in explaining certain observational details of long-runout landslides, some theoretical objections have been raised about the model. Hungr (1990) argues that the distance traveled by the center of gravity of a landslide should not vary with the mode of deposition, but rather in all instances should have the form of Equation 3a. He drew this conclusion from the observation that the change in kinetic and potential energy of the system of particles should equal the total work done on the landslide by external forces in the zone of accumulation:

$$W = MLg\,(\sin\beta - \mu_k\cos\beta) = -K \qquad (4)$$

In this equation, W, in Joules, equals the total work done by external forces on the landslide, M is the mass of the slide in kg, L is the final displacement of the center of gravity in m, g is gravitational acceleration in m/s^2, ß is the slope of the depositional surface in degrees, μ_k is the coefficient of kinetic friction of the landslide over the substrate and K equals the kinetic energy, in Joules, of the slide mass as it enters the runout surface. He further states that, "the theory developed in the paper incorrectly implies the existence of a rocket engine, propelling the slide mass along the runout surface. The magnitude of the implied thrust force for the Frank slide is in the order of 10^{11} N, or about 5000 times that of the largest rockets." In Van Gassen and Cruden (1990), the authors respond to both criticisms. To the first argument they reply:

> ...we agree with Hungr that the change in kinetic and potential energy of the system of particles should equal the total work done by external forces in the accumulation zone. However, an independent estimate of the kinetic energy of our system on its entry to the accumulation zone requires a knowledge of the distribution of velocities in the system and the processes by which the particles are moving. Their kinetic energy will certainly be substantially greater than $1/2\ Mv_o^2$.

Thus, they argue that the total energy of the system is greater than that represented by the kinetic energy of the center of mass of the landslide alone. In response to the second criticism they state:

> Hungr's...is a statement that the change of linear momentum of a system of particles is equal to the external forces on the system...u is the relative velocity of the particles expelled from the system with respect to the system velocity v. In our paper, the expelled particles are those at rest. They are no longer part of the rock avalanche, which is moving with average velocity v. Thus u = -v. As particles are expelled, their contribution to the change in linear momentum is counted. Once the particles are at rest they do not contribute to the changing momentum, they are outside the system.

These responses dispel the arguments made against the momentum transfer model by Hungr (1990). Based on the description of the mechanism as presented in Van Gassen and Cruden (1989; 1990), the model does not appear to contain any major flaws in theory.

The momentum transfer model of Van Gassen and Cruden (1989) provides an interesting new view of the process of long runout in large landslides. The model can successfully account for a number of important features of large landslides not properly described by any other theory. However, the model also fails to account for a substantial number of other critical characteristics. The principle drawbacks with the theory are its failure to describe the kinematics of mass loss from the system and its incorrect prediction that runout length should vary with the profile shape.

4. *Individual-Case Mechanisms*

All of the theories discussed to this point have been proposed as general solutions to the problem of long-runout landslides. However, a single overriding mechanism might not exist to explain the long-runout phenomenon. Instead, many different mechanisms can operate in large landslides that lead to a common set of characteristics, such as their high velocity, preserved stratigraphy and long runout. As in the general case theories, the individual case models fall into broad categories, which include bulk fluidization theories, basal lubrication theories and one theory that combines facets of both bulk fluidization and basal lubrication (Table 3).

One **individual-case bulk fluidization** theory suggests that large landslides can experience fluidization because of emplacement during strong

Table 3. Theories Proposed to Explain Long Runout in Large Landslides on a Case-by-Case Basis

The following list gives the major reference and title of theories proposed to explain long runout in large landslides on a case-by-case basis. They appear in the order of appearance in the text:

1. Earthquake fluidization: proposed by Solonenko (1972) for the Khait landslide and by Hazlett, et al. (in press) for the Vesuvius 1-7 landslides;

2. Basal lubrication by vaporized pore fluids: proposed independently by Habib (1975) and Goguel (1978) to explain the long runout of the large coherent translational Vaiont and Mt. Granier landslides;

3. Basal lubrication by a weak stratum in the landslide debris: proposed by Johnson (1978) and Watson and Wright (1969) to respectively explain the long runout and sedimentology of the Blackhawk and Saidmarreh landslides;

4. Basal lubrication by entrained mud or moist soil: Evans (personal communication, 1990) proposed mud lubrication to explain the high velocities and long runout of numerous large landslides in the Canadian Cordillera, and Heim (1932) suggested that the Elm landslide was lubricated by moist soil during the latter third of its runout;

5. Combined basal lubrication by partially melted snow, together with earthquake bulk fluidization causing internal flow of the sliding sheet as a Bingham plastic: proposed by McSaveney (1978) for the Sherman landslide.

seismic events (Solonenko, 1972; McSaveney, 1978; Hazlett, et al., in press). ***Earthquake fluidization*** can be considered a subset of acoustic or mechanical fluidization, in which seismic waves provide the driving energy source for fluidization of the rock debris. This type of behavior was suggested for the seven large landslides reportedly triggered during the 1944 eruption of Mt. Vesuvius (Hazlett, et al., in press):

> Acoustic fluidization is an appealing mechanism to explain the Vesuvius avalanches because a high level of seismicity existed at the time movement was initiated. It is very likely that a relatively strong acoustic energy field of scattered wave energy existed during the initiation of motion and that this energy supplemented that generated by downslope movement. This may have provided [an] acoustic surcharge to the 1944 block/ash avalanches.

Solonenko (1972) was less specific in detailing by what precise mechanism seismic groundshaking might decrease the H/L of large landslides, but seemingly he had a similar idea in mind when he reported the following about the Khait landslide:

> The collapses and landslides produced by strong earthquakes are of specific dynamics. This was clearly expressed during the Khait earthquake (force 10, M=7.5) of December 10, 1949...The distance covered by the collapsed mass was 10.5 km compared to 1.5-2 km involved in the [non-seismogenic] phenomena. This 5-6-fold increase is due to the disturbance of the collapsed mass by seismic oscillations.

McSaveney (1978), in addition, suggested that seismic energy played an important role in the fluidization of the Sherman landslide. However, he also envisioned a role for snow lubrication of the base of the landslide. This model will be discussed below in this section.

Seismic energy fluidization is more energetically favorable than any of the various fluidization theories discussed previously in this chapter, because it is the only one in which the energy of fluidization is obtained from the depositional environment rather than strictly from the energy of fall of the detached slidemass. Problems nevertheless exist in attempting to model landslide runout according to this model. For example, Hazlett, et al. (in press) noted that each of the Vesuvius landslides proposed to have experienced earthquake-energy fluidization exhibited preserved stratigraphy, ruling out bulk fluidization as an important mechanism for transport of these landslides. Is is not known whether the Khait landslide exhibited preserved stratigraphy

or not. The available evidence therefore rules against earthquake-energy fluidization for the Vesuvius landslides, and only circumstantial evidence exists to link the long runout of the Khait landslide with emplacement during an earthquake.

Three individual-case models have been proposed to explain long runout via special **basal lubrication mechanisms**. These special case theories include lubrication by vaporized pore fluids (Habib, 1975; Goguel, 1978), by sliding on a weak, clay- or mica-rich stratum in the landslide debris (Johnson, 1978), or by sliding on water-saturated substrate sediments (Evans, personal communication, 1990).

Habib (1975) and later Goguel (1978) independently developed a model for long runout in large coherent translational landslides. They both believed that the rapid velocities and low H/L values in these landslides resulted from ***pore fluid vaporization*** along their bases due to frictional heating produced during sliding. This theory addressed long runout in landslides such as Vaiont and Mt. Granier (Appendix A) which did not become greatly disaggregated during emplacement, and in which movement was restricted to sliding on discrete slip surfaces. The theory may also have importance in describing the early movement stages of large translational landslides which evolved downslope into brecciated debris streams. Habib (1975) described the theory as follows:

> When a large rock mass slips on a structural surface, the work given by gravity forces is dissipated on the slip surface and heat appears. If the rate of shear becomes high enough, the heat liberated can transform the water inside the rock into vapour, creating a vapour cushion which sustains the rock mass and lubricates the motion. If the slip surface is deep enough and planar, the rock mass may be essentially a rigid body perfectly supported by gas pressure because vapour appears specifically on the very points of contact (asperities, local bends of the slip surface, etc.). The coefficient of friction remains constant and the shearing resistance decrease is due [to] the lowering of [the] effective normal stress. With zero friction, a rock slide can acquire great velocity and even climb up the other side of the valley, or over a hill, because of its kinetic energy.

Both authors developed this theory with a quantitative analysis estimating the acceleration a translational slide might achieve down a slope once movement was initiated by some outside influence, e.g., an earthquake. These analyses, not developed here, include both a consideration of the energy dissipated in

the slip surface, as well as the influence of speed on the development of gaseous pore pressure.

This theory has considerable value for helping to understand the low H/L values exhibited by large coherent landslides such as Mt. Granier (0.17) and Vaiont (0.34; Appendix A). The theory also appears applicable to the initial movement stages of large translational landslides which became brecciated during movement, such as Saidmarreh (Watson and Wright, 1969) and Flims (Heim, 1932). The theory nonetheless exhibits some major limitations. For example, it might provide a landslide mass too much mobility. Once a cohesive mass of rock began to descend a hill and develop a basal pore pressure, the speed would increase further, increasing frictional heating and developing more pore pressure, etc., producing boundless acceleration once the slidemass became entirely supported by vapor. By the very nature of the boundary conditions of this model, however, the mechanism must break down if the slide mass disaggregates into a sliding or flowing breccia sheet. This ultimately occurs to some extent for almost all large landslides, presumably when stresses placed on a sliding block due to its rapid speed and the changing geometry of its travel path overcome its lithologic strength or the strength of discontinuities in the rock mass. Once this happens, the base of the landslide no longer exhibits distinct slip surfaces of any great extent (Chapter III), so that vapor production would slow or stop, and any vapor constrained along the slip plane might escape upwards into or through the breccia, turning off the process. Thus, pore-fluid vaporization might provide a functional mechanism for large coherent slide blocks, allowing them to develop high velocities. Once these landslides reached high speeds, however, even minor disruption of the slide blocks due to movement-related stresses could provide a natural breaking mechanism by stopping the production of gas and allowing accumulated vapor to leak out. This mechanism could explain the emplacement of the Mt. Granier slide if it exhibited any disruption during motion, as is likely.

Both Johnson (1978) and Watson and Wright (1969) proposed a second form of individual-case basal lubrication, one in which ***a weak stratum in the landslide debris*** itself forms the lubricating agent. Johnson (1978) proposed this model for the Blackhawk landslide of southern California, while Watson and Wright (1969) proposed their version to explain the runout of the giant Saidmarreh, Iran landslide.

Johnson (1978) proposed basal self-lubrication as an alternative explanation of the low H/L and other characteristic features of the Blackhawk landslide that were ascribed by Shreve (1959; 1968a; 1987) to air-layer lubrication. The Blackhawk landslide apparently bulldozed a distal heap of sandstone ahead of it as it progressed downslope at high speed (Chapter III: Figure 28). The sandstone appears to have been derived primarily from sources in Blackhawk Canyon, so that the distal heap was pushed ahead of the landslide for almost its entire runout length. The material also outcrops locally along the base of the landslide, suggesting that bits and pieces of the distal wedge were overrun by the leading edge of the landslide as it traveled downslope (Shreve, 1968a; Johnson, 1978). Johnson (1978) believed that this overrun material may have provided an important lubricating agent for the landslide:

> For example, it may have been that the sandstone "breccia" at the front of the flow was being "smeared out" beneath the overriding marble breccia, providing a zone of high fluidity beneath the front of the debris lobe (i.e., a self-lubricating action). It is hypothesized that when the frontal mass of sandstone "breccia" either diminished in volume or thickness below some critical value or its physical state changed...frictional resistance markedly increased, deceleration increased and the forward motion of the debris flow quickly terminated. Within the context of this debris flow model, the existing spatial distribution of the sandstone "breccia" is not viewed as coincidental but is considered an essential consequence.

According to Johnson (personal communication, 1990), the high mica and clay content of the sandstone debris in the bulldozed wedge may have provided a sort of "grease" along which the landslide could readily slide.

This self-lubrication mechanism provides an intriguing explanation for the high velocities and low H/L values of the Blackhawk landslide, and perhaps others that bulldozed copious quantities of loose, weathered debris ahead of them during runout. Possible examples include the Silver Reef (Shreve, 1968a), Elm (Heim, 1932) and Sherman (Shreve, 1966) landslides, which respectively ploughed up micaceous sandstone, topsoil and snow during runout, leading to distal debris heaps. This mechanism cannot provide a universal mechanism for long runout in large landslides, because not all large landslides bulldozed heaps of material ahead of them during runout. Nevertheless, the model does support the idea that weak substrate materials,

whatever their source, may increase the velocities and travel distances of all long-runout landslides (c.f., Figure 12b).

Watson and Wright (1969) also developed a basal self-lubrication model to describe the runout of the Saidmarreh landslide. However, instead of proposing a model by which a basal lubricant was entrained from an external source, Watson and Wright (1969) suggested that a weak marl stratum located along the base of the in situ slide mass, and along which the initial planar slope failure occurred, formed the basal lubricant for the subsequent runout of the landslide. They stated their conclusion as follows:

> The Saidmarreh landslide mass did not travel with turbulent motion throughout like a mudflow but instead slid forward either on its base or on the comminuted Eocene limestones. The Asmari limestone plate remained on top, breaking and dispersing as blocks...

They also suggested a second possible mechanism, or contributing factor, in the runout of the landslide was sliding on a low-friction gypsum substrate:

> Gypsum underlies the area from the base of the Kabir Kuh almost entirely across the Saidmarreh Valley to Kuh-i-Malah. Although the intricate badland topography provided a gross topographic roughness, the naturally smooth and slippery gypsum outcrops may have supplied a low-friction surface over which the slide could move...

Thus, both the nature of the landslide debris and the substrate may have played important roles in the runout of the Saidmarreh landslide.

The remaining individual-case models of landslide basal lubrication proposed lubrication by ***moist or water-saturated substrate sediments*** traversed and entrained by the landslides during runout. Evans (personal communication, 1990) proposed that entrained mud lubricated many large landslides in the Canadian Cordillera that traveled down or across stream courses during runout. In addition, Heim (1932) proposed that moist soil may have lubricated the base of the Elm landslide during runout:

> ...the rubble stream of Elm moved along the valley floor from its upper end, scouring the ground deeply all the way...it was the thick, clayey and very wet topsoil that lubricated the base layer to a large extent during the third part of the movement...

The one remaining individual-case model proposes to explain long runout in large landslides by merging two previously discussed models: mechanical fluidization and sliding of landslide debris on a low-strength or lubricated

substrate (McSaveney, 1978). In his analysis of the Sherman, Alaska, landslide (Figure 6g), McSaveney (1978) viewed its kinematics as a complex mixture of ***sliding and flowing***. McSaveney (1978) began his analysis of the mechanics of the landslide by assuming that the landslide behaved as some type of fluid during runout:

> At 5:35 p.m., 27 March 1964, a block of rock on Shattered Peak was about 400 m long, 250 m wide and 100 m thick...within the next 3-4 minutes of continued shaking the block fell from the mountain, and, 3.5 minutes later, lay spread over an area of 8.25 km^2 to a depth of about 1.65 m. This deformation shows that the debris flowed, responding to the stress of avalanching as a fluid. The transverse fissures and folds, demonstrating brittle and flexible behavior, show that this 'fluid' was not a simple Newtonian fluid, but had a more complex rheology.

Based on the assumption of fluid behavior and on the premise that the landslide debris had reached optimum dilation just after hitting the depositional surface (so that the volume of the landslide did not change significantly during runout) McSaveney (1978) stated that the "average thickness is a linear function of the area of the deforming avalanche." In other words, he viewed the landslide as a fluid that uniformly decreased in thickness as it spread out onto the Sherman glacier. By assuming that the leading edge of the landslide slid over the snow substrate with an angle of sliding friction of 0.11, he used the surface slope of the depositional surface to back-calculate a velocity profile for different debris trains on the landslide (Figure 15a). The slope of the velocity profile in the diagram gives the rate of change in thickness of the landslide along calculated sections of the travel path between the point of impact of the rockfall on Andres Glacier and the toe of the deposit on Sherman glacier. By expressing the slope as vertical strain rate, (1/h)(dh/dt), McSaveney (1978) found significant discontinuities in curves of vertical strain rate versus time, which he ascribed to changes in rheology of the flowing debris. He further stated that "When effective strain rate (which is the vertical strain rate if there is no lateral strain or change in volume) is plotted against effective shear stress (basal shear stress)...the debris appears to show a different response to high shear stress than to low shear stress" (Figure 15b). From the relations in Figure 15b, McSaveney (1978) also stated that:

> During the avalanche, the debris behaved as a complex, perhaps dilatent, Bingham plastic with a yield stress of about 2 kN/m^2 and two

Figure 15a. Plot from McSaveney (1978) showing the calculated velocity profile of the leading edge of the Sherman landslide from the impact point of the rockfall on the wast side of Andres Glacier to the toe of the deposit on Sherman glacier.

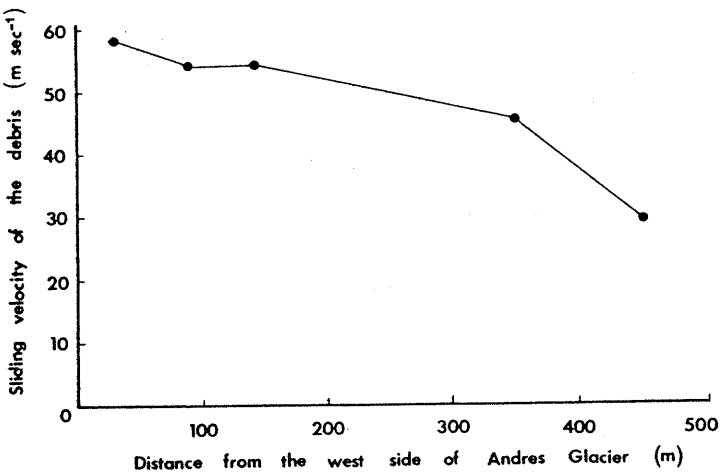
Sliding velocity of the debris (m sec⁻¹)
60
50
40
30
20
10
0
100
200
300
400
500
Distance from the west side of Andres Glacier (m)

Figure 15b. Plot from McSaveney (1978) showing the calculated effective strain rate versus effective shear stress relations for four different debris trains on the surface of the Sherman landslide. These relations are based on changes in the calculated slopes of the longitudinal velocity profiles of the debris trains, such as the profile shown in Figure 15a.

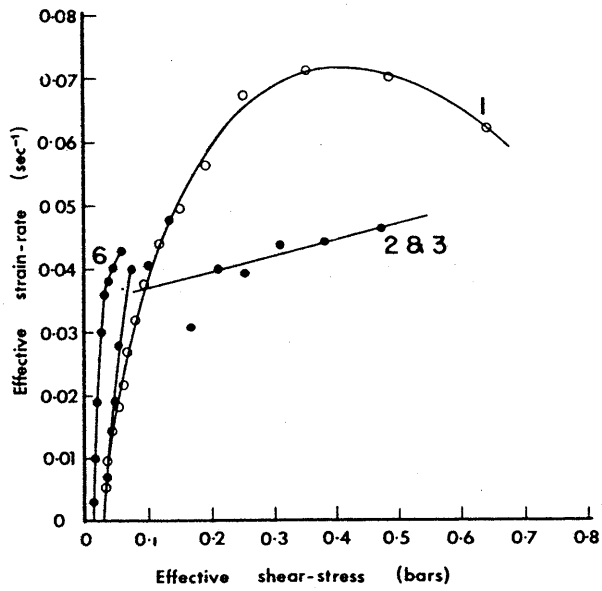
0·08
0·07
0·06
0 05
0·04
0·03
0·02
0·01
0
Effective strain-rate (sec⁻¹)
0
0·1
0·2
0·3
0·4
0·5
0·6
0·7
0·8
Effective shear-stress (bars)
1
2 & 3
6

> viscosities. At thicknesses greater than about 2.5 m, it deformed with a viscosity of 4 X 10^6 N s/m^2. When it had thinned to about 2.5 m, the viscosity dropped to about 1 X 10^5 N s/m^2. These very high viscosities prevented turbulence and kept deformation in the avalanche largely confined to shear at the base of the debris, so that for the most part, the avalanche slid as a thin flexible sheet, with solid rather than fluid behavior being the more visible. This was particularly so because of the additional effect of a rigid surface crust where the shear stress was low, and because the very rapidly moving fluid flow was supercritical.

McSaveney (1978) believed that the fluid behavior of the landslide resulted from the fact that it experienced mechanical fluidization during runout. He postulated that the Sherman landslide was fluidized by energy derived from "its motion and [from] the vibration of the earthquake." McSaveney (1978) concluded that:

> The Sherman Glacier rock avalanche fell during the continued strong shaking of the Great Alaska earthquake. The 10.1 X 10^6 m^3 of well-jointed and fractured graywacke and argillite, and about 2 X 10^6 m^3 of snow and ice, was perhaps at least partially fluidized by the violent shaking...
>
> Along most of its path, the avalanche slid on snow with a coefficient of basal kinetic friction of 0.11: it probably quickly gathered a basal plaster of ice and compact snow and essentially slid with ice sliding on wet snow.

The mechanical model of the Sherman landslide described by McSaveney (1978) allowed him to describe three important depositional characteristics of the deposit: the preservation of headscarp stratigraphy and three-dimensional jigsaw-puzzle blocks in the final deposit, and the low H/L value achieved by the landslide. McSaveney (1978) attributed the first two characteristics to the high viscosity of the landslide, which presumably prevented turbulent mixing of clasts within the flowing landslide. The observation that the landslide experienced an extremely low H/L value of 0.22 was accounted for in the model by assuming that most of the movement of the landslide across Sherman Glacier took place by sliding over ice and snow with a low coefficient of sliding friction.

The composite model of long runout postulated by McSaveney (1978) has some important drawbacks, in theory as well as in explaining some important geological relations in the landslide. The theoretical problems result from circular reasoning and contradictory logic in his discussion of the model. For

example, McSaveney (1978) began his discussion by assuming that the landslide traveled as a fluid and then used his data to determine the rheology of that fluid. He then concluded that the landslide had a Bingham plastic rheology that was capable of flowing beyond a certain yield stress, in a manner that confirmed his initial premise. In his calculation of the velocity profile of the landslide shown in Figure 15a, he assumed that the landslide only moved forward by sliding over the snow substrate, with a frictional coefficient of 0.11. No forward progress of the landslide by flow was taken into account in this calculation. The model would therefore only be valid if spreading and sliding occurred at precisely the same rate and that all of the internal deformation parallel to the ground surface was taken up by sliding at the base. Furthermore, the model rheology plotted in Figure 15b was based on discontinuities in the slope of the time/velocity plot (Figure 15a). These discontinuities appear to occur between different datapoints in the diagram, and thus appear entirely artificial. McSaveney (1978) also viewed the apparent fluidity of the landslide as arising from mechanical fluidization of the mass, a process which results from turbulent motion of constituent clasts in a grain flow. However, he states that the landslide actually experienced very little internal turbulence due to a high viscosity. These two concepts are not readily compatible; the preservation of stratigraphy in the mass, in fact, gives good evidence that the landslide was not fluidized during transport. Thus, though sliding and flowing may indeed occur together in long-runout landslides as proposed by McSaveney (1978), his analysis of the Sherman landslide fails to meaningfully address the mechanics of the problem.

Appendix EE: Calculations Regarding Block-on-Inclined-Plane Model of Landslide Runout

a = acceleration, m/s^2

m = mass of slide block, kg

g = gravitational acceleration, m/s^2

H = vertical height of scarp, m

v = velocity, m/s

Subscripts E, M, Mn, o, f refer to Earth, Mars, the Moon, initial conditions and final conditions, respectively.

β = slope of landslide scarp, degrees

μ_s = coefficient of static friction

μ_k = coefficient of kinetic friction

t = time, in seconds

x = distance in slope-parallel coordinates, m

y = distance in plain-parallel coordinates, m

Slope: Static Case:

$$ma_{x,o} = mg\sin(\beta) - \mu_s mg\cos(\beta)^{*} \quad \text{(see Figure 47)}$$

$$a_{x,o} = 0$$

$$mg\sin(\beta) = \mu_s mg\cos(\beta)$$

$$\sin(\beta) = \mu_s \cos(\beta)$$

$$\therefore \mu_s = \frac{\sin(\beta)}{\cos(\beta)} = \tan(\beta)$$

Slope: Sliding Case:

$$ma_x = mg\sin(\beta) - \mu_k mg\cos(\beta) \quad \text{(see Figure 47)}$$

$$a_x = g[\sin(\beta) - \mu_k \cos(\beta)]$$

For case where $\beta = 30°$ and $\mu_k = 0.5$, we have:

$$a_x = g[\,0.067]$$

$a_E = 0.656\ m/s^2$

$a_M = 0.249\ m/s^2$

$a_{Mn} = 0.112\ m/s^2$

Appendix EE, con't:

$$x = \frac{H}{\sin(\theta)} = \frac{500}{\sin(30°)} = 1000 \text{ m}$$

$$\underline{V_{f,x}^2 = V_{o,x}^2 + 2a_x(x - x_o)}$$

Because $V_{o,x}$ and x_o both = 0:

$$V_{f,x}^2 = 2a_x x$$

$$V_{f,x} = \sqrt{2a_x x}$$

V_E = 36.2 m/s

V_M = 22.3 m/s

V_{Mn} = 15.0 m/s

$$\underline{v_x = a_x t}$$

$$t = v_x / a_x$$

t_E = 55.2 s

t_M = 89.6 s

t_{Mn} = 133.6 s

Plain: Sliding Case:

$$\underline{ma_y = -mg\mu_k}$$ **(see Figure 47)**

$$a_y = -g\mu_k$$

a_E = -4.9 m/s

a_M = -1.86 m/s

a_{Mn} = -0.835 m/s

Appendix EE, con't:

$$\underline{\underline{V_{f,y}^2 = V_{o,y}^2 + 2a_y(y - y_o)}}$$

Because $V_{f,y}$ and y_o both = 0:

$$-V_{o,y}^2 + 2a_y y$$

$$y = \frac{-V_{o,y}^2}{2a_y}$$

$y_E = 133.7$ m

$y_M = 133.7$ m

$y_{Mn} = 133.7$ m

$$\underline{\underline{V_{f,y} = V_{o,y} + a_y t_y}}$$

Because the landslide comes to rest during this stage, $V_{f,y} = 0$:

$$-V_{o,y} = a_y t_y$$

$$\frac{-V_{o,y}}{a_y} = t_y$$

$t_E = 7.39$ s

$t_M = 12.0$ s

$t_{Mn} = 18.0$ s

total expended time, Earth = 62.6 s

total expended time, Mars = 101.6 s

total expended time, Moon = 151.6 s

*formulas with double underlines from Resnick and Halliday (1977)

Appendix F: Bibliography

Adams, J., 1981. Earthquake-dammed lakes in New Zealand: Geology, 9, 215-219.

Albee, A. L., et al., 1981. Geologic map of the Telescope Peak quadrangle, California, U. S. Geol. Survey Geol. Quadrangle Map GQ-1532, scale 1:62,500.

Alden, W. C., 1928. Landslide and flood at Gros Ventre, Wyoming, Trans. Am. Inst. Min. Metall. Eng., 76, 347-360.

Alder, H. L. and Roessler, E. B., 1977. Introduction to Probability and Statistics, 6th ed., W. H. Freeman and Company, San Francisco, 426 pp.

Atwater, B. F., 1987. Status of glacial Lake Columbia during the last floods from glacial Lake Missoula, Quart. Res., 27, 182-201.

Bagnold, R. A., 1954. Experiments on a gravity-free dispersion of large solid spheres in a Newton fluid under shear, Roy. Soc. London Proc., ser. A, 225, 49-63.

Bagnold, R. A., 1956. The flow of cohesionless grains in fluids, Roy. Soc. London Proc., ser. A, 249, 235-297.

Baker, V. R., 1983. The Channels of Mars, University of Texas Press, Austin, 198 pp.

Baker, V. R. and Bunker, R. C., 1985. Cataclysmic Late Pleistocene flooding from glacial lake Missoula: A review, Quart. Sci. Rev., 4, 1-41.

Baldwin, J. E. II, 1986. Martinez Mountain rock avalanche: in: Geology of the Imperial Valley, California, Annual Field Trip Guidebook #14, South Coast Geological Society, 37-48.

Blasius, K. R., et al., 1977. Geology of the Valles Marineris: First analysis of imaging from the Viking 1 Orbiter primary mission, J. G. R., 82, 4067-4091.

Blasius, K. R., et al., 1980. Viking Orbiter Stereo Imaging Catalog, NASA Contractor Report 3277, pp. 1-1 to 1-3.

Bock, C. G., 1977. Martinez Mountain rock avalanche, G. S. A. Rev. in Eng. Geol., vol. 3, 155-168.

Borg, I., et al., 1960. Experimental deformation of St. Peter Sand: A study of cataclastic flow: Rock deformation, D. Griggs and J. Handin, eds., G. S. A. Memoir 79, 133-191.

Brown, R. L. and Richards, J. C., 1970. Principles of Powder Mechanics, Pergamon Press, Oxford, UK, 223 pp.

Bull, C. and Marangunic, C., 1967. The earthquake-induced slide on the Sherman glacier, south-central Alaska, and its glaciological effects: Physics of snow and ice, H. Wura, ed., Hokkaido Univ. Inst. Low Temp. Sci., 1966 Int'l. Cong. Low Temp. Sci., vol. 1, Sapporo, Japan, 395-408.

Burchfiel, B. C., 1966. Tin Mountain landslide, southeastern California, and the origin of megabreccia, G. S. A. Bull., 77, 95-100.

Caldwell, D. H. and Babbitt, H. E., 1941. Flow of muds, sludges and suspensions in circular pipe, Ind. Eng. Chem., 33, 249-256.

Campbell, C. S., 1989. Self-lubrication for long runout landslides, J. Geol., 97, 653-665.

Campbell, D. B. and Shaw, W. H., 1978. Performance of a waste rock dump on moderate to steeply sloping foundations, Proc. Int. Symp. Stability in Coal Mining, 395-405.

Carmichael, R. S., ed., 1982. CRC Handbook of Physical Properties of Rocks, Vol. III, 146-152.

Carr, M. H., 1981. The Surface of Mars, Yale University Press, New Haven, CT, 232 pp.

Carr, M. H., 1986. Mars: A water-rich planet?, Icarus, 68, 187-216.

Carr, M. H., 1987. Water on Mars, Nature, 326, 30-35.

Chyba, C. F., et al., 1989. Depth to unoxidized material in the martian regolith, 20th Lunar and Planetary Science Conf., 157-158.

Costa, J. E. and Schuster, R. L., 1988. The formation and failure of natural dams, G. S. A. Bull., 100, 1054-1068.

Crandell, D. R., 1989. Gigantic debris avalanche of Pleistocene age from ancestral Mount Shasta volcano, California, and debris-avalanche hazard zonation, U. S. G. S. Bull. 1861, 32 pp.

Crandell, D. R. and Fahnestock, R. K., 1965. Rockfalls and avalanches from Little Tahoma Peak on Mount Ranier, Washington, U. S. G. S. Bull. 1221-A, 30 pp.

Crandell, D. R., et. al., 1984. Catastrophic debris avalanche from ancestral Mount Shasta volcano, California: Geology, 12, 143-146.

Cruden, D. M., 1976. Major rock slides of the Rockies, Can. Geotech. J., 13, 8-20.

Cruden, D. M., 1980. A large landslide on Mars: Discussion and reply, G. S. A. Bull., 91, 63.

Cruden, D. M., 1982. The Brazeau Lake slide, Jasper National Park, Alberta: Can. J. Earth Sci., 19, 975-981.

Cruden, D. M., 1985. Rock slope movements in the Canadian Cordillera: Can. Geotech. J., 22, 528-540.

Cruden, D. M. and Antoine, P., 1984. The slide from Mt. Granier, Isere and Savoie, France on November 24, 1248, IV Int. Symp. on Landslides, Vol. 1, 475-481.

Cruden, D. M. and Krahn, J., 1978. Frank rockslide, Alberta, Canada, In: Rockslides and Avalanches, 1, B. Voight, ed., Elsevier Pub. Co., New York, 97-112.

Cruden, D. M. and Hungr, O., 1986. The debris of the Frank Slide and theories of rockslide-avalanche mobility: Can. J. Earth Sci., 23, 425-432.

Curry, B. B. and Melhorn, W. N., 1990. Summit Lake landslide and geomorphic history of Summit Lake basin, northwestern Nevada, Geomorphology, 4, 1-17.

Daly, R. A., et al., 1912. Report of the Commission appointed to investigate Turtle Mountain, Frank, Alberta, Can. Geol. Surv., Mem., 27, 34 pp.

Daugherty, R. L., 1937. Hydraulics, 4th ed., McGraw-Hill Book Co., Inc., New York, 460 pp.

Davies, T. R. H., 1982. Spreading of rock avalanche debris by mechanical fluidization, Rock Mechanics, 15, 9-24.

Davis, J. C., 1986. Statistics and Data Analysis in Geology, 2nd ed., John Wiley & Sons, New York, 646 pp.

Delaney, P. T., et al., 1990. Deep magma body beneath the summit and rift zones of Kilauea volcano, Hawaii, Science, 247, 1311-1316.

Dibblee, T. W., Jr., 1964. Geologic map of the Lucerne Valley quadrangle, San Bernardino County, California, U.S. Geological Survey Misc. Invest. Map I-426.

Dobrin, M. B., 1976. Introduction to Geophysical Prospecting, 3rd ed., McGraw-Hill Book Co., 630 pp.

Drake, T. G., 1990. Structural features in granular flows, J. G. R., 95(B6), 8681-8696.

Eisbacher, G. H., 1979. Cliff collapse and rock avalanches (sturzstroms) in the Mackenzie Mountains, northwestern Canada, Can. Geotech. J., 309-334.

Eisbacher, G. H. and Clague, J. J., 1984. Destructive mass movements in high mountains: Hazard and management, Geol. Surv. Can., Pap. 84-16, 230 pp..

Eissler, H. K. and Kanamori, H., 1987. A single-force model for the 1975 Kalapana, Hawaii, earthquake, J. G. R., 92(B6), 4827-4836.

El-Baz, F., 1972. New geological findings in Apollo 15 lunar orbital photography, Proc. 3rd Lunar Science Conf., Vol. 1, 39-61.

Eppler, D. B., et. al., 1987. Rheologic properties and kinematics of emplacement of the Chaos Jumbles rockfall avalanche, Lassen Volcanic National Park, California. J. G. R., 92(B5), 3623-3633.

Erismann, T. H., 1979. Mechanisms of large landslides, Rock Mechanics, 12, 15-46.

Evans, S. G., et. al., 1987. A rock avalanche triggered by the October 1985 North Nahanni earthquake, District of Mackenzie, N.W.T.: Can. J. Earth Sci., 24, 176-184.

Evans, S. G., et. al., 1989. The Pandemonium Creek rock avalanche, British Columbia, Can. Geotech. J., 26, 427-446.

Fahnestock, R. K., 1978. Little Tahoma Peak rockfalls and avalanches, Mount Rainier, Washington, U.S.A., In: Rockslides and Avalanches, 1, B. Voight, ed., Elsevier Pub. Co., New York, 181-196.

Fairbridge, R. W., 1950. Landslide patterns on oceanic volcanoes and atolls, Geogr. J., 115, 84-88.

Fauque, L. and M. R. Strecker, 1988. Large rock avalanche deposits (Sturzstrome, sturzstroms) at Sierra Aconquija, northern Sierras Pameanas, Argentina: Eclogae geol. Helv., 81(3), 579-592.

Fornari, D. J., et. al., 1979. A large submarine sand-rubble flow on Kilauea volcano, Hawaii: J. Volcan. Geotherm. Res., 5, 239-256.

Francis, P. W., et. al., 1985. Catastrophic debris avalanche deposit of Socompa volcano, northern Chile: Geology, 13, 600-603.

Galitzin, B., 1915. Sur le tremblement de terre du 18 février 1911, Comptes rendus de l'Academie des Sciences, 160, 810-814.

Gaziev, E., 1984. Study of the Usoy landslide in Pamir, IV International Symposium on Landslides, Volume 1, 511-515.

Goguel, J., 1978. Scale-dependent rockslide mechanisms, with emphasis on the role of pore fluid vaporization: Rockslides and Avalanches, 1, B. Voight, ed., Elsevier Pub. Co., New York, 693-706.

Gongxian, W. and Bangdong, X., 1984. Brief introduction of landslides in loess in China, IV Int. Symp. on Landslides, Vol. 1, 197-207.

Greely, R. and Guest, J. E., 1987. Geologic map of the eastern equatorial region of Mars, U. S. Geological Survey Miscellaneous Investigations Series Map I-1802-B, scale 1:15,000,000.

Gregorian, S. S., et al., 1983. Mathematical modeling of mountain landslides and large landslide dams, Acad. Sci. U.S.S.R., Engineering Geology sect., 6, 61-72.

Gubin, I. E., 1960. Laws governing seismic phenomena in the Tadzhikistan region, Acad. Sci, U.S.S.R., 290.

Guest, J. E., 1971. Geology of the farside crater Tsiolkovsky: Geology and Physics of the Moon, G. Fielder, ed., Elsevier Publishing Co., Amsterdam, 93-103.

Habib, P., 1975. Production of gaseous pore pressure during rock slides, Rock Mechanics, 7, 193-197.

Hadley, J. B., 1959. The Madison Canyon landslide, Geotimes, 4(3), 14-17.

Hadley, J. B., 1960. The Madison landslide, Billings Geological Society, 11th Ann. Field Conf., 45-48.

Hadley, J. B., 1978. Madison Canyon rockslide, Montana, U.S.A.: Rockslides and Avalanches, 1, B. Voight, ed., Elsevier Pub. Co., New York, 167-180.

Haller, K. M., 1988. Proposed segmentation of the Lemhi and Beaverhead faults, Idaho, and Red Rock fault, Montana--Evidence from studies of fault-scarp morphology, G. S. A. Abst. Prog., 20(6), 418-419.

Hanes, D. M. and Inman, D. L., 1985. Observations of rapidly flowing granular-fluid materials, J. Fluid Mech., 150, 357-380.

Harrison, J. V. and Falcon, N. L., 1938. An ancient landslip at Saidmarreh in southwestern Iran, J. Geol., 46, 296-309.

Hazlett, R. W., et al., in press. Unusual slope failures and related deposits of the 1944 eruption of Mt. Vesuvius, Italy.

Heard, H. C., 1960. Transition from brittle fracture to ductile flow in solenhofen limestone as a function of temperature, confining pressure and interstitial fluid pressure: Rock deformation, G. S. A. Memoir 79, 193-226.

Hector, S.T., 1989. Beatty landslide, Santa Cruz County, California: California Geology, 37-39.

Heim, A., 1882. Der Bergsturz von Elm, Zeitschrift der Deutschen Geologischen Gesellschaft, 34, 74-115.

Heim, A., 1932. Bergsturz und Menschenleben, Fretz & Wasmuth A. G., Zurich, 218 p. (English translation by N. A. Skermer, BiTech Publishers, Vancouver, BC)

Heuberger, H., et. al., 1984. Quaternary landslides and rock fusion in central Nepal and in the Tyrolean Alps: Mountain Research and Development, 4(4), 345-362.

Hewett, K., 1988. Catastrophic landslide deposits in the Karakoram Himalaya; Science, 242, 64-67.

Hirth, G. and Tullis, J., 1989. The effects of pressure and porosity on the micromechanics of the brittle-ductile transition in quartz, J. G. R., 94, 17825-17838.

Holland, T. H., 1894. Report on the Gohna Landslip, Rec. Geol. Surv. India, 27(2), 55-64.

Howard, K. A., 1973a. Avalanche mode of motion: Implications from lunar examples, Science, 180, 1052-1055.

Howard, K. A., 1973b. Lunar Avalanches, Abst. Lunar Science IV Conf., 386-388.

Hoyer, M. C., 1971. Puget Peak avalanche, Alaska: G. S. A. Bull., 82, 1267-1284.

Hsü, K. J., 1975. Catastrophic debris streams (Sturzstroms) generated by rockfalls, G. S. A. Bull., 86, 129-140.

Hui, K. and Haff, P. K., 1986. Kinetic grain flow in a vertical channel, Int. J. Multiphase Flow, 12, 289-298.

Hulme, G., 1974. The interpretation of lava flow morphology, Geophys. J. R. Astr. Soc., 39, 361-383.

Hungr, O., 1990. Momentum transfer and friction in the debris of rock avalanches: Discussion, Can. Geotech. J., 27, 697.

Jahns, R. H. and Engel, E. J., 1949. Pliocene breccias in the Avawatz Mountains, San Bernardino County, California, G. S. A. Bull., 60, 1940.

JANAF Thermochemical Tables, 2nd Ed., 1971. National Bureau of Standards.

Jeffreys, H., 1923. The Pamir earthquake of 1911 February 18, in relation to the depths of earthquake foci, Roy. Astr. Soc., Monthly Notices, Geophys. Suppl., 1, 22-31.

Johnson, A. M., 1970. Physical Processes in Geology, Freeman, Cooper & Co., San Francisco, 577 p.

Johnson, A. M., 1984. Debris flow, in: Slope Instability, D. Brunsden and D. B. Prior, eds., John Wiley & Sons, New York, 257-361.

Johnson, B., 1978. Blackhawk landslide, California, U.S.A.: Rockslides and Avalanches, 1, B. Voight, ed., Elsevier Pub. Co., New York, 481-504.

Kanamori, H. and Given, J. W., 1982. Analysis of long-period seismic waves excited by the May 18, 1980 eruption of Mount St. Helens - A terrestrial monopole?, J. G. R., 87, 5422-5432.

Keefer, D. K., 1984. Landslides caused by earthquakes, G. S. A. Bull., 95, 406-421.

Kent, P. E., 1966. The transport mechanism in catastrophic rock falls, J. Geol., 74, 79-83.

Kerr, D. R., 1984. Early Neogene continental sedimentation in the Vallecito and Fish Creek mountains, western Salton trough, California, Sedimentary Geology, 38, 217-246.

Kojan, E. and Hutchinson, J. N., 1978. Mayunmarca rockslide and debris flow: Rockslides and Avalanches, 1, B. Voight, ed., 315-361.

Krieger, M. H., 1977. Large landslides, composed of megabreccia, interbedded in Miocene basin deposits, southeastern Arizona.

Krumdieck, M. A., 1984. On the mechanics of large landslides, IV Int. Symposium on Landslides, Vol. 1, Toronto, 539-544.

Lipman, P. W., et al., 1985. Ground deformation associated with the 1975 magnitude-7.2 earthquake and resulting changes in activity of Kilauea volcano, Hawaii, U. S. G. S. Prof. Pap. 1267, 45 pp.

Lipman, P. W., et. al., 1988. The giant submarine Alika debris slide, Mauna Loa, Hawaii: J. G. R., 93(B5), 4279-4299.

Longwell, C. R., 1951. Megabreccia developed downslope from large faults, Am. J. Sci., 249, 343-355.

Lucchitta, B. K., 1977. Crater clusters and light mantle at the Apollo 17 site; A result of secondary impact from Tycho, Icarus, 30, 80-96.

Lucchitta, B. K., 1978a. A large landslide on Mars, G. S. A. Bull., 89, 1601-1609.

Lucchitta, B. K., 1978b. Morphology of chasma walls, Mars, J. Res. U. S. Geol. Surv., 6(5), 651-662.

Lucchitta, B. K., 1979. Landslides in Valles Marineris, Mars, J. G. R., 84(B14), 8097-8113.

Lucchitta, B. K., 1987a. Valles Marineris, Mars: Wet debris flows and ground ice, Icarus, 72, 411-429.

Lucchitta, B. K., 1987b. Recent mafic volcanism on Mars, Science, 235, 565-567.

Malin, M. C., 1977. Comparison of volcanic features of Elysium (Mars) and Tibesti (Earth), G. S. A. Bull., 88, 908-919.

Mapel, W. J., et al., 1965. Geologic map and sections of the Doublespring Quadrangle, Custer and Lemhi Counties, Idaho, U. S. Geological Survey General Quadrangle Map GQ-464, scale 1:62500.

Mathews W. H. and McTaggart, K. C., 1969. The Hope landslide, British Columbia, Geol. Assoc. Canada, Proceedings, 20, 65-75.

Mathewson, C. C., 1981. Engineering Geology, Charles E. Merrill Pub. Co., Columbus, OH, 410 pp.

McCauley, J. F., 1978. Geologic map of the Coprates Quadrangle of Mars, U. S. Geol. Survey Misc. Inv. Series Map I-897, scale 1:5,000,000.

McEwen, A. S., 1989. Mobility of large rock avalanches: Evidence from Valles Marineris, Mars, Geology, 17, 1111-1114.

McKay, C. P., et al., 1985. Thickness of ice on perenially frozen lakes, Nature, 313, 561-562.

McSaveney, M. J., 1978. Sherman glacier rock avalanche: Rockslides and Avalanches, 1, B. Voight, ed., Elsevier Pub. Co., New York, 71-96.

Mellor, M., 1963. Polar Snow - A summary of engineering properties: Ice and Snow, Properties, Processes and Applications, W. D. Kingery, ed., M.I.T. Press, Cambridge, MA, 528-559.

Melosh, H. J., 1979. Acoustic fluidization: A new geologic process?, J. G. R., 84(B13), 7513-7520.

Melosh, H. J., 1983. Acoustic fluidization, American Scientist, 71, 158-165.

Melosh, H. J., 1986. The physics of very large landslides, Acta Mechanica, 64, 89-99.

Melosh, H. J., 1987. The mechanics of large rock avalanches, G. S. A. Rev. in Eng. Geol., Vol. VII, 41-49.

Mollard, J. D., 1977. Regional landslide types in Canada, G. S. A. Rev. in Eng. Geol., vol. 3, 29-56.

Moore, D. P. and Mathews, W. H., 1978. The Rubble Creek landslide, southwestern British Columbia, Can. J. Earth Sci., 15(7), 1039-1052.

Moore, J. G., 1964. Giant submarine landslides on the Hawaiian ridge: U. S. Geol. Surv. Prof. Pap. 501-D, D95-D98.

Moore, J. G., et al., 1989. Prodigious submarine landslides on the Hawaiian Ridge, J. G. R., 94(B12), 17465-17484.

Moore, J. G. and Moore, G. W., 1984. Deposit from a giant wave on the island of Lanai, Hawaii, Science, 226, 1312-1315.

Moore, W. J., 1972. Physical Chemistry, 977 pp.

Mudge, M. R., 1965. Rockfall-avalanche and rockslide-avalanche deposits at Sawtooth Ridge, Montana, G. S. A. Bull., 76, 1003-1014.

Müeller, L., 1964. The rock slide in the Vajont valley, Felsmechanik u. Ingenieurgeologie, 2, 148-212.

Müeller, L., 1968. New considerations of the Vajont slide, Rock Mech. Eng. Geol., 6, 1-91.

Mutch, T. A., et al., 1976. The Geology of Mars, Princeton University Press, Princeton, NJ, 400 pp.

Nedell, S. S., et al., 1987. Origin and evolution of the layered deposits in the Valles Marineris, Mars, Icarus, 70, 409-441.

Normark, W. R. and C. E. Gutmacher, 1988. Sur submarine slide, Monterey Fan, central California: Sedimentology, 35, 629-647.

Nye, J. F., 1951. The flow of glaciers and ice-sheets as a problem in plasticity, Roy. Soc. Lond. Proc. Series A, 207, 554-572.

Nye, J. F., 1967. Plasticity solution for a glacier snout, J. Glaciology, 6(47), 695-713.

Patterson, M. S., 1978. Experimental Rock Deformation - The Brittle Field, Springer-Verlag, New York, 254 pp.

Pierce, K. L. and Scott, W. E., 1982. Pleistocene episodes of alluvial-gravel deposition, southeastern Idaho: Cenozoic Geology of Idaho, Idaho Bureau of Mines and Geology Bulletin 26, B. Bonnichsen and R. M. Breckenridge, eds., 685-702.

Plafker, G. and Ericksen, G. E., 1978. Nevados Huascaran avalanches, Peru: Rockslides and Avalanches, 1, B. Voight, ed., 277-314.

Plaza-Nieto, G., et al., 1990. Landslide dam on the Pisque River, northern Ecuador, Landslide News, 4, 2-4.

Post, A., 1967. Effects of the March 1964 Alaska earthquake on glaciers, U. S. G. S. Prof. Pap. 544-D, 42 pp.

Potapov, A. V. and Ivanov, B. A., 1991. Landslide motion: Numerical simulation for Earth and Mars, 22nd Lunar and Planetary Science Conf., in press.

Preobrajensky, S., 1920. Eboulement D'Ousoi (Pamir), Geologischeskii Komitet Materialy, 14, 11-22.

Press, F., 1966. Seismic velocities: Handbook of physical constants, S. P. Clark, Jr., ed., G. S. A. Memoir 97, 197-212.

Press, F. and Siever, R., 1986. Earth, 4th ed., W. H. Freeman and Company, New York, 656 pp.

Prior, D. B., et al., 1984. Depositional characteristics of a submarine debris flow, J. Geol., 92, 707-727.

Ramuz, C. F., 1947. When the Mountain Fell, translated by S. F. Scott, Pantheon Books, New York, 221 pp.

Reiche, P., 1937. The Toreva-block - A distinctive landslide type, J. Geol., 45, 538-548.

Resnick, R. and Halliday, D., 1977. Physics, John Wiley & Sons, New York, 564 pp.

Robinson, M. S. and Tanaka, K. L., 1990. Magnitude of a catastrophic flood event at Kasei Valles, Mars, Geology, 18, 902-905.

Ross, C. P., 1947. Geology of the Borah Peak quadrangle, Idaho, G. S. A. Bull., 58, 1085-1160.

Rowland, S. M., et al., 1985. Characteristics of a high-strength, subaerial debris flow in the North Muddy Mountains of southern Nevada, G. S. A. Abst. w. Prog., 17, 703.

Salyards, S. L., 1985. Patterns of offset associated with the 1983 Borah Peak, Idaho, earthquake and previous events, in Proceedings of Workshop XXVIII on the Borah Peak, Idaho, Earthquake, R. S. Stein and R. C. Bucknam, Eds., U. S. G. S. Open File Rept. 85-290, 59-75.

Savage, S. B., 1984. The mechanics of rapid granular flows, Advances in Appl. Mech., 24, 289-366.

Scheller, E., 1971. Beitrag zum Bewegungsverhalten grosser Bergstürze, Eclogae Geol. Helvetiae, 64, 195-202.

Scheidegger, A. E., 1973. On the prediction and reach of catastrophic landslides, Rock Mechanics, 5, 231-236.

Schultz, P. H. and Gault, D. E., 1975. Seismically induced modification of lunar surface features, Proc. 6th Lunar Sci. Conf., 2845-2862.

Schuster, R.L. and Crandell, D.R., 1984. Catastrophic debris avalanches from volcanoes: IV International Symposium on Landslides, Vol. 1, 567-572.

Schwartz, D. P. and A. J. Crone, 1988. Paleoseismicity of the Lost River fault zone, Idaho: Earthquake recurrence and segmentation, G. S. A. Abst. with Prog., 20(3), 228.

Scott, D. H. and Tanaka, K. L., 1986. Geologic map of the western equatorial region of Mars, U. S. Geological Survey Miscellaneous Investigations Series Map I-1802-A, scale 1:15,000,000.

Scott, R. F., 1963. Principles of Soil Mechanics, Addison-Wesley Publishing Co., Inc., Palo Alto, CA, 97-98, 330.

Scott, W. E., et al., 1985. Quaternary tectonic setting of the 1983 Borah Peak earthquake, central Idaho, B. S. S. A., 75(4), 1053-1066.

Seed, H. B., 1968. Landslides during earthquakes due to liquifaction, J. Soil Mechanics and Foundations Division, ASCE, 94(SM5), 1053-1122.

Shaller, P. J., et al., 1989. Subaqueous landslides on Mars?, 20th Lunar and Planetary Science Conf., 990-991.

Sharp, R. P., 1973. Mars: Troughed terrain, J. G. R., 78, 4063-4072.

Sharp, R. P., 1976. Field Guide to Southern California Geology, Kendall/Hunt Publishing Co., Dubuque, IA, 208 pp.

Sharp, R. P., 1988. Living Ice: Understanding Glaciers and Glaciation, Cambridge University Press, New York, NY, 225 pp.

Sharpe, C. F. S., 1938. Landslides and Related Phenomena, Cooper Square Pub., New York, 137 pp.

Shelton, J. S., 1966. Geology Illustrated, W. H. Freeman and Company, San Francisco, 434 pp.

Shreve, R. L., 1959. Geology and mechanics of the Blackhawk landslide, Lucerne Valley, California, Ph.D. Thesis, California Institute of Technology, 79 pp.

Shreve, R. L., 1966. Sherman landslide, Alaska, Science, 154, 1639-1643.

Shreve, R. L., 1968a. The Blackhawk landslide, G. S. A. Spec. Pap. 108, 47 pp.

Shreve, R. L., 1968b. Leakage and fluidization in air-layer lubricated avalanches, G. S. A. Bull., 79, 653-658.

Shreve, R. L., 1987. Blackhawk landslide, southwestern San Bernardino County, California: G. S. A. Centennial Field Guide - Cordilleran Section, 109-114.

Siebert, L., 1984. Large volcanic debris avalanches: Characteristics of source areas, deposits, and associated eruptions, J. Volcanol. Geotherm. Res., 22, 163-197.

Sieh, K. E. and Bursik, M., 1986. Most recent eruption of the Mono craters, eastern central California: J. G. R., 91, B11, 12539-12571.

Size, W. B., ed., 1987. Use and Abuse of Statistical Methods in the Earth Sciences, International Association for Mathematical Geology, Studies in Mathematical Geology No. 1, Oxford University Press, New York, 169 pp.

Solonenko, V. P., 1972. Seismogenic destruction of mountain slopes, 24th Int. Geol. Congress, sect. 13, 284-290.

Solonenko, V. P., 1977. Landslides and collapses in seismic zones and their prediction, Bull. Int. Assoc. Eng. Geology, 15, 4-8.

Solonenko, V. P., 1979. Mapping the after-effects of disasterous earthquakes and estimation of hazard for engineering constructions, Bull. Int. Assoc. Eng. Geology, 19, 138-142.

Solonenko, V. P., et. al., 1984. The engineering seismogeology of the northern Muya Interrift Commissure (Baikal Rift Zone): Int. Assoc. Eng. Geol.. IV International Congress, pp 1-13.

Stickney, M. C. and Bartholomew, M. J., 1987. Seismicity and late Quaternary faulting of the northern Basin and Range Province, Montana and Idaho, B. S. S. A., 77(5), 1602-1625.

Stout, M. L., 1977. Radiocarbon dating of landslides in southern California, California Geology, 99-105.

Stout, M. L., 1988. Geology of Blackhawk Canyon, San Bernardino Mountains, southern California: G. S. A. Abst. w. Prog., 20(7), A55.

Stuiver, M. and Becker, B., 1986. High-precision decadal calibration of the radiocarbon time scale, AD 1950-2500 BC. Radiocarbon, **28**: 863-910.

Tanaka, K. L., 1986. The stratigraphy of Mars, J. G. R., 91(B13), E139-E158.

Tanaka, K. L. and Scott, D. H., 1987. Geologic map of the polar regions of Mars, U. S. Geological Survey Miscellaneous Investigations Series Map I-1802-C, scale 1:15,000,000.

Taylor, S. R., 1975. Lunar Science: A Post-Apollo View, Pergamon Press, Inc., New York, 372 pp.

Terzaghi, K., 1950. Mechanism of landslides, G. S. A. Engineering Geology (Berkey) Volume, 83-123.

Trunk, F. J., et al., 1986. Computer modeling of large rock slides, J. Geotechnical Engineering, 112(3), 348-360.

Ui, T., 1983. Volcanic dry avalanche deposits - Identification and comparison with nonvolcanic debris stream deposits, J. Volcan. Geotherm. Res., 18, 135-150.

Ui, T., et. al., 1986. Fragmentation of debris avalanche material during flowage - Evidence from the Pungarehu Formation, Mount Egmont, New Zealand: J. Volcanology and Geothermal Res., 27, 255-264.

U. S. Geological Survey, 1979. Controlled photomosaic of the Aeolis Southeast quadrangle of Mars, U. S. Geol. Survey Misc. Inv. Series Map I-1215, scale 1:2,000,000.

U. S. Geological Survey, 1980. Topographic orthophoto mosaic of the Tithonium Chasma region of Mars, U. S. Geol. Survey Misc. Inv. Series Map I-1294, scale 1:500,000.

U. S. Geological Survey, 1984a. Controlled photomosaic of part of the Valles Marineris region of Mars, U. S. Geol. Survey Misc. Inv. Series Map I-1591, scale 1:500,000.

U. S. Geological Survey, 1984b. Controlled photomosaic of part of the Valles Marineris region of Mars, U. S. Geol. Survey Misc. Inv. Series Map I-1593, scale 1:500,000.

U. S. Geological Survey, 1984c. Controlled photomosaic of part of the Valles Marineris region of Mars, U. S. Geol. Survey Misc. Inv. Series Map I-1592, scale 1:500,000.

U. S. Geological Survey, 1986a. Controlled photomosaic of part of the Candor Mensa region of Mars, U. S. Geol. Survey Misc. Inv. Series Map I-1841, scale 1:500,000.

U. S. Geological Survey, 1986b. Controlled photomosaic of part of the Candor Mensa region of Mars, U. S. Geol. Survey Misc. Inv. Series Map I-1842, scale 1:500,000.

U. S. Geological Survey, 1986c. Topographic map of the Coprates Northwest Quadrangle of Mars, U. S. Geol. Survey Misc. Inv. Series Map I-1712, scale 1:2,000,000.

Van Gassen, W. and Cruden, D. M., 1989. Momentum transfer and friction in the debris of rock avalanches, Can. Geotech. J., 26(4), 623-628.

Van Gassen, W. and Cruden, D. M., 1990. Momentum transfer and friction in the debris of rock avalanches: Reply, Can. Geotech. J., 27, 698-699.

Varnes, D. J., 1958. Landslide types and processes, In: Landslides and engineering practice, E. B. Eckel, ed., National Research Council, Highway Research Board, Special Report 29, 20-47.

Voight, B., 1978. Lower Gros Ventre slide, Wyoming, U.S.A., In: Rockslides and Avalanches, 1, B. Voight, ed., Elsevier Pub. Co., New York, 113-166.

Voight, B., et al., 1983. Nature and mechanics of the Mount St. Helens rockslide-avalanche of 18 May 1980, Geotechnique, 33, 243-273.

Voight, B. and Pariseau, W. G., 1978. Rockslides and avalanches: An introduction: Rockslides and Avalanches, 1, B. Voight, ed., Elsevier Pub. Co., New York, 1-67.

Wahrhaftig, C. and Cox, A., 1959. Rock glaciers in the Alaska Range, Geological Society of America Bulletin, **70**: 383-436.

Waitt, R. B., 1979. Rockslide-avalanche across distributary of Cordilleran ice in Pasayten Valley, northern Washington, Arctic and Alpine Res., 11(1), 33-40.

Watson, R. A. and Wright, H. E., Jr., 1969. The Saidmarreh landslide, Iran, G. S. A. Special Paper 123, 115-139.

Whitten, D. G. A. and Brooks, J. R. V., 1983. A Dictionary of Geology, Penguin Books, Ltd., Harmondsworth, England, 252.

Wilhelms, D. E., 1987. The geologic history of the Moon, U. S. Geological Survey Prof. Pap. 1348, 302 pp.

Yarnold, J. C. and Lombard, J. P., 1989. A facies model for large rock-avalanche deposits formed in dry climates: Conglomerates in Basin Analysis: A Symposium Dedicated to A. O. Woodford, I. P. Colburn, P. L. Abbott and J. Minch, eds., Pacific Section S. E. P. M., 62, 9-31.

Yosida, Z., 1963. Physical properties of snow: Ice and Snow, Properties, Processes and Applications, W. D. Kingery, ed., M.I.T. Press, Cambridge, MA, 485-527.

Appendix G: Table for Calculation of Significance from Z-Test Values (Alder and Roessler, 1977)

Areas Under the Normal Probability Curve

The entries under *A* denote the area between the line of symmetry (that is, $z = 0$) and the given *z*-value.

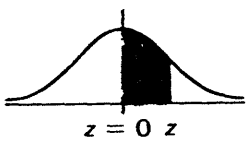

z	A	z	A	z	A	z	A
0.00	0.0000	0.30	0.1179	0.60	0.2258	0.90	0.3159
.01	.0040	.31	.1217	.61	.2291	.91	.3186
.02	.0080	.32	.1255	.62	.2324	.92	.3212
.03	.0120	.33	.1293	.63	.2357	.93	.3238
.04	.0160	.34	.1331	.64	.2389	.94	.3264
.05	.0199	.35	.1368	.65	.2422	.95	.3289
.06	.0239	.36	.1406	.66	.2454	.96	.3315
.07	.0279	.37	.1443	.67	.2486	.97	.3340
.08	.0319	.38	.1480	.68	.2518	.98	.3365
.09	.0359	.39	.1517	.69	.2549	.99	.3389
.10	.0398	.40	.1554	.70	.2580	1.00	.3413
.11	.0438	.41	.1591	.71	.2612	1.01	.3438
.12	.0478	.42	.1628	.72	.2642	1.02	.3461
.13	.0517	.43	.1664	.73	.2673	1.03	.3485
.14	.0557	.44	.1700	.74	.2704	1.04	.3508
.15	.0596	.45	.1736	.75	.2734	1.05	.3531
.16	.0636	.46	.1772	.76	.2764	1.06	.3554
.17	.0675	.47	.1808	.77	.2794	1.07	.3577
.18	.0714	.48	.1844	.78	.2823	1.08	.3599
.19	.0754	.49	.1879	.79	.2852	1.09	.3621
.20	.0793	.50	.1915	.80	.2881	1.10	.3643
.21	.0832	.51	.1950	.81	.2910	1.11	.3665
.22	.0871	.52	.1985	.82	.2939	1.12	.3686
.23	.0910	.53	.2019	.83	.2967	1.13	.3708
.24	.0948	.54	.2054	.84	.2996	1.14	.3729
.25	.0987	.55	.2088	.85	.3023	1.15	.3749
.26	.1026	.56	.2123	.86	.3051	1.16	.3770
.27	.1064	.57	.2157	.87	.3079	1.17	.3790
.28	.1103	.58	.2190	.88	.3106	1.18	.3810
.29	.1141	.59	.2224	.89	.3133	1.19	.3830

Areas Under the Normal Probability Curve

(*continued*)

z	A	z	A	z	A	z	A
1.20	0.3849	1.55	0.4394	1.90	0.4713	2.25	0.4878
1.21	.3869	1.56	.4406	1.91	.4719	2.26	.4881
1.22	.3888	1.57	.4418	1.92	.4726	2.27	.4884
1.23	.3907	1.58	.4430	1.93	.4732	2.28	.4887
1.24	.3925	1.59	.4441	1.94	.4738	2.29	.4890
1.25	.3944	1.60	.4452	1.95	.4744	2.30	.4893
1.26	.3962	1.61	.4463	1.96	.4750	2.31	.4896
1.27	.3980	1.62	.4474	1.97	.4756	2.32	.4898
1.28	.3997	1.63	.4485	1.98	.4762	2.33	.4901
1.29	.4015	1.64	.4495	1.99	.4767	2.34	.4904
1.30	.4032	1.65	.4505	2.00	.4773	2.35	.4906
1.31	.4049	1.66	.4515	2.01	.4778	2.36	.4909
1.32	.4066	1.67	.4525	2.02	.4783	2.37	.4911
1.33	.4082	1.68	.4535	2.03	.4788	2.38	.4913
1.34	.4099	1.69	.4545	2.04	.4793	2.39	.4916
1.35	.4155	1.70	.4554	2.05	.4798	2.40	.4918
1.36	.4131	1.71	.4564	2.06	.4803	2.41	.4920
1.37	.4147	1.72	.4573	2.07	.4808	2.42	.4922
1.38	.4162	1.73	.4582	2.08	.4812	2.43	.4925
1.39	.4177	1.74	.4591	2.09	.4817	2.44	.4927
1.40	.4192	1.75	.4599	2.10	.4821	2.45	.4929
1.41	.4207	1.76	.4608	2.11	.4826	2.46	.4931
1.42	.4222	1.77	.4616	2.12	.4830	2.47	.4932
1.43	.4236	1.78	.4625	2.13	.4834	2.48	.4934
1.44	.4251	1.79	.4633	2.14	.4838	2.49	.4936
1.45	.4265	1.80	.4641	2.15	.4842	2.50	.4938
1.46	.4279	1.81	.4649	2.16	.4846	2.51	.4940
1.47	.4292	1.82	.4656	2.17	.4850	2.52	.4941
1.48	.4306	1.83	.4664	2.18	.4854	2.53	.4943
1.49	.4319	1.84	.4671	2.19	.4857	2.54	.4945
1.50	.4332	1.85	.4678	2.20	.4861	2.55	.4946
1.51	.4345	1.86	.4686	2.21	.4865	2.56	.4948
1.52	.4357	1.87	.4693	2.22	.4868	2.57	.4949
1.53	.4370	1.88	.4700	2.23	.4871	2.58	.4951
1.54	.4382	1.89	.4706	2.24	.4875	2.59	.4952

Areas Under the Normal Probability Curve

(concluded)

z	A	z	A	z	A	z	A
2.60	0.4953	2.95	0.4984	3.30	0.4995	3.65	0.4999
2.61	.4955	2.96	.4985	3.31	.4995	3.66	.4999
2.62	.4956	2.97	.4985	3.32	.4996	3.67	.4999
2.63	.4957	2.98	.4986	3.33	.4996	3.68	.4999
2.64	.4959	2.99	.4986	3.34	.4996	3.69	.4999
2.65	.4960	3.00	.4987	3.35	.4996	3.70	.4999
2.66	.4961	3.01	.4987	3.36	.4996	3.71	.4999
2.67	.4962	3.02	.4987	3.37	.4996	3.72	.4999
2.68	.4963	3.03	.4988	3.38	.4996	3.73	.4999
2.69	.4964	3.04	.4988	3.39	.4997	3.74	.4999
2.70	.4965	3.05	.4989	3.40	.4997	3.75	.4999
2.71	.4966	3.06	.4989	3.41	.4997	3.76	.4999
2.72	.4967	3.07	.4989	3.42	.4997	3.77	.4999
2.73	.4968	3.08	.4990	3.43	.4997	3.78	.4999
2.74	.4969	3.09	.4990	3.44	.4997	3.79	.4999
2.75	.4970	3.10	.4990	3.45	.4997	3.80	.4999
2.76	.4971	3.11	.4991	3.46	.4997	3.81	.4999
2.77	.4972	3.12	.4991	3.47	.4997	3.82	.4999
2.78	.4973	3.13	.4991	3.48	.4998	3.83	.4999
2.79	.4974	3.14	.4992	3.49	.4998	3.84	.4999
2.80	.4974	3.15	.4992	3.50	.4998	3.85	.4999
2.81	.4975	3.16	.4992	3.51	.4998	3.86	.4999
2.82	.4976	3.17	.4992	3.52	.4998	3.87	.5000
2.83	.4977	3.18	.4993	3.53	.4998	3.88	.5000
2.84	.4977	3.19	.4993	3.54	.4998	3.89	.5000
2.85	.4978	3.20	.4993	3.55	.4998		
2.86	.4979	3.21	.4993	3.56	.4998		
2.87	.4980	3.22	.4994	3.57	.4998		
2.88	.4980	3.23	.4994	3.58	.4998		
2.89	.4981	3.24	.4994	3.59	.4998		
2.90	.4981	3.25	.4994	3.60	.4998		
2.91	.4982	3.26	.4994	3.61	.4999		
2.92	.4983	3.27	.4995	3.62	.4999		
2.93	.4983	3.28	.4995	3.63	.4999		
2.94	.4984	3.29	.4995	3.64	.4999		